IMPROVING VAPOR COMPRESSION CYCLE EFFICIENCIES IN SUPPORT OF CONVENTIONAL REFRIGERANT PHASEOUTS

A Dissertation

by

GUAN HUANG

Submitted to the Office of Graduate and Professional Studies of
Texas A&M University
in partial fulfillment of the requirements for the degree of

DOCTOR OF PHILOSOPHY

Chair of Committee,	Michael Pate
Co-Chair of Committee,	Andrea Strzelec
Committee Members,	Jorge L. Alvarado
	Eric L. Petersen
	Pavel V. Tsvetkov
Head of Department,	Andreas Polycarpou

December 2018

Major Subject: Mechanical Engineering

ABSTRACT

Finding replacements for R-410A is paramount, and it primarily focuses on issues such as energy efficiency, GWP, flammability, toxicity, and safety. The study reported herein supports replacing R-410A by investigating reconfigurations to vapor-compression cycles and then determining performance improvements for these modified cycles. In addition, a comprehensive climate zone model was developed so that modified cycle performances could be evaluated and compared for the full range of a cooling-season weather conditions found throughout the U.S, which was necessary because cycle performances are dependent on outdoor temperatures and humidities.

Using R-410A and other refrigerants, these evaluations and comparisons of modified vapor-compression cycles were first performed for outdoor air temperatures ranging from 26.7 to 35 ℃ and relative humidities ranging from 40% to 80% with assumed evaporator exit air temperatures of 7.2, 10, 12.8℃ and a typical compressor efficiency of 80%. The first set of modifications investigated are based on installing evaporative cooling at the condenser air inlet with external supply water sources being either producing COP highest improvements of 60% and internal water supplied by the evaporator condensate producing COP highest improvements 38%. The second set of modifications investigated are based on installing at the evaporator inlet HRV units with resulting COP improvements of 25% and ERV units with COP improvements reaching as high as 100%. The final two modifications both cool the refrigerant exiting the condenser and entering the evaporator by either using evaporator condensate water which resulted in COP improvement of less than 5%, or by transferring energy to the refrigerant exiting the evaporator and entering the compressor with the aid of an internal heat exchanger, which resulted in COP increase as high as 32%. As final step to determine the reconfiguration effectiveness for any

modified cycle with any phaseout replacement refrigerant at any location were combined the two sets of models, namely the climate zone models and the refrigeration cycle models, to perform a comprehensive analysis over full cooling seasons, for each climate zone. The results show that the performance ranking of modification and refrigerant types vary considerably with location, as defined by climate zones, throughout the U.S.

ACKNOWLEDGEMENTS

I would like to express my gratitude to Dr. Michael B. Pate and Dr. Andrea Strzelec for their guidance, support, and for imparting his knowledge and experience to me throughout this research study. I also sincerely appreciate Dr. Jorge Alvarado, Dr. Eric L. Petersen and Dr. Pavel V. Tsvetkov for their serving on my thesis committee. Finally, I would like to thank my mother and father for their support and encouragement.

CONTRIBUTORS AND FUNDING SOURCES

Contributors

A committee that included Dr. Michael Pate, Dr. Andrea Strzelec, Dr. Jorge Alvarado and Dr. Eric L. Petersen of the Department of Mechanical Engineering and Dr. Pavel V. Tsvetkov of the Department of Nuclear Engineering reviewed this thesis.

All other work conducted for this dissertation was completed by the student independently.

Funding Sources

Texas A&M Engineering Experiment Station (TEES), paid my third-year, fourth-year and fifth-year graduate tuition and fees.

NOMENCLATURE

C	Specific heat (Btu/lbm-°R)
D	Hydraulic diameter (in)
h_{ht}	Heat transfer coefficient ($W/m^2 \bullet K$)
h	Enthalpy (Btu/lbm)
K	Thermal conductivity (Btu/hr·ft·°F)
k	Specific heat ratio
$\dot{m}$	Mass flow rate (lb/s)
Nu	Nusselt number
P	Pressure (Psi)
Pr	Prandtl number
q	Refrigerating effect (Btu/lb)
R	Refrigerant ratios
Re	Reynolds number
RH	Relative humidity
T	Temperature (°F)
U	Overall heat transfer coefficient ($W/m^2 \bullet K$)
V	Volume (ft^3)
$\dot{V}$	Volume flow rate (ft^3/min)
$\dot{W}$	Compressor power (Btu/hr)
w	Specific work (Btu/lb)

Greek Symbols:

ρ	Density
ν	Specific volume
μ	Dynamic viscosity
η	Efficiency
ω	Humidity ratio
∅	Relative humidity

Subscripts:

a	Air
c	Condenser
comp	Compressor
db	Dry bulb
e	Evaporator
f	Fluid
fg	Enthalpy of vaporization
H	High side
in	Inlet
L	Low side
out	Outlet
p	At constant pressure
pc	Precooler
R	Refrigerating
s	Saturated

sat	Saturation
V	Volumetric
v	Vapor
w	Water
wb	Wet bulb

TABLE OF CONTENTS

Page

LIST OF FIGURES

Page

LIST OF TABLES

Page

1. INTRODUCTION

Refrigeration is defined as the process of moving heat from one place to another by using refrigerant in a closed cycle. Refrigeration, including all aspects of cooling the built environment, accounts for approximately 15% of worldwide electricity energy consumption and 8% of U.S electricity energy consumption, according to the International Institute of Refrigeration [1]. Space conditioning and HVAC equipment in commercial and residential buildings consume the majority of this energy. Therefore, finding new approaches to reduce the energy used to cool buildings without losing comfort and indoor air quality (IAQ) is an important challenge. Even with decades of searching and researching, the most energy efficient approach for cooling, is still the Rankine cycle, otherwise known as vapor compression refrigeration (VCR). However, when implementing new refrigerants, opportunities exist to improve the energy efficiency of existing vapor-compression technology and components by designing new systems that utilize creative configurations of individual components.

Refrigerants are the working fluids in refrigeration, air-conditioning, and heat-pump systems. Today, many residential and light commercial AC systems in use still contain R-22, which is being phased out globally and has been banned for use in new AC systems in the U.S since 2010. The vast majority of AC units sold today contain R-410A, which is an HFC mixture with a GWP (global warming potential), which is a measure of its climate-warming potential compared to CO2, of 2,088. Therefore, because of this high GWP, R-410A is soon to follow the path of R-22 in that its phase-out has also been mandated. Searching for a new replacement for R-410A are ongoing and paramount while considering Ozone Depleting Potential, GWP, flammability, toxicity, and safety issues. An important consideration when phasing out R-410A is that any replacement refrigerants should not have a lower COP compared to R-410A because the

net result could be an increase in global warming caused by increased power plant emissions. Therefore, as part of the R-410A phaseout, ongoing efforts must be made to improve the energy efficiency of existing vapor- compression technology and components.

2. BACKGROUND AND LITERATURE

2.1 NIST/ Dr. Domanski Research---4th Generation Refrigerant Investigation

Dr. Domanski NIST, the leader of the HVAC&R Equipment Performance Group of the Energy and Environment Division of the Engineering Laboratory, and his group have studied thermodynamic analysis of refrigerants [2] [3] for decades. Dr. Domanski created a new terminology called "exploration of thermodynamic space," which is defined the limits of what is allowed by thermodynamics, but without being constrained by presently known fluids. Four significant thermodynamic parameters, namely critical temperature, critical pressure, vapor heat capacity, and the acentric factor (a parameter related to the slope of the vapor-pressure curve) are identified as four fundamental parameters that can in turn be used to relate all other thermodynamic parameters. They denote a search domain containing refrigerant parameters under full range of possible thermodynamic behaviors. Then, they calculate the thermodynamic properties of a refrigerant by using these parameters and an equation of state. Next, they explore the thermodynamic space with a conventional vapor compression model by using the calculated refrigerant properties determined by the parameter values selected from the search domain. The goal of this exploration is to find an optimum combination of these parameters as as to maximize both COP and the Q_{vol}. With COP being an indicator of the energy efficiency (operating cost) of the system and Q_{vol} defining the refrigeration capacity per unit volume of refrigerant vapor flowing into the compressor; which is a measure of equipment size (first cost). By use of evolutionary algorithms, the most important thermodynamic parameters and their optimum values were determined, with this approach not being limited to only known fluids. This approach is further illustrated by the "Pareto front" on coordinates of inverse volumetric capacity versus inverse COP as shown in Figure 1 for a vapor compression cycle.

The Pareto front represents that a thermodynamic performance limit to for a given cycle and application. Also, it illustrates a fundamental tradeoff between volumetric capacity and COP- in that it is impossible to achieve high COP and high capacity simultaneously. Figure 1 shows refrigerants widely used currently, and it illustrates that the better refrigerants are the ones closer to the Pareto front.

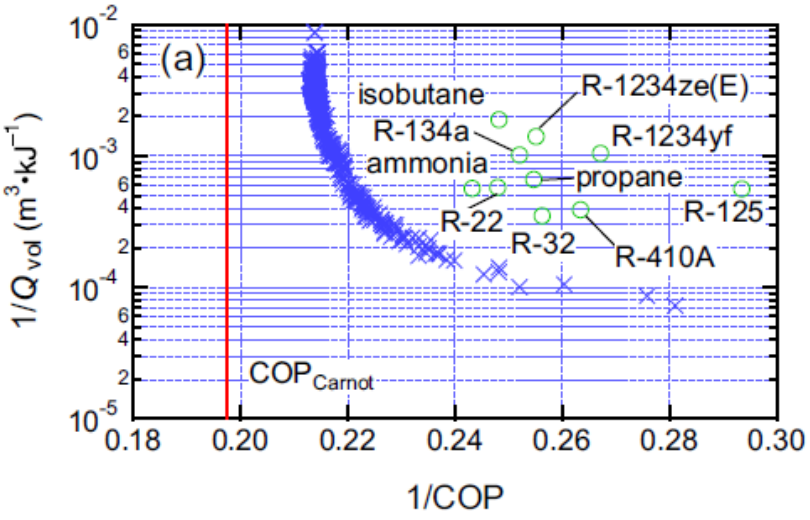

Figure 1 Pareto front and selected current refrigerant for the simple vapor compression cycle

Later in 2017, Dr. Domanski and his group published in Nature Communication [4] an important study that showed that there are limited options for low-global-warming-potential refrigerants. Furthermore, they concluded that the efficiency-versus-capacity trade-off that exists in an ideal analysis disappears when a more realistic system is considered that utilizes forced-convection, air-to-refrigerant heat exchangers, which are optimized for a particular refrigerant. For example, Figure 2 is shown for the primary vapor compression cycle with values being relative to those for R-410A and calculated for the optimized cycle model. The primary conclusion from this figure is that the viable candidates for single component low-GWP alternatives for small AC systems are very limited, especially for refrigerants with volumetric capacities similar to R410A.

Fluids with good COP and low toxicity are available, but all are slightly flammable. Nonflammable candidates exist among the fluid with low volumetric capacity, but the use of such fluids in small AC systems would require extensive redesign and may result in lower COP value. Blends offer possibilities, and refrigeration industries are actively reducing or eliminating flammability with the trade-off of increased GWP.

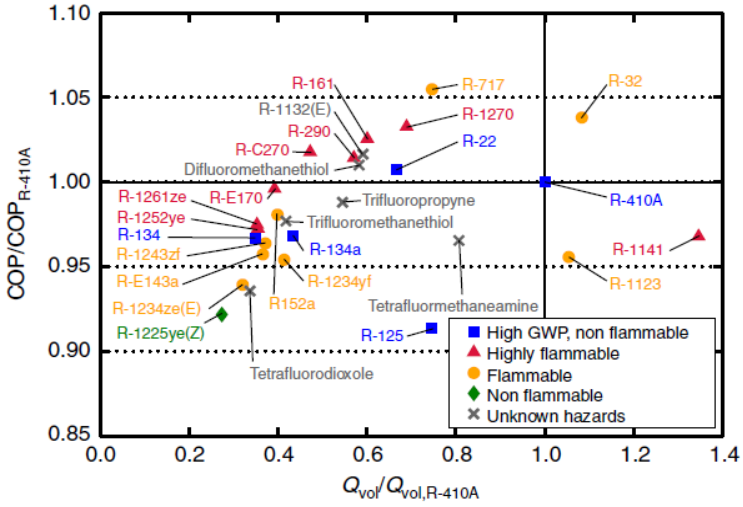

Figure 2 Different refrigerant values are relative to those for R-410A based on the optimized cycle model

From Dr. Domanski paper results, the R-410 replacement dilemma is summarized in Figure 3. To solve this problem, two different approaches are addressed in the study presented herein, namely: a) investigate performance enhancements for reconfigured systems b) identify new drop-in refrigerant types by property comparisons.

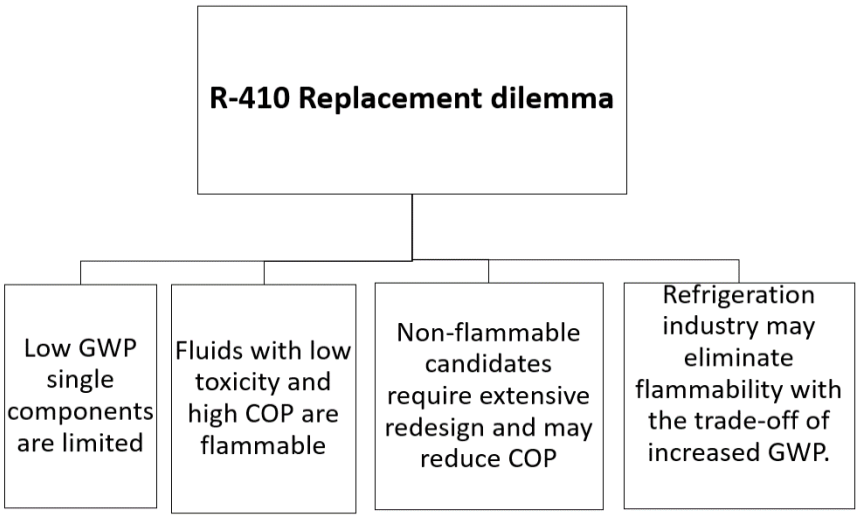

Figure 3 R-410 Replacement dilemma

2.1.1 System Reconfiguration

2.1.2 Conventional Vapor Compression System

A standard vapor-compression refrigeration cycle that one would expect to find in real-world HVAC cooling units has the four major components shown in Figure 4, namely a compressor, condenser, thermal expansion valve and evaporator. The refrigerant processes occurring in the four components are compression, condensation, throttling, and evaporation. In the compression stage, the refrigerant enters the compressor as a superheated vapor at low pressure and low temperature. The superheated vapor then leaves the compressor after being compressed adiabatically as a high pressure and high temperature superheated vapor. In the condensation stage, the high pressure and high-temperature vapor releases its thermal energy and condenses inside the condenser, resulting in the refrigerant leaving the condenser as a high pressure, subcooled liquid. In the throttling stage, the liquid refrigerant flows through the throttling valve in a constant enthalpy process so that the vapor and liquid refrigerant mixture enters the evaporator at a lower pressure and temperature. The low pressure refrigerant mixture is evaporated at a constant

temperature with the liquid absorbing heat from the low-temperature cold reservoir and continually evaporating. Finally, the refrigerant leaves the evaporator as a low-temperature, low-pressure vapor with some superheating occurring enters the compressor again, to complete the cycle. The refrigeration cycle comprising the above processes and states is shown in the Figure 5 Psychrometric chart at least for the air side and then in the Figure 6 T-s and Figure 7 P-h diagrams for the refrigerant side.

For air-side, which was shown previously in the Figure 5, Psychrometric chart, the focus is on processes in the evaporator and condenser, with the same outdoor air being supplied to both. In the case of the condenser, the air exits back to the outdoors. As the outdoor air in the case of the evaporator, the air is cooled and dehumidified as heat is transferred to the low-temperature refrigerant with the air temperature always being higher than the evaporator refrigerant temperature. Furthermore, as the air is cooled, the inlet air humidity ratio is maintained, until the dew point is reached at the 100% relative humidity point. Once the dew point is reached, condensate water is generated, which reduces the humidity ratio as shown in the Figure 5 Psychrometric Chart with the humidity ratio difference between the inlet and outlet of the evaporator being a measure of condensate formed and discharged from the system.

In addition to the evaporator, outdoor air also flows through the condenser and heat transfer occurs between the refrigerant and air, resulting in a higher temperature air being exhausted to the environment. This flowing air with in its increasing temperature is always lower than the condensing refrigerant temperature, was shown in Figure 6. Unlike air in the evaporator, no humidity ratio change occurs in the condenser because the dew point temperature cannot be reached by air heating. Of special note, the values of the refrigerant enthalpy change in all

components can be observed in the Figure 7 Ph diagram, which is important COP in that it is later defined as the ratio of Δh_e to Δh_{com} .

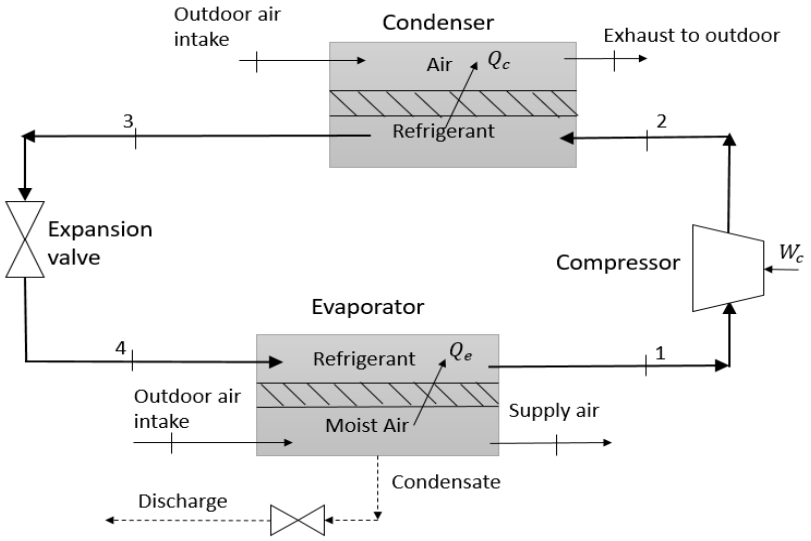

Figure 4 Schematic of conventional vapor-compression refrigeration cycles

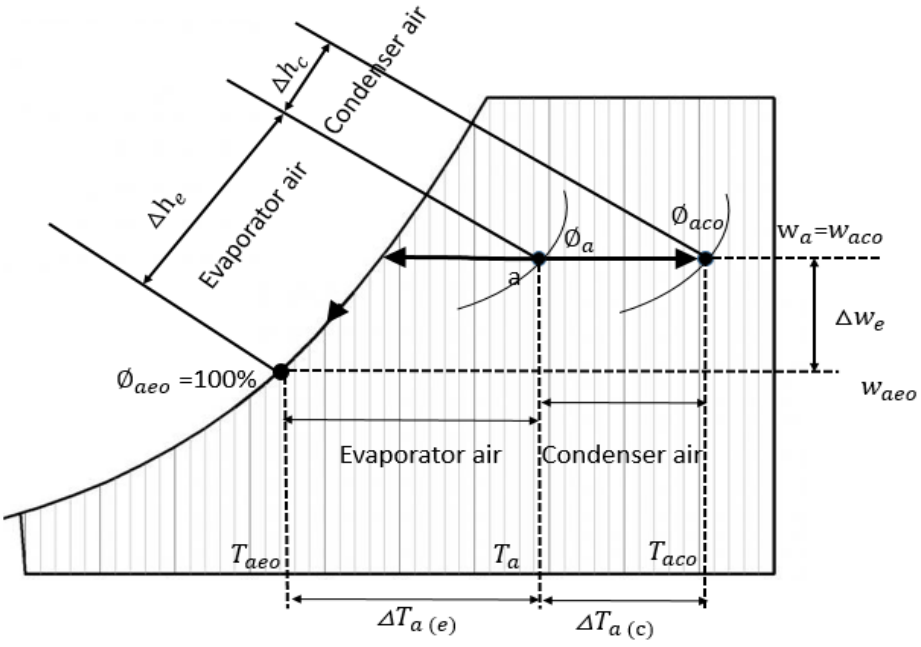

Figure 5 Psychrometric chart of air in the evaporator and condenser cooler

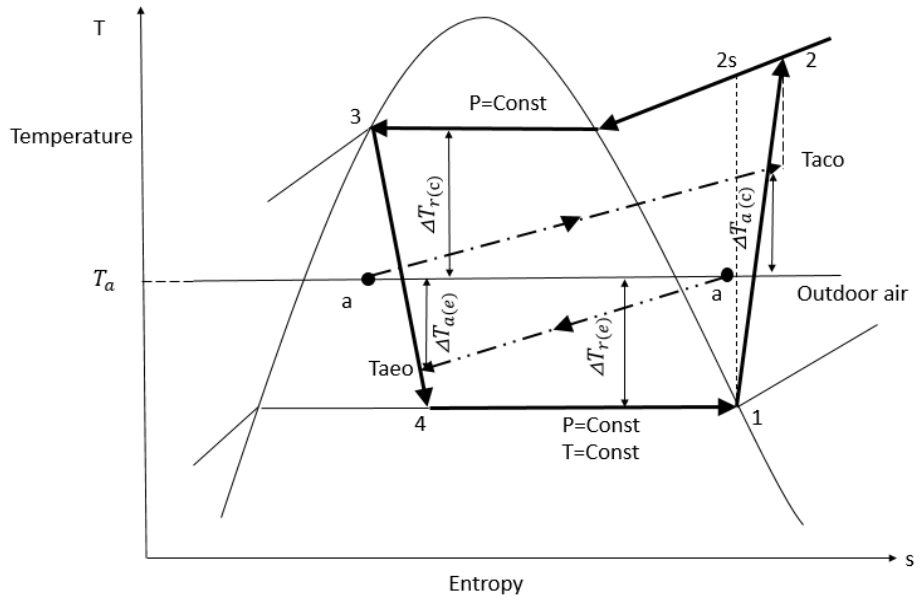

Figure 6 T-s diagram of conventional vapor-compression system

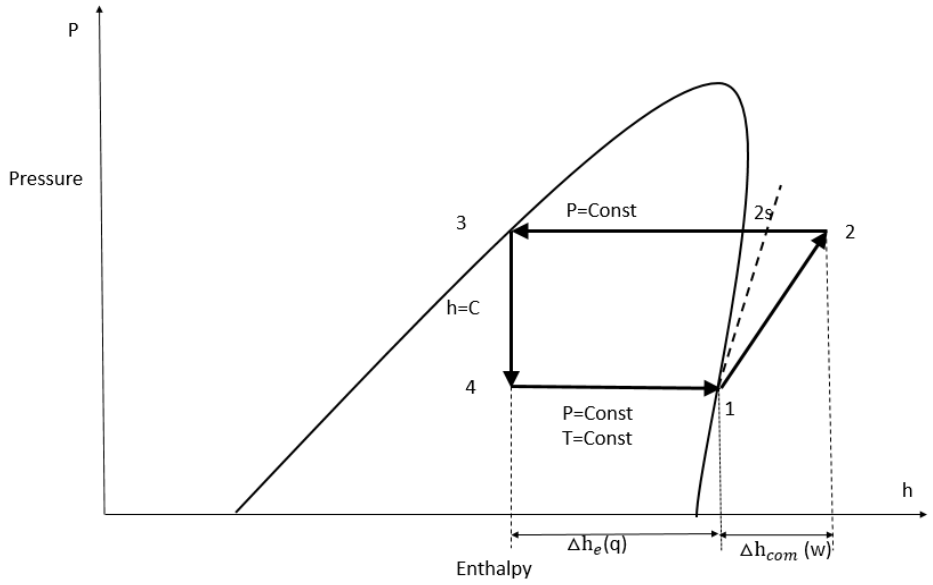

Figure 7 P-h diagram for conventional vapor compression system

Space conditioning and HVAC equipment in commercial and residential buildings consume the majority of the refrigeration energy. Therefore, finding new approaches to reduce the

energy used to cool buildings without sacrificing comfort and indoor air quality (IAQ) is a significant challenge. The approach that can have the highest probability of success in short-term is to improve the energy efficiency of individual components in HVAC systems and to design new systems utilizing creative configurations of existing vapor- compression technology and components, with the latter being an important focus of the study reported herein.

Modifying cycle components and configurations can improve conventional vapor-compression system performances by either indirect means when one changes outdoor air conditions supplied to the condensers, which then change refrigeration conditions or directly by changing refrigeration conditions. The net result from either of the above is to increase the cycle COP by increasing the refrigerating effect, decreasing compressor specific work or a combination of both effects.

2.1.3 Change Outdoor Air Condition

One such approach investigated herein for reducing energy consumption and operating costs by altering the supply air temperature to the heat exchanger which in our case is outdoor air is to modify or reconfigure the air-side of both the condenser and evaporator of a typical vapor-compression cycle. Specifically, an evaporative precooler can be added on the air-side before the condenser so that either external water or internal water, consisting of the evaporator condensate, is utilized to evaporatively precool outdoor air before it enters the condenser, resulting in a lower refrigerant condensing temperature. Of special note, it is sufficient with external water to always achieve a fully wet-bulb condition, which corresponds to the lowest possible condenser air-inlet temperature, regardless of the outdoor air conditions. However, with internal water usage, the degree to which evaporative cooler can reach a wet-bulb temperature and the amount of condensate formed in the evaporator are both dependent on the outdoor air dry-bulb temperature and relative

humidity. In other words, the internal condensate water collected for any specific outdoor air condition may or may not be sufficient to achieve a fully wet-bulb condition, which corresponds to the lowest possible condenser air-inlet temperature.

Another approach based on altering airside temperatures that is investigated herein is to modify only the air-side of the evaporator. Specifically, a heat recovery ventilator (HRV) or energy recovery ventilator (ERV) is added on the air-side before the evaporator. By using heat recovery/energy recovery ventilators between the incoming fresh outdoor air and the exhaust room air, the dry-bulb temperature of air entering the evaporator decreases while the relative humidity remains constant/decreasing, which in turn increases the refrigerating effect while lowering the compressor work so that the COP is increased.

A detailed literature review of past studies based on reconfiguring conventional vapor-compression refrigeration systems with evaporative cooling at the condenser air inlet based on utilizing a combination of external-sourced and internal-source water are limited and not systematic. Even so, as the first step in the modeling and analysis study performed herein, a literature survey was performed and specific results are reported in this section, with the literature falling in the categories of experimental and modeling studies for the case of external-sourced and internal-sourced to evaporatively cool the air entering the condenser.

External Experimental Studies Using external water only, Casvendi, B and Calli, Umit [5] experimentally investigated methods for improving the energy performance of air-cooled chillers with a WSMCST system installed upstream of the condenser air stream. Specifically, the WSMCST system consisted of three components, namely (1) a water treatment and control unit (2) a high-pressure pulverization unit with atomization nozzles and (3) a specially developed microprocessor. Based on the measurements from a factory located in Turkey, during a 3-months

period from June to August 2009 under ambient temperatures ranging from 25℃ to 39 ℃, the result of pre-cooling was to achieve a temperature reduction at the inlet of the condenser that varied between 5K to 20K. Furthermore, the use of mist-spray pre-cooling was reported to have increased the EER for a broad range of temperatures by as much as 14% along with a 5% increase in the COP. Also, they reported that the drawback of operating cost and external water purchase was negligible compared to its advantage. Specifically, the operation cost of the system accounted for only 2% of energy saving from the chiller while the water consumption price accounted for 10% of the energy conservation.

In another study, Hajidavalloo [6] used a 1.5-ton window air conditioner with media pads sprayed with external water for evaporative cooling. In this experiment, the ambient dry-bulb temperatures were 45 and 46 ℃ while the ambient wet-bulb temperatures were 24 and 25.5 ℃, with a decrease of condensing refrigerant temperature to 17 and 10℃, respectively. Using this approach, the power consumption could be decreased by as much as 16% and the coefficient of performance increased by around 55%. It was thus concluded that the application of evaporative cooling could result in an increase performances at least for a limited set of conditions and small size refrigeration systems.

Faramarzi, Ramin [7] set up a test comparing traditional air-cooled condensers and an evaporative –cooled condenser called (ECAC). The result revealed that ECAC performed more efficiently than the air-cooled system with a 51% higher EER for hot and dry conditions of 115 ℉ dry-bulb temperature and 74 ℉ wet-bulb temperature. However, the authors recommended that water usage efficiency, potential maintenance, reliability, corrosion, scaling and other water-related operational issues be investigated and considered.

Goswami, Mathur and Kulkarni [8] at the University of Florida did a specific evaluation of the impact of an indirect evaporative pre-cooler for the condenser, and the study showed a 20% reduction in overall energy use for an average of 14 °F air temperature drop before reaching the coil. Based on the above result, they predicted that the potential savings in drier climates with much lower dew points could be 30% with even more significant peak reductions.

Tianwei Wang [9] performed experimental research based on utilizing external water for evaporative cooling for air temperatures that ranged from 22-50 ℃ and 22-46 ℃ for the evaporator and condenser, respectively. The condenser inlet air was precooled with an evaporative cooling unit that consisted of a spray nozzle, a water supply pipe, a fan, a heater, a guiding plate, a cooling pad and a drainage pipe. The results showed an increase in the mass flow rate of refrigerant that went into the evaporator, which resulted in increases of COP ranging from 6.1% to 18%. A power reduction up to 14.3% on the compressor was also achieved.

Yang [10] investigated the effect on chiller efficiency of using water mist evaporative pre-cooling on air-cooled chillers during on-site experimental studies in a subtropical climate. Thus experimental results showed that the dry bulb temperature of air entering condenser with water mist pre-cooling dropped by up to 9.4 °C with the chiller COP being improved by up to 18.6%. As an aside, the study noted that the application of water mist pre-cooling associated with a chiller system is uncommon.

Adarsh Mohan Dixit [11] presented an experimental investigation of a high-efficiency air conditioner that utilized cellulose pads before the condenser in a 1.5 TR (refrigerating ton) air conditioner. They expected that the air conditioner performance could be improved due to the excellent water wet ability of the cellulose pads which causes a uniform water film over the entire surface of the pads and perfect contact between water and cooling air. The experimental results

reported showed that the COP reached a value of 8.03, which they concluded was higher than the standard value of 5.98 for conventional residential split air conditioners.

Hajidavalloo and Eghtedari [12] experimentally studied the effect on the performance of an air-cooled split-air conditioner of using an evaporatively cooled air condenser. Variable ambient air conditions up to 49℃ were examined to determine the effect on the COP and power consumption. Experimental results showed that by using evaporative-cooled air condenser under hot weather conditions, the COP could be improved up to 50% and the rate of improvement increased as the ambient air temperature was increased. They also found that the power consumption could be reduced up to 20%.

Chainarong and Doungsong [13] experimentally investigated the use of various indirect evaporative coolers to reduce energy consumption in a domestic split-type air conditioner. The condensing unit was retrofitted with a corrugated-media pad-type evaporative cooler, water sprayers, a water source, and a pump. The air-stream entering the condensing unit was cooled down at two positions, i.e., in the front of and within the cellulose corrugated pad. Moreover, injecting water into the air is divided into two types of distribution: water curtain and water spray. The study results showed that the electrical consumption and COP strongly depend on the ambient conditions. Due to the effects of condensing pressure, when the ambient temperature rises, the electrical consumption becomes higher, while the COP becomes lower. In addition, utilizing the indirect evaporative cooling system decreases the temperature of air entering the condensing unit, further enhancing the system performance. The maximum energy savings occurs when the water spray works together with the cellulose cooling pad. With the use of evaporative cooling systems, the COP is improved by around 6–48%, and electrical consumption is reduced by approximately 4–15%.

External Modeling Studies Yu and Chen [14] did a simulation analysis on an air-cooled chiller equipped with a direct evaporative cooler, with the outdoor dry bulb temperatures ranging from 15 to 35℃ and wet bulb temperatures ranging from 12.4 to 29.5 ℃. The model was operated under different schedules of condenser fan staging ---head pressure control (HPC). For any given heat rejection, there was a condensing temperature set point to control the staging of condenser fans. When the condensing temperature exceeded its set point, another condenser fan would be switched on to increase the heat rejection airflow, which enabled the condensing temperature to fall to slightly below its set point. Under HPC, the set point of the condensing temperature was fixed at 45℃ at all operating conditions. Fewer condenser fans were staged to limit the heat rejection airflow when the chiller load or outdoor temperature decreased. The result showed that when head pressure control is used, the cooler enables the condensing temperature to drop by 2.1-6.2℃, leading to a 1.4-14.4% decrease in chiller power and a 1.3-4.6% increase in the refrigeration effect.

Yu and Chan[15] attempted to improve the COP of air-cooled screw chillers when condensers are designed with evaporative pre-coolers and variable-speed fans. They developed a thermodynamic model for an air-cooled screw chiller with empirical equations describing the condenser components. Condenser components contained algorithms to determine the number and speed of staged condenser fans. The model was validated by using chiller specifications and a wide range of operating data in the steady-state mode. It was found that the optimum set-point condensing temperature is a function of the chiller load and the wet bulb temperature of the outdoor air. They reported that using the new condenser design and condenser fan operations could result in a 5.6–113.4% increase in chiller COP, depending on chiller loads and weather conditions. Also,

the cooling capacity can be enhanced by 3.8–28.2%, which enabled the chillers to operate at higher loads.

Bo Shen [16] theoretically demonstrated that commercially available evaporative pre-coolers offer an opportunity for low-cost retrofit for many existing packaged rooftop units, commercial unitary split systems, and cooled chillers under dry-bulb temperatures ranging from 20 to 45℃, and relative humidifies ranging from 20% to 80%. Additionally, a comparison of two working fluids, R410A and R22 showed that the benefits of pre-cooling with R410A were significantly higher than that for R22. Specifically, at low ambient temperatures, it is found that there is a 25% difference in the relative performances of R410A and R22.

Xiaoli [17] simulated an air-cooled chiller coupled with a direct evaporative-cooler to reduce the entering air temperature of the condenser and to improve the performance of air-cooled chiller. A mathematical model was developed for the energy performance of the evaporative air-cooled condenser (EACC), and the model was used to evaluate the energy-saving potential more accurately. The impacts of various factors on the energy saving potential were analyzed, and it was found that there exists an optimal evaporative-cooler pad thickness which maximizes the energy saving. Optimization results of the pad thickness in 31 main cities in China were presented, and the maximum energy saving potential of EACC in China was found to be between 2.4% and 14.0% depending on the climatic conditions. In general, it was shown that EACC has a more significant energy saving potential in dry and hot climate than in a humid and hot climate.

Youbi [18] proposed a water spraying system in front of an air-cooled condenser to reduce entering air temperatures. They developed a semi-local numerical model for the sprayed air-cooled condenser coupled with a refrigeration system. In their model, the air temperature was 25 ℃, RH was 30%, evaporating temperature was 5℃ and the subcooling/superheating temperature was 3/7

℃. They predicted the COP of the refrigeration system and found that it could be improved by up to 55%.

External Combined Experimentally and theoretical and Modeling studies Huan [19] performed an experimental study on the effect of evaporative cooling on an air-cooled chiller utilizing an evaporative precooler filled with corrugated-holed aluminum-foil fillers. It was shown that for an outdoor dry-bulb temperature of 28.5℃ and a wet-bulb temperature of 22.5℃, the use of a cooler pad caused an increase of 6.7% in the cooling capacity and a reduction of 6.9% in the electric demand, which in turn resulted in a COP increase of 14.7%. A regression analysis of the experimental data for the air temperature at the outlet and the energy loss through the filter based. It was concluded that the system is especially suitable for dry and hot areas, and it was suggested that the design for air-cooled chillers should be promoted.

Jia Yang [20] studied both experimentally and theoretically the effect of operating a water-mist precooling system to enhance the energy efficiency of air-cooled chillers under operating conditions with ambient dry-bulb temperatures of 32.7 and 28℃ and relative humidities of 20.1% and 78%. Using the conventional head pressure control, as noted previously, the COP was increased up to 21.3%. Considering an optimal water-mist generation rate under condensing temperature control, the chiller COP increased up to 51.5%.

Pongsakorn and Thepa [21] in an experimental and numerical study investigated the proper operating strategies and the appropriate capillary tube length of an optimal refrigerant charge for an inverter air conditioner system with an evaporative cooling system installed in the condensing unit. The adapting system was tested by varying frequencies, water flow rates, and spraying temperatures. The COP increased by 18.32% at the lowest frequency and spraying rate of 200l/h. Therefore, the flow rate of 100l/h tended to improve the COP at a higher range of frequency due

to water distribution complexly and lower total consumption with the efficiency being enhanced up to 31-35%.

Internal Experimental Studies Pengyu Li and Jinhua Chen [22] focused on a study of recovery and utilization of condensate drain in a split-type air conditioner under outdoor air dry-bulb temperatures ranging from 30-35 ℃ and relative humidities ranging from 60% to 70%. They found that by cooling the surface compressor with collected condensate water, the condensing temperature could be reduced. Also, making use of split air-conditioning and condensate water to cool the condenser the energy consumption could be reduced as much as 4.5%.

Dusan Licina [23] investigated utilizing the condensate from large air handling units (AHU) in hot and humid climates for pre-cooling outdoor air by utilizing an evaporative cooling unit in a separate AHU while simultaneously offsetting cooling tower water needs. The experiments were carried out for outdoor air dry-bulb temperatures ranging from 26-30.5 ℃ and relative humidities ranging from 60% to 90%. It was found that condensate production was sufficient for a pre-cooling that could produce approximately 10% energy saving while offsetting cooling tower demands more than 50%. Nevertheless, the usefulness of the results is limited because of a specific setup and a narrow set of conditions.

Internal Combined Experimentally and Modeling Studies R. Sawan [24] investigated utilizing the condensate drain in an evaporative cooling unit for pre-cooling the air entering the outdoor condensing unit by both simulations and experiments. The direct expansion vapor-compression system was designed to remove the total peak load at its rated capacity in order to control the indoor temperature at its set-point. At partial load, the system relies on the ON-OFF cycling of the compressor to maintain a temperature close to the set-point. The rated capacity of the system varied as the indoor and outdoor conditions deviated from the manufacturer's rated

conditions while the power consumption was computed from the energy input ratio depending on the indoor and outdoor conditions. The theoretical model simulated the ON-OFF operation of the DX unit in response to changes in the capacity of the system and indoor space load conditions. Furthermore, the model evaluated a case study of thermal conditions and energy demand for a typical office space in Beirut during June, August, and October. The simulation result revealed that the condensate would be sufficient in October only, resulting in a 5.3% energy saving for a whole day in that month. However, the spray of water was found to be last for six operating hours in June and eight hours in August, resulting in a reduction in the consumed energy of 5% in June and 4.5% in August.

Heat recovery/ Energy Recovery Most cases of heating, ventilating and air-conditioning (HVAC) systems currently in operation are all-air systems, meaning that they employ air not only for ventilation but also as a heat transfer medium. Indoor air quality, ventilation airflow rates and HVAC costs (capital and operating) are all related. Of special importance, energy loads for supply air cooling or heating sometimes can significantly reduce the need for dehumidifying or humidifying by using air-to-air heat/energy recovery devices. [25] Additionally, heat recovery technology also offers other optimal solutions: fresh air, better climate control, and energy efficiency.

Heat recovery in building applications is widely used in some Europe countries. For example, Lazzarin [26] discussed technical and economic aspects of using the HRV even for small ventilation flow rates in three cities (Milan, Rome, and Palermo) in Italy. Mats Fehrm [27] gave a comprehensive review of heat recovery in Sweden and Germany from both a development and an economic point of view. Air-to-air heat recovery ventilators for commercial buildings and the single-family houses is also widely used in China as well. [28]

Four systems were compared and investigated by J.L. Niu [29] in Hong Kong, namely all-air system, an all-air system with total heat recovery, chilled-ceiling with AHU, and chilled-ceiling with desiccant cooling. The annual energy consumptions for the four systems were compared, and the chilled-ceiling combined with desiccant cooling primary energy produce of saving up to 44% of compared to conventional constant volume all-air systems.

Carey J. Simonson [30] determined the performance of energy wheels using experiments and numerical simulations for a wide range of conditions of mass flux, temperature, and humidity. The agreement between simulated and measured results was well within the experimental uncertainty, and the three effectiveness values, namely sensible, latent and total were found to be unequal, and each has its unique sensitivity to operating conditions. The total effectiveness was shown to be a poor measurement of performance when the supply and exhaust inlet air enthalpies are almost the same.

Yaw Asiedu [31] presented a discussion on the design of dual air-to-air heat and energy exchangers within cabinet units located in Chicago. The example design problem presented for only a limited set of conditions showed that payback periods of a little over a year can be achieved for energy wheels and sometimes for heat exchangers.

Ambrose Dodoo [32] analyzed the impact of ventilation heat recovery on the operation of primary energy use in residential buildings for heating. It was found that heat recovery increases the electrical energy used for ventilation and reduces the heat energy used for space heating. Heat recovery is more effective (greater primary energy saving) in resistance heated building than in district heated buildings (almost no saving). Heat recovery systems can thus give substantial final energy reductions, but the primary energy saving is highly dependent on the heat supply system as well as the amount of electricity used for heat recovery and the airtightness of buildings.

Younness [33] compared the energy performance of HRV systems to other ventilation systems for low energy residential and commercial buildings. Three typical low energy buildings, namely a flat, a house and medium-sized office were studied. From the results of the simulation, was concluded that the adequacy of HRV systems in low energy buildings varies with the building type, heating loads and ventilation device characteristics.

Along with a reduction of ventilation heat loss, operating a heat recovery unit increases the pressure drop and fan power consumption in the system. J. Laverge [34] addresses the trade-off based on primary energy, carbon dioxide emission, household consumer energy price and exergy frameworks for the different climates found in Europe. It was concluded that for the moderate climate region of middle Europe, natural ventilation, simple exhaust mechanical ventilation and heat recovery ventilation have no clear advantage over each other, considering operating energy and associated ecologic (CO2) and economic (household consumer price) effects. However, by achieving realistic low specific fan power, heat recovery ventilation can be made profitable for many parts of Europe.

Roulet [35] addressed real energy recovery with air handling units from a theoretical point of view and presented the results of measurements on 13 units in Switzerland. The best three cases showed that the real heat recovery efficiency was between 60%, and 70%, with a 80% nominal efficiency for the worst three cases producing a real efficiency of only 10%.

Wahiba [36] presented a detailed numerical analysis of heat and membrane-based energy recovery ventilators by using computational fluid dynamics (CFD). The results showed a decrease in the HRV/ERV effectiveness with an increase in supply/exhaust air velocity. The results also indicated that the outdoor temperature and humidity had only minor effects on HRV/ERV performance.

The annual energy consumption of an air conditioner coupled with an enthalpy/membrane heat exchanger was studied and compared with a conventional air conditioning cycle by M. Nasif [37]. The result showed that in humid climates a saving of up to 8% in annual energy consumption could be achieved when membrane heat exchangers are used instead of a conventional HVAC system.

The applicability of ERVs with sensible and latent effectiveness values in a practical range was simulated by Mohammad [38]. A 10-story office building in four American cities as representatives of major climatic conditions was investigated, and the result showed that heat and moisture recovery (ERV) could lead to a significant reduction in the annual heating energy consumption up to 40% and 5% higher than the HRV. Also, an ERV with the capability of moisture recovery may reduce the annual cooling energy consumption by 20% provided there is proper controll.

A novel run-around membrane energy exchanger (RAMEE) system was designed, built and tested for HVAC by Khizir [39]. The system consisted of two counter cross-flow liquid-to-air membrane energy exchangers, one located in the supply and the other in the exhaust air streams of a building. Inside each exchanger, a microporous membrane separated the air and desiccant solution streams. During summer test conditions, the total system effectiveness increased with increasing desiccant flow rates, but decreased as the air flow rate increases. It was found that the maximum total effectiveness of the system can reach up to 55%.

Dominic [40] gave a review of utilizing six different heat recovery devices by analyzing and comparing their suitability for integration into passive ventilation systems. The result showed that heat pipes and rotary thermal wheels may be the technologies with the most potential for

integration due to high thermal efficiency and low-pressure loss across the heat recovery device in comparison to the other technologies.

2.1.4 Change Refrigerant Condition

Typically, the state of the refrigerant leaving the condenser of a conventional one-stage vapor compression cycle is usually assumed to be saturated liquid. Nevertheless, by cooling liquid refrigerant below the saturation condition, increases in the system coefficient of performance (COP) can occur. Specifically, the effect of subcooling is to lower the temperature of the refrigerant in the condenser exit, reducing the vapor quality at the evaporator inlet, increasing the enthalpy difference across the evaporator, which results in boosting the evaporator cooling capacity. Also, the utilization of subcooling ensures the refrigerant as a flashing liquid-phase at the inlet of the expansion device, which reduces the risk of vapor-phase at the expansion device inlet. Several approaches can be utilized to subcool the liquid refrigerant before the expansion processes, such as adding internal heat exchangers in single-stage cycles or two-stage cycles. Also, subcooling can be achieved by an auxiliary cooling system, such as a thermoelectric device or a secondary vapor compression system, which is also known as mechanical cooling.

Sub-cooling Effect Various researchers have studied the sub-cooling effect of condenser refrigerant in vapor compression refrigeration. Linton [41] investigated effect of the condenser liquid subcooling on a refrigeration system performance by experiment. The results show that with a constant condensing temperature, the COP and refrigeration capacity of three refrigerants benefited from the sub-cooling increases with COP increase being: R134a (12.5%), R12 (10.5%) and R152a (10%).

In addition, Yumrutas [42] studied a computational model-based exergy analysis, along with a first and second law analysis, of a vapor compression refrigeration cycle using ammonia as

the working fluid. According to the first law, the performance was significantly related to the degree of subcooling at the condenser. Specifically, subcooling of the refrigerant at the exit of the condenser causes the refrigerant to enter the cycle evaporator with lower quality, and thus it allows the refrigerant to absorb more heat in the evaporator, resulting in an increase in enthalpy difference across the evaporator, which improves the COP of the system.

Also, Dalkilic and Wongwises [43] studied the performance of a vapor-compression refrigeration system with several refrigerants at a condensation temperature of 50℃ with evaporating temperatures being varied from -30 ℃ to 10 ℃. The effect of subcooling degree on refrigeration was compared between R134a, R152a, R32, R290, R1270, and R600a. Similarly, Jensen [44] theoretically studied the optimality of sub-cooling in a simple refrigeration cycle using ammonia as the refrigerant and with subcooling to obtain savings in compressor power of about 2%.

Pottker [45] once presented a theoretical and experimental analysis of the effect of condenser subcooling on the performance of vapor-compression systems. The results showed that as the condenser subcooling increases, the COP reaches a maximum, as a trade-off between increasing refrigerating effects and specific compression work. In addition, from the simulation result, it was found that R1234yf would benefit the most from condenser subcooling in comparison to R410A, R134a, and R717. The experimental results showed that for a given operating condition, the system COP increased up to 18% for R1234yf and 9% for R134a.

Mechanical Sub-cooling by Adding a Sub-cooling Loop. Dedicated mechanical sub-cooling cycles typically utilize small mechanical vapor-compression cycles, coupled to the main cycle at the exit of the condenser, so as to provide sub-cooling to the main refrigeration cycle. The amount of sub-cooling, the thermal lift of the sub-cooling cycle, and the performance of the

overall cycle can be directly related to the temperature of the sub-cooling cycle. In practice, the components of the sub-cooling cycle are a fraction of the size of the main cycle components and operate through much smaller temperature extremes. Thus, the COP of the sub-cooling cycle is higher than that of the main refrigeration cycle, which in turn increases the overall cycle COP.

Zhang [46] added an auxiliary circuit to the main cycle to get the effect of sub-cooling using refrigerant R12 and R22. The results show that the COPs of the new cycle increase by 5 to 11% compared with those of a conventional cycle. Thornton [47] utilized dedicated mechanical sub-cooling design strategies for supermarket applications. The improvement in overall COP through the use of a sub-cooler was found to be approximately 10% over a range of conditions representative of supermarket applications. Khan [48] demonstrated by a model that the performance of the overall cycle (main cycle and sub-cooling cycle) can be improved over the original cycle, with this improvement found to be related to the refrigerant saturation temperature of the subcooler.

Qureshi [49] found that energy can be saved by incorporating a dedicated mechanical sub-cooling loops to existing refrigeration and air-conditioning systems. Comparing the R134a and R717 results, R134a used in both cycles produced the best results in terms of relative compressor size, COP and gain in COP. Qureshi [50] also experimentally investigated the mechanical sub-cooling cycle with a residential 1.5-ton simple vapor-compression refrigeration system. For the experiment, R22 was employed as the main cycle refrigerant while R12 was used in the sub-cooling loop, with the room temperature could be kept between 18 and 22℃. The results showed that the load carrying capacity of the evaporator increased by 0.5kW when R22 was subcooled in the main cycle by 5-8℃.

Syed [51] utilized a mechanical sub-cooling loop attached to the vapor-compression refrigeration cycle to increase the system performance and to reduce the energy consumption. It was found that the new system can significantly improve the system performance when operating in locations where the difference between the condensing and evaporating temperatures is large. The low-temperature refrigeration system, when operating at the optimum sub-cooler saturation temperature, will result in as much as a 85% reduction in power input and a 65% lower irreversibility rate. In another study, Syed [52] found that the system performance (with a sub-cooling loop) peaks at a sub-cooler saturation temperature midway between the condensing and evaporating temperatures. Simulations showed that the performance improvement could reach 20% during peak periods of high-condensing temperatures.

Yang [53] performed a model-based comprehensive analysis on the principles of sub-cooler sizing and optimal sub-cooling control of supermarket refrigeration systems, using mechanical sub-cooling operating between medium and low-temperature systems. The maximum energy saving was found to be around 27% for a R404A system and 20% for an R134a system.

Jianlin [54] described a new ejector refrigeration system with mechanical sub-cooling, which used an auxiliary liquid-gas ejector to enhance the sub-cooling for the refrigerant leaving the condenser. The new system had larger sub-coolings with the circulating pump consuming a little more power compared with the conventional ejector refrigeration system. The result showed that the COP of the new ejector refrigeration system was about 10% more than the conventional ejector refrigeration system for R142b, when the condensing temperature was 35℃, evaporating temperature was 5℃ and the mechanical sub-cooling degree was 15℃.

Xing [55] utilized a theoretical study of R404A and R290 with an ejector to evaluate improvements in the performance of a conventional single-stage vapor-compression. When the

evaporator temperature ranged from -40 to -10℃ and the condenser temperature was 45℃, the new cycle achieved COP improvements of 9.5% with R404 A and 7% with R290.

Using an internal heat exchanger generates superheating in the suction of the compressor, where the superheating ensures only the vapor phase of the refrigerant enters the compressor suction, thus preventing slugging of the compressor and sweating of the suction line. Internal heat exchangers have been adopted in vapor-compression refrigeration cycles for many years, but most applications are commonly used in vehicles, with most working fluids being carbon dioxide. Another validation of this heat exchanger is in home refrigerator when the small diameter capillary tube is connected to a larger diameter suction line leading to the compressor.

Internal Heat Exchanger Applied to Transcritical R-744 (CO2) Cycle and Vehicle Air-conditioning. Past studies indicate that carbon dioxide based systems associated with internal heat exchangers have great potential in two sectors—in automobile air conditioning and heat pumps for simultaneous cooling and heating.

Boewe [56] experimentally evaluated the effects of the internal heat exchanger on the performance of a well-instrumented transcritical mobile air-conditioning system using by R744 (CO2) as the refrigerant. The effect on cycle efficiency was as high as 25%. The optimal design for a COP-maximizing internal heat exchanger can also reduce material requirement up to 50% while increase effectiveness by 10%.

Cho [57] found that the maximum improvement of cooling capacity and COP can reach up to 11.9% and 9.1%, respectively owing to the internal heat exchanger in the transcritical carbon dioxide cycle. Aprea and Maiorino [58] experimentally examined the transcritical carbon dioxide refrigerator working as a traditional split-system for residential air conditioning when the internal

heat exchanger is used. The result showed that by using the internal heat exchanger, the COP is 10% better.

Sarkar [59] studied the transcritical carbon-dioxide heat pump system by energetic and exegetic analysis. It was found that the internal heat exchanger can increase the COP by 15% compared to those transcritical cycle at an evaporator temperature of 0℃ and a gas cooler outlet temperature of 60 ℃.

Torrella [60] studied the influence of the internal heat exchanger on the carbon dioxide transcritical refrigerating plant from the energetic point of view based on experimental tests. The results showed that the cooling capacity of the cycle could be increased up to 12% while the effect of the internal heat exchanger on the compressor power consumption is insignificant. Similarly, Aprea [61] found from experiments that improvements can be as much as 10%.

Preissner [62] tested the performance of an R14a automotive air-conditioning system in the laboratory with and without an internal heat exchanger. The results showed that at a higher condenser air temperature of 40℃, with an air flow rate of 1.0m/s, the COP, and the capacity increased by 5 to 10% with a liquid-suction line heat exchanger effectiveness of 60%.

Similarly, Chao [63] applied the internal heat exchanger as a drop-in component to a production vehicle in order to improve the performance of R134a A/C systems. The results showed the benefits are equal to or higher for cooling capacity, COP and performance with less charge.

Thermodynamic Analysis of subcooling and Superheating Effects. Selbas [64] studied an exergy-based thermo-economic optimization application associated with subcooled and superheated vapor-compression refrigeration systems. The application consists of determining the optimum heat exchanger areas with the corresponding optimum subcooling and superheating temperatures for R22, R134a, and R407.

Jarall [65] selected a wide range of superheating and subcooling temperatures as parameters to analyze the vapor-compression refrigeration cycles of R134a and R1234yf and then reported that the performance of the R1234yf system is influenced more significantly than that of R134a system by using subcooling and superheating temperatures.

Similarly, the effect of subcooling and superheating on the three refrigerants—R134a, R407c, and R410a were determined by Sencan [66]. It was found that subcooling and superheating applications affect the system performance with this effect is the same for R134a and R407c, but different for R410A.

Internal Heat Exchanger Applied to Vapor-Compression Refrigeration System. More literature is available on the topic of applying internal heat exchangers to the conventional vapor-compression refrigeration systems with residential and industrial refrigerants after 1990.

Hermes [67] explored the effects of the internal heat exchanger in vapor-compression refrigeration cycles under constrained cooling capacities and varied evaporating pressures for R134a, R22, R290, R410A, R600a, and R717. It was shown that the COP may either increase or decrease depending not only on the working pressures, but also on the heat exchanger effectiveness, the specific heat ratio, and the available latent heat to produce an additional refrigerating effect.

Klein [68] did a comprehensive investigation of R507A, R134a, R12, R404A, R290, R407, R600 and R410A as working fluid utilizing internal heat exchanger and found that the internal heat exchanger is useful in most cases. However, it is detrimental to system performance in systems using R22, R32, and R717.

Similarly, Navarro [69] used R22, R-134a, and R407c as working fluids for experimentally and theoretically verifying positive or negative influences on the overall energy efficiency when incorporating internal heat exchanger. Navarro [70] also presented an experimental analysis of the

influence of an internal heat exchanger on the performance of a vapor-compression system using R1234yf as a drop-in replacement for R134a. The result showed that reductions in cooling capacity and COP between 6 and 13% occurred when R1234yf replaces R-134 without internal heat exchanger while the reduction is lessened to 2 when the internal heat exchanger is used.

Vijayan [71] investigated the effects of internal heat exchangers experimentally in a window air conditioner using R22 and R407 as working fluid and finalized the maximum COP increase can reach 5.9% and 6.3%, respectively. When retrofitting R22 systems with R407C, the COP is found to drop with (6.26%) and without (6.64%) internal heat exchanger.

Pottker [72] experimentally studied the effect of the internal heat exchanger on the performance of an air conditioning system operating with R-134a and R1234yf under the same operating conditions. For both refrigerants, it was shown that the COP reaches a maximum as a consequence of the trade-off between increasing the refrigerating effect and increasing the specific compression work. For a given set of operating condition, the system COP increased with the heat exchanger up to 18% for R1234yf and 9% for R134a.

Dr. Domanski [73] theoretical evaluated the performance effects that can result from the installation of a liquid-line/suction-line heat exchanger. The study showed that the benefits of using the internal heat exchanger depends on a combination of operating conditions and fluid properties—such as heat capacity, latent heat, and coefficient of thermal expansion—with heat capacity being the most important property. The impact on COP may be positive or negative for the fluids that perform well in the basic cycle while the COP typically increases for the fluids that perform poorly in the basic cycle. Dr. Domanski [74] also compared the above system with two other novel systems---namely a system incorporated with an economizer and an ejector. The

results showed that the ejector cycle with a high level of ejector efficiency could reach the highest COP, while the liquid-line/suction-line heat exchanger cycles had the smallest COP improvement.

Similarly, Mastrullo [75] investigated the effects produced by a suction/liquid heat exchanger installed in a refrigeration cycle and focused that its use can improve or decrease the system performance depending on the operating conditions. Specifically, 19 different refrigerants were investigated, with the evaporating temperature being varied from -40 to 10 ℃ while condensing temperatures were varied from 25 to 50℃. Eventually, a simple chart was developed showing the effectiveness of the installation of the heat exchanger for each refrigerating fluid and specified operating condition.

2.2 Refrigerant Types and Properties

The working fluid used to transfer thermal energy from a low-temperature reservoir to a high-temperature reservoir is referred to as the refrigerant. There are three different types of refrigerant that are important for this study. For example, CFC refrigerants are molecules composed of carbon, chlorine, and fluorine, and they include R11, R12, R113, R500, etc. CFCs are stable, but they contribute to the destruction of the ozone layer. The HCFC refrigerants are molecules all composed of carbon, chlorine, fluorine, and hydrogen. They are less stable than CFC refrigerants, but destroy ozone as well. The HCFC refrigerants include R22, R123, R124, R401a, etc. A third refrigerant, HFCs are molecules composed of carbon, fluorine, and hydrogen and with the lack of chlorine, they will not destroy the ozone layer. The HFC refrigerants are widely used in the application of household refrigerators (R134a) and AC systems (R410A).

The most common refrigerants used early on were ammonia (R717), chloromethane (R40) and sulfur dioxide (R764), which all have some degree of toxicity and/or flammability. These refrigerants are called first-generation refrigerants with regards to refrigeration and air

conditioning applications. In 1928, Thomas Midgley, Jr. of Frigidaire and his colleagues developed the first commercially available CFC refrigerants, namely dichlorodifluoromethane (R12), and these chlorinated halocarbon refrigerants represent the second generation of refrigerants. Nevertheless, the second generation of refrigerants had drawback in that they could decrease the ozone layer in the stratosphere, which was highlighted in a 1974 paper by two University of California professors, Frank Rowland and Mario Molina. Replacement HFC refrigerants, third-generation, were developed following restrictions put into place due to CFC threats to the ozone layer. Although HFC refrigerants exclude chlorine and have no effect on stratospheric ozone, they have come under heavy scrutiny because of their global warming potential. As a newest, HFO refrigerants, which have significantly lower GWP values than HFCs, are being developed and promoted as alternatives to HFC refrigerants. Considering HFOs can be mildly flammable, which is an obvious barrier that exists, safety measures must be fully developed and widely implemented prior to the common use of mildly flammable refrigerants. The U.S. Environmental Protection Agency (EPA), and Underwriters Laboratories (UL) are working on coordinated agreements to allow for broad use of these fourth-generation [76]. A survey of the 4 generations of refrigerant can be seen below and then several presently used refrigerant are introduced in section that follows.

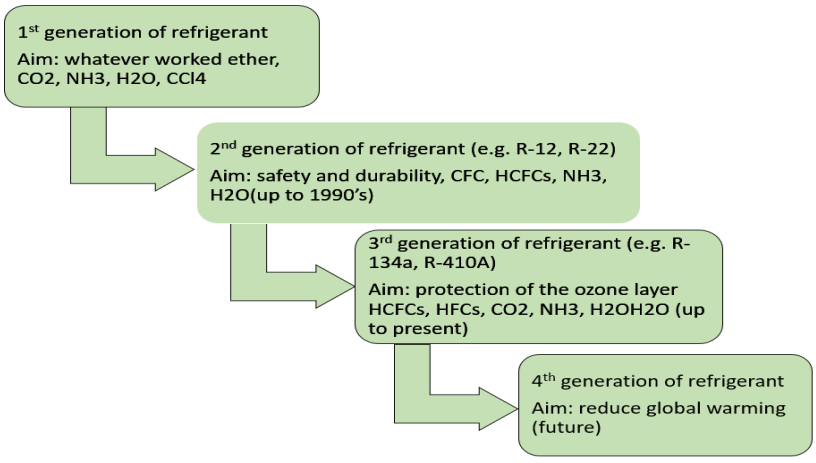

2.2.1 Categories of Conventional Refrigerants Presently Used in 3rd Generation (present)

- Refrigerant mixture
    - Zeotropic: In a state change, such as condensation and evaporation, the temperature varies, with examples including R404a, R407a, and R410a.
    - Azeotropes: They behave like pure refrigerants, with no change in temperature during the change of state, with examples including R500, R502, and R507a.
- Ammonia (NH3) or R717: Dangerously toxic and flammable but no negative environmental effects and generally used in industry
- Hydrocarbons: Common examples are propane (R290), butane (R600) and isobutene (R600a) with these fluids having good thermodynamic properties but being dangerous because of their flammability.
- Carbon dioxide or R744: This is inorganic, non-toxic, non-flammable, but can be inefficient from a thermodynamic standpoint depending on application and system components.

2.2.2 Example Results of a Property Comparison Methodology for R-134a Replacements (which are well-established compared to R-410A)

- R-134a is widely used in many air conditioning and refrigeration systems globally. It does not contribute to ozone depletion but it has an unacceptable GWP; it is also the first none-ozone-depleting fluorocarbon refrigerant to be commercialized.
- HFC-152a: It is almost a straight drop-in substitute for R-134a with its main drawback being that it is slightly flammable.
- Pure R1234ze is a satisfying option only in reconfigured vapor-compression systems and as a drop-in if combined with other refrigerants.

- R-1234yf: Developed by Honeywell and DuPont as a drop-in replacement for R-134a in vehicles because it has similar properties to R134a, with a lower global warming potential.

The influence of fluorocarbon refrigerants on the global warming has prompted countries throughout the world to pass legislation preventing or phasing out the use of such refrigerants. In the EU, regulations have already been enacted to replace R134a in mobile air conditioning systems by low global-warming potential (GWP) refrigerants, such as R1234yf, which as noted above has similar thermodynamic properties as R134a in comparison to other environmentally less harmful candidates.

The feasibility of using new low-GWP as refrigerants replacements for R134a has been investigated in a number previous studies that can be found in the published literature, shown in Table 1.

Table 1 A literature review of refrigerant replacement

Year	Author	Scope	Results
2010	Katsuyki Tanaka, Yukihiro Higashi[77]	Different methods used to conducte measurements of the thermodynamic properties of R-1234yf	In comparison with R-134a, almost all thermodynamic properties of R-1234yf are lower than those of R-134a.
2013	Ryo Akasaka, Katsuyuki Tanaka, Yukihiro Higashi[78]	The vapor-liquid coexistence curves near the critical point of the binary mixture of R-1234yf and R-32 were measured using the visual observation of meniscus disappearance.	The measurements of the saturated liquid and vapor densities were made for R-1234yf and R-32mixtures in the critical region, and the vapor-liquid coexistence curves were obtained for three different compositions. By the observations of the meniscus disappearing level and the intensity of the critical opalescence, the critical temperatures, critical densities, and critical molar volumes was determined.

Table 1 continued

Year	Author	Scope	Results
2016	Mota-Babiloni, Adrián Navarro-Esbrí, Joaquín Molés, Francisco Cervera, Ángel Barragán Peris, Bernardo Verdú, Gumersindo[79]	Investigated if R1234ze (E) has good environmental properties and can be used in most HVACR applications.	This study collected the most relevant research about R1234ze(E) thermophysical and compatibility properties, heat transfer, and pressure drop characteristics and vapor compression system performance. Base on the result, the pure R1234ze (E) is a good option only in new HVACR systems. However, when combined with other refrigerants, the final GWP value is also considerably reduced, maintaining efficiency parameters at levels that allow them to replace R134a in existing systems with minor modification.
2017	Agrawal, Neeraj Patil, Shriganesh Nanda, Prasant[80]	An in-house experimentatl test facility of a domestic refrigerator was developed to measure the mixture of R290/R600a (50%/50%) as a drop-in substitute for R134a.	The zeotropic blend can be acted as drop-in substitute. The cooling capacity of the system with a blend was comparatively more than R134a. The mass of refrigerant requirement is significantly lower by using R290/R600a (50%/50%) as a refrigerant.
2006	M.Fatouh M.EI Kafafy [81]	The possibility of using hydrocarbon mixtures as working fluids to replace R134a in domestic refrigerators was evaluated through a simulation analysis in this study.	The reported results confirmed that the propane/iso-butane/n-butane mixture with 60% propane is the best drop-in replacement for R134a in domestic refrigerators under normal, subtropical and tropical operating conditions.
2014	Katare, Pravin K Kriplani, Vilayat M [82]	It is important to estimate the thermodynamic properties of working fluids for simulation and efficient operation of thermal systems such as refrigerators and its performance.	As a result of the analysis in this study, the energy efficiency of HFOs is low, mixtures of medium GWP fluids such as R32 and low GWP refrigerants such as R1234yf may be the working fluids of choice in the immediate future.
2014	Sah, Ramesh P Das, Ranadip K Tiwari, Vidhika [83]	A simple vapor compression refrigeration system was studied with refrigerants, R134a, R143a, R152a, R290, and R32.	R290 has the lowest pressure ratio and the highest cooling capacity for an entire range of evaporating temperatures from -10 to 4 ℃ and condensing temperature from 40 to 54 ℃.

3. PURPOSE AND OBJECTIVES

The purpose of this study was to develop an optimization methodology based on studying the effect that refrigerant properties have on reconfigured residential air-conditioning systems with an emphasis on maximizing system performance.

Research objectives:

Identify and evaluate the efficiency of 4th Generation Refrigerants with a focus on improving vapor-compression system performance to facilitate the switch-over to replacement refrigerants:

- Step one—identify possible replacement refrigerant types---use property comparisons
- Investigate cycle performance improvements (COP ratios) for various reconfigurations---using COP ratios, climate zone models and conclusions

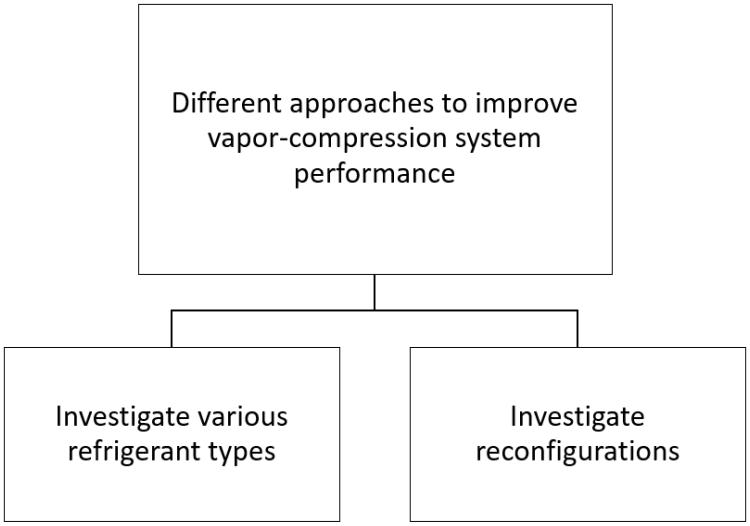

Fundamental research questions being addressed:

- How cycle performances vary when different refrigerants are used in the same vapor-compression system (based on property and condition comparison)?

*need to identify replacement refrigerants to be evaluated for different configurations

- How much can cycle performance be improved for four different categories (6 different cycles) of reconfigured systems?

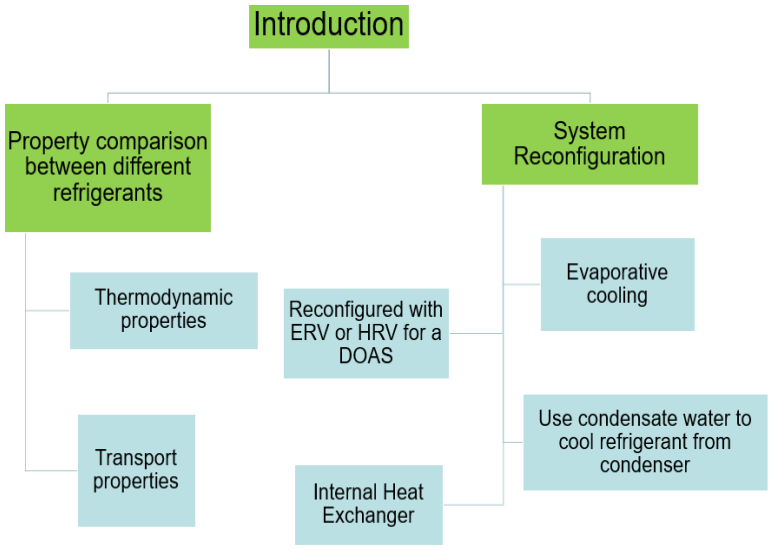

4. PROPERTY COMPARISON

The overall performance of a refrigeration system is dependent on the thermodynamic and transport properties of the working fluid, which directly affect component performances, such as energy transfers in the heat exchanger (heat transfer coefficients) and pressure drops in the piping systems (friction factors). As noted earlier, one approach to selecting a replacement refrigerant for R-134a and R-410A is by forming and evaluating property ratios and by knowing property trends that can increase overall and component performances.

4.1 Thermodynamic Property Comparison

Thermodynamic parameters and properties are particularly important because they determine state points, in addition to affecting component performance. Specifically, one would desire expect that the P and T values on state plots be as close as possible for the conventional and replacement fluids especially for the same application. Listed below are thermodynamic properties whose ratios are proportional (or inversely proportional) to system and component performances.

- Saturation pressure: P_{sat}
- Liquid density: ρ_f
- Vapor specific volume: v_v
- Velocity ratio comparison
- Specific heats: C_p
- Liquid and vapor enthalpy effects

    a. Saturation Pressure (same temperature):

    - Effects pipe pressure and joint strength

    b. Liquid Density

    - Effects pipe fluid velocity, heat transfer, and pressure drop

c. Vapor Specific Volume

- Effects pipe fluid velocity, heat transfer and pressure drop (see item d. below)

d. Velocity ratio Comparison- the ratio of vapor-to-liquid velocity during phase change

- For the same mass flow and tube:

$$\frac{V_v}{V_l} = \frac{\rho_l}{\rho_v} = \rho_l \ \nu_v$$

- Effects pressure drop and heat transfer during phase change

e. Specific heats

- The effect is on Pr= $\frac{\mu C_p}{k}$, which is proportional to the convective heat transfer coefficient.

f. Liquid and Vapor Enthalpy effects (most important)

- " enthalpy of vaporization," h_{fg}
- Effects, cooling capacity - $\dot{m}h_{fg}$

Thermodynamics Comparison between R-134a and R-1234yf In this thesis, the high-side (condenser) temperature is set as 30℃ and the low-side (evaporator) temperature as -20℃, for both R-1234yf and R-134a. At -20℃, the saturation pressure of R-1234yf is 13.6% higher than that of R-134a, which is 150.9 kPa to 132.8 kPa, respectively. However, at 30℃, the saturation pressure differences between the two kinds of refrigerants decreases to 1.7%, which is negligible. Refrigerant saturation pressure also affects pipe pressure and joint strength. Liquid densities for R-1234yf are 9% to 10% less than R-134a. Additionally, liquid density is a parameter that affects pipe fluid velocity, heat transfer, and pressure drop. R-1234yf has a 14% to 22% smaller specific volume than R-134a. Similar to liquid density, vapor specific volume is also a parameter that affects fluid pipe velocity, heat transfer, and pressure drop.

4.2 Transport Properties

Similar to thermodynamic properties above, transport properties are presented below.

- Viscosity : μ_v , μ_f
- Thermal conductivity : k_v , k_f
- Prandtl number : Pr_v , Pr_f

a. Viscosity

- The effect is on pressure drop (friction factors and Reynolds number)
- Reynolds number ($Re= \frac{4\dot{m}}{\pi D\mu}$) is inversely proportional to viscosity
- The friction factor is inversely proportional to $Re^{0.25}$
- Reynolds number affects Nusselt number (proportional to $Re^{0.8}$)
- The effect is on heat transfer coefficient

b. Thermal Conductivity

- Effects heat transfer

c. Prandtl number

- The definition is $Pr = \frac{\mu C_p}{k}$
- Refrigerant ratios: $R = \frac{Pr_{1234yf(1)}}{Pr_{134a(2)}} = \left(\frac{\mu_1}{\mu_2}\right)\left(\frac{C_{p1}}{C_{p2}}\right)\left(\frac{k_2}{k_1}\right)$

- Prandtl number affects Nusselt number (proportional to $Pr^{\frac{1}{3}}$)

Transport Properties Comparison between R-134a and R-1234yf The effect of specific heat is on $Pr= \frac{\mu C_p}{k}$, which is proportional to the convective heat transfer coefficient. For R-1234yf, the specific heat of the liquid phase is 6.7 to 5.5% lower than that of R-134a, and the specific heat of the vapor phase is 3.8 to 1.9% higher than that of R-134a. As a result, liquid R-1234yf has less heat transfer while vapor R-1234yf has greater heat transfer compared to that of R-134a. Enthalpy

is 4 to 6% less for liquid R-1234yf while 13 to 16% less for vapor R-1234yf compared to that of R-134a. The most important thermodynamic property effect is liquid and vapor enthalpy. The enthalpy of vaporization-- h_{fg} , for R-1234yf, is 18% less than that of R-134a at all temperatures. Moreover, according to the definition of cooling capacity--$\dot{m}h_{fg}$, we can conclude that the R-1234yf cooling capacity is 18% less than that of R-134ª for the same mass flow rate or the R-1234yf mass flow rate is 18% larger than that of R-134a for the same cooling capacity.

Compared to R-134a, liquid viscosities of R-1234yf are smaller by 17 to 18%, however, vapor viscosities are larger by 0.2 to 2.5%. As noted earlier, viscosity affects pressure drops, friction factors, and Reynolds number as well. According to the definition of Reynolds number, $Re=\frac{4\dot{m}}{\pi D\mu}$, the Reynolds number is inversely proportional to viscosity. Thus, for the liquid phase of the refrigerant, the Reynolds number is 18% larger for R-1234yf compared to R-134a. Friction factor is inversely proportional to $Re^{0.25}$, resulting in R-1234yf having a 4% smaller pressure drop for the same liquid flow rate. Moreover, Reynolds numbers affect the Nutsselt number, which is proportional to $Re^{0.8}$. As a result, the Nutsselt number is 14% larger for R-1234yf compared to R-134a. For R-1234yf compared to R-134a, liquid thermal conductivities are 20 to 22% smaller and vapor thermal conductivities are 23% to 25% smaller. Because of the lower liquid thermal conductivity, the heat transfer of R-1234yf will be reduced compared to that of R-134a. Besides thermal conductivity, other properties effect on heat transfer can be seen in Eqn (2). In fact, the three effect on heat transfer can be observed by forming R-1234yf to R-134a heat transfer ratios, namely R ratio. As an example, the liquid ratio is $R_f = (0.75)(0.72)(1.23) = 0.7$, while the vapor ratio is $R_v = (1.05)(1.03)(1) = 1.08$. To summarize, this means that for the liquid phase, the refrigerant ratio of R-1234yf is 30% smaller while for the vapor phase, the refrigerant ratio of R-1234yf is larger by 8%. Prandtl number affects the Nusselt number, which is proportional to $Pr^{\frac{1}{3}}$.

The Nusselt number of liquid phase R-1234yf is 10% smaller than that of R-134a. A comprehensive analysis between R-134a, R-1234yf and R-1234ze is shown in Appendix B.

4.3 Parameter Comparisons

To evaluate component performance, ratios of two important parameters, namely the heat transfer coefficient and the pressure drop, are formed from property ratios. One can easily surmize that selecting a replacement refrigerant that increases heat transfer while reducing pressure drop is desirable.

4.3.1 Heat transfer coefficient comparison

$$\mathrm{Nu} = 0.023\,\mathrm{Re}^{0.8}\mathrm{Pr}^{0.33} = \frac{\mathrm{hD}}{\mathrm{k}} \tag{1}$$

In our research, making a comparison of the convective heat transfer coefficient between two refrigerants, will use Eqn (1), where $\mathrm{Re} = \frac{4\dot{m}}{\pi D\mu}$, $\dot{m} = \rho V\frac{\pi}{4}D^2$, $\mathrm{Pr} = \frac{\mu C_p}{k}$. By substituting the Reynolds number and Prandtl number into Eqn (1), we obtain Eqn (2), which is shown as follows.

$$\mathrm{h} = 0.023\,\frac{\mathrm{k}}{\mathrm{D}}\left(\frac{\rho VD}{\mu}\right)^{0.8}\left(\frac{\mu C_p}{k}\right)^{0.33} \tag{2}$$

Assuming the same velocity, the ratio of refrigerant B to refrigerant A is defined as:

$$\frac{h_A}{h_B} = \frac{k_A}{k_B}\left(\frac{\rho_A}{\rho_B}\right)^{0.8}\left(\frac{\mu_B}{\mu_A}\right)^{0.8}\left(\frac{\mu_A}{\mu_B}\right)^{0.33}\left(\frac{C_{PA}}{C_{PB}}\right)^{0.33}\left(\frac{k_B}{k_A}\right)^{0.33} = \left(\frac{k_A}{k_B}\right)^{0.67}\left(\frac{\rho_A}{\rho_B}\right)^{0.8}\left(\frac{\mu_B}{\mu_A}\right)^{0.47}\left(\frac{C_{PA}}{C_{PB}}\right)^{0.33} \tag{3}$$

Assuming the same cooling capacity, yields

$$\dot{Q} = AGh_{fg} \tag{4}$$

$$\frac{G_B}{G_A} = \frac{h_{fg\,A}}{h_{fg\,B}} \tag{5}$$

The ratio of refrigerant B to refrigerant A is then defined as:

$$\frac{h_B}{h_A} = \frac{k_B}{k_A}\left(\frac{h_{fg\,A}}{h_{fg\,B}}\right)^{0.8}\left(\frac{\mu_A}{\mu_B}\right)^{0.8}\left(\frac{\mu_B}{\mu_A}\right)^{0.33}\left(\frac{C_{PB}}{C_{PA}}\right)^{0.33}\left(\frac{k_A}{k_B}\right)^{0.33} = \left(\frac{k_B}{k_A}\right)^{0.67}\left(\frac{h_{fg\,A}}{h_{fg\,B}}\right)^{0.8}\left(\frac{\mu_A}{\mu_B}\right)^{0.47}\left(\frac{C_{PA}}{C_{PB}}\right)^{0.33} \quad (6)$$

4.3.2 Pressure drop comparison

The pressure drop through a piping system is defined as $\Delta P = f_D \frac{\rho}{2} V^2 \frac{L}{D}$, where ρ is the density of the fluid, V is the average velocity in the pipe, f_D is the friction factor from the Moody Chart, L is the length of the pipe and D is the pipe diameter.

For laminar flow, $f_D = \frac{0.316}{Re^{0.25}}$ when Re$\leq$ 20000

For turbulent flow, $f_D = \frac{0.184}{Re^{0.25}}$ when Re$\geq$20000

where Re= $\frac{\rho VD}{\mu}$

Assuming the same velocity, results in

$$\frac{\Delta P_B}{\Delta P_A} = \frac{{\mu_B}^{0.25}}{{\mu_A}^{0.25}} \frac{{\rho_A}^{0.25}}{{\rho_B}^{0.25}} \frac{\rho_B}{\rho_A} = \frac{{\mu_B}^{0.25}}{{\mu_A}^{0.25}} \frac{{\rho_B}^{0.75}}{{\rho_A}^{0.75}} \quad (7)$$

While assuming the same cooling capacity results in

$$\frac{\Delta P_B}{\Delta P_A} = \frac{{\mu_B}^{0.25}}{{\mu_A}^{0.25}} \frac{{G_B}^{1.75}}{{G_A}^{1.75}} \frac{\rho_A}{\rho_B} = \frac{{\mu_B}^{0.25}}{{\mu_A}^{0.25}} \frac{{h_{fg\,A}}^{1.75}}{{h_{fg\,B}}^{1.75}} \frac{\rho_A}{\rho_B} \quad (8)$$

5. RECONFIGURED SYSTEMS

Promising refrigerant candidates were identified by screening for properties, then compared to R-410A in the proposed evaporative cooling systems. Two reconfiguration approaches were investigated to improve the performance of a conventional vapor-compression system: Approach A (Indirect) and Approach B (Direct). Four cases using these two approaches were considered:

Approach a example:

A. Install evaporative cooling with external water (A1) and internal water (A2) at condenser air inlet
B. Install HRV (B1) or ERV (B2) units at evaporator inlet (DOAS)

Approach b example:

C. Use evaporator condensate water to cool refrigerant exiting the condenser
D. Configure an internal heat exchanger (liquid-line and suction-line heat exchanger)—transfer refrigerant energy from high to low side

5.1 Evaporative Cooling Reconfigured System (A1 and A2)

5.1.1 Evaporative Cooling History and Category

Evaporative cooling has been used since ancient time, and it can be used independently in some applications or combined with other systems. For instance, zeer pot is an evaporative cooling device commonly used in rural Africa and the Middle East, utilizing earthenware pot, lined with wet sand, contains an inner pot within which the food is placed. With cool air and good ventilation conditions, the interior of a zeer pot can chill down to nearly 40 °F.

Basically, there are simple ways to implement evaporative cooling: directly evaporative precool the cooling air before it goes through a condenser; flood water over the condenser coil

while air is blown through it. Also, evaporative precoolers and evaporatively cooled condenser coils are the most commonly used technologies in the evaporative cooled residential condenser market.

This study is focused on evaporative precoolers using condensate water from the evaporator or external water. There are two kinds of precoolers---direct water-injection system and indirect water-injection systems. In the direct water-injection system, pumps and nozzles are used to spray water into the incoming air stream, where it evaporates, cooling the air before it enters the condenser. Indirect water-injection uses a cooling mesh that water is sprayed onto, when the air passes through the mesh, it is cooled before it reaches the condenser. Using the direct method may lead to fouling deposits as a result of the salt content of sprayed water and eventually corrode the coil; however, using condensate would avoid this problem.

5.1.2 System Description

For this study, 100% outdoor air is utilized, which means that the outdoor air is both the heat source and heat sink. Energy is removed from the outdoor air in the evaporator as the air is dehumidified and cooled. Next, this energy plus that of the compressor work is rejected to the outdoor air in the vapor compression system condenser. An advantage of the 100% outdoor fresh air application is that the analysis is simplified by having only one set of conditions.

By installing an evaporator cooler upstream of the condenser, shown in Figure 8, water is used to precool the outdoor air before it enters the condenser, resulting in a lower refrigerant condensing temperature. With externally sourced water, it is can achieve the wet-bulb condition, which corresponds to the lowest possible condenser air-inlet temperature. With internal water, where the condensate from the evaporator is used for precooling, both the degree to which

evaporative cooler can reach the wet-bulb temperature and the amount of condensate are dependent on the outdoor air temperature and relative humidity. Therefore, the internal condensate collected for a specific outdoor air condition may or may not be sufficient to achieve a fully wet-bulb condition.

Scenario A1 (externally sourced cooling water), is shown in Figure 8, with the outdoor air leaving the evaporative precooler being fully saturated to the wet bulb temperature. Figure 10 shows that the lower outdoor air wet-bulb temperature, leads to an even lower condensing refrigerant temperature for scenario A1. Thus, the refrigeration effect increases while specific work decreases as compared to the case without evaporative cooling, shown in Figure 12. The COP of this system should be the largest of the three scenarios due to the energy transfer and the lowest heat-sink temperature. While the performance of systems using only external water and those that use combination of internal and external are the same, there could be significant water savings achieved by supplementing with internal water.

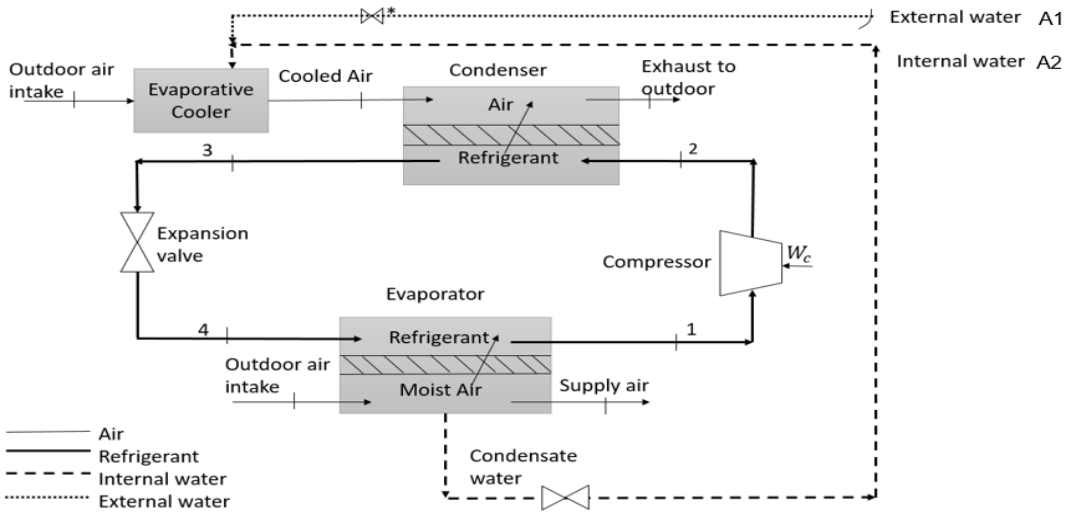

Figure 8 Schematic of the vapor-compression refrigeration cycles with evaporative cooling (external source and internal source) of the condenser-inlet air

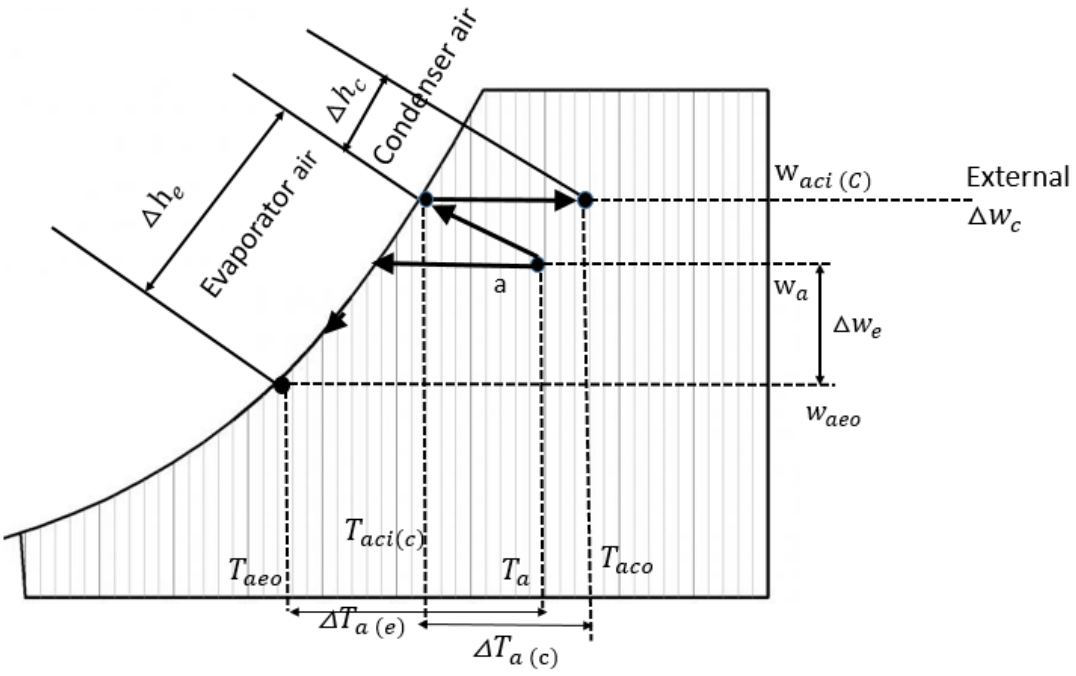

Figure 9 Psychrometric chart of air in the evaporator and condenser cooler for scenario A1

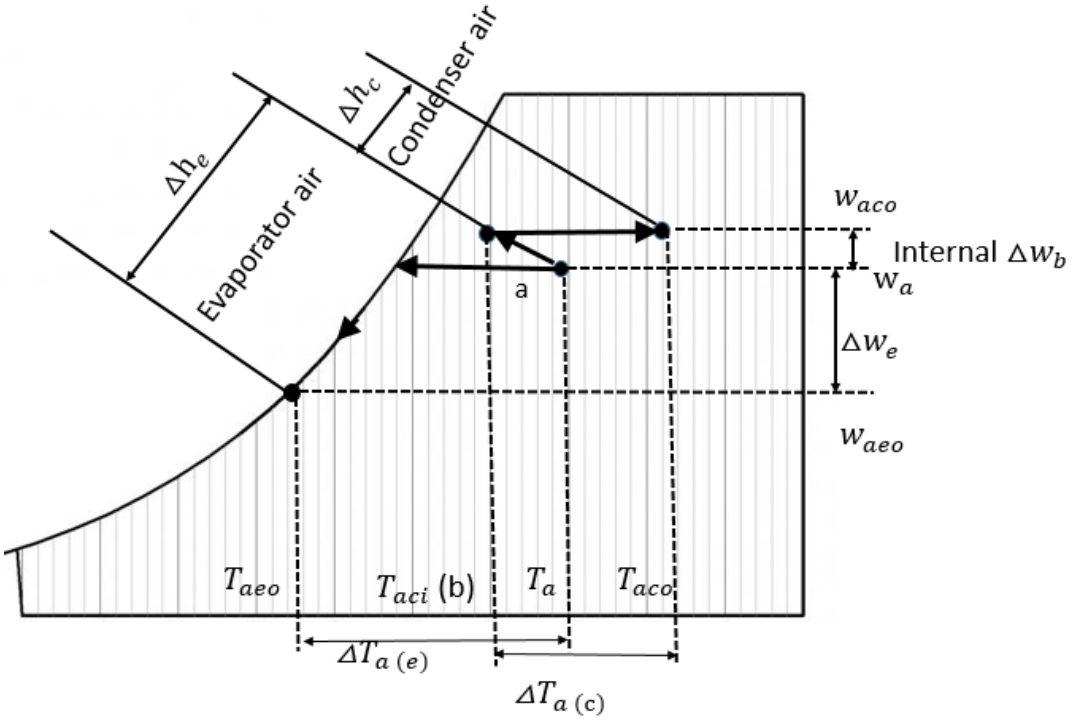

Figure 10 Psychrometric chart of air in the evaporator and condenser cooler for scenario A2

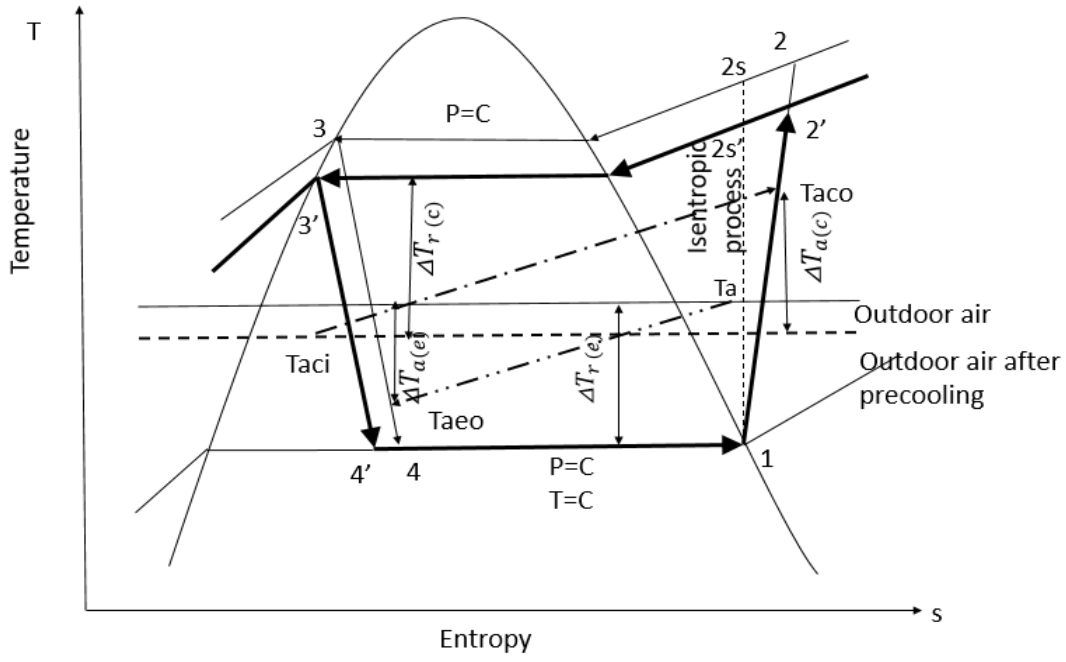

Figure 11 T-s diagram of a system with evaporative cooling utilizing external water (internal water)

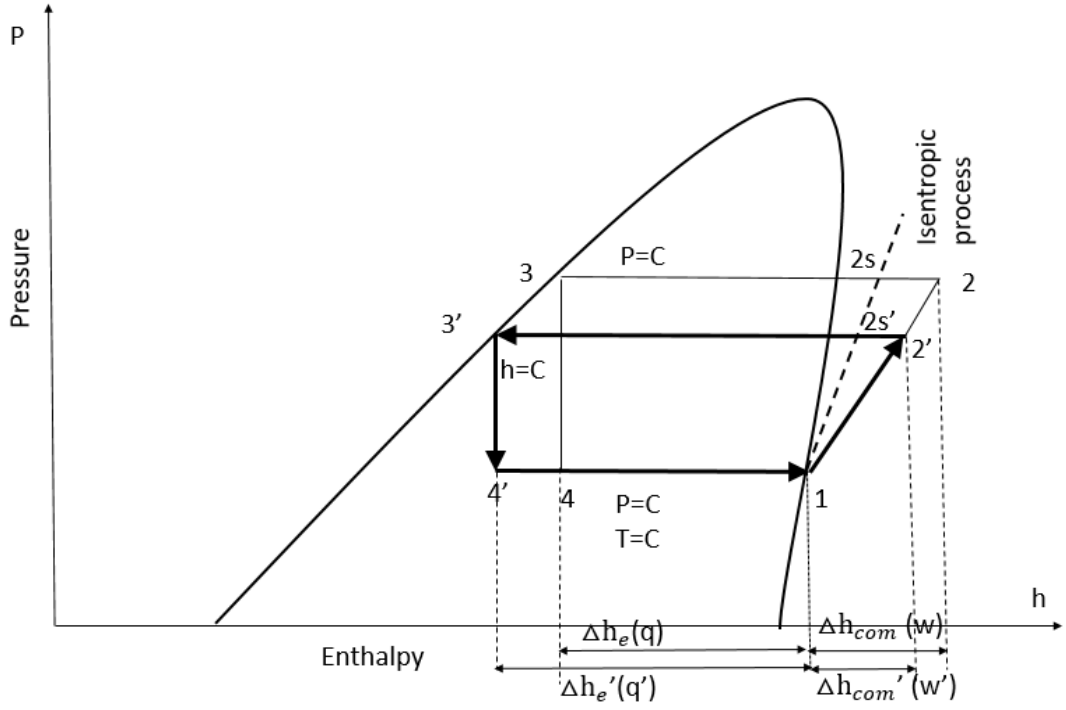

Figure 12 P-h diagram system with evaporative cooling utilizing external water and internal water

In scenario A2, a conventional vapor-compression cycle is reconfigured with an evaporative precooler before the condenser using only internal condensate water. As the humidity ratio of the outlet air is lower than that of inlet air in the evaporator, condensate water is formed and collected. This condensate then goes to the evaporative precooler to dehumidify and cool the outdoor air, as shown in Figure 10. In some cases, the internal condensate water is not sufficient foto saturate the outdoor air to the wet bulb temperature, which corresponds to the lowest possible condenser air-inlet temperature.

5.1.3 Proof-of-concept for a Reconfigured Cycle Higher Efficiency

A proof-of-concept is presented here to validate and support the approach to increase cycle performance by reconfiguring a vapor-compression cycle to evaporatively cool the outdoor air that is supplied to the condenser. This proof-of-concept is achieved by presenting explanations and descriptions of a typical vapor compression cycle compared to the reconfigured one. Also, the order-of-magnitude difference in performance parameters is identified. The next step after this validation of the approach to increase cycle efficiency is to quantify the performance increase by performing a detailed analysis in the section that follows.

The proof-of-concept states by increasing that system cooling capacity or evaporator heat transfer rate are the same for all three scenarios, namely A through A2, with the air-side being.

$$\dot{Q_{ae}}=\dot{m_{ae}}\ (h_{aei}\text{-}h_{aeo}\ ) \tag{9}$$

Moreover, then dividing by the mass flow rate of air in the evaporator, resulting in

$$q_{ae} = h_{aei} - h_{aeo} \tag{10}$$

Because the objective of the vapor compression cycle is to cool air, then it is necessary to compare all three scenarios namely A through A2 by performing the same cooling task for the same conditions. In other words, the outdoor air entering the evaporator regardless of its dry bulb temperature and relative humidity is cooled and dehumidified for all 3 cases to the same

temperature of 45 °F which is an assumed value, representing the real-world application. Therefore, values of the air-side inlet and exit enthalpy shown in the above equation are the same for all three scenarios.

The air-side and refrigerant-side heat transfer water, which are the same as cooling capacity, are equal to each other as follows

$$\dot{Q_{re}}=\dot{m_r}\ (h_{rei}\text{-}h_{reo}\ )=\dot{Q_{ae}} \tag{11}$$

As will be shown and explained later, the refrigerant-side mass flow rate differs from scenario to scenario because the entering and exiting enthalpy are different, under the case of the air-side.

Of special importance, the three scenarios result in different values for the refrigerant-side compressor work because the high-side refrigerant pressure that affects compressor work changes as the air-side temperature of the condenser change because of the use of an evaporative cooler. These differences in the compressor pressure and work can be better understood by focusing on the condenser-side inlet-air temperatures (T_{aci}) for the 3 scenarios, with a magnitude order as followed,

$$T_{Aac} > T_{A2ac} > T_{A1ac} \tag{12}$$

Scenario A as representing outdoor air being delivered directly to the condenser is the highest while scenario A1 and A2 have a lower temperature approaching the wet bulb condition because the air is evaporatively cooled. The above air-side temperature magnitude order is repeated for the condenser refrigerant-side ("a") saturation temperature as follows

$$T_{Arc} > T_{A2rc} > T_{A1rc} \tag{13}$$

which is, in turn, determining the compressor outlet pressure magnitude order that is essentially based on the refrigerant saturation temperature order of

$$P_{Arc} > P_{A2rc} > P_{A1rc} \tag{14}$$

With the result that the typical vapor-compression cycle without the evaporative cooler has the highest pressure.

Continuing the parameter order of the scenarios and the effect that one parameter has on the other, the magnitude order of the pressure rise across the compressor follows, assuming that the inlet pressure to the compressor is the same for all 3 scenarios,

$$\Delta P_{Arc} > \Delta P_{A2rc} > \Delta P_{A1rc} \tag{15}$$

which indicates that evaporatively cooling the condenser can reduce the pressure rise across the compressor. Even though the refrigerant cycle compressor work is not directly proportional to pressure rise because the process is irreversible and the refrigerant gas is compressible one can say in a general sense that more work is required to compress the gas to a higher pressure compared to a lower pressure. So that the compressor specific work magnitude order follows the pressure rise order as follows

$$w_{Ar} > w_{A2r} > w_{A1r} \tag{16}$$

The above magnitude order for the three scenarios has now been established with the baseline refrigerant cycle (scenario A) requiring more work than the two evaporative cooler scenarios. This order is important because it affects the order of the three cycle performances regarding the COP increasing its magnitude with the addition of the evaporator cooler. The COP performance parameter is especially important because it motivates this study, also provides observing how COP is affected by changes in other parameters and insight into how the evaporative cooler upstream of the condenser improves cycle performance and reduces energy consumption.

The vapor-compression cycle performance is directly related to the value of the coefficient of performance (COP), which is defined as the ratio of useful energy and energy usage or the ratio of cooling capacity and compressor power. Either way, the result is as follows

$$\text{COP}=\dot{Q_{er}}/\dot{W_r} \tag{17}$$

Because cooling capacities are the same for all three scenarios, operating with the same outside air condition, then the heat transfer rate into the refrigerant flowing through the evaporator is the same for all of the scenarios. However, the energy transfer per unit mass into the refrigerant may not be equal. To show the magnitude order for three scenarios, one can replace the rate value for energy transfer in the COP with specific values per unit mass as follows

$$\dot{W_r}=\dot{m}_r\ w_r \tag{18}$$

and

$$Q_{re} = \dot{m}_r\ q_{re} \tag{19}$$

So that compression work and evaporator energy become:

$$w_r= \dot{W_r}/\dot{m}_r \tag{20}$$

And

$$q_{re} = \dot{Q_{re}}/\dot{m}_r \tag{21}$$

With the final result for the COP being

$$\text{COP}=q_{re}/w_r \tag{22}$$

As noted previously, the specific work for the compressor decrease with evaporative cooling from scenario A through C so that the inverse of each work, which is proportional to COP, is as follows,

$$\frac{1}{w_{A1r}} > \frac{1}{w_{A2r}} > \frac{1}{w_{Ar}} \tag{23}$$

All of the specific energy transfer in the evaporator, q_{re} , were the same for each scenario then the COPs would be ordered as follows

$$COP_{A1} > COP_{A2} > COP_{A} \tag{24}$$

However, a complicating fact is that the unit energy transfer on the refrigerant side of the evaporator is not equal so that

$$q_{Are} \neq q_{A2re} \neq q_{A1re} \tag{25}$$

The state exiting the evaporator (i.e., entering the compressor), for all scenarios is the same based on assuming a fixed condition saturated vapor and evaporator saturation temperature and pressure, but the refrigerant state entering the evaporator, namely h_{rei} is different from scenario to scenario. Specifically, the reason for this difference, even for the same cooling capacity, is that the refrigerant temperature exiting the condenser is different for each scenario, meaning that the refrigerant state exiting the condenser (i.e. entering the expansion device) and then entering the evaporator on the refrigerant side is different for each scenario. Observations of the process on a Ts diagram or Ph diagram shows the following scenario magnitude order,

$$h_{Arei} > h_{A2rei} > h_{A1rei} \tag{26}$$

which measure that the evaporative cooling reconfiguration. Therefore, for a fixed evaporator outlet state for all three scenarios, magnitude order for the enthalpy difference, namely

$$\Delta\, h_{re} = h_{reo} - h_{rei} \tag{27}$$

which represents unit energy transfer, q_{re} is as follows

$$\Delta h_{A1r} > \Delta h_{A2r} > \Delta h_{Ar} \tag{28}$$

So that the specific energy transfer to the refrigerant in the evaporator is

$$q_{A1re} > q_{A2re} > q_{Are} \tag{29}$$

which essentially means that the evaporative cooling effect on the cycle is to increase the results for a unit mass of refrigerant flowing into the system to transfer heat. It would thus appear from the above that the COP of the baseline vapor compression cycle can be improved by decreasing the air heat sink temperature (or decreasing the high-side refrigerant temperature) with the installation of an air-side evaporative cooler upstream of the condenser as the result of two effects with one being more obvious than the other. The obvious effect is increasing the COP as the result of decreasing the specific work required by the compressor where the less obvious effect is because the cooling energy transfer per unit also increases. In other words, the COP increase due to decreasing the pressure rise of the compressor is more easily observed than the second effect of increasing the enthalpy change across the evaporator on the refrigerant side.

Another view of the above duel effects is that for a large evaporator enthalpy change, as the result of the evaporative cooler reconfiguration, then a smaller refrigerant mass transfer is needed to achieve the same cooling capacity, and as a result the lower refrigerant mass flow rate reduces the compressor power even more than the specific work reduction caused by, the lower compression pressure rise.

The reduction in compressor work with evaporative cooling for the same cooling capacity can be determined by the following several steps presented below focusing only on the two extreme scenarios of A and A1 means air at the dry bulb temperature and wet bulb temperature entering the condenser, respectively, and recalling that the cooling capacity is,

$$\dot{Q}_{Ar}=\dot{Q}_{A1r} \tag{30}$$

So that

$$\dot{m}_{Ar}q_{Are}=\dot{m}_{A1r}\ q_{A1re} \tag{31}$$

And

$$\dot{m}_{Ar}\,\Delta h_{Are}=\dot{m}_{A1r}\,\Delta h_{A1re} \tag{32}$$

As noted before, the enthalpy change through the evaporator is larger for scenario C with evaporative cooling causing a reduction in the condensing refrigerant temperature, which in turn decreases the enthalpy entering the evaporator, so that

$$\Delta h_{A1re} > \Delta h_{Are} \tag{33}$$

Moreover, as a result, the refrigerant mass flow rate required for the typical system is higher than that of the reconfigured cycle

$$\dot{m}_{Ar} > \dot{m}_{A1r} \tag{34}$$

, which can then be applied to the compressor power. Recalling for compressor power, of special importance, this difference is mass flow rate along with

$$\dot{W}_{Ar}=\dot{m}_{Ar}w_{Ar} \tag{35}$$

$$\dot{W}_{A1r}=\dot{m}_{A1r}\,w_{A1r} \tag{36}$$

Moreover, considering the effect of both mass flow rate and specific work regarding enthalpy with the latter, and being smaller for scenario A1 as follows

$$w_{Ar} > w_{A1r} \tag{37}$$

Then the result as follows is that compressor power for scenario A is larger than Scenario A1

$$\dot{m}_{Ar}\,w_{Ar} > \dot{m}_{A1r}\,w_{A1r} \tag{38}$$

And

$$\dot{W}_{Ar} > \dot{W}_{A1r} \tag{39}$$

Instead of using “greater than” equations for parameters, one can also form ratios shown as follows

$$\frac{w_{Ar}}{w_{A1r}} > 1 \tag{40}$$

$$\frac{\dot{m}_{Ar}}{\dot{m}_{A1r}} > 1 \tag{41}$$

So that $\frac{\dot{W}_{Ar}}{\dot{W}_{A1r}} > 1$

Moreover, by representing a power ratio in terms of mass flow rate ratios and specific work ratios as above, it is easier to see how scenario A compressor power compares to scenario A1 (and by inference scenario A2).

This ratio approach can also be used to show how COP s are affected by reconfiguring a vapor compression cycle with an evaporative cooler (i.e., different scenarios), especially because all three scenarios have the same cooling capacity.

Forming a COP ratio as follows,

$$\frac{COP_{A1}}{COP_A} = (\frac{\dot{W_{Ar}}}{\dot{W_{A1r}}})(\frac{\dot{Q_{A1re}}}{\dot{Q_{Are}}}) \tag{42}$$

Moreover, with the last ratio or term being unity, (i.e., equal cooling capacity) so that

$$\frac{COP_{A1}}{COP_A} = \frac{\dot{W_{Ar}}}{\dot{W_{A1r}}} \tag{43}$$

Because the scenario A to A1 compressor power ratio is greater than unity, then the COP ratio is greater than unity meaning that

$$\frac{COP_{A1}}{COP_A} > 1 \tag{44}$$

So that

$$COP_{A1} > COP_{A2} > COP_A \tag{45}$$

The above analysis provides an understanding of how each parameter affects other parameters and proves a validity that reconfiguring a baseline vapor-compressor cycle with a

condenser inlet evaporative cooler increase the cycle performance. However, of special importance is quantifying this performance increase or COP increase for different outdoor conditions, namely dry bulb temperatures and relative humidities, which is the subject and focus of this study. A section that follows a detailed model, both refrigerant, and air-side, is formulated for both a typical vapor compression cycle and one that is reconfigured with an evaporative cooler to reduce the temperature of the outdoor air entering the condenser. This model is then solved for a variety of outdoor conditions and COPs are tabulated, graphed and compared to different scenarios.

5.1.4 Model Development and Formulation

To calculate the critical refrigerant cycle performance parameters, such as the refrigeration cooling effect, the compressor work, and COP, it is necessary to specify or determine the thermodynamic state properties of the cooling refrigerant at each point in the vapor compression cycle. To accomplish this, it is also necessary to know the state properties and flow conditions of the moist air entering and leaving the evaporator and condenser, along with the condition of the condensate draining from the air-side of the evaporator. Therefore, determining the performance parameters, such as COP, that will allow for evaluating the effect of the upstream evaporative cooler requires developing, deriving, and solving four separate models, namely: 1) moist air properties 2) condensing refrigerant temperature calculation 3) evaporative cooling process 4) vapor-compression refrigeration cycle.

5.1.4.1 Moist Air Properties

An accurate method to calculate the moist air properties of the air entering and exiting the heat exchangers is especially important for the evaporator and the evaporative cooler because the internal water that condenses and drains from the evaporator is used in the evaporative cooler, which is a major focus for this study. As a start, the following equations (R.G.Wylie & T.Lalas)

can be used to determine the saturated water-vapor pressure for the outdoor air at dry-bulb temperatures that are within the limits of the earth's climate.

$$P_s = 610.78 \exp\left[\left(\frac{t_{db}}{t_{db}+238.3}\right) \times 17.2694\right] \quad (46)$$

In this equation, the water-vapor saturation pressure, P_s is in units of pascals and the dry-bulb temperature $t_{db}$is in degrees Celsius.

Next, the moist-air humidity ratio, w, defined as the ratio of water vapor mass to dry air mass can be determined from a relationship that is easily derived from the ideal gas assumption and ideal gas equations to both dry air and water vapor:

$$w=0.622 \frac{p_v}{p_{tot}-p_v} \quad (47)$$

where P_v is the actual water vapor pressure and p_{tot} is the total air pressure or in the case of outdoor air, the atmospheric pressure.

Another important moist air parameter used in this study is relative humidity, RH, because outdoor air is typically defined by not only the dry-bulb temperature but also by a value for relative humidity. This relative humidity (RH) is defined as follows: the ratio of the actual water-vapor pressure, P_v to the saturated water-vapor pressure, P_s, which was found from Eqn 46.

$$RH=\frac{p_v}{p_s} \quad (48)$$

As one can see, the above three equations can be rearranged and combined to determine the various parameters and properties of the moist air for any state or process. Specifically, for this study, this moist air model can be used to calculate the amount of condensate formed in the refrigerant system evaporator and, for the case of an evaporative cooler, the outlet state when liquid water is added to the flowing moist- air stream entering the condenser.

Once the moist air properties and state are known, then the moist air enthalpy can be determined. Moist air enthalpy is a particularly important parameter because it is a major

component of the energy balance equation as written for the two HXs, regardless of the dependent parameters of interest. Therefore, knowing that the moist air is at the dry-bulb temperature and has a humidity ratio w, then the enthalpy of moist air, in terms of dry air mass, kJ/kg, can be calculated as follows:

$$h=h_a+wh_g \tag{49}$$

The enthalpy of dry air in kJ/kg, at any temperature (t), between 0 and 60 ℃ is approximately:

$$h_a = 1.007t - 0.026 \tag{50}$$

and at the same temperature the enthalpy of water vapor is:

$$h_g = 2501 + 1.84t \tag{51}$$

Combining the above terms and inserting dry-bulb temperature result in moist air enthalpy in terms of energy per unit dry air mass, kJ/kg,

$$h=1.007\ t_{db}-0.026+ w\ [2501 + 1.84t_{db}] \tag{52}$$

5.1.4.2 Condensing Refrigerant Temperature Calculation

In order to calculate the significant refrigerant cycle performance parameters, it is necessary to know the condensing refrigerant temperature. As a start, the following paragraphs will introduce the assumptions and temperature calculations in the evaporator.

Refrigerant and Air Temperatures in Evaporator As several outdoor air conditions and evaporator outlet temperatures are fixed, the enthalpy change through the evaporator is known as follows,

$$\Delta h_e = h_{aei}-h_{aeo} \tag{53}$$

As shown in Figure 13, another assumption is made that the evaporating refrigeration temperature is 10°F lower than the evaporator outlet air temperature, which is expressed as followed,

$$T_1 = T_{aeo} - 10 \tag{54}$$

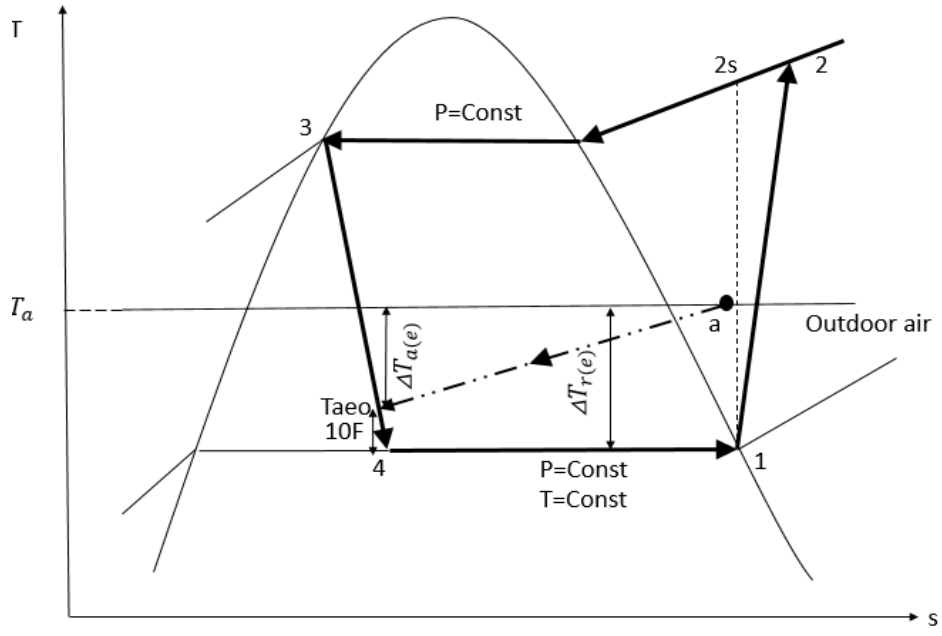

Figure 13 Evaporator outlet temperature difference of two streams

Energy balance equation By using the thermodynamics first law, considering the whole vapor-compression refrigeration system as a control system, as shown in the figure below, the energy transfer in equals energy transfer out,

$$\dot{Q}_{in} = \dot{Q}_{out} \tag{55}$$

Also, energy transfer in the system is the compressor work ($\dot{W}_{comp}$) plus the cooling capacity of the evaporator and energy transfer out of the system is the heat rejection of condenser ($\dot{Q}_c$), which yields,

$$\dot{Q}_c=\dot{Q}_e+\dot{W}_{comp} \quad (56)$$

Heat rejection of the condenser, $\dot{Q}_c$, was calculated by Eqn (57)

$$\dot{Q}_c=\dot{m}_{ac}\triangle h_c = \dot{m}_{ac}\, C_p\, \triangle T_{ac} \quad (57)$$

where $\dot{m}_{ac}$ is the air mass flow rate in the condenser, $\triangle h_c$ is the enthalpy change of air across the condenser, C_p is the specific heat capacity of air, $\triangle T_{ac}$ is the temperature change of air across the condenser.

The cooling capacity, as discussed in the previous part, is expressed as

$$\dot{Q}_e=\dot{m}_{ae}\, \Delta h_e \quad (58)$$

The air conditioner COP is expressed cooling capacity, $\dot{Q}_e$ over power consumption $\dot{W}_{comp}$, as follow,

$$COP=\frac{\dot{Q}_e}{\dot{W}_{comp}} \quad (59)$$

Move the power consumption to the left, yielding

$$\dot{W}_{comp}=\frac{\dot{Q}_e}{COP} \quad (60)$$

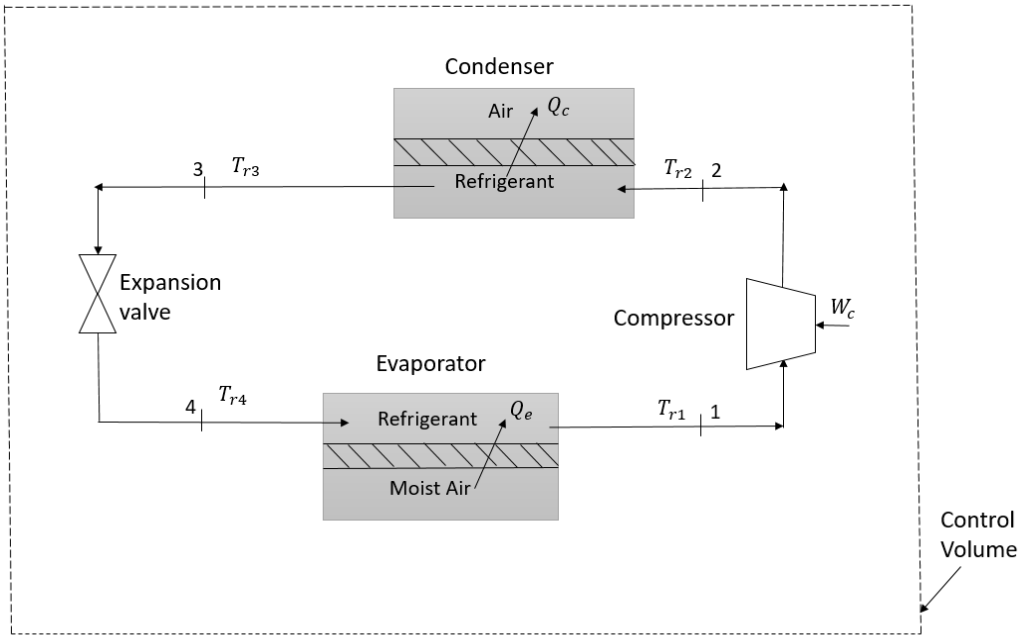

Figure 14 Control Volume of vapor-compression refrigeration system

By substituting Eqn (57), (58) and (60) into equation (56), a final equation is generated as follows:

$$\dot{m}_{ac}\, C_p \triangle T_{ac} = \dot{m}_{ae} \Delta h_e \left(1+\frac{1}{COP}\right) \tag{61}$$

Where

$$\dot{m}_{ac} = \boldsymbol{\rho}\ cfm_c \tag{62}$$

$$\dot{m}_{ae} = \boldsymbol{\rho}\ cfm_e \tag{63}$$

The above two equations, Eqn (62) and Eqn (63) are used to calculate the mass flow rate of air in the condenser, evaporator and one make an assumption that density of air is constant. It is figured out the cfm ratio in ASHRAE handbook ---cfm value in the condenser is about two and a half times of that in the evaporator. One can assume that the densities are similar in the evaporator air and condenser air with the colder air in the evaporator having a slightly larger density. Therefore, the condenser-to-evaporator mass ratio is about 2.5, meaning that the air mass flow rate

in the condenser is 2.5 times of the evaporator. A comprehensive table and figure of cfm ratio with a refrigerant cooling ton and manufacture is listed in Appendix B and C.

Finally, by simplifying Eqn (61), the relationship of air temperature change across condenser ($\triangle \mathrm{T_{ac}}$) is expressed as,

$$\frac{\mathrm{C_p} \triangle \mathrm{T_{ac}}}{\Delta h_e} = \frac{\dot{\mathrm{m}}_{\mathrm{ae}}}{\dot{\mathrm{m}}_{\mathrm{ac}}} \left(1+\frac{1}{COP}\right) \tag{64}$$

After inserting the approximate mass ratio, then the reduced equation is

$$\triangle \mathrm{T_{ac}} = T_{aco} - T_a = \frac{\Delta h_e}{2.5\mathrm{C_p}} \left(1+\frac{1}{COP}\right) \tag{65}$$

Refrigerant and Air Temperatures in Condenser As the condenser is the counter-flow heat exchanger and according to the Second Law, heat flows from high temperature to low temperature. Thus, the outlet refrigerant temperature of the condenser is greater than the inlet air temperature in the condenser; one assumption is made that the temperature difference is 30 °F, as shown in Figure 15,

$$T_3 = T_{aci} + 30 \tag{66}$$

where T_3 is the outlet refrigerant temperature of condenser and T_{aci} is the inlet air temperature in the condenser.

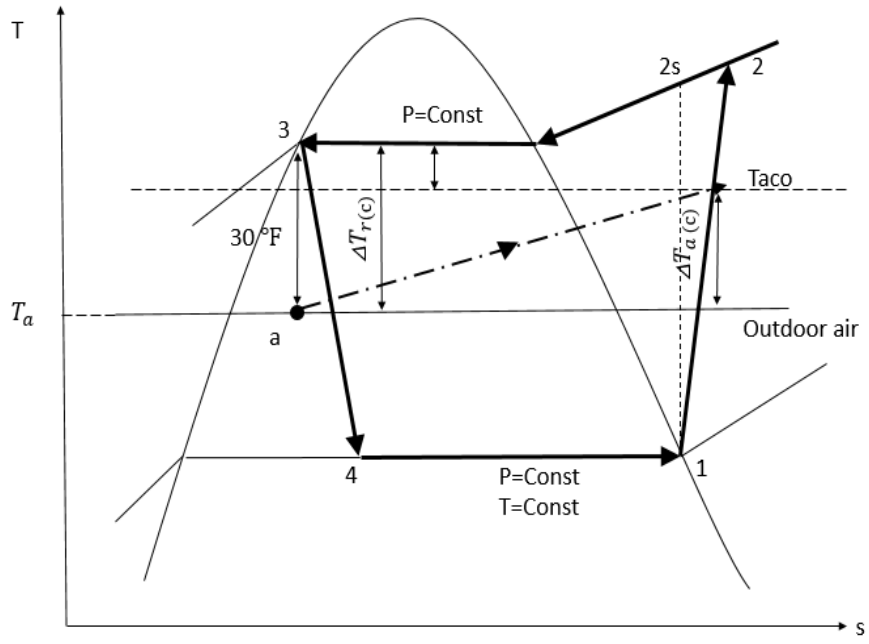

Figure 15 Refrigerant condensing temperature and condenser outlet air temperature

5.1.4.3 Evaporative Cooling Process

The model of the evaporator cooling process is important because it takes into the outdoor air and then determines the dry-bulb temperature and humidity ratio (namely the moist air state and properties), that is delivered to the air-side of the refrigerant-cycle condenser. The evaporative cooling process model for reconfigured system A1 consists of 2 processes, namely, 1) heat transfer between external water and air in the precooler 2) condensing refrigerant temperature determination. However, for reconfigured system A2, three processes are involved: 1) condensate from the evaporator, 2) heat transfer between condensate and air in the precooler, 3) moist-air refrigerant condenser temperature leaving precooler. The process of heat transfer between water and air in the precooler is quite similar, however, the process of scenario of A2 is much more complicated than A1.

5.1.4.3.1 Evaporative Cooling Process for A1

Heat transfer between external water and air in the precooler Heat transfer occurs as the injected external water gained energy from the outdoor air entering the evaporative precooler with the energy transfer causing the external water to evaporate and the moist air to cool. Considering the evaporative precooler as a control volume, there is no heat absorbed or rejected to the surrounding, which means the heat absorption of the water equals to the heat rejection from the air, so that

$$\dot{Q}_w = \dot{Q}_a \tag{67}$$

where $\dot{Q}_w$ is the heat transfer to the water

$$\dot{Q}_w = \dot{m}_w \, (h_{fe} - h_{fi}) \tag{68}$$

where $\dot{m}_w$ is the mass flow rate of water and we assume it is equal to the amount of water we need to get humidity air from dry-bulb to wet-bulb. h_{fi} is the liquid enthalpy of the entering external water and h_{fe} is the water enthalpy at the exit temperature. It is considered that the entering external water temperature is identical to evaporator outlet air temperature, yielding,

$$\dot{m}_w = \dot{m}_{a\,pc} \, (w_{sat} - w_e) \tag{69}$$

$$\dot{Q}_a = \dot{m}_{a\,pc} C_{pa} (T_{a\,pc} - T_e) \tag{70}$$

where $\dot{Q}_a$ is the heat rejected from the air, $\dot{m}_{a\,pc}$ is the mass flow rate of air in the precooler, C_{pa} is the air specific heat, $T_{a\,pc}$ is the inlet air (outdoor air) temperature in the precooler and T_e is the equilibrium temperature of the air after rejecting heat to the external water and the whole process along with the control volume is shown in Figure 16.

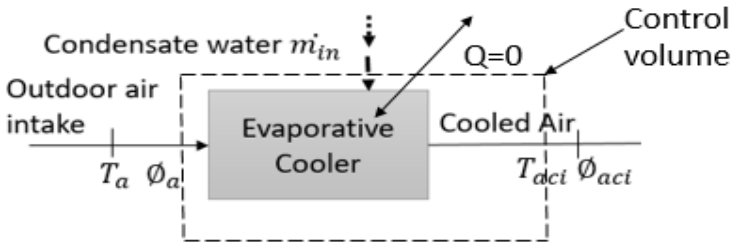

Figure 16 Control volume of precooler

Combing Eqn (67) (68) (69) and (70), which yields,

$$(w_{sat}\text{-}w_e)\, C_{pw}\, (T_e - T_{aeo}) = C_{pa}\, (T_{a\,pc} - T_e) \tag{71}$$

The equilibrium temperature of air in the evaporative cooler could then be calculated, and it is also known that humidity ratio of air remains constant through heat transfer process. Finally, equilibrium state point and final state point after evaporative cooling can be determined.

5.1.4.3.2 Evaporative Cooling Process for A2

Condensate from the evaporator Condensate water is generated in the refrigerant cycle evaporator on the air-side because of the humidity ratio difference between moist air entering and exiting the evaporator, and it is expressed as follows,

$$\dot{m_w} = \dot{m_{a\,e}}\, (w_{aei}\text{-}w_{aeo}) \tag{72}$$

where w_{aei} and w_{aeo} are the inlet and outlet air humidity ratios respectively for the evaporator, which $\dot{m_{a\,e}}$ is the mass flow rate of dry air flowing through the evaporator. This condensate is then either delivered to the condenser or else discharged out of the system.

Heat transfer between condensate and air in the precooler Heat transfer occurs as the injected condensate water gained energy from the outdoor air entering the evaporative precooler

with the energy transfer causing the condensate to evaporate and the moist air to cool. Considering the evaporative precooler as a control volume, there is no heat absorbed or rejected to the surrounding, which means the heat absorption of the water equals to the heat rejection from the air, so that $\dot{Q}_w$=$\dot{Q}_a$ and $\dot{Q}_w$= $\dot{m}_w$ ($h_{fe} - h_{fi}$), further resulting in $\dot{Q}_a = \dot{m}_{a\,pc} C_{pa}(T_{a\,pc} - T_e)$. This process is the exactly the same as that of reconfigured system A1.

It is assumed that condensate water from evaporator which was modeled in another section can be fully utilized in the precooler; however, in some cases, it is possible that excess water could be formed that has to be disposed of.

As mentioned above, cfm_c = 2.5 cfm_e and combing the above three questions, which yields,

$$(w_{aei}\text{-}w_{aeo})\ C_{pw}\ (T_e - T_w) = 2.5\ C_{pa}\ (T_{a\,pc} - T_e) \qquad (73)$$

The equilibrium temperature of air in the evaporative cooler could then be calculated, and we also know that humidity ratio of air remains constant through heat transfer process. Finally, the equilibrium state point can be determined.

Moist-air Refrigerant Condenser Temperature Leaving Precooler In the evaporative cooling process, the enthalpy of air remains constant, which means the state point moves from outdoor air to the saturated point along the constant enthalpy line. However, the humidity ratio increases, the final state being somewhere between the original entering outdoor air condition and the saturating point, which corresponds to 100% RH with no additional condensate evaporation and hence a terminal temperature point, which is depending on the amount of condensate water is generated from the evaporator and how much water is required for saturation. Under this circumstance, a judgment is necessary to make the facts that determine whether the outdoor air can reach the saturated state.

The condensate draining from the evaporator based on the change of the air-side humidity ratio is expressed as,

$$\dot{m}_{w\,out} = \dot{m}_{a\,e}\,(w_{aei}\text{-}w_{aeo}) \tag{74}$$

while the water rejected to the evaporator cooler that in turn evaporate to increase the moist air humidity ratio, is shown as follows,

$$\dot{m}_{w\,in} = \dot{m}_{a\,pc}\,(w_{final}\text{-}w_e) \tag{75}$$

where $\dot{m_{a\,e}}$ and $\dot{m_{a\,pc}}$ is the mass flow rate of dry air flowing through the evaporator and the evaporative cooler, respectively. w_e is the humidity ratio of moist-air at equilibrium state after rejected heat to the water, which remains the same as outdoor air entering the precooler. w_{final} is the final humidity ratio of moist-air after evaporative coothe ling process, somewhere between original state point and saturated point.

As noted previously, the flow rate of the condenser air is typically 2.5 times that of the evaporator in HVAC application. Therefore, with the assumption that dry air density is not a strong function of temperature so that that flow rates can refer to either mass or volume. Because the condenser and precooler are in series, the flow rates of dry air through the two components are equal, meaning,

$$\dot{m}_{a\,pc}=\dot{m}_{a\,c}=2.5\dot{m}_{a\,e} \tag{76}$$

Combing the above three equations, the correlation of humidity ratio could then be simplified as follows, assuming the pro cooler water and evaporator drain water are equal,

If the air will reach saturated state and excess water would be disposed of,

$$\dot{m}_{a\,e}\,(w_{aei}\text{-}w_{aeo}) \geq \dot{m}_{a\,pc}\,(w_{sat}\text{-}w_e) \tag{77}$$

By canceling the mass flow rates of both sides, yielding,

$$(w_{aei}\text{-}w_{aeo}) \geq 2.5\,(w_{sat}\text{-}w_e) \tag{78}$$

where w_{sat} is the saturated point humidity ratio, then the corresponding dry bulb temperature to the saturated point is the outdoor air temperature after evaporative cooling.

If the air will not reach saturated state point, which follows the relationship below,

$$\dot{m}_{a\,e}\,(w_{aei}\text{-}w_{aeo}) \leq \dot{m}_{a\,pc}\,(w_{sat}\text{-}w_{e}) \tag{79}$$

By canceling the mass flow rates of both sides, yielding,

$$(w_{aei}\text{-}w_{aeo}) \leq 2.5(w_{sat}\text{-}w_{e}) \tag{80}$$

The humidity ratio after evaporative cooling could then be calculated using the following equations,

$$\dot{m}_{a\,e}\,(w_{aei}\text{-}w_{aeo}) = \dot{m}_{a\,pc}\,(w_{final}\text{-}w_{e}) \tag{81}$$

By canceling the mass flow rates of both sides, which yields

$$(w_{aei}\text{-}w_{aeo}) = 2.5\,(w_{final}\text{-}w_{e}) \tag{82}$$

$$w_{final}=w_{e}+0.4\triangle w_{1} \tag{83}$$

Then the final temperature of the air can be calculated.

5.1.4.4 Refrigeration Cycle Models

5.1.4.4.1 Overview

Vapor compression refrigeration is the most widely used refrigeration method and as such is considered to be the conventional approach to cooling and this process is the same for all the reconfigured systems.

The vapor compression cycle performance as measured by its COP is the primary parameter for determining the effect of installing upstream of the condenser the airside evaporative cooling unit that uses internal water from the system evaporator. As mentioned previously, the effect of this evaporative cooler on the refrigeration cycle is to change the high-side condenser pressure and temperature. Other than changing the refrigerant state points, the refrigerant cycle

model for the case with and without the evaporative cooler is the same, meaning all refrigerant components and their refrigerant-side models are unchanged for the two situations.

5.1.4.4.2 Component Models Assumptions

The theoretical refrigeration cycle modeled for this study is based on the following assumptions:

1. The isentropic efficiency of the compressor is 80%

2. Pressure drops in the condenser and evaporator are neglected.

3. The kinetic and potential energy changes in all cycle processes are neglected.

4. Both the evaporator and condenser HXs are insulated from heat losses and gains to/from the surroundings.

The four components modeled comprise the refrigerant cycle model, and they are described below starts at the compressor inlet in the order that they are connected, namely, the compressor, condenser, expansion device, and evaporator.

For the compressor process, the compressor efficiency is important and defined as:

$$\eta = \frac{(h_{2s} - h_1)}{(h_2 - h_1)} \tag{84}$$

where h_{2s} is the isentropic enthalpy of refrigerant from inlet condenser while h_2 is the actual enthalpy of refrigerant from condenser inlet and h_1 is the enthalpy of refrigerant from evaporator outlet. Once the isentropic efficiency is known, then the equation can be used to find h_2 from entering condition and exit condition.

Because the compressor increases the pressure of saturated vapor exiting the evaporator to a more heated state, then the specific work done during compression, which is essential for the COP calculation, is determined as follows

$$w = h_2 - h_1 \tag{85}$$

The superheated refrigerant gas exiting the compressor then loses heat to air-side cooling as it passes through the condenser at a constant high-side pressure, assuming the exit is either a saturated or subcooled liquid state. The specific heat transfer in the condenser in terms of the refrigerant-side enthalpy is given by

$$q_c = h_3 - h_2 \tag{86}$$

h3 is enthalpy of the refrigerant at condenser outlet.

Refrigerant exiting the condenser passes through the thermal expansion valve to the low-side pressure, assuming a constant enthalpy process, where it then enters the evaporator,

$$h_3 = h_4 \tag{87}$$

Liquid refrigerant entering the evaporator absorbs heat at a constant low-side pressure from the air-side that is being cooled. The refrigerant state exiting the evaporator after the liquid has evaporated is either a saturated vapor or a superheated vapor and the refrigerant-side heat transfer is given as follows

$$q_e = h_1 - h_4 \tag{88}$$

where h_4 is the enthalpy of the refrigerant at the evaporator inlet.

5.1.4.4.3 The Coefficient of Performance

The coefficient of performance (COP), defined as the ratio of cooling capacity to work input, is often used as a measure of cycle performance and is the parameter of interest in terms of evaluating and analyzing the effect of adding the evaporative precooler. For the vapor-compression cycle in this study, an assumption is made that the only input or output is the net input to the compressor that the cooling capacity is the total heat transfer to the refrigerant side of the evaporator from the moist air being cooled. Therefore, the defining equation is shown as follows,

$$\text{COP} = \frac{\text{Q}_{\text{evaporator}}}{\text{W}_{\text{compressor}}} = \frac{q}{w} = \frac{h_1 - h_3}{h_2 - h_1} \tag{89}$$

In preparation for introducing a percent performance change parameter, the COP_{ref} is calculated without evaporative cooling, namely a typical cycle of the baseline case (scenario A), while COP is calculated with evaporative cooling utilizing either internal water or a combination of internal and external water, which are scenarios B and C, repectively. The COP% is the COP percentage difference between scenario B or C (COP) and scenario A (COP_{ref}), which reconfiguring a vapor-compression allows for one to analyze the utility of the cycle with an evaporative cooler, is defined as follows,

$$\text{COP\%}=\frac{COP-COP_{ref}}{COP_{ref}} \tag{90}$$

Carnot refrigeration cycle The Carnot refrigeration cycle, which is also called a reverse Carnot cycle, is an ideal or theoretical thermodynamic cycle based on all processes being reversible, and it is the most efficient cycle for transferring thermal energy from a low to high-temperature reservoir, even though it is an ideal impractical cycle. Furthermore, all processes within this cycle are internally reversible, so that heat transfer is assumed to occur when there are no temperature differences. Also, there are no external irreversibilities. The Carnot COP can be determined based on the second law and calculated as follows,

$$\text{COP}_{\text{carnot}} = \frac{\text{T}_\text{L}}{\text{T}_\text{H}-\text{T}_\text{L}} \tag{91}$$

where T_H is the high-side temperature (i.e. condenser) and T_L is the low-side temperature (i.e.evaporator).

A comparison between a vapor-compression cycle and the idealized Carnot refrigeration cycle is necessary, and it can be made by forming a ratio of the two as follows, which is called the refrigerating efficiency,

$$\eta_\text{R} = \frac{\text{COP}}{\text{COP}_{\text{carnot}}} \tag{92}$$

An analysis of quantitative values can provide a direction on how to improve the efficiency of a vapor-compression refrigerant system.

5.1.5 Simulation Input and Output

A comprehensive simulation model was developed and programmed in Engineering Equation Solver 2016 for a vapor-compression conditioning system comprising air-to-refrigerant evaporator and condenser, a compressor, a thermal expansion valve, and evaporative cooler before condenser. The possible parameters affecting the final results of the model such as 1) outdoor air temperature (T_a) 2) outdoor air relative humidity ($\emptyset a$) 3) air temperature exiting evaporator (T_{aeo}). Typical outcomes of the model are 1) specific work (w) 2) refrigerating effect (q) 3) vapor-compression system coefficient of performance (COP).

5.1.6 Simulation Data Set-up and Overview

In this section, outdoor air temperatures of 26.7, 29.4, 32.2, 35 ℃ (80, 85, 90, 95℉) and relative humidities of 40%, 50%, 60%, 70%, 80% over a range of assumed evaporator exit air temperatures of 7.2, 10, 12.8℃ (45, 50, 55℉) with a typical compressor efficiency of 80%.

5.1.7 Simulation Results and Analysis

In this section, two different scenarios, namely reconfigured system A1---external evaporative cooling and reconfigured system A2--- internal evaporative cooling are investigated and compared. Each reconfigured system will be compared to the baseline system (system A) with quantitative analysis. Then further results will be shown that under which condition, internal condensate will be enough for fully evaporative cooling.

5.1.7.1 Results and Analysis for Reconfigured System A1

In this section, the first step is to investigate Reconfigured system A1 alone---how COP varied with different conditions. The second step is to further evaluate the improvement of

Reconfigured system A1 over the baseline system A and get a comprehensive analysis of how COP improvement related to different variables. The final step is to build a correlation of COP/COP ratio with external evaporative cooling related to outdoor air temperature, relative humidity along with Taeo. Also, a compressive table with all test results would be shown in Appendix B.

5.1.7.1.1 Scenario A1 alone (external case)

In this section, the first step is to study how condenser inlet air temperature after precooling related to different variables and the second step is to further investigate how modification COP related to different variables.

5.1.7.1.1.1 Evaporative Cooling Effect

Figure 17, 18 and 19 show the relationship between condenser inlet air temperature after precooler and outdoor air condition (temperature and relative humidity) under three different evaporator outlet air temperatures, 7.2, 10, 12.8 ℃(45, 50, 55 ℉), respectively . Thus, evaporative cooling effect, which is defined as outdoor air temperature minus condenser inlet air temperature after precooler, could be seen from the plots as well. Evaporative cooling effect does not change a lot with Taeo and outdoor air temperature, but significant varies with relative humidity. With the boosting relative humidity, the evaporative cooling effect is decreasing in that the higher relative humidity has a higher saturation temperature (wet-bulb) temperature.

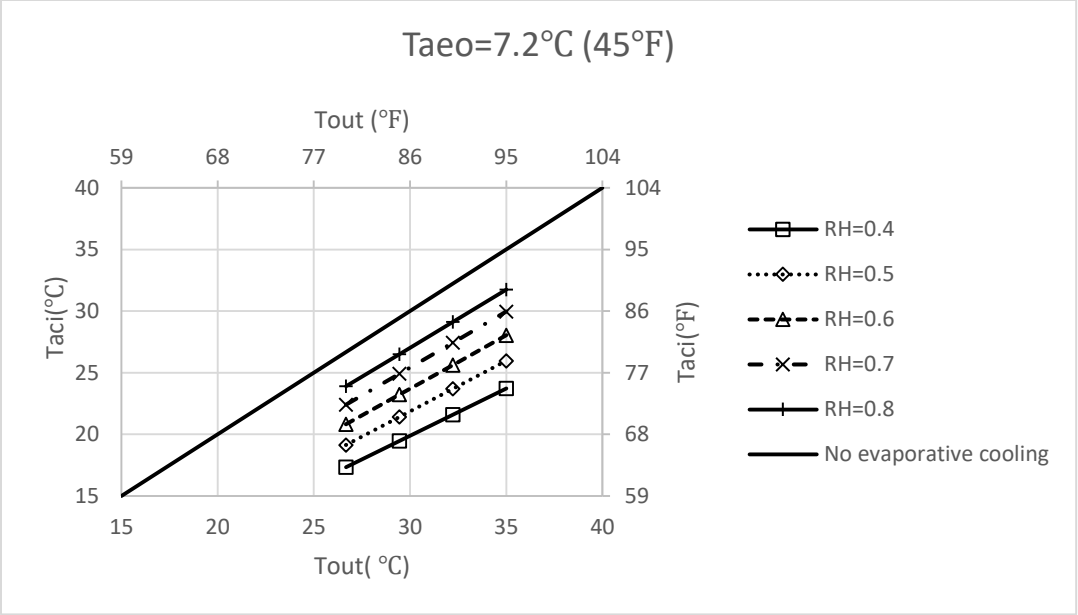

Figure 17 Condenser air inlet versus outdoor air temperature at Taeo=7.2 ℃

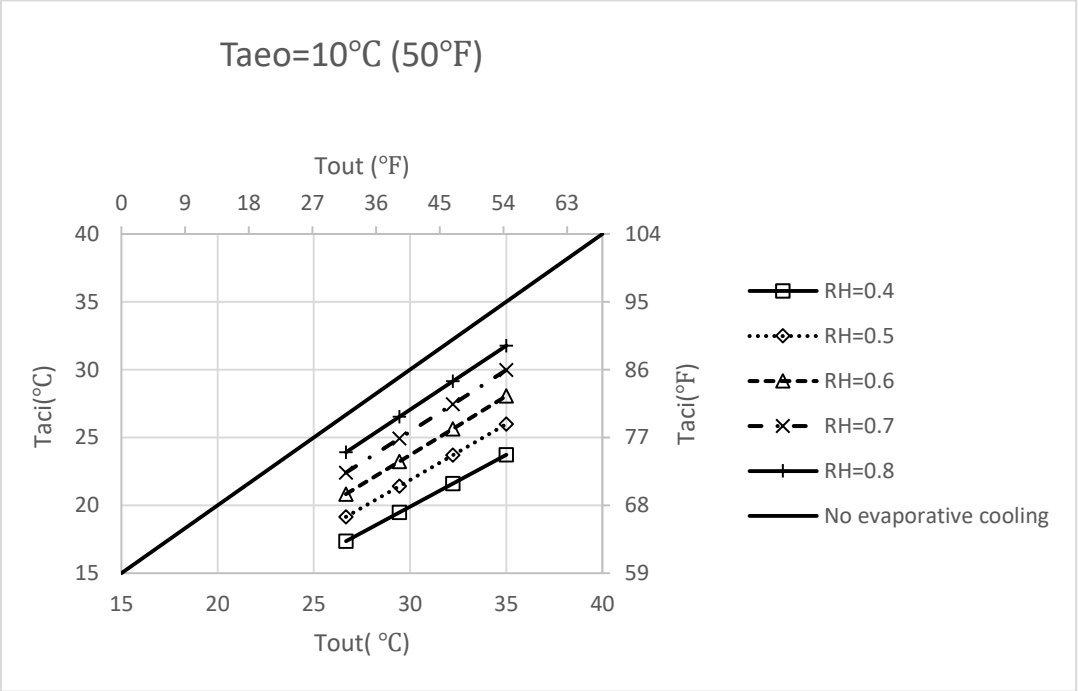

Figure 18 Condenser air inlet versus outdoor air temperature at Taeo=10 ℃

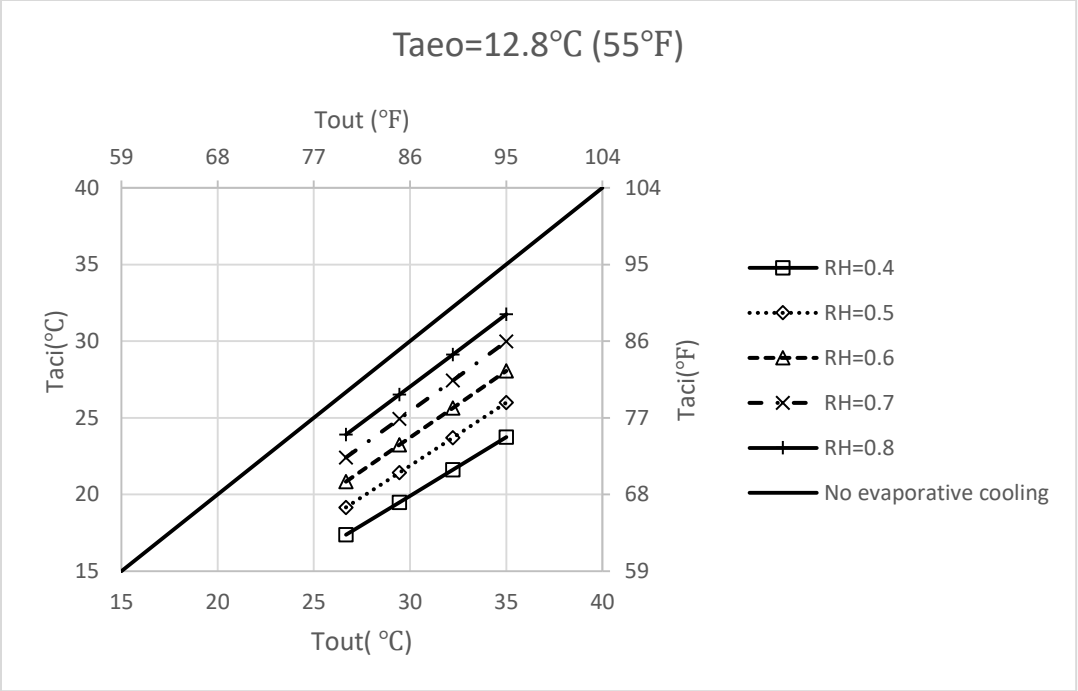

Figure 19 Condenser air inlet versus outdoor air temperature at Taeo=12.8 ℃

5.1.7.1.1.2 Scenario A1 COP Overview

Figure 20 gives an overview of how reconfigured system A1 system performance related to three variables, namely ourdoor air temperatures, relative humidities and Taeo, and it further shows that COP decreases with relative humidity because with the boosting relative humidity, the evaporative cooling effect is decreasing, which is discussed in the previous section. Figure 21, 22, 23 and 24 show how COP varies with different Taeo under the same outdoor air temperature, and it is observed that COP increases with the increasing Taeo. Figure 25, 26 and 27 show how COP varies with different outdoor air temperature under the same Taeo and these three plots illustrate that COP decreases with the increasing outdoor air temperature. The trend of COP varied with the three parameters is further summarized in Table 2.

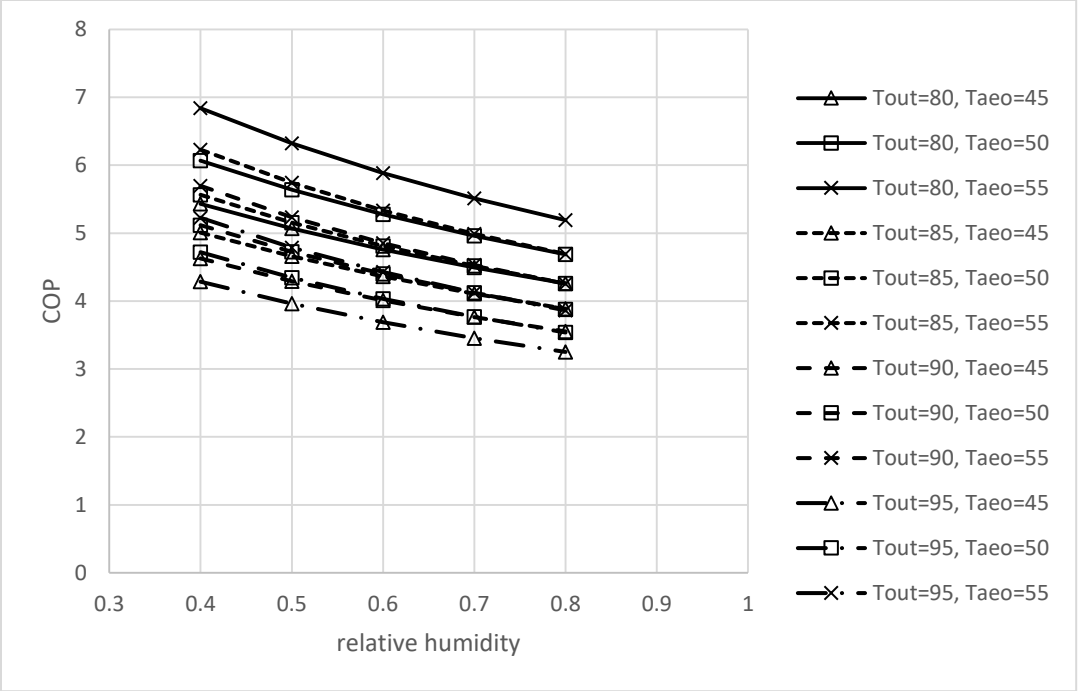

Figure 20 COP versus relative humidity at different conditions

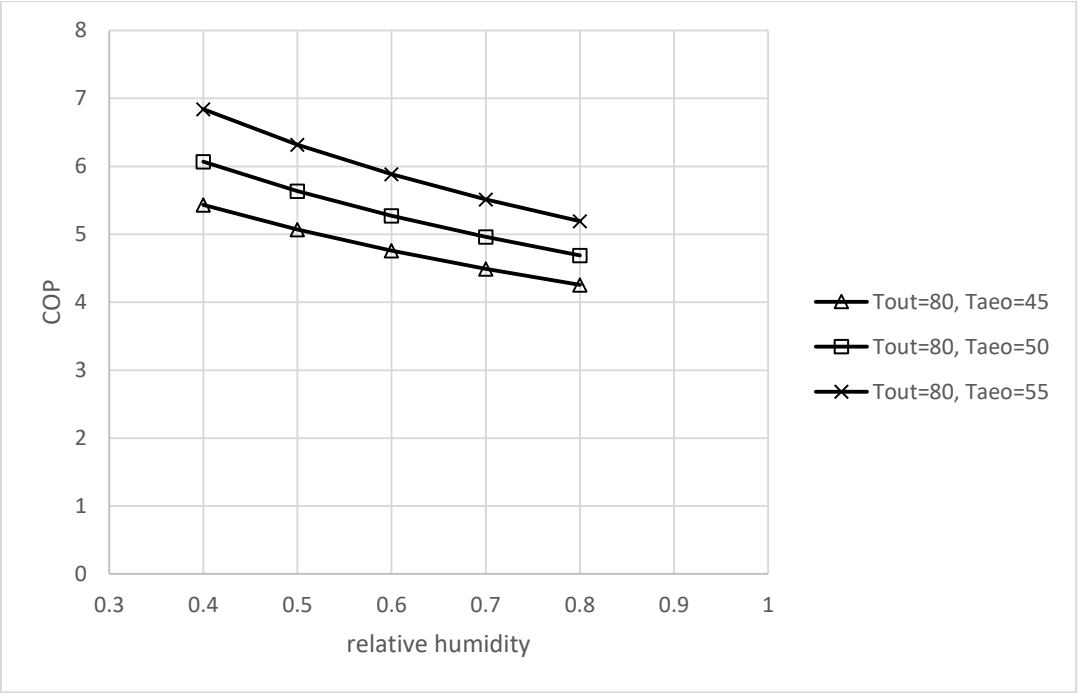

Figure 21 COP versus relative humidity when Tout=80 ℉

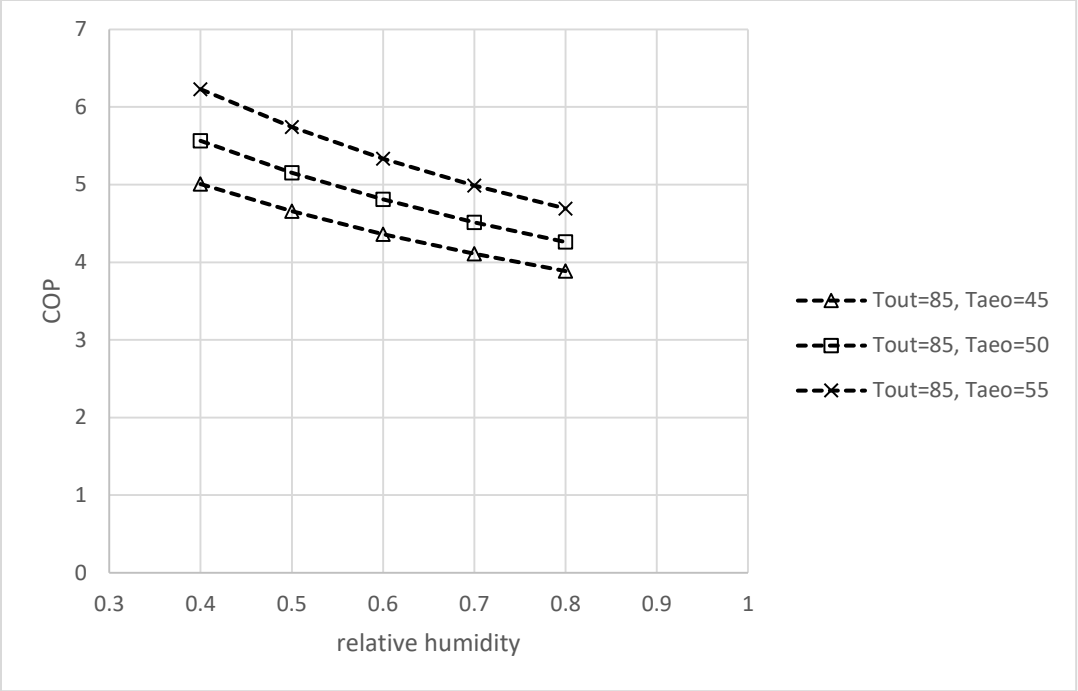

Figure 22 COP versus relative humidity when Tout=85 ℉

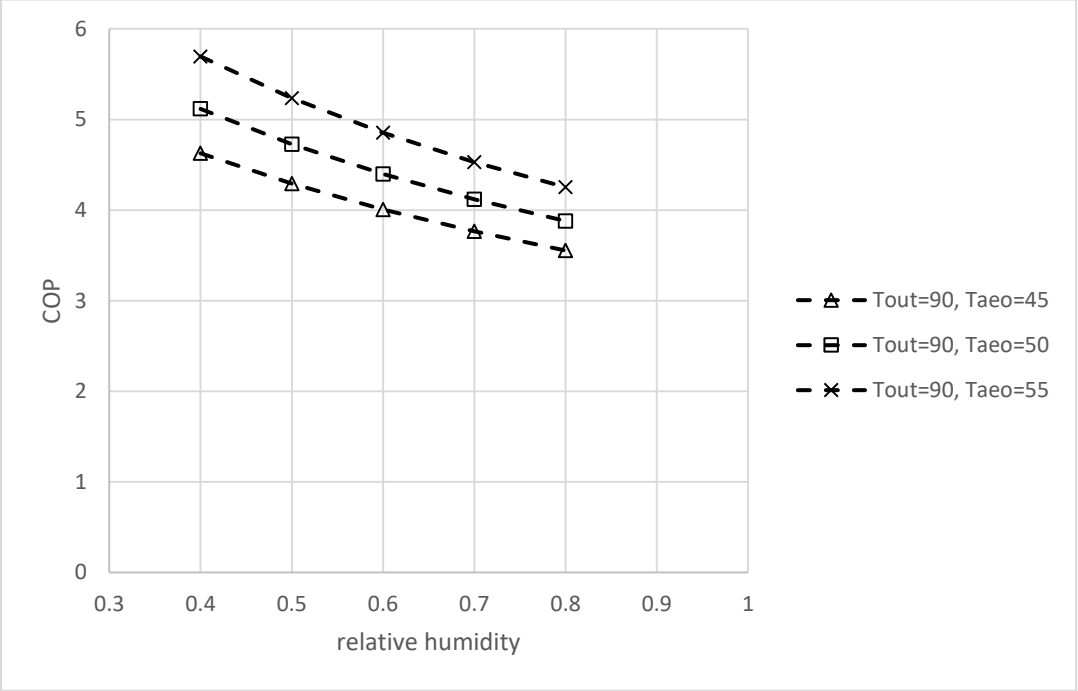

Figure 23 COP versus relative humidity when Tout=90 ℉

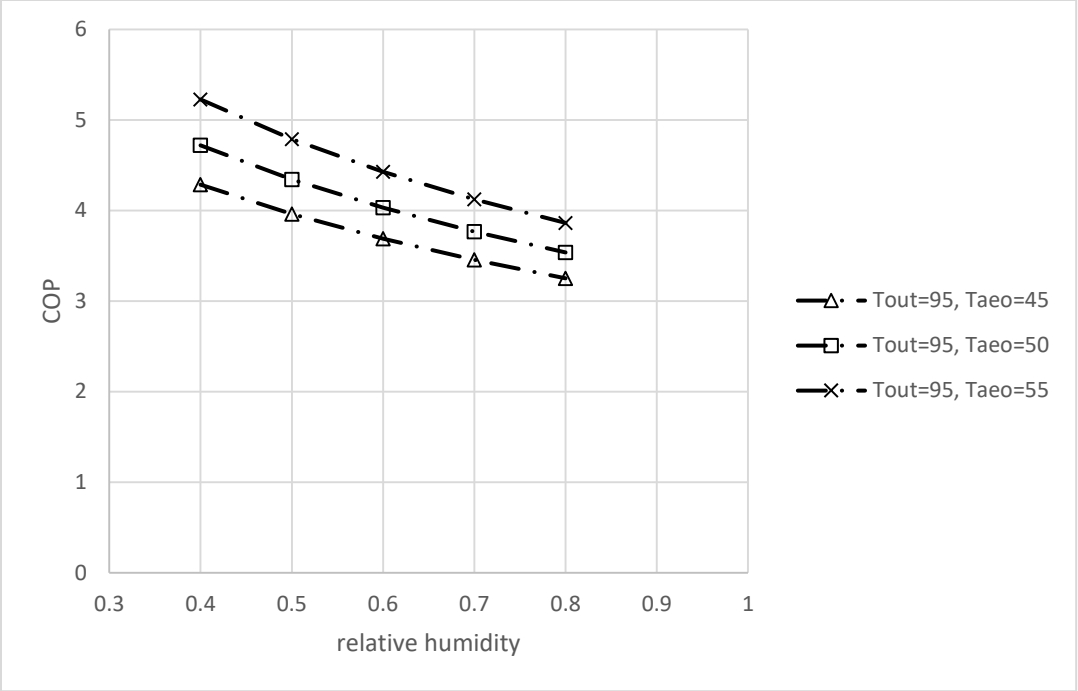

Figure 24 COP versus relative humidity when Tout=95 ℉

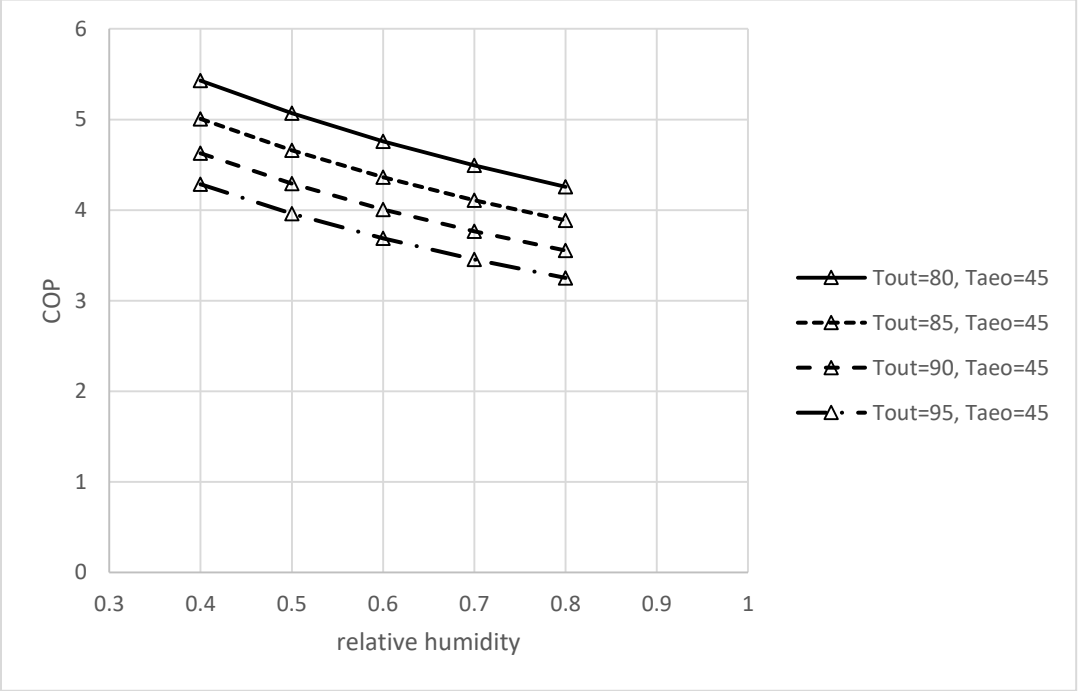

Figure 25 COP versus relative humidity when Taeo=45 ℉

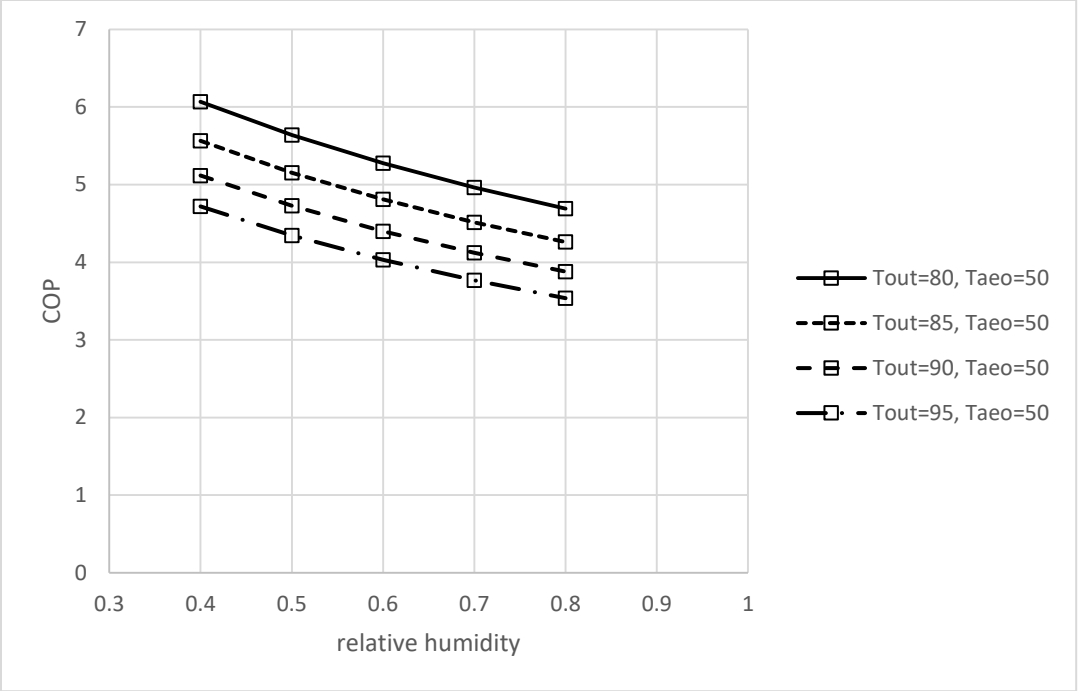

Figure 26 COP versus relative humidity when Taeo=50 ℉

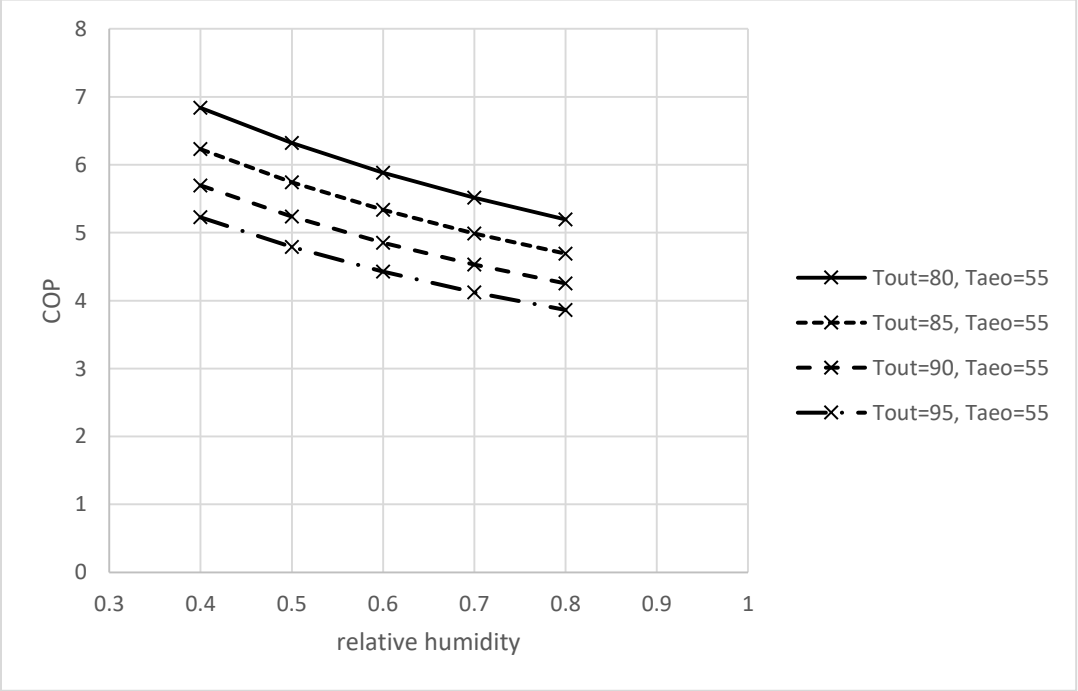

Figure 27 COP versus relative humidity when Taeo=55 ℉

Table 2 COP varied with Tout, RH and Taeo

case	T_{out}	RH	T_{aeo}	COP with EC
1	↑	→	→	↓
2	→	↑	→	↓
3	→	→	↑	↑

5.1.7.1.2 Compare Scenario A1 to Scenario A

5.1.7.1.2.1 COP Improvement Due to Evaporative Cooling Overview

Figure 28 shows the relationship between COP with and without evaporative cooling when COP ranges from 1 to 10. The highest increase can reach as much as 60%. Figure 29 shows the same plot but COP ranging from 1 to 4. The greatest increase can reach up to 40%.

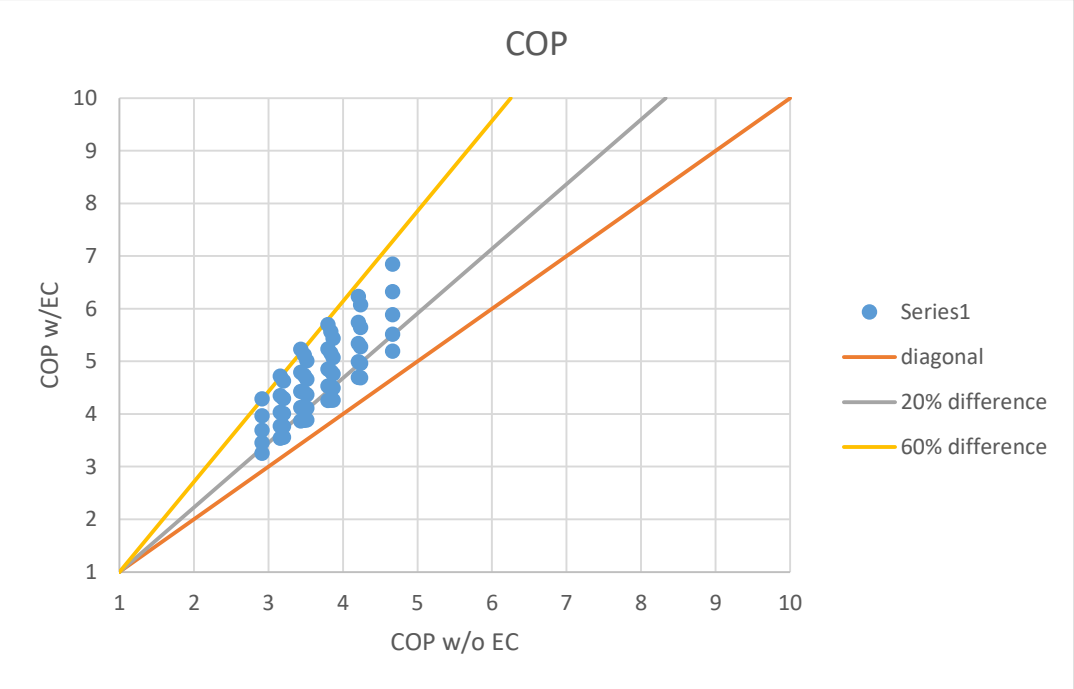

Figure 28 COP with/without external evaporative cooling with the range of 1 to 10

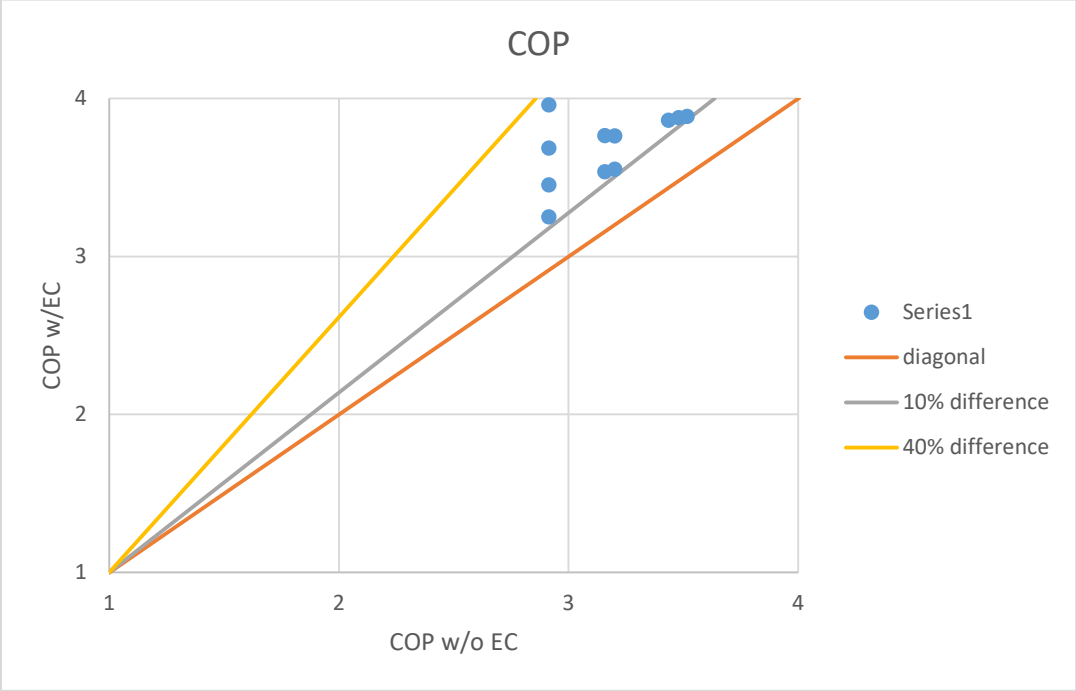

Figure 29 COP with/without external evaporative cooling with the range of 1 to 4

5.1.7.1.2.2 COP Enhancement Analysis

Figure 30 and 31 give the overview of COP improvement varied with outdoor air conditions---temperatures and relative humidites, along with different Taeo. It is observed that COP percentage difference decrease with increasing relative humidity. Figure 32, 33, 34 and 35 show how COP percentage difference varies with different Taeo under the same outdoor air temperature, and it is further observed that COP percentage difference increase with the increasing Taeo. Figure 36, 37, and 38 show how COP percentage difference varies with different outdoor air temperature under the same Taeo and these figures illustrate that percentage difference increase with the increasing outdoor air temperature. The trend of COP improvement varied with aforementioned three variables are summarized in Table 3.

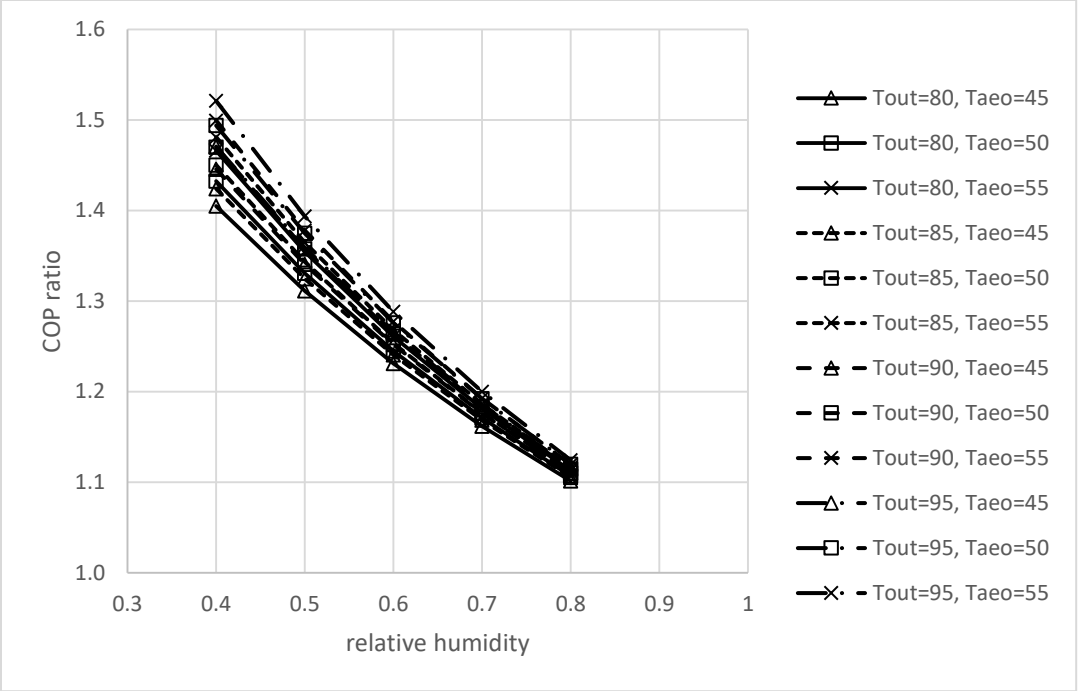

Figure 30 COP ratio (external evaporative cooling/baseline) versus relative humidity under different conditions

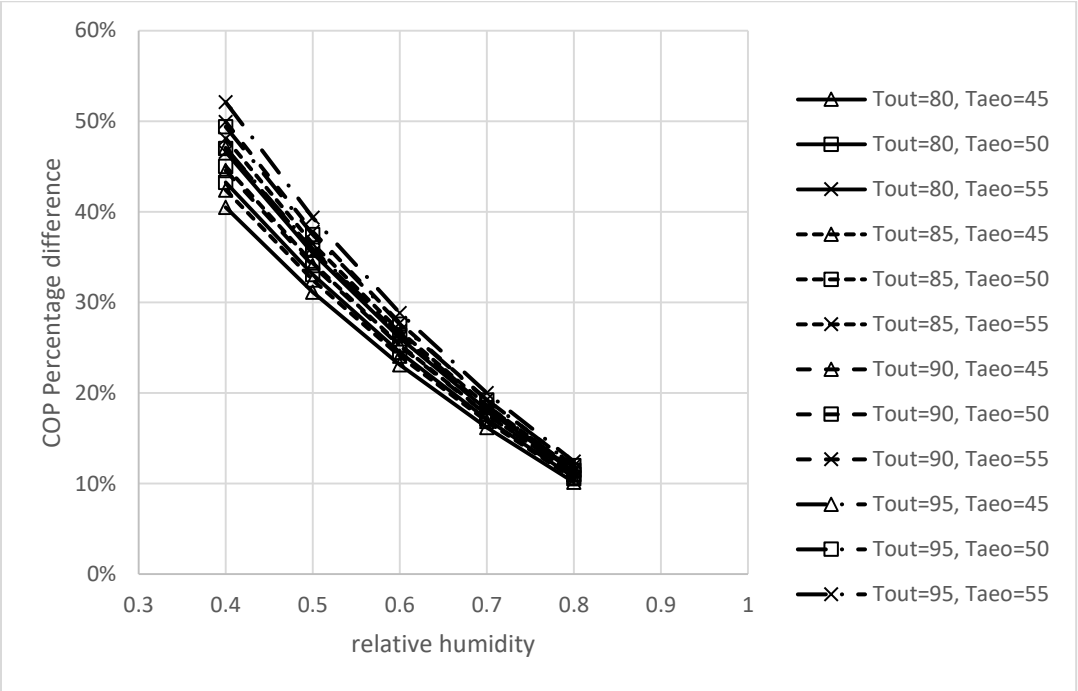

Figure 31 COP percentage difference (external evaporative cooling over baseline) versus relative humidity under different conditions

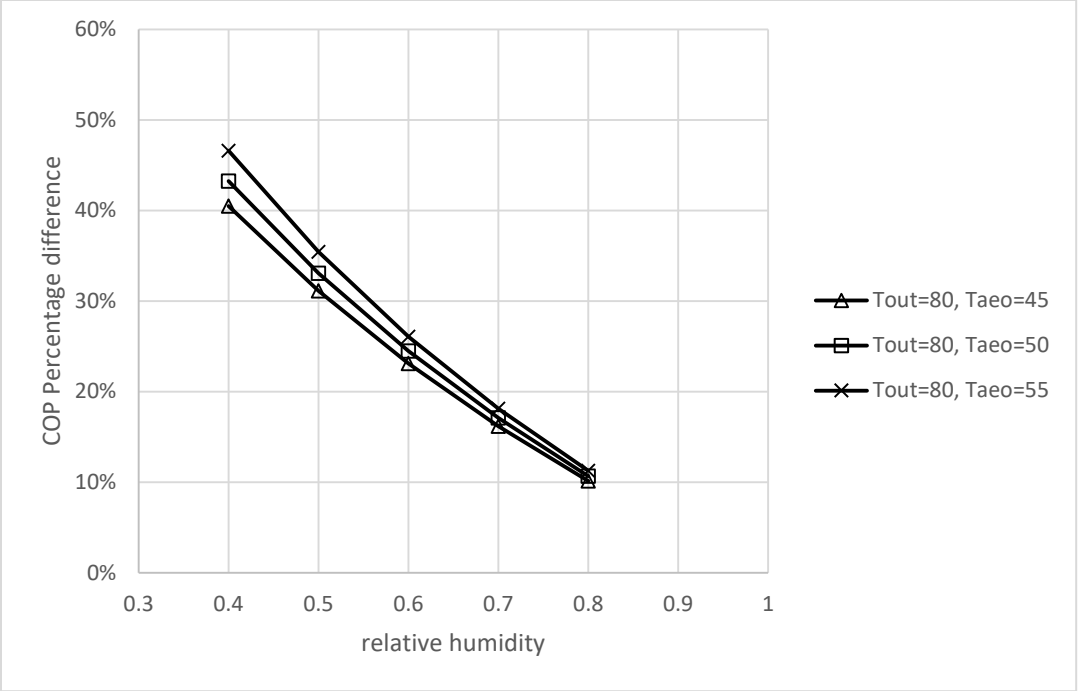

Figure 32 COP percentage difference (external evaporative cooling over baseline) versus relative humidity when Tout=80 ℉

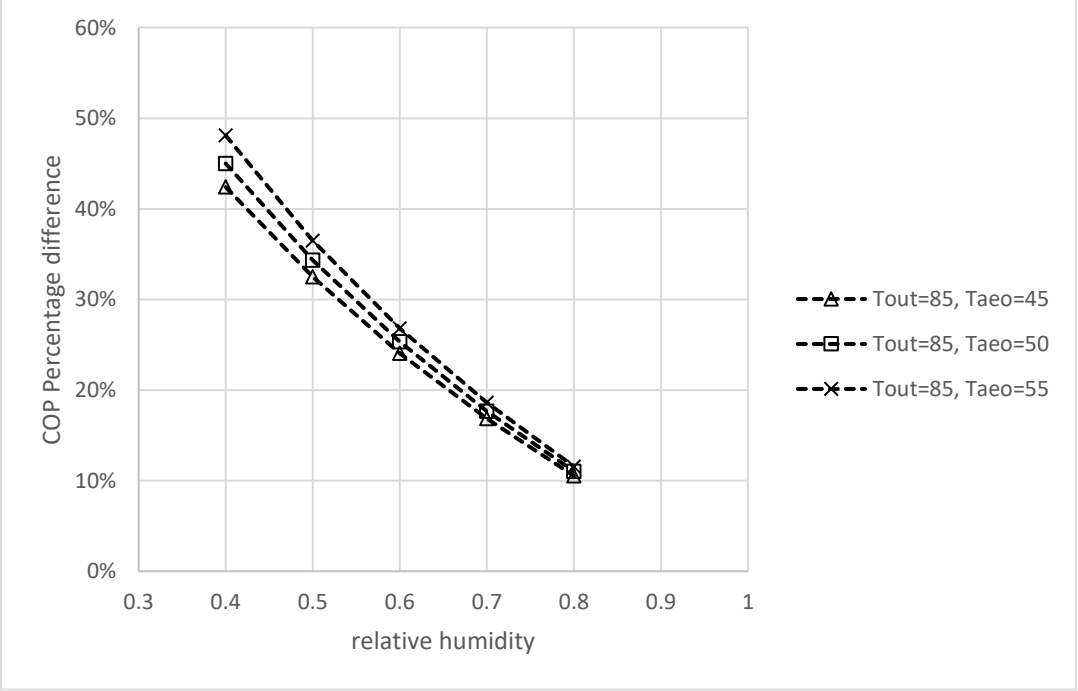

Figure 33 COP percentage difference (external evaporative cooling over baseline) versus relative humidity when Tout=85 ℉

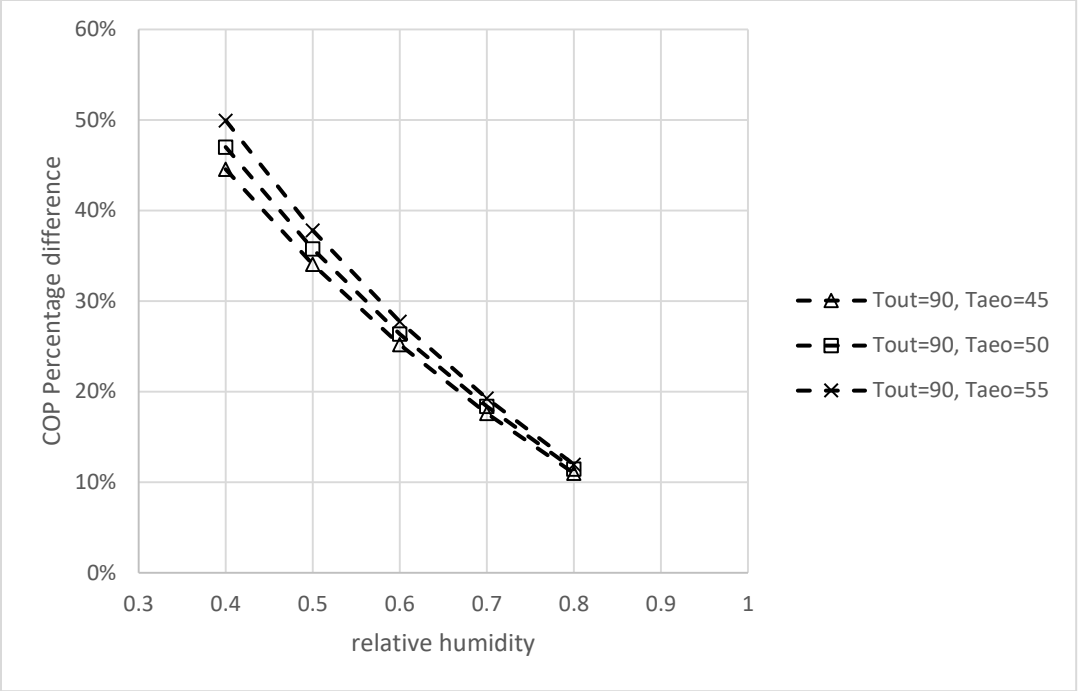

Figure 34 COP percentage difference (external evaporative cooling over baseline) versus relative humidity when Tout=90 ℉

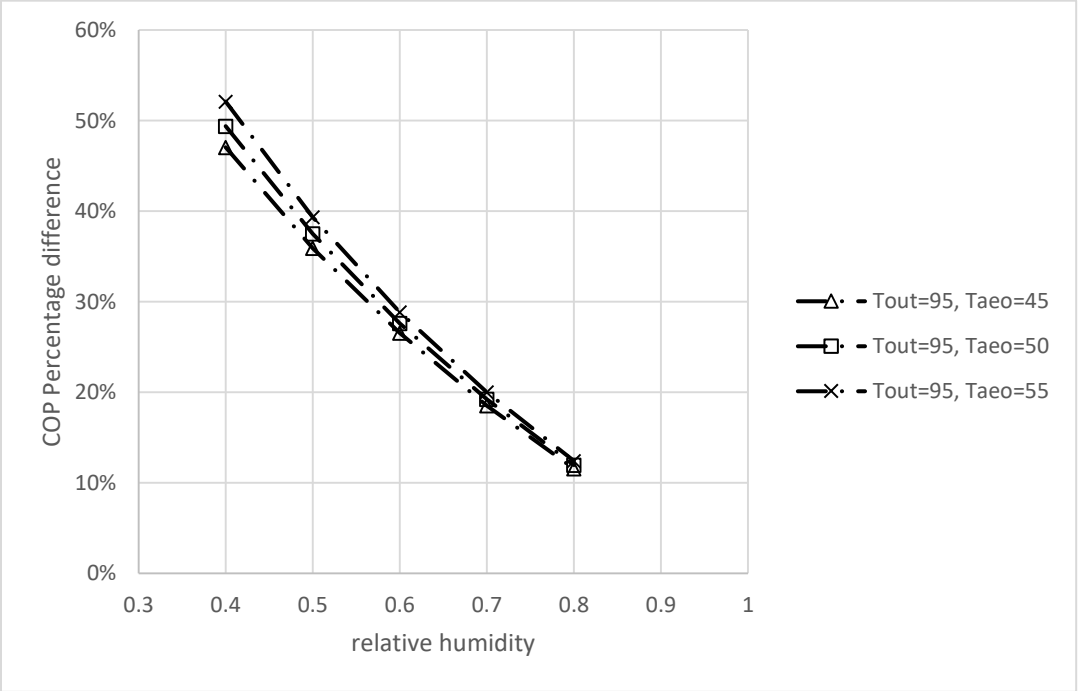

Figure 35 COP percentage difference (external evaporative cooling over baseline) versus relative humidity when Tout=95 ℉

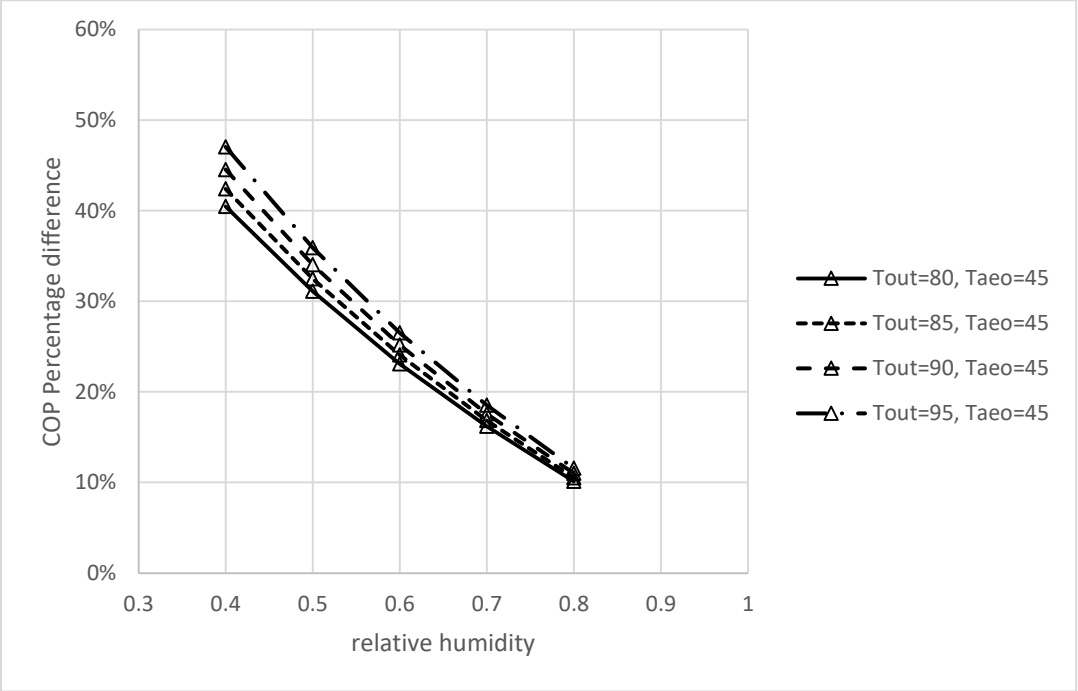

Figure 36 COP percentage difference (external evaporative cooling over baseline) versus relative humidity when Taeo=45 ℉

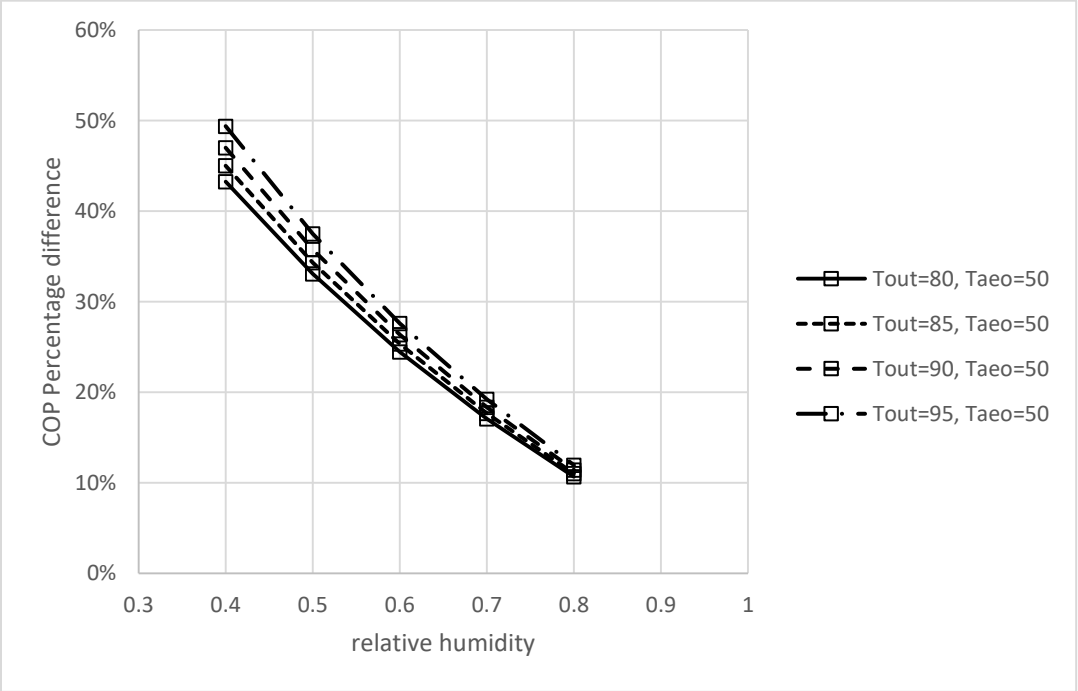

Figure 37 COP percentage difference (external evaporative cooling over baseline) versus relative humidity when Taeo=50 ℉

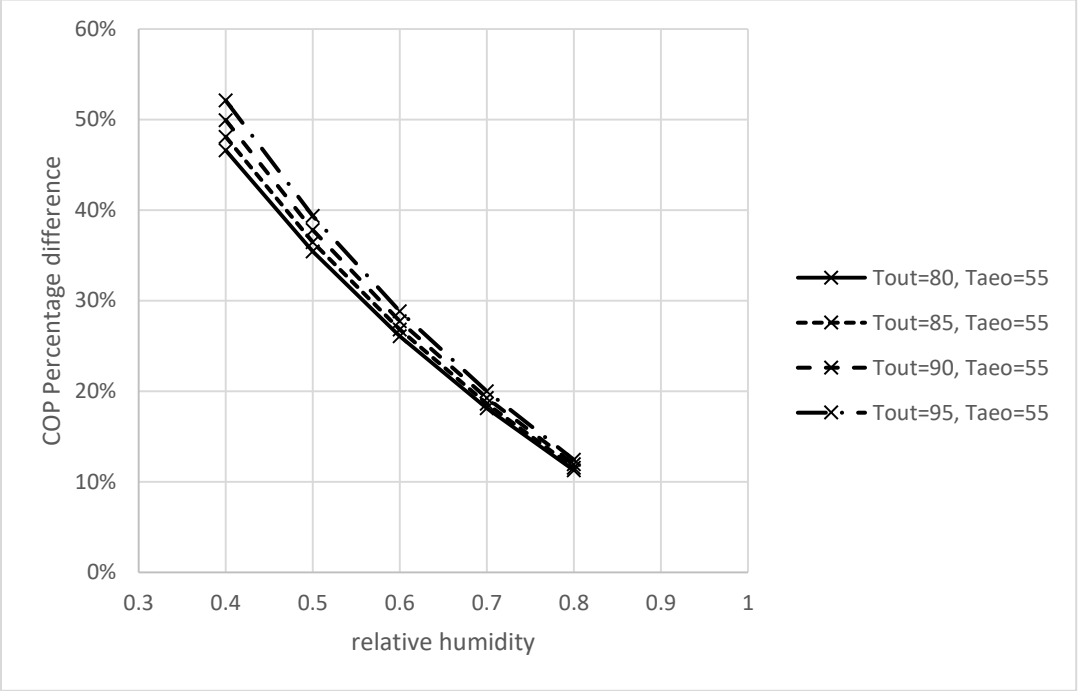

Figure 38 COP percentage difference (external evaporative cooling over baseline) versus relative humidity when Taeo=55 ℉

Table 3 COP percentage difference (external evaporative cooling over baseline) varied with Tout, RH, and Taeo

case	T_{out}	RH	T_{aeo}	% difference
1	↑	→	→	↑
2	→	↑	→	↓
3	→	→	↑	↑

5.1.7.1.3 Equation Derivation

5.1.7.1.3.1 Statistical Analysis of Data

For the analysis above, the $\mathrm{COP_{w/o\,EC}}$ is just related to outdoor air temperature and evaporator outlet air temperature, but $\mathrm{COP_{w/EC}}$ is related to outdoor air temperature and relative

humidity along with evaporator outlet air temperature. Multivariate correlations and scatterplot matrix between Tout, RH, Taeo and two COPs, COP ratios are shown in Table 4 and Figure 39. It is observed from the scatterplot that COP value has a strong negative relationship with outdoor air temperature, but COP ratio has a weak positive relationship with outdoor air temperature. Strong or weak depend on how Person's correlation coefficient close to -1 or 1. When the outdoor air temperature is greater than its mean value, $COP_{w/oEC}$, $COP_{w/EC}$ are less than their mean values and vice versa. When the outdoor air temperature is greater than its mean value, COP ratio is larger than its mean value and vice versa. Correlation between RH and $COP_{w/EC}$has a weak negative relationship, while RH and COP ratio has a strong negative relationship. When daily RH is greater than its mean value, $COP_{w/oEC}$ or $COP_{w/EC}$, COP ratio are less than their mean values and vice versa. Correlation between Taeo and $Cop_{w/oEC}$ or $COP_{w/EC}$, has a strong positive relationship, while Taeo and COP ratio has a weak positive relationship. When Taeo is greater than its mean value, $COP_{w/oEC}$ or $COP_{w/EC}$, COP ratio are also larger than their mean values and vice versa.

Table 4 Multivariate Correlations

	Tout	**RH**	**Taeo**	**COP**	**COP ex**	**COP ratio**
Tout	1.0000	-0.0000	-0.0000	-0.8311	-0.6141	0.1006
RH	-0.0000	1.0000	-0.0000	-0.0000	-0.5941	-0.9830
Taeo	-0.0000	-0.0000	1.0000	0.5472	0.5020	0.0962
COP	-0.8311	-0.0000	0.5472	1.0000	0.7937	-0.0299
COP ex	-0.6141	-0.5941	0.5020	0.7937	1.0000	0.5791
COP ratio	0.1006	-0.9830	0.0962	-0.0299	0.5791	1.0000

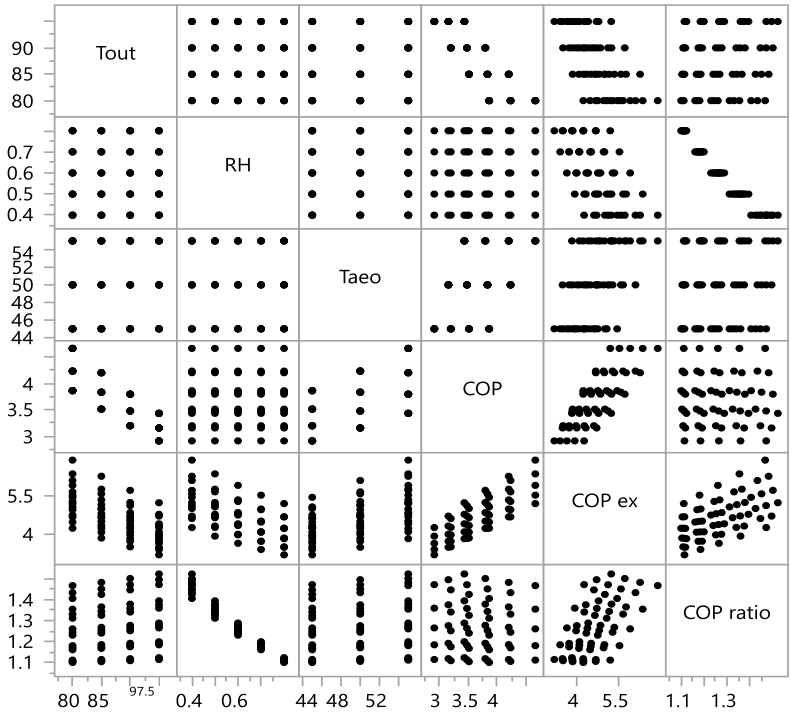

Figure 39 Scatterplot Matrix

5.1.7.1.3.2 Correlation Development

Based on the upper limit and lower limit of the cooling season weather report, the conditions below are used to derive regression equations. Outdoor air condition is set as: 26.7, 29.4, 32.2, 35 ℃ (80, 85, 90, 95℉); RH=40%, 50%, 60%, 70%, 80%; Taeo=7.2, 10, 12.8℃ (45, 50, 55℉); compressor efficiency: 80%. The conditions mentioned above have a wider range than the real-world weather conditions, thus, derivation of equations is based on these typical conditions. Two models are simulated, a baseline system without evaporative cooling and a evaporative cooling system using utilizing external water.

$\boldsymbol{COP_{w/oEC}}$ **Correlation** For the simulation under the dry condition, based on the equations aforementioned, it is indicated that COP is a function of Taeo and outdoor air temperature, namely, COP=f(Taeo, Tout). First of all, a quadratic function is assumed. However,

according to Figure 40, the residual vs. predicated data plot, the scatterplot for quadratic function looks not flat at all and the vertical scatter of the data increase with the boosting x, which both indicated that quadratic function is not the perfect model formula for COP.

To make a remedy, another fitting model is come out---log COP is used instead of COP. In another word, log COP is a function of Taeo, outdoor air temperature and relative humidity, log COP=f(Taeo, Tout). A quadratic function is still assumed for log COP and all the coefficients are shown in Table 5 as follows,

Table 5 log $COP_{w/oEC}$ Model Coefficient

a0+a1*RH^2+a2*RH+a3*Taeo^2+a4*Taeo+a5*Tout^2+a6*Tout+a7*RH*Taeo+a8*Taeo*Tout+a9*RH*Tout									
a0	a1	a2	a3	a4	a5	a6	a7	a8	a9
1.82	0	0	8.18e-5	0.0231	2.21e-5	-0.0156	0	-0.000157	0

The residual in this section is defined as the difference between the actual value and the predicted value. According to Figure 40, the residual vs. predicted data plot, it is shown that the scatterplot looks flat for the exponential function. Also, the vertical scatter of the data does not increase or decrease when x is changing, it is concluded that the conditional variance does not depend on x and thus the exponential function is the correct model. Figure 41 and 42, the actual vs. predicted plots, show the error between predicted data and actual data for both models is negligible. Although quadratic and exponential both have small error, the residua plot (Figure 40) indicates quadratic function is worse than exponential method. Thus, exponential model is a better choice in this section and the error between predicted data and actual data is indicated in Figure 43---always less than 1%.

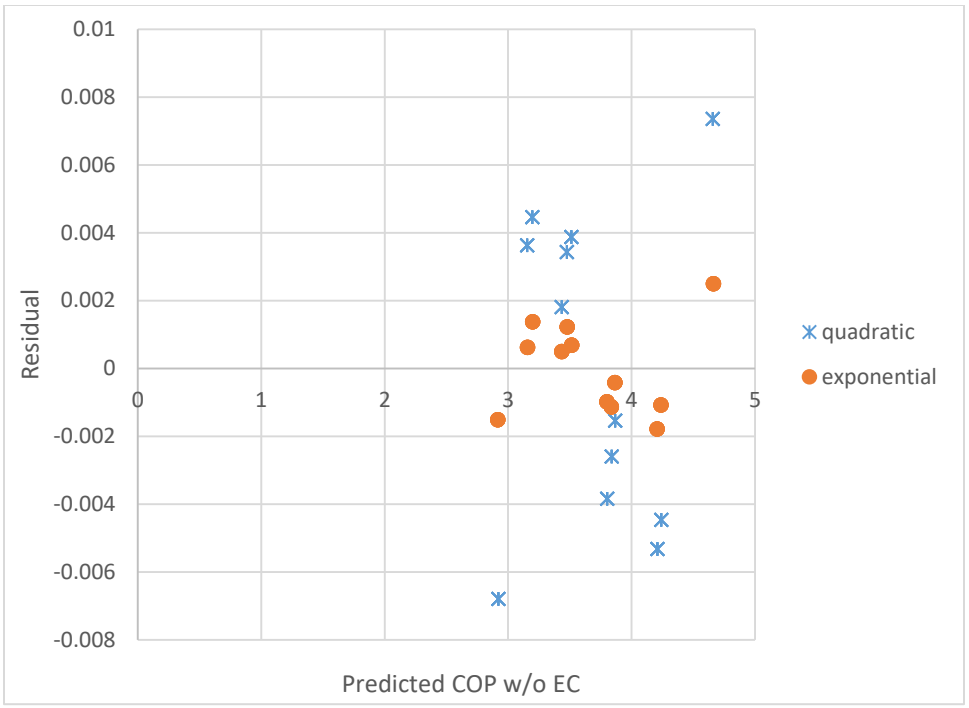

Figure 40 Actual and Predicted comparison between exponential and quadratic methods for baseline COP

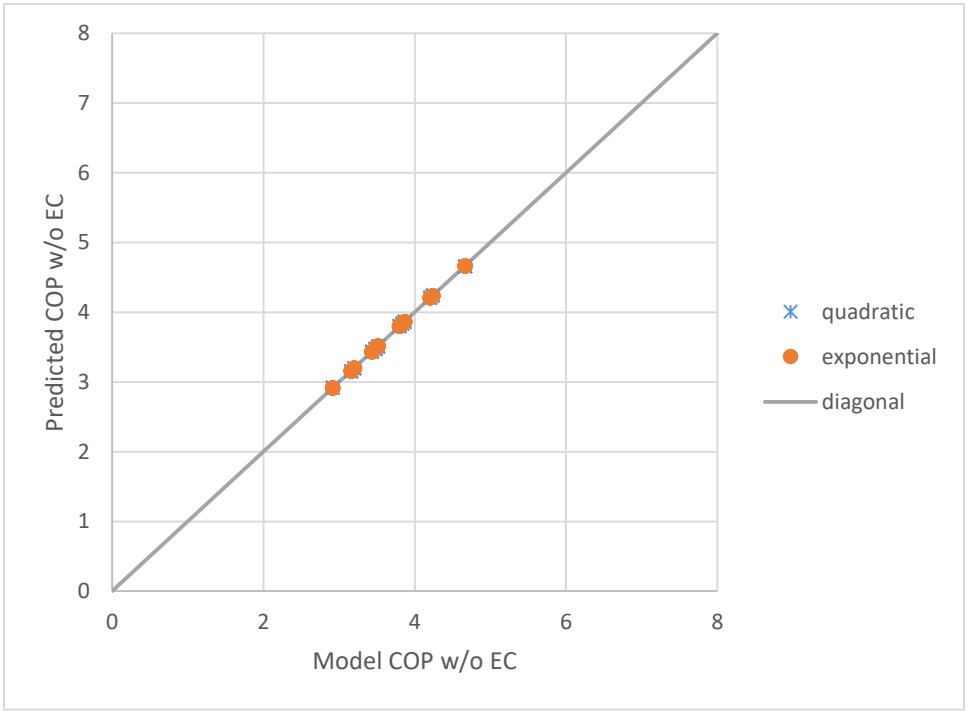

Figure 41 Percentage difference comparison between exponential and quadratic methods for baseline COP

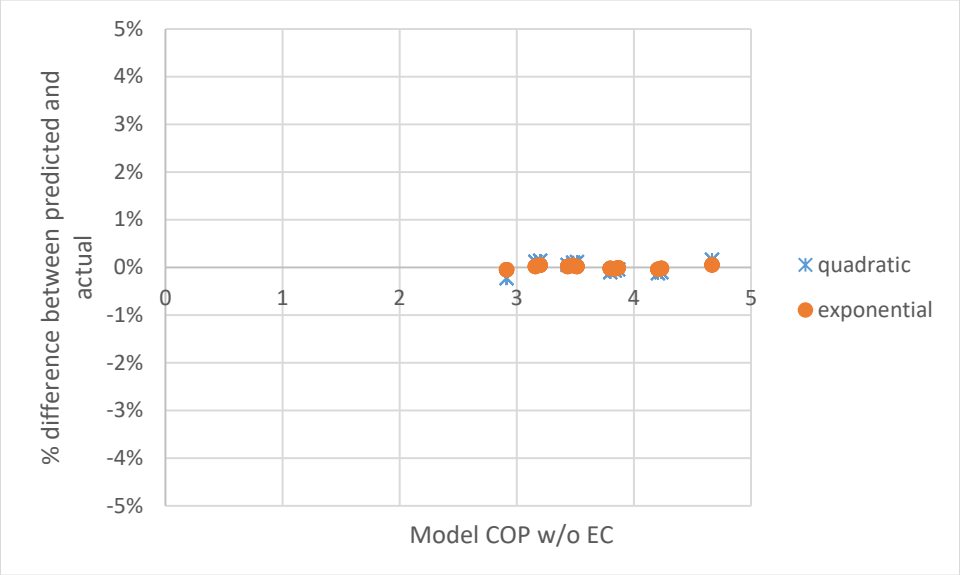

Figure 42 Predicted and actual data difference of quadratic and exponential methods for baseline COP

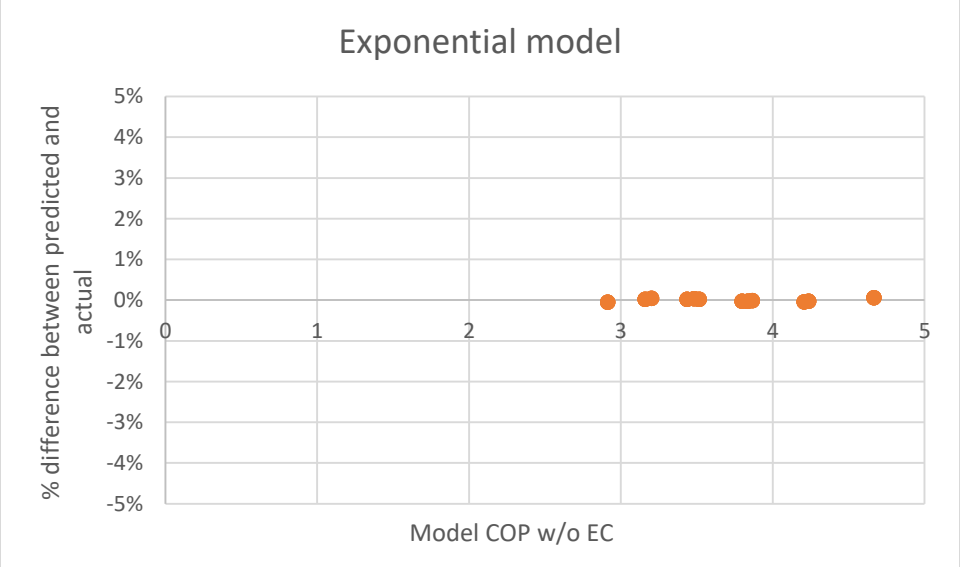

Figure 43 Predicted and actual data difference of exponential method for baseline COP

$\boldsymbol{COP_{external}}$ **Correlation** According to the equations mentioned previously, plus several assumptions made for this model, it is known that COP with external evaporative cooling is a

function of relative humidity, Taeo and outdoor air temperature. Both quadratic model and exponential model are considered, namely COP=f (RH, Taeo, Tout) and log COP=f (RH, Taeo, Tout). However, exponential model is better than quadratic model and comprehensive model coefficients of the exponential function is built in Table 6, shown as follows,

Table 6 $log\ COP_{external}$ *Model Coefficients*

a0+a1*RH^2+a2*RH+a3*Taeo^2+a4*Taeo+a5*Tout^2+a6*Tout+a7*RH*Taeo+a8*Taeo*Tout+a9*RH*Tout									
a0	a1	a2	a3	a4	a5	a6	a7	a8	a9
1.96	0.314	-0.265	0.000114	0.0297	4.98e-5	-0.0140	-0.00723	-0.000194	-0.00495

According to Figure 44, the residual vs. predicted data plot, it is shown that the scatterplot looks flat for the exponential method, which means it is the correct model; the scatterplot does not flat for the quadratic method, which means it is not a perfect model. Also, the vertical scatter of the data does not increase or decrease when x is changing for expoential method, it is concluded that the conditional variance does not depend on x. Figure 45 and 46, the actual vs. predicted plots, indicate the error between predicted data and actual data for both methods is negligible but quadratic method has two outliers. Although quadratic and exponential both have small error, the residual plot (Figure 44) indicates quadratic model is worse than exponential model. Thus, exponential model is a better choice in this section and the error between predicted data and actual data is indicated in Figure 43---always less than 1%.

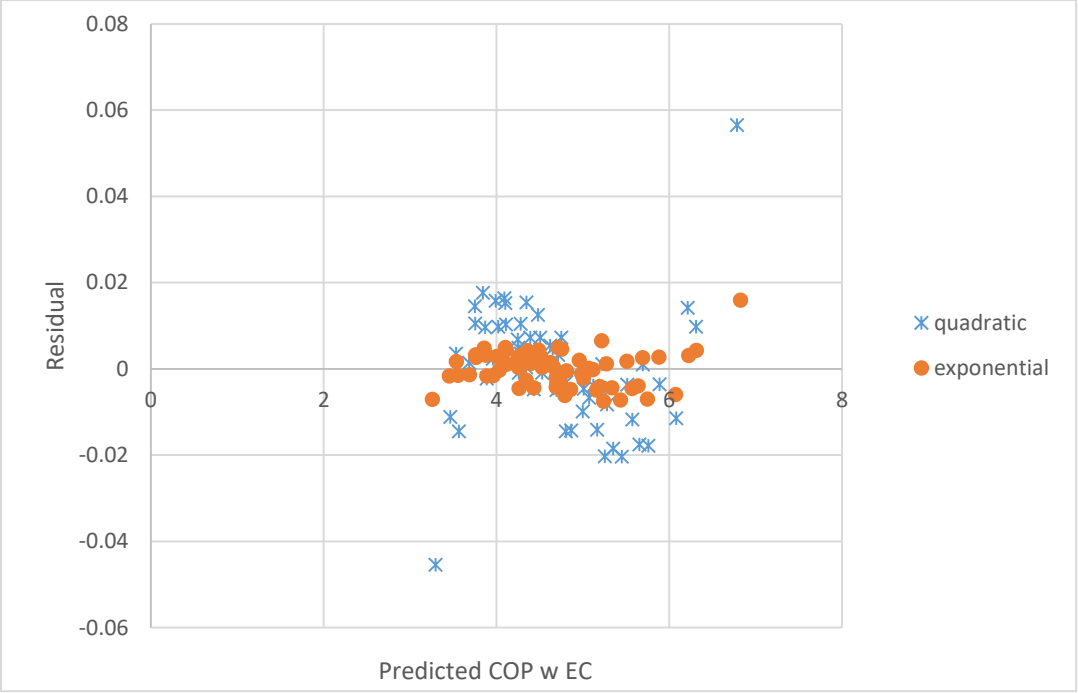

Figure 44 Residual comparison between exponential and quadratic methods for system with external evaporative cooling

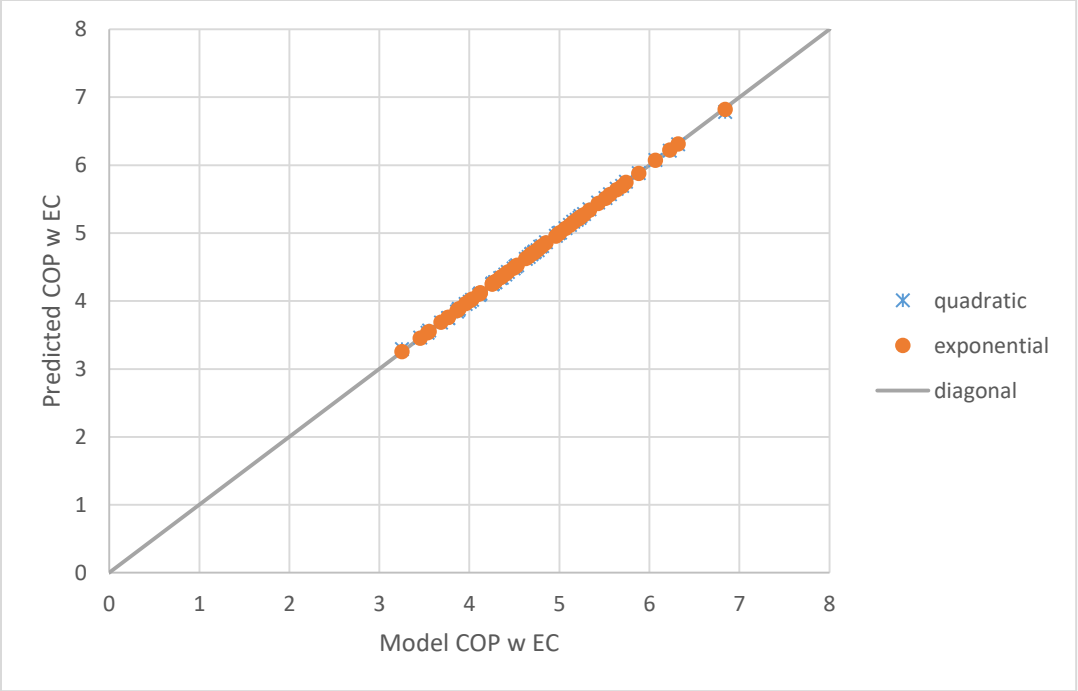

Figure 45 Actual and Predicted comparison between exponential and quadratic methods for system with external evaporative cooling

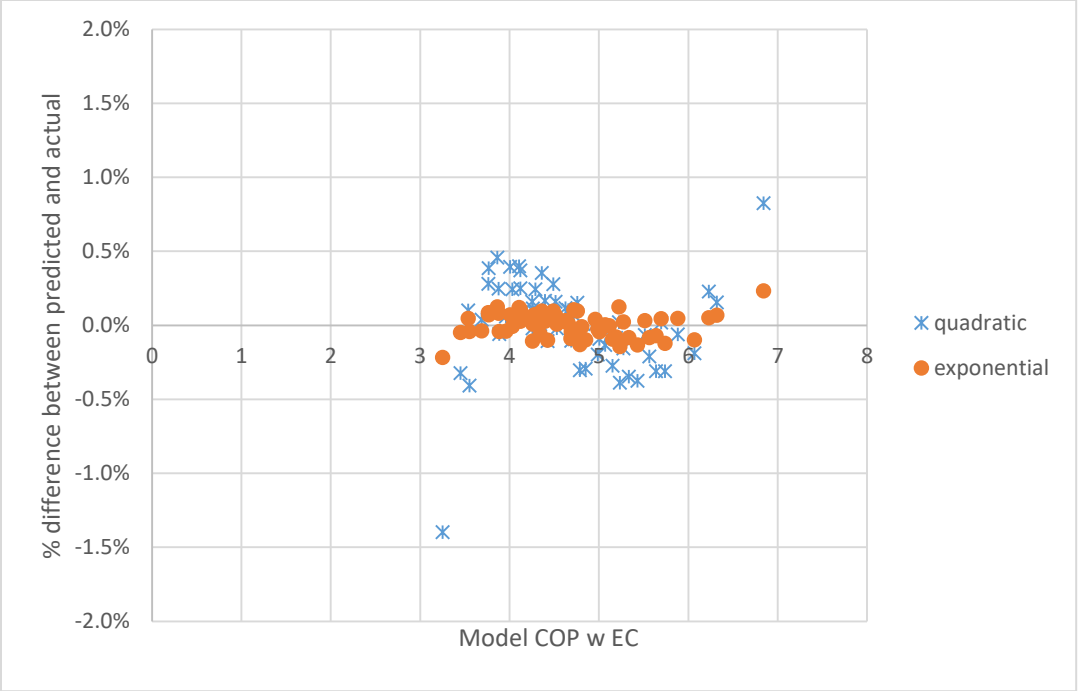

Figure 46 Percentage difference comparison between exponential and quadratic methods for system with external evaporative cooling

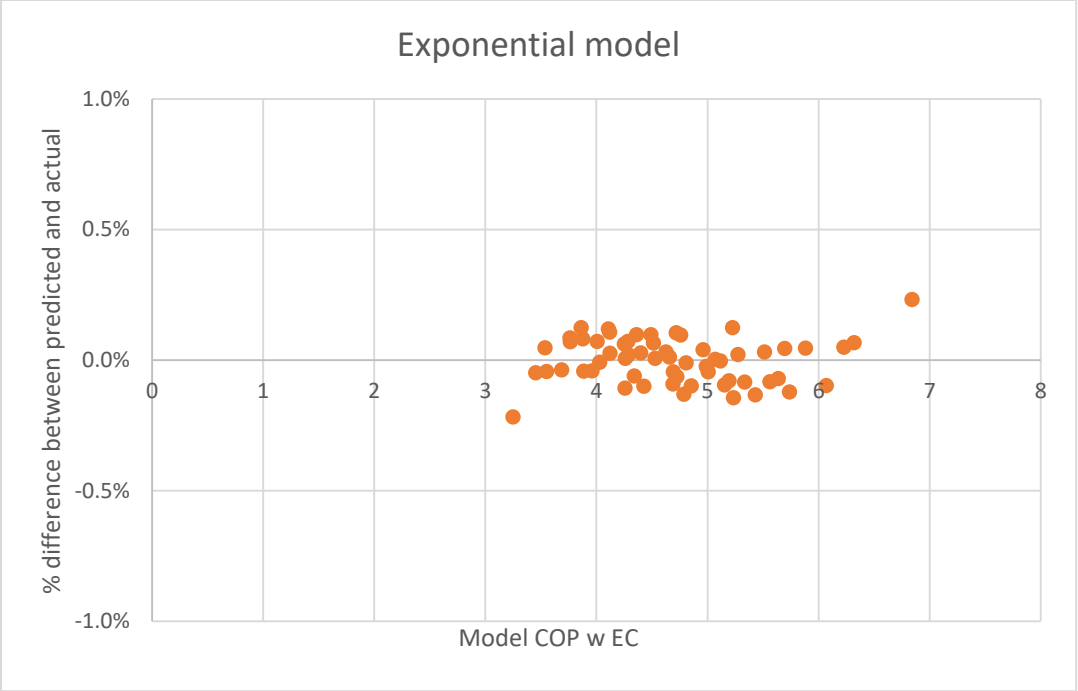

Figure 47 Percentage difference between predicted and actual data of exponential method for system with external evaporative cooling

5.1.7.1.3.3 COP Accuracy Analysis

It is necessary to compare the error of the model without evaporative cooling and the improvement due to evaporative cooling since if the error is higher than the improvement, the equations derived above will become useless. Thus, the points under the diagonal in Figure 48 are OK and the ones above diagonal are not OK. Figure 48 shows absolute difference between actual and predicted is negligible compared to COP improvement, which indicates the model built previously is correct.

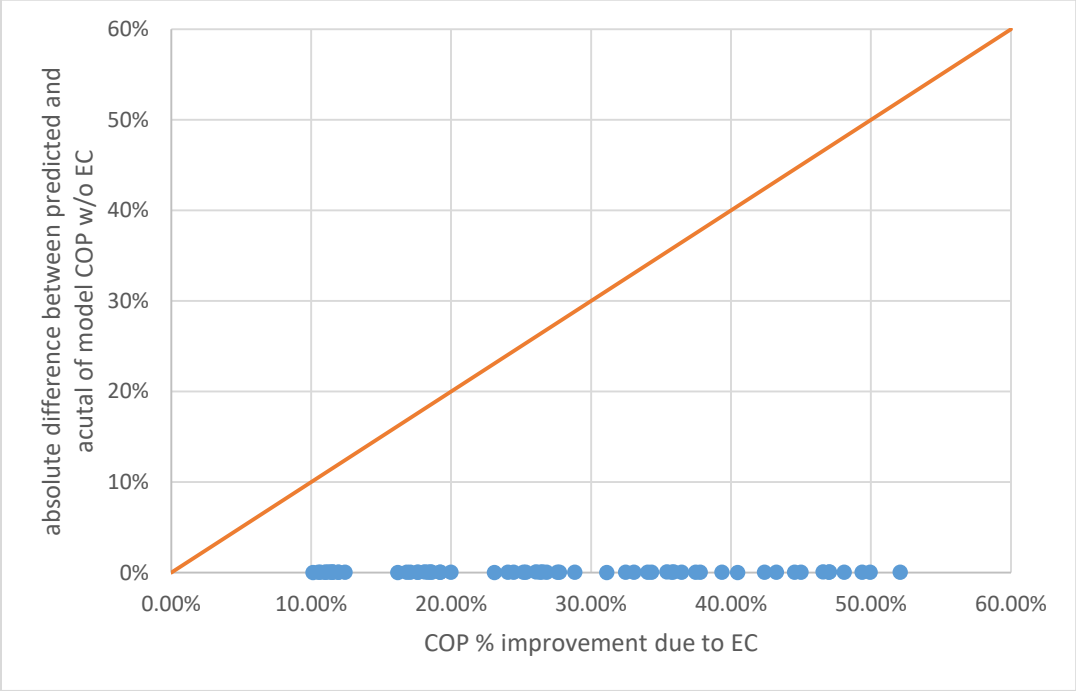

Figure 48 Error and improvement comparison from 0 to 60% due to external evaporative cooling

$\boldsymbol{COP_{ratio}}$ **Correlation** According to the equations mentioned previously, plus several assumptions made for this model, COP ratio of the system with external evaporative cooling over the baseline system is a function of relative humidity, Taeo and outdoor air temperature. Both

quadratic model and exponential model are considered, namely COP ratio=f (RH, Taeo, Tout) and log COP ratio=f (RH, Taeo, Tout). However, exponential model is better than quadratic model and comprehensive model coefficients of the exponential function is built in Table 7, shown as follows,

Table 7 log COP ratio (external evaporative cooling over baseline system) Model Coefficients

a0+a1*RH^2+a2*RH+a3*Taeo^2+a4*Taeo+a5*Tout^2+a6*Tout+a7*RH*Taeo+a8*Taeo*Tout+a9*RH*Tout									
a0	a1	a2	a3	a4	a5	a6	a7	a8	a9
0.144	0.314	-0.265	3.24e-5	0.00661	2.76e-5	0.00171	-0.00723	-3.75e-5	-0.00495

According to Figure 49, the residual vs. predicted data plot, it is shown that the scatterplot looks flat for the exponential method, which means it is the correct model; the scatterplot does not flat for the quadratic method, which means it is not a perfect model. Also, the vertical scatter of the data does not increase or decrease when x is changing for expoential method, it is concluded that the conditional variance does not depend on x. Figure 50 and 51, the actual vs. predicted plots, indicate the error between predicted data and actual data for both methods is negligible. Although quadratic and exponential both have small error, the residual plot (Figure 49) indicates quadratic model is worse than exponential model. Thus, exponential model is a better choice in this section and the error between predicted data and actual data is indicated in Figure 52---always less than 0.5%.

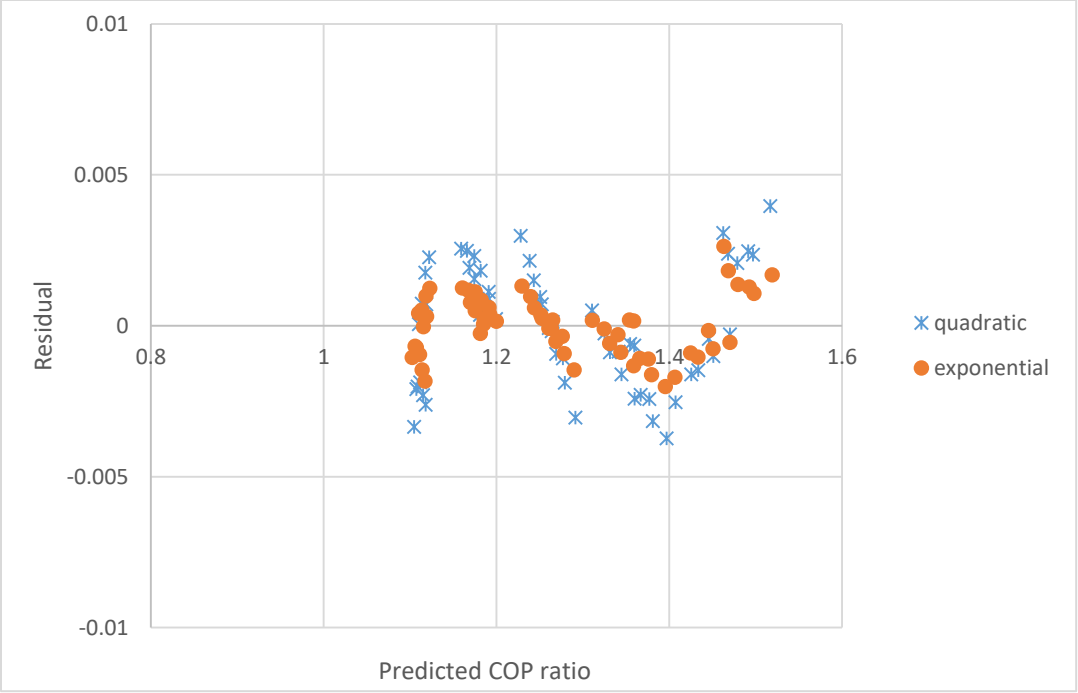

Figure 49 Residual comparison between exponential and quadratic methods for COP ratio of external evaporative cooling over baseline system

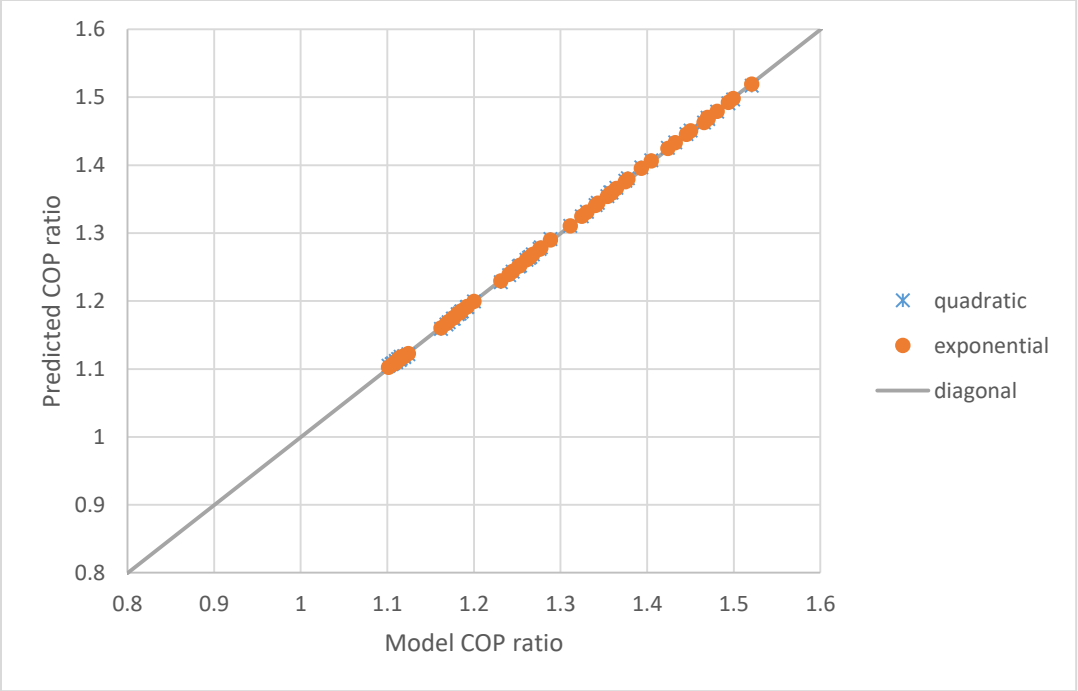

Figure 50 Actual and Predicted comparison between exponential and quadratic methods for COP ratio of external evaporative cooling over baseline system

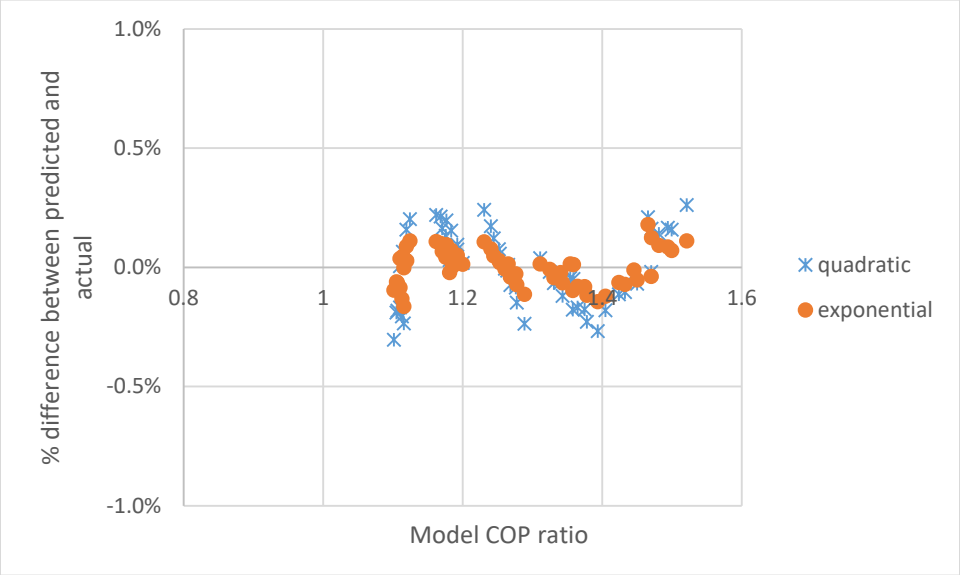

Figure 51 Percentage difference comparison between exponential and quadratic methods for COP ratio of external evaporative cooling over baseline system

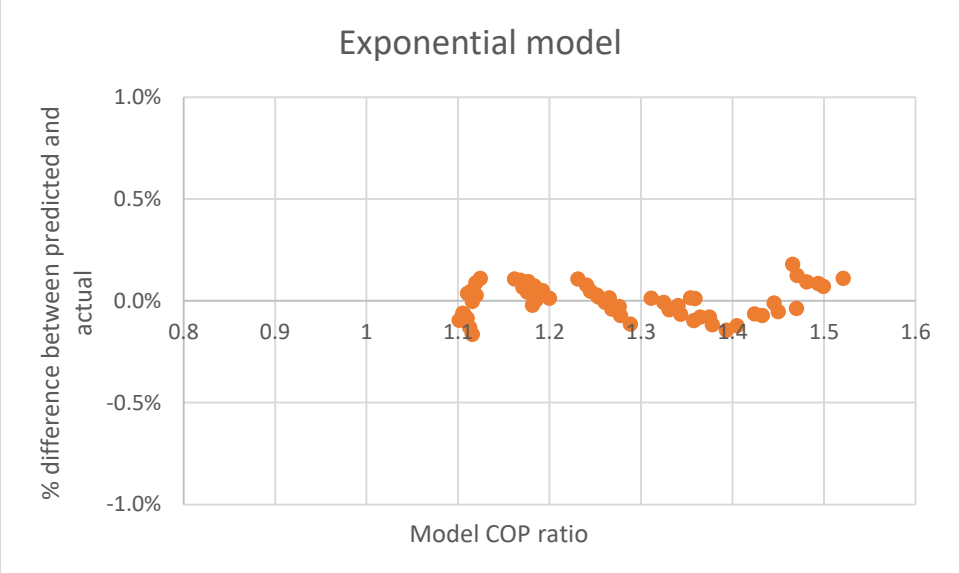

Figure 52 Predicted and model data difference of exponential method for COP ratio of external evaporative cooling over baseline system

5.1.7.1.4 Conclusions

This research studied the effect of external water to precool outdoor air before entering condenser on the vapor-compression system coefficient of performance (COP) using R410A. The possible parameters affecting the final results of the model such as outdoor air temperature; outdoor relative humidity; evaporator outlet air temperature. Typical outcomes of the model are specific work (w), refrigerating effect (q), and vapor-compression system coefficient of performance (COP).

It is shown that with evaporative cooling before condenser, refrigerating effect increases while specific work decreases, which results in an increasing COP. According to the results with the conditions of outdoor air temperatures of 26.7, 29.4, 32.2, 35 ℃ (80, 85, 90, 95°F) and relative humidities of 40%, 50%, 60%, 70%, 80% over a range of assumed evaporator exit air temperatures of 7.2, 10, 12.8℃ (45, 50, 55°F) with a typical compressor efficiency of 80%, the highest benefit of COP percentage difference with R410A can reach as much as 60% by taking advantage of external water.

5.1.7.2 Results and Analysis for Reconfigured System A2

As there are three different variables (outdoor conditions---dry-bulb temperature, relative humidity and indoor supply air temperature---Taeo) having impacts on COP/ COP improvement of this model, the section will discuss how these three variables contribute to the COP and COP improvement separately. Also, a compressive table with all test results would be shown in Appendix B.

5.1.7.2.1 Scenario A2 Alone (Internal Case)

In this section, the first step is to study how condenser inlet air temperature after precooling with internal condensate evaporative cooling related to different variables and the second step is to further investigate how modification COP related to different variables.

5.1.7.2.1.1 Evaporative Cooling Effect

Table 8 shows the relationship of wet-bulb (saturated point) temperatures, final outdoor air temperatures (utilizing internal water) with varied outdoor air conditions (dry-bulb temperatures and relative humidity) and supply air temperatures (Taeo). The blank filled in yellow is the case that internal condensate is enough for evaporative cooling outdoor temperatures to wet-bulb temperatures.

For a specific outdoor air temperature ($26.67\,℃, 80\,℉$), with the constant supply (evaporator outlet) air temperature, increasing relative humidity results in the final outdoor air entering the condenser getting close to the wet bulb (saturated point) and away from original outdoor air point. When outdoor air relative humidity gets to 70%, outdoor air temperature could even reach wet bulb temperature under all three supply (evaporator outlet) air temperatures (45,50,55℉).

For a specific outdoor air temperature (90℉,32.22℃), it is observed that the lowest relative humidity (critical relative humidity) for getting incoming air to condenser fully saturated is changing for different supply air temperature. With lower supply temperature ($45\,℉$), the condensate drain is sufficient for evaporative cooling even when outdoor air relative humidity reaches 50%.

For a specific supply air temperature (Taeo) 50°F, it is concluded that the case with a higher outdoor temperature has a lower critical outdoor air relative humidity (the outdoor relative humidity corresponding to fully precool air to wet-bulb). For instance, the critical relative humidity is 50% when the outdoor dry-bulb temperature is 95°F while 70% when the outdoor dry-bulb temperature is 80°F.

The results are summarized in Table 9, with higher relative humidity, higher outdoor air temperature and lower supply air temperature (Taeo), condensate water is easier to be sufficient for evaporative cooling.

Table 8 Wet-bulb temperatures for outdoor air and incoming air temperatures for the condenser under different conditions

Tout	T supply air °F	RH	Tsat°F	Taci °F
80	45	0.4	63.36	75.71
		0.5	66.5	71.74
		0.6	69.46	69.46
		0.7	72.26	72.26
		0.8	74.9	74.9
	50	0.4	63.38	78.12
		0.5	66.53	74.15
		0.6	69.5	70.19
		0.7	72.3	72.3
		0.8	74.94	74.94
	55	0.4	63.41	80.94
		0.5	66.56	76.97
		0.6	69.53	73.01
		0.7	72.33	72.33
		0.8	74.98	74.98
85	45	0.4	67.16	77.89
		0.5	70.56	73.21
		0.6	73.75	73.75
		0.7	76.74	76.74
		0.8	79.56	79.56
	50	0.4	67.19	80.31

Table 8 continued

Tout	T supply air °F	RH	Tsat°F	Taci °F
		0.5	70.6	75.63
		0.6	73.79	73.79
		0.7	76.78	76.78
		0.8	79.6	79.6
	55	0.4	67.22	83.15
		0.5	70.63	78.47
		0.6	73.83	73.83
		0.7	76.82	76.82
		0.8	79.64	79.64
90	45	0.4	70.96	79.62
		0.5	74.63	74.63
		0.6	78.04	78.04
		0.7	81.23	81.23
		0.8	84.21	84.21
	50	0.4	71	82.06
		0.5	74.67	76.57
		0.6	78.09	78.09
		0.7	81.27	81.27
		0.8	84.26	84.26
	55	0.4	71.03	84.91
		0.5	74.71	79.42
		0.6	78.13	78.13
		0.7	81.32	81.32
		0.8	84.31	84.31
95	45	0.4	74.77	80.85
		0.5	78.71	78.71
		0.6	82.34	82.34
		0.7	85.72	85.72
		0.8	88.87	88.87
	50	0.4	74.81	83.31
		0.5	78.75	78.75
		0.6	82.39	82.39
		0.7	85.77	85.77
		0.8	88.93	88.93
	55	0.4	74.85	86.18
		0.5	78.8	79.75
		0.6	82.44	82.44
		0.7	85.82	85.82
		0.8	88.98	88.98

Table 9 Different conditions lead sufficient condensate

T_{out}	RH	T_{aeo}	Sufficient condensate
↑	→	→	
→	↑	→	
→	→	↓	

Table 10 shows the humidity ratio difference of utilizing condensate water from the evaporator---$\triangle w_{internal}$, and the situation of maximum ---$\triangle w_{max}$ (saturated point) along with the ratio of them when outdoor air temperature is 80 °F, the data corresponding to other outdoor air temperatures is shown in the Appendix B. The ratio whose value is larger than one indicates that condensate water is sufficient for evaporative cooling. At a constant supply air temperature (Taeo), with a boosting relative humidity, $\triangle w_{internal}$ increase while $\triangle w_{external}$ decreases, which means the final state point of outdoor air gets close to the saturated point and then stays at saturated point even when $\triangle w_{internal}$ boosts beyond $\triangle w_{max}$. Table 10 also indicates that when relative humidity reaches to 70% or a higher value, final outdoor air will become saturated under all evaporator outlet temperatures. When relative humidity remains constant, higher evaporator outlet temperature (°F) results in lower $\triangle w_{internal}$ while $\triangle w_{external}$ stays almost constant because $\triangle w_{external}$ is only highly related to the outdoor air relative humidity.

Table 10 Wet-bulb temperatures of outdoor air, incoming air temperatures for the condenser and different humidity ratios when the outdoor air temperature is 80 ℉

Tout	T supply air	RH	Tsat	Taci	△w internal	△w total	△w internal/△w total/2.5
80	45	0.4	63.36	75.71	0.00232	0.003703	0.250607615
		0.5	66.5	71.74	0.00449	0.002977	0.603291905
		0.6	69.46	69.46	0.006674	0.002289	1.166273482
		0.7	72.26	72.26	0.008874	0.001636	2.169682152
		0.8	74.9	74.9	0.01109	0.001012	4.383399209

Table 10 continued

Tout	T supply air	RH	Tsat	Taci	△w internal	△w total	△w internal/△w total/2.5
80	50	0.4	63.38	78.12	0.001024	0.003715	0.11025572
		0.5	66.53	74.15	0.003193	0.002993	0.426729034
		0.6	69.5	70.19	0.005378	0.002308	0.932062392
		0.7	72.3	72.3	0.007577	0.001658	1.827985525
		0.8	74.94	74.94	0.009792	0.001038	3.773410405
	55	0.4	63.41	80.94	0	0.003726	0
		0.5	66.56	76.97	0.00166	0.003006	0.22089155
		0.6	69.53	73.01	0.003845	0.002325	0.661505376
		0.7	72.33	72.33	0.006044	0.001678	1.440762813
		0.8	74.98	74.98	0.008259	0.001062	3.110734463

Figure 53, 54 and 55 show the relationship between condenser inlet air temperature after precooler and outdoor air condition (temperature and relative humidity) under three different evaporator outlet air temperatures, 7.2, 10, 12.8 ℃ (45, 50, 55 ℉), respectively. Thus, evaporative cooling effect, which is defined as outdoor air temperature minus condenser inlet air temperature after precooler, could be further observed. Unlike the case of external water evaporative cooling, the evaporative cooling effect for internal evaporative cooling is related to all three variables, as discussed above. The lines which are parallel to the diagonal line indicate the condensate drain is sufficient for evaporative cooling; otherwise, the condensate is not enough. The internal evaporative cooling is most effective in the hot and humid region, especially when relative humidity higher than 60%. For the dry region (relative humidity is 40% or lower), the evaporative cooling effect with internal condensate is very limited, and there is even no evaporative cooling effect with the highest evaporator outlet air temperature--- 55 ℉.

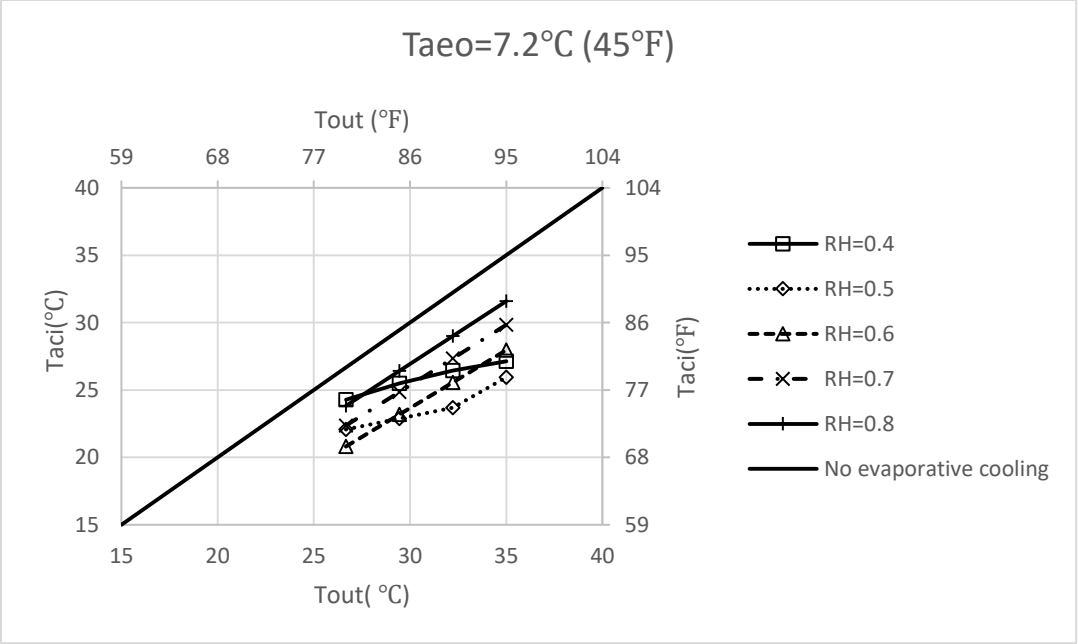

Figure 53 Condenser air inlet after precooler varied with different outdoor air conditions when Taeo=7.2 ℃

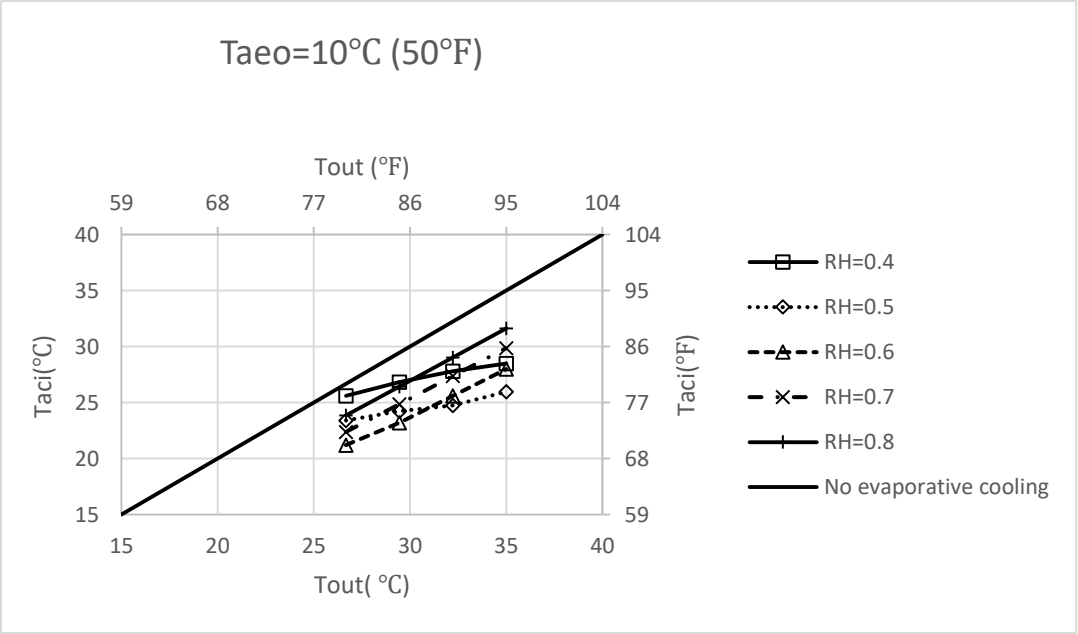

Figure 54 Condenser air inlet after precooler varied with different outdoor air conditions when Taeo=10 ℃

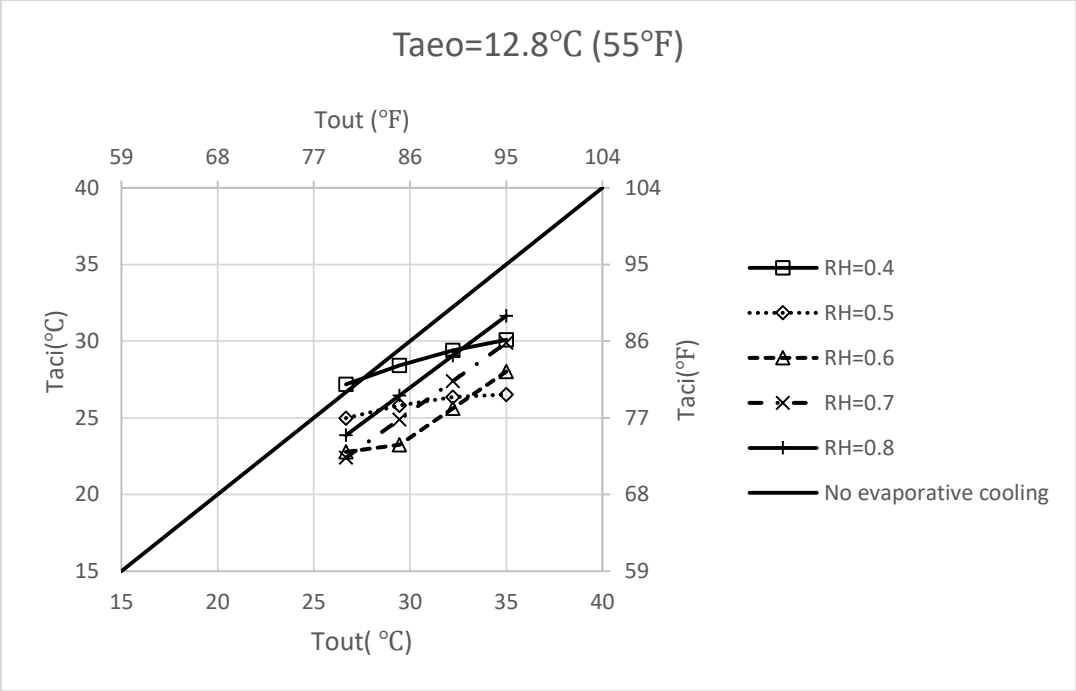

Figure 55 Condenser air inlet after precooler varied with different outdoor air conditions when Taeo=12.8 ℃

5.1.7.2.1.2 Scenario A2 COP Overview

Figure 56 gives an overview of how COP related to outdoor air temperatures, relative humidities and evaporator outlet air temperature---Taeo, this Figure further indicates that for all working conditions, with increasing relative humidity, COP first increases slowly with relative humidity varied from 40%-60% and then decreases of relative humidity varied from 60%-80% because final outdoor air become saturated when relative humidity reaches 60%. This optimum relative humidity condition is understandable based on the fact that relative humidities below 50% may not produce enough condensate draining from the evaporator for the outdoor air to fully reach the wet-bulb temperature, which is the lowest possible heat sink temperature, relative humidities above 70% means achievable gains from evaporative cooling are limited because even though sufficient internal water is obtained the dry and wet bulb temperature are already close to each

other. Figure 57, 58, 59 and 60 show how COP is related to Taeo under the same outdoor air temperature and these plots indicate that COP increases with the increasing Taeo. Figure 61, 62 and 63 show how COP is changing with different outdoor air temperatures under the same Taeo, and these plots illustrate that COP decreases with the increasing outdoor air temperature. The results are summarized in Table 11---a reconfigured system with internal evaporative cooling has the best evaporative cooling effect for the hot and moderately humid region (50%-70%) with a higher supply air (evaporator outlet air) temperature.

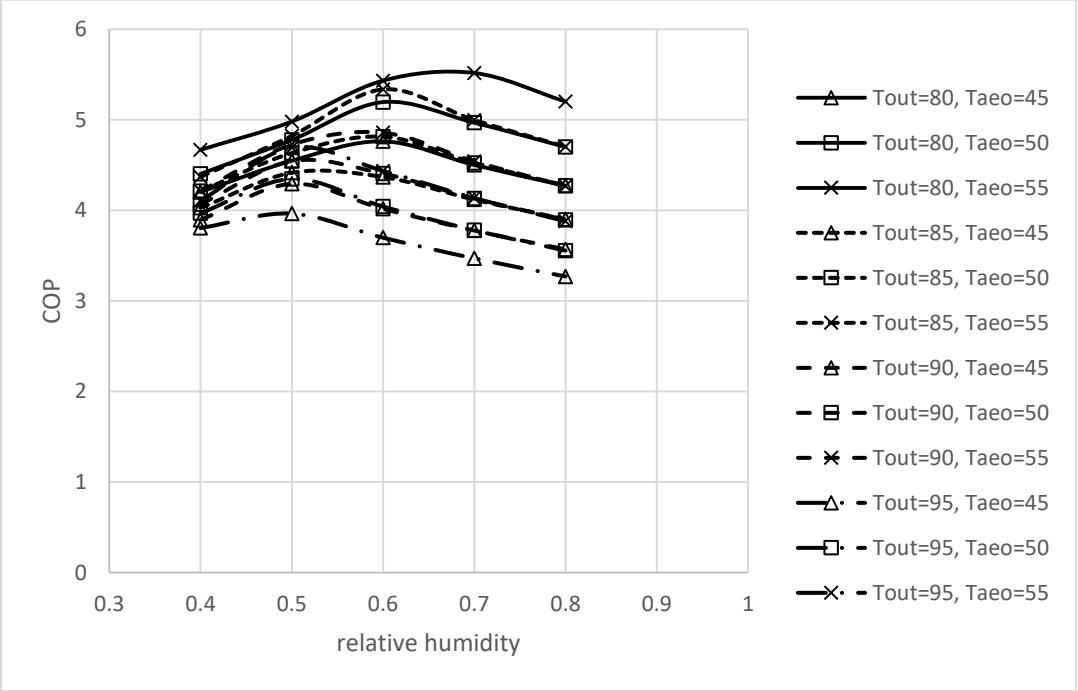

Figure 56 COP for system with internal evaporative cooing varied with relative humidity under different conditions

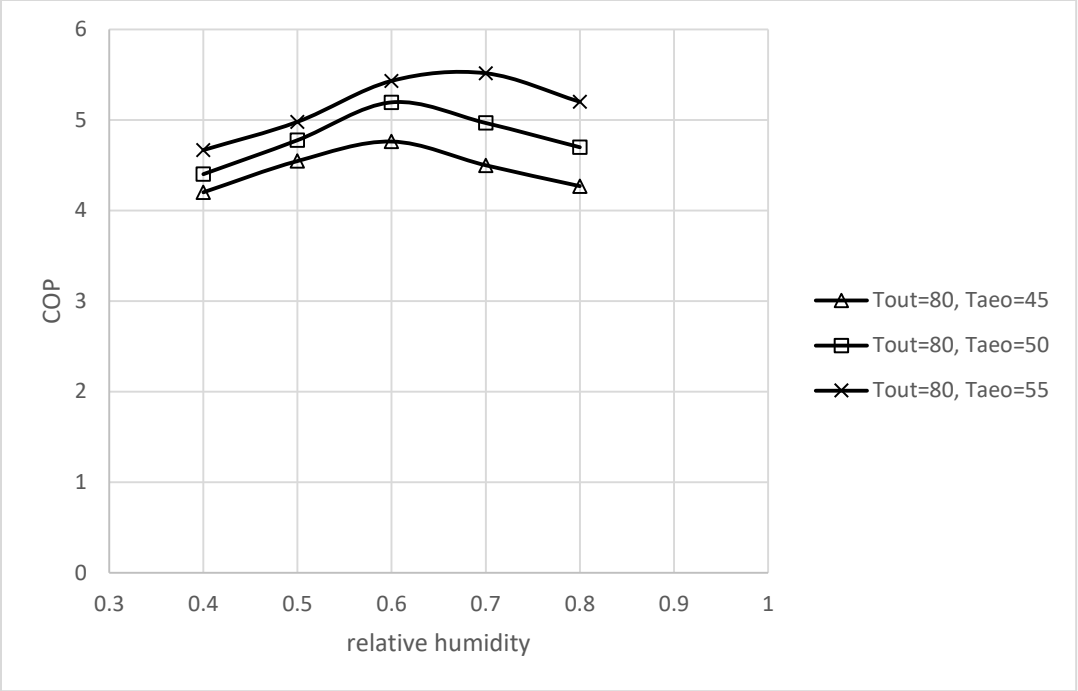

Figure 57 COP for system with internal evaporative cooing varied with relative humidity when Tout=80 ℉

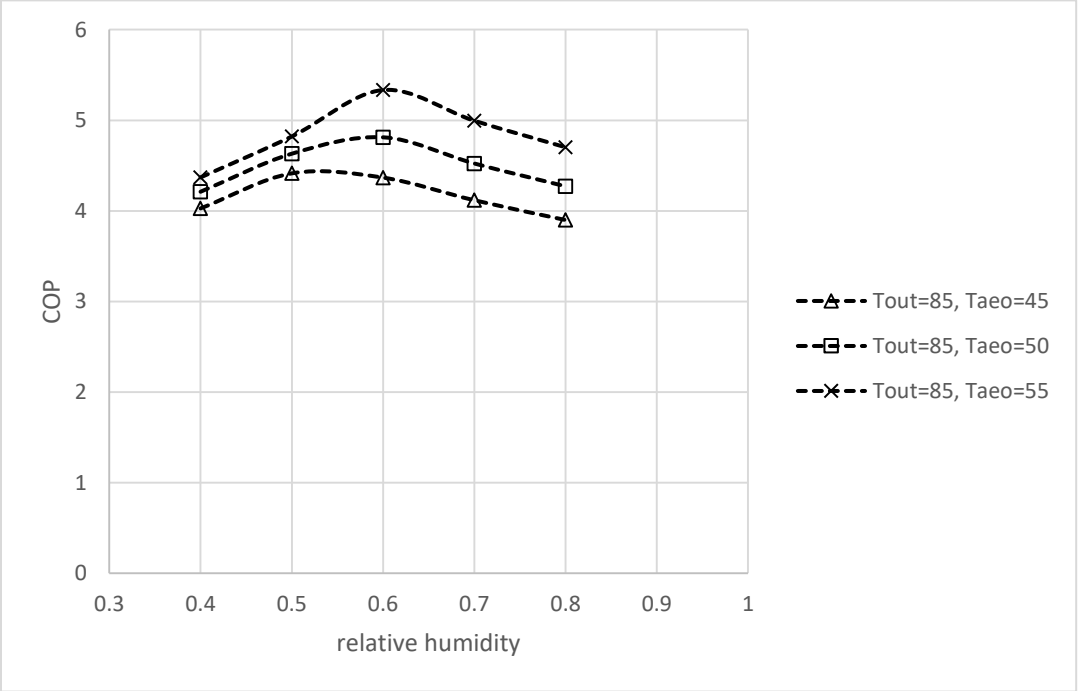

Figure 58 COP for system with internal evaporative cooing varied with relative humidity when Tout=85 ℉

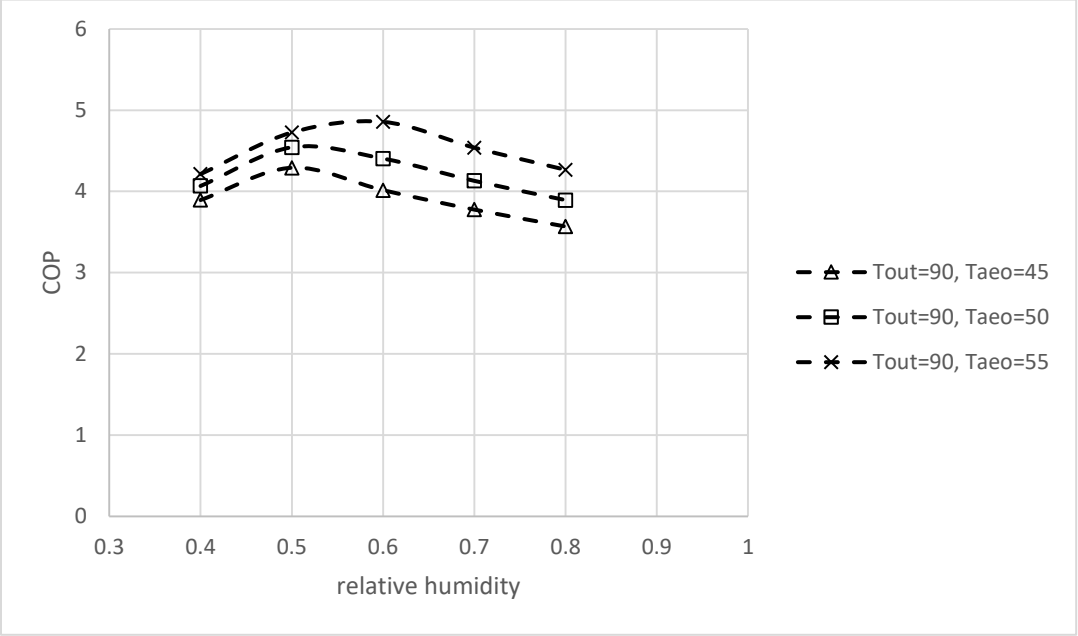

Figure 59 COP for system with internal evaporative cooing varied with relative humidity when Tout=90 °F

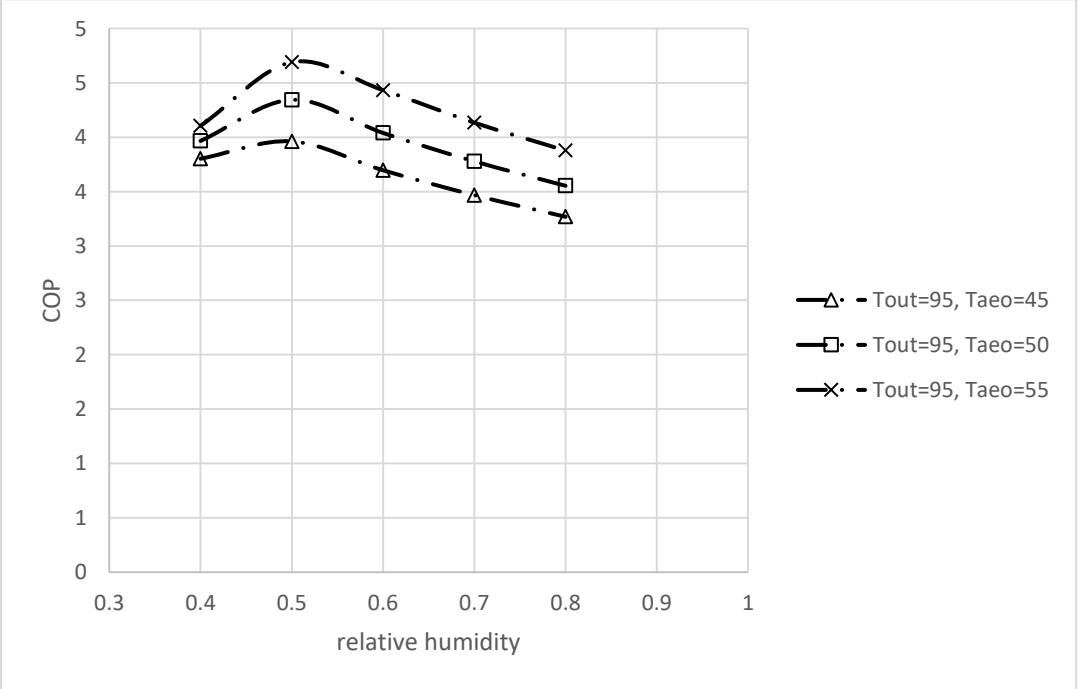

Figure 60 COP for system with internal evaporative cooing varied with relative humidity when Tout=95 °F

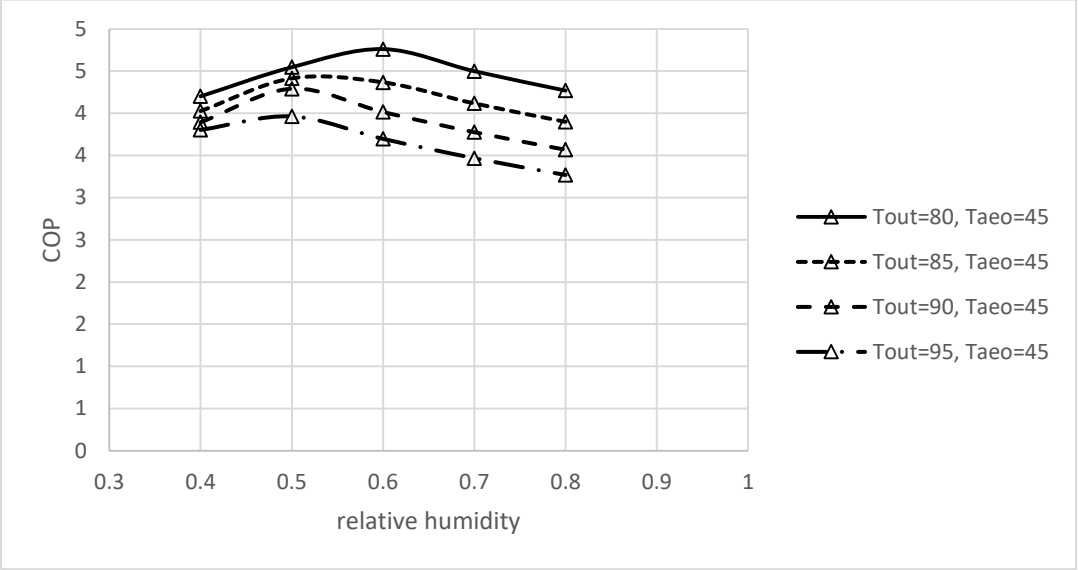

Figure 61 COP for system with internal evaporative cooing varied with relative humidity when Taeo=45 °F

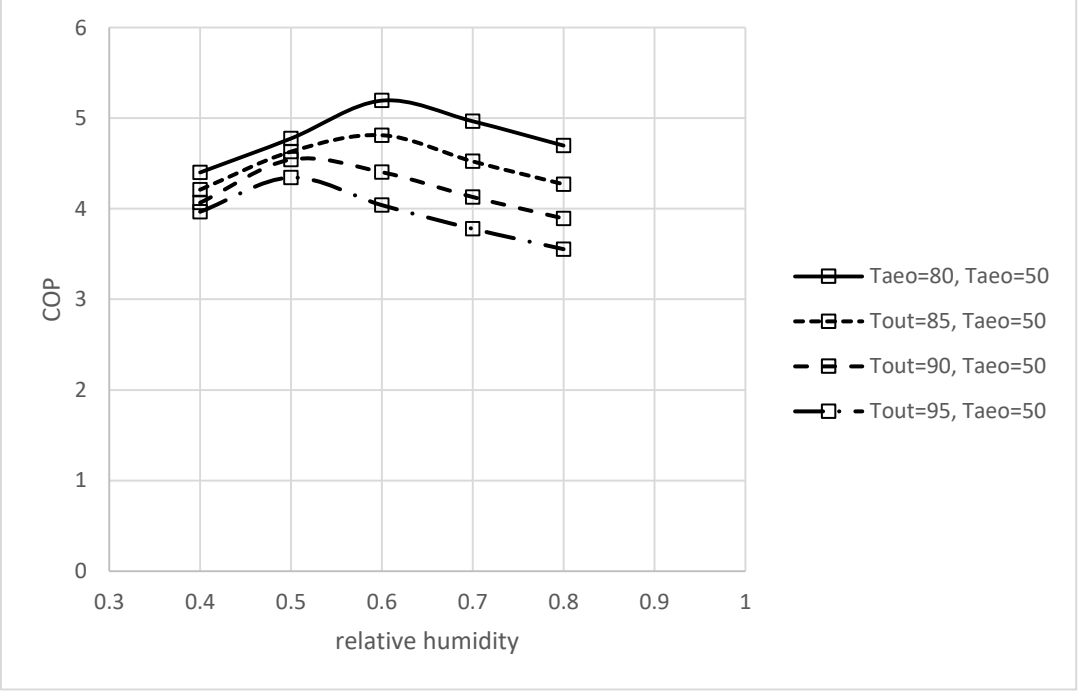

Figure 62 COP for system with internal evaporative cooing varied with relative humidity when Taeo=50 °F

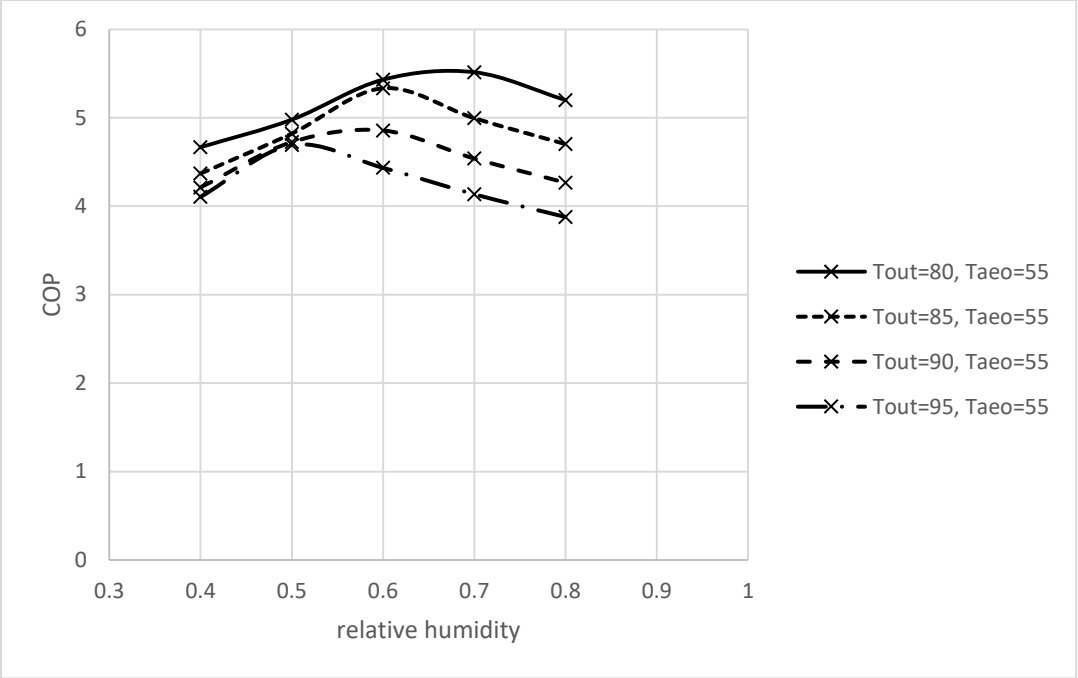

Figure 63 COP for system with internal evaporative cooing varied with relative humidity when Taeo=55 °F

Table 11 COP with internal evaporative cooling varied with Tout RH and Taeo

case	T_{out}	RH	T_{aeo}	COP with EC
1	↑	→	→	↓
2	→	↑	→	↑ $first\ then$ ↓
3	→	→	↑	↑

5.1.7.2.2 Compare Scenario A2 to Scenario A

5.1.7.2.2.1 COP Improvement Due to Evaporative Cooling Overview

Figure 64 shows the relationship between COP with/without internal evaporative cooling when COP is ranging from 1 to 6. This plot also indicate that improvement is obvious for half of

the conditions but negligible for the other half. The improvement is highly depending on how much water generated in the evaporator. The highest improvement can reach 38%.

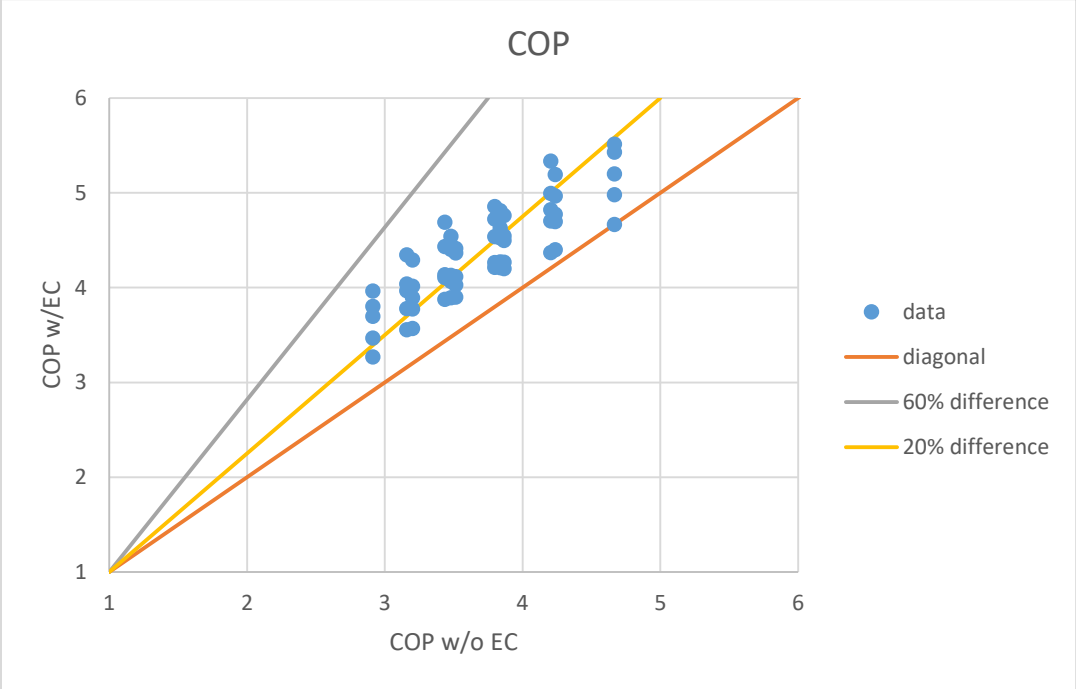

Figure 64 COP with/without internal evaporative cooling with the range of 1 to 6

5.1.7.2.2.2 COP Enhancement Analysis

For the reconfigured COP enhancement analysis, COP percentage difference is defined as follows, COP (in)%= $\frac{COP_{in}-COP_{ref}}{COP_{ref}}$.

Figure 65 gives an overview of how COP percentage related to outdoor air temperature, relative humidities and Taeos. This figure shows that COP percentage difference first increases slowly with relative humidity ranging from 40%-60% and then decreases with relative humidity ranging from 60%-80% because final outdoor air become saturated when relative humidity reaches 60%. This optimum relative humidity condition is understandable based on the fact that relative humidities below 50% may not produce enough condensate draining from the evaporator for the outdoor air to fully reach the wet-bulb temperature, which is the lowest possible heat sink

temperature, relative humidities above 70% means achievable gains from evaporative cooling are limited because even though sufficient internal water is obtained the dry and wet bulb temperature are already close to each other. Figure 66, 67, 68 and 69 show the relationship between COP percentage difference and Taeo under the same outdoor air temperature, and these figures show that COP percentage difference increase with the decreasing Taeo. The percentage difference is biggest at lower relative humidity (40%) and becoming negligible after high relative humidity (70%). Figure 70, 71 and 72 show the relationship between COP percentage difference and outdoor air temperatures at same Taeo and these figures illustrate that COP percentage difference increases with the boosting outdoor air temperature. The results mentioned above is summarized in Table 12--a reconfigured system with internal evaporative cooling has the best COP improvement for the hot and moderately humid region (50%-70%) with a lower supply air (evaporator outlet air) temperature.

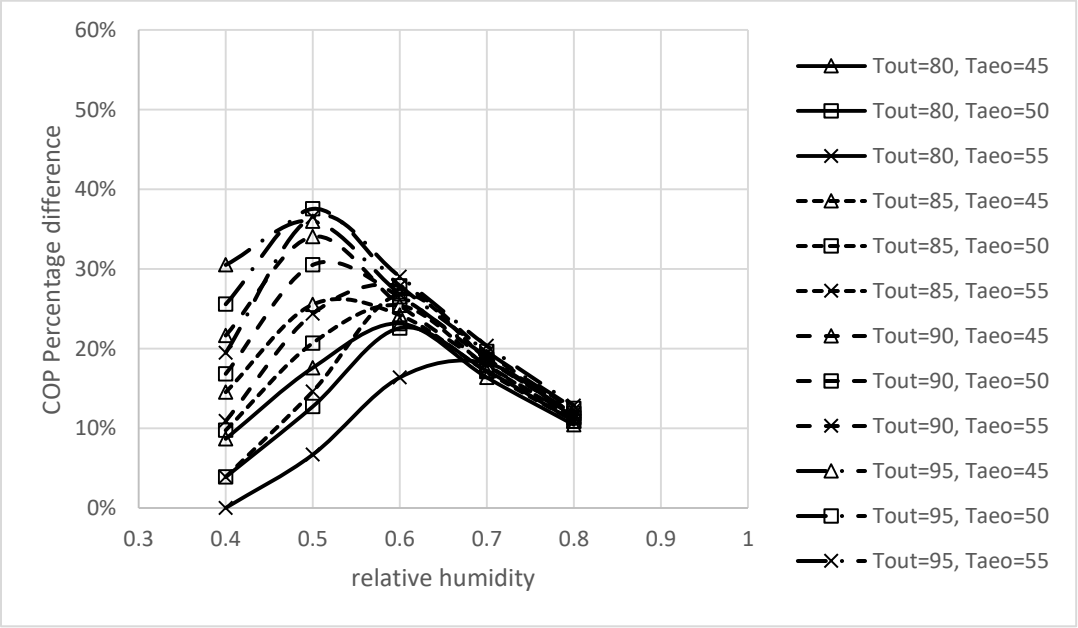

Figure 65 COP percentage difference (internal evaporative cooling/baseline) versus relative humidity under different conditions

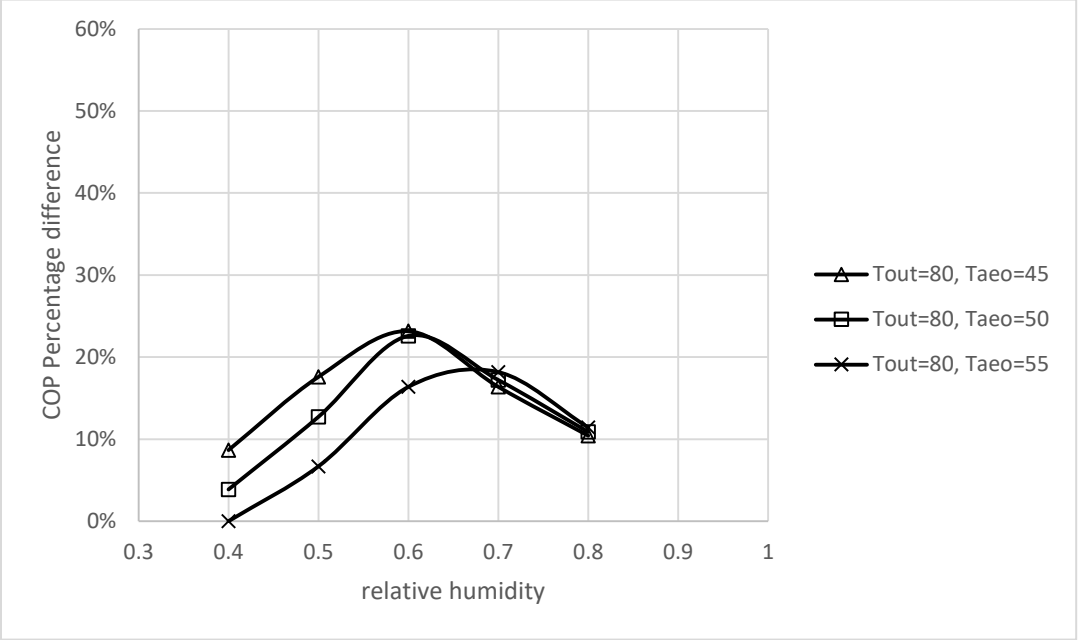

Figure 66 COP percentage difference (internal evaporative cooling over baseline) versus relative humidity when Tout=80 ℉

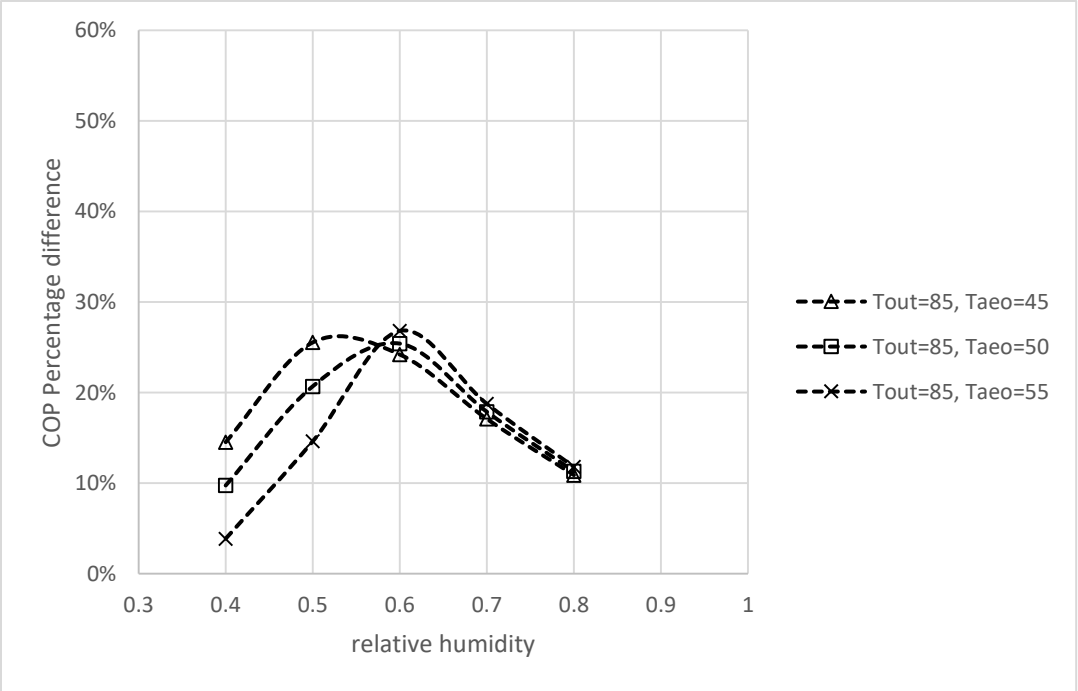

Figure 67 COP percentage difference (internal evaporative cooling over baseline) versus relative humidity when Tout=85 ℉

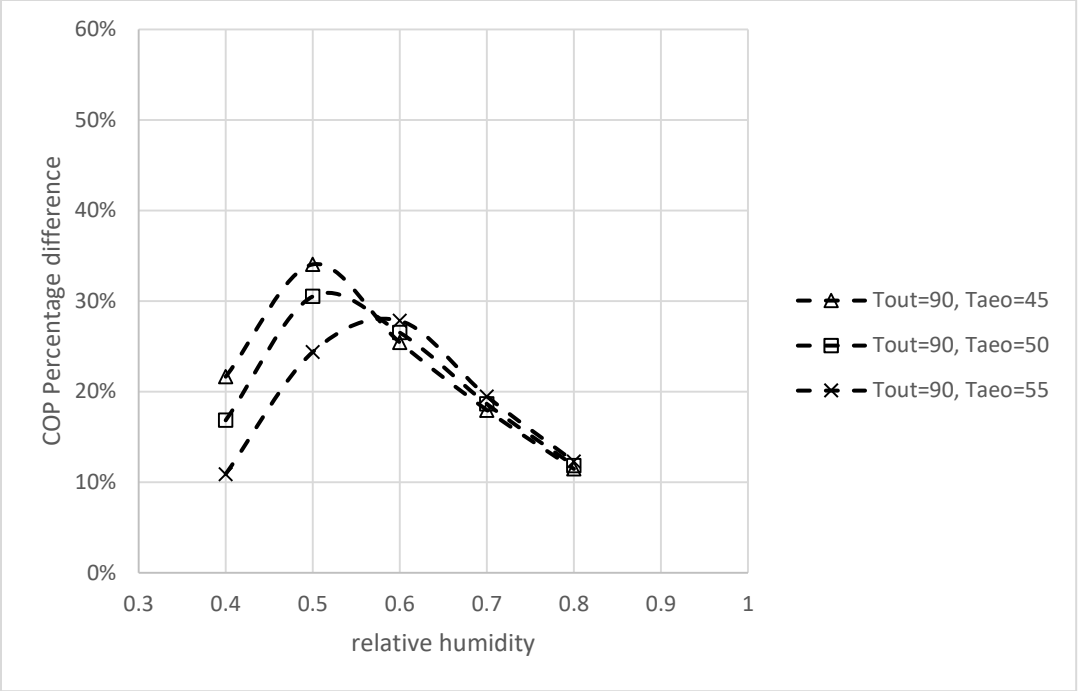

Figure 68 COP percentage difference (internal evaporative cooling over baseline) versus relative humidity when Tout=90 ℉

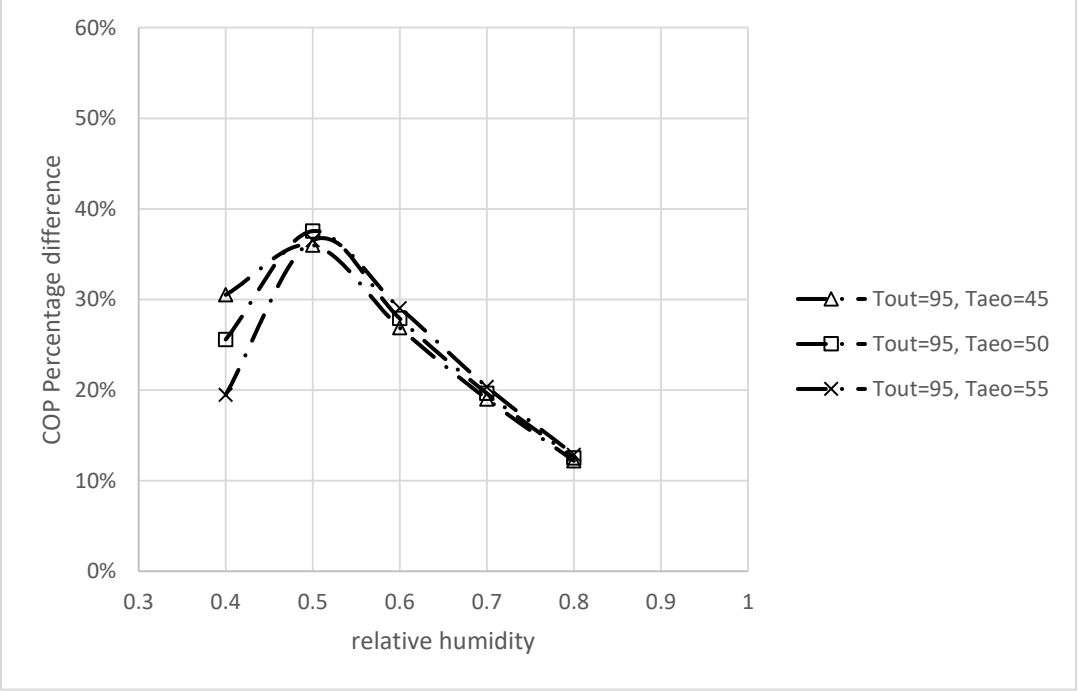

Figure 69 COP percentage difference (internal evaporative cooling over baseline) versus relative humidity when Tout=95 ℉

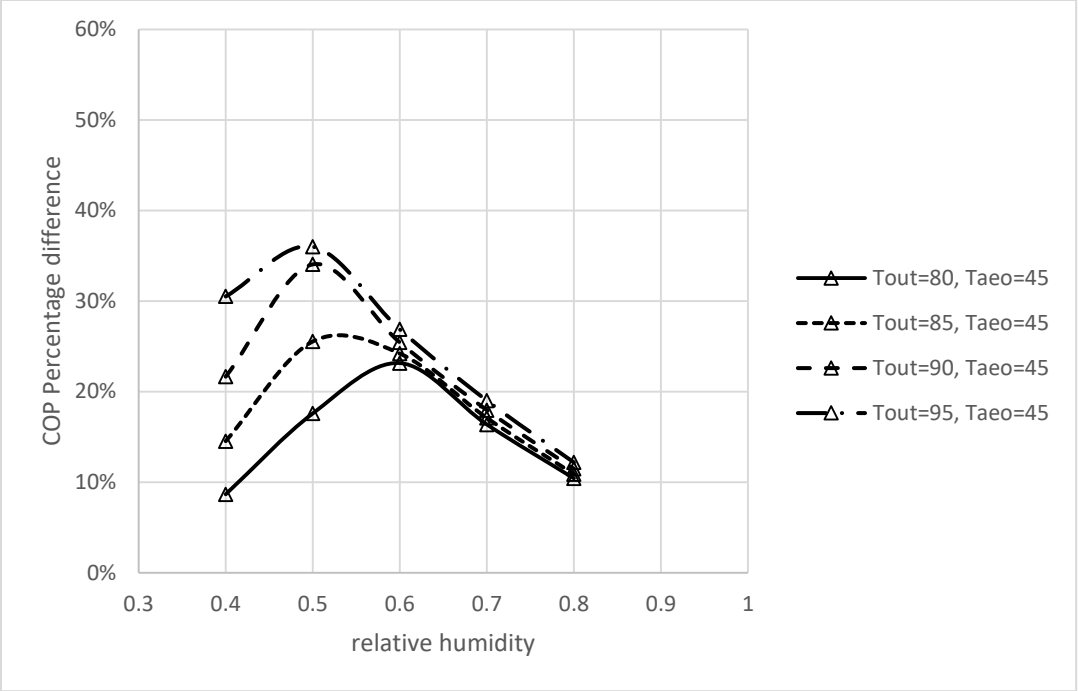

Figure 70 COP percentage difference (internal evaporative cooling over baseline) versus relative humidity when Taeo=45°F

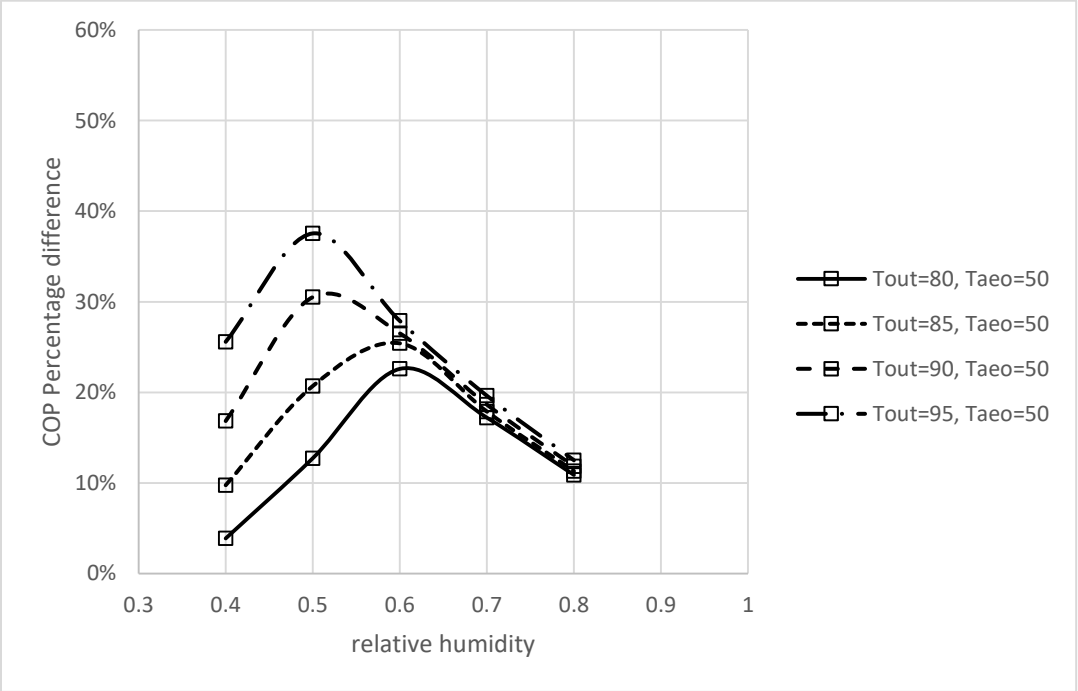

Figure 71 COP percentage difference (internal evaporative cooling over baseline) versus relative humidity when Taeo=50 ℉

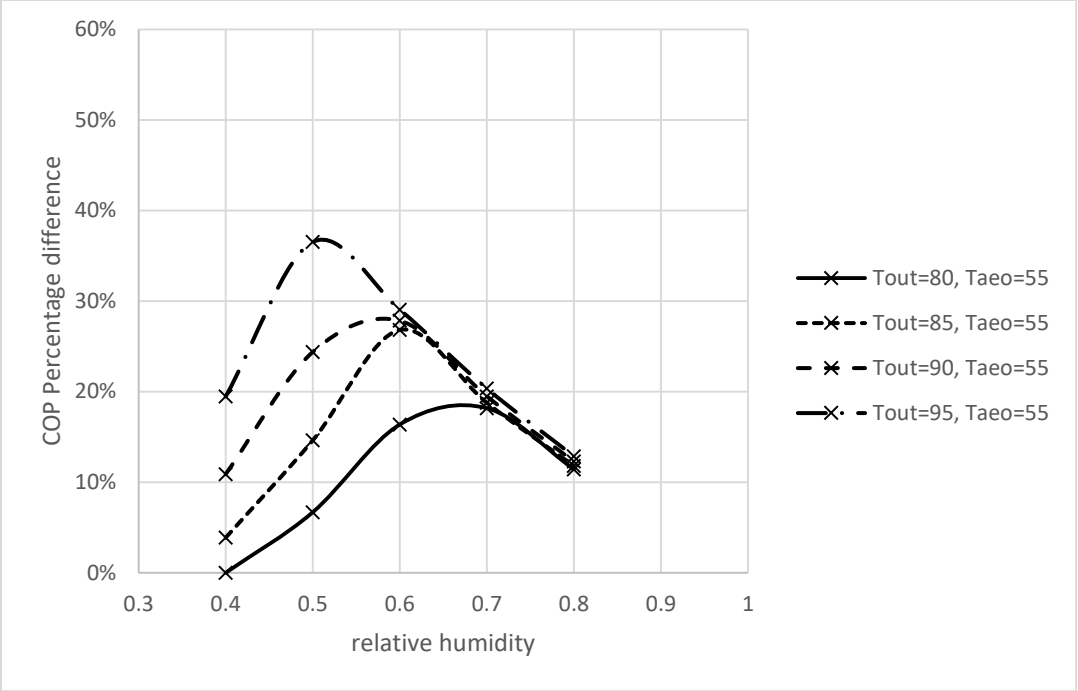

Figure 72 COP percentage difference (internal evaporative cooling over baseline) versus relative humidity when Taeo=55 ℉

Table 12 COP percentage difference (internal evaporative cooling over baseline) varied with Tout, RH, and Taeo

case	T_{out}	RH	T_{aeo}	% difference
1	↑	→	→	↑
2	→	↑	→	$\uparrow first\ then \downarrow$
3	→	→	↑	↓

5.1.7.2.3 Equation Derivation

5.1.7.2.3.1 Correlation Development

Based on the upper limit and lower limit of the cooling season weather report, the conditions below are used to derive regression equations. Outdoor air condition is set as: 26.7, 29.4, 32.2, 35 ℃ (80, 85, 90, 95℉); RH=40%, 50%, 60%, 70%, 80%; Taeo=7.2, 10, 12.8℃ (45,

50, 55°F); compressor efficiency: 80%. The conditions above have a wider range than the conditions in the real weather report thus derivation of equations are based on these data. The simulation is based on two systems, namely a baseline system (derived in the previous section), and a reconfigured system with evaporative cooling utilizing internal condensate water.

$COP_{internal}$ Correlation Similarly to Reconfigured system A1, regression method containing quadratic and exponential methods are used and compared in this section as well.

According to the equations aforementioned, plus several assumptions made for this model, it is known that COP with internal evaporative cooling is a function of relative humidity, Taeo and outdoor air temperature, namely log COP=f (RH, Taeo, Tout). A complete quadratic regression of log COP is built in Table 13, shown as follows,

Table 13 log $COP_{internal}$ Model Coefficients

a0+a1*RH^2+a2*RH+a3*Taeo^2+a4*Taeo+a5*Tout^2+a6*Tout+a7*RH*Taeo+a8*Taeo*Tout+a9*RH*Tout									
a0	a1	a2	a3	a4	a5	a6	a7	a8	a9
0.0703	-2.59	4.68	-0.0000485	-0.000632	-8.70e-6	0.00675	0.0274	0.0000448	-0.0346

According to Figure 73, the residual vs. predicted data plot, it is shown that the scatterplot looks flat for the exponential method, which means it is the correct model; the scatterplot is not flat for the quadratic method, which means it is not a perfect model. Also, the vertical scatter of the data does not increase or decrease when x is changing for exponential method, it is concluded that the conditional variance does not depend on x. Figure 74 and 75, the actual vs. predicted plots, indicate the error between predicted data and actual data for exponential model is always smaller than that of quadratic model. Although quadratic and exponential both have small error---less than 10%, the residual plot (Figure 73) indicates quadratic model is worse than exponential model. Thus, exponential model is a better choice in this section and the error between predicted data and actual

data is indicated in Figure 76---always less than 5%. However, the error of exponential model for internal evaporative cooling system is still larger than that of external evaporative cooling system (less than 1% error) since the data used for internal evaporative cooling model is highly depending on the amount of water generated in the evaporator.

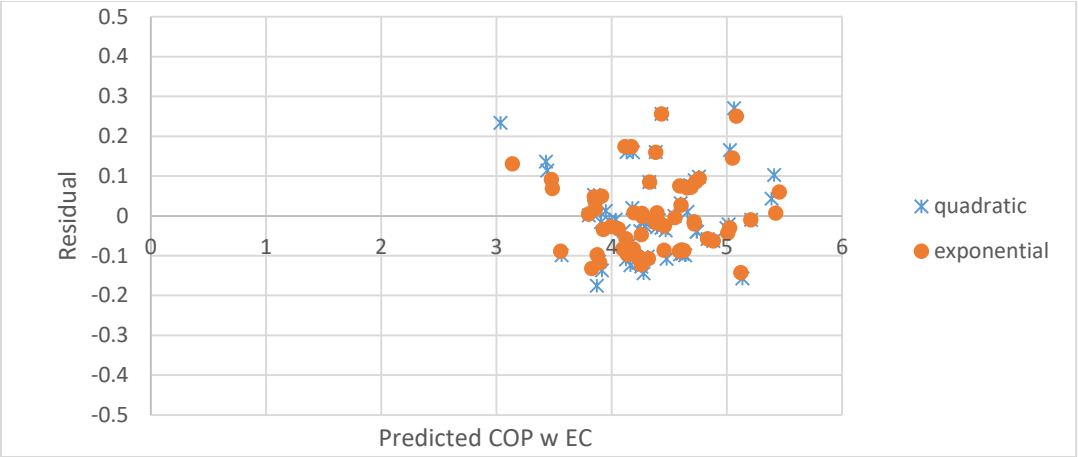

Figure 73 Residual comparison between exponential and quadratic methods for system with internal evaporative cooing

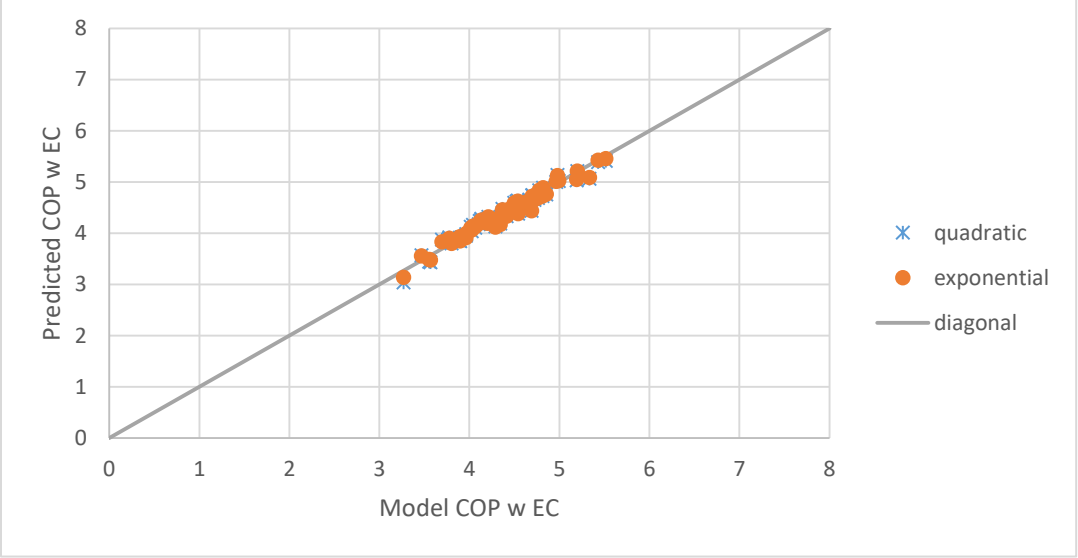

Figure 74 Actual and Predicted comparison between exponential and quadratic methods for system with internal evaporative cooing

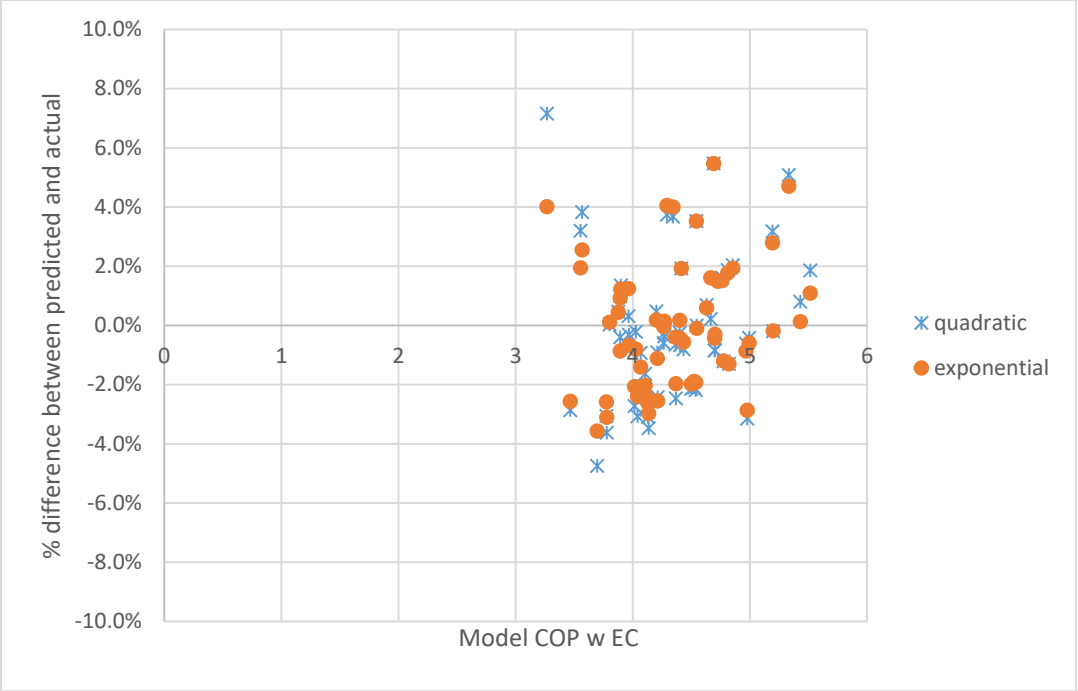

Figure 75 Percentage difference comparison between exponential and quadratic methods for system with internal evaporative cooing

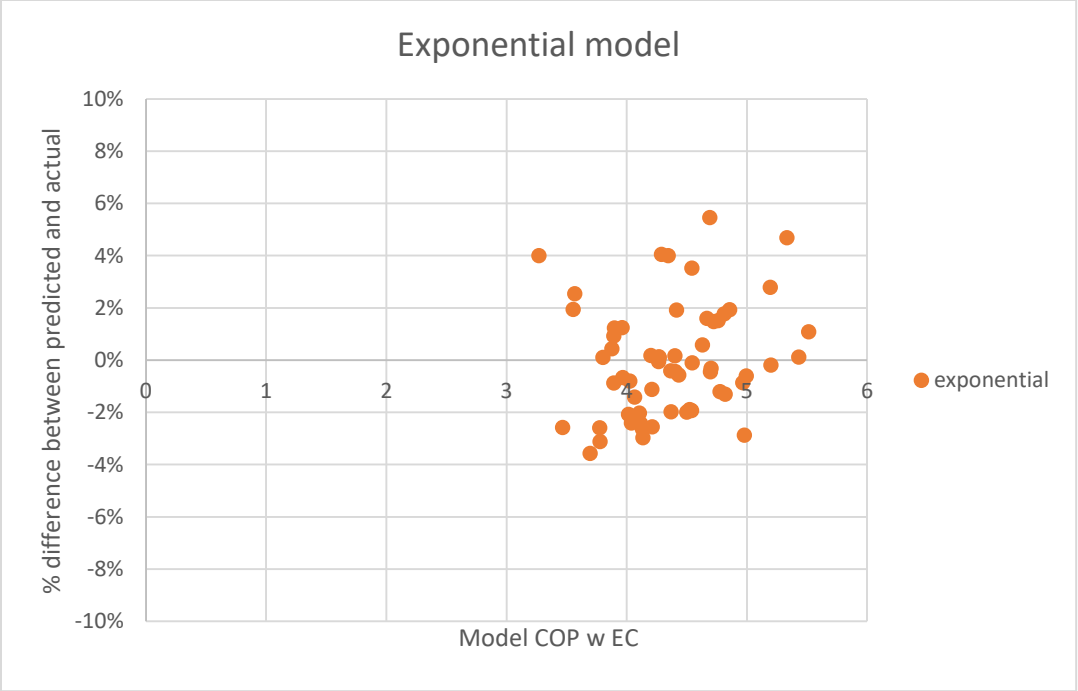

Figure 76 Percentage difference comparison of predicted and actual data of exponential method for system with internal evaporative cooing

5.1.7.2.3.2 COP Accuracy Analysis

It is necessary to compare the error of the model without evaporative cooling and the improvement due to evaporative cooling since if the error is higher than the improvement, the equations derived above will become useless. Thus, the points under the diagonal in Figure 77 are OK and the ones above diagonal are not OK. Figure 77 shows absolute difference between actual and predicted is negligible compared to COP improvement, which indicates the model built previously is correct.

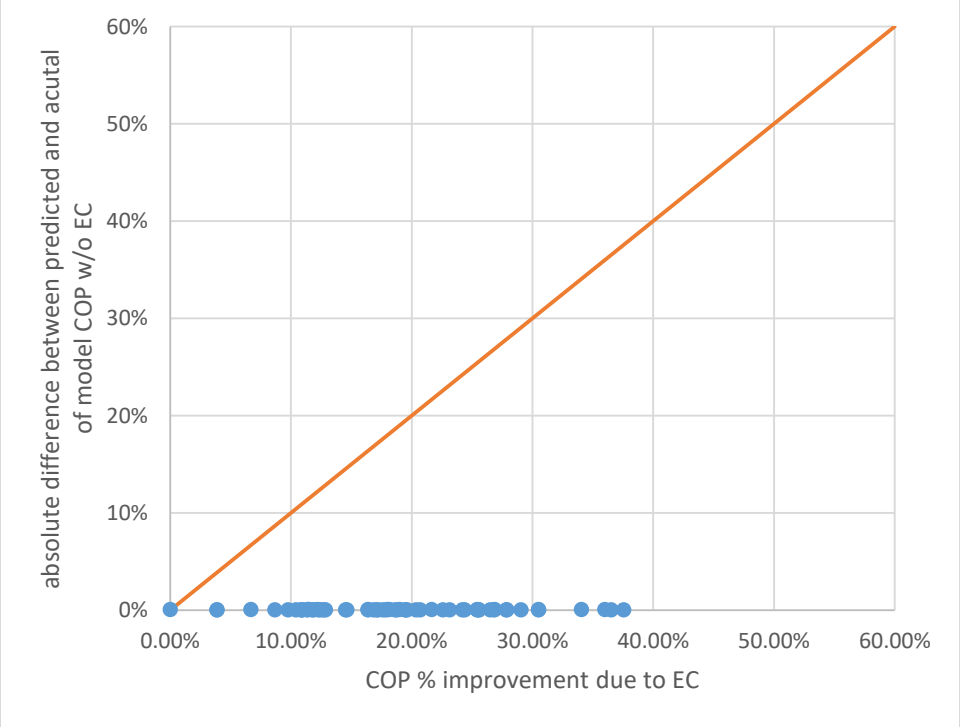

Figure 77 Error and improvement comparison due to internal evaporative cooing

$\boldsymbol{COP_{ratio}}$ **Correlation** According to the equations mentioned previously, plus several assumptions made for this model, COP ratio of the system with internal evaporative cooling over the baseline system is a function of relative humidity, Taeo and outdoor air temperature. Both

quadratic model and exponential model are considered, namely COP ratio=f (RH, Taeo, Tout) and log COP ratio=f (RH, Taeo, Tout). However, exponential model is better than quadratic model and comprehensive model coefficients of the exponential function is built in Table 14, shown as follows,

Table 14 log COP ratio (internal evaporative cooling over baseline system) Model Coefficients

a0+a1*RH^2+a2*RH+a3*Taeo^2+a4*Taeo+a5*Tout^2+a6*Tout+a7*RH*Taeo+a8*Taeo*Tout+a9*RH*Tout									
a0	a1	a2	a3	a4	a5	a6	a7	a8	a9
-1.75	-2.59	4.68	-0.000130	-0.0238	-3.08e-5	0.0224	0.0274	0.000202	-0.0346

According to Figure 78, the residual vs. predicted data plot, it is shown that the scatterplot looks flat for the exponential method, which means it is the correct model; the scatterplot is flat for the quadratic method, which means it is also a perfect model. Also, the vertical scatter of the data does not increase or decrease when x is changing for both models, it is concluded that the conditional variance does not depend on x. Figure 79 and 80, the actual vs. predicted plots, indicate the error between predicted data and actual data for both methods is within 6% and the error of exponential model is slightly smaller. Thus, exponential model is a better choice in this section and the error between predicted data and actual data is indicated in Figure 81---always less than 6%. However, the error of exponential model for internal evaporative cooling system is still larger than that of external evaporative cooling system (less than 0.5% error) since the data used for internal evaporative cooling model is highly depending on the amount of water generated in the evaporator.

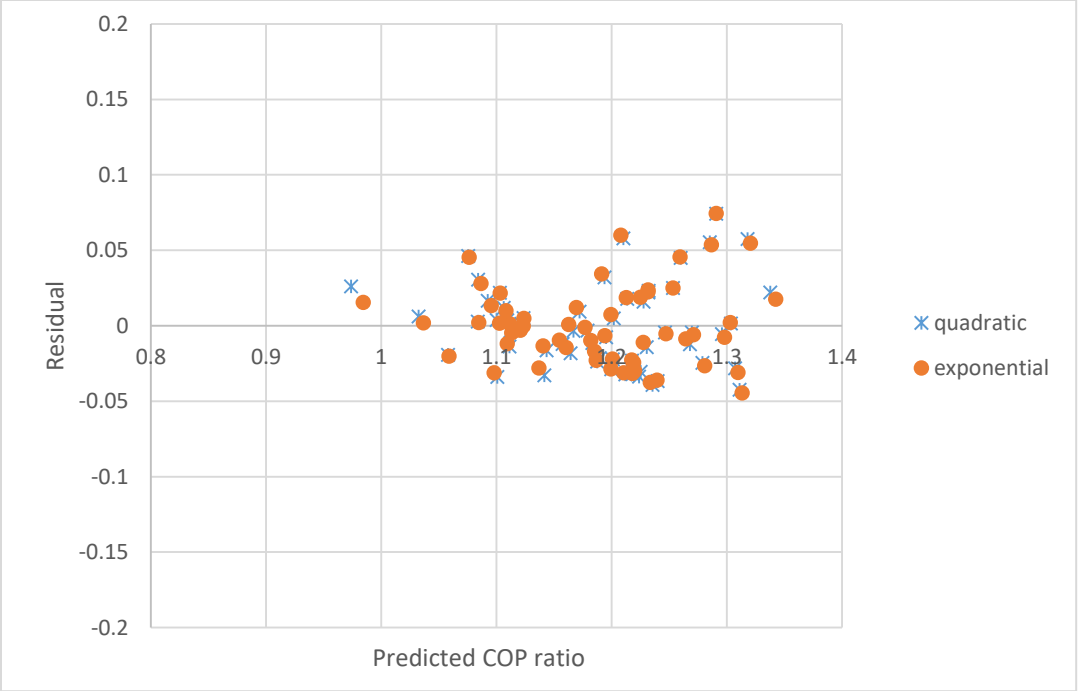

Figure 78 Residual comparison between exponential and quadratic methods for system with internal evaporative cooing

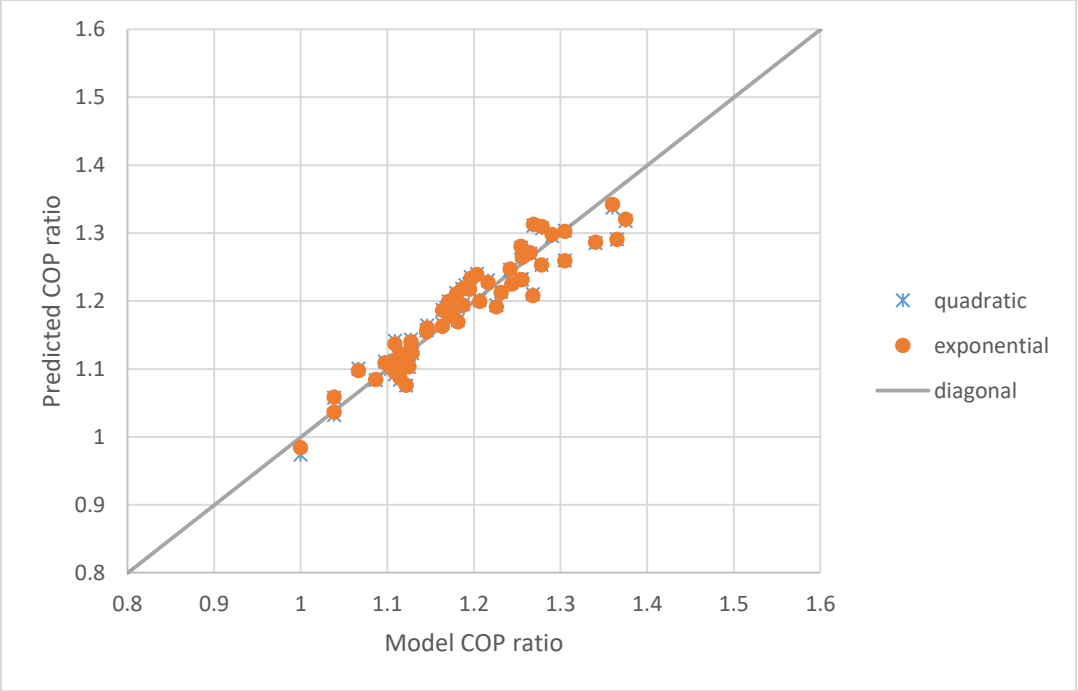

Figure 79 Actual and Predicted comparison between exponential and quadratic methods for system with internal evaporative cooing

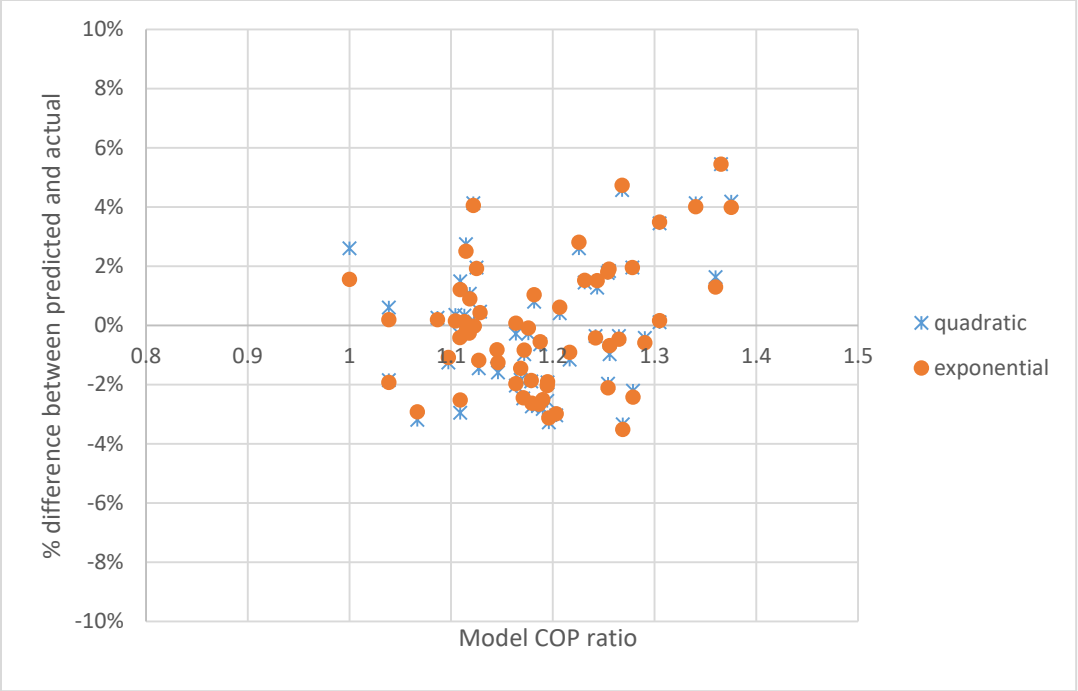

Figure 80 Percentage difference comparison between exponential and quadratic methods for system with internal evaporative cooing

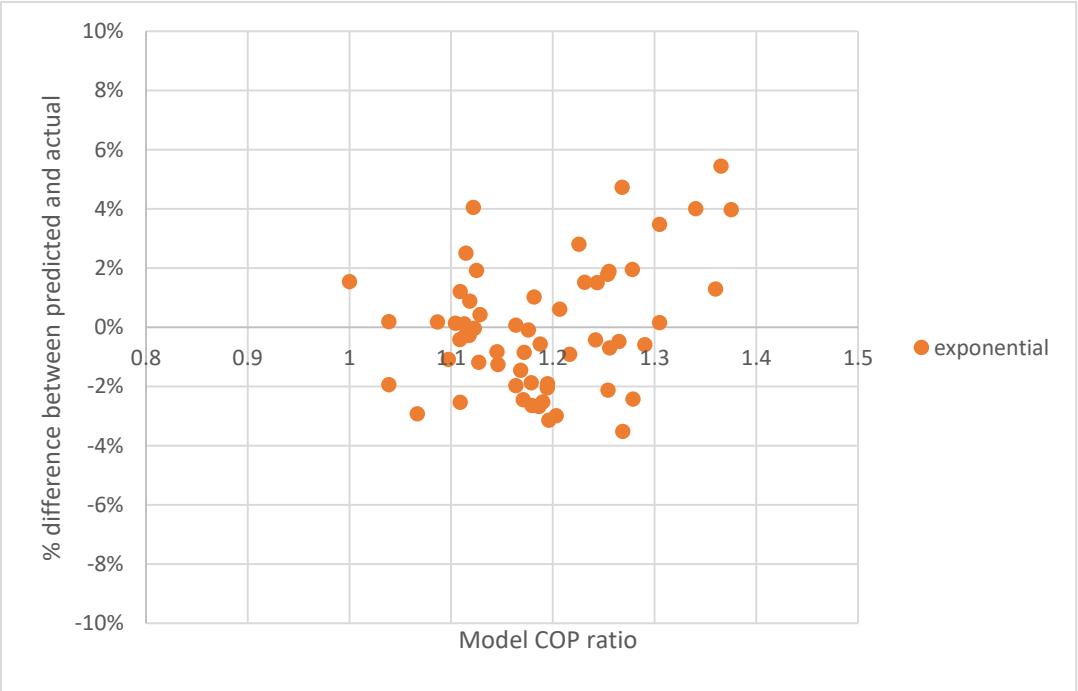

Figure 81 Percentage difference between predicted and actual data of exponential method for system with internal evaporative cooing

5.1.7.2.4 Conclusions

This research studied the effect of utilizing condensate water or total water to precool outdoor air before entering condenser on the vapor-compression system coefficient of performance (COP) using R410A. The possible parameters affecting the final results of the model such as outdoor air temperature; outdoor relative humidity; evaporator outlet air temperature. Typical outcomes of the model are specific work (w), refrigerating effect (q), and vapor-compression system coefficient of performance (COP).

It is shown that with evaporative cooling before condenser, refrigerating effect increases while specific work decreases, which results in an increasing COP. According to the results, with the conditions of outdoor air temperatures of 26.7, 29.4, 32.2, 35 ℃ (80, 85, 90, 95°F) and relative humidities of 40%, 50%, 60%, 70%, 80% over a range of assumed evaporator exit air temperatures of 7.2, 10, 12.8℃ (45, 50, 55°F) with a typical compressor efficiency of 80%, the highest benefit of COP percentage difference with R410A can reach as much as 38% by taking advantage of internal water.

The final result illustrated that, in most humid climate areas (especially when RH higher than 70%), condensate water is sufficient to precool air to wet-bulb temperature while in dry/moderate humid region areas, external water is necessary to make a supplement to get 100% evaporative cooling effect.

The simulation result revealed that the COP percentage difference increase with boosting outdoor air temperature and decreasing Taeo (supply temperature) by taking advantage of internal condensate water. Also, the cycle was found to be most effective when RH within 50%-70%. Thus, it is recommended to use the condensate water cycle in hot and moderate humid (RH within 50%--70%) region.

However, COP percentage difference increase with boosting outdoor air temperature, rising Taeo (supply air temperature) and decreasing relative humidity by taking advantage of the total water. Therefore, it is recommended to use the total water cycle in the hot and dry region while the expense of supplemental water expense should be considered.

5.2 Cooling and Dehumidifying Outdoor Air Efficiency with a DOAS Vapor Compression Cycle Reconfigured with an HRV or ERV (B1 and B2)

Reducing energy consumption in refrigeration and air-conditioning system used in industrial, commercial and residential applications is both an ongoing and major concern, especially when one considers that 40% of the energy use in the U.S is associated with building energy. A dedicated outdoor air system (DOAS), decouples the HVAC sensible/latent load by separating outdoor air and return air into two HVAC systems, has become more and more popular in both residential and commercial buildings. This paper investigates performance limits for a range of outdoor air conditions of DOAS (dedicated outdoor/outside air system) incorporating HRVs (heat recovery ventilator) or ERVs (energy recovery ventilator) installed upstream of the air entering the evaporator. By using heat recovery/energy recovery between the incoming fresh outdoor air and exhaust room air, the dry-bulb temperature of air entering a vapor-compression cooling system, specifically the evaporator, decreases while the humidity ratio remains either constant or else decreases. This energy performance of a vapor-compression refrigeration system reconfigured with an HRV or ERV before the evaporator was investigated for a wide range of outdoor temperatures and humidity conditions representing all U.S climate zones.

It is shown that by using heat recovery (e.g. sensible heat) or energy recovery (e.g. latent heat) of outdoor air before it enters the evaporator, the overall refrigeration cooling effect increases,

which includes the HRV and ERV, while the compressor specific work remains constant, resulting in an increasing COP, defined as the ratio of refrigerating effect (cooling capacity) and compression work. Specifically, by using the exhaust air from buildings to precool, using an HRV, the incoming outdoor air entering the evaporator, the highest percentage increase in COP, with R410A as the working fluid can be as much as 25%. Similarly, by using the exhaust air from buildings to precool and pre-dehumidify, using an ERV, the incoming outdoor air entering the evaporator then increase in COP can reach as much as more than 100%. However, at dry and moderate temperature climate zones, systems reconfigured with HRVs perform enough well, and the added capital costs of an ERV may not be beneficial, with the focus of this study being to quantify the DOAS performance for different climate zones.

5.2.1 HRV ERV Definition

Air-to-air energy recovery is the process of recovering heat or/and moisture between airstreams at different temperatures and humidities. This process is essential in maintaining acceptable indoor air quality (IAQ) while maintaining low energy costs and reducing overall energy consumption. Energy can be recovered either by its sensible (temperature only) or latent (moisture) form, or combination of both from multiple sources. Units for extracting sensible energy are called sensible heat exchange devices or heat recovery ventilators (HRVs). Devices that transfer both heat and moisture are known as energy or enthalpy devices or energy recovery ventilators (ERVs). HRVs and ERVs are available for commercial and industrial applications as well as for residential and small-scale commercial uses. Types of ERVs include fixed-plate heat exchangers, rotary wheels, heat pipes, runaround loops, thermosiphons, and twin-tower enthalpy

recovery loops. In energy recovery ventilators, effectiveness refers to the ratio of actual energy or moisture recovered to the maximum possible amount of energy and moisture that can be recovered.

One such approach investigated herein for reducing energy consumptions and operating costs is to modify or reconfigure a typical vapor-compression cycle that is made up of the four major components, namely an evaporator, a compressor, a condenser, and a thermal expansion valve, by modifying the air-side of the evaporator. Specifically, a heat recovery ventilator or energy recovery ventilator is added on the air-side before the evaporator. By using heat recovery/energy recovery ventilators between the incoming fresh outdoor air and exhaust room air, the dry-bulb temperature of air entering the evaporator decreases while the relative humidity remains constant/decreasing, which in turn increase the refrigerating effect and lower the compressor work, finally COP increases.

The focus of the study presented here is to compare the performance of the above vapor-compression cooling system before and after it is modified to utilize HRV or ERV. This comparison is based on simulating both the typical system and the system after being reconfigured with HRV or ERV to reduce the air-side temperature. The performance variable of interest in this study in the refrigeration system coefficient of performance (COP), and differences are expected for the three scenarios of interest that are distinguished from each other either a typical system (scenario A) or a system with HRV before evaporator (scenario B1), or a system with ERV before evaporator (scenario B2), the relative performance value of COP of these three scenarios vary with the outdoor air conditions.

5.2.2 DOAS

For this particular study, it is assumed a dedicated outdoor air system (DOAS) so that the outdoor air is both the heat source and heat sink, meaning that energy is removed in the vapor-

compression system evaporator from outdoor air as the air is dehumidified and cooled and then this energy plus compressor work rejected in the vapor compression system condenser to the same outdoor air.

The above scenario is used in the practical application as noted is commonly called a dedicated outdoor air system (DOAS), which has become more and more popular in both residential and commercial buildings. DOAS in this article and its simplest terms is defined as: “before it enters the building, the outdoor air is conditioned separately from the return air.” By separating outdoor air and return air to two HVAC systems, a DOAS effectively separates handling the sensible load and latent load. The outdoor air HVAC unit, which is distinguished from the return-air HVAC unit, is used to remove the latent load to control humidity and remove part of the sensible load to produce a comfort temperature simultaneously while the return-air HVAC unit is used to remove the sensible load to produce a comfortable temperature. Decoupling the sensible/latent load after a reasonable approach because the problems associated with controlling building humidity in most climate zones where cooling predominates are almost always related to supplying fresh outdoor ventilation air, with one possible exception being low humidity region such as the southwest of the US, which typically are not densely populated.

The benefits of DOAS are obvious: easier to control humidity, more accurate delivery of ventilation air quantity, increasing energy efficiency and providing designers a flexible choice of HVAC components. It would appear that a DOAS setup provides one of the best opportunities for achieving an energy saving by using the proposed reconfiguration of HRV or ERV upstream of the reconfigured system evaporator. As a final note, the theoretical analysis and system performance evaluation are simplified if only one set of conditions, which is achieved by the DOAS representing both the high and low side air, are assumed rather than two sets.

5.2.3 System Description

5.2.3.1 Scenario B1. System Reconfigured with HRV

The scenario A typical vapor-compression cycle is reconfigured with an HRV before the evaporator, as shown in Figure 82. As stated in the second law of thermodynamics, heat energy always transfers from a region of high temperature to one of low temperature. Specifically, as the outdoor air temperature is higher than that of exhaust air from building, heat energy transfer from outdoor air to exhaust air from building through HRV, resulting in a lower temperature entering the evaporator. As only sensible heat recovery occurs, outdoor air relative humidity remains constant during this process. In the condenser, heat transfer occurs from the refrigerant to the air, outdoor air without a humidity ratio change being exhausted to the environment, which can be seen on the right side of Figure 83.

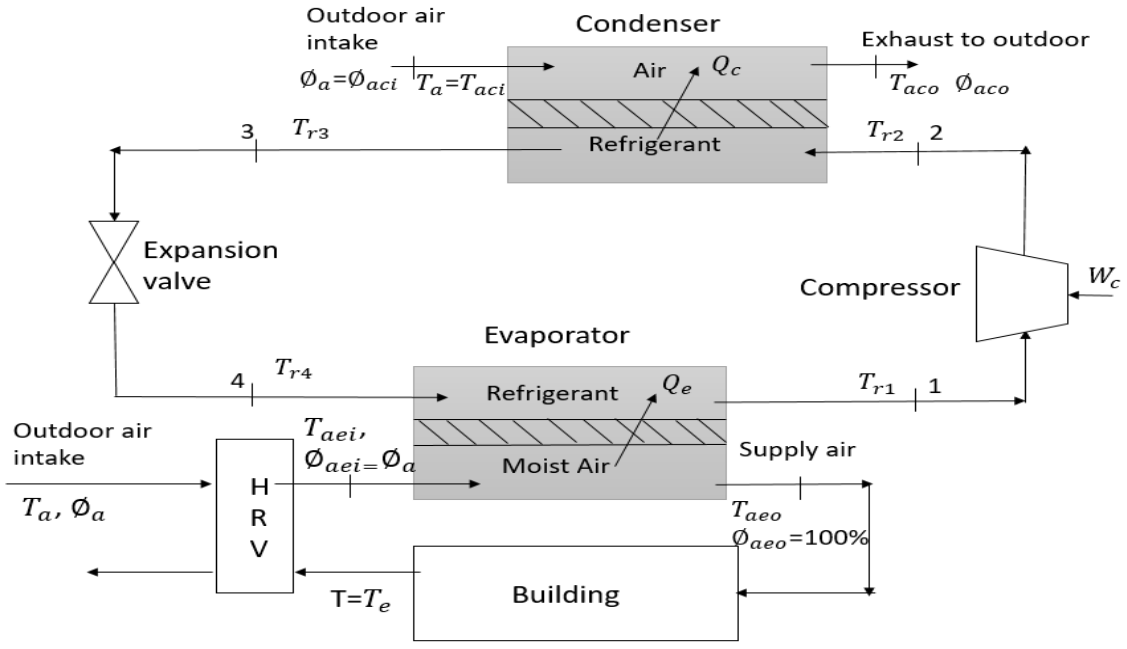

Figure 82 Schematic of the vapor-compression refrigeration cycles with HRV

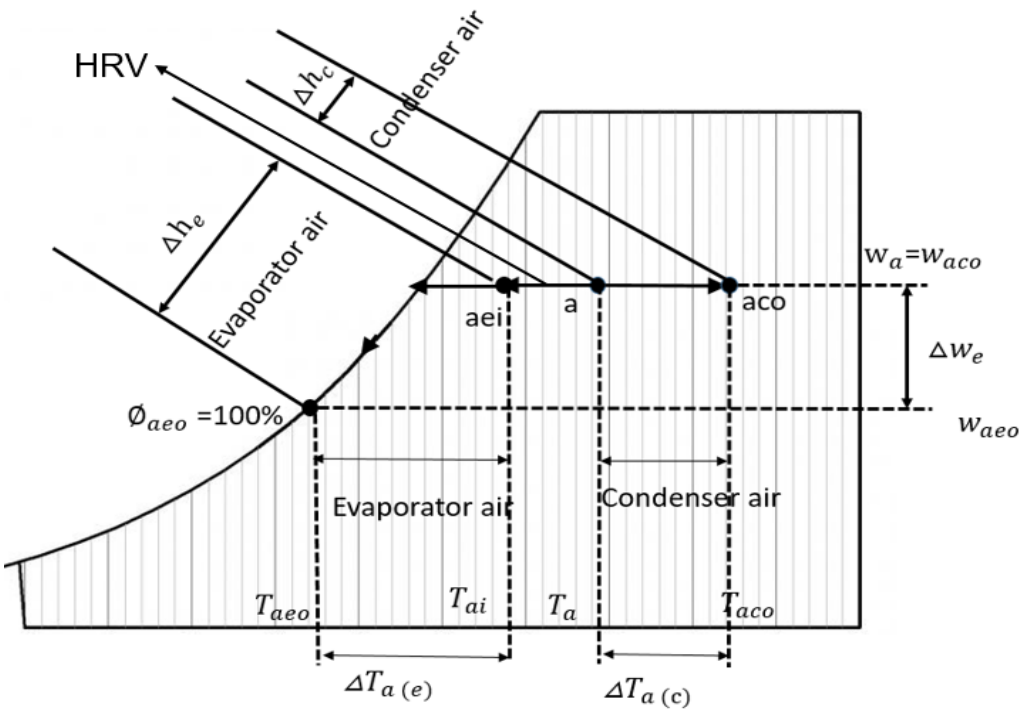

Figure 83 Psychrometric chart of air in the evaporator and condenser (Point state a: Outdoor air into the HRV before the evaporator and condenser)

5.2.3.2 Scenario B2. System Reconfigured with ERV Before the Evaporator

Scenario B2, differed from scenario B1, with ERV before the condenser, is shown in Figure 84. The second law can be extended to say that mass transfer always occurs from a region of high vapor pressure to one of low vapor pressure. The ERV facilitates this transfer across a separating wall made of a material that conducts heat and is permeable to water vapor. Moisture is transferred when there is a difference in vapor pressure between the two airstreams. Specifically, as the outdoor air temperature is higher than that of exhaust air from building, heat energy transfer from outdoor air to exhaust air from building through HRV, resulting in a lower temperature entering the evaporator. On top of that, the latent due to the difference in water vapor pressures is generated and results in a humidity decrease of air entering the evaporator, as shown on the left side of Figure

85. In the condenser, heat transfer occurs from the refrigerant to the air, outdoor air without a humidity ratio change being exhausted to the environment, which can be seen on the right side of Figure 85.

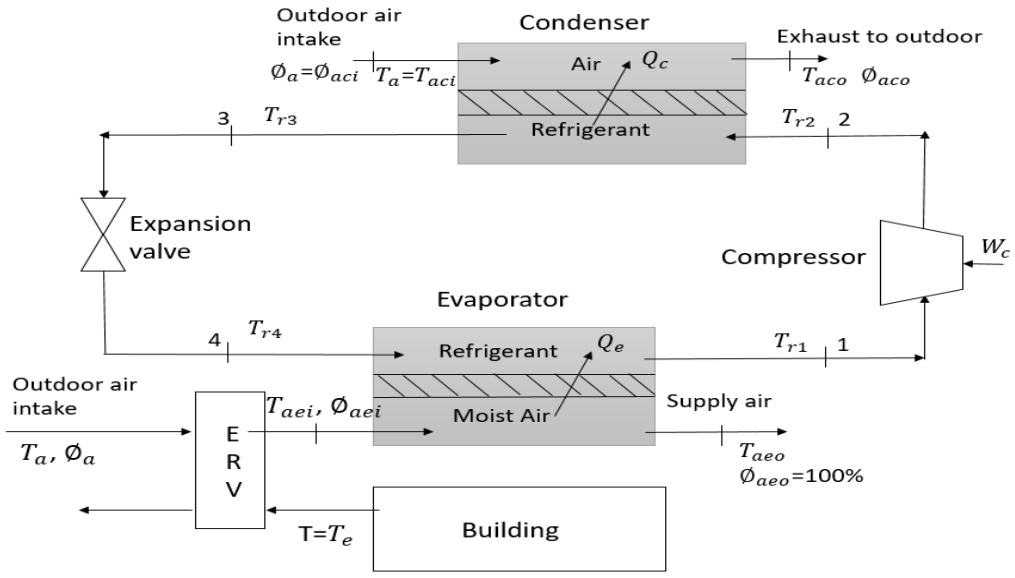

Figure 84 Schematic of the vapor-compression refrigeration cycles with ERV before the evaporator

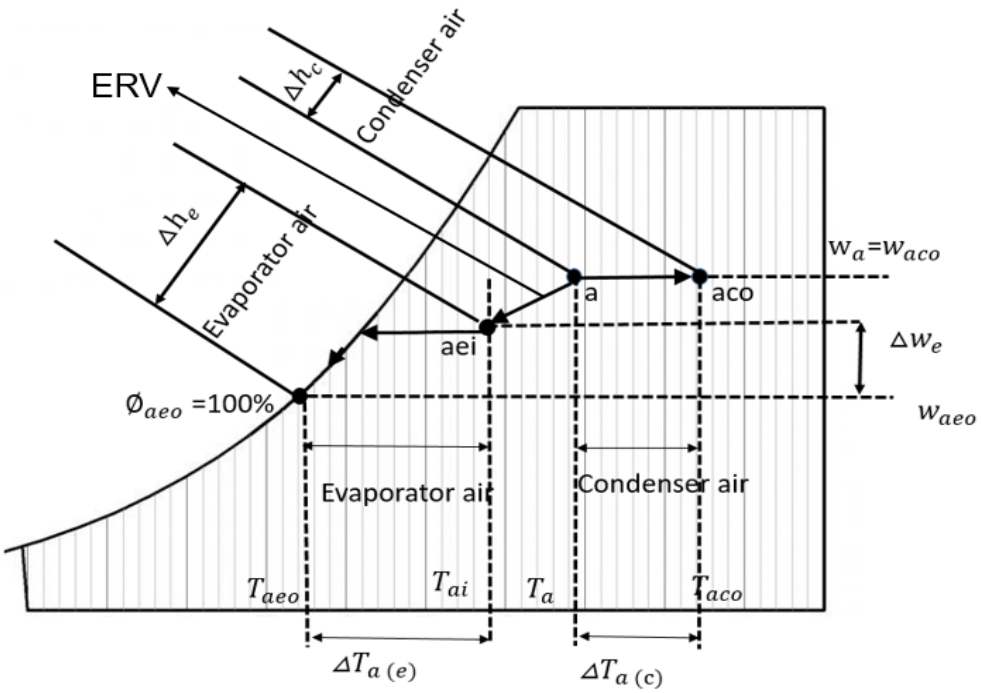

Figure 85 Psychrometric chart of air in the evaporator and condenser for Scenario B2

5.2.4 Model Development and Formulation

In order to calculate the important refrigerant cycle performance parameters, such as the refrigeration cooling effect, the compressor work, and COP, it is necessary to specify or determine the thermodynamic state properties of the cooling refrigerant at each point in the vapor compression cycle. To accomplish this task, it is also necessary to know the state properties and flow conditions of the moist air entering and leaving the evaporator and condenser, along with the condition of the condensate draining from the air-side of the evaporator. Therefore, determining the performance parameters, such as COP, that will allow for evaluating the effect of the upstream evaporator requires developing, deriving, and solving four separate models, namely: 1) moist air properties 2) heat recovery and/or energy recovery process 3) condensing refrigerant temperature calculation 4) vapor-compression refrigeration cycle. Process 1, 3 and 4 are the same as

Reconfigured System A1, thus process two heat recovery and/or energy recovery process is the focus of this section.

5.2.4.1 Sensible and Latent Effectiveness

5.2.4.1.1 Sensible Heat Transfer

On a typical summer day, supply air at temperature, humidity, or enthalpy h_a and mass flow rate m_a enters the ERV, while exhaust air from the conditioned space enters at conditions h_e and m_e. Because conditions at h_e are lower than that of h_a, heat and mass transfer from the supply airstream to the exhaust airstream because of differences in temperature and vapor pressures across the separating wall. Consequently, the supply air exit properties decrease, while those of the exhaust air increase. Exit properties of these two streams can be estimated, knowing the flow rates and the effectiveness of the heat exchanger.

According to ASHRAE Standard 84, effectiveness is defined as

$$\varepsilon=\frac{Actual\ transfer\ of\ moisture\ or\ energy}{Maximum\ possible\ transfer\ between\ airstreams} \tag{93}$$

From Figure 86, assuming no water vapor condensation in the HRV, the sensible effectiveness $\varepsilon_s$of a heat recovery ventilator is given as,

$$\varepsilon_s = \frac{q_s}{q_{s,max}}=\frac{m_a C_{pa}(T_a-T_{aei})}{C_{min}(T_a-T_e)} \tag{94}$$

As the mass flow rate and heat capacity of exhaust air and supply air are quite similar, the above equation can be simplified as

$$\varepsilon_s=\frac{T_a-T_{aei}}{T_a-T_e} \tag{95}$$

$$T_{aei} = T_a - \varepsilon_s(T_a - T_e) \tag{96}$$

where q_s=sensible heat transfer rate, But/h,

$q_{s,max}$= maximum sensible heat transfer rate, Btu/h

ε_s=sensible effectiveness

T_a=Outdoor air dry-bulb temperature

T_e=inlet exhaust dry-bulb temperature

T_{aei}=dry-bulb temperature entering the evaporator

5.2.4.2 Latent Heat Transfer

The ERV allows the transfer of both sensible and latent heat, the latter due to the difference in water vapor pressures between the airstreams. From Figure 86, assuming no condensation in the ERV, the latent effectiveness ε_L of an energy recovery ventilator is given as,

$$\varepsilon_L = \frac{q_L}{q_{L,max}} = \frac{m_a h_{fg}(w_a - w_{aei})}{m_{min} h_{fg}(w_a - w_e)} \quad (97)$$

Because we assume that the mass flow rate is the same for exhaust air and supply air and the enthalpy of vaporization can be dropped out from numerator and denominator, the above equation can be rewritten as

$$\varepsilon_L = \frac{w_a - w_{aei}}{w_a - w_e} \quad (98)$$

$$w_{aei} = w_a - \varepsilon_L(w_a - w_e) \quad (99)$$

where q_L=latent heat transfer rate, But/h,

$q_{L,max}$= maximum latent heat transfer rate, Btu/h

ε_L=latent effectiveness

w_a=Outdoor air humidity ratio

w_e=inlet exhaust humidity ratio

T_{aei}=air humidity ratio entering the evaporator

h_{fg} =enthalpy of vaporization, Btu/lb

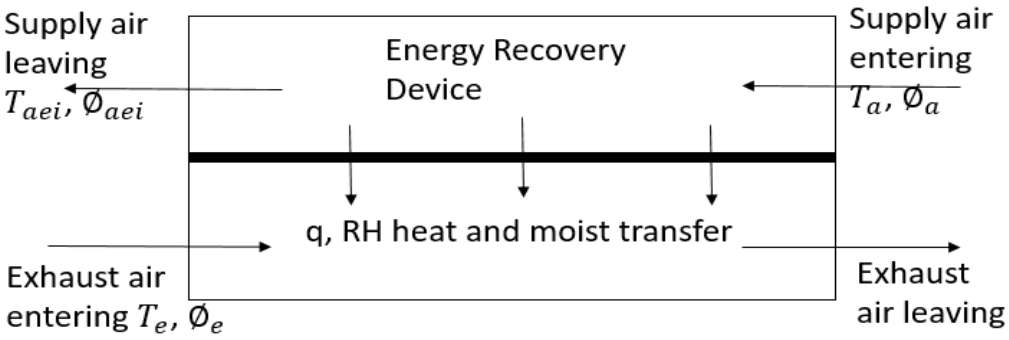

Figure 86 Airstream convection---heat and moist transfer

5.2.4.3 New COP Definition

The coefficient of Performance Coefficient of performance (COP), defined as the ratio of useful cooling load to work input, is often used as a measure of cycle performance and is the parameter of interest in terms of evaluating and analyzing the effect of adding the HRV or ERV before evaporator. For the vapor-compression cycle in this study, an assumption is made that the compressor work is the only input and the cooling capacity of evaporator and cooling load of HRV/ERV are the total heat transfer. Therefore, the new defining equation is shown as follows,

$$COP_{new}=\frac{\mathrm{Q_{useful}}}{\mathrm{W_{compressor}}} \tag{100}$$

$$Q_{useful}=Q_e + Q_{recovery} \tag{101}$$

Based on the old definition of COP described previously and new definition listed above, a relationship between new and old definition of COP is derived as follows,

$$COP_{new} = COP_{old}\ (1+\frac{Q_{recovery}}{Q_e}) \tag{102}$$

$$Q_e=m_{ae}\Delta h_e=m_{ae}(h_{aei} - h_{aeo}) \tag{103}$$

where

$$Q_{recovery}=m_{ae}(h_a - h_{aei}) \quad (104)$$

5.2.5 Simulation Input and Output

A simulation comprehensive model was developed and programmed in Engineering Equation Solver 2016 for a vapor-compression conditioning system comprising air-to-refrigerant evaporator and condenser, a compressor, a thermal expansion valve and evaporative cooler before condenser. The possible parameters affecting final results of the model such as 1) outdoor air temperature (T_a) 2) outdoor air relative humidity ($\emptyset a$) 3) air temperature exiting evaporator (T_{aeo}). Typical outcomes of the model are 1) specific work (w) 2) refrigerating effect (q) 3) vapor-compression system coefficient of performance (COP).

5.2.6 Simulation Data Set-up and Overview

In this article, outdoor air temperatures of 26.7, 29.4, 32.2, 35 ℃ (80, 85, 90, 95℉) and relative humidities of 40%, 50%, 60%, 70%, 80% over a range of assumed evaporator exit air temperatures of 7.2, 10, 12.8℃ (45, 50, 55℉) with a typical compressor efficiency of 80%.HRV or ERV effectiveness is 60%.

5.2.7 Results and Analysis

When selecting a heat or energy recovery device, the indoor and outdoor design conditions and yearly weather data are significant because enthalpy differences between the outdoor and indoor air govern the energy recovery rate.

5.2.7.1 HRV Limitations

HRVs are suitable when outdoor air humidity is low and latent space loads are high for most of the year, and also for use with swimming pools, chemical exhaust, paint booths, and indirect evaporative coolers.

Furthermore, condensation or frosting does not occur or is negligible for HRV, which is nearly true for larger commercial HRV applications. Note that HRV only allows transfer of sensible heat energy associated with heat transfer because of the temperature difference between the airstreams. Since for the case without HRV or ERV, a wide range of data is set as: outdoor air condition is set as: 26.7, 29.4, 32.2, 35 ℃ (80, 85, 90, 95°F); RH=40%, 50%, 60% 70%, 80%; Taeo=7.2, 10, 12.8 ℃(45, 50, 55°F); indoor air condition (exhaust air) is set as: 23.9℃ (75°F), RH=50%, which is based on the second law. Thus, it is necessary to check if all the data is under the condition that no condensation occurred. For the HRV limitation study, ERV/HRV effectiveness range from 60%-100%, namely 60%, 80% and 100%.

It is concluded that if the temperature after heat recovery decreased below dew point temperature, condensation occurred. From table 15, it is found that for some cases condensation occurred (the ones filled in with pink). Thus it is necessary to calculate the boundary of critical relative humidity to the corresponding outdoor air temperature (26.7, 29.4, 32.2, 35 ℃ (80, 85, 90, 95°F)), which is listed in table 16.

According to Figure 87, when the points with relative humidity are below the critical relative humidity curve, no condensation occurred; otherwise, condensation occurred. With the increasing HRV effectiveness, the limitation is becoming narrower.

Of special note, according to the definition of ERV, it is assumed no condensation occurred as well, and the humidity ratio of incoming air should be greater than that of exhaust air. For this study, all the conditions worked. Thus there is no need to discuss the limitation of ERV for this study.

Table 15 Critical temperatures under different conditions

Tout	RH	T aeo	T dew	T indoor	T 2ae 60%	Tae 80%	Tae 100%
80	0.4	45	53.43	75	77	76	75
80	0.5	45	59.62	75	77	76	75
80	0.6	45	64.81	75	77	76	75
80	0.7	45	69.29	75	77	76	75
80	0.8	45	73.24	75	77	76	75
80	0.4	50	53.43	75	77	76	75
80	0.5	50	59.62	75	77	76	75
80	0.6	50	64.81	75	77	76	75
80	0.7	50	69.29	75	77	76	75
80	0.8	50	73.24	75	77	76	75
80	0.4	55	53.43	75	77	76	75
80	0.5	55	59.62	75	77	76	75
80	0.6	55	64.81	75	77	76	75
80	0.7	55	69.29	75	77	76	75
80	0.8	55	73.24	75	77	76	75
85	0.4	45	57.89	75	79	77	75
85	0.5	45	64.2	75	79	77	75
85	0.6	45	69.5	75	79	77	75
85	0.7	45	74.07	75	79	77	75
85	0.8	45	78.1	75	79	77	75
85	0.4	50	57.89	75	79	77	75
85	0.5	50	64.2	75	79	77	75
85	0.6	50	69.5	75	79	77	75
85	0.7	50	74.07	75	79	77	75
85	0.8	50	78.1	75	79	77	75
85	0.4	55	57.89	75	79	77	75
85	0.5	55	64.2	75	79	77	75
85	0.6	55	69.5	75	79	77	75
85	0.7	55	74.07	75	79	77	75
85	0.8	55	78.1	75	79	77	75
90	0.4	45	62.34	75	81	78	75
90	0.5	45	68.78	75	81	78	75
90	0.6	45	74.18	75	81	78	75
90	0.7	45	78.84	75	81	78	75
90	0.8	45	82.96	75	81	78	75
90	0.4	50	62.34	75	81	78	75
90	0.5	50	68.78	75	81	78	75

Table 15 continued

Tout	RH	T aeo	T dew	T indoor	T 2ae 60%	Tae 80%	Tae 100%
90	0.6	50	74.18	75	81	78	75
90	0.7	50	78.84	75	81	78	75
90	0.8	50	82.96	75	81	78	75
90	0.4	55	62.34	75	81	78	75
90	0.5	55	68.78	75	81	78	75
90	0.6	55	74.18	75	81	78	75
90	0.7	55	78.84	75	81	78	75
90	0.8	55	82.96	75	81	78	75
95	0.4	45	66.78	75	83	79	75
95	0.5	45	73.35	75	83	79	75
95	0.6	45	78.86	75	83	79	75
95	0.7	45	83.62	75	83	79	75
95	0.8	45	87.82	75	83	79	75
95	0.4	50	66.78	75	83	79	75
95	0.5	50	73.35	75	83	79	75
95	0.6	50	78.86	75	83	79	75
95	0.7	50	83.62	75	83	79	75
95	0.8	50	87.82	75	83	79	75
95	0.4	55	66.78	75	83	79	75
95	0.5	55	73.35	75	83	79	75
95	0.6	55	78.86	75	83	79	75
95	0.7	55	83.62	75	83	79	75
95	0.8	55	87.82	75	83	79	75

Table 16 Critical relative humidities according to different outdoor temperatures

Tout (IP)	Tout (SI)	EF 60% RH	EF 80% RH	EF 100% RH
80	26.66667	0.9064	0.8769	0.8483
85	29.44444	0.8238	0.7715	0.722
90	32.22222	0.7509	0.6809	0.6166
95	35	0.6863	0.6028	0.5283

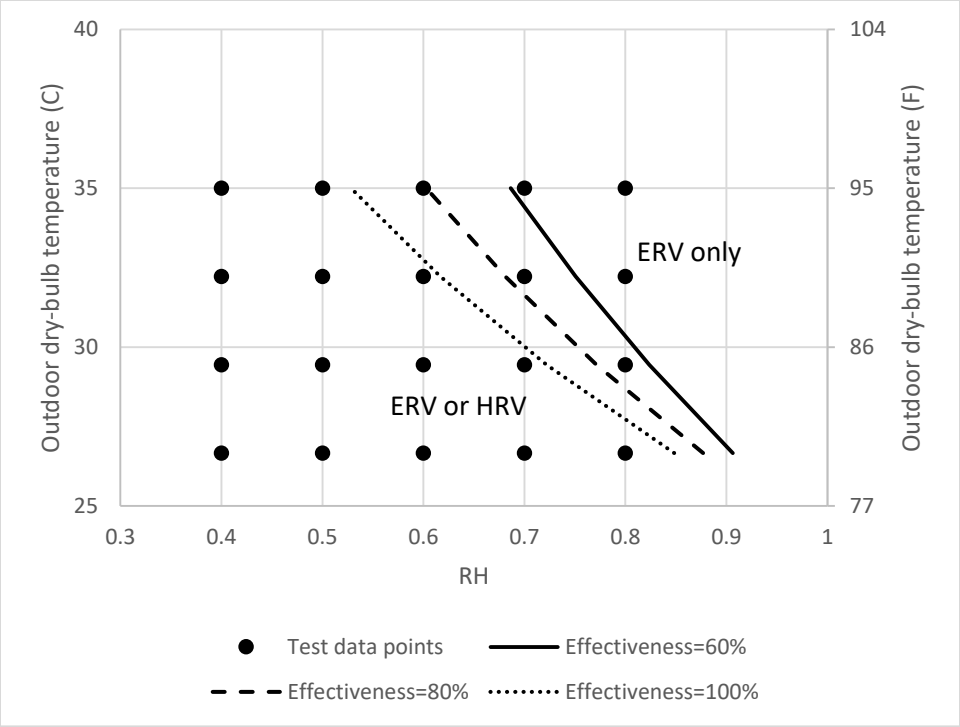

Figure 87 HRV limitation

5.2.7.2 Scenario B1 Compared with Scenario A (HRV compared with baseline)

5.2.7.2.1 COP Improvement Due to HRV Overview

When comparing scenario B1 (HRV) and B2 (ERV) with Scenario A (baseline system, only heat/energy recovery effectiveness of 60% is considered.

Figure 88 shows the relationship between COP with and without HRV with COP ranging from 1 to 10. This figure also illustrates that for most cases the improvement is within 20% and the highest improvement can reach 25%.

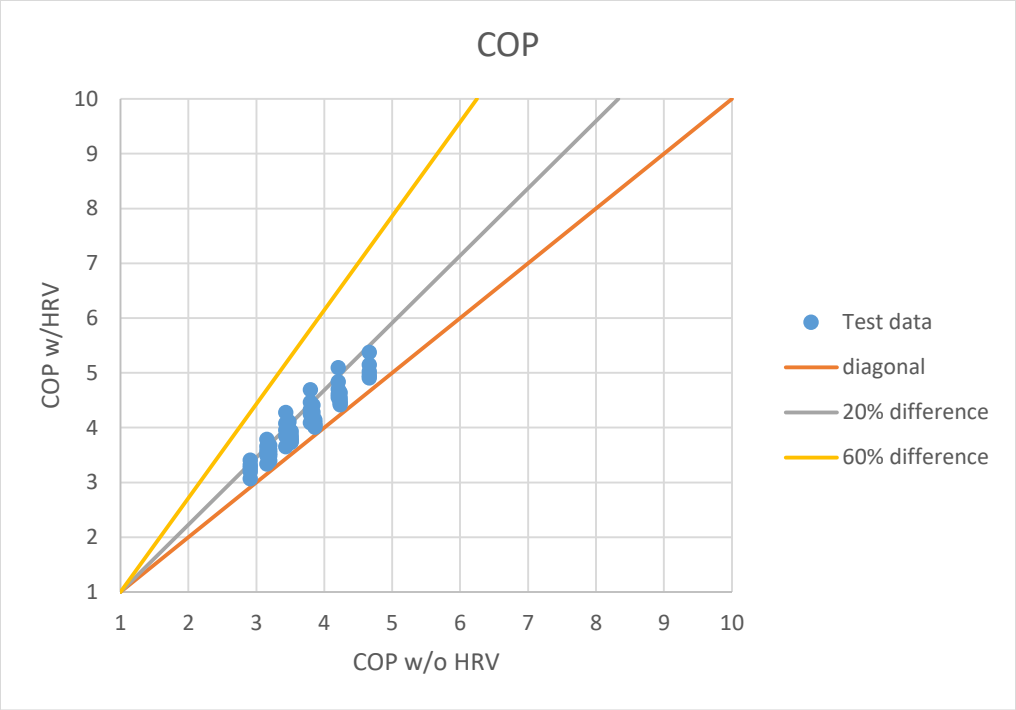

Figure 88 COP with/without HRV

5.2.7.2.2 Scenario B1 COP Overview

Figure 89 gives an overview of how reconfigured system B1 system performance related to three variables, namely ourdoor air temperatures, relative humidities and Taeo, and it further shows that COP slightly decreases with the increasing relative humidity. Figure 90, 91, 92 and 93 show how COP varies with different Taeo under the same outdoor air temperature, and it is observed that COP increases with the increasing Taeo. Figure 94, 94 and 96 show how COP varies with different outdoor air temperature under the same Taeo and these three plots illustrate that COP decreases with the increasing outdoor air temperature. The trend of COP varied with the three parameters is further summarized in Table 17.

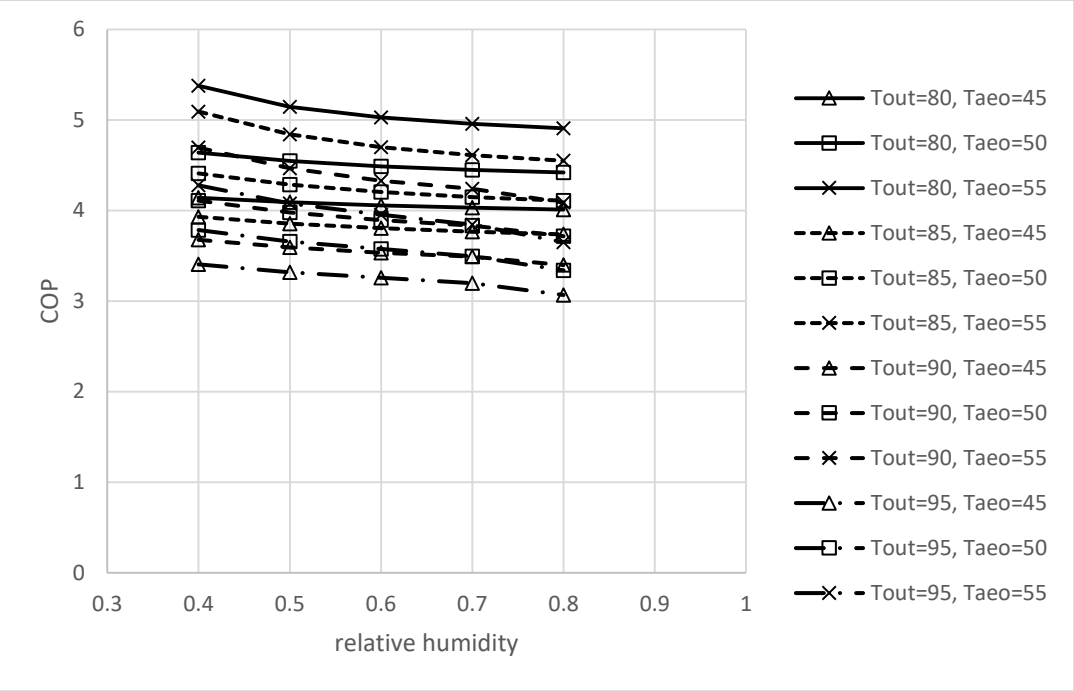

Figure 89 COP with HRV varied with relative humidity under different conditions

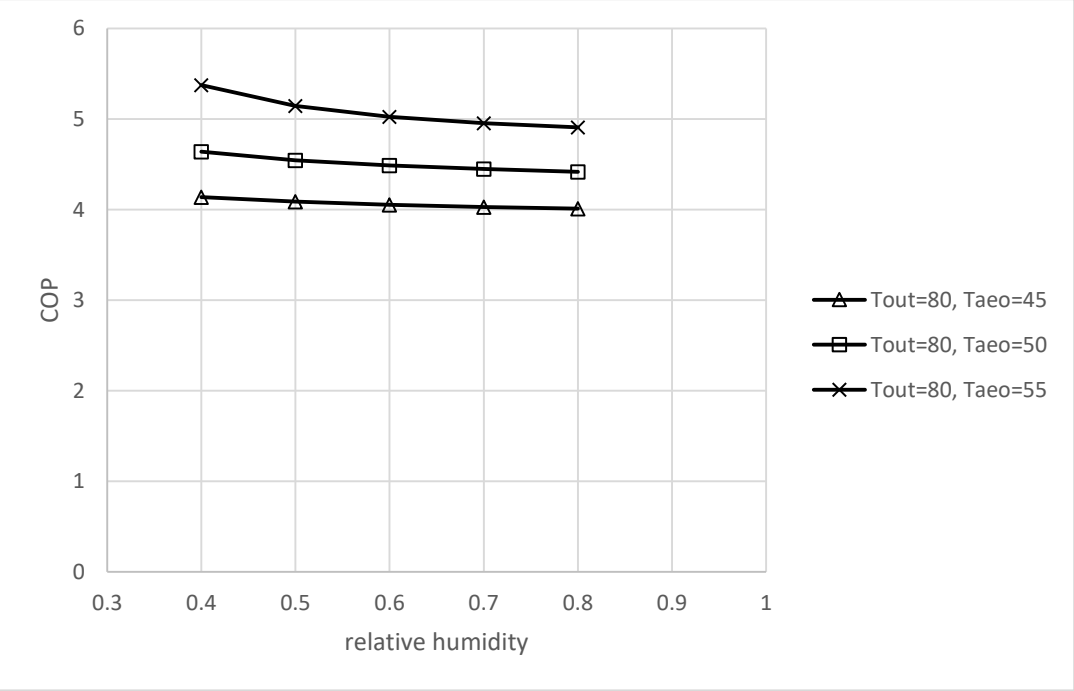

Figure 90 COP with HRV varied with relative humidity when Tout=80 °F

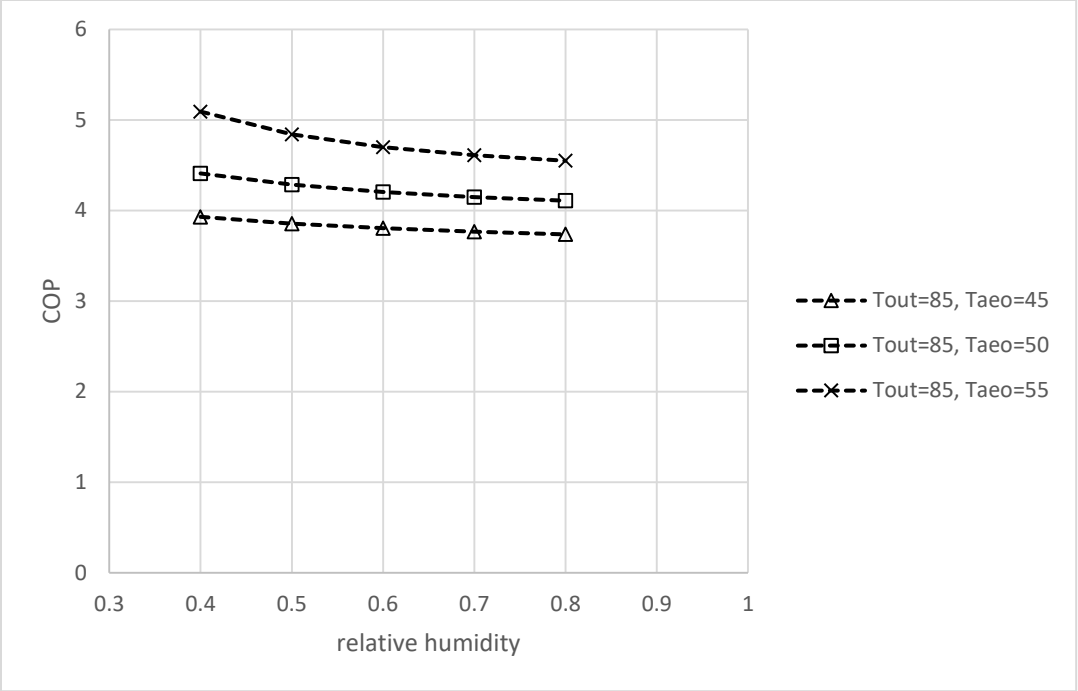

Figure 91 COP with HRV varied with relative humidity when Tout=85 °F

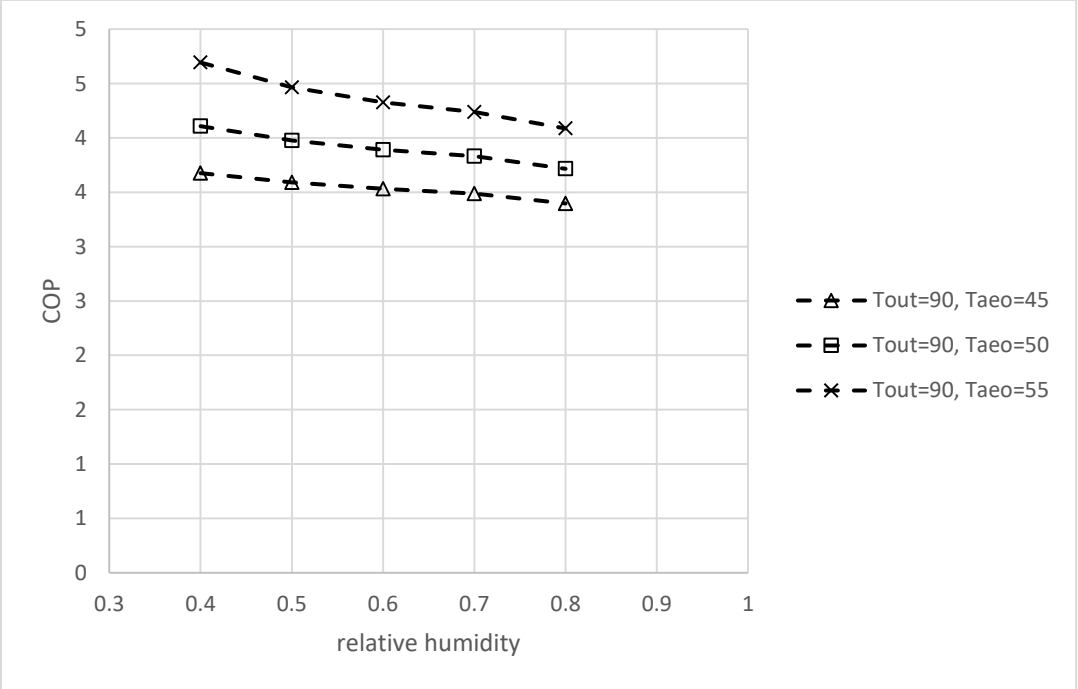

Figure 92 COP with HRV varied with relative humidity when Tout=90 °F

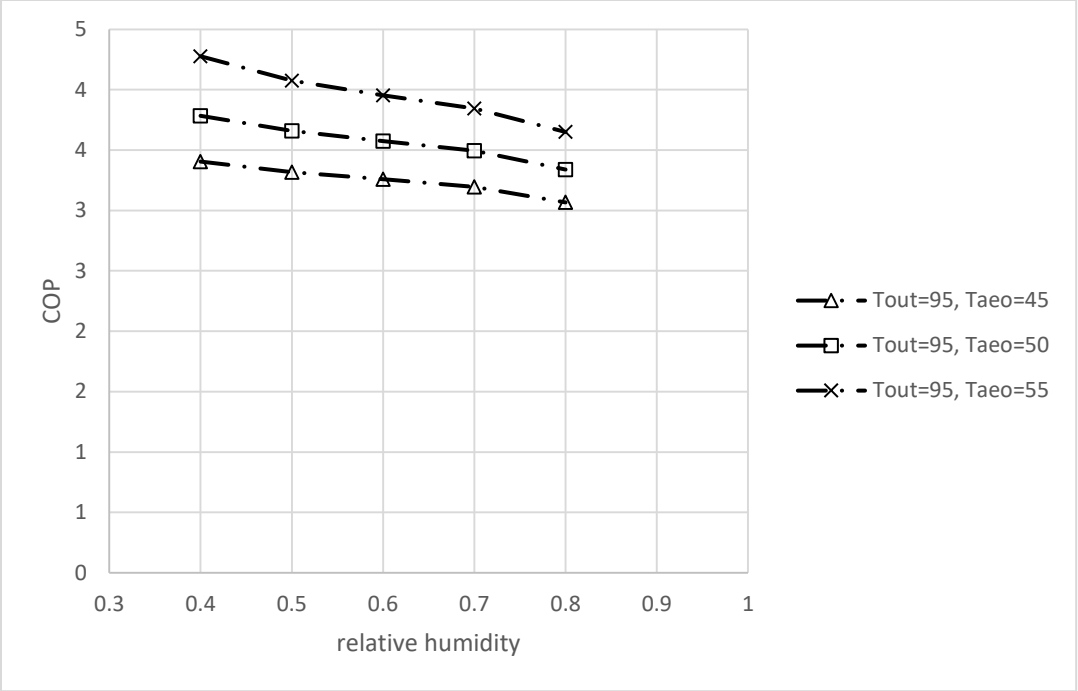

Figure 93 COP with HRV varied with relative humidity when Tout=95 ℉

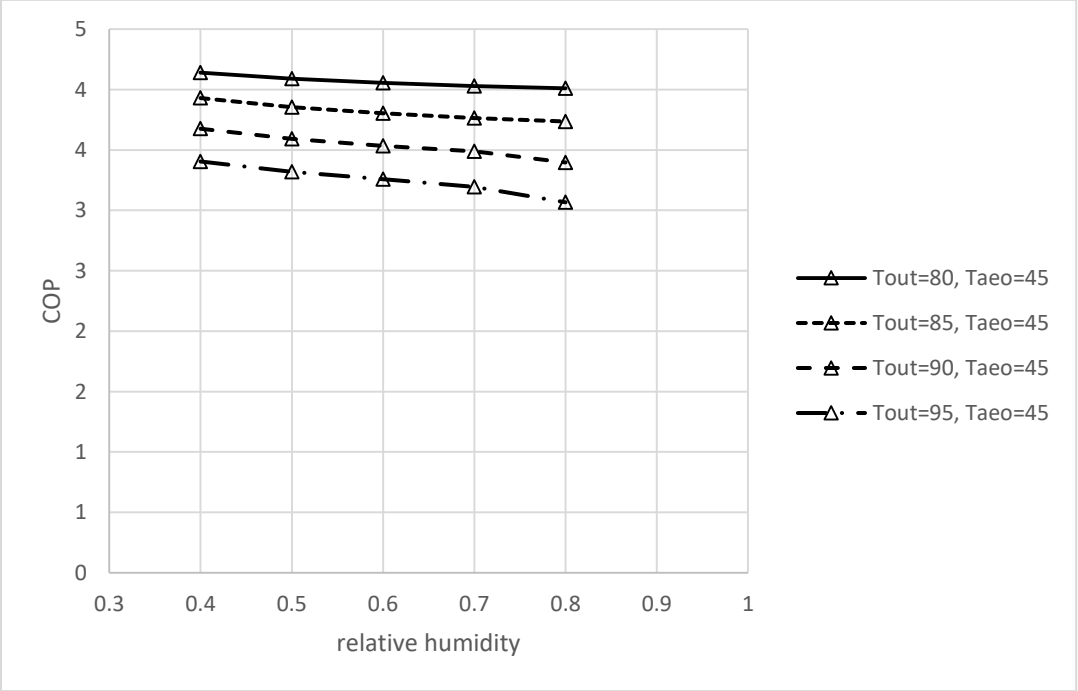

Figure 94 COP with HRV varied with relative humidity when Taeo=45 ℉

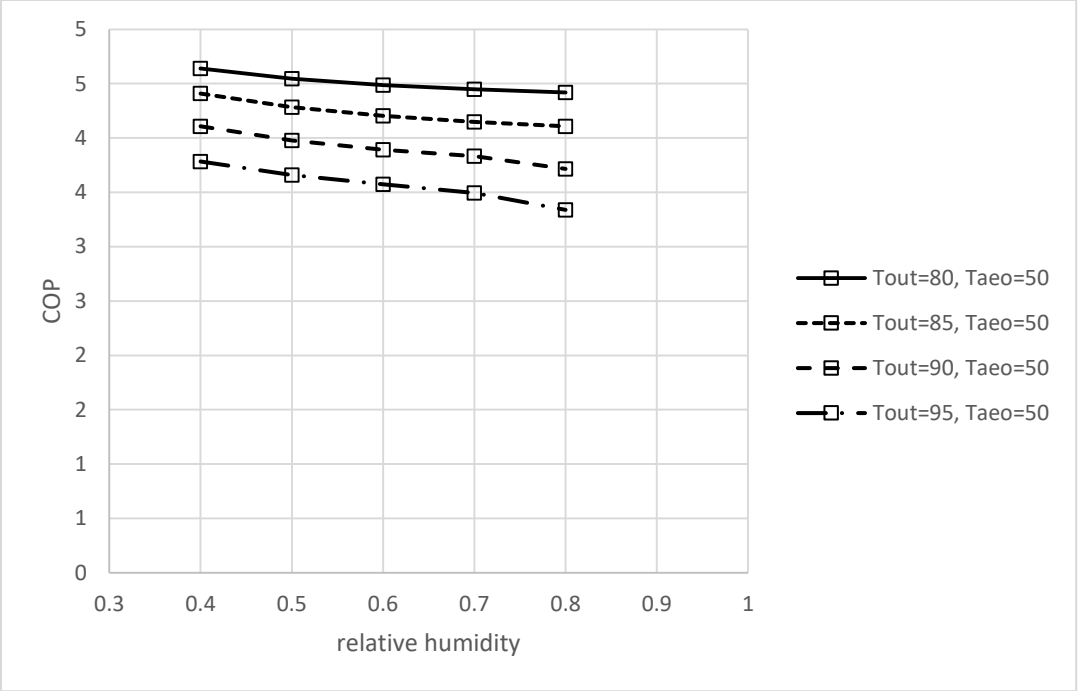

Figure 95 COP with HRV varied with relative humidity when Taeo=50 °F

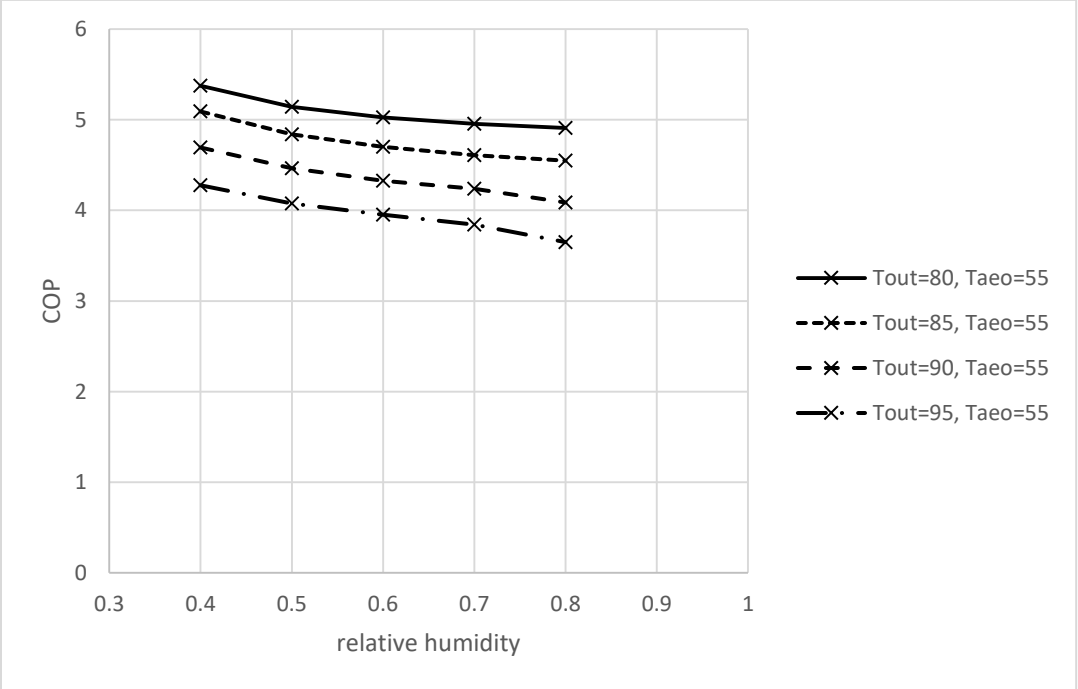

Figure 96 COP with HRV varied with relative humidity when Taeo=55 °F

Table 17 COP with HRV varied with Tout RH and Taeo

case	T_{out}	RH	T_{aeo}	COP with HRV
1	↑	→	→	↓
2	→	↑	→	↓
3	→	→	↑	↑

5.2.7.2.3 COP Enhancement Analysis (with HRV)

Figure 97 gives an overview of how percentage difference (reconfigured system B1 compared to baseline system A) related to the three variables, namely outdoor air temperatures, relative humidities and Taeo, and Figure 97 further shows that that COP percentage difference decrease with increasing relative humidity. Figure 98, 99, 100 and 101 show how COP percentage difference varies with different Taeo under the same outdoor air temperature, and it is indicated that COP percentage difference increase with the boosting Taeo at low relative humidity; when RH is over 70%, COP improvement is very similar for different Taeo. Figure 102, 103 and 104 show how COP percentage difference varies with different outdoor air temperature under the same Taeo and these three plots illustrate that COP percentage difference increase with the boosting outdoor air temperature when relative humidity is low; however, when RH is over 70%, COP improvement is very similar for different outdoor air temperatures. The trend of COP improvement varied with aforementioned three variables are summarized in Table 18.

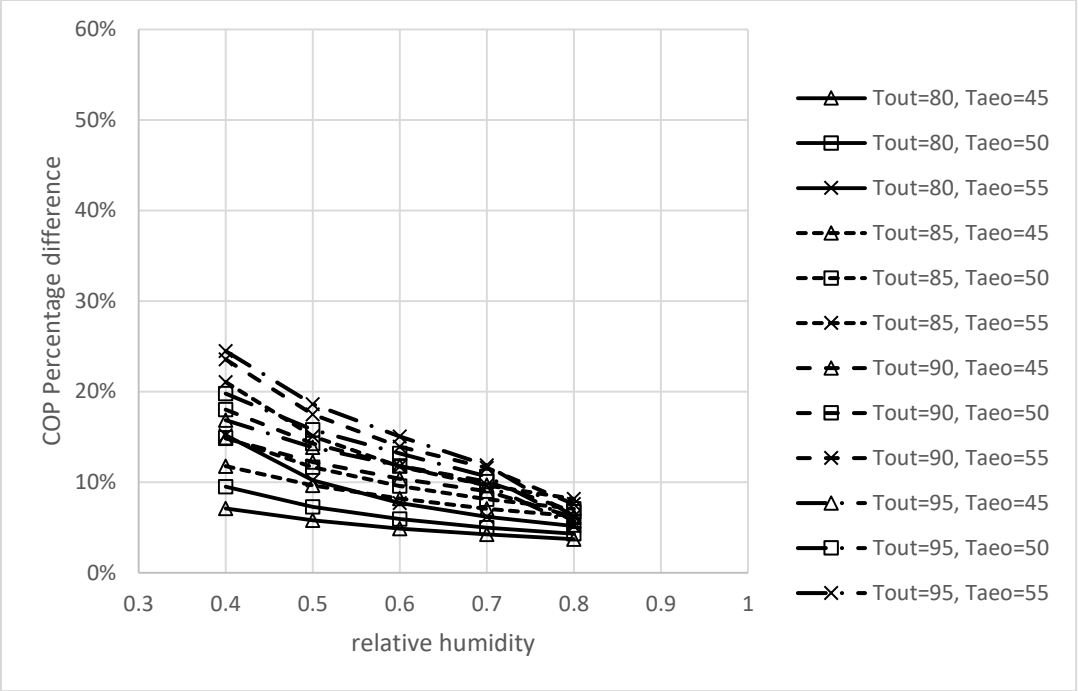

Figure 97 COP percentage difference (HRV over baseline) versus relative humidity under different conditions

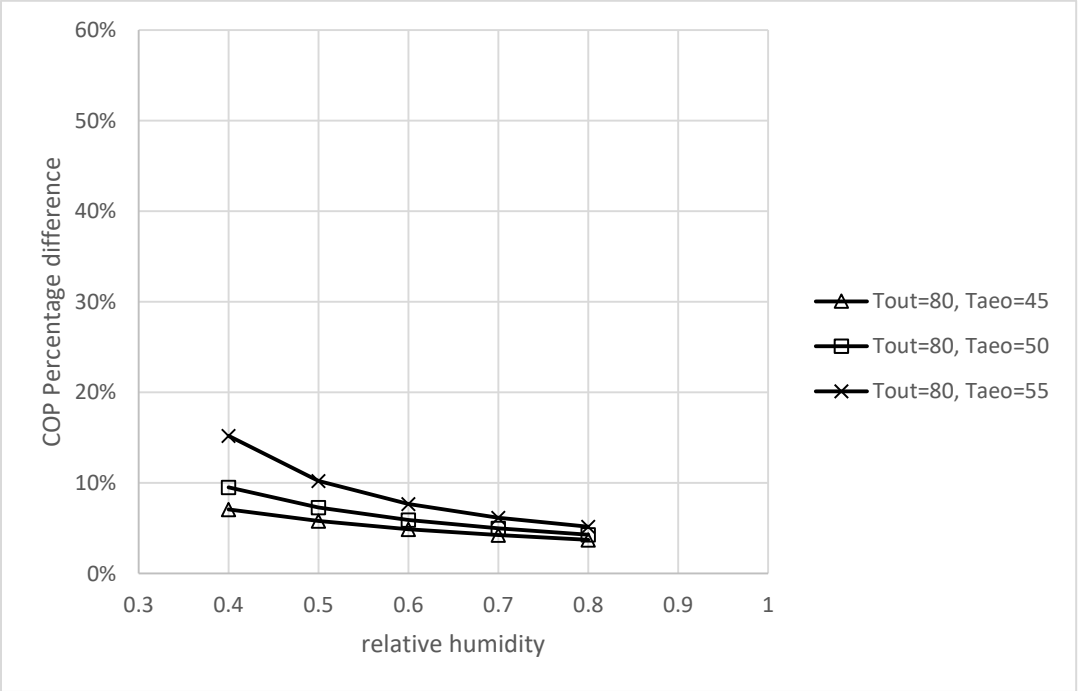

Figure 98 COP percentage difference (HRV over baseline) versus relative humidity when Tout=80°F

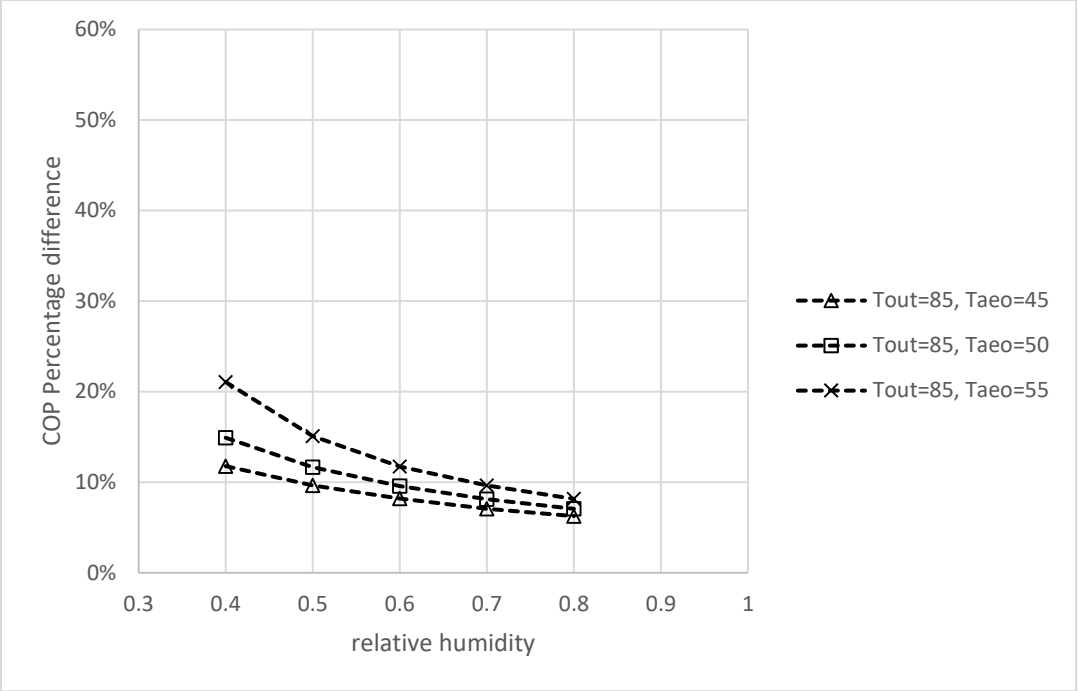

Figure 99 COP percentage difference (HRV over baseline) versus relative humidity when Tout=85°F

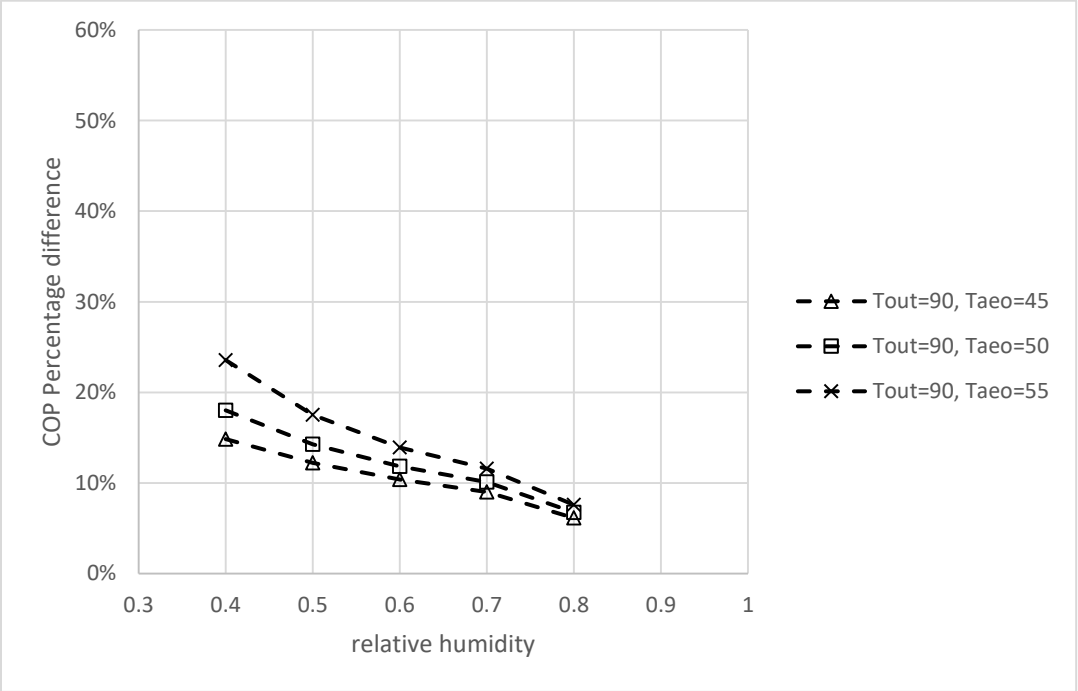

Figure 100 COP percentage difference (HRV over baseline) versus relative humidity when Tout=90°F

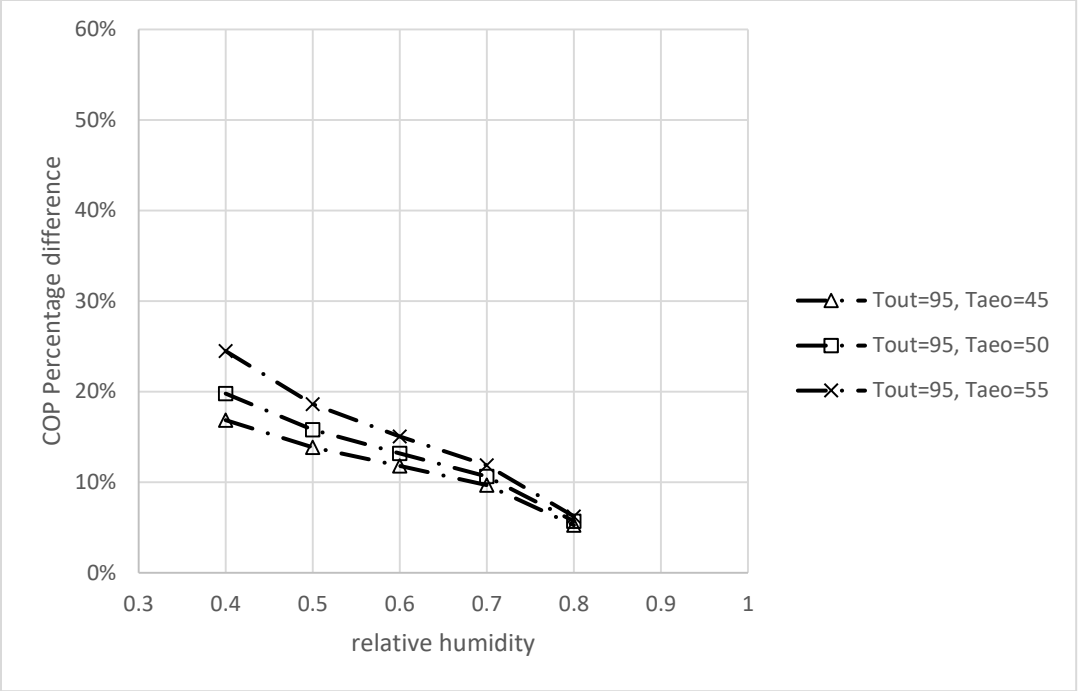

Figure 101 COP percentage difference (HRV over baseline) versus relative humidity when Tout=95°F

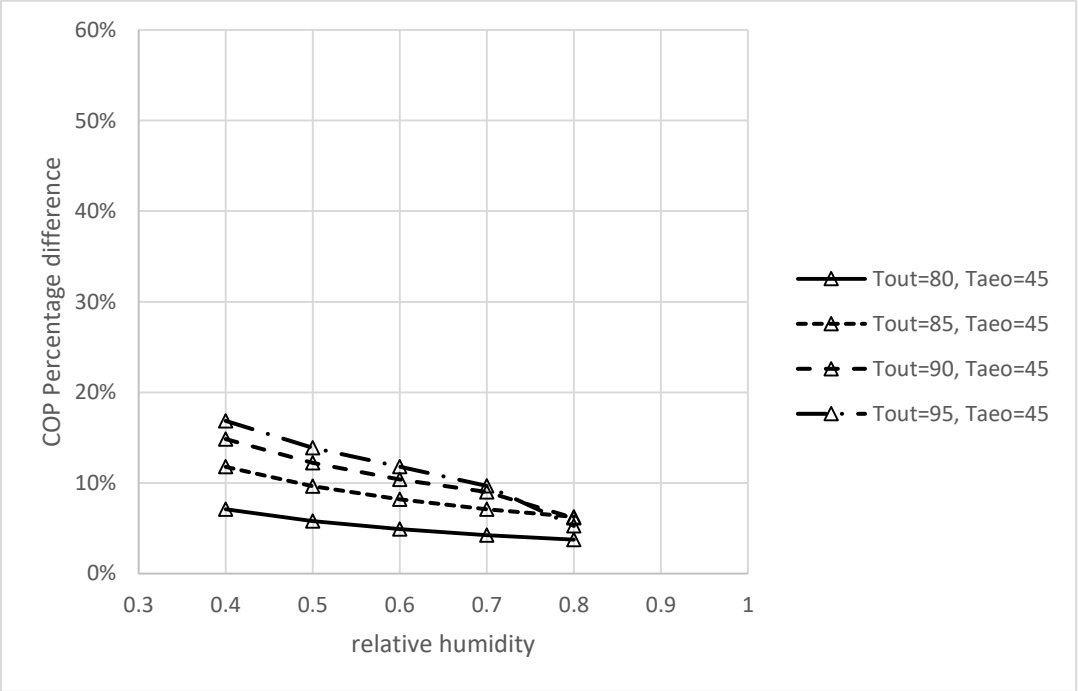

Figure 102 COP percentage difference (HRV over baseline) versus relative humidity when Taeo=45°F

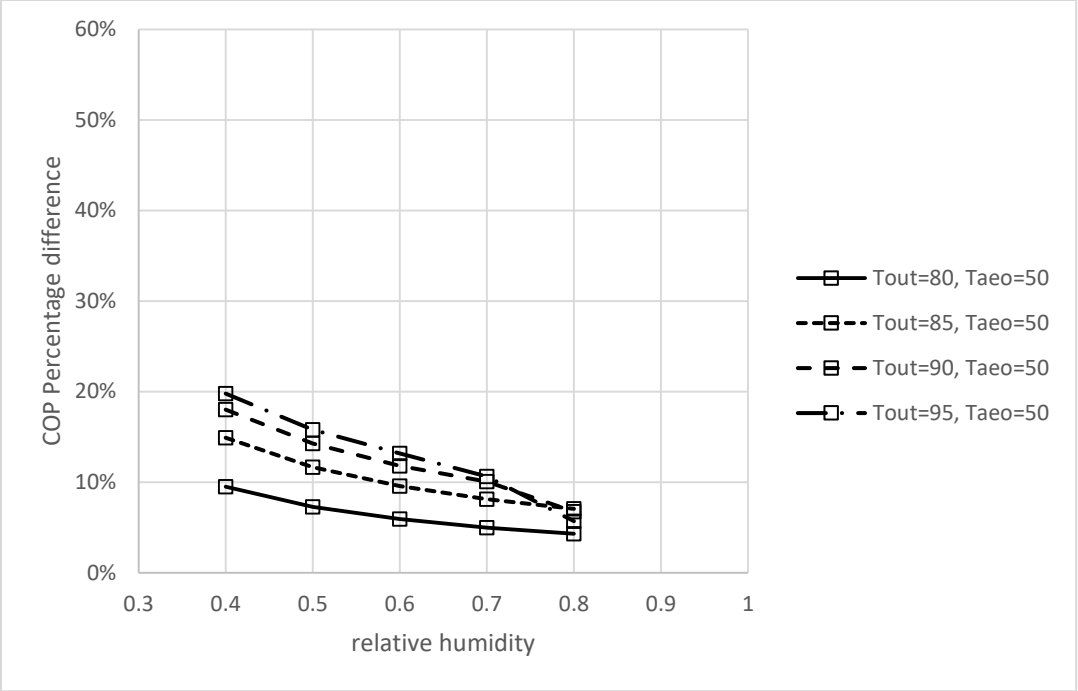

Figure 103 COP percentage difference (HRV over baseline) versus relative humidity when Taeo=50°F

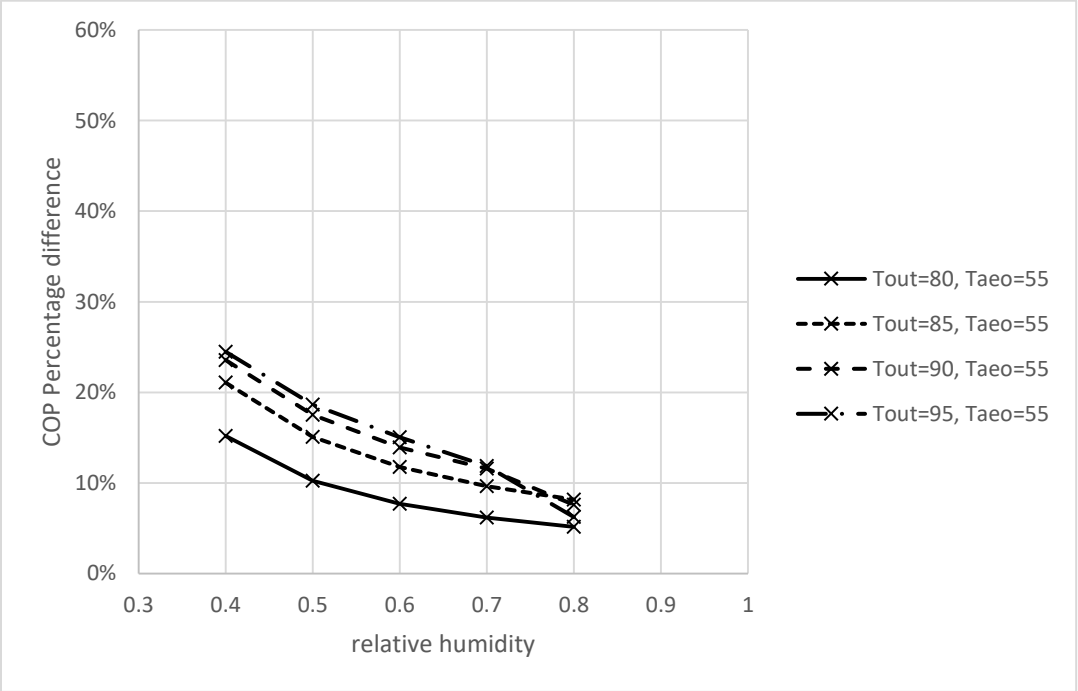

Figure 104 COP percentage difference (HRV over baseline) versus relative humidity when Taeo=50°F

Table 18 COP percentage difference (HRV over baseline) varied with Tout, RH, and Taeo

case	T_{out}	RH	T_{aeo}	% difference with HRV
A	↑	→	→	↑
B	→	↑	→	↓
C	→	→	↑	↑

5.2.7.2.4 Correlation Development

Based on the upper limit and lower limit of the cooling season weather report, the conditions below are used to derive regression equations. Outdoor air condition is set as: 26.7, 29.4, 32.2, 35 ℃ (80, 85, 90, 95℉); RH=40%, 50%, 60%, 70%, 80%; Taeo=7.2, 10, 12.8℃ (45, 50, 55℉); indoor air condition (exhaust air) is set as: 23.9℃ (75℉), RH=50%; compressor efficiency: 80%; HRV effectiveness 60%. The conditions above have a wider range than the conditions in the real weather report thus derivation of equations are based on these data. The simulation is based on two systems, namely a baseline system (derived in the previous section), and a reconfigured system with HRV (B1).

5.2.7.2.4.1 COP with HRV Correlation

Similarly to Reconfigured system A1 and A2, only exponential model is considered in this section. According to the equations aforementioned, plus several assumptions made for this model, it is known that COP with HRV is a function of outdoor air temperature and relative humidity, Taeo and heat exchanger effectiveness. Since effectiveness of heat exchanger is 60%, which is a fixed value, then the exponential model is set as log COP=f (RH, Taeo, Tout). A complete quadratic regression of log COP is built in Table 19. The error between predicted data and actual data is indicated in Figure 105---always less than 2%.

Table 19 log COP_{HRV} Model Coefficients

a0+a1*RH^2+a2*RH+a3*Taeo^2+a4*Taeo+a5*Tout^2+a6*Tout+a7*RH*Taeo+a8*Taeo*Tout+a9*RH*Tout									
a0	a1	a2	a3	a4	a5	a6	a7	a8	a9
-1.27	0.158	1.27	0.000255	0.0194	-0.000267	0.0463	-0.014	0.158	-0.0112

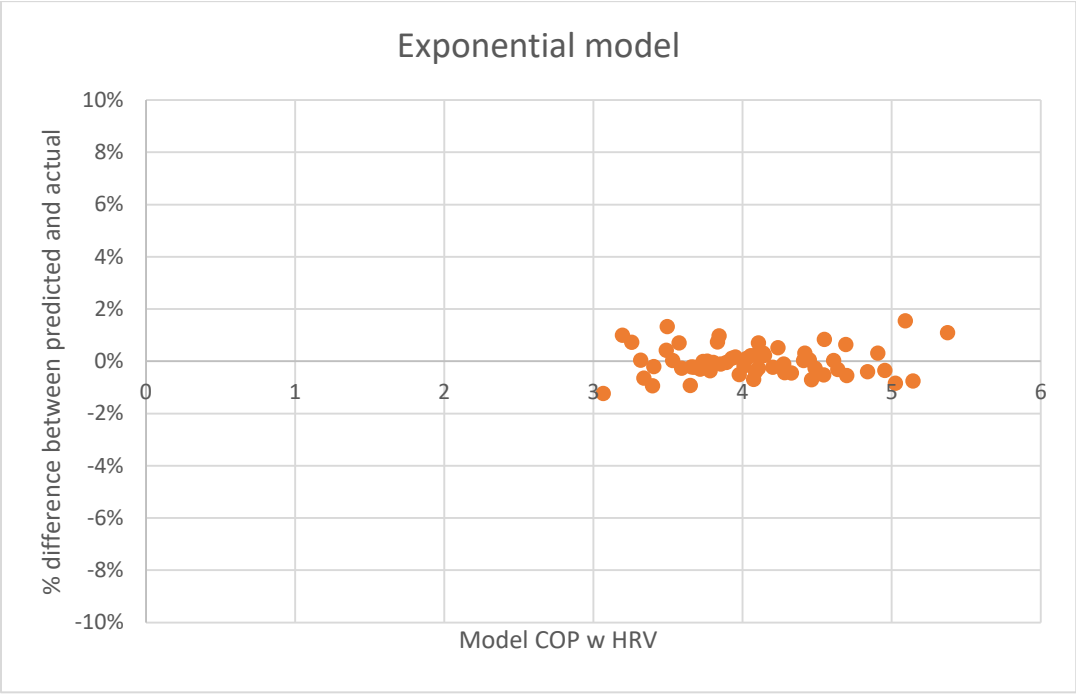

Figure 105 Percentage difference comparison of predicted and actual data of exponential method for COP with HRV

5.2.7.2.4.2 COP Ratio of HRV (B1) over Baseline (A) Correlation

Only exponential model is considered in this section. According to the equations aforementioned, plus several assumptions made for this model, it is known that COP ratio with HRV is a function of outdoor air temperature and relative humidity, Taeo and heat exchanger effectiveness. Since effectiveness of heat exchanger is 60%, which is a fixed value, then the exponential model is set as log COP ratio=f (RH, Taeo, Tout). A complete quadratic regression of

log COP ratio is built in Table 20. The error between predicted data and actual data is indicated in Figure 106---always less than 2%.

Table 20 log COP ratio (HRV over baseline system) Model Coefficients

a0+a1*RH^2+a2*RH+a3*Taeo^2+a4*Taeo+a5*Tout^2+a6*Tout+a7*RH*Taeo+a8*Taeo*Tout+a9*RH*Tout									
a0	a1	a2	a3	a4	a5	a6	a7	a8	a9
-3.09	0.158	1.27	0.000173	-0.00369	-0.000289	0.0620	-0.014	-1.82e-5	-0.0112

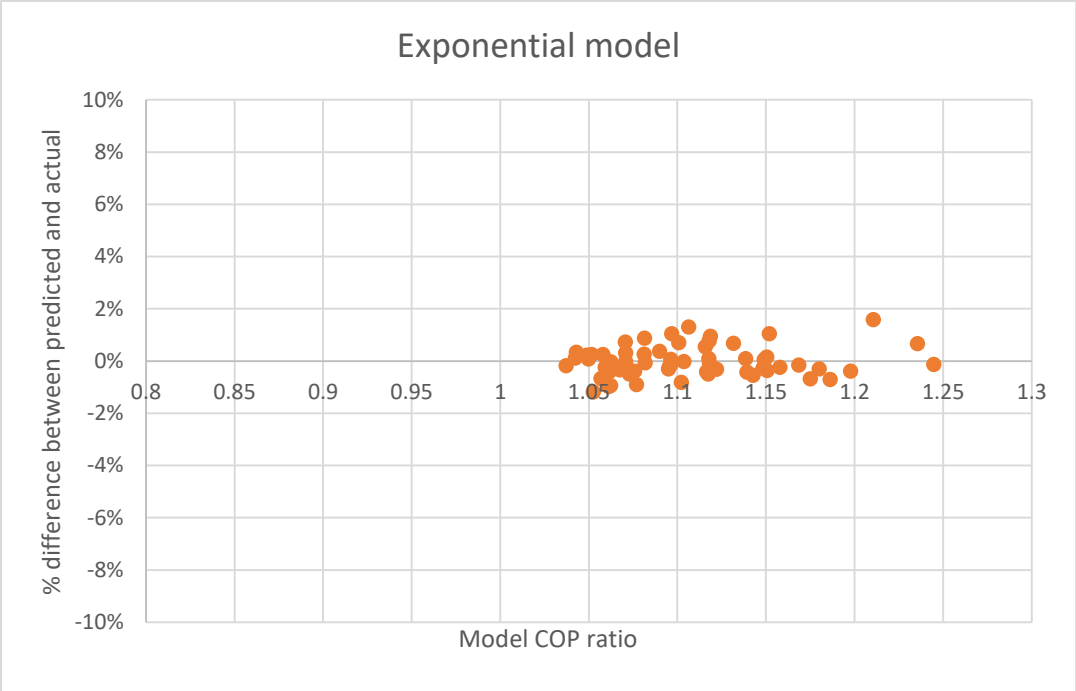

Figure 106 Percentage difference comparison of predicted and actual data of exponential method for COP ratio of HRV over baseline

5.2.7.3 Scenario B2 Compared with Scenario A

5.2.7.3.1 COP Improvement Due to ERV Overview

Figure 106 shows the relationship between COP with and without ERV when COP is ranging from 1 to 10. It is observed that for most data, the improvement is within 20% to 80%, however, the highest increase can go beyond 100%.

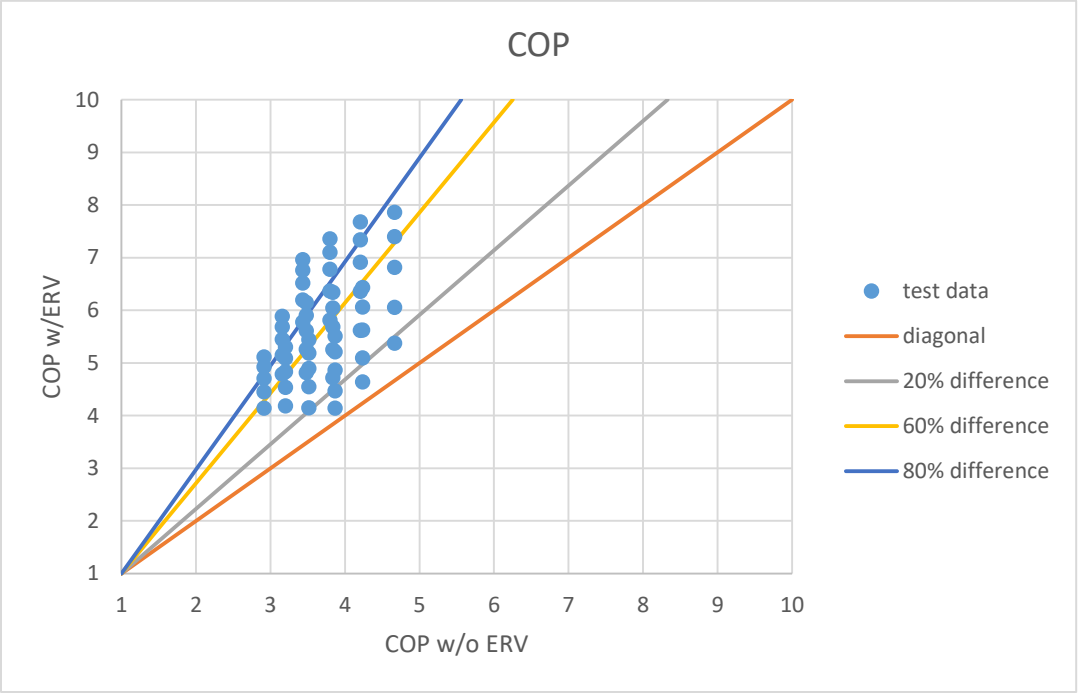

Figure 107 COP with/without ERV

5.2.7.3.2 Scenario B2 COP Review (with ERV)

Figure 108 gives an overview of how reconfigured system B2 (ERV) system performance related to three variables, namely ourdoor air temperatures, relative humidities and Taeo, and it further shows that COP increases with the boosting relative humidity. Figure 109, 110, 111 and 112 show how COP varies with different Taeo under the same outdoor air temperature, and it is observed that COP increases with the increasing Taeo. Figure 113, 114 and 115 show how COP varies with different outdoor air temperature under the same Taeo and these three plots illustrate that COP may increase or decrease with the increasing outdoor air temperature. The trend of COP varied with the three parameters is further summarized in Table 21.

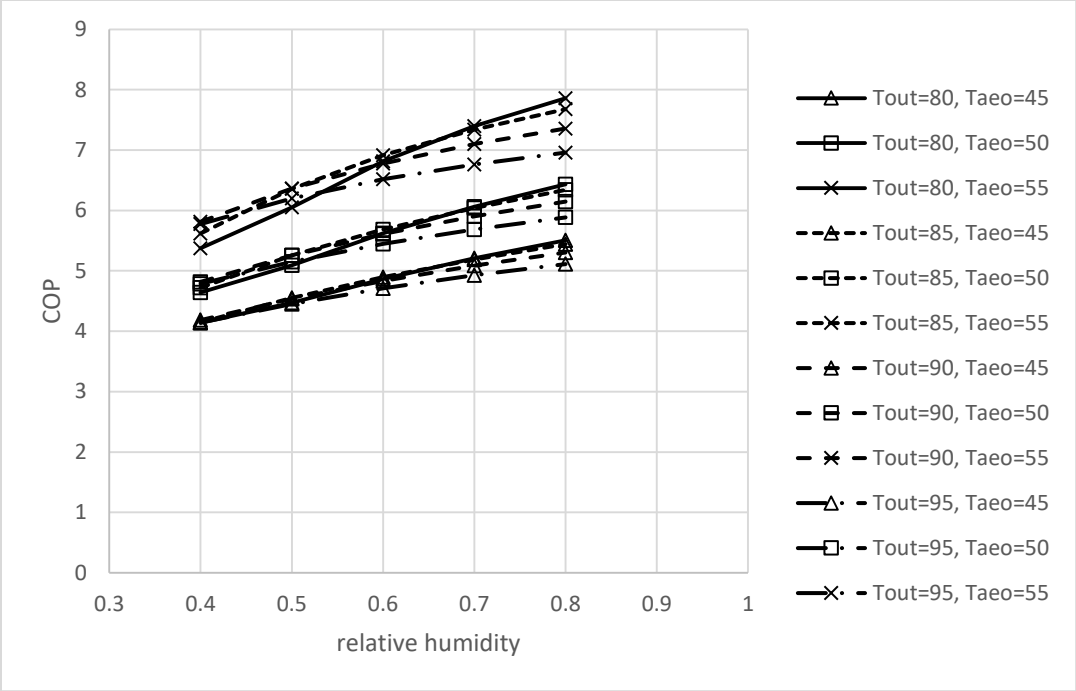

Figure 108 COP with ERV varied with relative humidity under different conditions

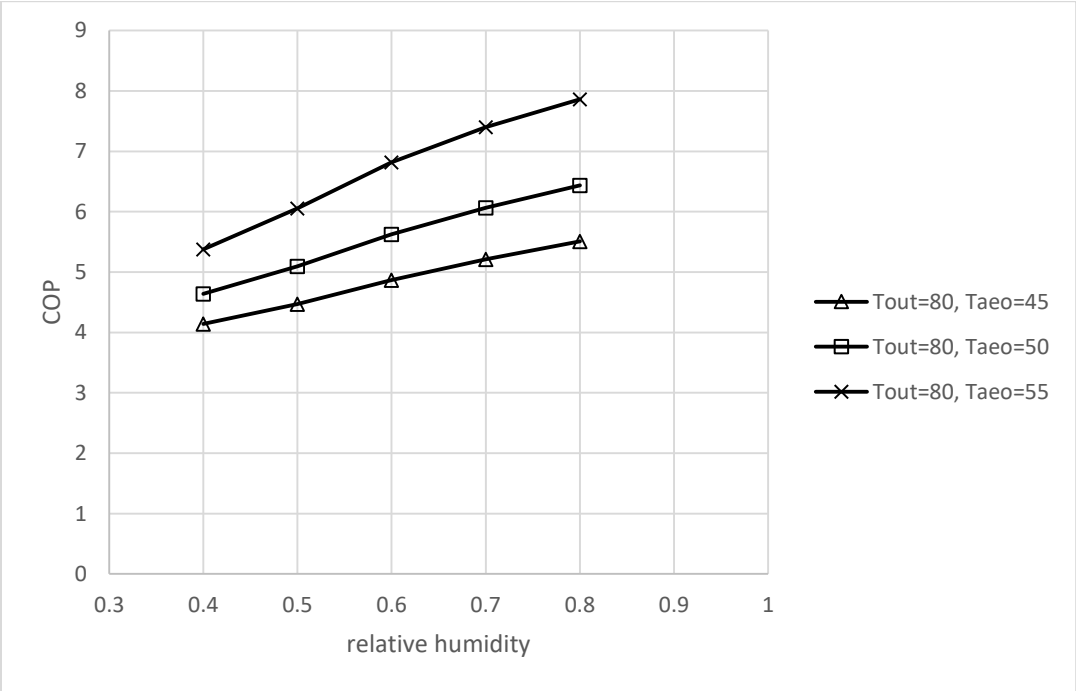

Figure 109 COP with ERV varied with relative humidity when Tout=80 °F

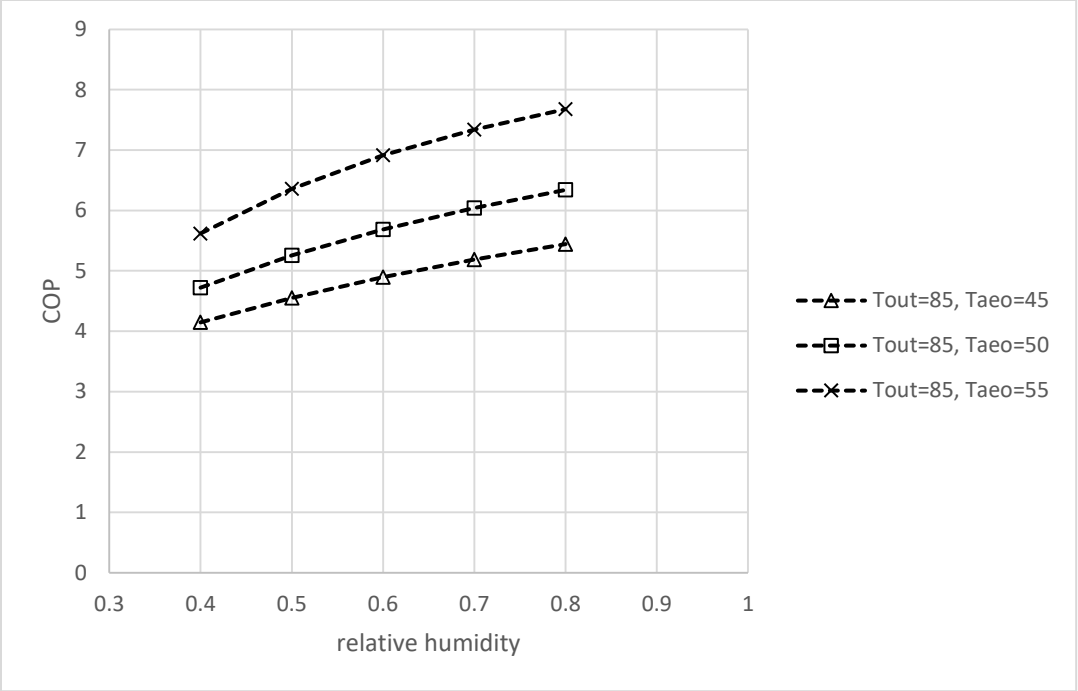

Figure 110 COP with ERV varied with relative humidity when Tout=85 °F

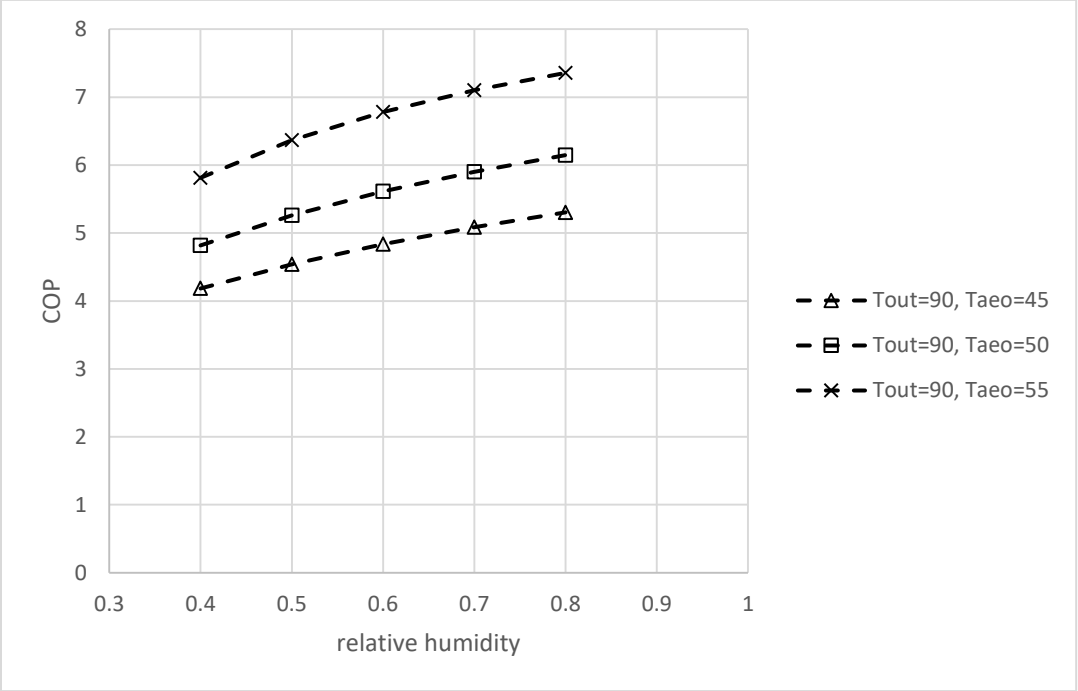

Figure 111 COP with ERV varied with relative humidity when Tout=90 °F

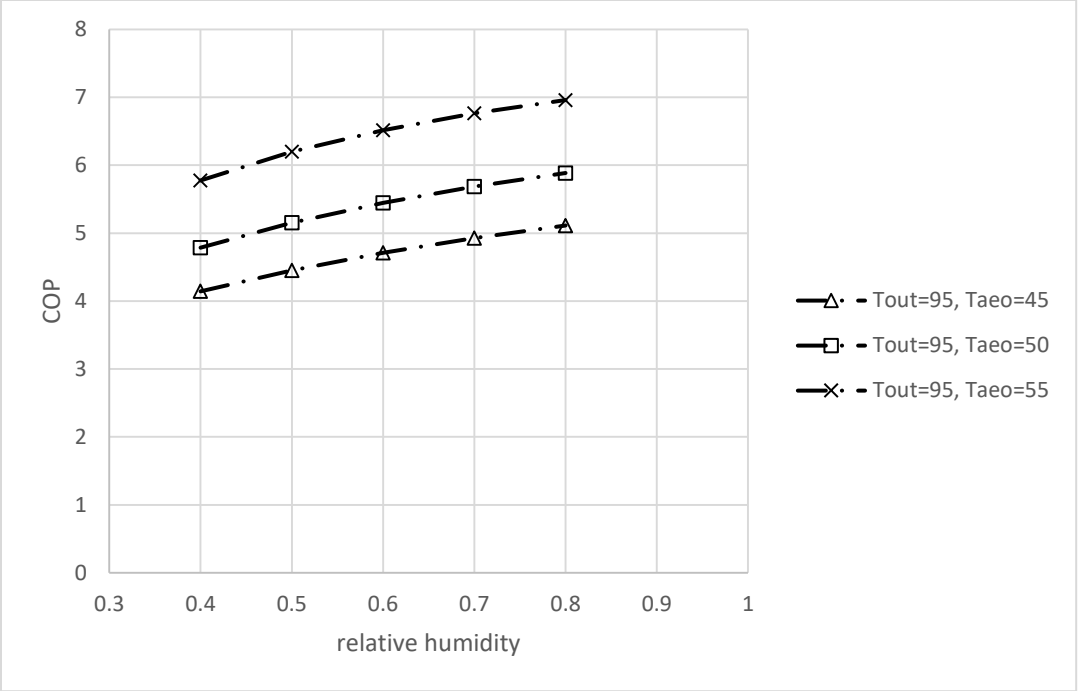

Figure 112 COP with ERV varied with relative humidity when Tout=95 °F

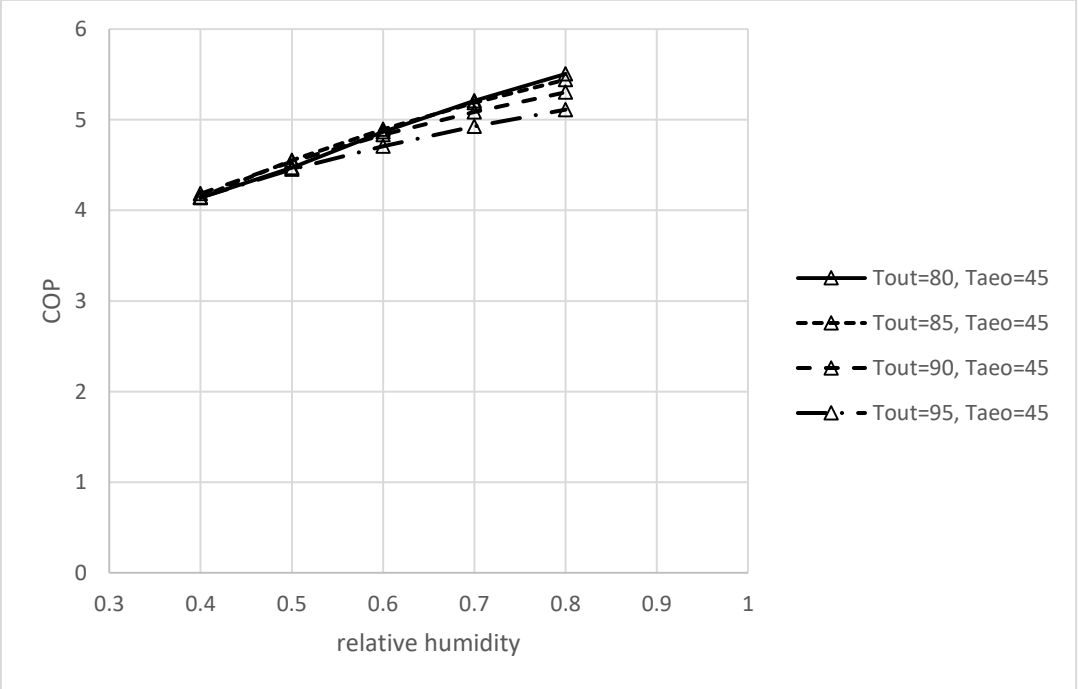

Figure 113 COP with ERV varied with relative humidity when Taeo=45 °F

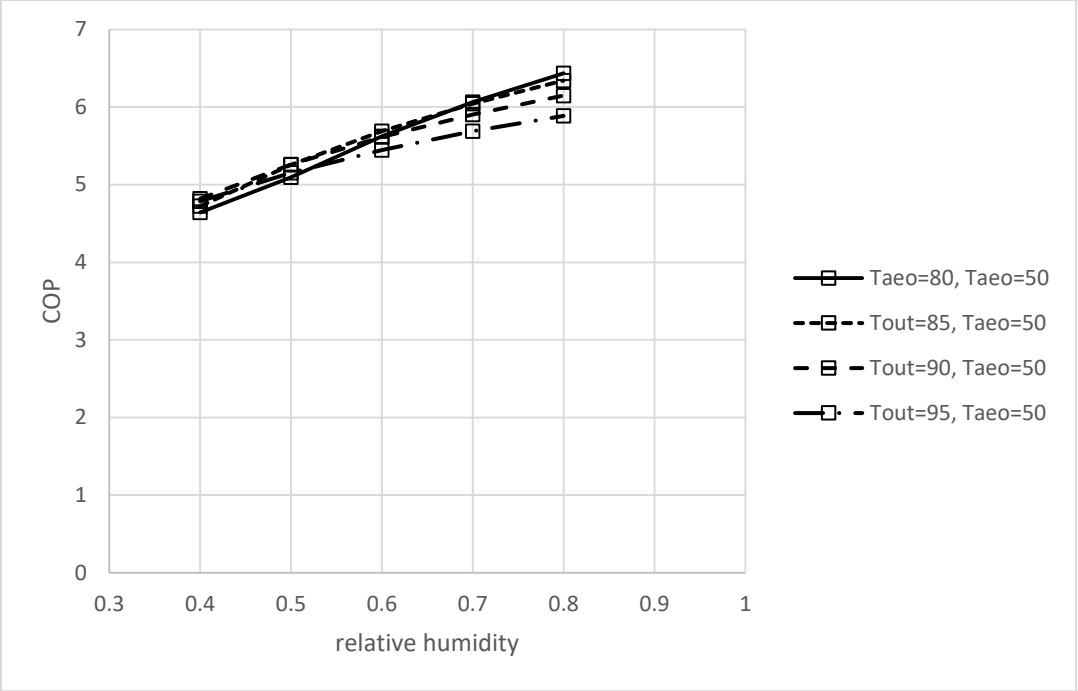

Figure 114 COP with ERV varied with relative humidity when Taeo=50 °F

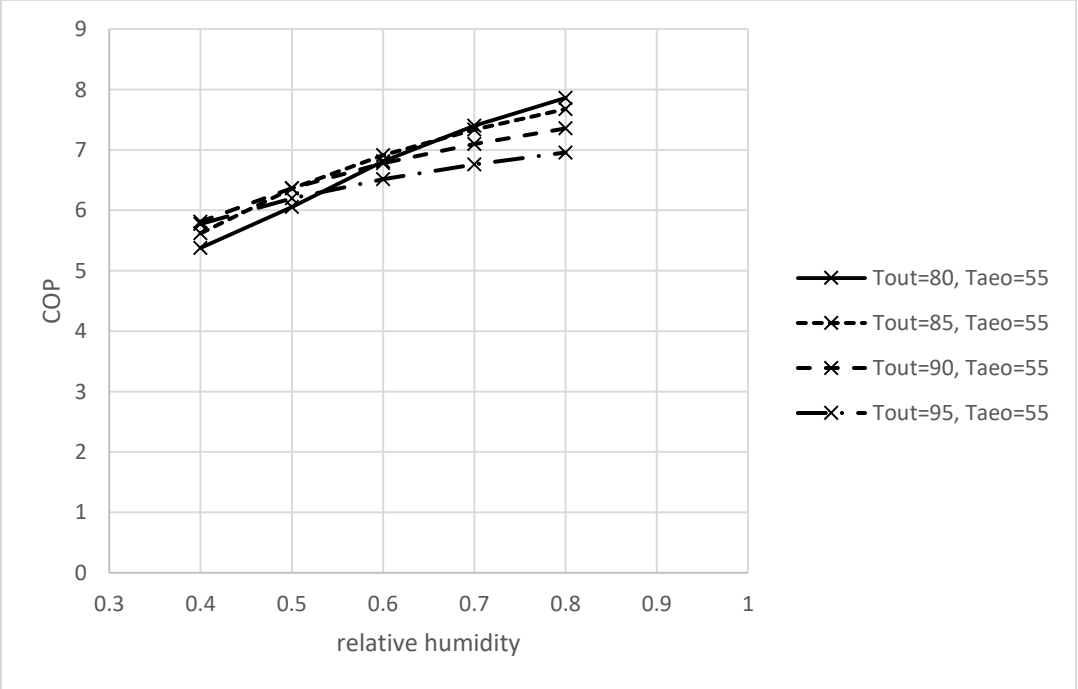

Figure 115 COP with ERV varied with relative humidity when Taeo=55 °F

Table 21 COP with ERV varied with Tout, RH and Taeo

case	T_{out}	RH	T_{aeo}	COP with ERV
1	↑	→	→	It depends
2	→	↑	→	↑
3	→	→	↑	↑

5.2.7.3.3 COP Enhancement Analysis (The system with ERV compared to the system without ERV)

Figure 116 gives an overview of how percentage difference (reconfigured system B1 compared to baseline system A) related to the three variables, namely outdoor air temperatures, relative humidities and Taeo, and Figure 116 further shows that COP percentage difference increase with boosting relative humidity. Figure 117, 118, 119 and 120 show how COP percentage difference varies with different Taeo under the same outdoor air temperature, and it is indicated that COP percentage difference increase with the boosting Taeo. Figure 121, 122 and 123 show how COP percentage difference varies with different outdoor air temperature under the same Taeo and these three plots illustrate that COP percentage difference increase with the boosting outdoor air temperature. The trend of COP improvement varied with aforementioned three variables are summarized in Table 22.

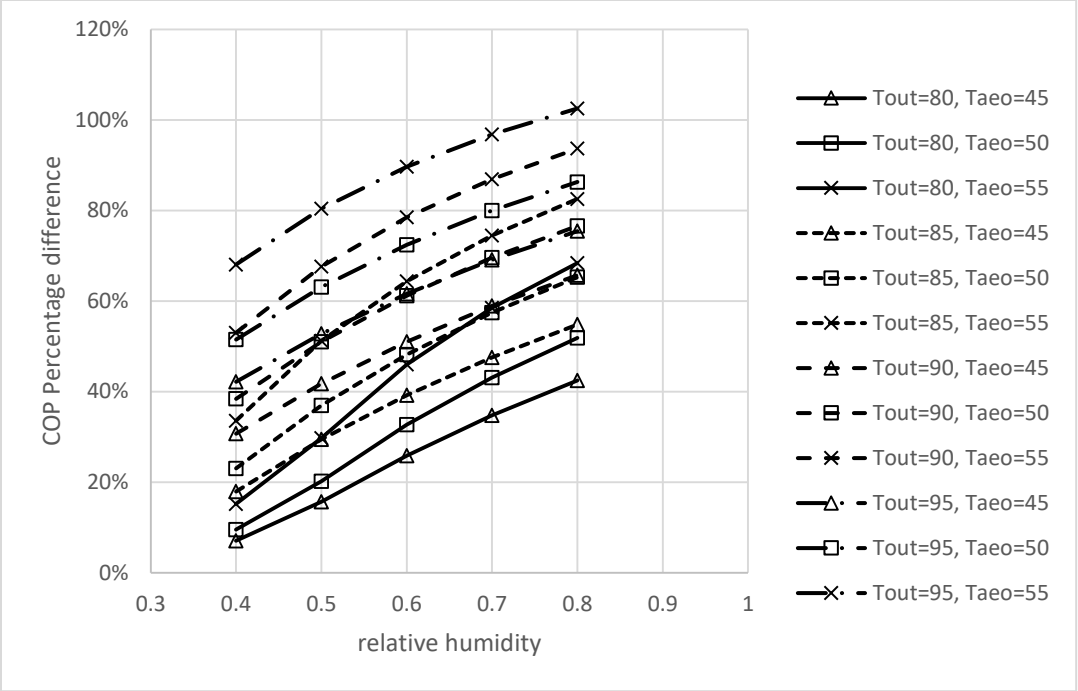

Figure 116 COP percentage difference (ERV over baseline) versus relative humidity under different conditions

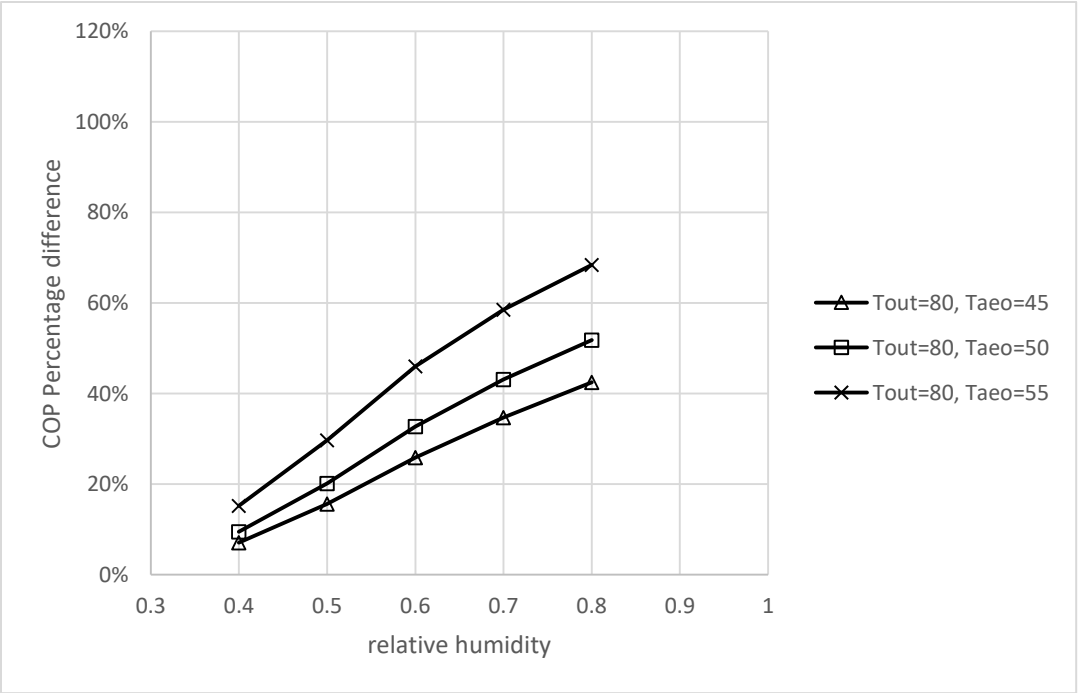

Figure 117 COP percentage difference (ERV over baseline) versus relative humidity when Tout=80°F

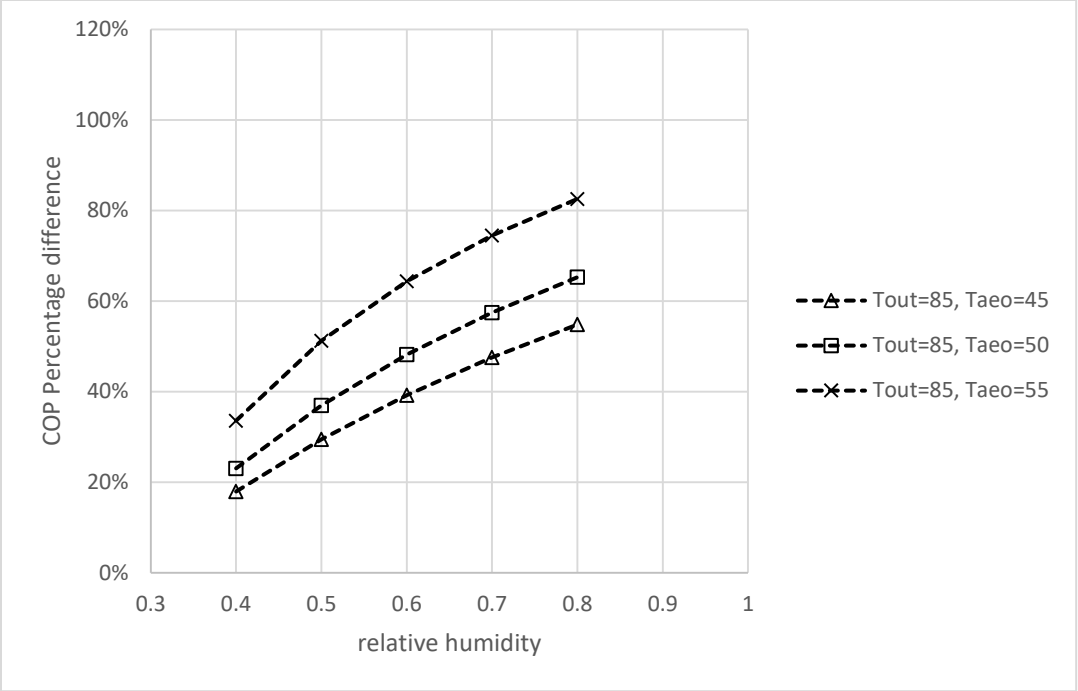

Figure 118 COP percentage difference (ERV over baseline) versus relative humidity when Tout=85°F

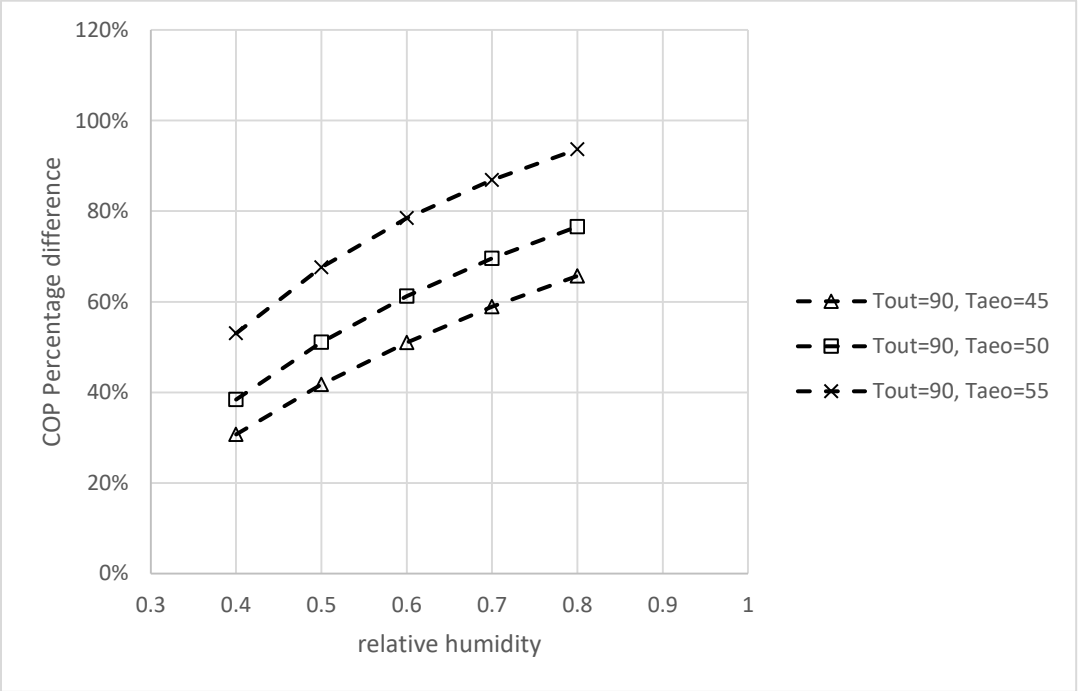

Figure 119 COP percentage difference (ERV over baseline) versus relative humidity when Tout=90°F

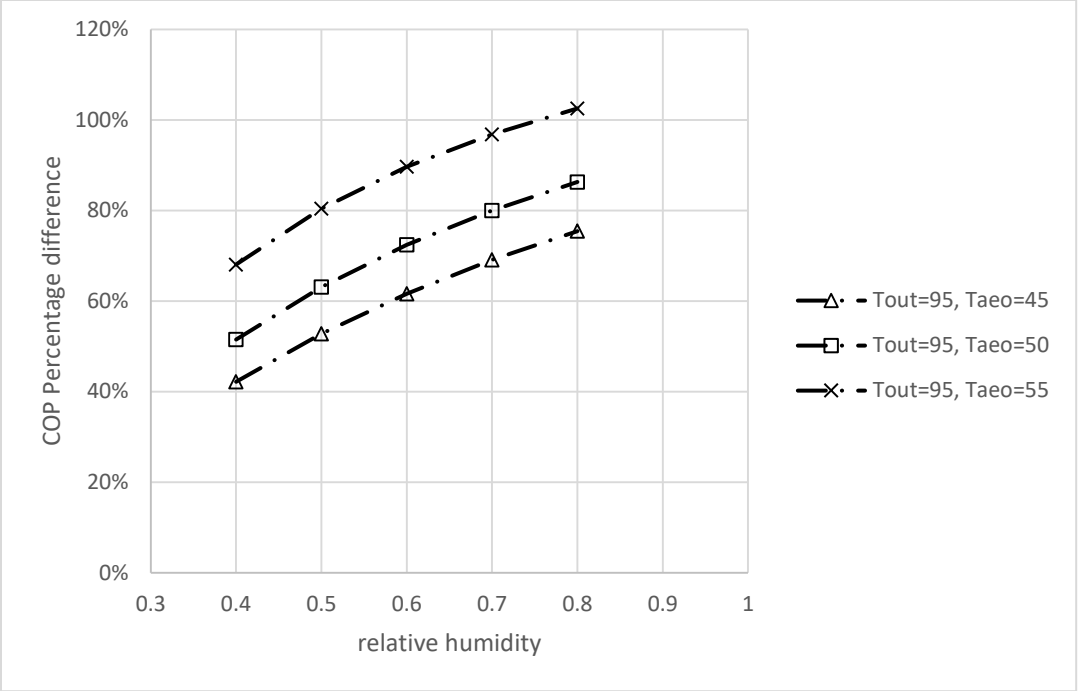

Figure 120 COP percentage difference (ERV over baseline) versus relative humidity when Tout=95°F

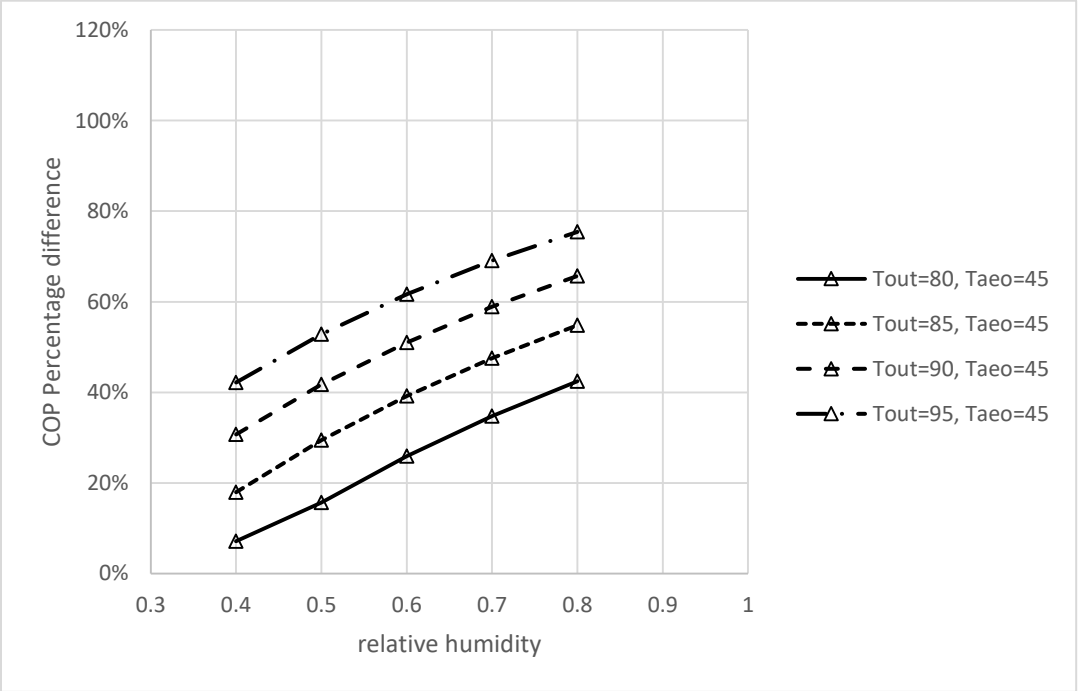

Figure 121 COP percentage difference (ERV over baseline) versus relative humidity when Taeo=45°F

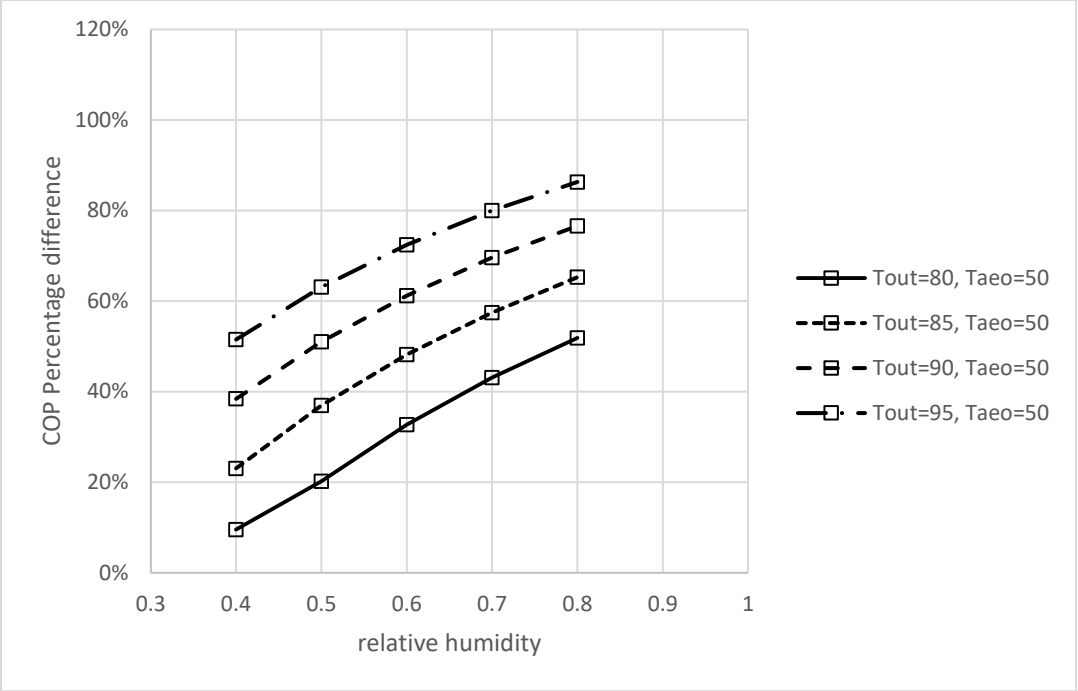

Figure 122 COP percentage difference (ERV over baseline) versus relative humidity when Taeo=50°F

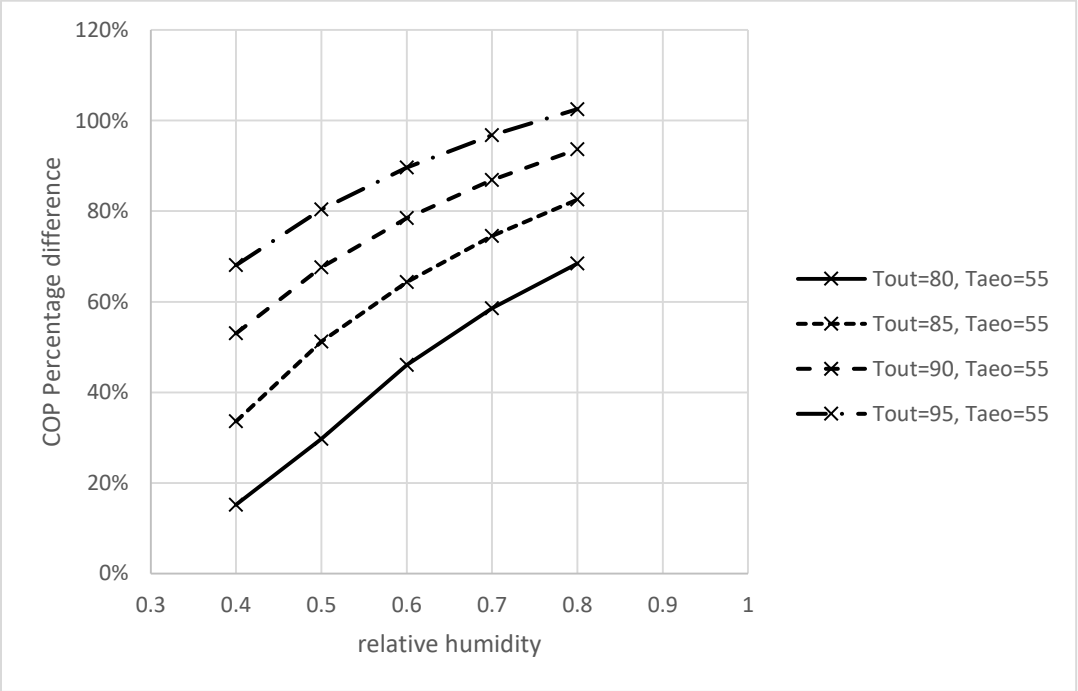

Figure 123 COP percentage difference (ERV over baseline) versus relative humidity when Taeo=55°F

Table 22 COP percentage difference (ERV over baseline) varied with Tout, RH, and Taeo

case	T_{out}	RH	T_{aeo}	% difference with ERV
1	↑	→	→	↑
2	→	↑	→	↑
3	→	→	↑	↑

5.2.7.3.4 Correlation Development

5.2.7.3.4.1 COP with ERV Correlation

Similarly to Reconfigured system B1, only exponential model is considered in this section. According to the equations aforementioned, plus several assumptions made for this model, it is known that COP with ERV is a function of outdoor air temperature and relative humidity, Taeo and heat exchanger effectiveness. Since effectiveness of heat exchanger is 60%, which is a fixed value, then the exponential model is set as log COP=f (RH, Taeo, Tout). A complete quadratic regression of log COP is built in Table 23. The error between predicted data and actual data is indicated in Figure 124---always less than 4%.

Table 23 log COP_{HRV} Model Coefficients

a0+a1*RH^2+a2*RH+a3*Taeo^2+a4*Taeo+a5*Tout^2+a6*Tout+a7*RH*Taeo+a8*Taeo*Tout+a9*RH*Tout									
a0	a1	a2	a3	a4	a5	a6	a7	a8	a9
-2.29	-0.786	3.30	0.000805	-0.0518	-0.000378	0.0778	0.000649	2.53e-6	-0.0230

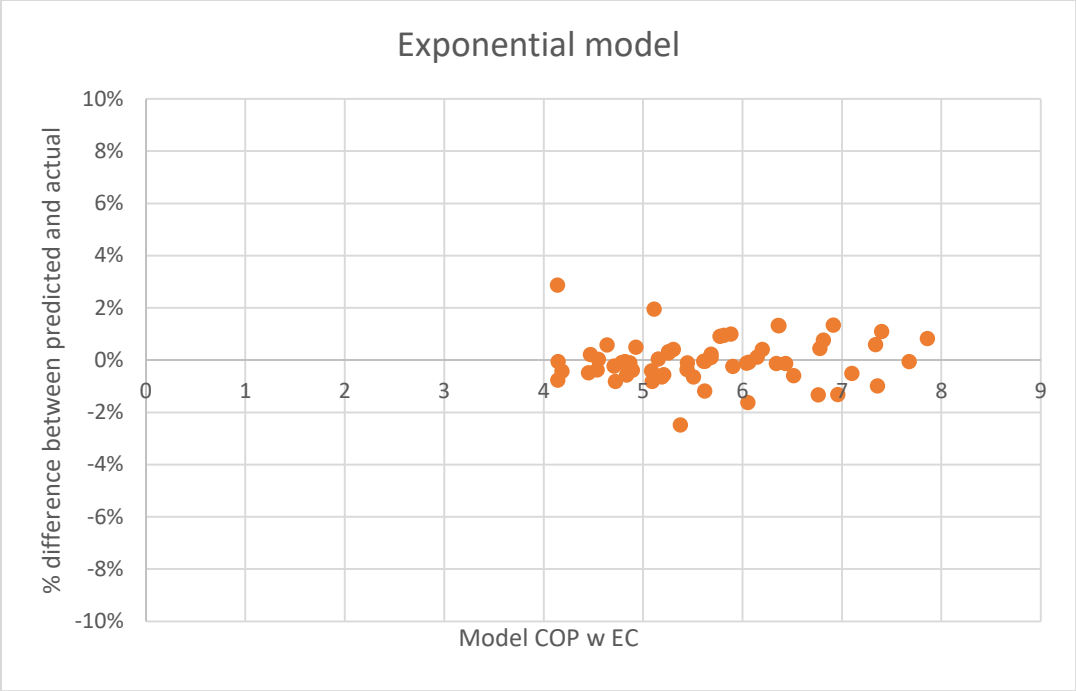

Figure 124 Percentage difference comparison of predicted and actual data of exponential method for COP with HRV

5.2.7.3.4.2 COP Ratio of ERV (B2) over Baseline (A) Correlation

Only exponential model is considered in this section. According to the equations aforementioned, plus several assumptions made for this model, it is known that COP ratio with ERV is a function of outdoor air temperature and relative humidity, Taeo and heat exchanger effectiveness. Since effectiveness of heat exchanger is 60%, which is a fixed value, then the exponential model is set as log COP ratio=f (RH, Taeo, Tout). A complete quadratic regression of log COP ratio is built in Table 24. The error between predicted data and actual data is indicated in Figure 125---always less than 4%.

Table 24 log COP ratio (ERV over baseline system) Model Coefficients

a0+a1*RH^2+a2*RH+a3*Taeo^2+a4*Taeo+a5*Tout^2+a6*Tout+a7*RH*Taeo+a8*Taeo*Tout+a9*RH*Tout									
a0	a1	a2	a3	a4	a5	a6	a7	a8	a9
-4.11	-0.786	3.30	0.000724	-0.0750	-0.000400	0.0934	0.00649	0.000159	0.0230

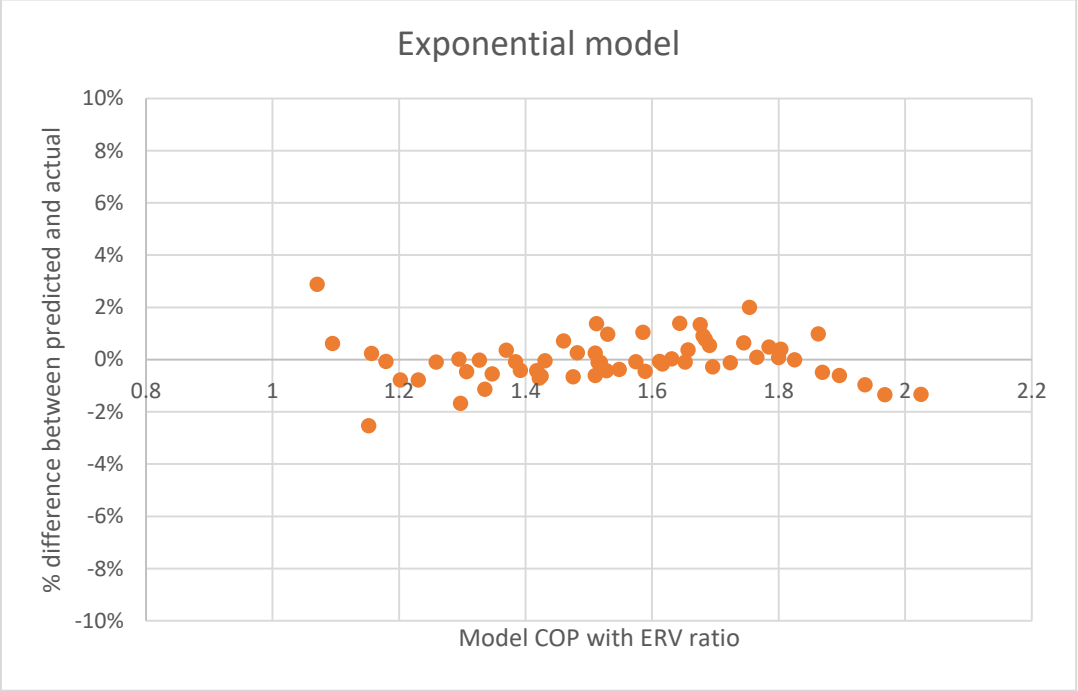

Figure 125 Percentage difference comparison of predicted and actual data of exponential method for COP ratio of ERV over baseline

5.2.7.4 Scenario B1 Compared to Scenario B2 (HRV system compared to ERV system)

HRVs and ERVs are available for commercial and industrial applications as well as for residential and small-scale commercial uses. However, ERV has greater maintenance requirement and costly than HRV. Thus, it is necessary to study the ratio of systems with ERV with systems with HRV. In other words, if the ratio is close to 1, there is very limited latent heat recovery potential and no need to use ERV instead of HRV.

Figure 126 shows how COP ratio of system with ERV over system with HRV varied with outdoor air temperatures, relative humidities and Taeo. It is further observed that the COP ratio increase with boosting relative humidity. Figure 127, 128, 129 and 130 show how COP ratio varied with different Taeo under the same outdoor air temperature and these plots illustrate that COP ratio increase with the boosting Taeo. Figure 131, 132 and 133 demonstrate how COP ratio varied with different outdoor air temperature at the same Taeo and the result show that COP ratio increase with the increasing outdoor air temperature. Thus, the benefit of system with ERV with system of HRV is obvious at hot and humid regions.

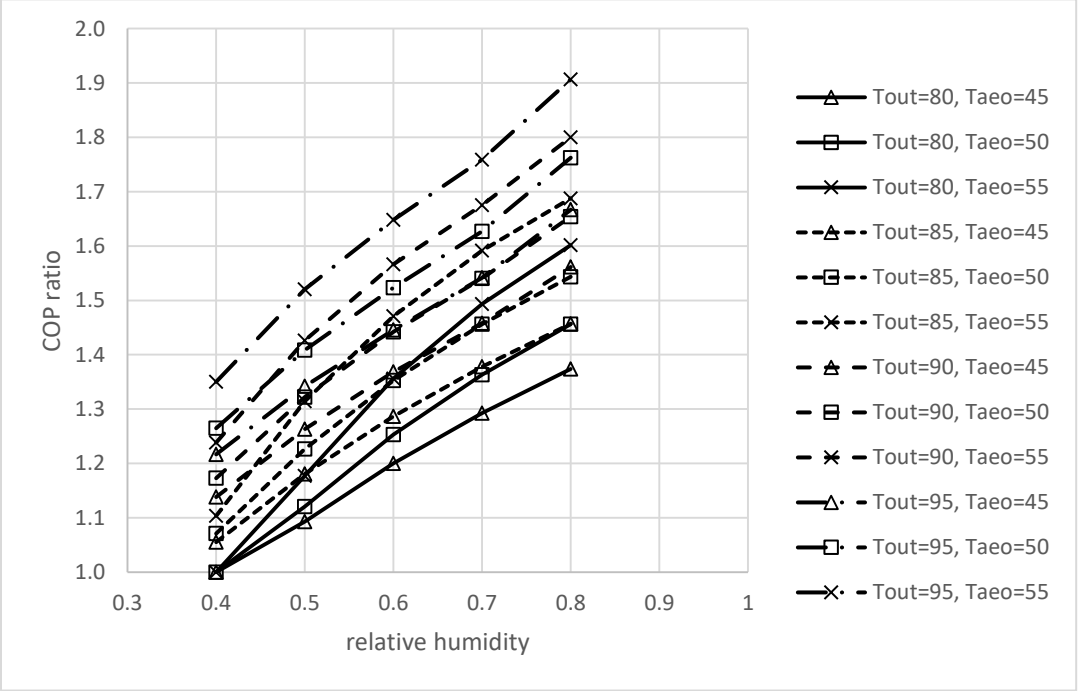

Figure 126 COP ratio of ERV over HRV versus relative humidity under different conditions

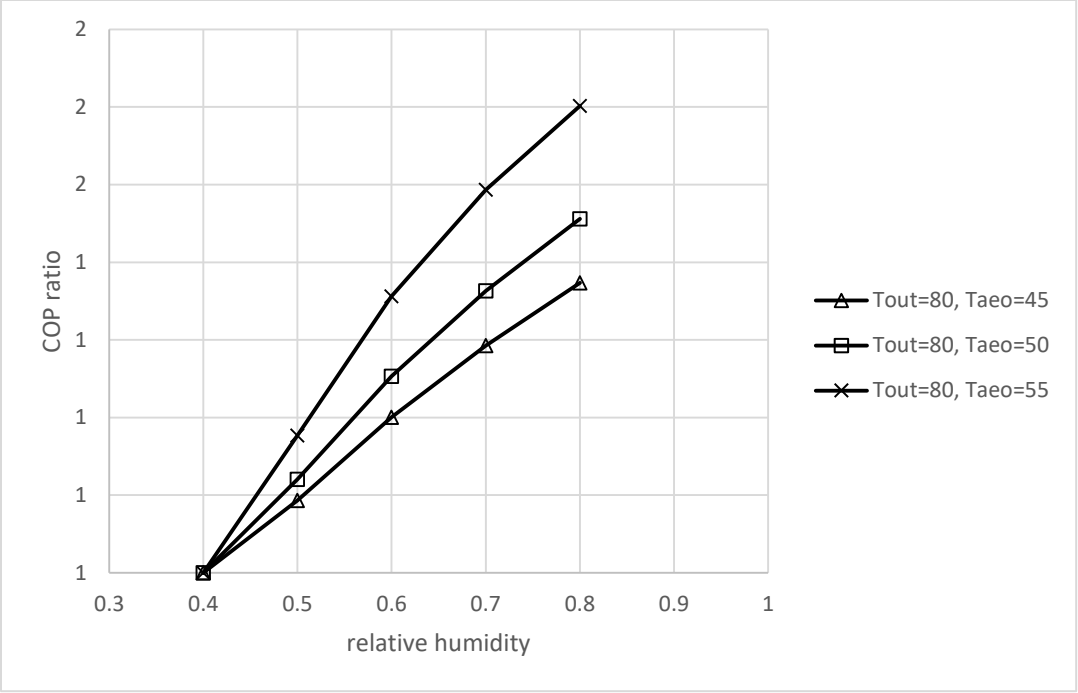

Figure 127 COP ratio of ERV over HRV versus relative humidity when Tout=80 °F

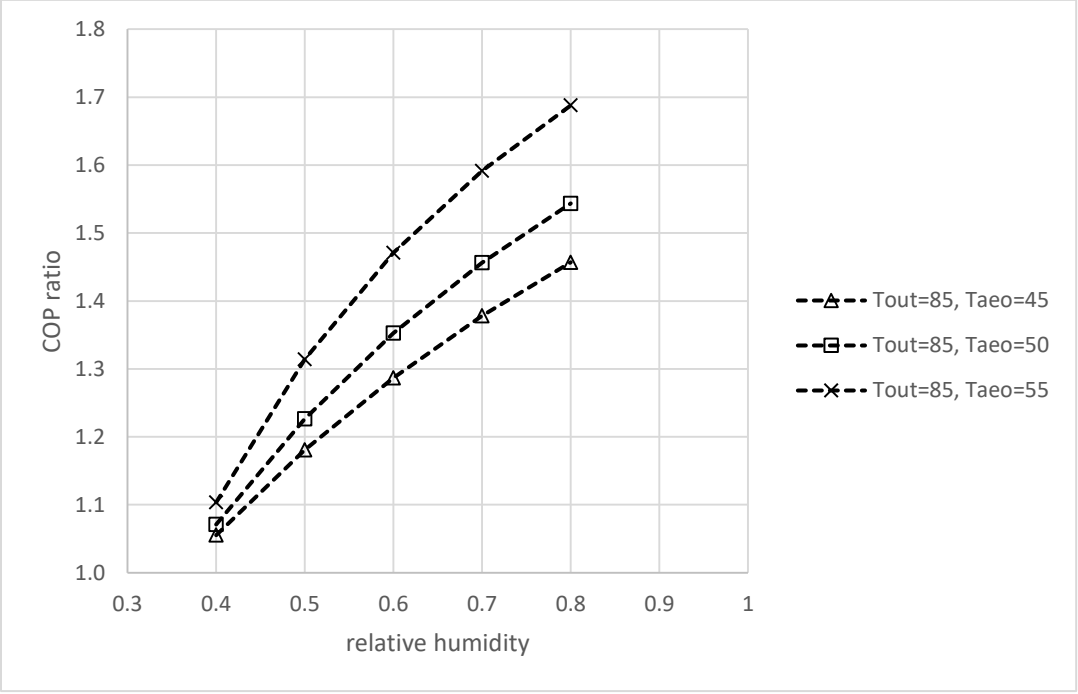

Figure 128 COP ratio of ERV over HRV versus relative humidity when Tout=85 °F

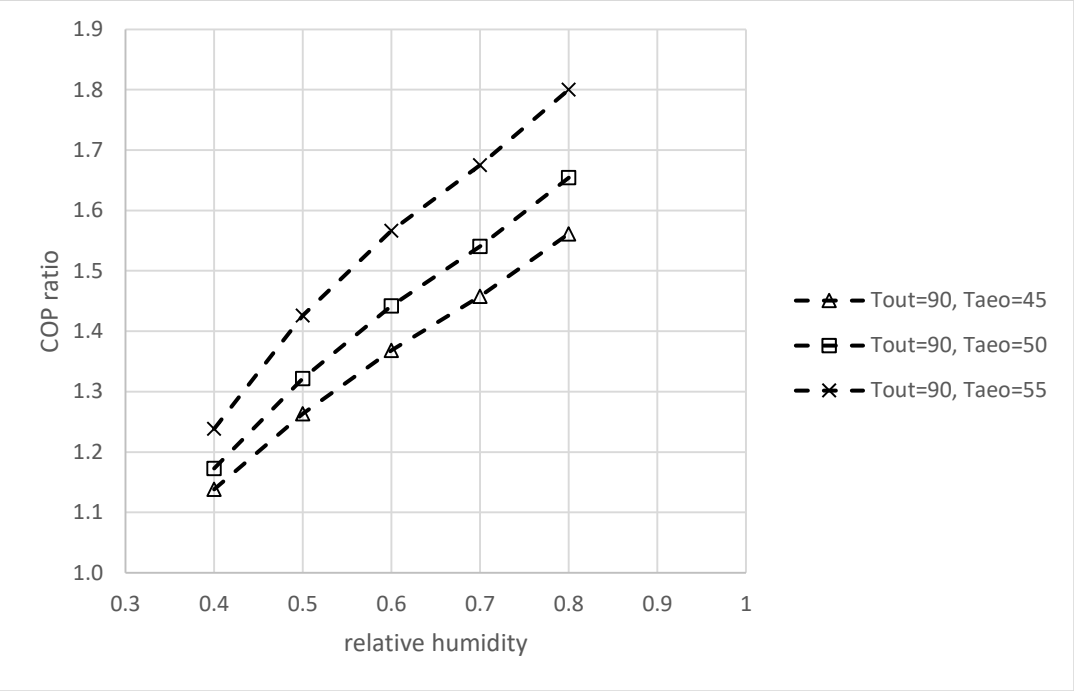

Figure 129 COP ratio of ERV over HRV versus relative humidity when Tout=90 °F

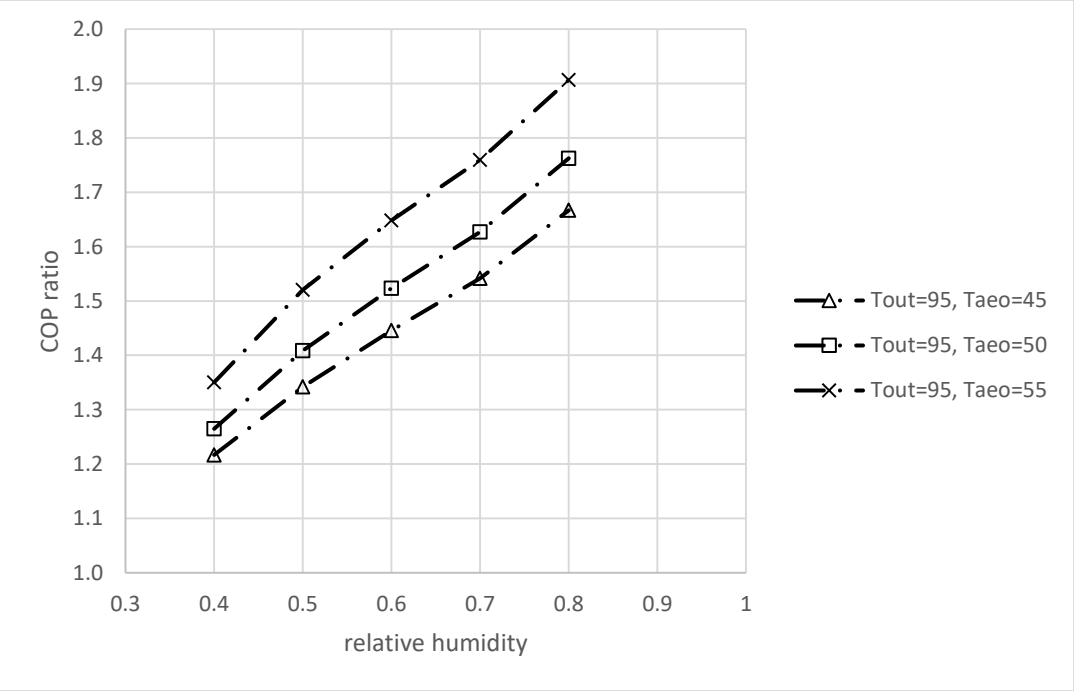

Figure 130 COP ratio of ERV over HRV versus relative humidity when Tout=95 °F

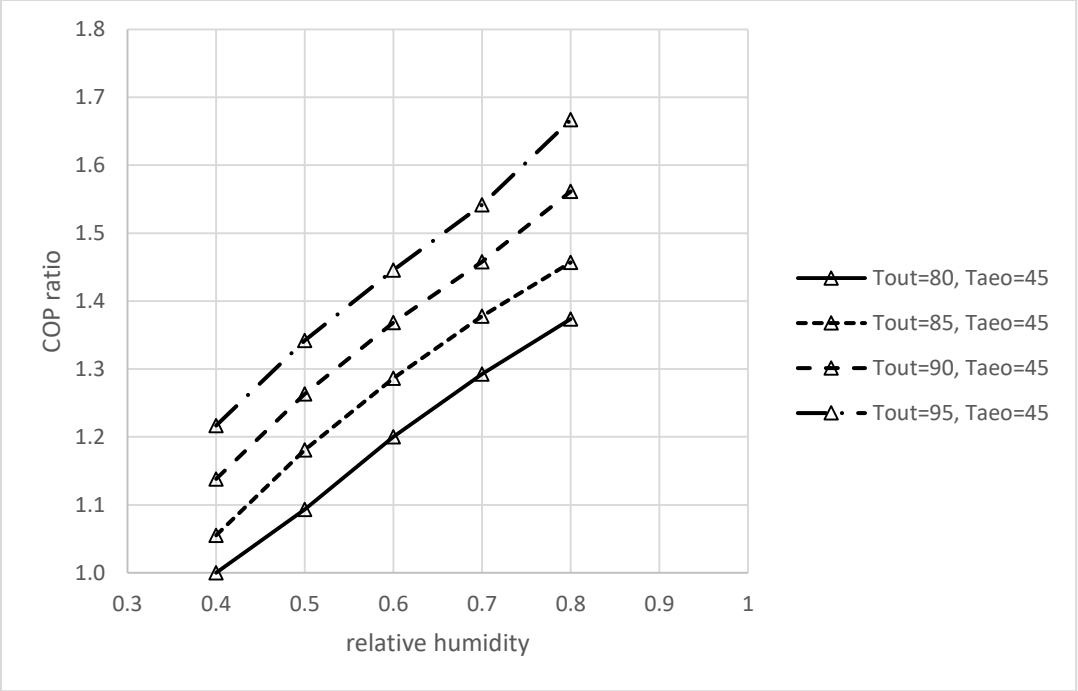

Figure 131 COP ratio of ERV over HRV versus relative humidity when Taeo=45 °F

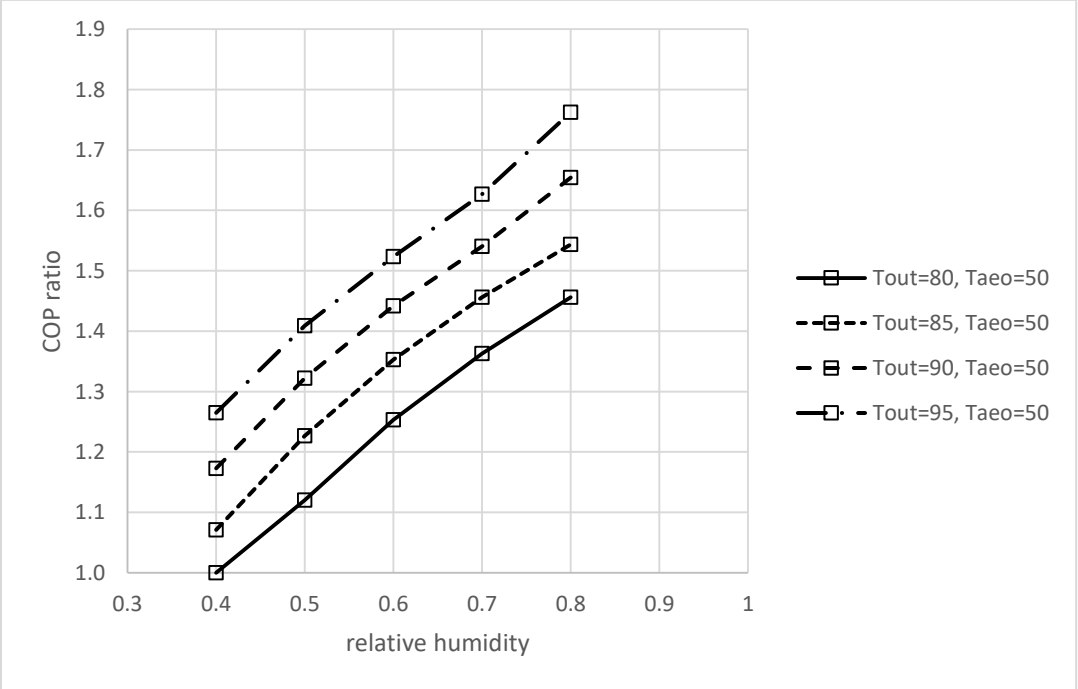

Figure 132 COP ratio of ERV over HRV versus relative humidity when Taeo=50 °F

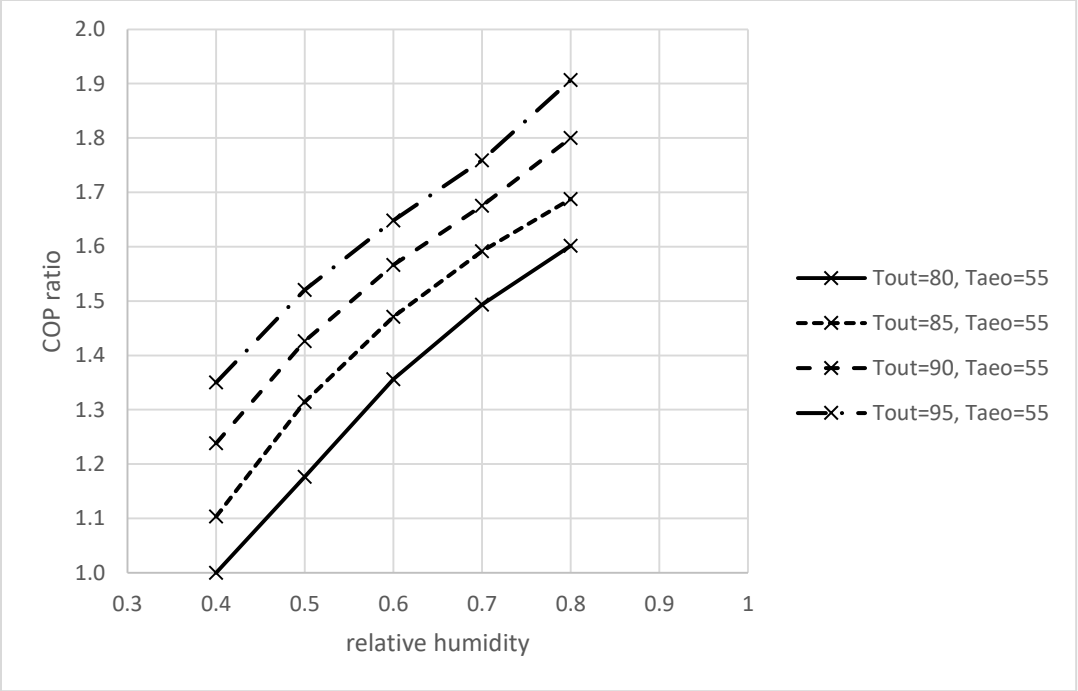

Figure 133 COP ratio of ERV over HRV versus relative humidity when Taeo=55 °F

5.2.7.5 Recovery Energy Factor

One important factor is the so-called recovery energy proportion, which is defined as the recovery energy over the total energy output of the system, which is also equal to 1-COPold/COP new. Another one important factor is the evaporator energy proportion, which is defined as the refrigerating effect over the total energy and is equal to COP old/COP new. It is observed that one factor can be calculated by another factor.

For this study, COP old is always the baseline system COP without ERV/HRV. Thus, the ratio of recovery energy (q recovery) over evaporator energy (q) is exactly the percentage difference of the reconfigured system and the baseline system. Finally, the recovery energy proportion could be calculated by the percentage difference between reconfigured system and baseline system.

5.2.8 Conclusions

1. Using the exhaust air from buildings to precool or dehumidify incoming outdoor air with an ERV and/or HRV is well-known; however when this same system using outdoor air entering the evaporator, then a DOAS (dedicated outdoor air system) is formed, which is the focus of this study. It is shown that with an HRV precooling evaporator air, the percentage increase in COP with R410A as the working fluid can be as much as almost 25%, depending on the outdoor conditions. In addition, by using the exhaust air from building to precool and pre-dehumidify the incoming outdoor air entering the evaporator with an ERV, then the increasing effect can be over 100%. Of special note, the ERV is shown to always have a better improvement than the HRV; however, the degree of improvement is dependent on outdoor conditions.

2. Improvement of HRV system increase with boosting Tout, Taeo but decrease with boosting RH. Thus, reconfigured system of HRV is usually best for the hot and dry climate zone areas. Improvement of ERV system increase with boosting Tout, RH and Taeo. Therefore, reconfigured system of ERV can get the best benefit for the hot and humid climate zone areas.

3. The benefit of ERV over HRV is pretty low at dry humid (especially at 40% RH), and this benefit increase with the boosting Taeo but decrease with the boosting outdoor air temperature. Thus, at dry and moderate temperature climate zone, reconfigured system D (HRV) performs quite well and no need for ERV since the retrofit of ERV needs further capital cost but little benefit. For the humid and hot climate zone, it is necessary to consider using an ERV instead of HRV since the benefit is significant, but the trade-off effect of increasing capital cost and boosting energy saving.

5.3 Use Evaporator Condensate Water to Cool Refrigerant Exiting the Condenser (Reconfigured System C)

Typically the state of the refrigerant going out from the condenser of conventional one-stage vapor compression cycle is usually assumed to be saturated liquid. Nevertheless, by cooling liquid refrigerant below saturation, the refrigerant becomes subcooling liquid with refrigerating effect increases while specific work stays constant, finally resulting in an increasing system coefficient of performance (COP).

Although different methods above to get condenser subcooling are quite common in refrigeration and air conditioning systems, as far as author's knowledge, utilizing condensate water from the evaporator to get condenser subcooling has not been systematically studied in the open literature. As a result, this study attempts to fill up this gap.

5.3.1 System Description

As cooling systems rely on evaporator coils, which produce moisture, instead of draining this high-quality water into sewers, we can easily capture the condensate water. By utilizing the condensate water as available coolant supplies, we can obtain subcooled liquid prior to the expansion device by adding a heat exchanger between the condenser and expansion valve, as shown in Figure 134. The first law is carried out for refrigerant R410A during simulation, and the effect on subcooling utilizing condensate water from the evaporator is investigated. From Figure 135 Ts diagram and Figure 136 ph diagram, it is observed that refrigerating effect increases while specific work stays constant, finally resulting in an increasing system coefficient of performance (COP). All simulations, analysis and thermodynamic properties of refrigerants are performed using EES under several different conditions. Finally, one would get an evaluation of COP

improvement from the simulation for R410A and verify the estimated results by comparing with the data from Riverside Energy Efficiency lab.

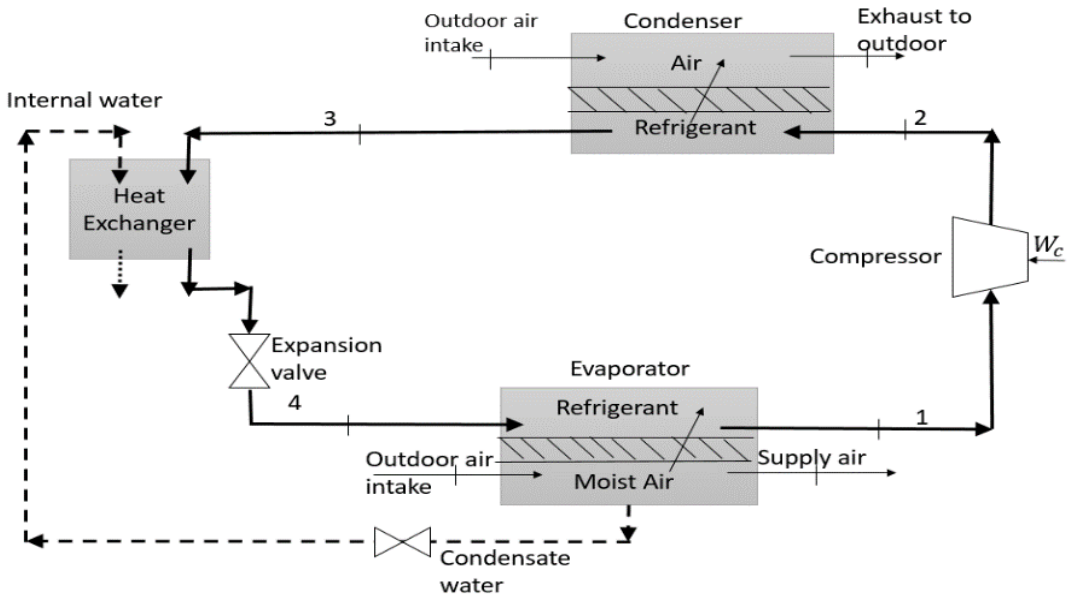

Figure 134 Schematic of reconfigured system C

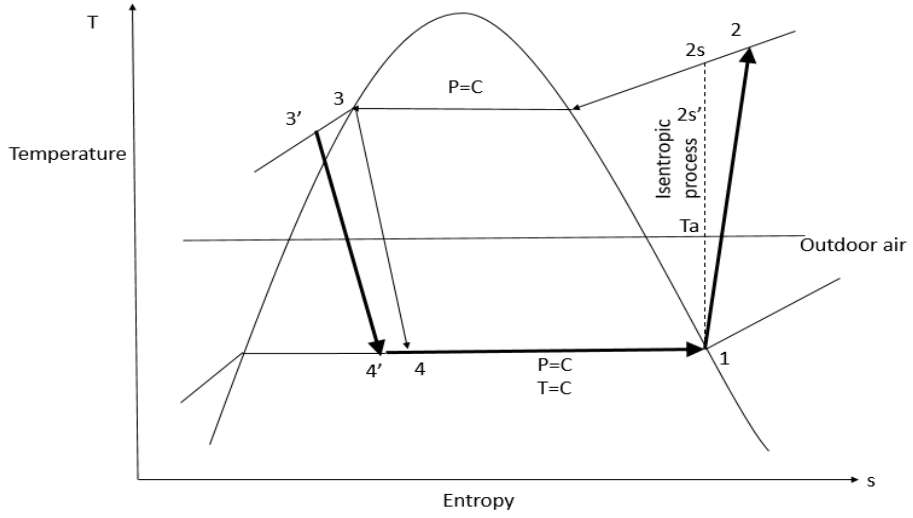

Figure 135 Ts diagram of reconfigured system C

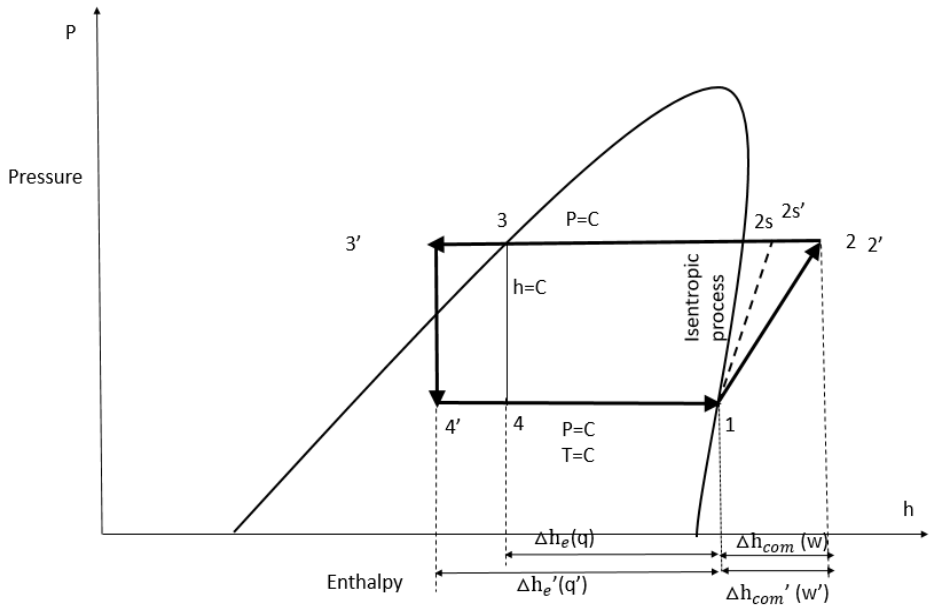

Figure 136 Ph diagram of reconfigured system C

5.3.2 Model Develop and Formulation

To calculate the critical refrigerant cycle performance parameters, such as the refrigeration cooling effect, the compressor work, and COP, it is necessary to specify or determine the thermodynamic state properties of the cooling refrigerant at each point in the vapor compression cycle. To accomplish this task, it is also necessary to know the state properties and flow conditions of the moist air entering and leaving the evaporator and condenser, along with the condition of the condensate draining from the air-side of the evaporator. Therefore, determining the performance parameters, such as COP, that will allow for evaluating the effect of the upstream heat exchanger requires developing, deriving, and solving four separate models, namely: 1) moist air properties 2) evaporating and condensing refrigerant temperature calculation 3) heat transfer in heat exchanger 4) vapor-compression refrigeration cycle. Only the third step—heat transfer in heat exchanger is different from the previous reconfigured systems, and this step is also the focus of this section.

5.3.2.1 Heat Transfer in Different Heat Exchangers

5.3.2.1.1 Heat Transfer in the Evaporator

In the evaporator,

$$\dot{m}_w = \dot{m}_a\ (w_1 - w_2) \tag{105}$$

where w_1 and w_2 are humidity ratio of inlet and outlet air in the evaporator. $\dot{m}_a$ is the mass flow rate of dry air while $\dot{m}_w$ is the mass flow rate of water.

Heat transfer occurs as the refrigerant mixture in the evaporator gained energy from the outdoor air entering the evaporator with the energy transfer causing the refrigerant to evaporate and outdoor air to cool. Consider the evaporator as a control volume; there is no heat absorbed or rejected to the surrounding, which means the heat absorption of the refrigerant equals to the heat rejection from the air, so that,

$$\dot{Q}_R = \dot{Q}_a \tag{106}$$

where $\dot{Q}_R$ is the heat transfer to the refrigerant,

$$\dot{Q}_R = \dot{m}_R\ (h_1 - h_3') \tag{107}$$

where $\dot{m}_R$ is the mass flow rate of refrigerant, h_1 is the enthalpy of outlet refrigerant (saturated vapor) in the evaporator, h3' is the enthalpy of outlet refrigerant (subcooled liquid) from the condenser after heat exchanger.

Heat rejected from the air can be expressed as,

$$\dot{Q}_a = \dot{m}_a\ (h_{1a} - h_{2a}) \tag{108}$$

where $\dot{m}_a$ is the mass flow rate of air, h_{1a} and h_{2a} are the inlet and outlet air enthalpy in the evaporator.

By combining Eqn 107 and 108,

$$\dot{m}_a\ (h_{1a} - h_{2a}) = \dot{m}_R\ (h_1 - h_3') \tag{109}$$

5.3.2.1.2 Heat Transfer in the Heat Exchanger

According to ASHRAE Standard 84, effectiveness is defined as $\varepsilon = \frac{Actual\ transfer\ of\ moisture\ or\ energy}{Maximum\ possible\ transfer\ between\ airstreams}$. By simplification, it is yield as, $\text{Ɛ} = \frac{Q}{Q_{max}} = \frac{(\dot{m}Cp)H20\ (T_{c,o} - T_{c,i})}{(\dot{m}Cp)\min(T_{h,i} - T_{c,i})}$, which is introduced in section 5.2 already.

As the mass of condensation water is negligible compared to the refrigerant, as a result,

$$(\dot{m}Cp)\min = (\dot{m}Cp)H20 \tag{110}$$

Heat exchanger effectiveness is then simplified as

$$\text{Ɛ} = \frac{(T_{c,o} - T_{c,i})}{(T_{h,i} - T_{c,i})} \tag{111}$$

In equation (111), $T_{c,o}$ is the outlet water temperature after heat exchanger, $T_{c,i}$ is the inlet water temperature of the heat exchanger, which is equal to the outlet air temperature of the evaporator. $T_{h,i}$ is the outlet refrigerant temperature exiting from condenser before entering heat exchanger.

Heat transfer occurs as the injected condensate water gained energy from the refrigerant entering the heat exchanger with the energy transfer causing the condensate water evaporate and hot liquid refrigerant to cool. Considering the heat exchanger as a control volume, there is no heat absorbed or rejected to the surrounding, which means the heat absorption of the condensate water equals to the heat rejection from the hot refrigerant liquid,

$$\dot{Q}_R = \dot{Q}_w \tag{112}$$

where $\dot{Q}_w$ is the heat transfer to the water,

$$\dot{Q}_w = \dot{m}_w\ C_{PW}\ (T_{c,o} - T_{c,i}) \tag{113}$$

where $\dot{m}_w$ is the mass flow rate of condensation water, Cpw is the specific heat of water.

$\dot{Q}_R$ is the heat transfer to the refrigerant,

$$\dot{Q}_R = \dot{m}_R (h_3 - h_3') \quad (114)$$

where, $\dot{m}_R$ is the mass flow rate of refrigerant, h_3' is the enthalpy of outlet refrigerant from condenser after heat exchanger and h_3 is the enthalpy of outlet refrigerant entering the heat exchanger

By combining Eqn 113 and 114,

$$\dot{m}_w C_{PW} (T_{c,o} - T_{c,i}) = \dot{m}_R (h_3 - h_3') \quad (115)$$

Since the mass flow rate of refrigerant is the same through the whole system, by combing equation (109), (111) and equation (115), a final equation is yield as,

$$(h_1 - h_3')(w_1 - w_2)\, Cpw\, (T_{c,o} - T_{c,i}) = (h_{1a} - h_{2a})(h_3 - h_3') \quad (116)$$

By using the above equation, we can obtain the final enthalpy of outlet refrigerant after heat exchanger is a function of outdoor air conditions (temperature and relative humidity), supply air temperature (evaporator outlet air temperature) and heat exchanger effectiveness, namely h_3'=f($T_{evap\ inlet\ air}$, RH, $T_{evap\ outlet\ air}$, Ɛ).

5.3.3 Simulation Input and Output

A comprehensive model was developed and programmed in EES 2017 for a vapor-compression conditioning system comprising air-to-refrigerant evaporator and condenser, a compressor, a thermal expansion valve and a heat exchanger connected between condenser outlet and evaporator. The heat transfer occurs between the outlet refrigerant of the condenser and condensation water in the evaporator. As a result, the outlet refrigerant from condenser will drop from saturated state to subcooling state. For the compressor, a fixed isentropic efficiency of 80% was assumed for this model. For the outdoor air, uniform temperature and velocity were also

assumed. The input variables of the model were outdoor air temperature (T_a), relative humidity ($\emptyset a$); evaporator outlet air temperature (T_{aeo}); heat exchanger effectiveness (ε). Typical outcomes of the model are specific work (w), refrigerating effect (q), vapor-compression system coefficient of performance (COP).

5.3.4 Simulation Data Set-up and Overview

In this section, outdoor air temperatures of 26.7, 29.4, 32.2, 35 ℃ (80, 85, 90, 95℉) and relative humidities of 40%, 50%, 60%, 70%, 80% over a range of assumed evaporator exit air temperatures of 7.2, 10, 12.8℃ (45, 50, 55℉) with a typical compressor efficiency of 80%. Heat Exchanger Effectiveness is 0, 20%, 50%, 80%, and 100%.

5.3.5 Results and Analysis

5.3.5.1 Scenario C Alone (Take Effectiveness 80% for Example)

Since COP of the reconfigured system increase with the increasing effectiveness, thus take the case of 80% effectiveness for example in this section. Figure 137 gives an overview of how reconfigured system C (subcooling) system performance related to three variables, namely ourdoor air temperatures, relative humidities and Taeo, and it further shows that COP of the reconfigured system remained quite constant with the increase relative humidity. Figure 138, 139, 140 and 141 show how COP varies with different Taeo under the same outdoor air temperature, and it is observed that COP increases with the boosting Taeo. Figure 142, 143 and 144 show how COP varies with different outdoor air temperatures under the same Taeo and it is further observed that COP decreases with the increasing outdoor air temperature. The trend of COP varied with the three parameters is further summarized in Table 25.

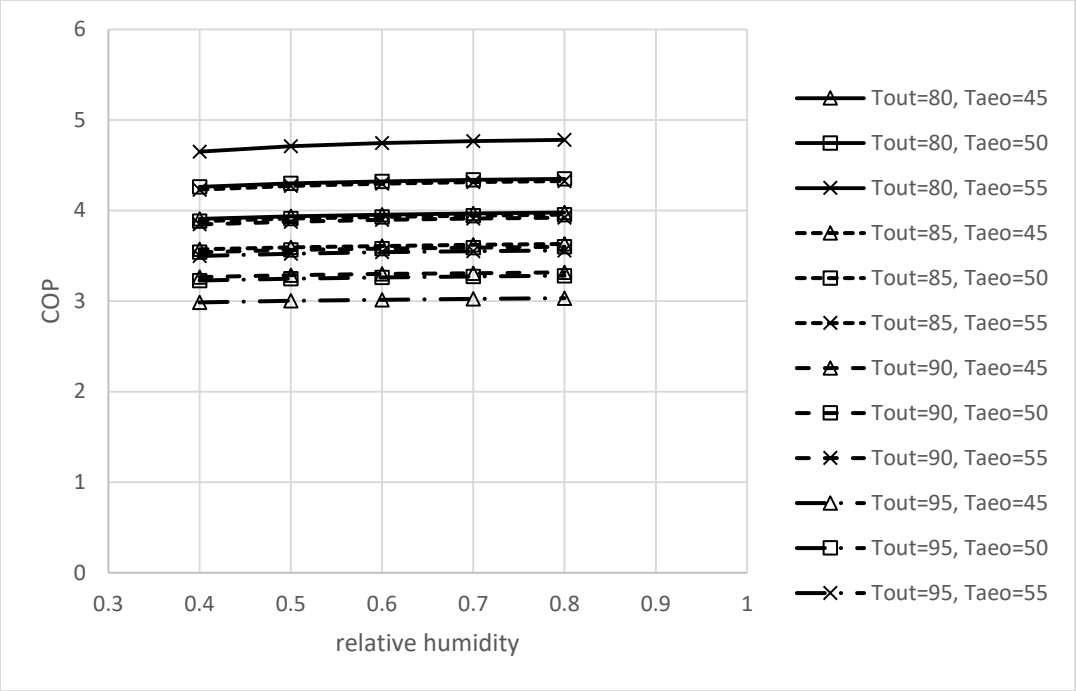

Figure 137 COP with condensing refrigerant subcooling varied with relative humidity under different conditions

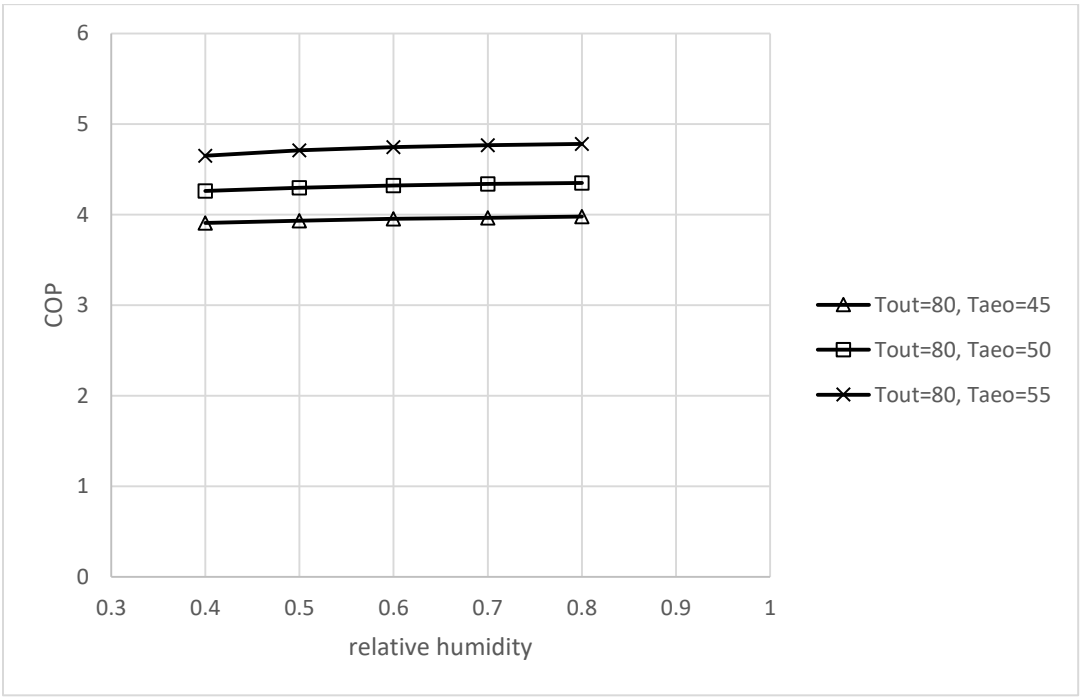

Figure 138 COP with condensing refrigerant subcooling varied with relative humidity when Tout=80 °F

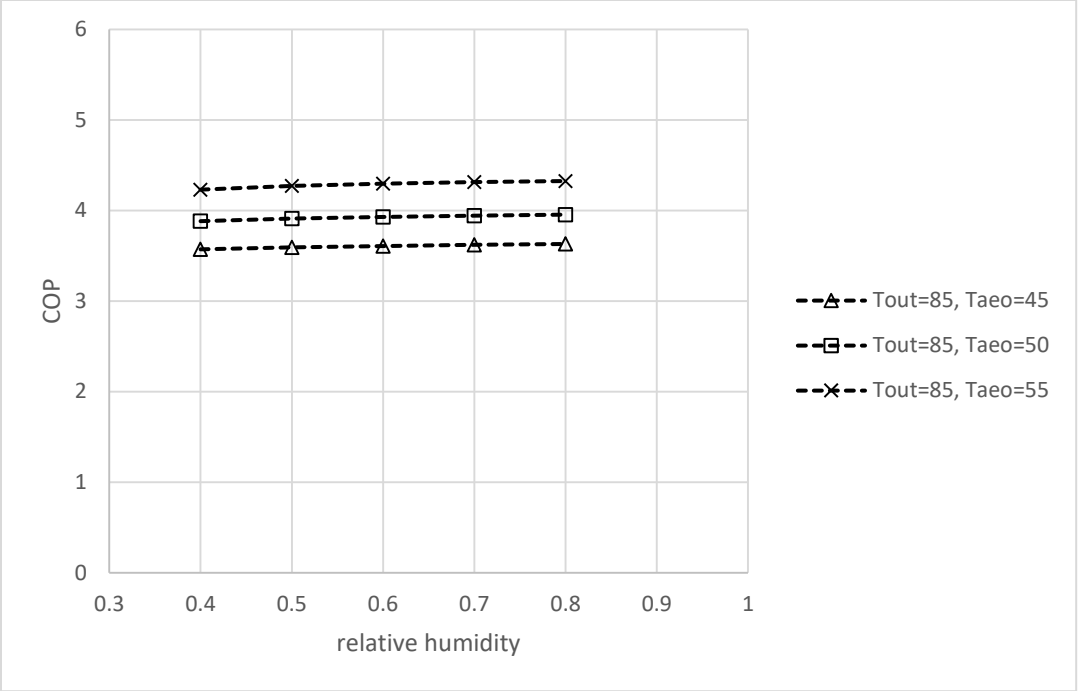

Figure 139 COP with condensing refrigerant subcooling varied with relative humidity when Tout=85 °F

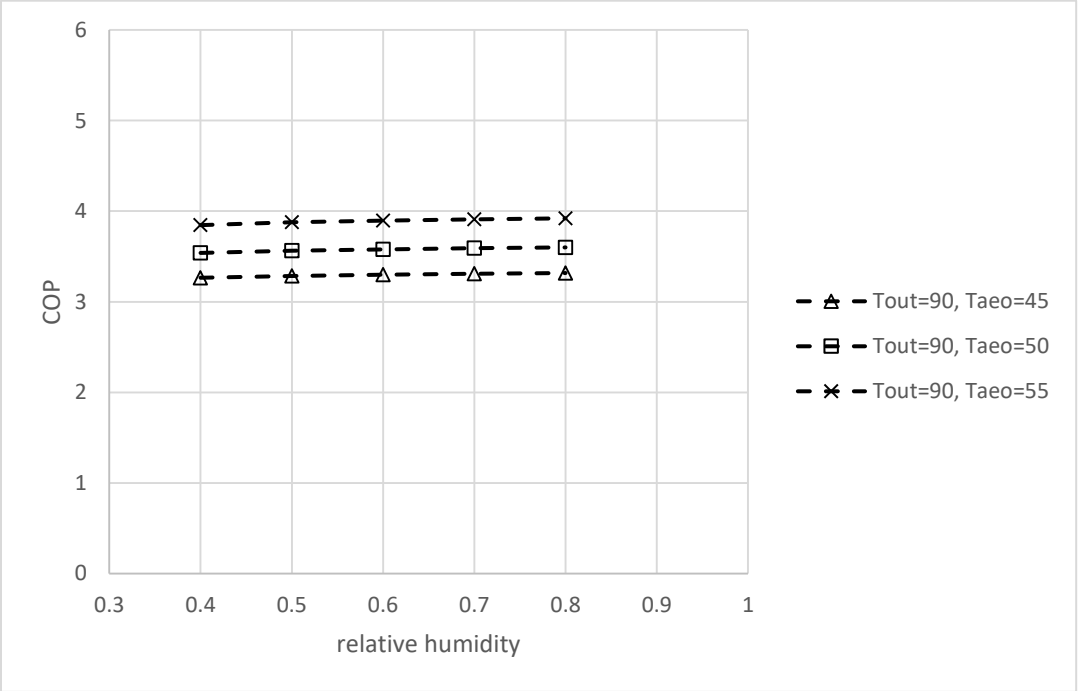

Figure 140 COP with condensing refrigerant subcooling varied with relative humidity when Tout=90 °F

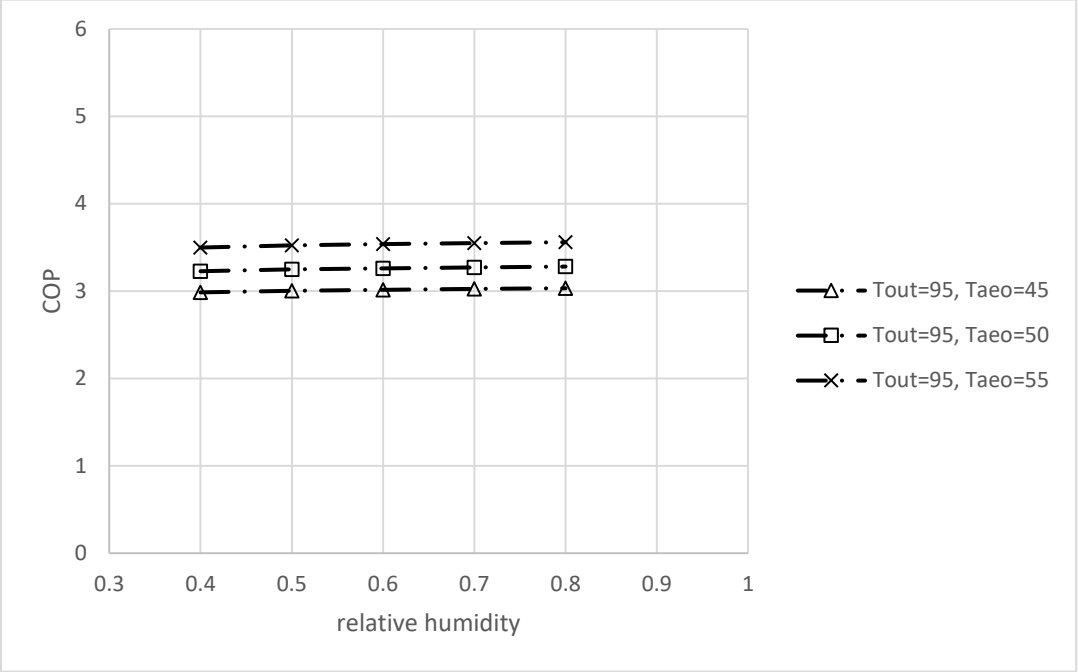

Figure 141 COP with condensing refrigerant subcooling varied with relative humidity when Tout=95 °F

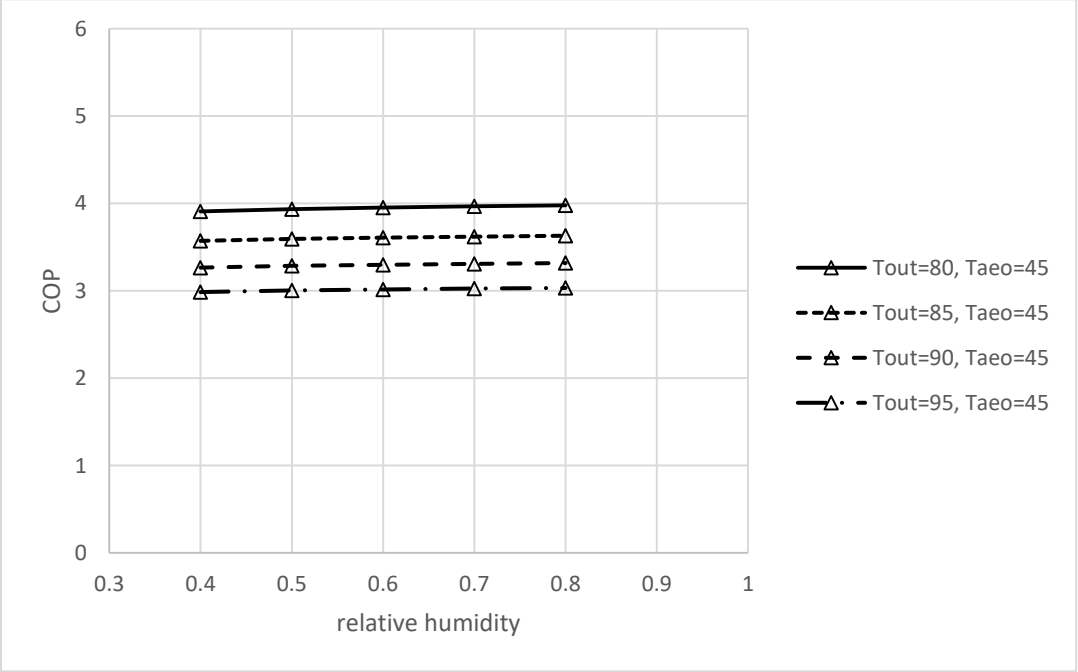

Figure 142 COP with condensing refrigerant subcooling varied with relative humidity when Taeo=45 °F

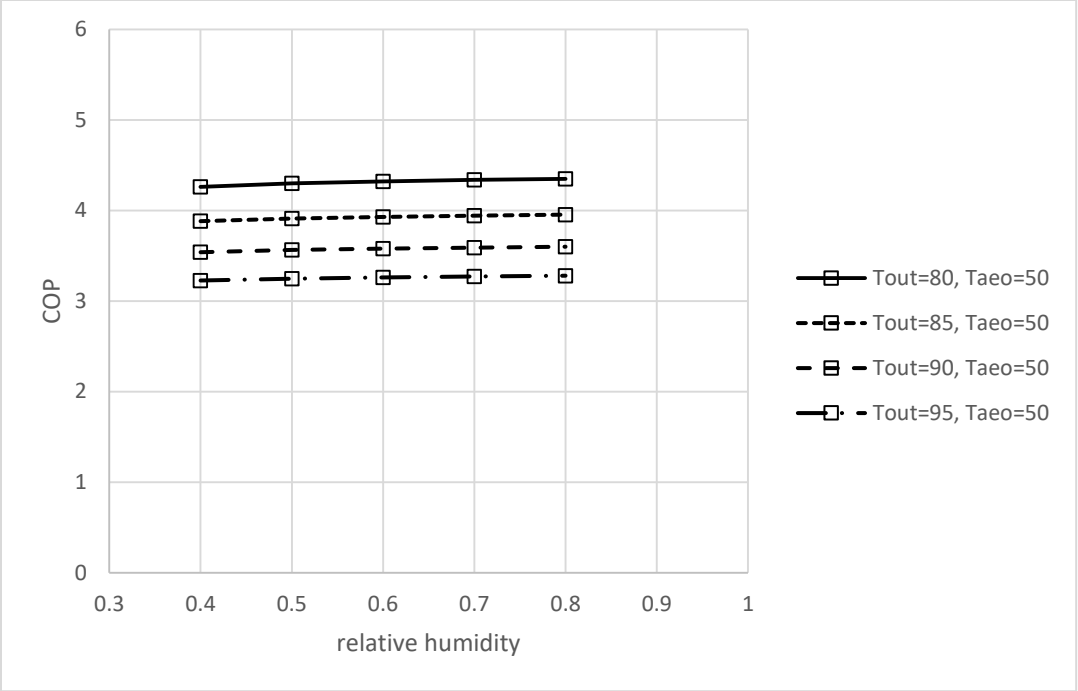

Figure 143 COP with condensing refrigerant subcooling varied with relative humidity when Taeo=50 °F

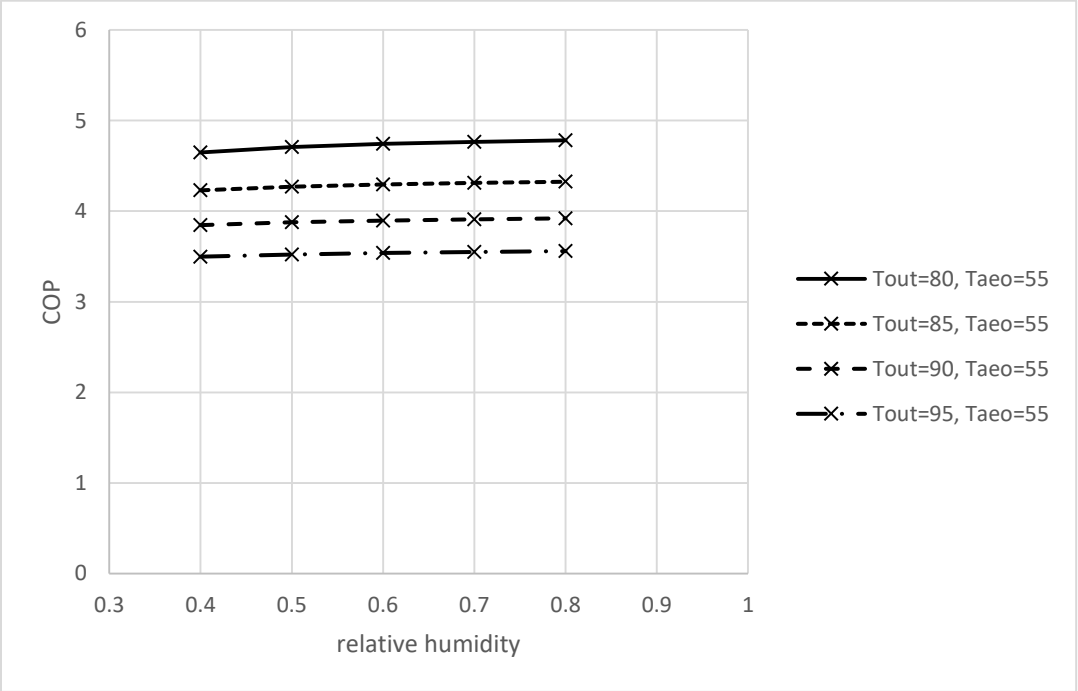

Figure 144 COP with condensing refrigerant subcooling varied with relative humidity when Taeo=55 °F

Table 25 COP with condensing refrigerant subcooling varied with Tout, RH and Taeo

case	T_{out}	RH	T_{aeo}	COP with subcooling
1	↑	→	→	↓
2	→	↑	→	→
3	→	→	↑	↑

5.3.5.2 Compare Scenario B to Scenario A

5.3.5.2.1 COP improvement due to subcooling overview

Figure 145 shows the relationship between COP with and without subcooling. It is observed that the improvement of all the data is within 10% and the highest improvement can reach around 5%.

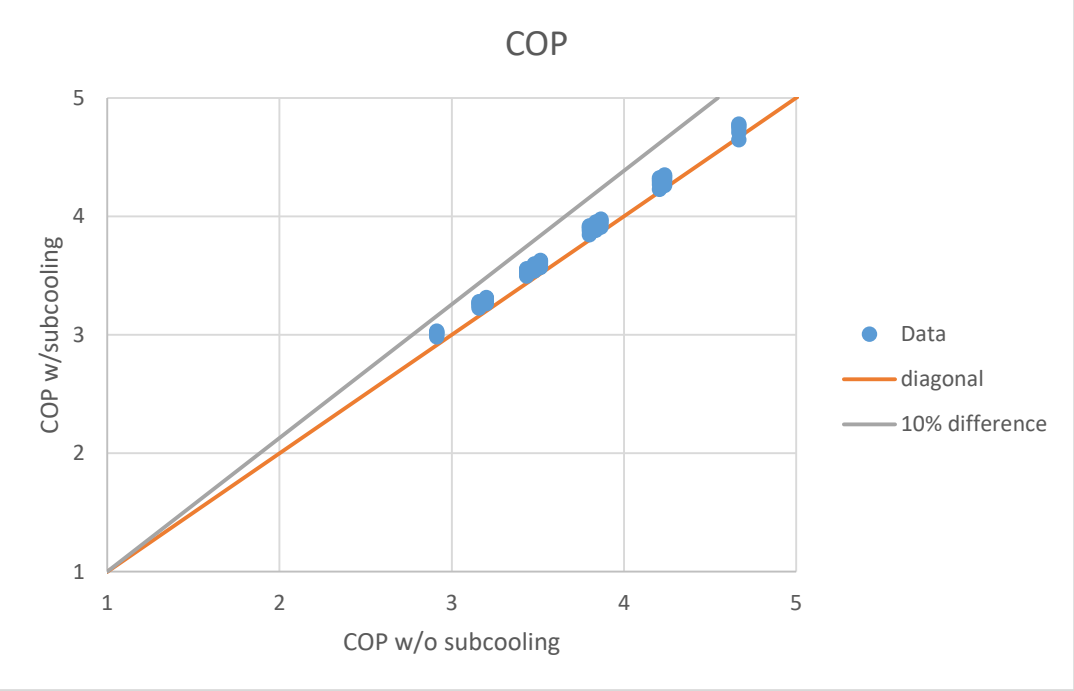

Figure 145 COP improvement with condensing refrigerant subcooling

5.3.5.2.2 COP Enhancement Analysis

Figure 146 gives an overview of how percentage difference (reconfigured system C compared to baseline system A) related to the three variables, namely outdoor air temperatures, relative humidities and Taeo, and Figure 146 further shows that COP percentage difference increase with boosting relative humidity. Figure 147, 148, 149 and 150 show how COP percentage difference varies with different Taeo under the same outdoor air temperature, and it is indicated that COP percentage difference decreases with the boosting Taeo. Figure 151, 152 and 153 show how COP percentage difference varies with different outdoor air temperature under the same Taeo and these three plots illustrate that COP percentage difference increases with the boosting outdoor air temperature. The trend of COP improvement varied with aforementioned three variables are summarized in Table 26.

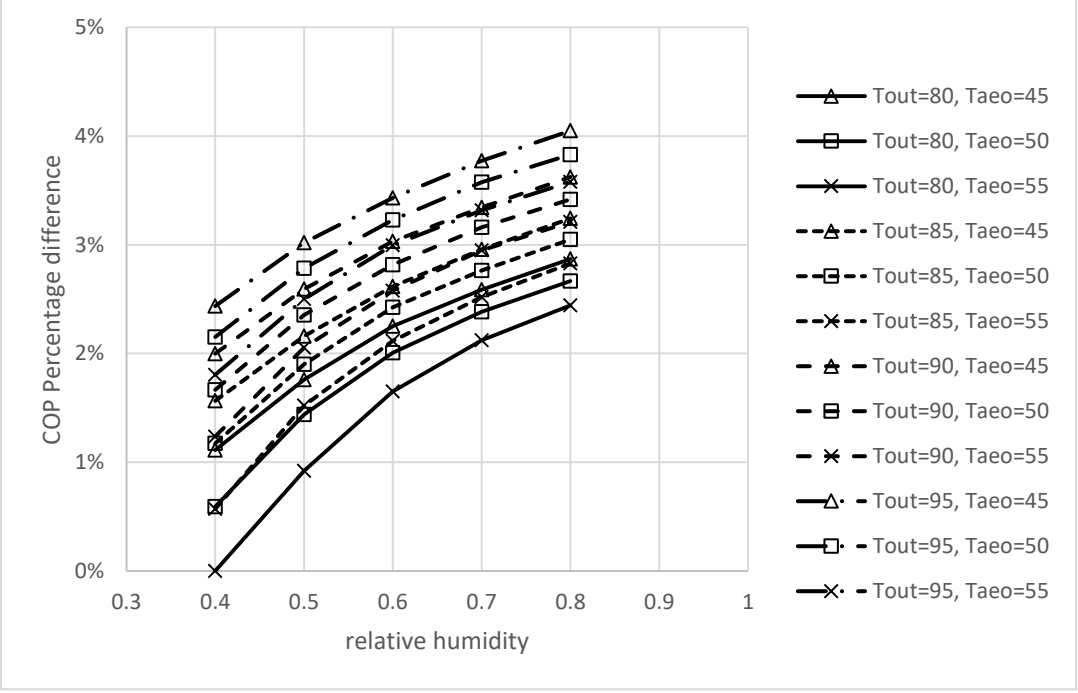

Figure 146 COP percentage difference (system with condensing refrigerant subcooling over baseline) versus relative humidity under different conditions

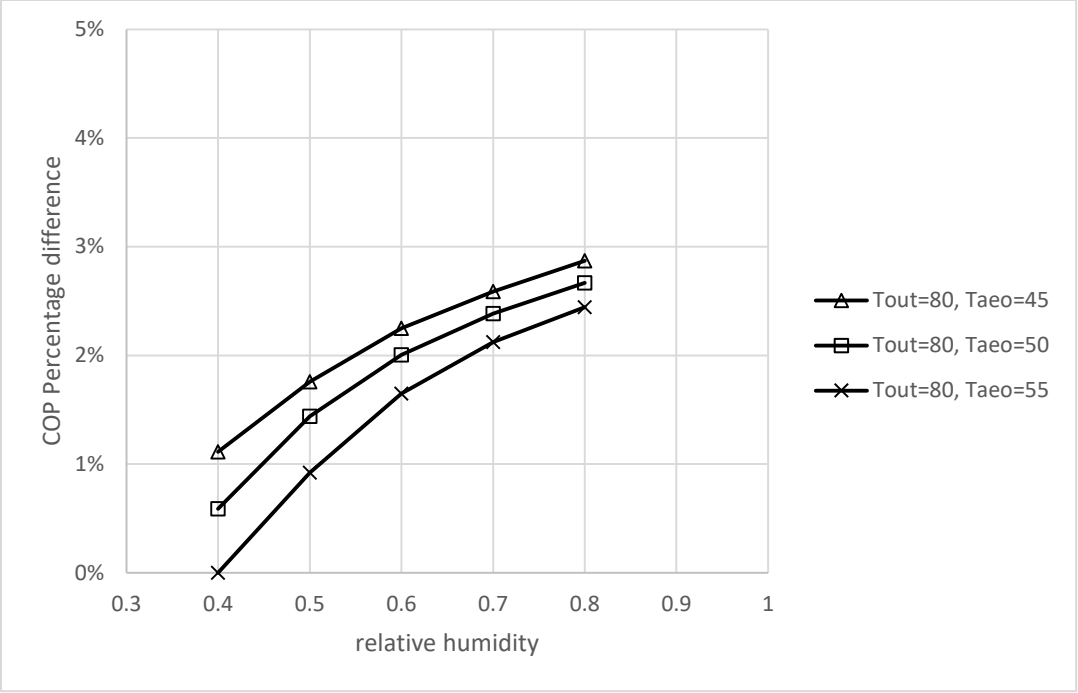

Figure 147 COP percentage difference (system with condensing refrigerant subcooling over baseline) versus relative humidity when Tout=80°F

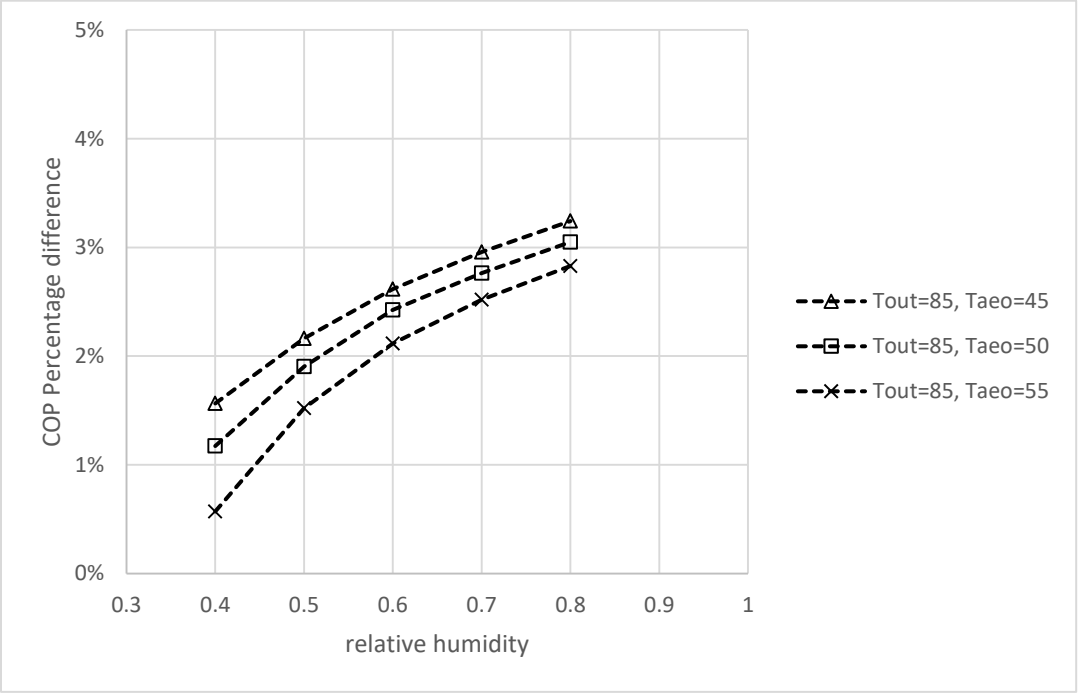

Figure 148 COP percentage difference (system with condensing refrigerant subcooling over baseline) versus relative humidity when Tout=85°F

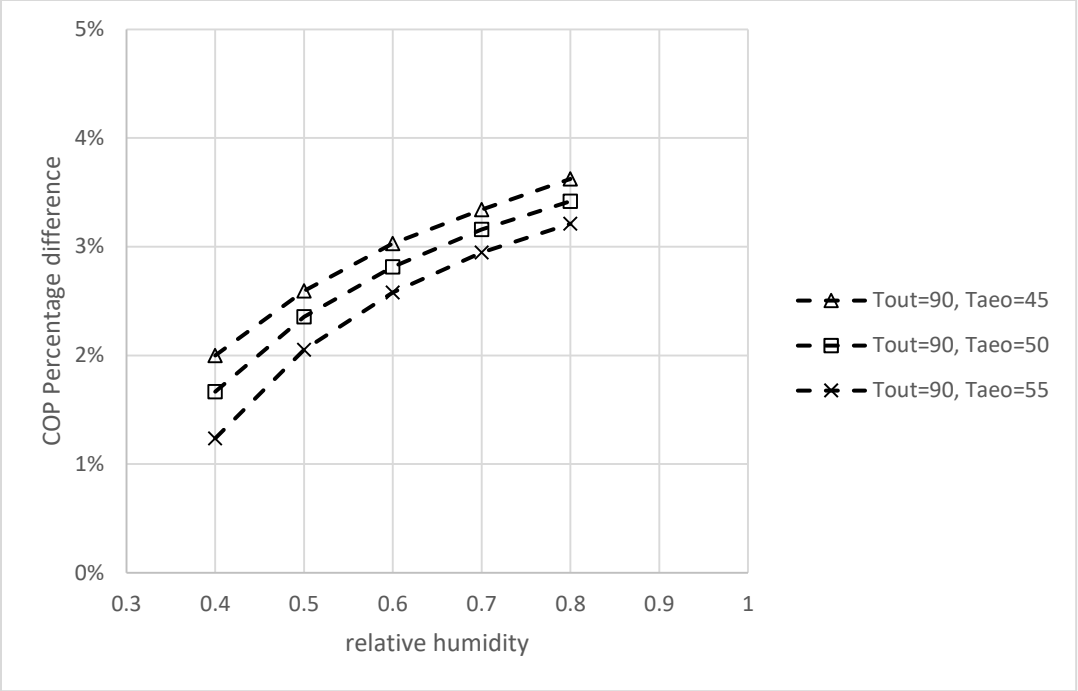

Figure 149 COP percentage difference (system with condensing refrigerant subcooling over baseline) versus relative humidity when Tout=90°F

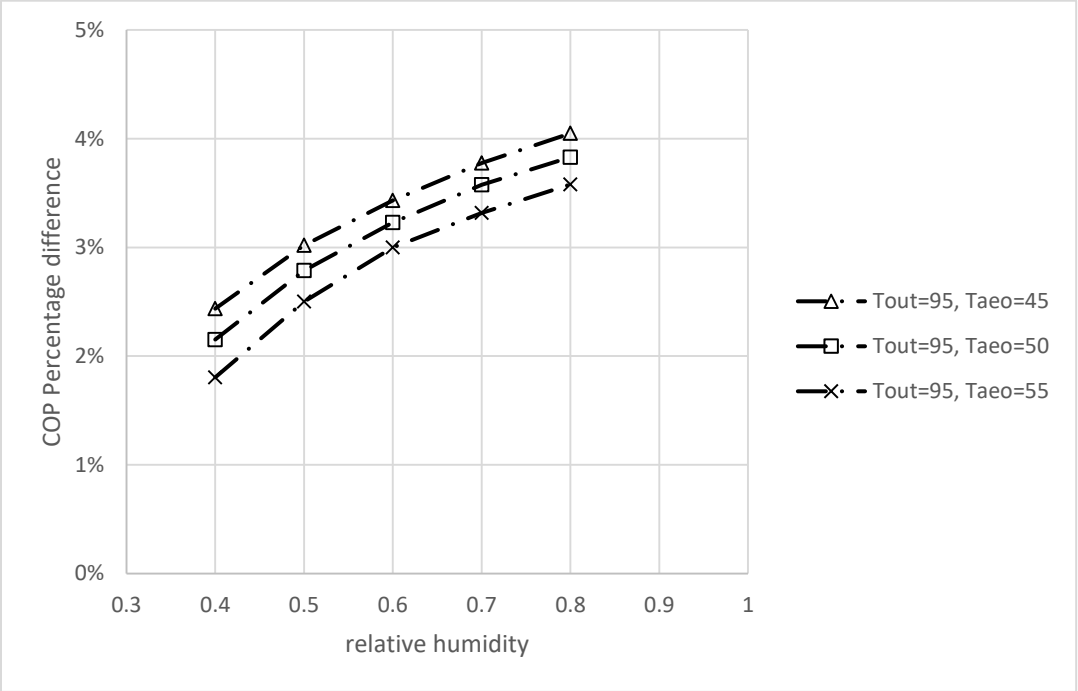

Figure 150 COP percentage difference (system with condensing refrigerant subcooling over baseline) versus relative humidity when Tout=95°F

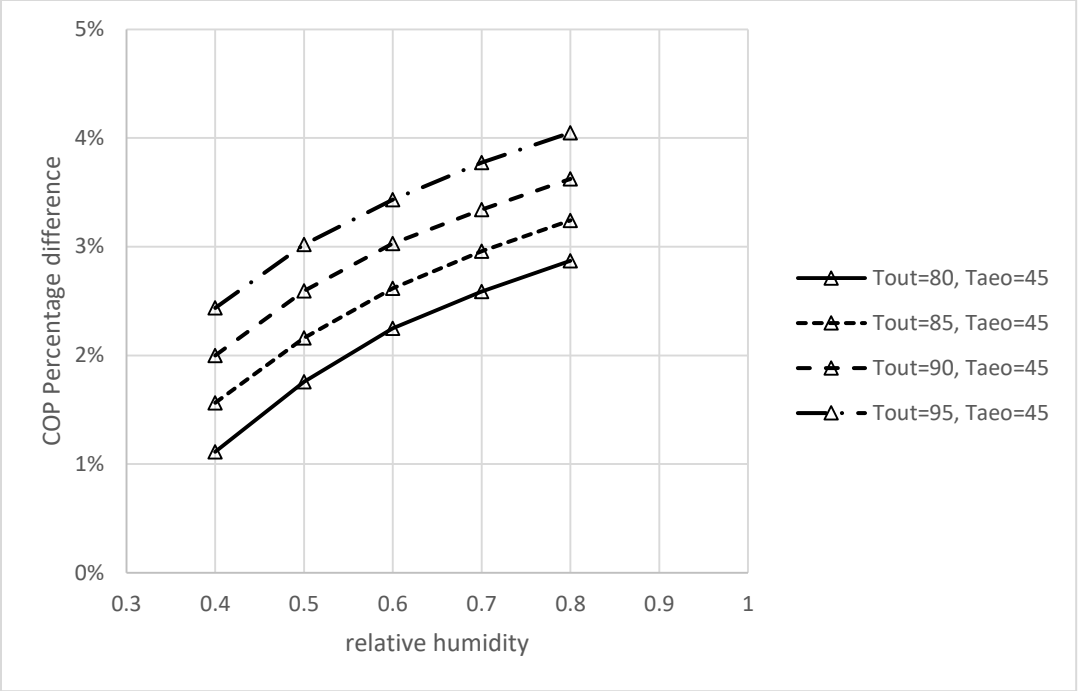

Figure 151 COP percentage difference (system with condensing refrigerant subcooling over baseline) versus relative humidity when Taeo=45°F

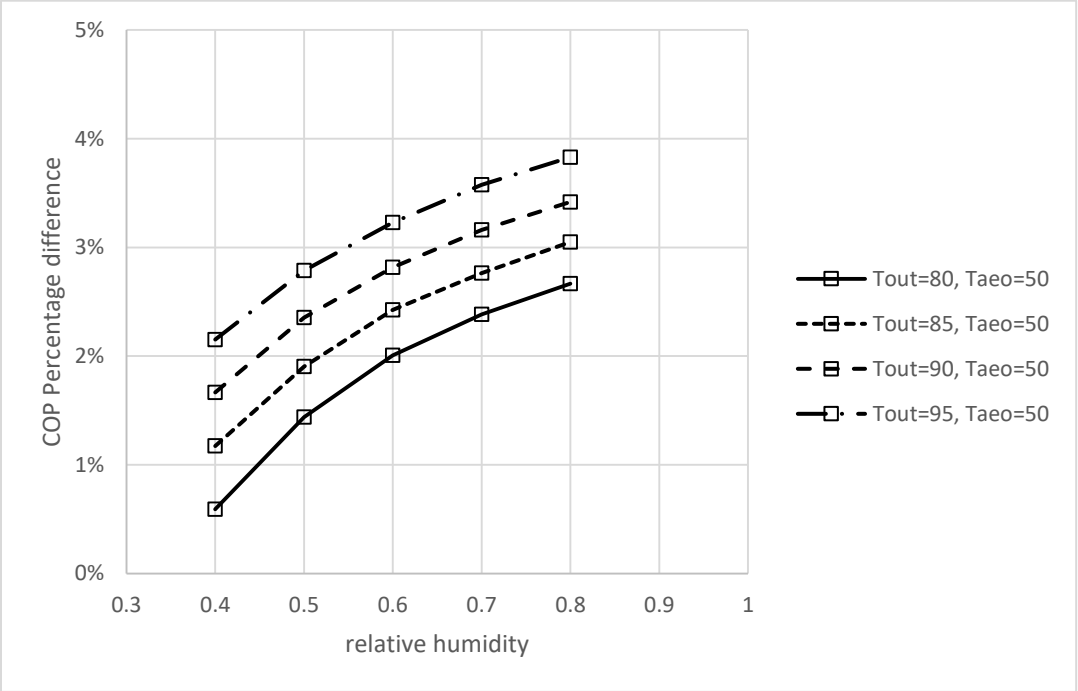

Figure 152 COP percentage difference (system with condensing refrigerant subcooling over baseline) versus relative humidity when Taeo=50°F

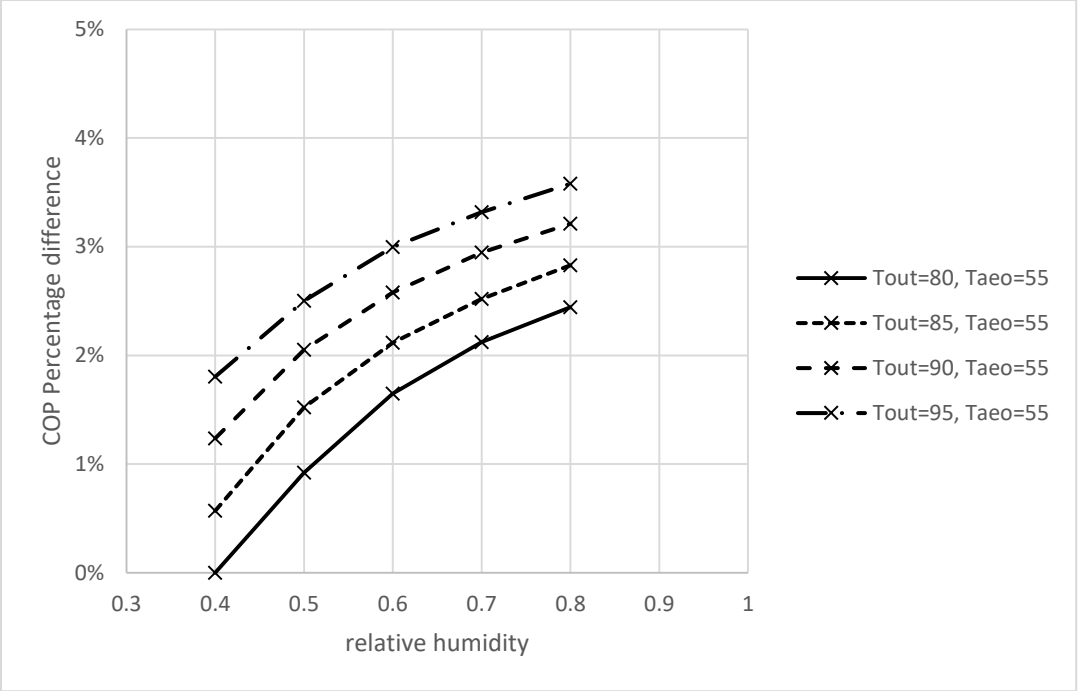

*Figure 153 COP percentage difference (system with condensing refrigerant subcooling over baseline) versus relative humidity when Taeo=50°*F

Table 26 COP percentage difference (system with condensing refrigerant subcooling over baseline) varied with Tout, RH, and Taeo

case	T_{out}	RH	T_{aeo}	% difference
1	↑	→	→	↑
2	→	↑	→	↑
3	→	→	↑	↓

5.3.5.3 Heat Exchanger Effectiveness Influence

From the result of Section 5.3.5.2, reconfigured system COP benefits the most when outdoor temperature and relative humidity is high. Thus, it is necessary to study that case with difference heat exchanger effectiveness. Figure 154 show the COP improvement with heat

exchanger effectiveness from 0 to 100% when outdoor air temperature is 95 °F and relative humidity is 80% for different Taeo. It is further observed that COP can improve as much as 5% when heat exchanger effectiveness is 100% and negligible when heat exchanger effectiveness is 20%.

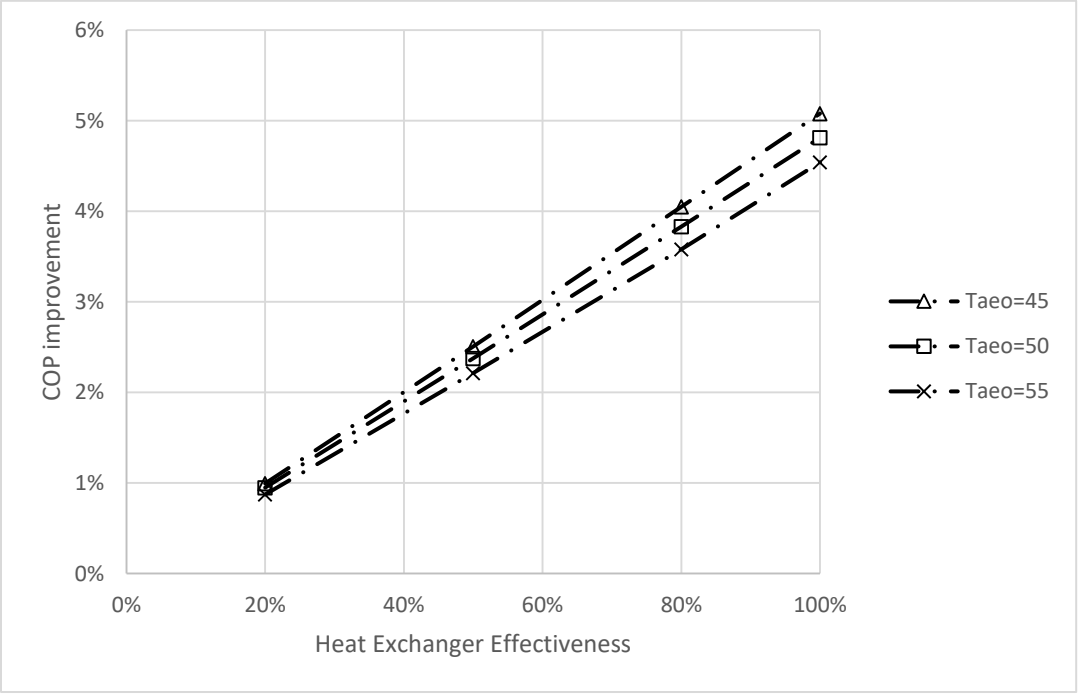

Figure 154 COP percentage difference (system with condensing refrigerant subcooling over baseline) versus relative humidity when Tout=95°F and RH=80%

5.3.5.4 Correlation Development

5.3.5.4.1 COP with Condensing Refrigerant Subcooling Correlation

Similarly to Reconfigured system B1 and B2, only exponential model is considered in this section. According to the equations aforementioned, plus several assumptions made for this model, it is known that COP with condensing refrigerant subcooling is a function of outdoor air temperature and relative humidity, Taeo and heat exchanger effectiveness. Since effectiveness of heat exchanger is 20%, 50%, 80% and 100%, which are fixed values, then the exponential model is set as log COP=f (RH, Taeo, Tout) for each different heat exchanger effectiveness. For this

section, heat exchanger effectiveness of 20% is taken as an example, all the other heat exchanger effectiveness data is in Appendix B and C. A complete quadratic regression of log COP is built in Table 27. The error between predicted data and actual data is indicated in Figure 155---always less than 1%.

Table 27 log $COP_{subcooling}$ Model Coefficients when HX effectiveness is 20%

a0+a1*RH^2+a2*RH+a3*Taeo^2+a4*Taeo+a5*Tout^2+a6*Tout+a7*RH*Taeo+a8*Taeo*Tout+a9*RH*Tout									
a0	a1	a2	a3	a4	a5	a6	a7	a8	a9
1.80	-0.0196	0.0370	7.52e-5	0.0231	2.26e-5	-0.0156	0.000338	-0.000153	-0.000218

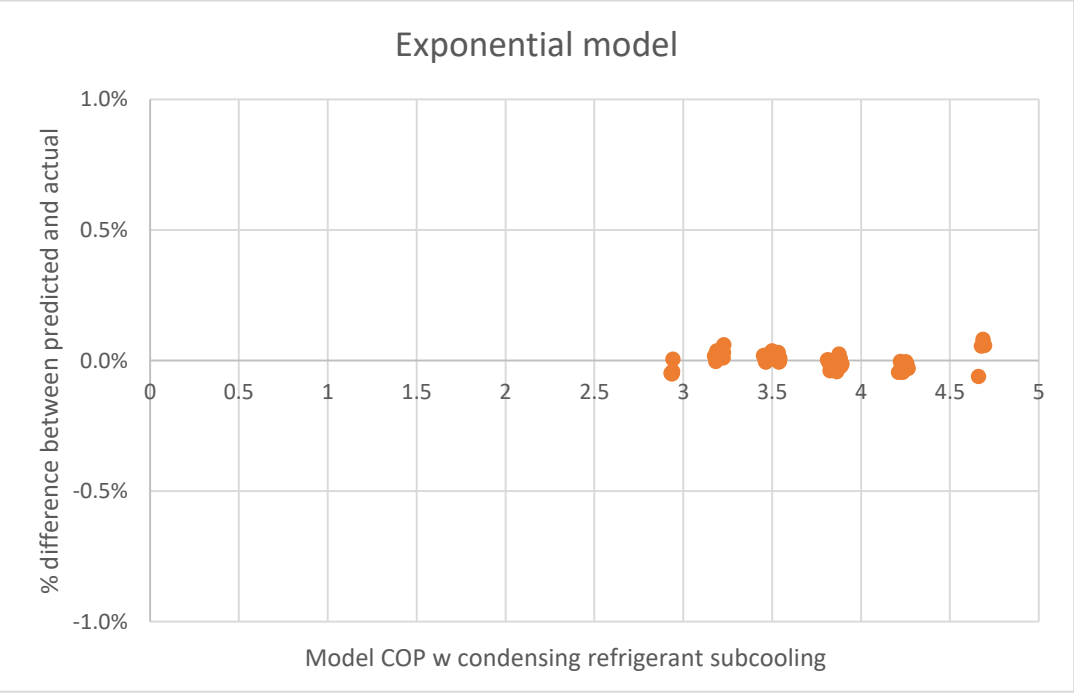

Figure 155 Percentage difference comparison of predicted and actual data of exponential method for COP with condensing refrigerant subcooling when HX effectiveness is 20%

5.3.5.4.1.1 COP Ratio of Condensing Refrigerant Subcooing (C) over Baseline (A) Correlation

Only exponential model is considered in this section. According to the equations aforementioned, plus several assumptions made for this model, it is known that COP ratio with condensing refrigerant subcooling is a function of outdoor air temperature and relative humidity, Taeo and heat exchanger effectiveness. Since effectiveness of heat exchanger is 20%, 50%, 80% and 100%, which are fixed values, then the exponential model is set as log COP ratio=f (RH, Taeo, Tout) for each different heat exchanger effectiveness. For this section, heat exchanger effectiveness of 20% is taken as an example, all the other heat exchanger effectiveness data is in Appendix A and B. A complete quadratic regression of log COP ratio is built in Table 28. The error between predicted data and actual data is indicated in Figure 156---always less than 4%.

Table 28 log COP ratio (condensing refrigerant subcooling over baseline system) Model Coefficients for HX effectiveness=20%

a0+a1*RH^2+a2*RH+a3*Taeo^2+a4*Taeo+a5*Tout^2+a6*Tout+a7*RH*Taeo+a8*Taeo*Tout+a9*RH*Tout									
a0	a1	a2	a3	a4	a5	a6	a7	a8	a9
-0.0158	-0.0196	0.0370	-6.61e-6	-0.360e-5	5.010e-7	6.07e-5	0.0370	4.01e-6	-0.000218

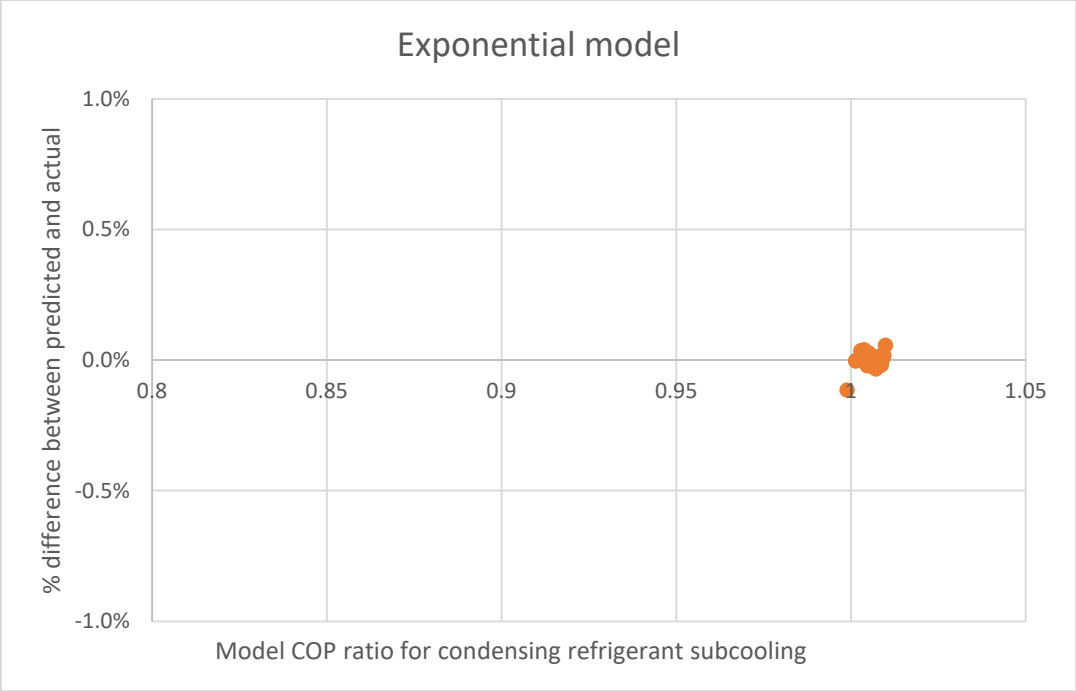

Figure 156 Percentage difference comparison of predicted and actual data of exponential method for COP ratio of condensing refrigerant subcooling over baseline when HX effectiveness is 20%

5.3.5.5 Comparisons to Experimental Results

On top of using software (EES) to simulate the model, Riverside Energy Efficiency Laboratory did series of experiments to verify the results. The AC Boost Standard device has room to improve as a heat exchanger with an effectiveness of 36%, and removed about 0.8% of the total cooling capacity of the evaporator; while AC Boost Turbo is a more effective heat exchanger reaching an effectiveness of 80%, which can remove 1.1% of the total cooling capacity. Even if with a perfect heat exchanger the condensate alone could only remove the heat of about 1.4% of the total cooling capacity. The AC Boost Turbo showed the greatest change in cooling capacity and COP In addition, the AC Boost Turbo device has little or no effect on the rate the humidity drops compared to the baseline unit for the conditions the device was tested in. Nevertheless, the

Mini Evaporator Device was ineffective at increasing the cooling capacity of the system for different testing conditions.

5.3.6 Conclusions

This section studied the effect of utilizing condensate water through a heat exchanger with condenser outlet refrigerant on the vapor-compression system coefficient of performance (COP) using R410A. Based on the result, it is concluded as follows:

1. For all different working conditions, COP percentage difference is less than 5%.

2. It is concluded that COP of the reconfigured system remained quite constant with the increase relative humidity, COP increased with the increasing Taeo and decreased with the increasing outdoor air temperature.

3. It is concluded that COP percentage difference increase with increasing relative humidity, decrease with the increasing Taeo and increase with the increasing outdoor air temperature, increase with the boosting heat exchanger effectiveness. Thus, this reconfigured system is suitable for the hot and humid region with low supply room temperature.

4. The effect of utilizing condensate water through a heat exchanger with condenser outlet refrigerant on the vapor-compression system coefficient of performance (COP) is not significant compared to other subcooling method shown in introduction. However, instead of draining this high-quality water into sewers, utilizing condensate water will not cost much compared to other subcooling methods.

5.4 Internal Heat Exchanger (Liquid-to-Suction HX) Reconfigured system D

Internal heat exchangers (liquid-to-suction heat exchanger) have been adopted in vapor-compression cycles, not only to reduce the vapor quality at the evaporator inlet, thus increasing

the evaporator capacity but also to prevent slugging of the compressor and sweating of the suction line. The internal heat exchanger may either increase or reduce the cycle efficiency, as measured by the Coefficient of Performance (COP), depending on the relative effect of an increasing refrigerating effect and an increasing compression work. Thus, the net effect on the performance of the installation of an internal heat exchanger (liquid-line/suction line heat exchanger) is analyzed theoretically for a conditional representative of HVAC cooling which is unlike residential refrigeration that has been studied in the past. The most commonly used refrigerant namely R410A for vapor-compression HVAC building systems will be used as working fluid. The coefficient of performance (COP) with/without internal heat exchanger is evaluated for a wide range of heat exchanger effectivenesses and working conditions. It is shown that for all conditions, the boosting of the refrigerating effect caused by the internal heat exchanger is much more significant than the increasing compression work, resulting in an increasing COP, which is defined as the refrigerating effect divided by compression work. Also, as expected, the COP increase with heat exchanger effectiveness. Of special note, it was found that the highest COP increase with an internal heat exchanger system compared to a baseline system is 32% when effectiveness is 100%. At the other extreme, the COP improvement is always less than 10% when heat exchanger effectiveness is at the low end of its range, such as 20%. In sum, the reconfigured system with the installation of an internal heat exchanger gets the most benefit for hot temperature climate zones along with low room supply air temperature (evaporator outlet air temperature).

5.4.1 Introduction

The state of refrigerant evaporator outlet and condenser outlet will be changed from saturated to superheating and subcooling, respectively. The effect of subcooling is to lower the temperature of the refrigerant in the condenser exit, reducing the vapor quality at the evaporator

inlet, increasing in enthalpy difference through the evaporator, which results in boosting the evaporator cooling capacity. In addition, the utilization of subcooling ensures the phase of refrigerant as liquid-phase at the inlet of the expansion device, which reduces the risk of flashing vapor-phase at the expansion device inlet. Using Internal Heat Exchanger generates superheating in the suction of the compressor, where the superheating ensures only vapor phase of refrigerant entering the compressor suction and prevents slugging of the compressor and sweating of the suction line.

One can note that employing the internal heat exchanger increases the specific refrigerating effect. On the other hand, the specific volume of the refrigerating vapor at the beginning of the compression rises and, as a consequence, the specific compression work increases too. The system coefficient of performance (COP), namely the ratio of the refrigerating effect to the compression work, could be higher or lower than the baseline cycle (without internal heat exchanger). Furthermore, the so-called internal heat exchanger may either increase or reduce the system performance, which is depending on the combination of refrigerant properties (particular those that affect the volumetric refrigerating effect) and operating conditions.

Therefore, the aim of the present study is to verify the effect of the internal heat exchanger by utilizing software (EES) of simulating a model and getting accurate data of refrigerating effect, specific compression work, system COP with/without internal heat exchanger under a wide range operating conditions with R410A as working fluid.

5.4.2 System Description

As it is known to all, an Internal Heat Exchanger, also called liquid-to-suction heat exchanger, consists of one inner chamber and one outer chamber. Hot liquid refrigerant from the condenser flows through the inner chamber, and it is surrounded by cool refrigerant vapor flowing

from the evaporator through the outer chamber, as shown in Figure 157. Finally, heat transfer occurs between the inner chamber and outer chamber. The state of refrigerant evaporator outlet and condenser outlet will be changed from saturated to superheating and subcooling, respectively. The effect of subcooling is to lower the temperature of the refrigerant in the condenser exit, reducing the vapor quality at the evaporator inlet, increasing in enthalpy difference through the evaporator, which results in boosting the evaporator cooling capacity. Also, the utilization of subcooling ensures the phase of refrigerant as liquid-phase at the inlet of the expansion device, which reduces the risk of flashing vapor-phase at the expansion device inlet. Using Internal Heat Exchanger generates superheating in the suction of the compressor, where the superheating ensures only vapor phase of refrigerant entering the compressor suction and prevents slugging of the compressor and sweating of the suction line. From Figure 158, with Internal Heat Exchanger, refrigerating effect increases and the compressor work variation will be decided by the result of the simulation.

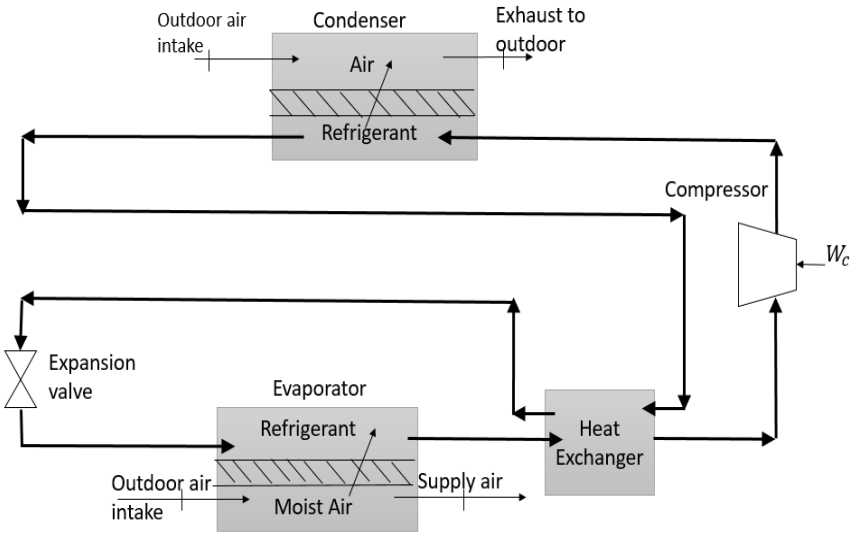

Figure 157 Reconfigured system by using Internal Heat Exchanger

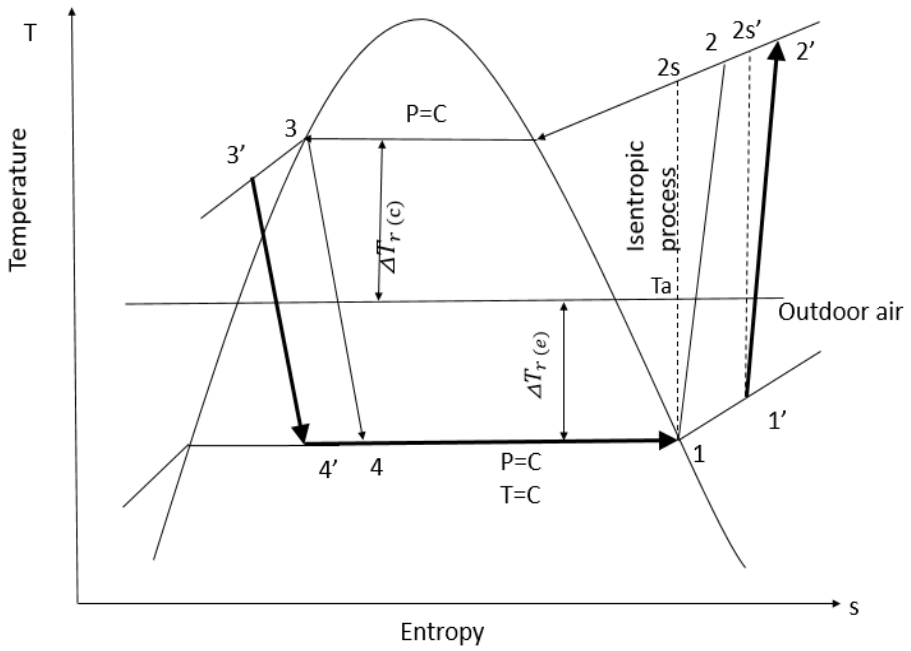

Figure 158 Ts diagram by using Internal Heat Exchanger

5.4.3 Model Formulation and Development

To calculate the critical refrigerant cycle performance parameters, such as the refrigeration cooling effect, the compressor work, and COP, it is necessary to specify or determine the thermodynamic state properties of the cooling refrigerant at each point in the vapor compression cycle. To accomplish this task, it is also necessary to know the state properties and flow conditions of the moist air entering and leaving the evaporator and condenser. Therefore, determining the performance parameters, such as COP, that will allow for evaluating the effect of the internal heat exchanger (liquid-suction line heat exchanger) requires developing, deriving, and solving three separate processes, namely: 1) evaporating and condensing refrigerant temperature calculation 2) heat transfer in internal heat exchanger 3) vapor-compression refrigeration cycle. Only the second process differs from the previous reconfigured system, and this process is the focus of this section.

5.4.3.1 Heat Transfer in Internal Heat Exchanger

According to ASHRAE Standard 84, effectiveness is defined as $\varepsilon = \frac{Actual\ transfer\ of\ moisture\ or\ energy}{Maximum\ possible\ transfer\ between\ airstreams}$ and it is then simplified as $\varepsilon = \frac{Q}{Q_{max}} = \frac{(\dot{m}Cpg)\ (T_{c,o} - T_{c,i})}{(\dot{m}Cp)\min(T_{h,i} - T_{c,i})}$, which is also defined in the previous section, where $T_{h,i}$ and $T_{h,o}$ are the inlet and outlet of the condenser refrigerant while $T_{c,o}$ and $T_{c,i}$ are the outlet and inlet of the evaporator refrigerant. C_{pf} and C_{pg} are fluid and vapor specific heat. As fluid specific heat is larger than vapor specific heat, we can simplify equation (117) as

$$\varepsilon = \frac{(T_{c,o} - T_{c,i})}{(T_{h,i} - T_{c,i})} \tag{117}$$

Heat transfer occurs as the injected cold refrigerant vapor gained energy from the hot liquid refrigerant entering the internal heat exchanger with the energy transfer causing the saturated refrigerant vapor get superheated and hot liquid refrigerant to cool. Considering the internal heat exchanger as a control volume, there is no heat absorbed or rejected to the surrounding, which means the heat absorption of the cold refrigerant vapor equals to the heat rejection from the hot refrigerant liquid,

$$\dot{Q}_{Rv} = \dot{Q}_{Rl} \tag{118}$$

where $\dot{Q}_{Rv}$ is the heat transfer to the refrigerant vapor,

$$\dot{Q}_{Rv} = \dot{m}_R\ (h_1' - h_1) \tag{119}$$

where $\dot{m}_R$ is the mass flow rate of the refrigerant, h_1' is the enthalpy of outlet refrigerant from evaporator after internal heat exchanger and h_1 is the enthalpy of evaporator outlet refrigerant entering the internal heat exchanger.

$\dot{Q}_{Rl}$ is the heat transfer to the refrigerant liquid,

$$\dot{Q}_{Rl} = \dot{m}_R\ (h_3 - h_3') \tag{120}$$

Where h_3' is the enthalpy of outlet refrigerant from condenser after the internal heat exchanger and h_3 is the enthalpy of outlet refrigerant entering the internal heat exchanger.

By combining Eqn (119) and (120),

$$\dot{m}_R (h_1' - h_1) = \dot{m}_R (h_3 - h_3') \quad (121)$$

Since the mass flow rate of refrigerant is the same through the whole system, a final equation is yield as,

$$h_1' - h_1 = h_3 - h_3' \quad (122)$$

5.4.4 Simulation Input and Output

A comprehensive model was developed and programmed in EES 2017 for a vapor-compression conditioning system comprising air-to-refrigerant evaporator and condenser, a compressor, a thermal expansion valve and a heat exchanger connected between condenser outlet and evaporator. The heat transfer occurs between the outlet refrigerant of the condenser and the outlet refrigerant of the evaporator. As a result, the outlet refrigerant from condenser will drop from saturated state to subcooling state, and the outlet refrigerant from evaporator will rise from saturated state to superheated state. For the compressor, a fixed isentropic efficiency of 80% was assumed for this model. For the outdoor air, uniform temperature and velocity were also assumed. The input variables of the model were outdoor air temperature (T_a); evaporator outlet air temperature (T_{aeo}); internal heat exchanger effectiveness (ε). Typical outcomes of the model are specific work (w), refrigerating effect (q), and vapor-compression system coefficient of performance (COP).

5.4.5 Simulation Data Set-up and Overview

In this section, outdoor air temperatures of 26.7, 29.4, 32.2, 35 ℃ (80, 85, 90, 95℉) and relative humidities of 40%, 50%, 60%, 70%, 80% over a range of assumed evaporator exit air temperatures of 7.2, 10, 12.8℃ (45, 50, 55℉) with a typical compressor efficiency of 80%. Internal heat exchanger effectiveness is 0, 20%, 50%, 80% and 100%.

5.4.6 Results and Analysis

5.4.6.1 Scenario D Alone

Figure 159, 160, 161, 162 show how COP with internal heat exchanger varies with different outdoor air temperatures, Taeos are four heat exchanger effectiveness---20%, 50%, 80% and 100%, respectively. It is easy to understand that with the boosting effectiveness of the internal heat exchanger, the COP of the reconfigured system is increased as well. However, according to these four plots, the COP ranges corresponding to heat exchanger effectiveness from 20%, 50%, 80%, and 100% are 3.1---4.9, 3.4---5.2, 3.7---5.4, and 3.9---5.6, respectively. Thus, with the boosting effectiveness of the internal heat exchanger, the COP of the reconfigured system is increased slightly. From a single plot mentioned above, it is concluded that COP of the reconfigured system decrease with the boosting outdoor air temperature and increase with the rise of evaporator outlet air temperature. The result of how COP with internal heat exchanger related to outdoor air temperature, Taeo and internal heat exchanger effectiveness is summarized in Table 29.

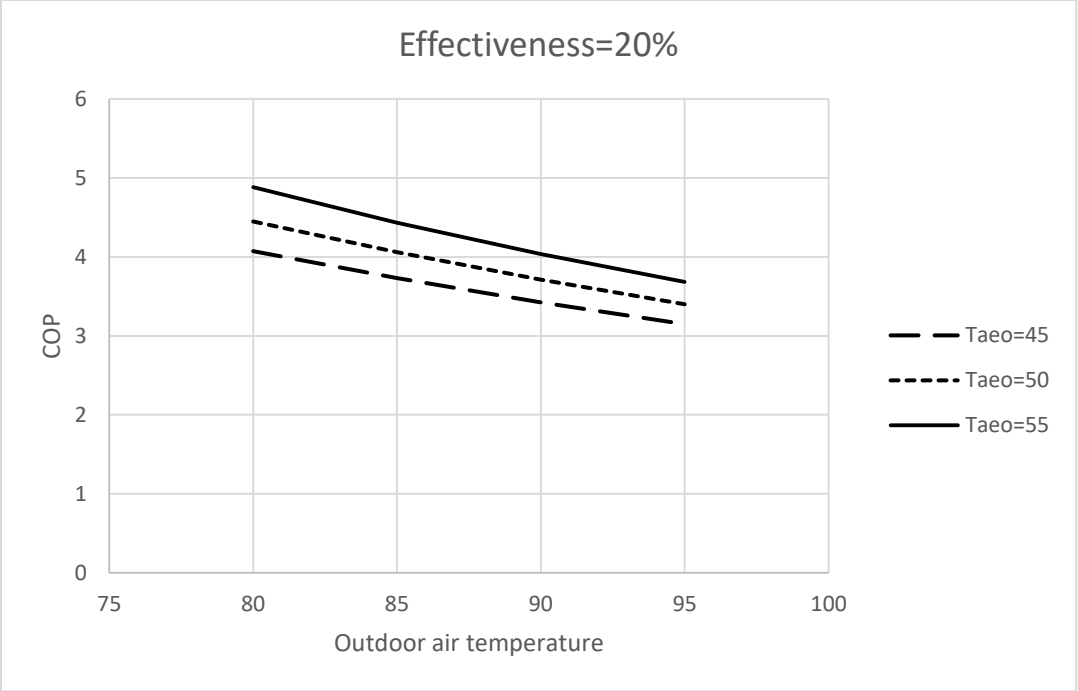

Figure 159 COP with internal heat exchanger effectiveness 20% varied with outdoor air temperature and Taeo

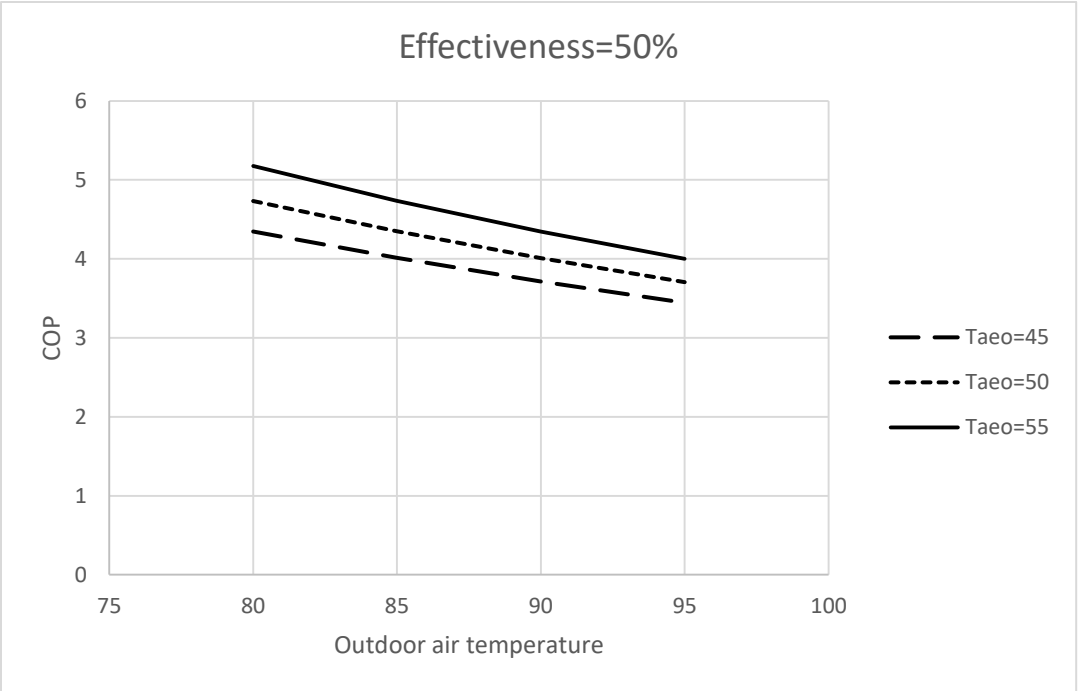

Figure 160 COP with internal heat exchanger effectiveness 50% varied with outdoor air temperature and Taeo

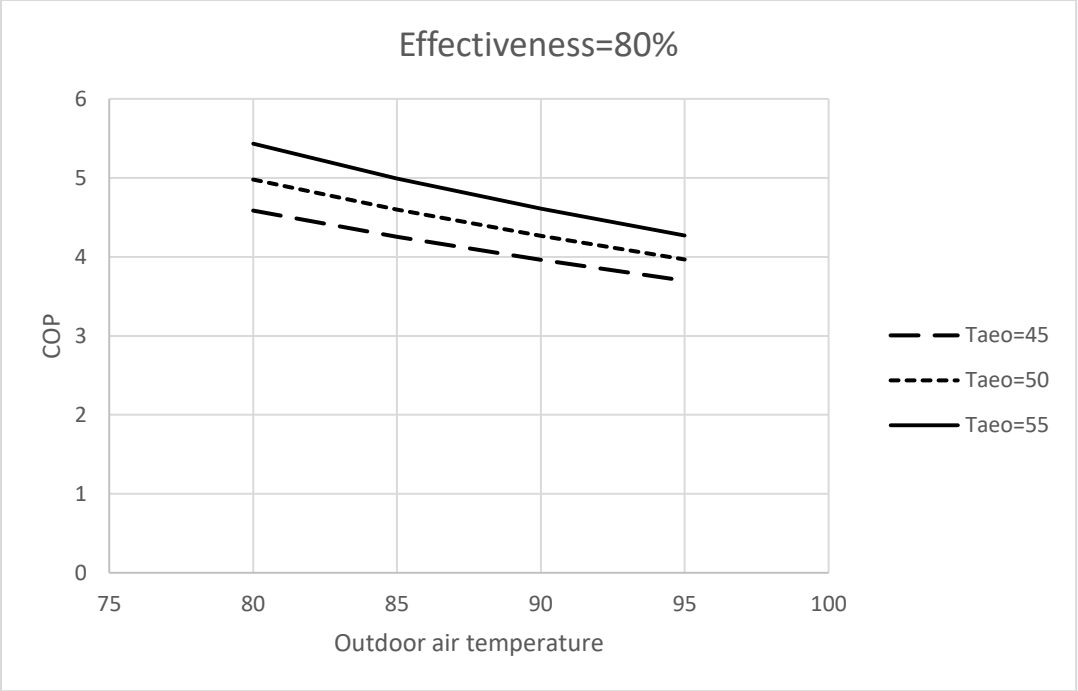

Figure 161 COP with internal heat exchanger effectiveness 80% varied with outdoor air temperature and Taeo

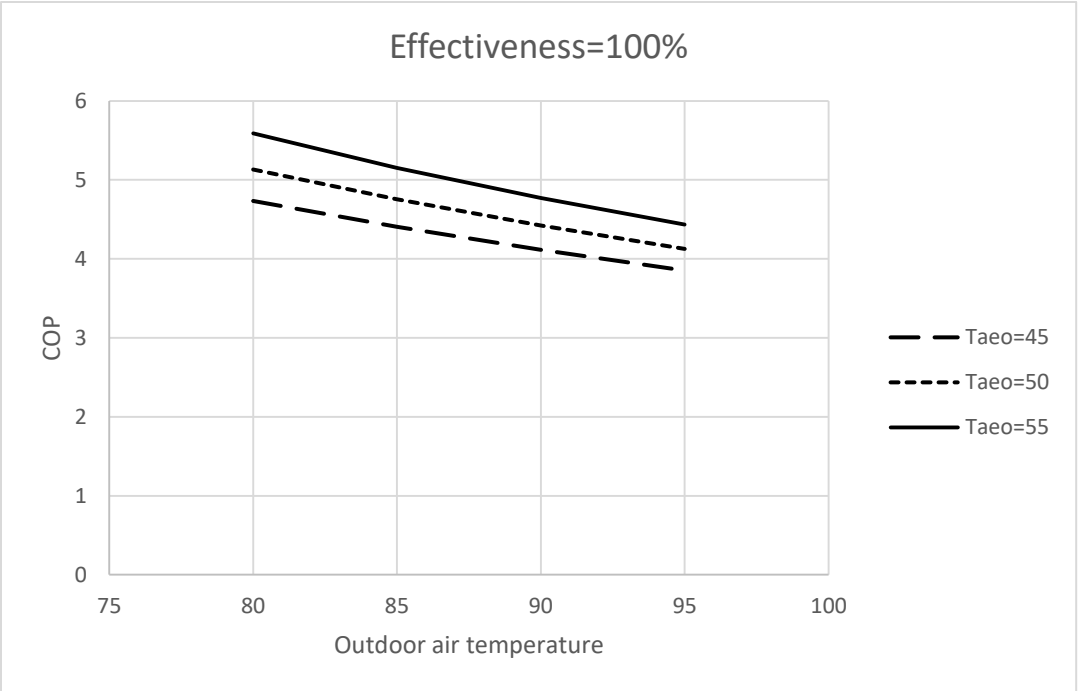

Figure 162 COP with internal heat exchanger effectiveness 100% varied with outdoor air temperature and Taeo

Table 29 COP with internal heat exchanger varied with different variables

case	T_{out}	Internal heat exchanger effectiveness	T_{aeo}	COP with subcooling
1	↑	→	→	↓
2	→	↑	→	↑
3	→	→	↑	↑

5.4.6.2 Compare Scenario D to Scenario A (baseline system)

5.4.6.2.1 COP Improvement Due to the Internal Heat Exchanger Overview

Figure 163 shows the relationship between COP with and without an internal heat exchanger. It is observed form the figure that the highest increase can reach as much as 32% when effectiveness is 100%. However, the improvement is always lower than 10% when heat exchanger effectiveness is 20%.

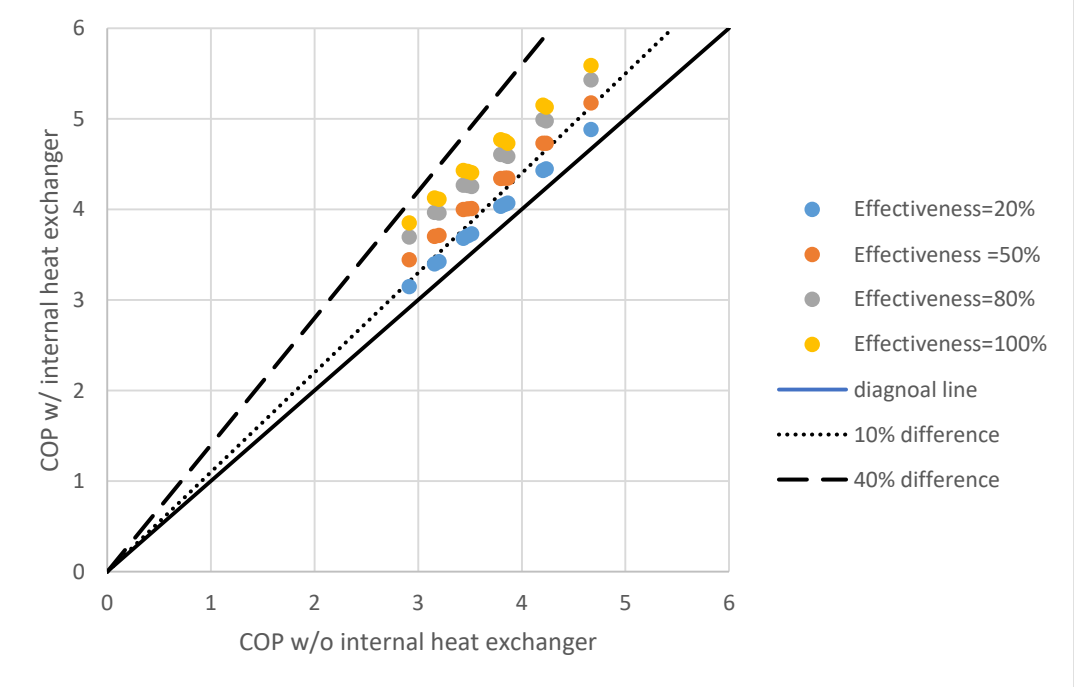

Figure 163 COP improvement due to internal heat exchanger

5.4.6.2.2 COP Enhancement Analysis

Figure 164, 165, 166, and 167 show how COP improvement with internal heat exchanger varies with different outdoor air temperatures, Taeos are four heat exchanger effectiveness---20%, 50%, 80% and 100%, respectively. It is easy to understand that with the boosting effectiveness of the internal heat exchanger, the COP improvement of the reconfigured system is increased as well. However, according to these four plots, the COP improvement ranges corresponding to heat exchanger effectiveness from 20%, 50%, 80%, and 100% are 5%---8%, 11%---18%, 16%---26%, and 19%---32%, respectively. Thus, with the boosting effectiveness of the internal heat exchanger, the COP improvement of the reconfigured system is increased obviously. From a single plot mentioned above, it is concluded that COP improvement of the reconfigured system increases with the boosting outdoor air temperature and decreases with the rise of evaporator outlet air temperature. The result of how COP with internal heat exchanger related to outdoor air temperature, Taeo and internal heat exchanger effectiveness is summarized in Table 30.

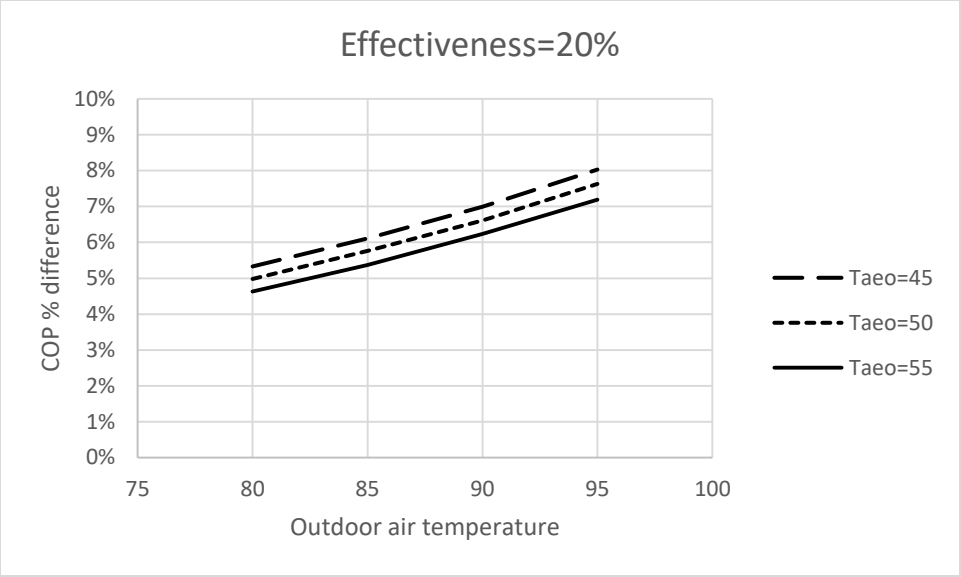

Figure 164 COP improvement with internal heat exchanger effectiveness 20% varied with outdoor air temperature and Taeo

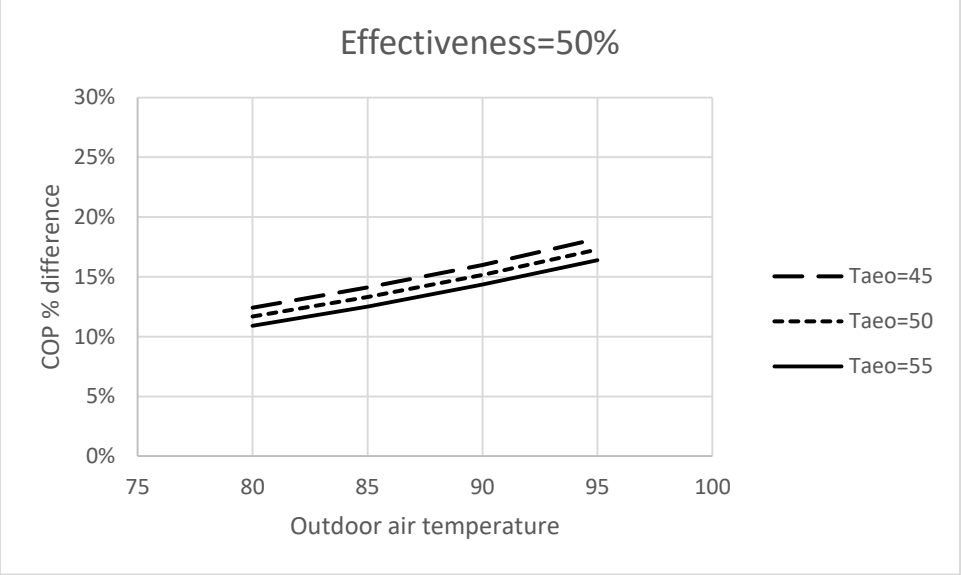

Figure 165 COP improvement with internal heat exchanger effectiveness 50% varied with outdoor air temperature and Taeo

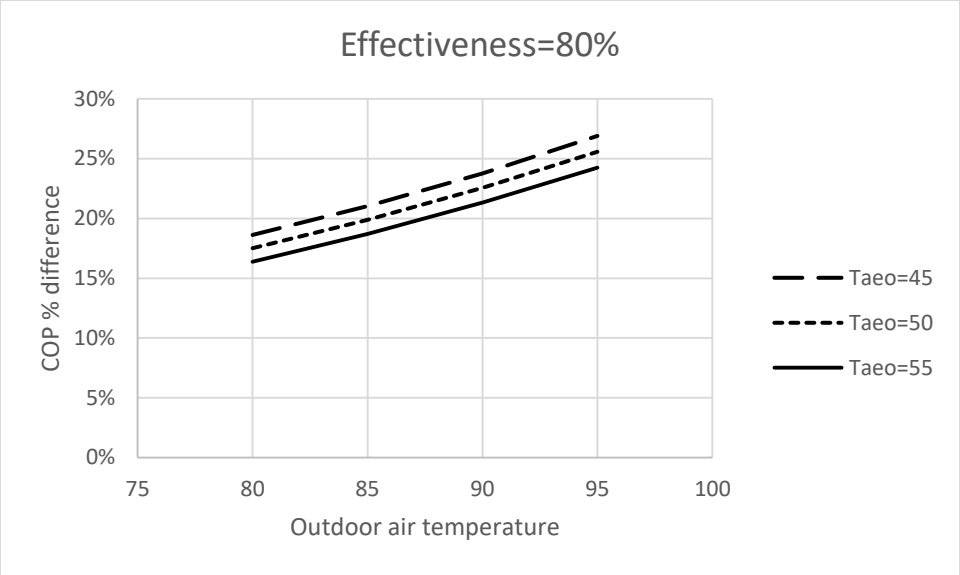

Figure 166 COP improvement with internal heat exchanger effectiveness 80% varied with outdoor air temperature and Taeo

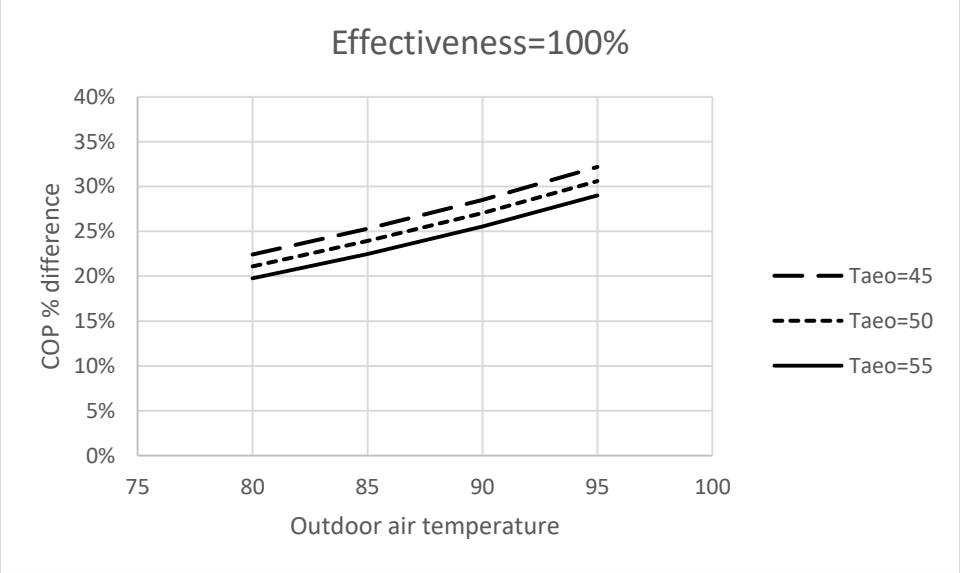

Figure 167 COP improvement with internal heat exchanger effectiveness 100% varied with outdoor air temperature and Taeo

Table 30 COP improvement with internal heat exchanger varied with different variables

case	T_{out}	Effectiveness	T_{aeo}	% difference
1	↑	→	→	↑
2	→	↑	→	↑
3	→	→	↑	↓

5.4.6.3 Correlation Development

5.4.6.3.1 COP with Internal Heat Exchanger Correlation

Unlike the previous reconfigured system models, COP with internal heat exchanger is a function of outdoor air temperature, Taeo and heat exchanger effectiveness. Thus, for simplification, only quadratic model is considered in this section. Since effectiveness of heat exchanger is 20%, 50%, 80% and 100%, which are fixed values, then the quadratic model is set as COP=f (Taeo, Tout) for each different heat exchanger effectiveness. For this section, heat exchanger effectiveness of 20% is taken as an example, all the other heat exchanger effectiveness data is in Appendix A and B. A complete quadratic regression of COP is built in Table 31. The error between predicted data and actual data is indicated in Figure 168---always less than 0.5%.

Table 31 COP_{IHX} Model Coefficients when HX effectiveness is 20%

a0+a1*Taeo^2+a2*Taeo+a3*Tout^2+a4*Tout+a5*Taeo*Tout					
a0	a1	a2	a3	a4	a5
7.04	0.00088	0.139	0.000803	-0.119	-0.00184

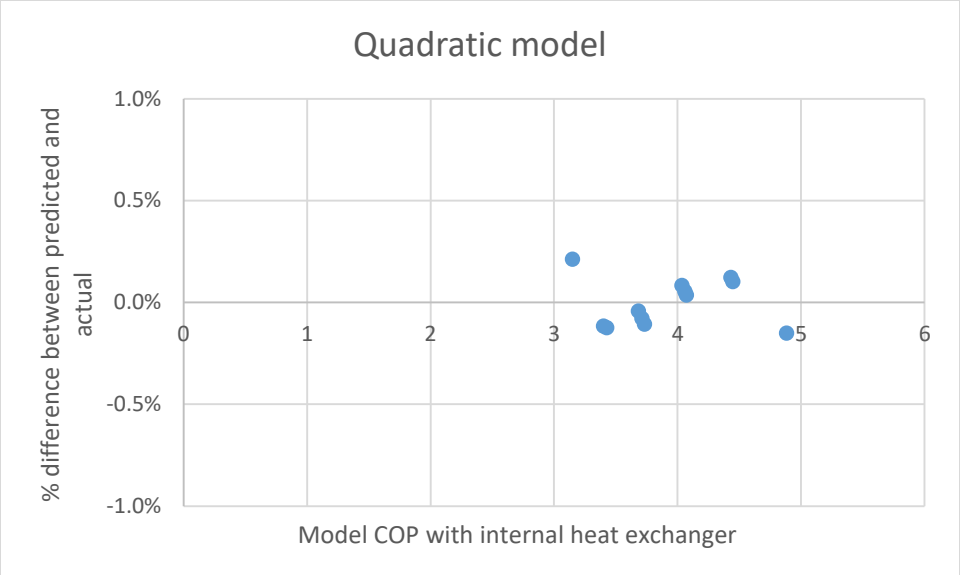

Figure 168 Percentage difference comparison of predicted and actual data of exponential method for COP with internal heat exchanger when HX effectiveness is 20%

5.4.6.3.2 COP Ratio of Internal Heat Exchanger (D) over Baseline (A) Correlation

Unlike the previous reconfigured system models, COP ratio with internal heat exchanger is a function of outdoor air temperature, Taeo and heat exchanger effectiveness. Thus, for simplification, only quadratic model is considered in this section. Since effectiveness of heat exchanger is 20%, 50%, 80% and 100%, which are fixed values, then the quadratic model is set as COP ratio=f (Taeo, Tout) for each different heat exchanger effectiveness. For this section, heat exchanger effectiveness of 20% is taken as an example, all the other heat exchanger effectiveness data is in Appendix A and B. A complete quadratic regression of COP ratio is built in Table 32. The error between predicted data and actual data is indicated in Figure 168---always less than 0.5%.

Table 32 COP_{IHX} ratio Model Coefficients when HX effectiveness is 20%

a0+a1*Taeo^2+a2*Taeo+a3*Tout^2+a4*Tout+a5*Taeo*Tout					
a0	a1	a2	a3	a4	a5
1.0779	-2.59e-6	0.000272	2.31e-5	-0.00185	-8.84e-6

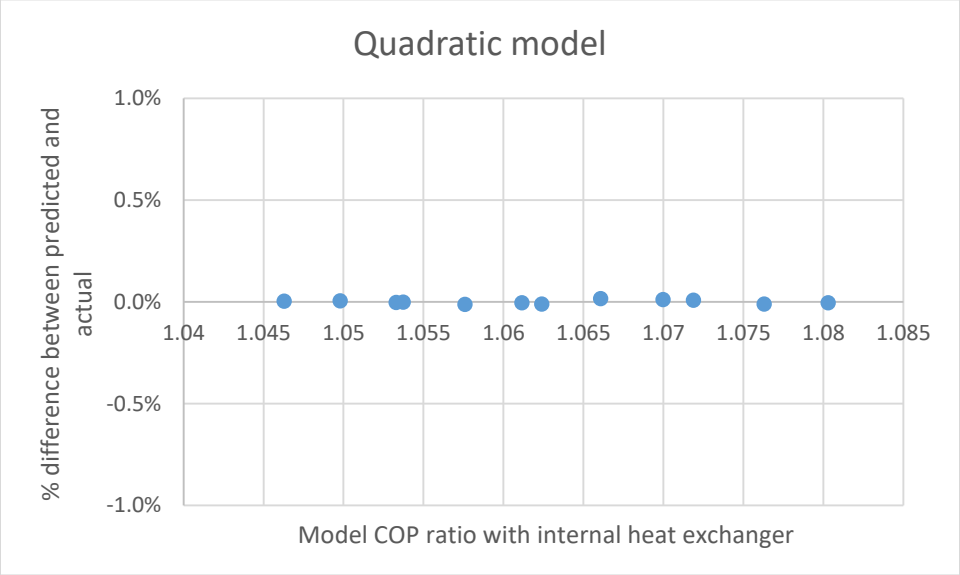

Figure 169 Percentage difference comparison of predicted and actual data of exponential method for COP ratio of internal heat exchanger over baseline when HX effectiveness is 20%

5.4.7 Conclusions

This section studied the effect on the coefficient of performance (COP) of utilizing internal heat exchangers on vapor-compression systems using R410A. Based on the result of this study, it can be concluded:

1. It is shown that the internal heat exchanger effectiveness boosts, both the refrigerating effect (cooling capacity) and specific compression work. Nevertheless, the boosting of refrigerating effect is more significant than the compression work, resulting in an increasing COP for all conditions and heat exchanger effectiveness. For heat exchanger effectiveness of 20%, 50%, 80% and 100%, refrigerating effect increase as 11%---16%, 26%---39%, 41%---61%, 51%---76%

while compression work only increase as 6%---8%, 14%---18%, 21%---27% and 26%---33%, respectively.

2. The COP ranges corresponding to heat exchanger effectiveness from 20%, 50%, 80%, and 100% are 3.1---4.9, 3.4---5.2, 3.7---5.4, and 3.9---5.6, respectively. Thus, with the boosting effectiveness of the internal heat exchanger, the COP of the reconfigured system is increased slightly. Take heat exchanger effectiveness of 80% as an example, with outdoor air temperature increase from 80 ℉ to 95 ℉, the corresponding COP range is decreasing from 4.6---5.4 to 3.7---4.3; with evaporator outlet air temperature increase from 45℉ to 55℉, the corresponding COP range is increasing from 3.7---4.6 to 4.3---5.4. Thus, the COP of the reconfigured system decreases with the boosting outdoor air temperature and increase with the rise of evaporator outlet air temperature.

3. The highest increase in COP for an internal heat exchanger system compared to a baseline system is 32% when effectiveness is 100% with this decreasing to 27%, 18% and 8% when heat exchanger effectiveness drops to 80%, 50%, and 20%, respectively.

4. COP improvement of installing an internal heat exchanger increases with increasing outdoor air temperature and decreases with increasing evaporator outlet air temperature. Thus, an HVAC system reconfigured with an internal heat exchanger is more suitable for hot temperature regions and for these situations where lower room supply air temperatures (evaporator outlet air temperature) are required, which also coincides with conditions that result in the highest energy consumption.

6. CLIMATE ZONE MODEL

Since the focus of this study is to investigate reconfigurations of the conventional vapor-compression cycle (for each, find COPs and ratios), it is important to use appropriate approach and simulation to develop models and find COP functions (outdoor air temperature and relative humidity).

COPs and COP ratios vary depending on outdoor temperature and relative humidity, so the effectiveness of reconfiguration varies as well. Furthermore, outdoor temperature and relative humidity are highly related to location (climate zone) and time of year. Thus, a further study of climate zone is necessary.

6.1 Climate Zone Temperature and Relative Humidity Development

This section presents an investigation of dry-bulb temperature, relative humidity and wet-bulb temperature correlation development based on climate data for the time of year (month/day) from 53 cities. These 53 cities represent special locations spread out over several climate zones, categorize 1 through 7, along with humid, dry, and marine sub-zones represented by A, B, and C respectively, for a total of 18 different climate regions or climate zones. These 53 cities were selected based on their population size, their distribution around the U.S. to the point of comprising all 14 climate zones, and the availability of average climate data that is accurate and complete while being representative of past and future years. It should be noted that some of the climate zones were represented by 2 or more cities and in these cases represented in climate zone data files were created by averaging the city data.

Furthermore, it was necessary in several cases to divide some of the 14 zones into subzones because two cities representing different locations in a particular climate zone might have had quite different climates, meaning temperatures and relative humidities. In these cases, the climate

zone might be divided into an East (e), a North (n) region and a west (w) region. The average monthly data generalized equations for dry-bulb temperature, relative humidity, and wet-bulb temperature were decided through cubic regression for each climate zone. After this derivation, the equations were validated by comparing predicted data with climate zone data. Of special importance, to calculate the monthly average relative humidity and dry/wet bulb temperature for any location in the U.S., it is assumed that the period for data selection is during an approximate cooling season or outdoor temperature greater than 10℃ (50°F).

6.1.1 Introduction and Literature

In the US, the heating and cooling residential and commercial buildings with HVAC system consume about 40% of total energy usage and emit about 39% of the total CO2 emissions. Thus, increasing the energy efficiency of buildings are paramount to reducing energy costs and emissions. Building codes, as used by local and state enforcement entities are typically tied to the prevailing climate within an enforcement jurisdiction, where the dominant climate is based upon a 30-year average of local to regional surface observations.

Climate has a major impact on the energy use of residential buildings/commercial buildings and energy codes and standards rely on a clear definition of climate zones to convey information and requirements to builders. Nevertheless, the unique and agreed-upon climate zone map for the U.S. for use with building codes was built after 2004. Guidelines for these codes, applied to residential and commercial buildings, are developed by the Department of Energy (DOE) and ASHRAE. Based on surface observations ASHRAE, in partnership with the Department of Energy, have developed climate zone maps for which building codes are developed. In this article, the author focus on climate zone 1A, 2A, ,2B, 3A, 3B, 3C, 4A, 4B, 4C, 5A, 5B, 6A, 6B, 7A. The

number in the above code stands for temperature, which varies from very hot to very cold; the letter in the code means humidity level, and they are humid, dry and marine, respectively.

As outside dry-bulb temperature and relative humidity during cooling seasons are significant parameters for the evaluation of system performance, the correlation of these two parameters with a time of year (month/day) and climate zone become more critical. The focus of the study presented herein is to develop correlations of dry-bulb temperature, relative humidity and a wet-bulb temperature of each climate zone to the time of year (month/day) and climate zone, respectively. However, studies of that topic are limited and not systematical. As a result, this study attempts to fill up this gap and derive approximation equations.

In recent years, calibrated energy modeling of residential and commercial buildings have gained importance. Thus, accurate weather data play an important role in this calibration process and projected energy savings.

6.1.1.1 TMY Definition and Comparison with Historical Weather Data

The U.S. Department of Energy's National Renewable Energy Laboratory (NREL) first developed TMY files in 1981, serving as a representation of average weather conditions for specific locations. Files are based on 15 to 30 years of hourly weather data, which mostly collected from a local weather station and including data on various weather characteristics such as solar radiation and temperature. Statistical methods are used to select each of the twelve months considered to be "typical" for that location. For instance, January might come from 1975, but February comes from 1990. Subsequent iterations of TMY data were created based on weather data for different periods. The Typical Meteorological Year version 2 (TMY2) files were developed using weather station data from 1961 to 1990 including 239 locations in the U.S. After that, the updated version (TMY3) covers only 15 years (1991-2005) and includes weather

information for more than 1400 sites in the U.S. with even more information of variables compared to TMY 2, including precipitation.

Although the TMY data help public a lot to generalize weather conditions and simplify the forecasting process, there are some drawbacks associated with their usage [84]. Firstly, TMY data is assumed to be representative of the average climatic conditions. Methods used to construct them disregard periods of extreme weather conditions or anomalies. The oversimplification of assumed localized weather conditions may produce some bias in the results and lead to some inaccurate expectations of building performance. Secondly, TMY 3 is based on only 15 years-period. Thus a lack of 15 years (compared to TMY 2) of consistent data in some locations could limit the robustness of the generated data. Thus, the drawbacks discussed above could potentially lead to a bias in the simulation results, with modeled performance being over or underestimated.

Huang and Crawley [85] [86] presented results from the DOE-2.1 E hourly energy simulation program for a prototype office building as influenced by locally measured weather data for multiple years and several weather data sets for a set of North American locations. They compared the influence of the various weather data sets on simulated annual energy use and energy costs. The results showed that TMY 2 should be used rather than the older TMY data.

Hong and Change[87] compared the impacts of TMY3 data and actual collected weather data during 30 years on energy consumption and peak electricity demands for large-scale buildings across all 17 ASHRAE climate zones. The result showed that the TMY3 data could over-estimate actual weather results as much as 18% and under-predict as much as 37%. The author also concluded that the lack of agreement between the series of weather flies is mostly attributed to the TMY3 files not capturing average weather conditions in each location. Similarly, Wang[88] found that based on the annual energy prediction using TMY data, the uncertainties in annual energy

consumption introduced by real historical weather during the period 10-15 years, ranged from -4.0% to 6.1% for the four typical climatic zones.

6.1.1.2 ASHRAE Definition of Different Climate Zones

Building codes, as used by local and state enforcement entities are typically tied to the dominant climate within an enforcement jurisdiction, where the dominant climate is based upon a 30-year average of local to regional surface observations. The climate zone is intended as an aid in helping builders to identify the appropriate climate designation for the counties in which they are building. The climate regions described here are based on the climate designations used by ASHRAE 169-2006 defined by cooling degree-days, heat degree-days and is listed in Table 33. Climate zone boundaries follow county boundary lines Since this study is focused on the cooling season for large regions. Thus climate zones 1B, 5C (region area too small) 7B, 8A and 8B (too cold) are disregard. Of special note, seven of the eight U.S climate zones recognized by ASHRAE occur in the continental United States. The sub-arctic U.S. climate zone, not shown on the climate zone map, appears only in Alaska.

Table 33 Climate Zones Definition

Climate Zones	CDD	HDD
1A Very Hot – Humid	IP Units 9000 < CDD50°F and SI Units 5000 < CDD10℃	
1B Dry	IP Units 9000 < CDD50°F and SI Units 5000 < CDD10℃	
2A Hot	IP Units 6300 < CDD50°F ≤ 9000 and SI Units 3500 < CDD10℃ ≤ 5000	
2B Dry	IP Units 6300 < CDD50°F ≤ 9000 and SI Units 3500 < CDD10℃ ≤ 5000	
3A Warm-Humid	IP Units 4500 < CDD50°F ≤ 6300 and SI Units 2500 < CDD10℃ < 3500	
3B Dry	IP Units 4500 < CDD50°F ≤ 6300 and SI Units 2500 < CDD10℃ < 3500	

Table 33 Continued

Climate Zones	CDD	HDD
3C Warm-Marine	IP Units CDD50°F≤ 4500 and SI Units CDD10℃ ≤ 2500	IP units HDD65°F ≤ 3600 and SI units HDD18℃ ≤ 2000
4A Mixed-Humid	IP Units CDD50°F≤ 4500 and SI Units CDD10℃≤ 2500	IP units HDD65°F≤ 5400 and SI units HDD18℃ ≤ 3000
4B Dry	IP Units CDD50°F ≤ 4500 and SI Units CDD10℃ ≤ 2500	IP units 3600 < HDD65°F ≤ 5400 and HDD18℃ ≤ 3000
4C Mixed-Marine		IP Units 3600 < HDD65°F ≤ 5400 and SI Units 2000 < HDD18℃ ≤ 3000
5A Cool-Humid		IP Units 5400 < HDD65°F ≤ 7200 and SI Units 3000 < HDD18℃ ≤ 4000
5B Dry		IP Units 5400 < HDD65°F ≤ 7200 and SI Units 3000 < HDD18℃ ≤ 4000
5C Marine		IP Units 5400 < HDD65°F ≤ 7200 and SI Units 3000 < HDD18℃ ≤ 4000
6A Cold-Humid		IP Units 7200 < HDD65°F ≤ 9000 and SI Units 4000 < HDD18℃ ≤ 5000
6B Dry		IP Units 7200 < HDD65°F ≤ 9000 and SI Units 4000 < HDD18℃ ≤ 5000
7A Very cold		IP Units 9000 < HDD65°F ≤ 12600 and SI Units 5000 < HDD18℃ ≤ 7000
7B Very cold		IP Units 9000 < HDD65°F ≤ 12600 and SI Units 5000 < HDD18℃ ≤ 7000
8A Subarctic		IP Units 12600 < HDD65 °F and SI Units 7000 < HDD18℃
8B Subarctic		IP Units 12600 < HDD65 °F and SI Units 7000 < HDD18℃

6.1.1.3 Statistical Weather Data Products

Lots of other statistical weather data products except TMY and NOAA are available to the public as well, and they are listed below. The only drawback of them is that the process for a specific city (county) data lookup is complicated and time-wasting. Based on the background of climate zone information discussed above, the author is trying to derive a correlation of dry-bulb temperature/relative humidity/wet-bulb temperature related to the time of year (month/day) for 14

climate zones across the U.S. during the cooling season. As long as any specific location (city/county) climate zone code is known, the weather data could be calibrated as well.

U.S. Records This tool lists and maps records tied or broken on a given date for weather stations across the 50 United States. Records are distinguished as daily (largest/smallest for that day on the calendar), monthly (largest/smallest value during that month), or all-time (largest/smallest value ever observed at that station). Summary information for recent periods (year-to-date, month-to-date, last 30 days) is provided in tabular format.

Climate Extremes Index This index charts the occurrence of specific extreme events over time since 1910. In most cases, extreme events are defined as lying in the outermost ("most unusual") ten percent of a place's history. Analyses are available at national and regional levels.

Global Climate at a Glance The Global Climate at a Glance (GCAG) web application can be used to retrieve monthly and annual global temperature anomaly maps that date back to 1880. Users can also create time series for locations around the globe by selecting a point on the map. The interactive interface allows users to adjust the vertical and horizontal axes of the time series plots to view selected range of months or years of data or to view the entire period of record.

Global Temperature Anomalies This page provides direct access and explanatory material for NCEI's global-scale and near-global-scale temperature anomalies products. Values are broken out by hemisphere (southern, northern) or by surface type (land, ocean). The values are compared to the 20th-century average (positive numbers: warmer than the 20th-century average; negative numbers: cooler).

Global Temperature and Precipitation Maps The user can select temperature or precipitation anomalies as they were reported by NCEI's Climate Monitoring Branch.

Global-Scale Microwave Sounding Unit Temperatures Microwave Sounding Units (MSU) measure radiation emitted by the Earth's atmosphere from NOAA polar-orbiting satellites. The MSU products provide insight into the temperature trends and patterns in three different slabs of the atmosphere, from the lowest: lower troposphere, middle troposphere, and lower stratosphere.

6.1.1.4 Dry-bulb Temperature and Relative Humidity Importance

Two useful properties for environmental analysis in most buildings would be dry-bulb temperature and relative humidity. Dry-bulb temperature is commonly used for the calculation of cooling degree, and cooling/heating load and relative humidity is an indicator of how much moisture is in the air compared to desirable moisture conditions.

M.R. Bran[89] obtained equations in the analysis use the humidity ratio derived from the dry-bulb temperature and the relative humidity in conjunction with the actual dry-bulb temperature. These equations are used to estimate the consumption for the base year period (1961-1990) and the predicted climate period 2030-2059. The results showed that the energy consumption of supermarket depends more on temperature than humidity and electricity use will increase by 2.1% whereas gas consumption will drop by 13% for the future estimate.

Kody M.Powell [90] used weather (dry-bulb temperature, wet-bulb temperature, and relative humidity) and time variables (month, hour, and day) as inputs to evaluate several different models and discusses each model’s ability to accurately forecast hourly loads for a district energy system up to 24 hours in advance. A nonlinear autoregressive model with exogenous inputs shows the best fit to data.

Mahabir Bhandari [91] once evaluated the weather datasets for building energy simulations. Since there are data sources publicly available with high temporal sampling rates but at relatively poor geospatial sampling locations. This study is aiming to compare provided weather

characteristics with data collected from a weather station inaccessible to the service providers. Serval weather parameters are compared: monthly average dry-bulb temperature; relative humidity; direct normal, diffuse and global solar radiation; wind speed and wind direction.

Fei Lei [92] investigated a model which is aiming at identifying energy savings in energy retrofitting projects or energy management programs. Most baseline models are developed by regressing the energy consumption versus weather and other independent variables while this baseline model is based on the characteristics of building and weather. Eleven office buildings from Wuhan (a city of the hot summer and cold winter region of China) were modeled. The result shows that monthly mean outdoor dry-bulb temperature was the most important variable and other weather variables, such as relative humidity and global solar radiation were weak correlations with the whole building energy consumption. The author concluded a single variable linear model based on outdoor dry-bulb temperature is sufficient for the baseline model in hot summer and cold winter condition.

The weather parameter data is also widely used in Energy Management and Control Systems [93] in buildings. A commercial EMCS is installed in the demonstration building. Additional sensors were installed to provide the measurements for outdoor air dry-bulb temperature and relative humidity, wind speed and direction, direct normal solar radiation. High-quality sensors were used to minimize the impacts from the weather on the model output uncertainties.

6.1.2 Results and Analysis

6.1.2.1 U.S. cities (climate zones)

The U.S. is divided into 7 climate zones 1---7: 1A---very hot and humid; 1B---very hot and dry; 2A---hot and humid; 2B---hot and dry; 3A---warm and humid; 3B---warm and dry; 3C---

warm and marine; 4A---mixed and humid; 4B---mixed and dry; 5A---cool and humid; 5B cool and dry; 5C---cool and marine; 6A---cold and humid; 6B---cold and dry; 7---very cold. Moreover, the above zones are based on thermal criteria, CDD (cooling degree day) and HDD (heating degree day). According to ASHRAE standard, 50 °F is referred as the base temperature for cooling degree-day calculation (cooling is the focus of this study) since they are the most commonly used bases for building energy applications, the cooling season is defined as the range of the monthly dry-bulb temperature above 50 °F. Take Miami (1A) for example, the monthly temperatures from January to December are all higher than 50°F. Thus the cooling season for Miami is from January to December. However, some cities like Chicago (5A), the monthly temperatures from April to October are higher than 50°F. Thus the cooling season is only ranged from April to October.

For each climate zone, the largest area or the city with most population is chosen. Of special note, climate zone 3A and 3B, as the special geographical condition, even the weather of several cities in the same climate zone are still significantly differed. Thus they are further divided into a sub-category--- 3A west, 3A east; 3B west, 3B east, 3B north and 3B Las Vegas.

The weather data for the report of 53 cities across the U.S. that used to develop a correlation for the 14 climate zones were from NOAA (National Oceanic and Atmospheric) during the past 30 years (1981-2010). This daily data from NOAA consisted of:

Dry-bulb temperature—high, low, average

Relative humidity—high, low, average

Wet-bulb temperature –average only (calculated from dry-bulb temperature and relative humidity)

It should be noted that the daily average temperature and daily average for each city were calculated based on the daily highest and daily lowest data while the wet-bulb temperature was

calculated based on the daily average temperature and daily average relative humidity. A survey of the cooling season climate data for all 53 cities shows that most outdoor dry-bulb temperatures range from 55°F to 95°F while most relative humidities ranging from 15% to 75%. The full data consists of more than 3000 data points, which are numerous to include herein; however, a sample of cooling season data is shown in Table 34 (Appendix has a comprehensive table, only climate zone 1A is shown as follows). For one city, namely, Albuquerque, which is in climate zone 4B.

Another indication of how extensive the data set can be seen in Figure 1 for two of the 7 climate data sets, namely monthly average dry-bulb temperature and monthly average relative humidity covering all 14 climate zones. Significant insight can be gained by studying the climate data in Figure 170 and 171. For example, the climate zones are numbered 1 through 7, representing hot to cold climate, and this trend can be seen in the fact that dry-bulb temperature decreases from left to right as does the cooling season length. The highest temperature in the middle of the cooling season can also be observed. In Figure 171, it can be seen that the humid region designated by "B" have daily average relative humidity around 70% while the dryer region has 20% to 40%.

Table 34 Weather report of 53 cities (1A for example, other climate zones are in the Appendix)

City	Month	Daily Highest(°F)	Daily lowest(°F)	Daily Temp (°F)	Daily Highest RH	Daily Lowest RH	Daily Average RH	wet bulb Temp (°F)
Miami	Jan	76	60	68	0.84	0.59	0.72	62.01
	Feb	78	62	70	0.83	0.57	0.7	63.36
	March	80	65	72.5	0.82	0.56	0.69	65.37
	April	83	68	75.5	0.8	0.53	0.67	67.55
	May	87	73	80	0.83	0.59	0.71	72.67
	June	90	76	83	0.86	0.65	0.76	76.8
	July	91	77	84	0.86	0.63	0.74	77.17

Table 34 Continued

City	Month	Daily Highest(°F)	Daily lowest(°F)	Daily Temp (°F)	Daily Highest RH	Daily Lowest RH	Daily Average RH	wet bulb Temp (°F)
Miami	August	91	77	84	0.86	0.65	0.75	77.45
	Sep	89	77	83	0.88	0.66	0.77	77.08
	Oct	86	74	80	0.86	0.62	0.74	73.49
	Nov	82	68	75	0.85	0.61	0.73	68.64
	Dec	78	63	70.5	0.83	0.59	0.71	64.05
Key west	Jan	74	64	69	0.81	0.69	0.75	63.61
	Feb	76	66	71	0.8	0.67	0.73	64.98
	March	78	68	73	0.79	0.66	0.72	66.56
	April	81	72	76.5	0.77	0.63	0.7	69.23
	May	85	76	80.5	0.77	0.65	0.71	73.13
	June	88	79	83.5	0.79	0.68	0.74	76.71
	July	89	80	84.5	0.78	0.66	0.72	77.06
	August	89	80	84.5	0.79	0.68	0.73	77.34
	Sep	88	79	83.5	0.81	0.69	0.75	76.99
	Oct	85	76	80.5	0.81	0.68	0.75	74.21
	Nov	80	72	76	0.82	0.69	0.76	70.31
	Dec	76	67	71.5	0.82	0.69	0.75	65.91

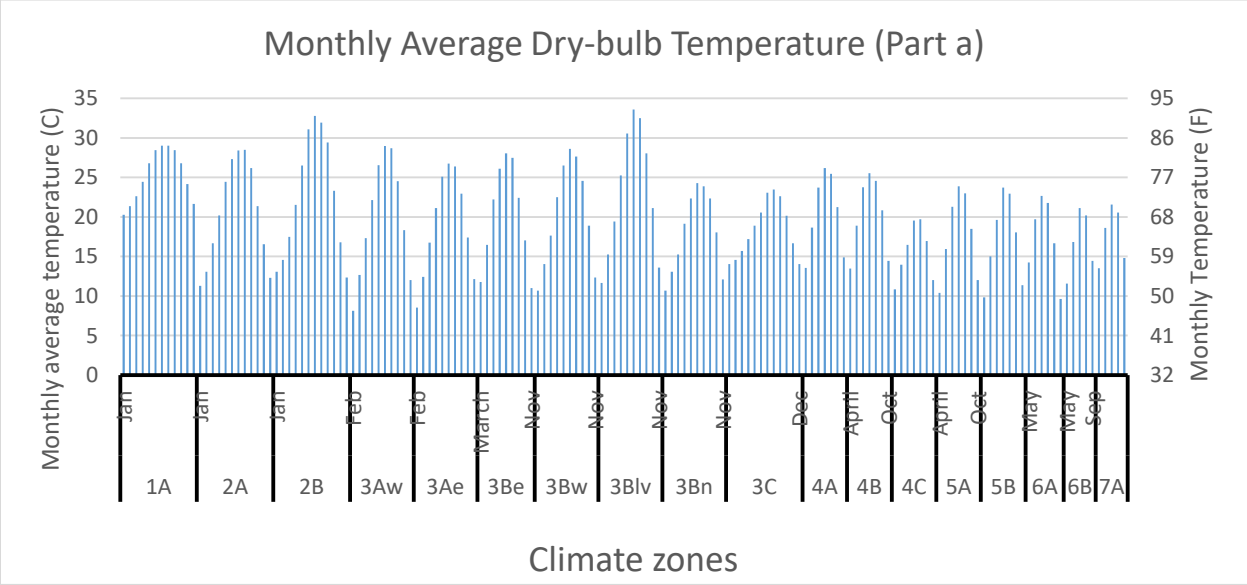

Figure 170 Monthly average dry-bulb temperature for different climate zones

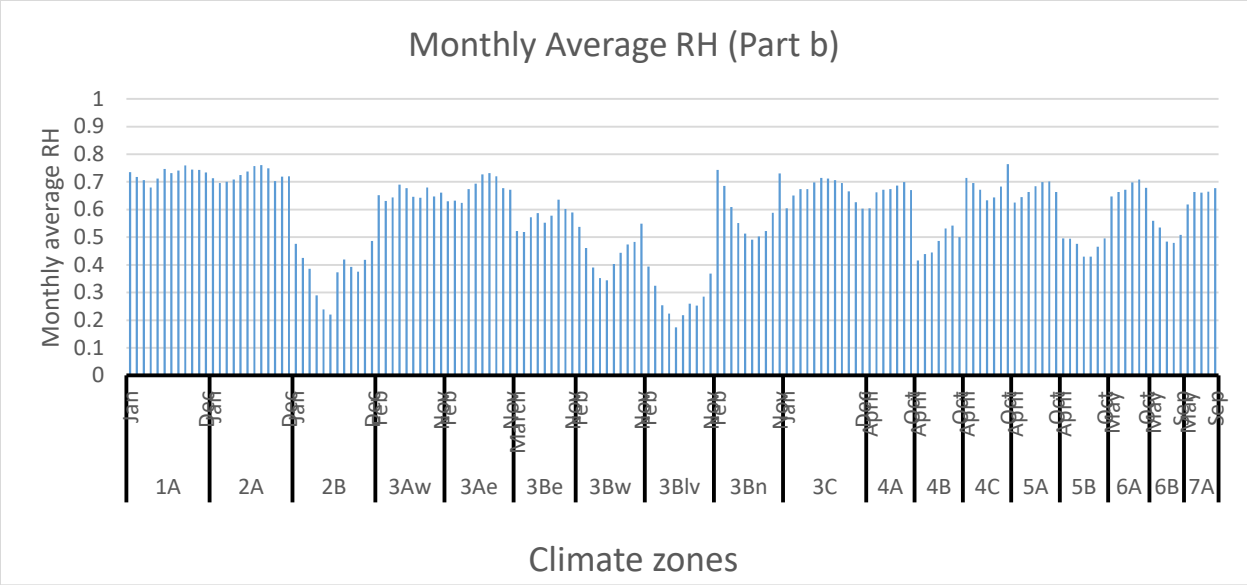

Figure 171 Monthly average relative humidity for different climate zones

6.1.2.2 TMY Data and NOAA Data Comparison

The most well-known climate data available to the public is called Typical Meteorological Year data (TMY). The TMY data is based on meteorological measurements made at hourly intervals over a number of years that were then assumed to build up a picture of local climate regions throughout the U.S. A particular characteristic of TMY data is that a simple average of the yearly data underestimates the amount of variability, so the month that is most representative of the location is selected, regardless of what year that was measured. Specifically, for each month, the average radiation over the whole measurement period is determined, together with the average radiation in each month during the measurement period. The data for the month that has the average radiation most closely equal to the monthly average over the whole measurement period is then chosen as the TMY data for that month. This process is then repeated for each month in the year. The months are added together to give a full year of hourly samples with the possibility existing that data of "June" come from 1998 while "July" data maybe from 1996.

Climate conditions can have significant variability changing hourly, daily, monthly or yearly. Thus, it is necessary to verify the accuracy of NOAA data, used to develop climate zone weather data correlation with the TMY data commonly accepted climate data-set for building energy analysis. Six cities with the range of different climate from all across the U.S, namely Dallas (3Aw), Orlando (2A), Los Angeles (3C), Richmond (4A), Albuquerque (4B) and Omaha (5A) were selected to compare between TMY data and NOAA data (Dallas and Orlando plots are shown in this section, all the other four cities are in the Appendix C). Since TMY data is based on the specific location hourly data, then the TMY daily data is averaged based on the hourly data. We also assume that the average monthly data of NOAA is exactly in the middle of each month. Thus, the plot of TMY daily temperatures/RH versus 30-year-average NOAA data is shown in Figure 172, 173, 174 and 175 (only Dallas and Orlando, the other four cities are left in Appendix C). During the cooling season, the two data source are quite similar; the NOAA data is all within in the range of the fluctuation of the TMY data, which further approved the accuracy of the weather report used in this study. Of special note, January 1st is always counted as Day 1 and Dec 31th as Day 365, even if the cooling season for a specified city does not last from January to December.

Since TMY daily data is calculated, the TMY monthly data is then calculated based on the average of daily data. Thus, TMY monthly data and NOAA 30-year-average monthly data is compared in Table 35. For most cases, the monthly average data between two sources is within 3℃. The monthly average relative humidity deviation is generally less than 0.1

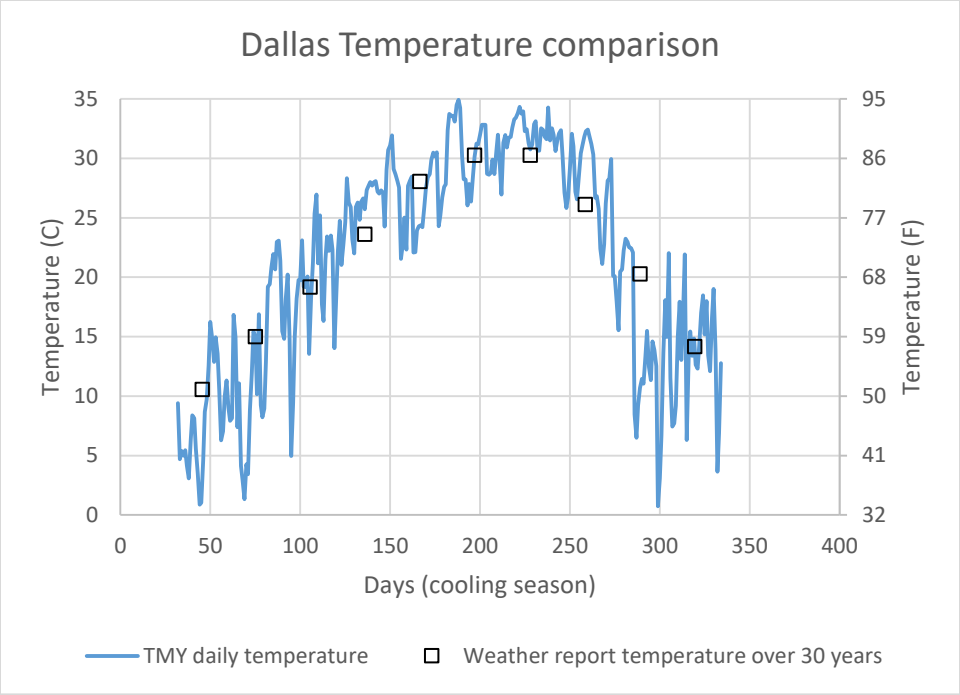

Figure 172 Temperature for Dallas comparison between TMY data and NOAA

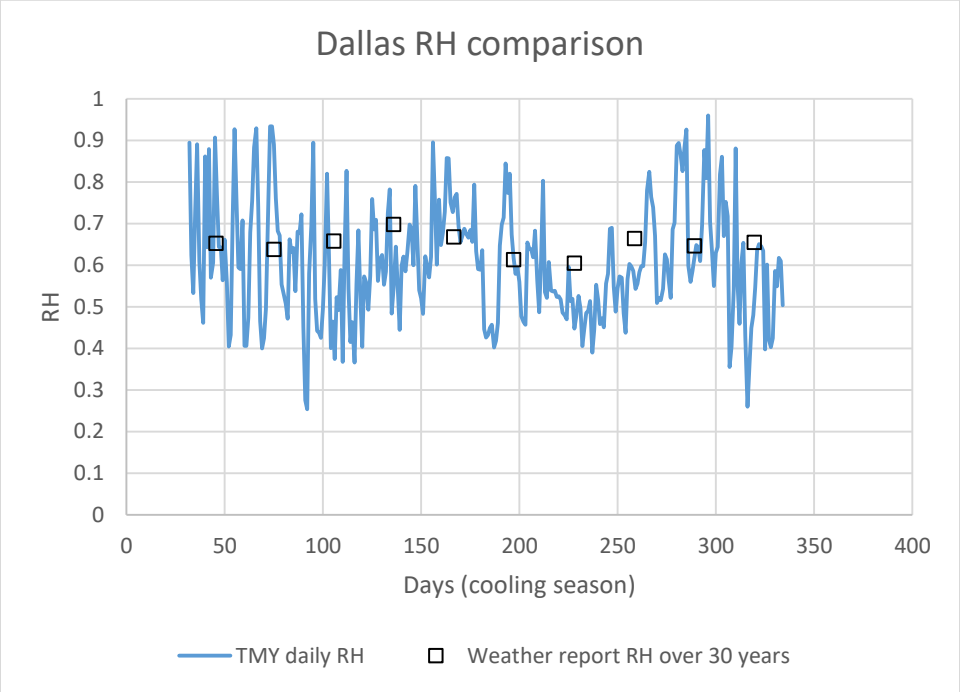

Figure 173 Relative humidity for Dallas comparison between TMY data and NOAA

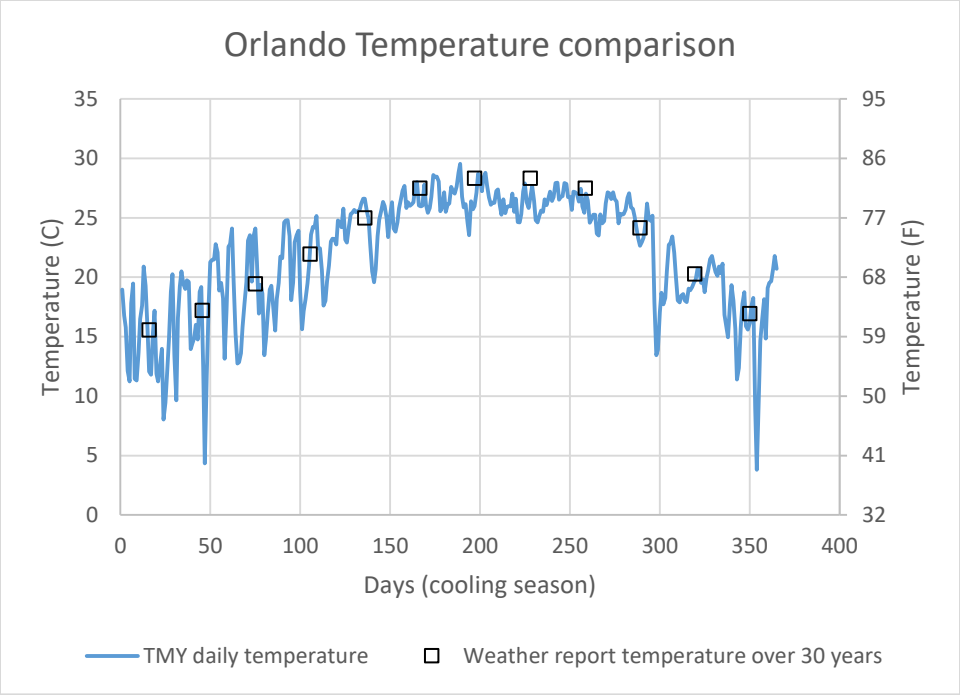

Figure 174 Temperature for Orlando comparison between TMY data and NOAA

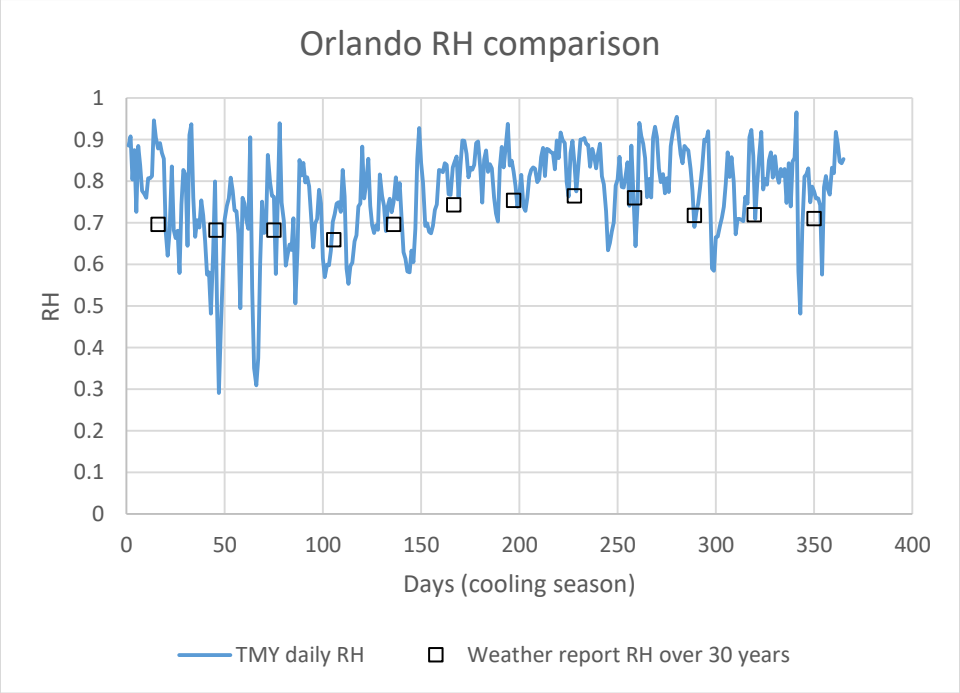

Figure 175 Relative humidity for Orlando comparison between TMY data and NOAA

Table 35 TMY and NOAA monthly average comparison

City	Month	TMY		NOAA		Difference		% difference	
		Dry-bulb (C)	RH	Dry-bulb	RH	Dry-bulb	RH	Dry-bulb	RH
Dallas	Feb	8.0	0.67	10.6	0.65	-2.5	0.01	-24.12%	2.22%
	March	12.7	0.64	15.0	0.64	-2.3	0.00	-15.30%	-0.46%
	April	18.9	0.52	19.2	0.66	-0.2	-0.13	-1.25%	-20.49%
	May	26.4	0.61	23.6	0.70	2.8	-0.09	11.94%	-12.81%
	June	26.5	0.69	28.1	0.67	-1.6	0.03	-5.61%	3.94%
	July	30.7	0.58	30.3	0.61	0.4	-0.03	1.42%	-4.77%
	August	32.2	0.50	30.3	0.61	1.9	-0.11	6.43%	-17.46%
	Sep	28.6	0.60	26.1	0.66	2.5	-0.07	9.56%	-10.12%
	Oct	14.8	0.71	20.3	0.65	-5.5	0.07	-27.07%	10.28%
	Nov	13.7	0.54	14.2	0.66	-0.4	-0.12	-2.98%	-17.95%
Orlando	Jan	14.6	0.79	15.6	0.70	-1.0	0.09	-6.44%	13.24%
	Feb	17.4	0.67	17.2	0.68	0.2	-0.01	1.26%	-1.32%
	March	18.8	0.68	19.4	0.68	-0.6	0.00	-3.09%	-0.22%
	April	21.6	0.70	21.9	0.66	-0.4	0.04	-1.73%	5.96%
	May	24.6	0.73	25.0	0.70	-0.4	0.04	-1.67%	5.11%
	June	26.5	0.80	27.5	0.74	-1.0	0.06	-3.67%	8.03%
	July	26.9	0.81	28.3	0.75	-1.5	0.06	-5.19%	8.09%
	August	26.2	0.86	28.3	0.76	-2.1	0.09	-7.50%	12.33%
	Sep	26.1	0.80	27.5	0.76	-1.4	0.04	-5.00%	5.06%
	Oct	23.1	0.80	24.2	0.72	-1.1	0.08	-4.42%	11.56%
	Nov	20.1	0.80	20.3	0.72	-0.2	0.08	-0.92%	11.76%
	Dec	16.4	0.78	16.9	0.71	-0.6	0.07	-3.49%	10.47%
Los Angeles	Jan	16.7	0.73	14.4	0.60	2.3	0.13	15.76%	21.98%
	Feb	14.2	0.74	15.0	0.66	-0.8	0.09	-5.16%	13.01%
	March	14.6	0.67	15.8	0.69	-1.3	-0.03	-8.02%	-3.78%
	April	15.8	0.70	17.5	0.70	-1.7	0.00	-9.86%	0.65%
	May	17.0	0.73	18.9	0.73	-1.9	0.00	-10.13%	0.40%
	June	18.2	0.79	20.6	0.75	-2.4	0.04	-11.52%	5.86%
	July	19.9	0.77	23.1	0.75	-3.2	0.02	-13.84%	2.06%
	August	20.0	0.76	23.3	0.75	-3.3	0.01	-14.09%	1.92%
	Sep	19.8	0.81	22.8	0.72	-3.0	0.09	-13.03%	12.39%
	Oct	18.1	0.72	20.6	0.68	-2.4	0.04	-11.75%	6.23%
	Nov	16.2	0.66	16.9	0.62	-0.7	0.04	-4.14%	6.65%
	Dec	14.3	0.67	14.4	0.59	-0.1	0.08	-0.86%	13.29%

Table 35 Continued

City	Month	TMY		NOAA		Difference		% difference	
		Dry-bulb (C)	RH	Dry-bulb	RH	Dry-bulb	RH	Dry-bulb	RH
Richmond	April	14.4	0.66	14.4	0.6	-0.1	0.06	-0.60%	10.08%
	May	19.9	0.66	19.2	0.69	0.7	-0.03	3.83%	-4.14%
	June	23.5	0.65	24.2	0.69	-0.7	-0.03	-2.91%	-5.04%
	July	26.3	0.73	26.4	0.72	-0.1	0.02	-0.32%	2.27%
	August	25.2	0.71	25.3	0.74	-0.1	-0.02	-0.30%	-2.99%
	Sep	20.8	0.84	21.4	0.74	-0.6	0.1	-2.78%	14.06%
	Oct	14.3	0.78	15.3	0.7	-1	0.07	-6.41%	10.60%
Albuquerque	April	13.9	0.26	13.3	0.34	0.6	-0.08	4.32%	-24.21%
	May	17.8	0.33	18.9	0.33	-1.1	0	-5.64%	-0.68%
	June	23.2	0.35	23.9	0.32	-0.7	0.03	-2.84%	10.78%
	July	25.6	0.44	25.6	0.42	0.1	0.02	0.27%	3.90%
	August	24.1	0.46	24.4	0.48	-0.4	-0.01	-1.51%	-2.86%
	Sep	20.5	0.48	20.8	0.48	-0.3	0	-1.66%	-0.08%
	Oct	13.7	0.42	14.2	0.46	-0.5	-0.04	-3.26%	-8.21%
Omaha	April	12.2	0.69	11.1	0.61	1.1	0.08	9.94%	13.65%
	May	17.6	0.7	16.9	0.64	0.7	0.06	3.90%	9.54%
	June	23.6	0.74	22.2	0.66	1.4	0.08	6.30%	12.55%
	July	25.7	0.67	24.7	0.68	1	-0.01	3.88%	-0.87%
	August	23.9	0.83	23.6	0.7	0.3	0.13	1.28%	18.05%
	Sep	19.1	0.76	18.9	0.7	0.2	0.06	1.24%	7.95%
	Oct	12.6	0.66	11.9	0.65	0.6	0.01	5.41%	2.02%

6.1.2.3 Different Cities in One Climate Zone Comparison

Average monthly data during cooling season of outdoor dry-bulb temperature and relative humidity for each climate zone are shown in Appendix C. These two sets of figures show two important information: 1. outdoor temperature decreases with increasing climate zones 2. climate zone A compared to B represents more humid regions.

An important task in this study is to verify if all cities in the same climate zone have similar weather data. Since for the purpose of dividing the U.S. into different climate zones and further dividing into sub-climate zones to get the weather data correlation with time of year, it is necessary

to keep all the climate data (outdoor dry-bulb temperature and RH) of different cities in one climate zone (or sub-climate zone) similar to each other . The plots of dry-bulb temperature and relative humidity for different cities in the same climate zone are presented in Appendix C. For most cases, the largest deviation between the single city temperature and the average temperature is within 2℃. Compared to temperature plot, RH plot has larger deviation, but the difference between city RH and average RH is still within 10%.

By averaging different city data in one climate zone, a table with climate zone average data is achieved in Table 36, with the data of daily highest, daily lowest, daily average temperature and daily highest, daily lowest, daily average relative humidity and wet-bulb temperature from NOAA (National Oceanic and Atmospheric) during the past 30 years (1981-2010).

Table 36 Average data for each climate zone

		Daily Highest	Daily lowest	Daily Temp (°F)	Daily Highest RH	Daily Lowest RH	Daily Average RH	wet bulb Temp (°F)
1A	Jan	75.0	62.0	68.5	0.83	0.64	0.73	62.8
	Feb	77.0	64.0	70.5	0.82	0.62	0.72	64.2
	March	79.0	66.5	72.8	0.80	0.61	0.71	66.0
	April	82.0	70.0	76.0	0.78	0.58	0.68	68.4
	May	86.0	74.5	80.3	0.80	0.62	0.71	72.9
	June	89.0	77.5	83.3	0.83	0.66	0.75	76.8
	July	90.0	78.5	84.3	0.82	0.65	0.73	77.1
	August	90.0	78.5	84.3	0.82	0.66	0.74	77.4
	Sep	88.5	78.0	83.3	0.84	0.68	0.76	77.0
	Oct	85.5	75.0	80.3	0.84	0.65	0.74	73.9
	Nov	81.0	70.0	75.5	0.83	0.65	0.74	69.5
	Dec	77.0	65.0	71.0	0.83	0.64	0.73	65.0
2A	Jan	62.0	42.7	52.3	0.84	0.59	0.71	47.7
	Feb	65.0	46.0	55.5	0.84	0.55	0.70	50.3
	March	72.0	52.0	62.0	0.85	0.55	0.70	56.2

Table 36 continued

		Daily Highest	Daily lowest	Daily Temp (°F)	Daily Highest RH	Daily Lowest RH	Daily Average RH	wet bulb Temp (°F)
	April	78.7	58.0	68.3	0.88	0.54	0.71	62.0
	May	85.3	66.7	76.0	0.89	0.56	0.72	69.5
	June	90.0	72.3	81.2	0.90	0.58	0.74	74.6
	July	92.0	74.3	83.2	0.91	0.60	0.76	77.0
	August	92.3	74.3	83.3	0.92	0.60	0.76	77.2
	Sep	88.3	70.0	79.2	0.90	0.60	0.75	73.0
	Oct	80.3	60.7	70.5	0.88	0.53	0.70	64.0
	Nov	72.0	51.7	61.8	0.87	0.57	0.72	56.4
	Dec	63.7	44.7	54.2	0.85	0.59	0.72	49.5
2B	Jan	67.0	44.0	55.5	0.64	0.31	0.48	46.0
	Feb	70.0	46.5	58.3	0.59	0.26	0.43	47.2
	March	76.0	51.0	63.5	0.54	0.23	0.39	50.5
	April	84.0	57.5	70.8	0.42	0.16	0.29	53.2
	May	93.0	66.5	79.8	0.35	0.13	0.24	57.7
	June	101.5	74.5	88.0	0.32	0.12	0.22	62.3
	July	102.5	79.5	91.0	0.51	0.23	0.37	70.7
	August	100.5	78.5	89.5	0.58	0.26	0.42	71.3
	Sep	97.0	73.0	85.0	0.54	0.25	0.39	67.0
	Oct	86.5	61.5	74.0	0.52	0.23	0.38	58.1
	Nov	74.5	50.0	62.3	0.57	0.27	0.42	50.3
	Dec	65.5	43.0	54.3	0.65	0.33	0.49	45.2
3Aw	Feb	57.0	36.3	46.7	0.79	0.52	0.65	41.6
	March	65.3	44.3	54.8	0.78	0.48	0.63	48.5
	April	74.0	52.3	63.2	0.80	0.49	0.64	56.1
	May	81.7	62.0	71.8	0.85	0.53	0.69	64.8
	June	89.7	70.0	79.8	0.85	0.50	0.68	71.6
	July	94.3	74.0	84.2	0.83	0.47	0.65	74.6
	August	94.0	73.3	83.7	0.83	0.46	0.64	74.0
	Sep	86.7	65.7	76.2	0.86	0.50	0.68	68.3
	Oct	75.7	54.3	65.0	0.82	0.47	0.65	57.7
	Nov	64.0	43.3	53.7	0.81	0.51	0.66	47.9
3Ae	Feb	58.0	36.7	47.3	0.77	0.49	0.63	41.8
	March	66.0	42.7	54.3	0.80	0.47	0.63	48.0
	April	74.0	50.3	62.2	0.80	0.45	0.62	54.7
	May	81.0	59.0	70.0	0.85	0.50	0.67	62.7

Table 36 continued

		Daily Highest	Daily lowest	Daily Temp (°F)	Daily Highest RH	Daily Lowest RH	Daily Average RH	wet bulb Temp (°F)
	June	87.3	67.0	77.2	0.86	0.53	0.69	69.7
	July	90.0	70.3	80.2	0.89	0.57	0.73	73.3
	August	89.3	69.7	79.5	0.90	0.57	0.73	72.8
	Sep	83.3	63.3	73.3	0.89	0.55	0.72	66.9
	Oct	74.3	52.3	63.3	0.86	0.49	0.68	56.9
	Nov	65.0	42.7	53.8	0.84	0.51	0.67	48.3
3Be	March	68.0	38.3	53.2	0.71	0.34	0.52	45.0
	April	76.3	47.0	61.7	0.71	0.33	0.52	51.9
	May	85.3	58.7	72.0	0.78	0.36	0.57	61.9
	June	91.7	66.3	79.0	0.80	0.38	0.59	68.3
	July	95.0	70.0	82.5	0.75	0.36	0.55	70.3
	August	94.0	69.0	81.5	0.77	0.38	0.58	70.3
	Sep	86.7	58.0	72.3	0.83	0.44	0.64	63.9
	Oct	76.0	49.3	62.7	0.80	0.40	0.60	54.7
	Nov	65.3	38.3	51.8	0.77	0.40	0.59	45.1
3Bw	Feb	63.0	39.5	51.3	0.69	0.39	0.54	43.7
	March	69.5	45.0	57.3	0.61	0.31	0.46	47.1
	April	77.0	50.5	63.8	0.53	0.25	0.39	50.6
	May	86.0	59.0	72.5	0.49	0.21	0.35	56.3
	June	93.5	66.0	79.8	0.48	0.21	0.34	61.3
	July	96.0	71.0	83.5	0.56	0.25	0.40	66.2
	August	94.0	69.5	81.8	0.60	0.28	0.44	66.2
	Sep	89.0	63.5	76.3	0.64	0.31	0.47	62.8
	Oct	78.5	53.5	66.0	0.65	0.32	0.48	54.8
	Nov	66.0	42.5	54.3	0.70	0.40	0.55	46.5
3Blv	Feb	63.0	43.0	53.0	0.52	0.26	0.39	42.4
	March	70.0	49.0	59.5	0.44	0.21	0.33	46.1
	April	78.0	56.0	67.0	0.35	0.16	0.25	49.4
	May	89.0	66.0	77.5	0.31	0.13	0.22	55.5
	June	99.0	75.0	87.0	0.24	0.11	0.17	59.5
	July	104.0	81.0	92.5	0.29	0.15	0.22	65.2
	August	102.0	79.0	90.5	0.35	0.17	0.26	65.7
	Sep	94.0	71.0	82.5	0.34	0.17	0.25	59.9
	Oct	81.0	59.0	70.0	0.38	0.19	0.29	52.7

Table 36 continued

		Daily Highest	Daily lowest	Daily Temp (°F)	Daily Highest RH	Daily Lowest RH	Daily Average RH	wet bulb Temp (°F)
	Nov	66.0	47.0	56.5	0.47	0.26	0.37	44.7
3Bn	Feb	61.5	41.0	51.3	0.89	0.60	0.74	47.2
	March	66.5	44.5	55.5	0.85	0.52	0.69	50.0
	April	72.5	46.5	59.5	0.80	0.42	0.61	52.1
	May	81.0	52.0	66.5	0.77	0.34	0.55	56.7
	June	88.0	56.5	72.3	0.73	0.30	0.51	60.5
	July	93.0	58.5	75.8	0.71	0.27	0.49	62.8
	August	92.0	58.0	75.0	0.72	0.28	0.50	62.5
	Sep	88.5	56.0	72.3	0.74	0.31	0.52	60.8
	Oct	79.0	50.0	64.5	0.80	0.38	0.59	56.0
	Nov	65.0	42.5	53.8	0.87	0.59	0.73	49.2
3C	Jan	67.5	47.0	57.3	0.72	0.49	0.60	50.0
	Feb	68.0	48.5	58.3	0.76	0.54	0.65	51.8
	March	69.5	51.0	60.3	0.78	0.57	0.67	54.1
	April	72.5	53.5	63.0	0.80	0.55	0.67	56.5
	May	74.5	57.5	66.0	0.81	0.58	0.70	59.8
	June	77.5	60.5	69.0	0.83	0.60	0.71	62.8
	July	82.5	64.5	73.5	0.84	0.58	0.71	66.8
	August	84.0	64.5	74.3	0.83	0.58	0.71	67.4
	Sep	82.5	63.0	72.8	0.82	0.57	0.70	65.7
	Oct	78.0	58.5	68.3	0.79	0.54	0.67	61.0
	Nov	72.5	51.5	62.0	0.75	0.50	0.63	54.6
	Dec	67.5	47.0	57.3	0.73	0.48	0.60	49.9
4A	April	66.9	46.0	56.4	0.75	0.46	0.60	49.3
	May	75.6	55.6	65.6	0.82	0.51	0.66	58.6
	June	84.3	65.1	74.7	0.83	0.52	0.67	66.9
	July	88.4	69.9	79.1	0.83	0.52	0.67	70.9
	August	87.3	68.4	77.9	0.85	0.52	0.69	70.1
	Sep	80.1	60.4	70.3	0.86	0.54	0.70	63.6
	Oct	68.7	48.9	58.8	0.83	0.51	0.67	52.7
4B	April	70.0	42.5	56.3	0.59	0.25	0.42	45.4
	May	79.5	52.5	66.0	0.61	0.27	0.44	53.6
	June	88.0	61.5	74.8	0.61	0.27	0.44	60.6
	July	90.5	65.5	78.0	0.67	0.30	0.49	64.5
	August	88.0	64.5	76.3	0.72	0.35	0.53	64.5

Table 36 continued

		Daily Highest	Daily lowest	Daily Temp (°F)	Daily Highest RH	Daily Lowest RH	Daily Average RH	wet bulb Temp (°F)
	Sep	82.0	57.0	69.5	0.73	0.36	0.54	59.1
	Oct	70.5	45.5	58.0	0.67	0.33	0.50	48.6
5A	April	60.6	40.8	50.7	0.75	0.50	0.63	44.7
	May	70.6	50.8	60.7	0.78	0.51	0.65	53.8
	June	80.0	60.6	70.3	0.80	0.52	0.66	62.8
	July	84.2	65.8	75.0	0.83	0.54	0.68	67.5
	August	82.4	64.4	73.4	0.85	0.55	0.70	66.4
	Sep	75.0	55.6	65.3	0.85	0.55	0.70	59.2
	Oct	63.0	44.2	53.6	0.80	0.52	0.66	47.9
5B	April	62.3	37.0	49.7	0.67	0.32	0.50	41.6
	May	72.3	45.7	59.0	0.68	0.31	0.49	49.3
	June	81.7	53.0	67.3	0.67	0.28	0.48	55.6
	July	90.3	59.0	74.7	0.62	0.24	0.43	60.2
	August	89.0	57.7	73.3	0.62	0.24	0.43	59.1
	Sep	79.3	49.7	64.5	0.66	0.27	0.47	53.0
	Oct	66.3	38.7	52.5	0.68	0.31	0.50	43.9
6A	May	68.0	47.3	57.7	0.78	0.51	0.65	51.1
	June	77.7	57.3	67.5	0.80	0.53	0.66	60.3
	July	82.3	63.3	72.8	0.82	0.52	0.67	65.2
	August	80.7	61.7	71.2	0.85	0.55	0.70	64.3
	Sep	72.0	52.0	62.0	0.86	0.56	0.71	56.4
	Oct	59.0	39.7	49.3	0.81	0.54	0.68	44.4
6B	May	66.3	39.3	52.8	0.73	0.38	0.56	45.4
	June	76.7	48.0	62.3	0.73	0.35	0.54	52.9
	July	85.7	54.3	70.0	0.68	0.29	0.48	58.0
	August	84.0	52.7	68.3	0.67	0.29	0.48	56.4
	Sep	73.0	43.0	58.0	0.69	0.33	0.51	48.7
7A	May	68.7	44.0	56.3	0.79	0.45	0.62	49.5
	June	77.3	53.7	65.5	0.84	0.49	0.66	58.5
	July	83.3	58.3	70.8	0.86	0.47	0.66	63.1
	August	81.7	56.3	69.0	0.87	0.46	0.66	61.7
	Sep	71.0	46.3	58.7	0.86	0.49	0.68	52.7
4C	April	61.0	42.0	51.5	0.9	0.6	0.7	46.9
	May	67.3	47.0	57.2	0.9	0.5	0.7	51.7
	June	72.3	51.0	61.7	0.8	0.5	0.7	55.2
	July	79.7	54.7	67.2	0.8	0.4	0.6	59.3
	August	80.0	55.0	67.5	0.8	0.4	0.6	59.9

Table 36 continued

		Daily Highest	Daily lowest	Daily Temp (°F)	Daily Highest RH	Daily Lowest RH	Daily Average RH	wet bulb Temp (°F)
	Sep	74.3	50.7	62.5	0.9	0.5	0.7	56.2
	Oct	62.3	45.0	53.7	0.9	0.6	0.8	49.7

6.1.2.4 Temperature and Relative Humidity for Climate Zone A and B

The monthly temperature of climate zone A and zone B are shown in Figure 176 and 177, the curve of temperature versus month fits like quadratic but not symmetric, the peak temperature occurred in July for most climate zones. Also, the climate zones with large zone numbers always have more fluctuation during the cooling season.

The monthly relative humidity of climate zone A and zone B are shown in Figure 178 and 179, the data for climate zone A is quite stable, almost no fluctuation during the cooling season with the range of RH 60%-80%. Also, the difference between zone numbers is negligible. However, the curve for climate zone B fits like quadratic and the minimum relative humidity occurred in June or July. Also, different climate zones in zone B differs a lot from each other.

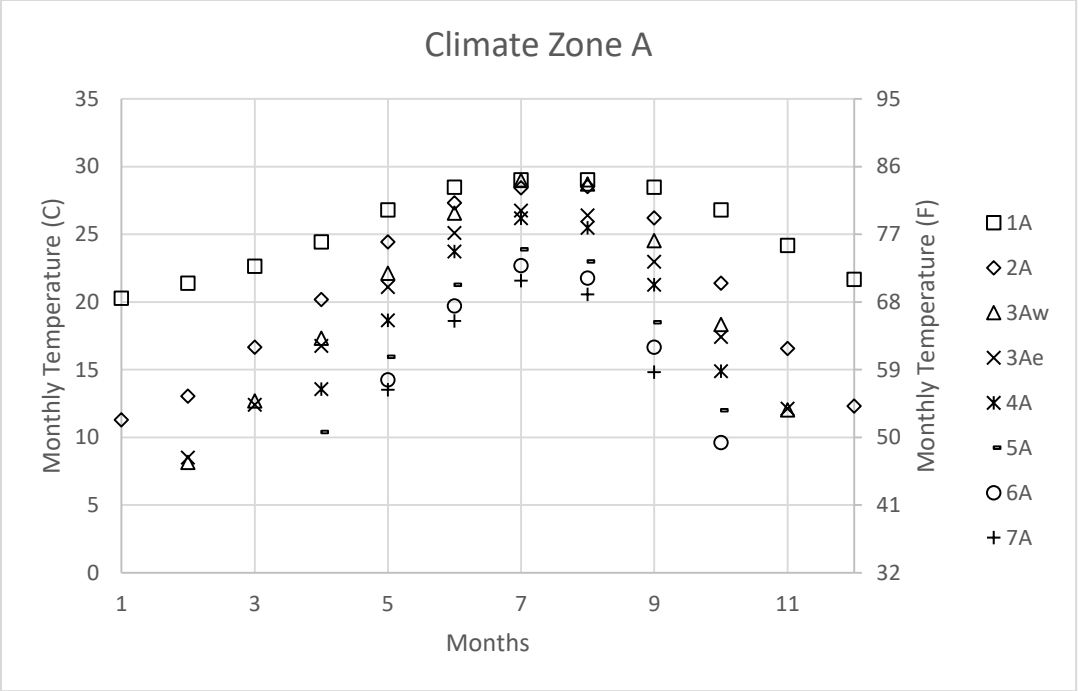

Figure 176 Monthly temperature for climate zone A

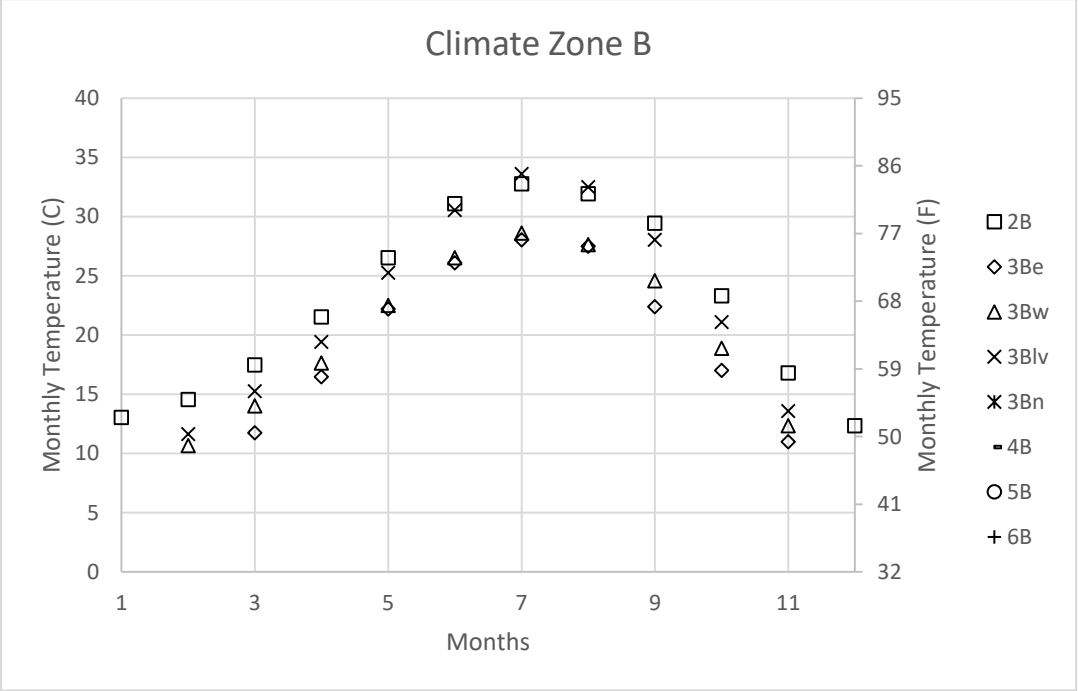

Figure 177 Monthly temperature for climate zone B

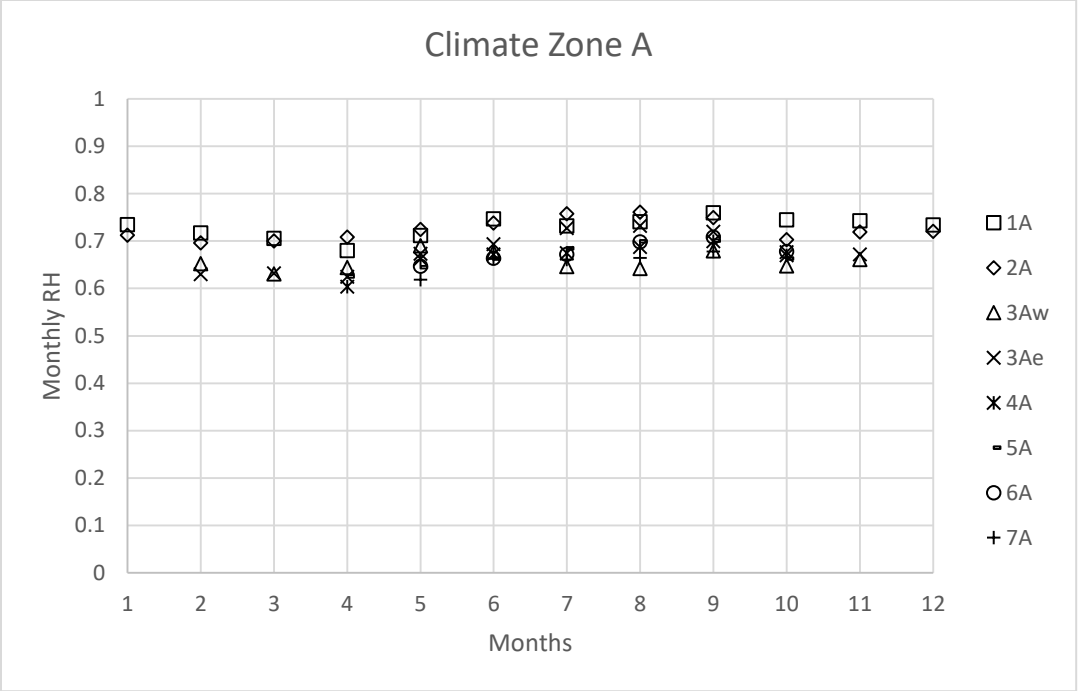

Figure 178 Monthly relative humidity for climate zone A

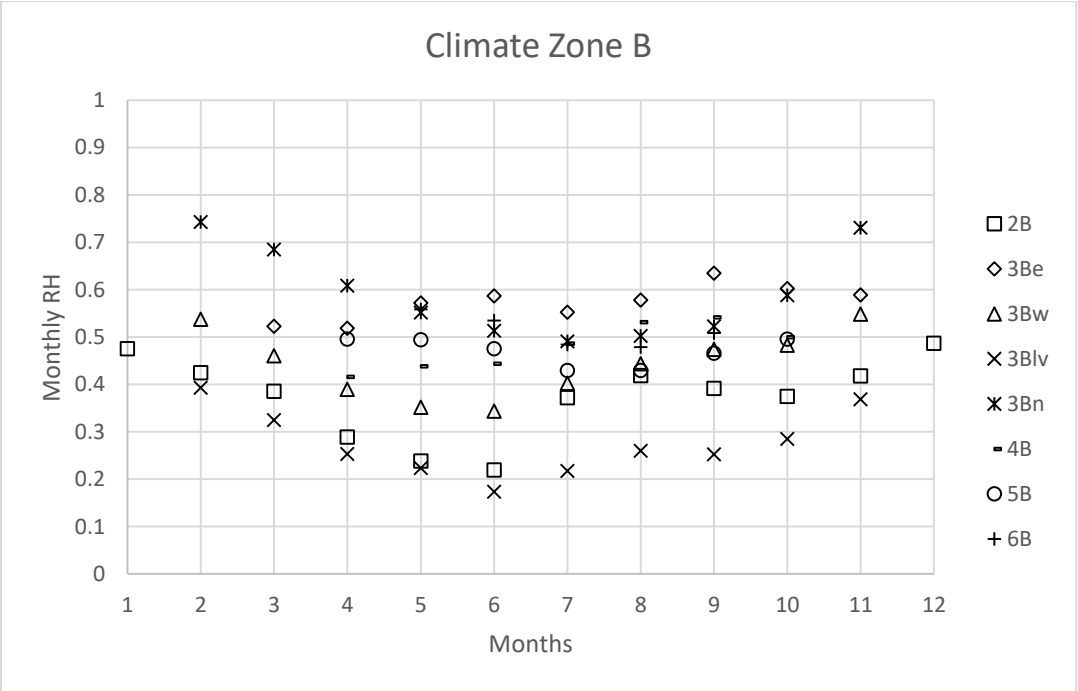

Figure 179 Monthly relative humidity for climate zone B

6.1.2.5 Wet-bulb Temperature Analysis

The wet-bulb temperature is the temperature a parcel of air would have if it were cooled to saturation (100% relative humidity) by the evaporation of water into it, with the latent heat being supplied by the parcel.

The wet-bulb temperature is the lowest temperature which may be achieved by evaporative cooling of a water-wetted ventilation surface. Lower wet-bulb temperatures that correspond with drier air in the cooling season can translate to energy savings in air-conditioned buildings due to: 1. Reduced dehumidification load for ventilation air, 2. Increased efficiency of the cooling tower. The difference of dry-bulb temperature and wet-bulb temperature represented the potential of evaporative cooling. The bigger the difference, the more potential there is.

Figure 180 and 181 show wet-bulb temperature/dry-wet versus dry-bulb temperature for climate zone A, B, and C respectively. At the same dry-bulb temperature, climate B always has a lower wet-bulb temperature, which means climate zone B always has more significant evaporative cooling potential than climate zone A and C.

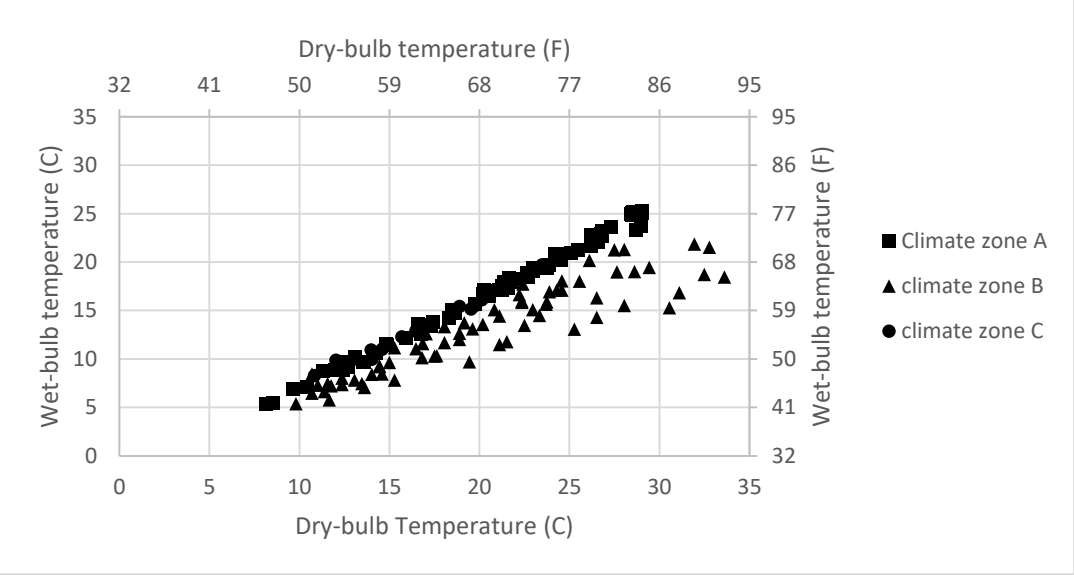

Figure 180 Wet-bulb temperature and dry-bulb temperature

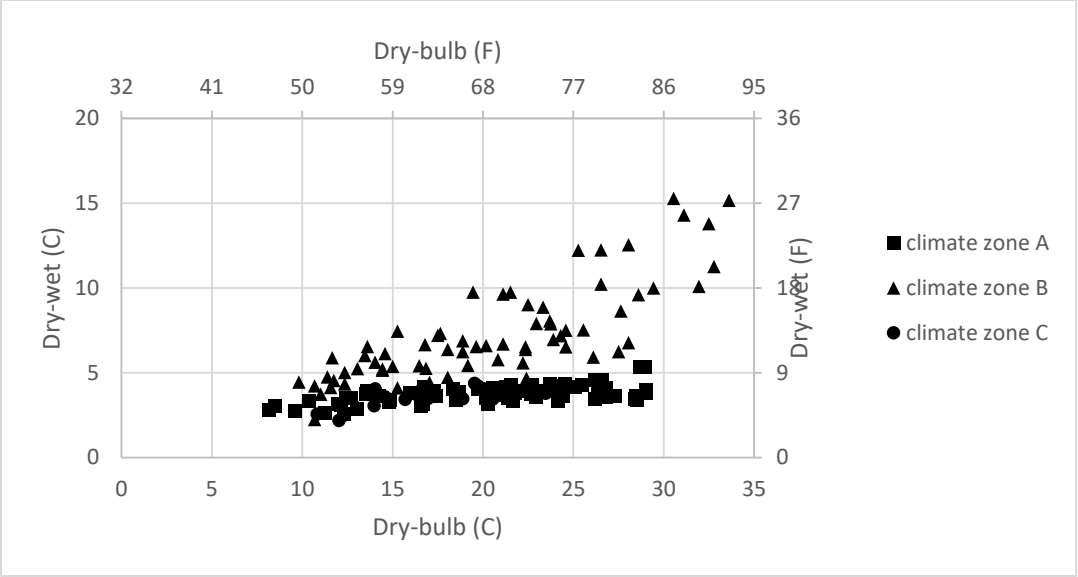

Figure 181 Dry-bulb temperarture-wet-bulb temperature versus wet-bulb temperature

Figure 182---188 showed evaporative cooling potential versus month for all climate zones (zone 1 to zone 7). For climate zone A, the potential is quite low and steady during the whole cooling season since climate zone A is humid region along with steady RH all over the year. However, for climate zone B, the peak potential always occurred between June and August. As for most regions in climate zone B, months during June and August had the lowest RH value.

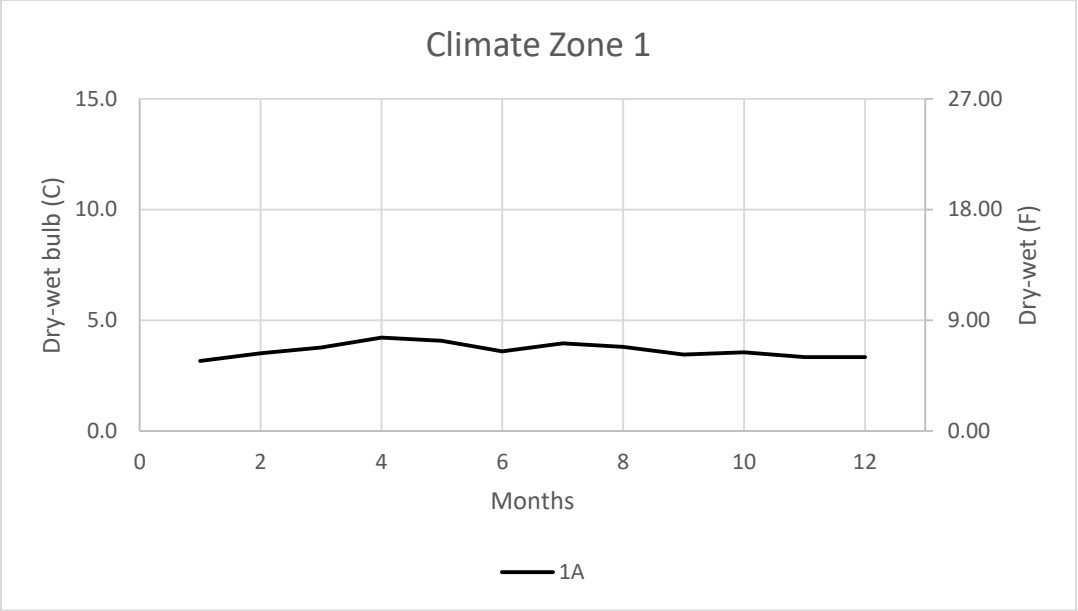

Figure 182 Dry-wet versus month for climate zone 1

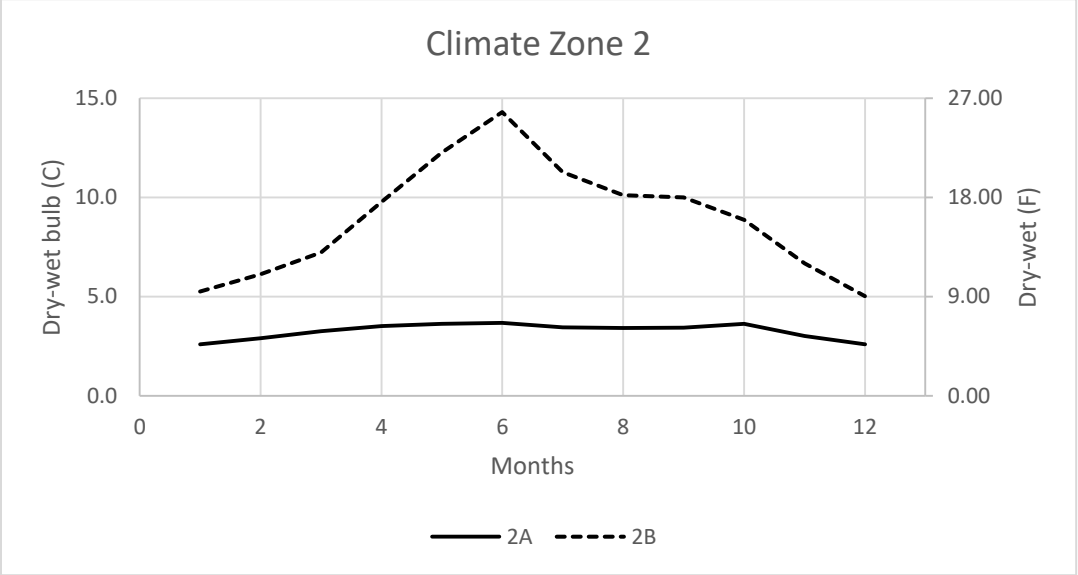

Figure 183 Dry-wet versus month for climate zone 2

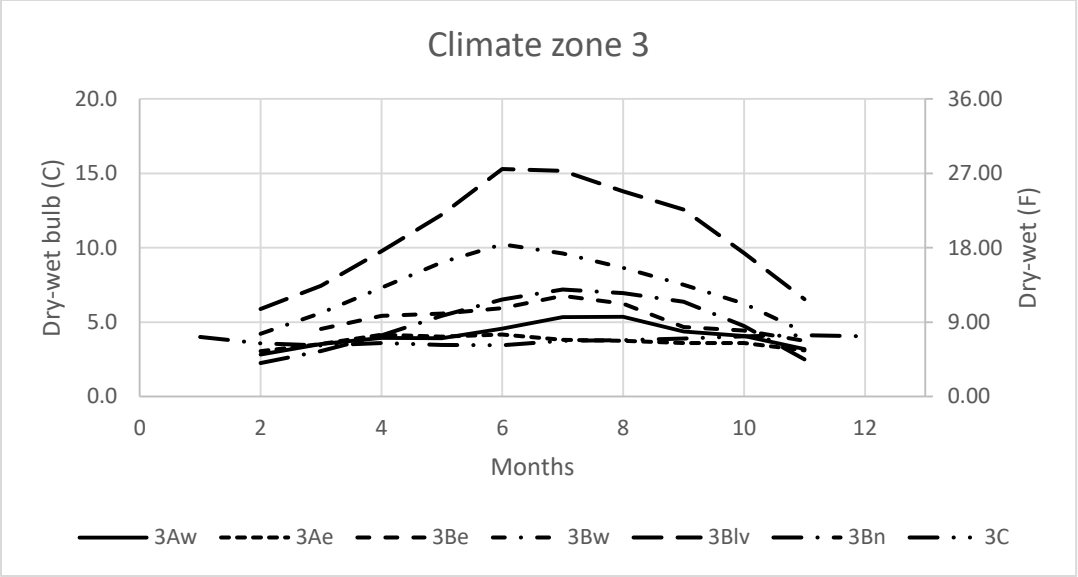

Figure 184 Dry-wet versus month for climate zone 3

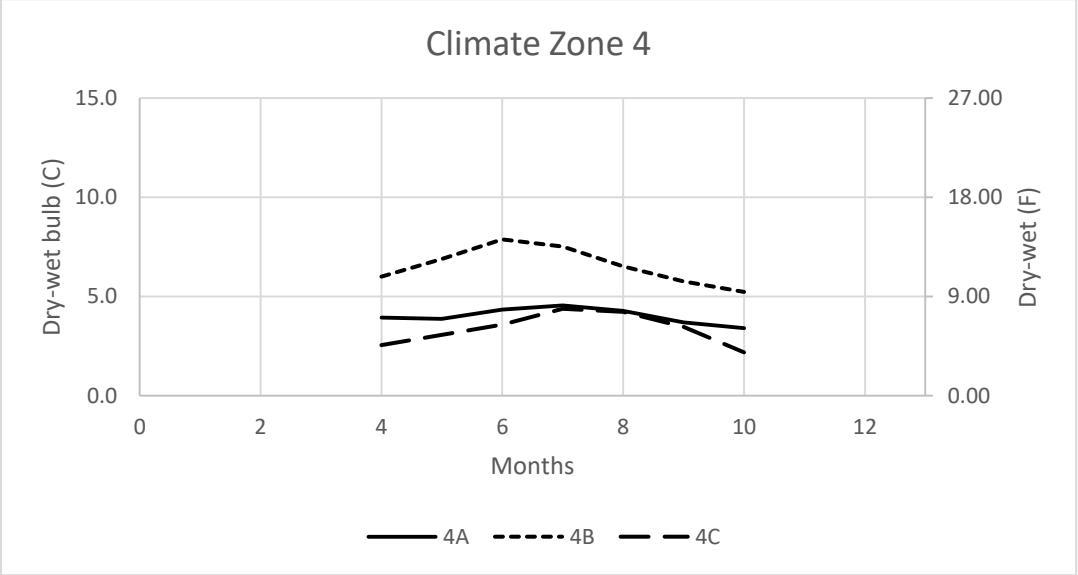

Figure 185 Dry-wet versus month for climate zone 4

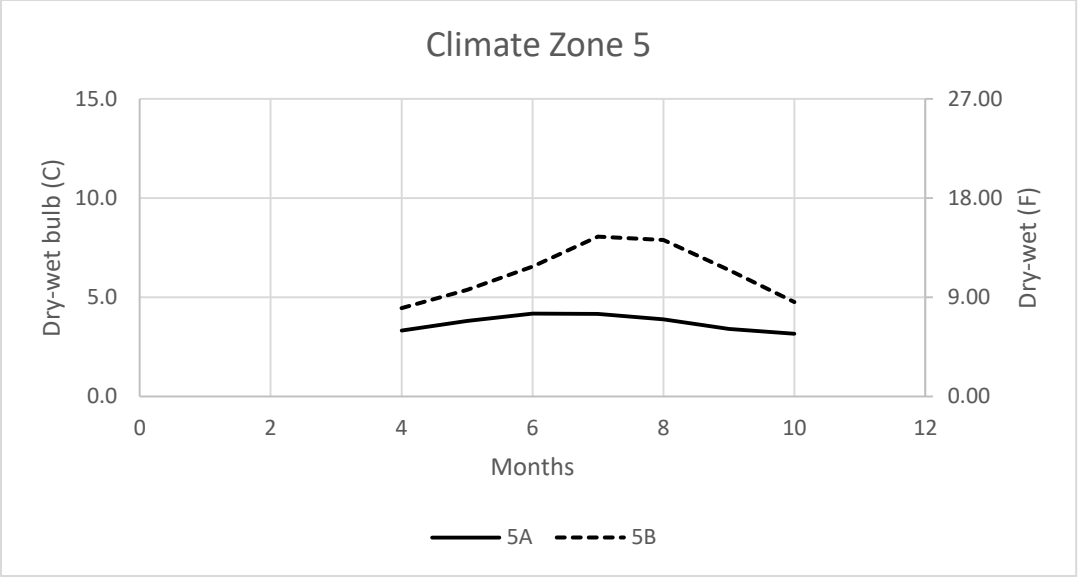

Figure 186 Dry-wet versus month for climate zone 5

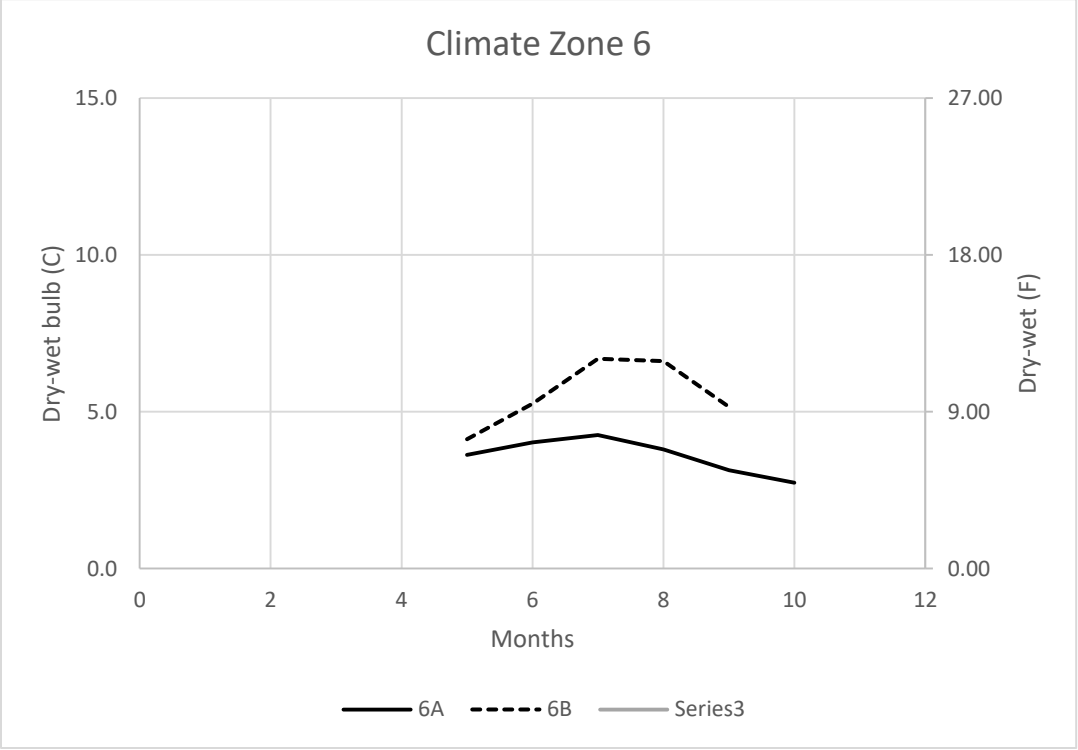

Figure 187 Dry-wet versus month for climate zone 6

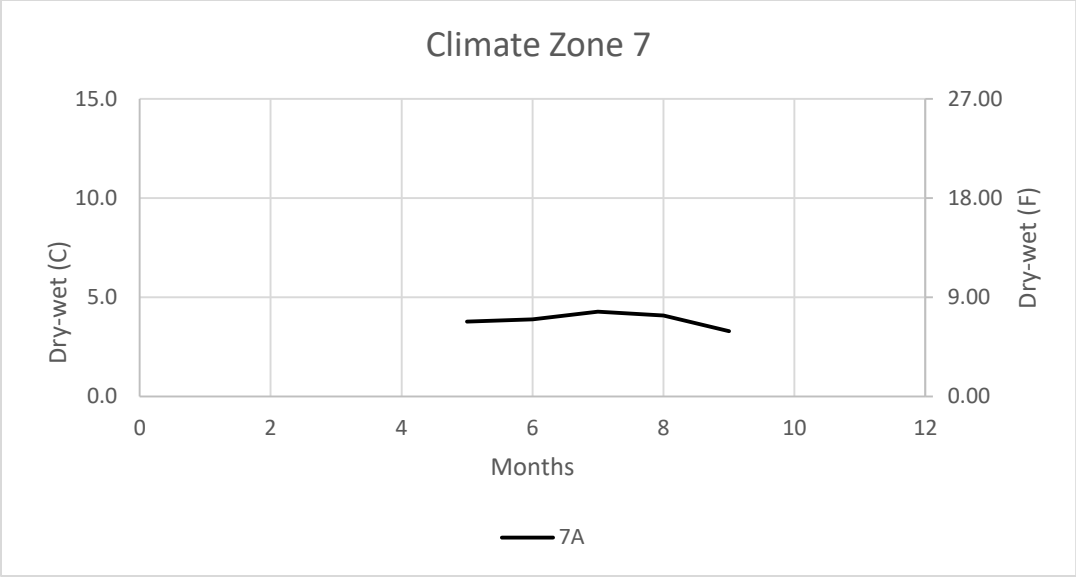

Figure 188 Dry-wet versus month for climate zone 7

6.1.2.6 Correlation Development

Multiple regression has been selected as the method for building predictive models to investigate the relationship between dry-bulb (relative humidity, wet-bulb) to the time of year (month/day) and climate zones.

For the derivation of the equation, a specific cubic regression model is assumed as follows for the monthly average model (take dry-bulb temperature as an example, relative humidity and the wet-bulb temperature had the same formula)

$$\boldsymbol{T = a + bx + cx^2 + dx^3} \quad (123)$$

Where x is the month number and coefficients of a, b, c and d are all climate zone related.

Residual in this section is defined as the actual data minus the predicted data in the following plots, which is the same as previous sections. Figure 189 shows the predicted data versus actual data of dry-bulb temperature and all the data is close to the diagonal line. All the residuals are within 2.5℃ according to Figure 190. Figure 191 indicates the inaccuracy only occurred in climate zone 2B and 3Blv (3B Las Vegas).

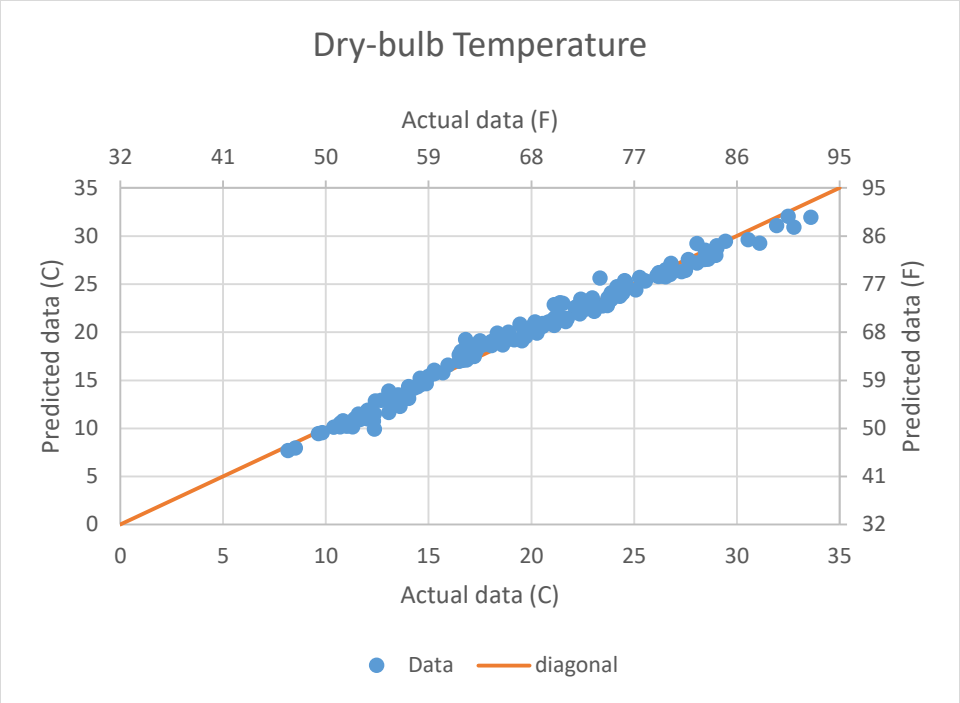

Figure 189 Predicted versus actual data of dry-bulb temperature

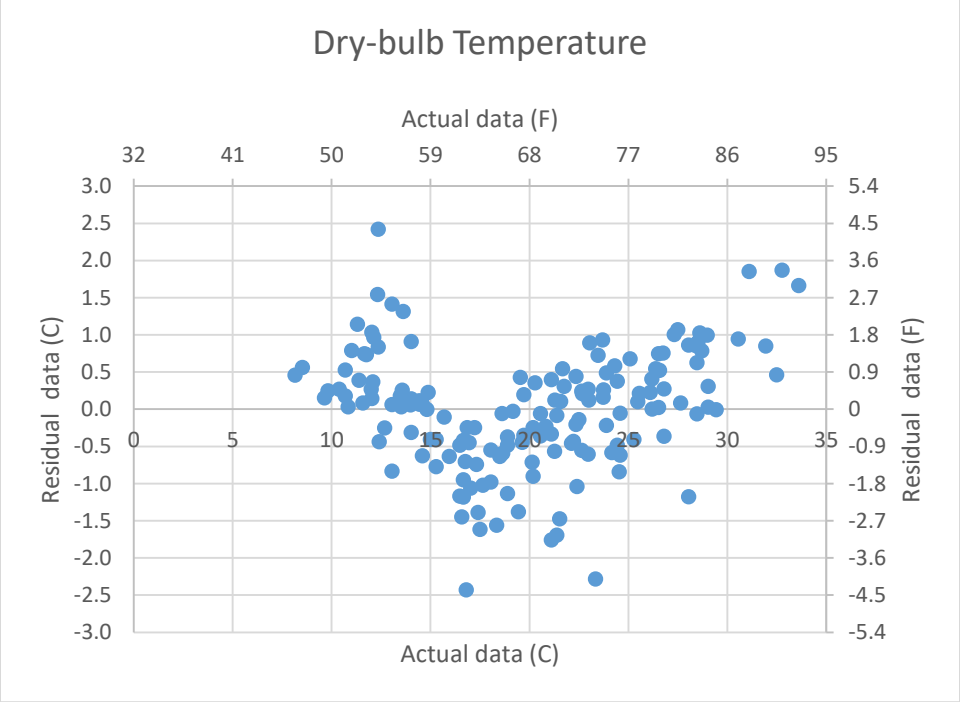

Figure 190 Residual data vsersus actual data of dry-bulb temperature

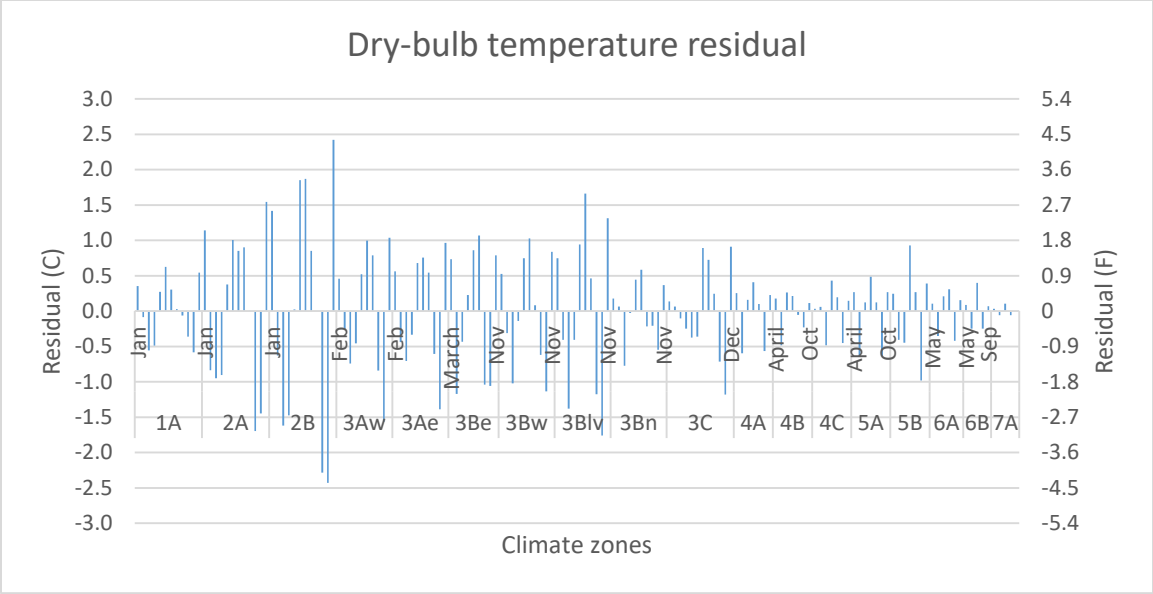

Figure 191 Predicted vs. actual dry-bulb temperature for different climate zones

Figure 192 shows the predicted data versus actual data of relative humidity and all the data is close to the diagonal line. All the residuals are within 0.1 according to Figure 193, and the inaccuracy only occurred in climate zone 2B according to Figure 194.

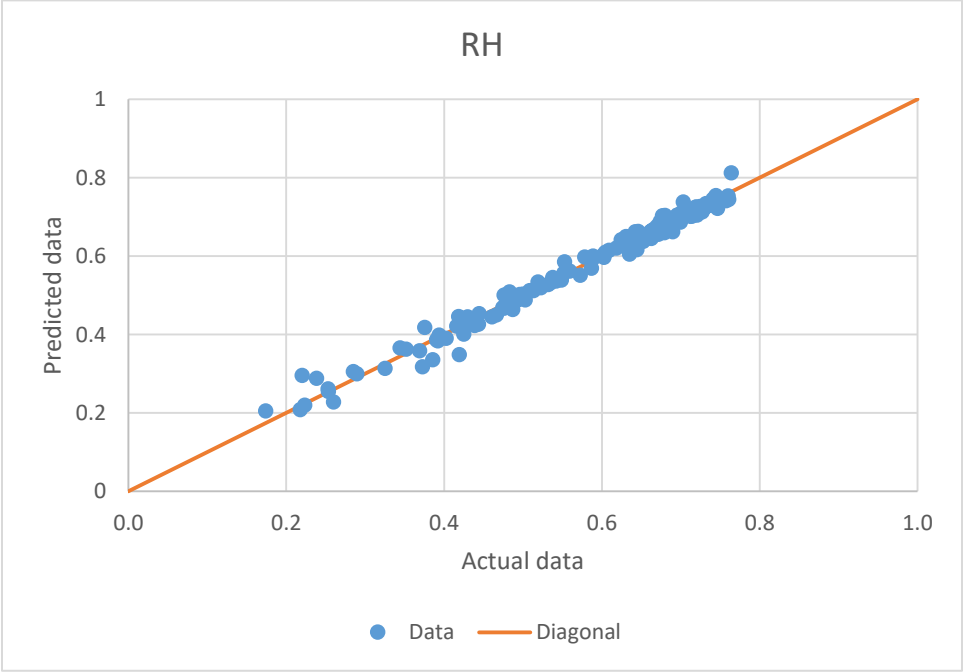

Figure 192 Predicted versus actual data of relative humidity

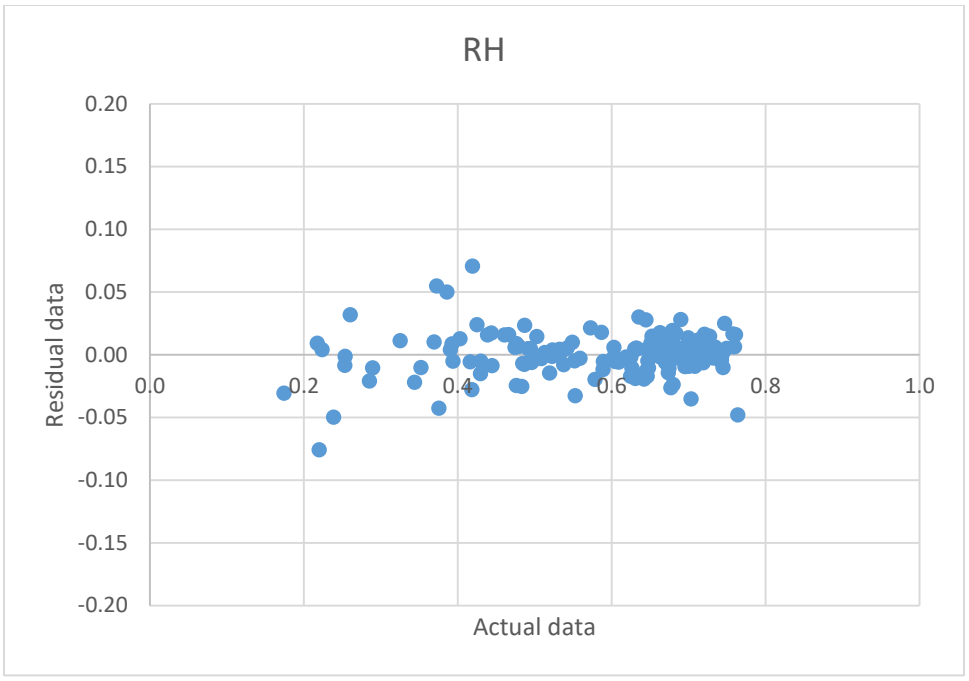

Figure 193 Residual data vsersus actual data of relative humidity

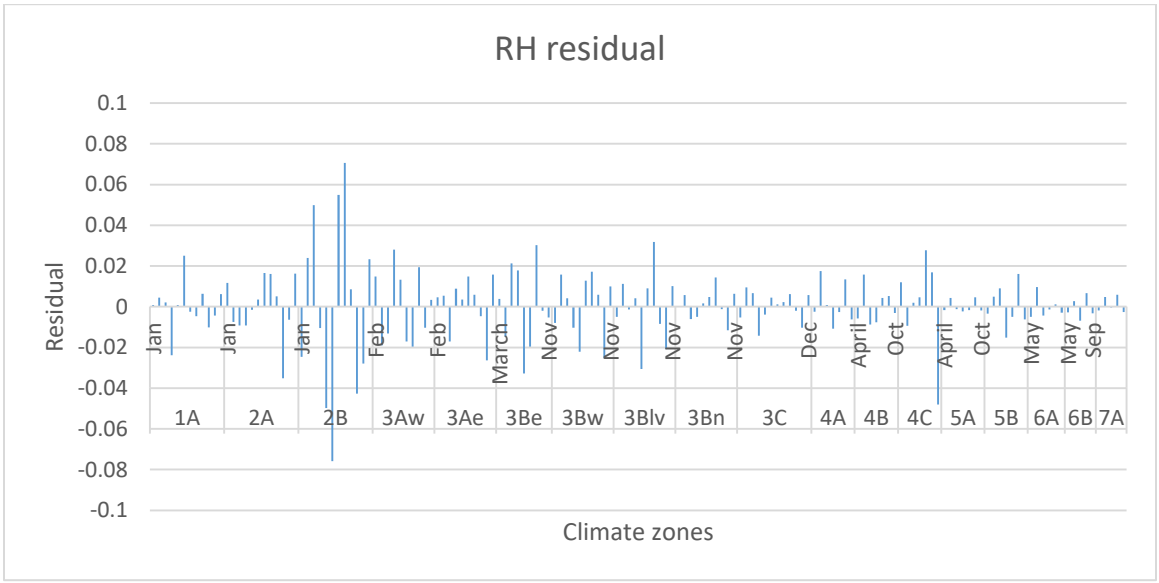

Figure 194 Predicted vs. actual relative humidity

Figure 187 showed the predicted data versus actual data of wet-bulb temperature. All the residuals are within 2.5℃ according to Figure 188, and the inaccuracy only occurred in climate zone 2B according to Figure 189.

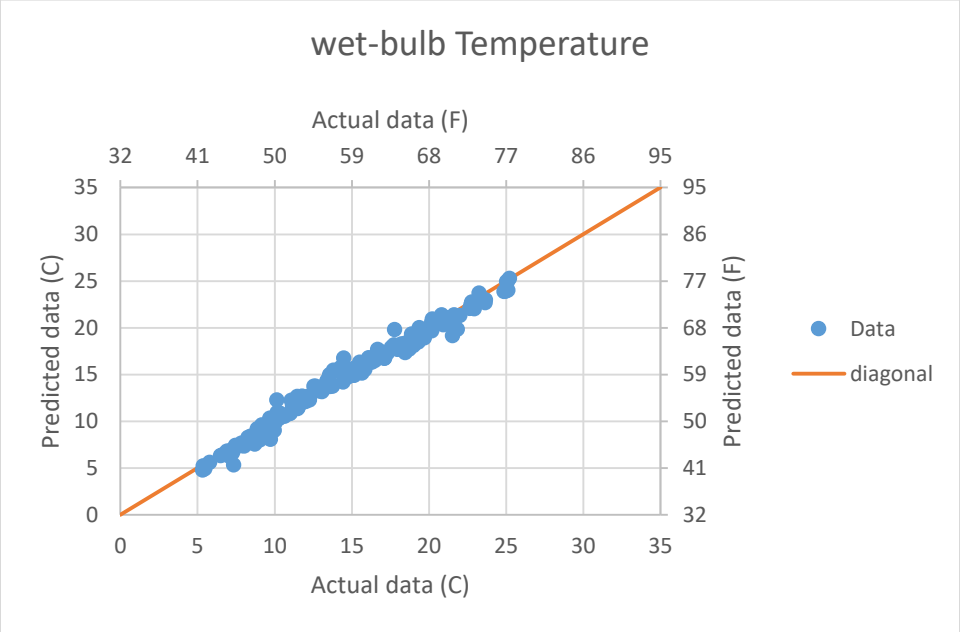

Figure 195 Predicted versus actual data of wet-bulb temperature

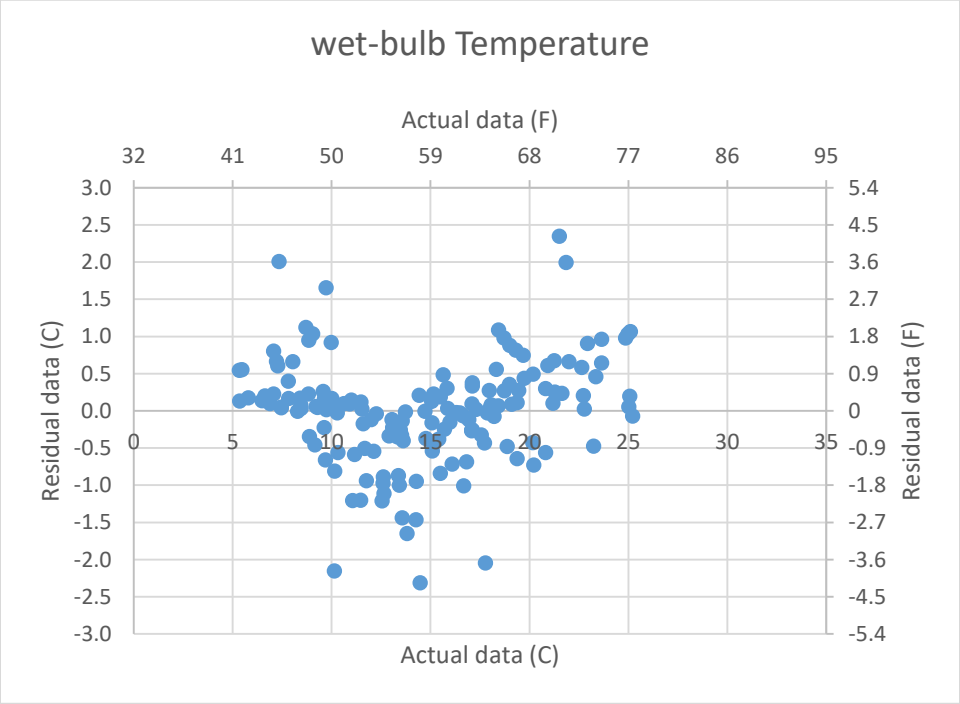

Figure 196 Residual data vsersus actual data of wet-bulb temperature

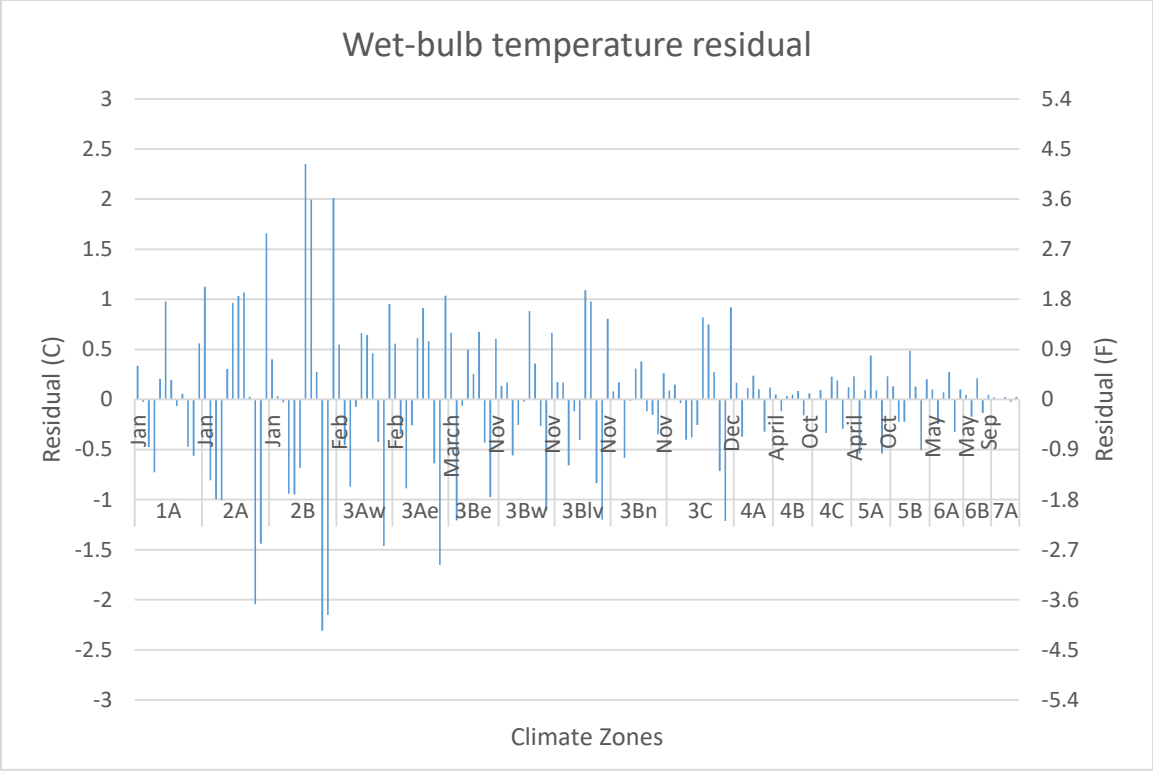

Figure 197 Predicted vs actual wet-bulb temperature

Similarly, assuming the monthly average temperature is exactly the middle of each month, the daily temperature is then derived by the similar method.

For the derivation of the equation of daily average model, a specific cubic regression model is assumed as follows, which is the exactly the same formula as the monthly average model (take dry-bulb temperature as an example, relative humidity and the wet-bulb temperature had the same formula)

$$\boldsymbol{T = a + by + cy^2 + dy^3} \qquad (124)$$

Where y is the day number and coefficients of a, b, c and d are all climate zone related. Again, January 1st is always counted as day 1. All monthly average data from January to December

(totally 12 months) is corresponding to day 16, 45.5, 75, 105.5, 136, 166.5, 197, 228, 258.5, 289, 319.5, and 350 of daily data derivation.

The cubic curve of dry-bulb temperature, relative humidity and wet-bulb temperature for 18 climate zones are shown in Appendix B. The coefficient of a, b, c, d for monthly and daily data of dry-bulb temperature, relative humidity, and wet-bulb temperature are shown in Appendix A. All the figures indicate that cubic curve fits well for all three functions, namely dry-bulb temperature, RH, and wet-bulb during the whole cooling season.

6.2 Cooling Degree-Days and Weighting Factor Correlations for U.S. Locations and Climate Zones

Cooling degree-days are an important climatic indicator and have been used in many applications designing and operating energy efficient buildings along with estimating energy consumption. Of special importance, cooling degree days are based on outdoor temperature weather data, and using any approaches and assumptions can be formed from these types of data. The author first calibrated the monthly cooling degree-days by using correlation daily dry-bulb temperature in section 6.1 by exploring 53 cities in 18 climate zones across the U.S. In fact, tables of Cooling Degree Days (CDD) are tabulated in any number of past papers and reports, usually for specific locations and applications. Typically, for an annual or monthly basis for specific locations. In an effort to provide each to use, tools for those performing cooling analysis based on the use of cooling degree concepts, the study is reported herein developing by using time of year(month) weather data and presenting equations for monthly cooling degree-days and weighting factors for each U.S. climate zone (totally 18). The results reveal that a cubic non-linear

analysis related monthly cooling degree-days and weighting factors to the time of year for each climate zone.

6.2.1 Introduction and Literature

The cooling degree-days method is one of the most common and simplest methods used in the ventilation and air-conditioning industry estimating cooling energy requirements. Furthermore, cooling degree-days are a significant climatic design indicator that captures the extremity and duration of ambient temperature.[94] Essentially, cooling degree-days are the summation of temperature differences between outdoor air temperature and a reference temperature, which is also known as the base temperature. The base temperature,T_b is referred to as the outdoor air temperature at which the cooling system does not need to run in order to maintain comfort conditions. In other words, when the outdoor air temperature is below the base temperature, there is no need for the cooling system to provide cooling. On the other hand, cooling systems need to operate when the outdoor temperature is above the base temperature. Meanwhile, the summed temperature differences or cooling degree-days also have a relationship with cooling energy consumption. Of special note, four common degree-day base temperatures are used to correlate cooling energy to the local climate for various systems applications and requirements in 5 °F increasing that result in 50°F, 55°F, 60°F and 65°F, which in turn corresponds to 10, 12.8, 15.6 and 18.3 in℃.

Past literature has discussed and presented bases temperature and different methodologies to predict cooling degree-days. In many cases, the approach is to use the historical data to further predict the future climate in terms of temperature and relative humidity. A summary of literature is listed in Table 37.

Table 37 Literature summary table

Year	Author	Scope	Results
2014	Kyoungmi Lee	Kyoungmi Lee [95] determined real base temperatures to accurately calculate HDD and CDD for South Korea by using monthly electric energy consumption and mean temperature data from 2001 to 2010.	The results revealed that the regional electricity demand depends on air temperature and the sensitivity of electricity demand to the temperature change is in turn affected by the size of cities. The South Korean regional base temperatures, defined by a piecewise linear regression method, are ranging from 14.7 to 19.4℃.
2011	Monjur Mourshed	Monjur Mourshed [96] researched predicting future weather data (the 2020s, 2050s, and 2080s) in Dhaka (the capital of Bangladesh) by using a statistically averaged baseline present-day hourly weather data.	Analysis showed that cooling degree-days continue to increase in future climates. The magnitude of change in monthly cooling degree-days is uneven and is greater in winter months than in summer and monsoon. The duration of outdoor air dry-bulb temperature in the form of increased cooling degree-days in future climates will result in a surge in demand for energy for comfort cooling, which will add further stress to the already stressed energy infrastructure in the country
2012	Monjur Mourshed	The author [97] also developed an equation for calculating degree-days from low-resolution temperature data by exploring the relationship between degree-days and annual mean temperature for 5511 different locations around the world by using multiple non-linear regression.	The equation can be used to calculate degree-days of locations for which daily temperature data may not be available. The equations can also be used to calculate degree-days from low-resolution global circulation model of increasing temperature, for investigating the impact of climate change on building heating and cooling energy demand at a global scale without the need to create synthetic weather series through morphing or downscaling.
2011	Z.Oktay	Z.Oktay [98] investigated a new approach for predicting cooling degree –hours.	The study showed a novel approach to predict the outdoor temperature fluctuations during daytime as a dimensionless temperature variation coefficient. The daily outdoor temperature trend is established by using the daily maximum and minimum temperatures. A case study of 58 cities in different geographical regions of Turkey is utilized, and the results are then compared between the simulated data and published data.

Table 37 continued

Year	Author	Scope	Results
2015	Yana Petri	Yana Petri [99] evaluated the impacts of global warming on residential heat and cooling degree-days in the United States.	They projected future (2080-2099) HDD and CDD values by adding changes to values based on historical observations (1981-2010) of US climate. The sum HDD +CDD is an indicator of locations that are thermally comfortable, with low heating and cooling demand. By the end of the century, station median HDD+CDD will be reduced in the contiguous US, decreasing in the North and increasing in the South. BY considering HDD and CDD values separately, future New York, NY, is anticipated to become more like present Oklahoma City, OK; Denver, CO becomes more like Raleigh, NC, and Seattle, WA, becomes more like San Jose, CA. These results serve as an indicator of projected climate change and can help inform decision-making.

6.2.2 Model Development and Formulation

6.2.2.1 Model Description

Several different methods are used for calculating cooling degree-days. The hourly method produces the most accurate estimate and this use of the complicated hourly method for energy, or building simulation has now been widely used. Nevertheless, the hourly method is not suitable for all applications due to the unavailability of hourly temperature data for many locations. Thus, degree-days retain their usefulness because they are accurate climate indicator and daily data is more easily accessed for many different locations.

Of special note, ASHRAE Standard 90.1 2007 relies mostly on cooling degree-days data at a 10℃ (50℉) base temperature to classify U.S. locations into climate zones from zone 1 (hottest) to zone 7 (coldest) followed by an A or B symbol, represents humid and dry conditions, respectively. By analyzing the monthly dry-bulb temperature of 53 cities in 18 climate zones during the past 30 years (1980-2010, NOAA), it is concluded that the monthly dry-bulb

temperature related to month for each climate zone. Furthermore, it is assumed that the monthly temperature falls exactly in the middle of each month so that the daily temperature is then derived using a daily correlation for each month based on the mid-month temperature for each month during the cooling season. Specifically, January 1st is Day 1, and Dec 31st is Day 365 even though for some climate zones the cooling season does not start from January. From the results in section 6.1 developed above, it suggests a very strong cubic non-linear regression relationship between daily temperature and day. For this study, all the result from Section 6.1 is herein used for cooling degree-day model development.

Monthly cooling degree-days during the cooling season are calculated by the following formula,

$$CDD_{month} = \sum_{i=starting\ day}^{ending\ day} (T_i - T_b) \tag{125}$$

where T_b base-temperature and 10℃ (50°F), 12.8℃ (55°F), 15.6℃ (60°F) and 18.3℃ (65°F) are studied in this paper. T_i is the daily temperature which is calibrated from the correlation in section 6.1. Of special note, cooling degree-day is counted from the daily temperature above base temperature and end at the daily temperature above base temperature since when the outdoor air temperature is below the base temperature, there is no need for the cooling system to provide cooling. If the daily temperatures in one month are all above base temperature, the month is called a full month. If some daily temperatures in one month are below the base temperature, the month is called a residual month.

Similarly, the total cooling degree-days for a whole year is the summation of monthly cooling degree-days for a year and is calibrated as follows,

$$CDD_{year} = \sum_{i=1}^{365} (T_i - T_b) \tag{126}$$

The monthly weighting factor is defined as the monthly cooling degree-days divide by the total year cooling degree days, as shown in Eqn 127, which represents the portion of the annual cooling that is required during each month,

$$WF=\frac{CDD_{month}}{CDD_{year}} \quad (127)$$

6.2.2.2 Data Statistics and Analysis

By using the methodology discussed above, monthly/total cooling degree-days and weighting factor under base-temperature 10℃ (50℉), 12.8℃ (55℉), 15.6℃ (60℉) and 18.3℃ (65℉) for each climate zone (totally 18 zones) are shown in Appendix B. Of special note, in some climate zone, the month for cooling does not start from January, but in this table, the month is ranged from January to December and the month with no cooling is left with a blank. Also, the starting month may or may not be the same for different base-temperatures.

Since 10℃ (50℉) is the focus of this study, Figure 198 shows the actual monthly cooling degree-days varied with monthly average dry-bulb temperature (derived from the correlation in section 6.1.2) for all climate zones during the cooling season under ten 10℃ base-temperature. The plot is roughly a straight line according to Eqn (125) in methodology. The reason some data with a monthly average dry-bulb temperature below 10℃ still have cooling degree-days is that even monthly average temperature is below the base temperature. However, some daily temperatures in that month are above the base temperature. Thus cooling degree-days still exist for these outliers.

Figure 199 shows the total cooling degree-days varied with climate zones (totally 18) under 10℃ (50℉) base temperature. As discussed in section 6.1, the focus is on climate zone 1A, 2A, 2B, 3A, 3B, 3C, 4A, 4B, 4C, 5A, 5B, 6A, 6B, 7A. The number in the above code stands for temperature, which varies from very hot to very cold; the letter in the code means humidity level,

and they are humid, dry and marine, respectively. For each climate zone, the largest area or the city with most population is chosen. Of special note, climate zone 3A and 3B, as the special geographical condition, even the weather of several cities in the same climate zone are still significantly differed. Thus they are further divided into a sub-category--- 3A west, 3A east; 3B west, 3B east, 3B north and 3B Las Vegas. By averaging different city data in one climate zone, a climate zone average data is achieved.

Since the number in the climate zone code stands for temperature, which varies from very hot to very cold (1 to 7), climate zone 1A had the greatest cooling degree-days, almost four times of climate zone 7A. In climate zone 3, Las Vegas daily temperature is higher than the others all year around. Thus Las Vegas cooling degree-days are significantly higher than other zones. Since the letter in the code just means humidity level, all climate zones with same zone number had similar total cooling degree-days.

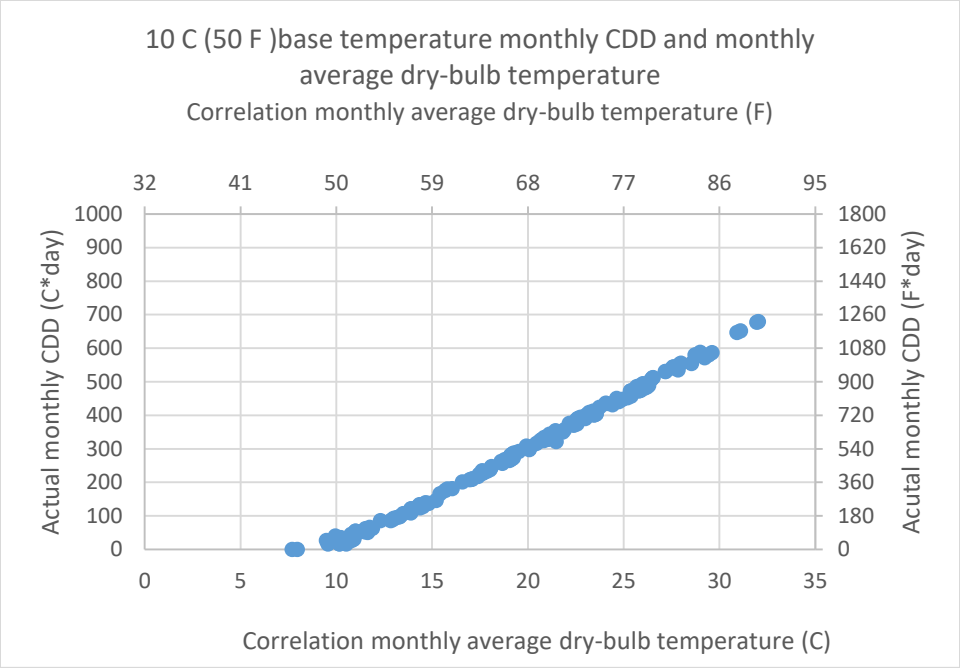

Figure 198 Actual monthly CDD varied with correlation monthly average dry-bulb temperature

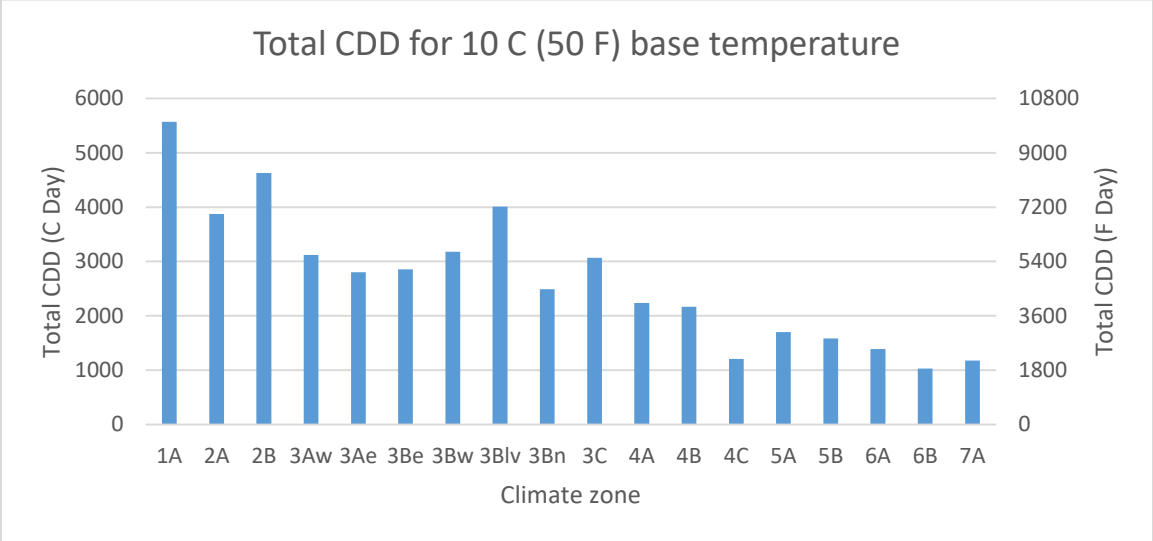

Figure 199 Total cooling degree days varied with climate zone

Table 38 shows cooling season starting day/ending day and length during a year under base-temperature 10℃ (50°F), all the outdoor temperatures above the base temperature are counted. Figure 200 and 201 further illustrate that for most cases that lower climate zone numbers have

longer cooling season since the smaller number, the hotter. Nevertheless, climate zone 3C also has significant long cooling season since it is a marine climate zone and the daily temperatures are almost all above base temperature 10℃ (50°F), but do not fluctuate a lot during the whole year.

Table 38 Cooling season length for 10 ℃ base temperature

	Cooling season				
Climate zones	start	end	length	Percentage	CDD (C*day)
1A	1	365	365	100%	5570.484
2A	15	352	338	93%	3873.809
2B	2	349	348	95%	4628.598
3Aw	59	322	264	72%	3120.059
3Ae	58	323	266	73%	2801.002
3Be	71	320	250	68%	2858.121
3Bw	45	323	279	76%	3176.398
3Blv	40	324	285	78%	4010.682
3Bn	38	325	288	79%	2487.779
3C	1	365	365	100%	3069.488
4A	91	304	214	59%	2235.25
4B	92	303	212	58%	2167.013
4C	97	296	200	55%	1208.672
5A	105	295	191	52%	1703.043
5B	108	292	185	51%	1584.076
6A	122	287	166	45%	1390.114
6B	129	270	142	39%	1029.372
7A	121	272	152	42%	1174.098

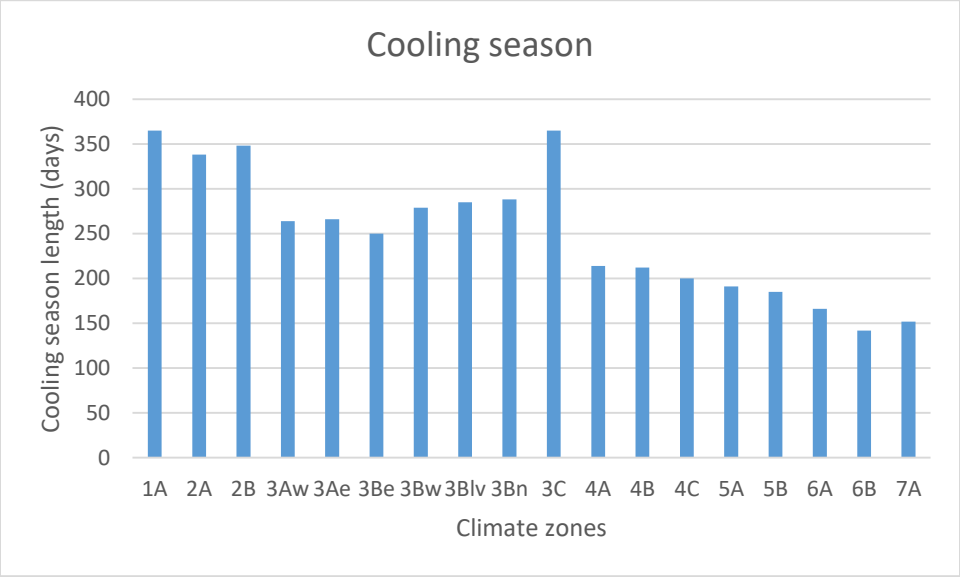

Figure 200 cooling season length varied with different climate zones

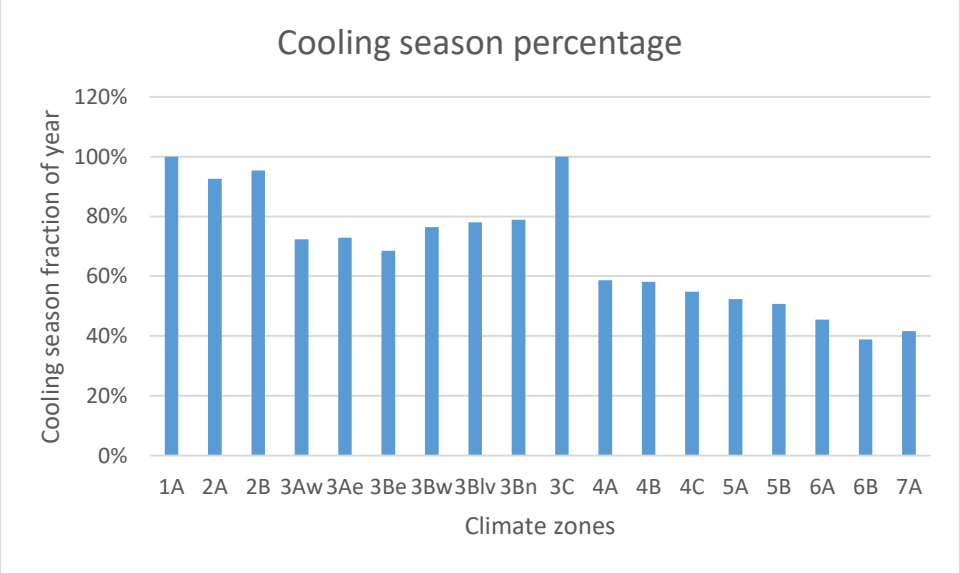

Figure 201 Cooling season length varied with different climate zones

Figure 202 and 203 show the cooling season length varied with total cooling degree-days for all climate zones under base-temperature 10℃ (50°F). It is observed from Figure 202 that, for most cases, the longer the cooling season, the greater cooling degree-days. However, Figure 203 indicates that climate zone 3C is an exception since its daily temperatures are all slightly higher

than the base temperature. However, these daily temperatures are quite stable for the whole year. Even in the summer, the daily temperatures are not that high compared to climate zone 1A, 2A, 2B.

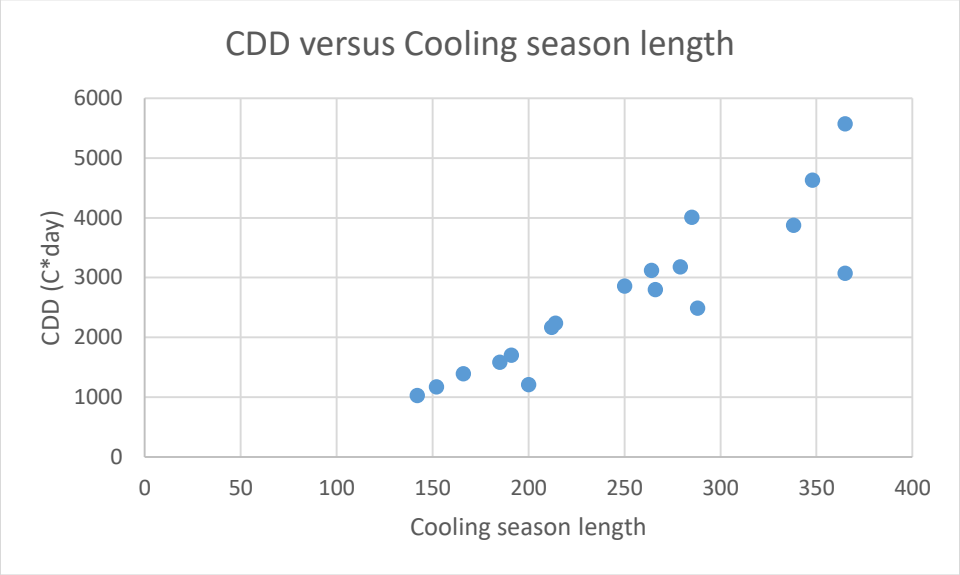

Figure 202 CDD versus cooling season length

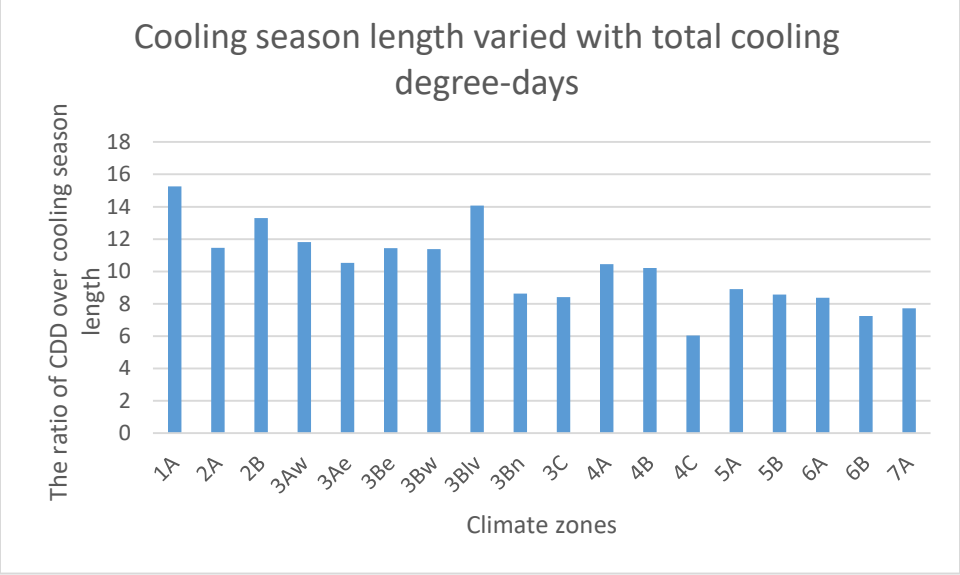

Figure 203 Cooling season length varied with total cooling degree-days for different climate zones

According to the result of section 6.1, a very strong cubic non-linear regression relationship between monthly/daily cooling dry-bulb temperature and month/day for each climate zone is derived. Similarly, it is also assumed that the cubic regression relationship exists between monthly cooling degree-days/weighting factors and month number. Since the raw data is in English unit, the equation derived below is in English units as well----for cooling degree days, use °F · day.

As mentioned previously, if the daily temperatures in one month are all above base temperature, the month is called a full month; if some daily temperatures (one or more) in one month are below the base temperature, the month is called a residual month. The residual month in the early of the year is called lower residual month while in the later of the year is called an upper residual month. To improve the accuracy of the correlation, only full month data is correlated in this study. The residual month data is the actual data of cooling degree-days/weighting factor, which is summarized in Table 39. Of special note, there is no residual month in climate zone 1A and 3C. Only upper residual month exists in climate zone 4A and 7A.

Table 39 Lower and upper residual data

Climate Zone	Month Lower	CDD Lower	WF Lower	Month Upper	CDD Upper	WF Upper
1A						
2A	Jan	31.5	0.0045	Dec	80.8	0.0116
2B	Jan	91.3	0.0110	Dec	72.0	0.0086
3Aw	Feb	0.1	0.0000	Nov	97.1	0.0173
3Ae	Feb	0.4	0.0001	Nov	93.3	0.0185
3Be	March	83.0	0.0161	Nov	64.0	0.0124
3Bw	Feb	28.6	0.0050	Nov	111.9	0.0196
3Blv	Feb	55.6	0.0077	Nov	153.8	0.0213
3Bn	Feb	30.0	0.0067	Nov	108.6	0.0243
3C						
4A				Oct	250.6	0.0623

Table 39 continued

Climate Zone	Month Lower	CDD Lower	WF Lower	Month Upper	CDD Upper	WF Upper
4B	April	174.7	0.0448	Oct	233.8	0.0599
4C	April	47.8	0.0220	Oct	113.3	0.0521
5A	April	49.8	0.0162	Oct	118.5	0.0387
5B	April	29.5	0.0104	Oct	98.6	0.0346
6A	May	223.5	0.0893	Oct	47.6	0.0190
6B	May	93.7	0.0506	Sep	223.2	0.1205
7A				Sep	246.9	0.1168

Cooling degree-days and weighting factors are predicted in the formula shown as follows,

$$\boldsymbol{CDD_{monthly}/WF = a + bx + cx^2 + dx^3} \quad (128)$$

Where x is month number and coefficients of a, b, c and d are all climate zone related. All the results of coefficients are summarized in Table 40.

Table 40 Coefficient of two models

	Cooling degree days				Weighting factor			
	a	b	c	d	a	b	c	d
1A	465.1485	56.09368	13.55867	-1.4371	0.046321	0.005616	0.001351	-0.00014
2A	-219.413	195.0584	11.65909	-2.18411	-0.03139	0.027916	0.001683	-0.00031
2B	-114.851	150.7751	27.03106	-3.24557	-0.01389	0.018144	0.003238	-0.00039
3Aw	-625.052	192.581	35.85476	-4.35	-0.11099	0.034131	0.006409	-0.00078
3Ae	-617.988	217.2295	23.53723	-3.43106	-0.12257	0.043109	0.004662	-0.00068
3Be	-1595.5	654.6018	-33.6987	-1.13989	-0.31013	0.12724	-0.00655	-0.00022
3Bw	-307.171	84.21028	46.29113	-4.62045	-0.05368	0.014698	0.008103	-0.00081
3Blv	-252.819	45.03041	66.07641	-6.10682	-0.03509	0.006256	0.009152	-0.00085
3Bn	-24.8458	-70.4171	58.57836	-4.66178	-0.00555	-0.01573	0.013081	-0.00104

Table 40 continued

	Cooling degree days				Weighting factor			
	a	b	c	d	a	b	c	d
3C	192.6764	-30.8192	30.70797	-2.36368	0.034873	-0.00558	0.005558	-0.00043
4A	-1096.21	191.9037	57.22817	-6.35648	-0.27279	0.047849	0.014201	-0.00158
4B	-203.389	-163.167	103.3643	-8.38333	-0.05524	-0.04053	0.026325	-0.00214
4C	1213.006	-822.167	178.9321	-10.8583	0.560694	-0.3793	0.082443	-0.005
5A	-560.289	-123.95	105.4143	-8.75	-0.1841	-0.03985	0.0343	-0.00285
5B	248.9246	-539.103	168.6234	-11.7672	0.087301	-0.18907	0.059138	-0.00413
6A	-5461	1809.5	-147	2	-2.1902	0.726233	-0.05915	0.000817
6B	-5706.36	1704.001	-114.96	0	-3.07974	0.919655	-0.06204	0
7A	1439.4	-1273.67	303.25	-19.6833	0.6853	-0.60482	0.14385	-0.00933

Figure 204---217 show the predicted monthly cooling degree-days and weighting factors for all 18 climate zones during the cooling season under base temperature 10℃ (50℉). Specifically, the author chooses climate zone 3Aw to represent 3A, 3Be to represent 3B. These figures indicate that July and August always have the largest cooling degree-days and weighting factors. These figures also illustrate that the trends of these cooling degree-days/weighting factors varied with month are extremely similar to that of monthly dry-bulb temperatures versus month.

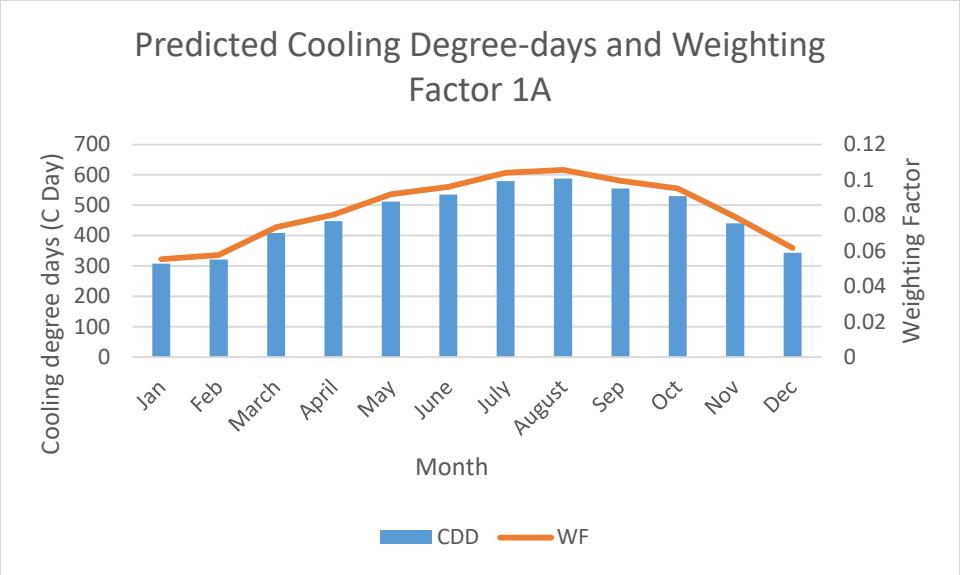

Figure 204 Monthly cooling degree-days and weighting factors versus month for climate zone 1A

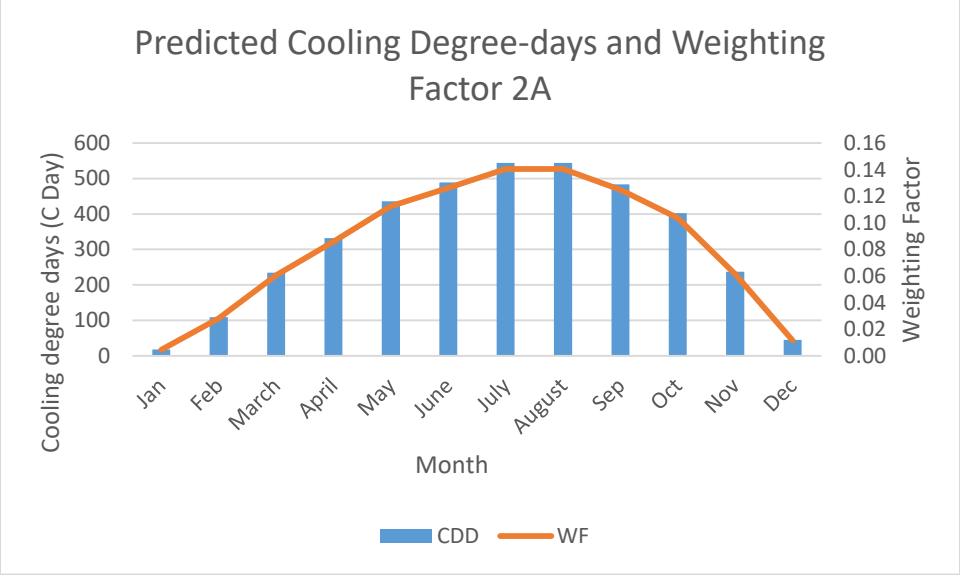

Figure 205 Monthly cooling degree-days and weighting factors versus month for climate zone 2A

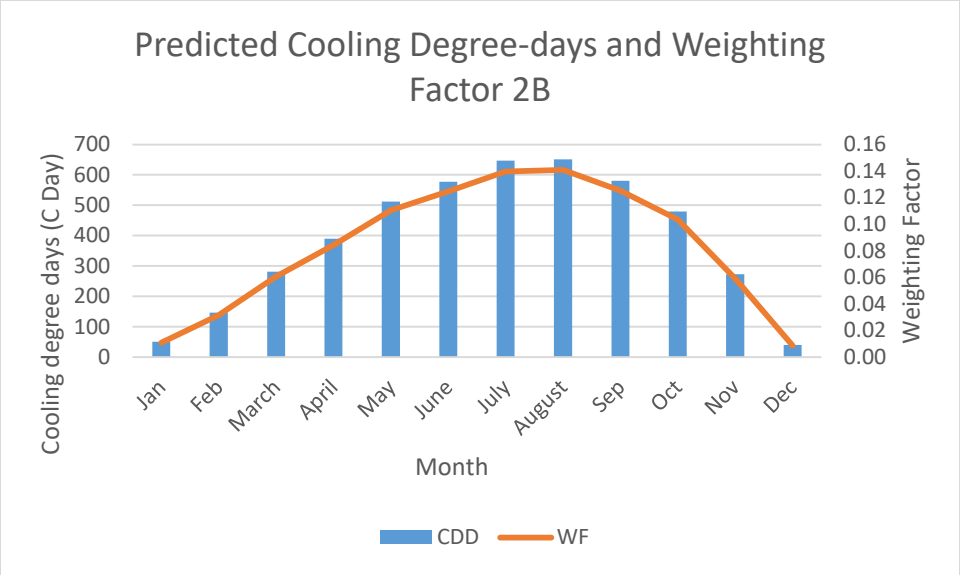

Figure 206 Monthly cooling degree-days and weighting factors versus month for climate zone 2B

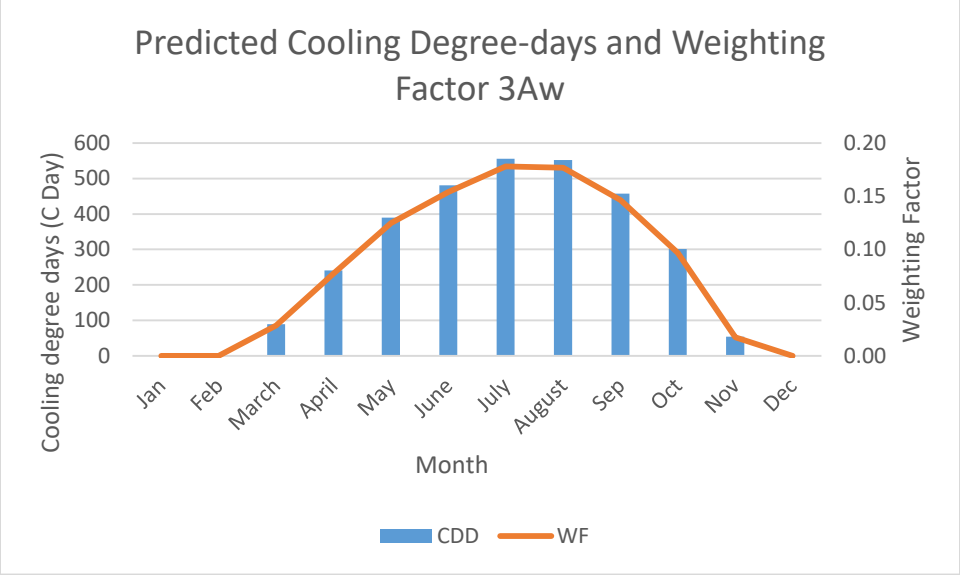

Figure 207 Monthly cooling degree-days and weighting factors versus month for climate zone 3Aw

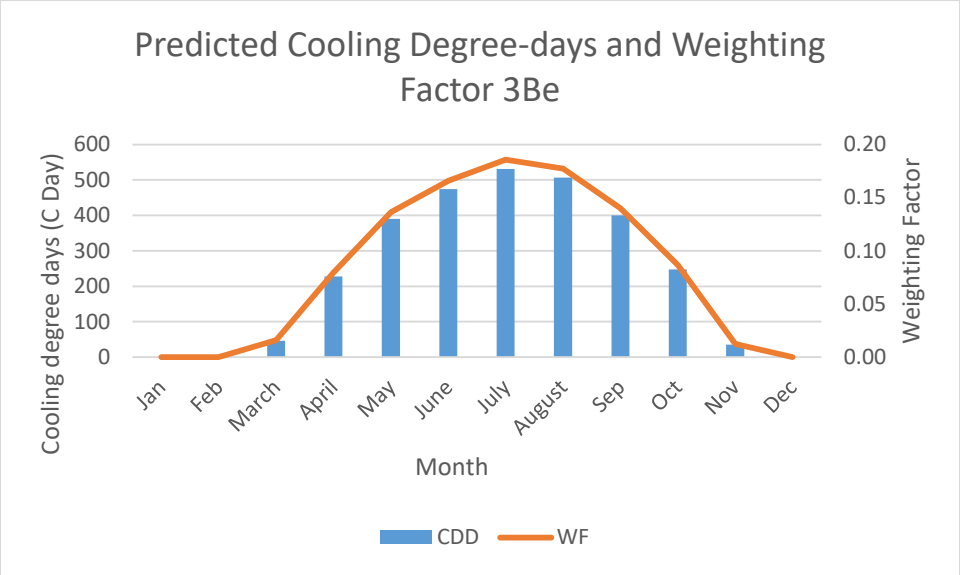

Figure 208 Monthly cooling degree-days and weighting factors versus month for climate zone 3Be

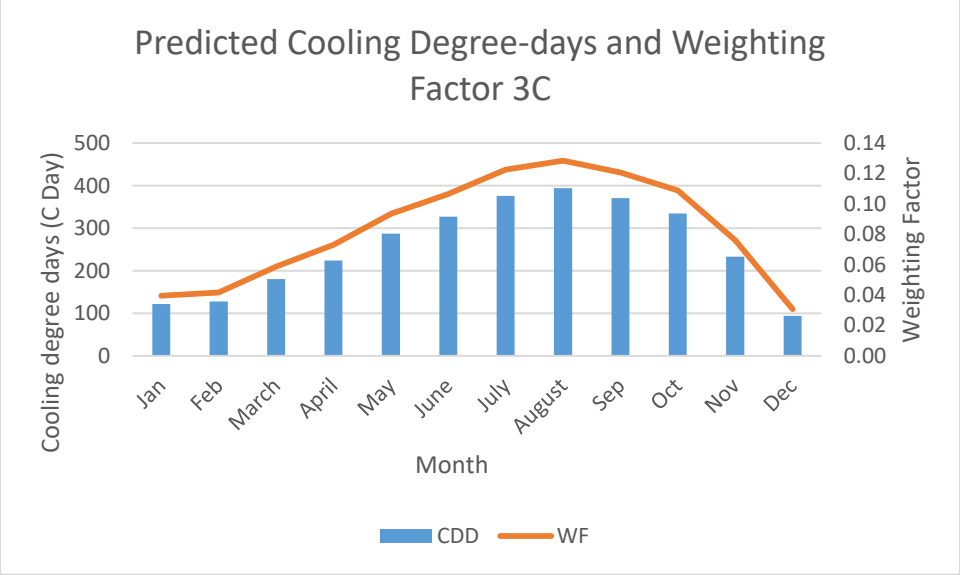

Figure 209 Monthly cooling degree-days and weighting factors versus month for climate zone 3C

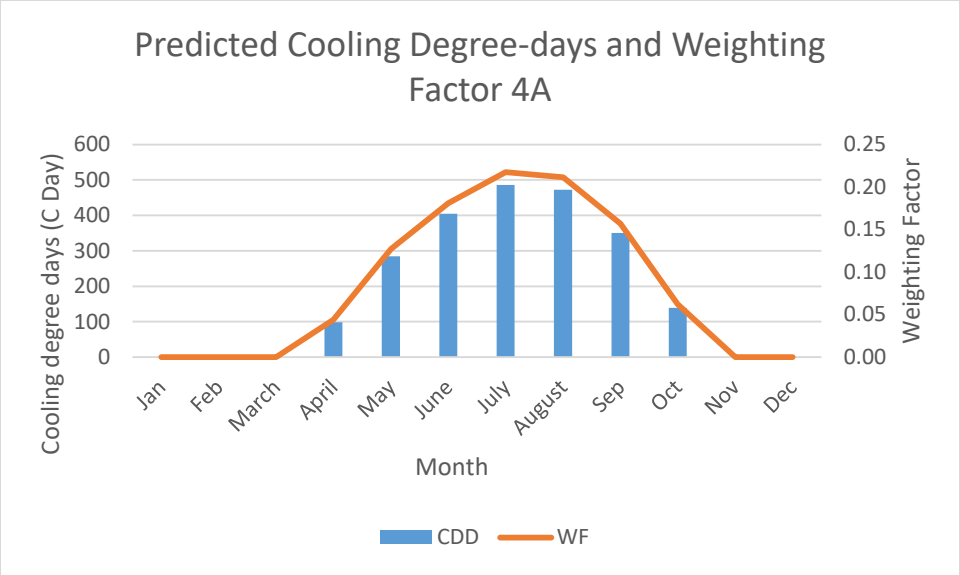

Figure 210 Monthly cooling degree-days and weighting factors versus month for climate zone 4A

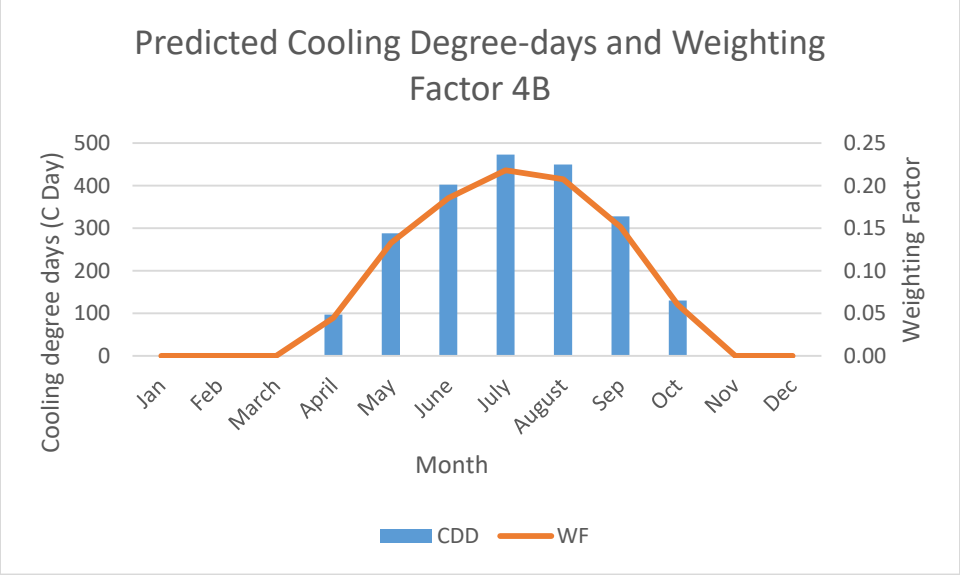

Figure 211 Monthly cooling degree-days and weighting factors versus month for climate zone 4B

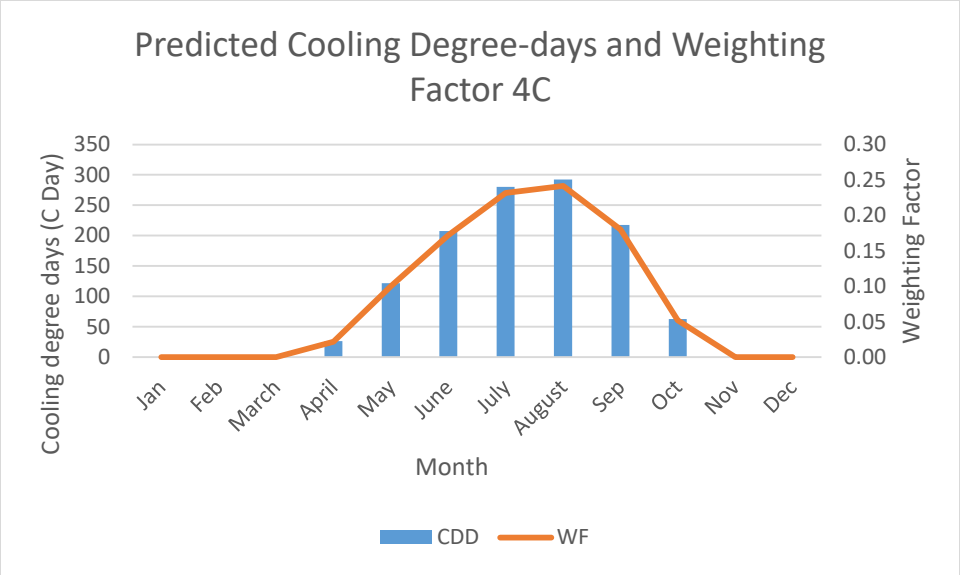

Figure 212 Monthly cooling degree-days and weighting factors versus month for climate zone 4C

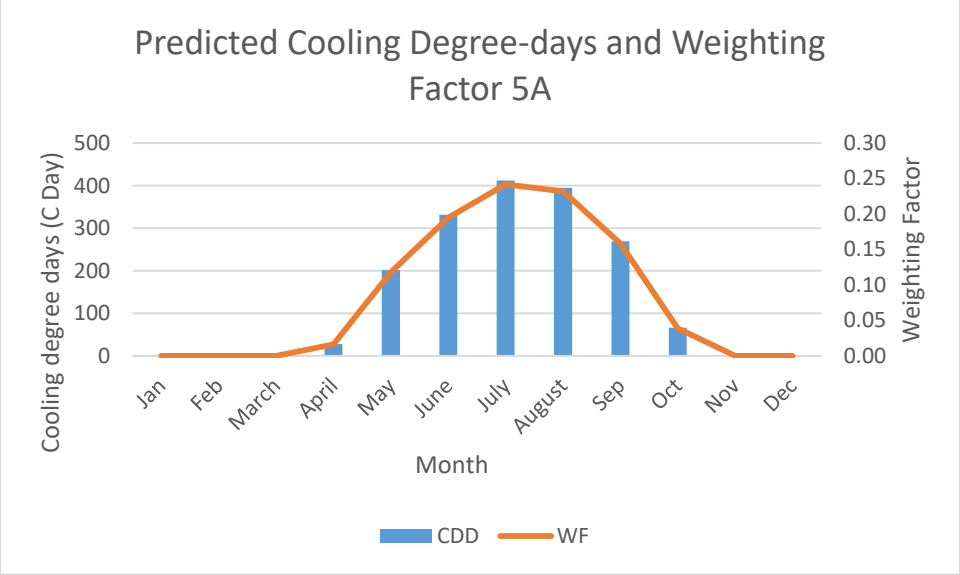

Figure 213 Monthly cooling degree-days and weighting factors versus month for climate zone 5A

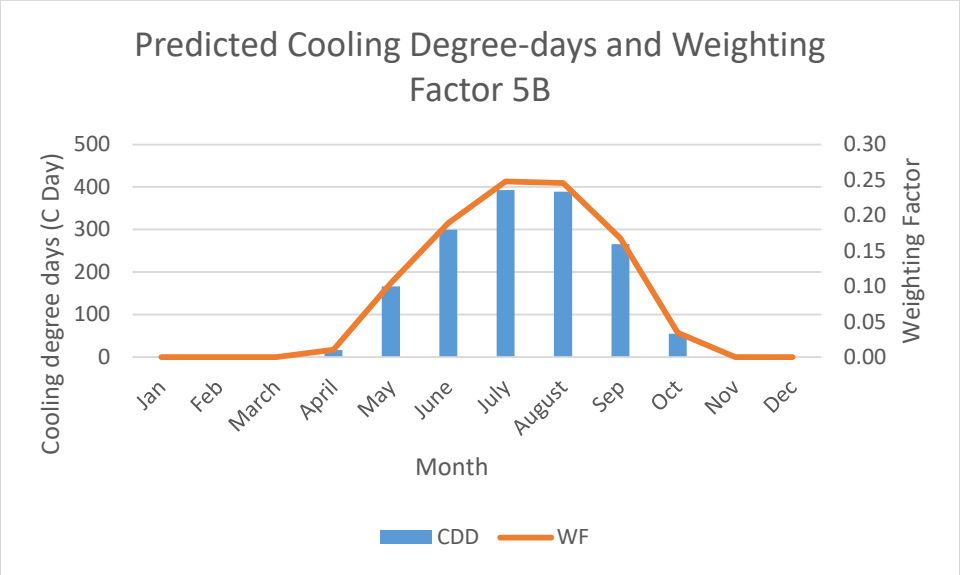

Figure 214 Monthly cooling degree-days and weighting factors versus month for climate zone 5B

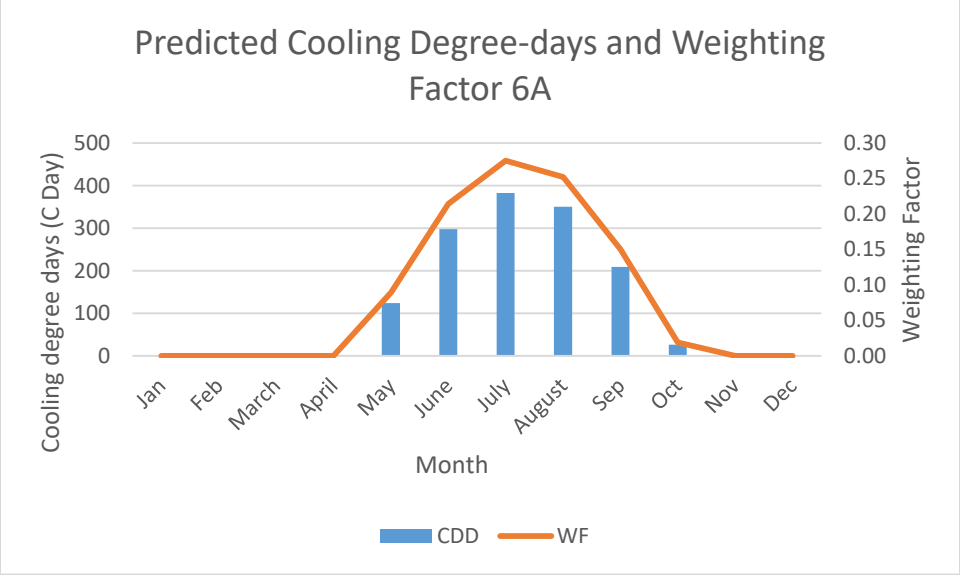

Figure 215 Monthly cooling degree-days and weighting factors versus month for climate zone 6A

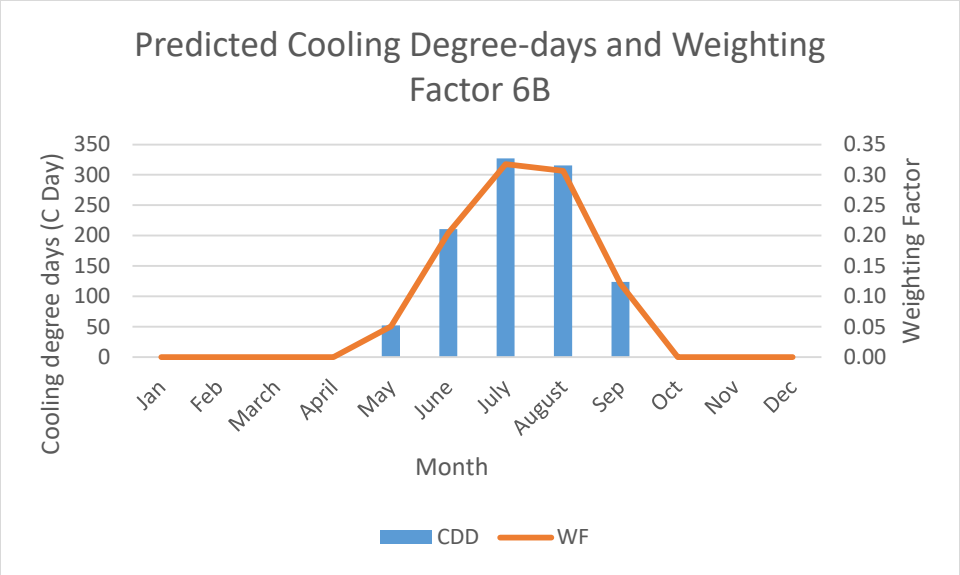

Figure 216 Monthly cooling degree-days and weighting factors versus month for climate zone 6B

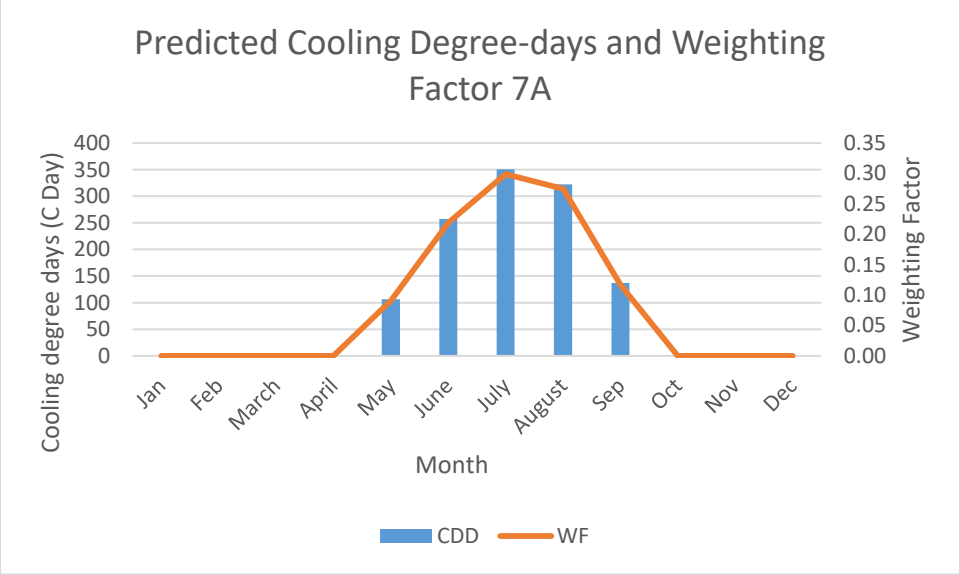

Figure 217 Monthly cooling degree-days and weighting factors versus month for climate zone 7A

Figure 218 and Figure 219 show the predicted data versus actual data for cooling degree-day and weighting factor, respectively. These two figures indicate that all the data is quite near the diagonal line, which further proves the cubic regression equation utilized in this section fits the

data quite well. Percentage error is defined as $\frac{predicted-actual}{actual}$ in this section. Figure 220 and 221 show the percentage error of cooling degree-days and weighing factors, respectively. These two plots all indicate that the percentage errors are mostly within 4%. The residual defined in this section remains the same as section 6.1, namely the difference between actual data and predicted data. Figure 222 shows the cooling degree-day residual for all 18 climate zones. Climate zone 5A, 5B, 6A, 6B and 7A data are the most accurate zones since the cooling season lasts quite short for these zones.

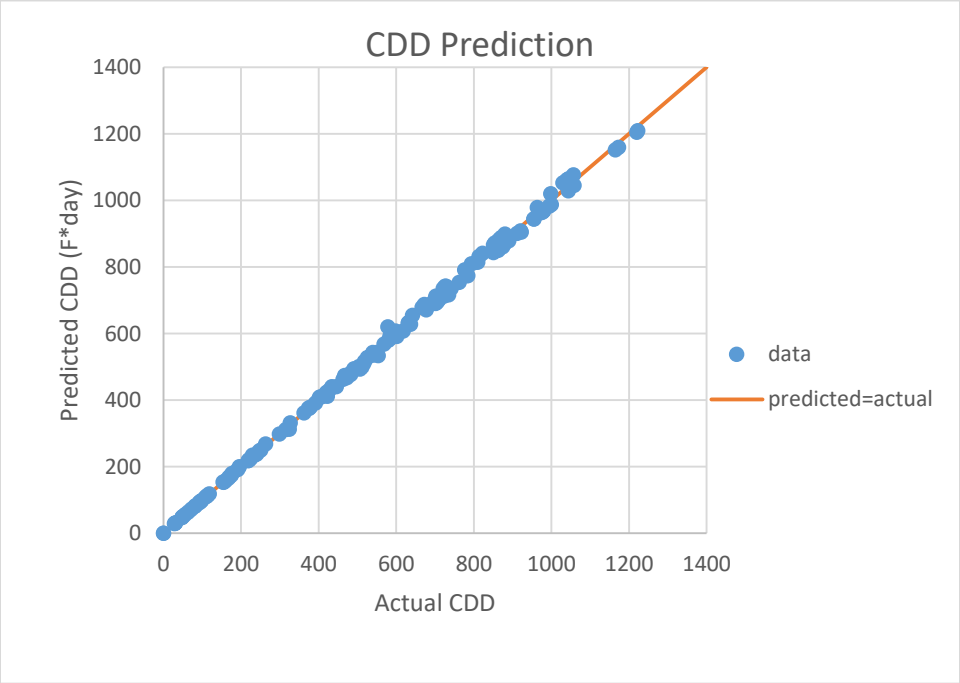

Figure 218 Predicted data versus actual data for cooling degree-days

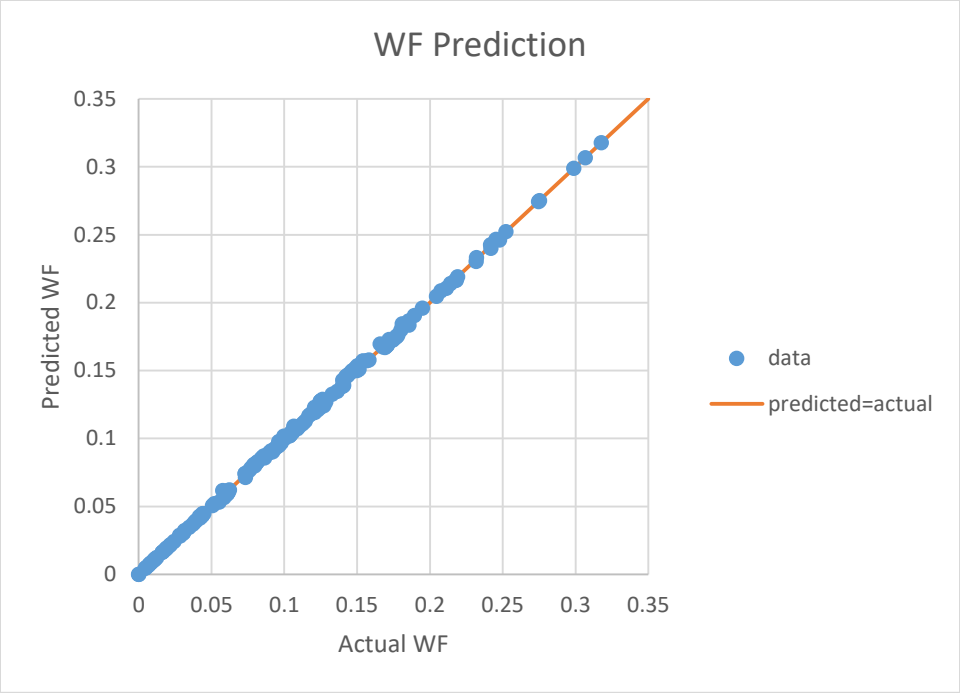

Figure 219 Predicted data versus actual data for weighting factors

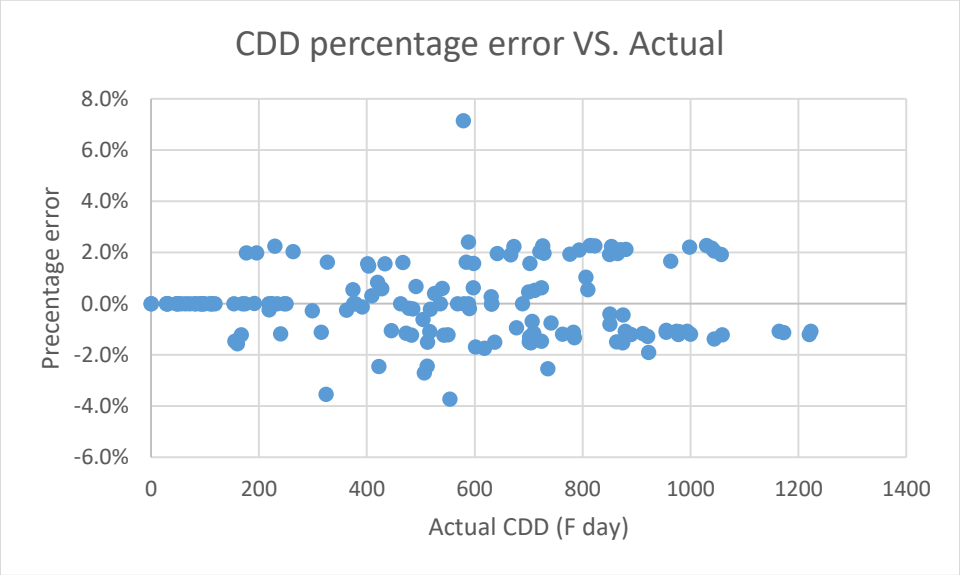

Figure 220 Percentage error for cooling degree-days

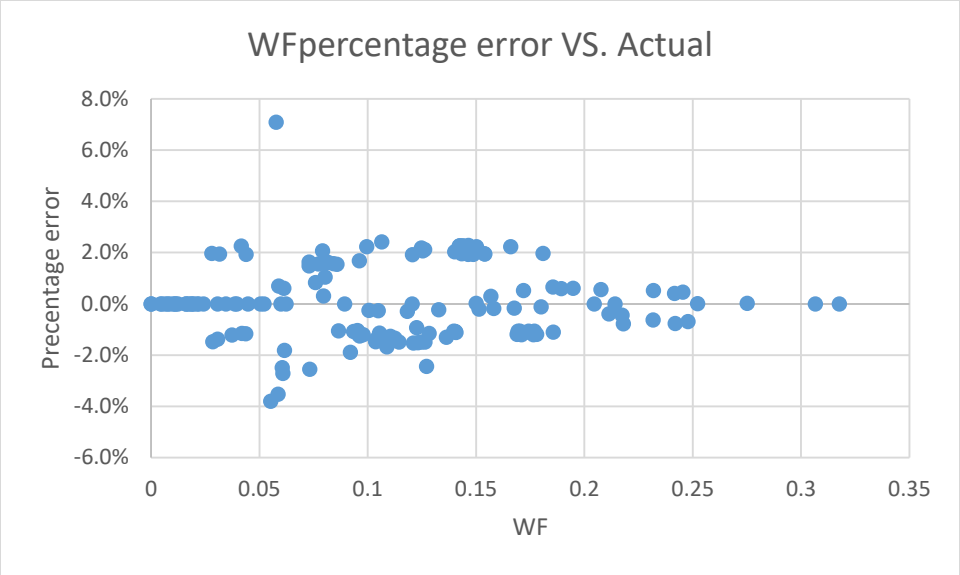

Figure 221 Percentage error for weighting factors

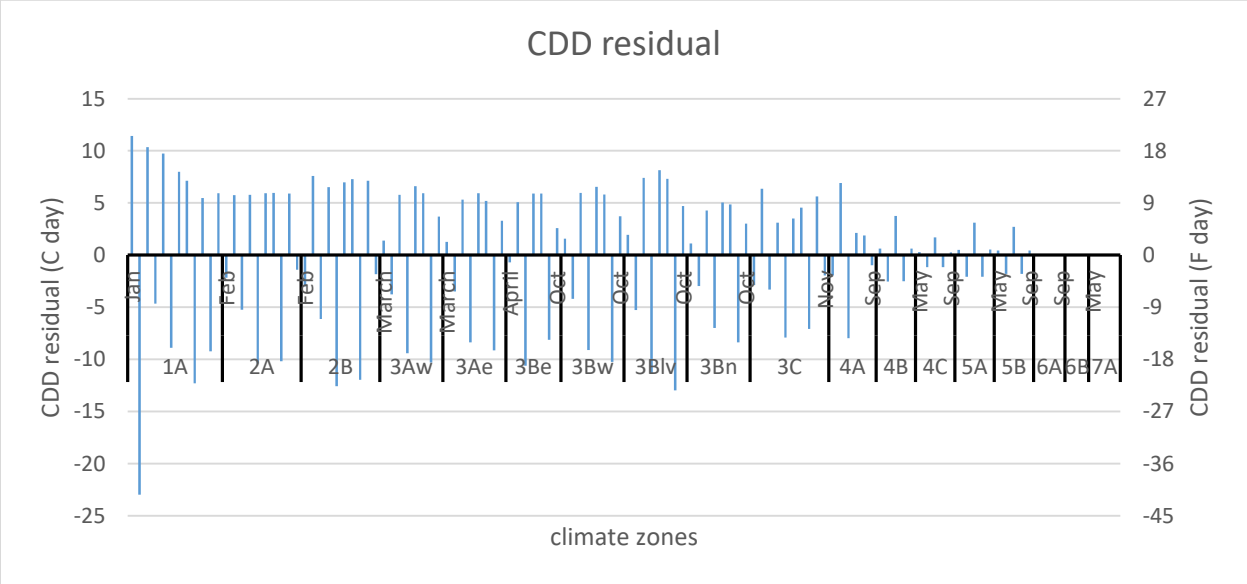

Figure 222 Cooling degree-days residual for all 18 climate zones

6.3 Cooling Building Energy COP Evaluation: A simplified Model

The energy consumption associated with space cooling accounts for a significant proportion of building electricity use and space cooling also plays a major role in determining the magnitude of electricity demand. Thus predicting the energy consumption/efficiency in buildings

has become one of the primary topics for most countries. In this context, the present paper proposes a simple vapor-compression system model to simulate the system COP. This simplified vapor-compression system COP is correlated to outdoor dry-bulb temperature only, which is also the baseline system COP. The weighting factor has been widely used for predicting the total COP of a conventional vapor-compression system during the cooling season. The weighting factors correlated with the time of year for each climate zone (totally 18) across the U.S. have been derived in section 6.2. The total COP during the cooling season is calibrated by using the monthly COP and weighting factor, and it is the focus of this section.

6.3.1 Introduction and Literature

Energy consumption of buildings has become a relevant international issue, and different policy measures for energy saving are under discussion in many countries. The relationship between climate and energy is a hot issue which the world's governments and scholars focused on. The prediction of energy use in buildings is therefore significant to improve the energy performance with the aim of achieving every conservation and reducing environmental impact. Since the energy performance in buildings is influenced by many factors, such as ambient weather conditions, building constructions and characteristics, the operation of sub-level components like lighting and occupancy. Due to the complexity of the problem, precise energy efficiency predictions is quite difficult. This section is only focused on a simplified vapor-compression model, and the coefficient of performance is outdoor air dry-bulb temperature related only.

Two basic methods are used to predict building energy consumption and efficiency, namely, engineering method and statistical method. Engineering method includes mechanical/architecture engineering calculations as principles for building energy consumption, and this software includes DOE-2 and Energy Plus. On the other hand, statistical methods have also been developed to predict

building energy consumption/efficiency that uses correlations among influencing variable such as weather data. Correlations are typically determined using a linear/non-linear regression model that represents the relationship between the building's energy consumption/efficiency and corresponding weather data. (Outdoor dry-bulb temperature, cooling degree-days and weighting factor) The statistical method is the focus of this study.

Energy consumption/efficiency in buildings has been increasing globally, and the increase in building energy efficiency has become one of the primary topics of interest for most developed/developing countries. Cooling degree days are the summation of temperature differences between the outside air and a reference base temperature over time, which could be applied to estimate building energy consumption or to monitor the energy performance of existing buildings.

Gorazd Krese [100] once analyzed real electric energy consumption data using the cooling degree method which neglects the influence of latent cooling loads and the improved wet-bulb cooling degree method considering latent loads simultaneously. The result showed that the improved wet-bulb cooling degree approach performed better on the metered data.

Minjae Shin [101] investigated the prediction of cooling energy use in buildings using an enthalpy-based cooling degree days method in a hot and humid climate. By proposing an enthalpy-based CDD method, latent heat and sensible heat are taking into account simultaneously. The new method is compared to the traditional cooling degree method by examining two institutional buildings, and the result showed that the enthalpy-based CDD method resulted in a percent error of approximately 2% less than that of the temperature-based CDD method.

K. Papakostas [102] researched the impact of the ambient temperature rise on the energy consumption for cooling in residential buildings of Greece. Two main cities, namely Athens and

Thessaloniki are chosen from 1983 to 2002. The decade average (1983-1992 and 1993-2002) values of cooling degree days of the two cities are compared, for various base temperatures (20-28℃). The author concluded that the average cooling degree days from period 1983-1992 and 1993-2002 of Athens are increasing from 25% to 69% while 10% to 21% for Thessaloniki. The result showed an increase in the cooling energy demand by 26% and 10% for Athens and Thessaloniki respectively.

L.M. Al-Hadhrami [103] presented the annual and seasonal cooling degree day values over Saudi Arabia by utilizing the long-term daily average temperatures from 38 meteorological stations based on a reference temperature of 18.3℃. The values of CDD in that paper could be used to estimate the fuel or energy required for cooling or heating of buildings in respective areas. Imre Csaky [104] did a similar study of analyzing cooling degree day variation in the last five years in Debrecen.

Yan Cheng-wen [105] investigated a fast and effective method for predicting building energy consumption at different climate zones by using the artificial neural network with 20 input parameters, including 18 building envelope performance parameters, heating degree day and cooling degree day. The study proved that the method prediction rate is over 96%.

Mattia De Rosa [106] simulated heating and cooling building energy demand by a simplified model and a modified degree days approach. The model consists of several transient energy balance equations for external walls and internal air according to a lumped-capacitance approach, and it has been implemented utilizing the Matlab. The energy consumption for cooling is analyzed in different locations, showing that for low degree days the inertia effect assumes paramount importance, affecting the common linear behavior of the building consumption against the standard degree days. Also, in this situation, other factors such as solar irradiation have an

important role. Considering these effects, a correction to CDD is proposed, demonstrating that by taking into account all the contributions the linear relationship between energy consumption and degree days is maintained.

Peng Xu [107] utilized archived General Circulation Model (GCM) projections and statistically downscaled these data to the site scale for use in building cooling and heating simulations. Building energy usage was projected out to the years of 2040, 2070 and 2100. This study found that under the condition that the cooling technology stays at the same level in the future, electricity use for cooling will increase by 50% over the next 100 years in certain areas of California under the IPCC (Intergovernmental Panel on Climate Change)'s worst-case carbon emission scenario. Under the IPCC's most likely carbon emission scenario, cooling electricity usage will increase by about 25%.

6.3.2 Methodology

6.3.2.1 A Simplified Model

A simplified vapor-compression model is set as model A (baseline system), which is mentioned previously. However, slightly changes are made to the simulation assumptions and all the other processes are the same as the baseline system:

- Isentropic efficiency of the compressor is 70%
- Pressure drops in the condenser and evaporator are neglected.
- Kinetic and potential energy changes in all cycle processes are neglected.
- Both the evaporator and condenser HXs are insulated from heat losses and gains to/from the surroundings.
- Refrigerant evaporating temperature is 35°F (T1), so enthalpy of state 1 (saturated vapor) is known

- Assume the outdoor air temperature is 40, 50, 60, 70, 80, 90, 100 °F
- Refrigerant condensing temperature is always 30 °F higher than that of outdoor air temperature, so condensing pressure and enthalpy of state 3 (saturated liquid) are known

A result of how a simplified vapor-compression system performance related to outdoor dry-bulb temperature is shown in Table 41. When outdoor air temperature increase from 40 to 100°F, the coefficient of system performance is decreasing from 8.7 to 2.3. It is observed that COP is a function of outdoor dry-bulb temperature---COP=f (Tout).

Table 41 COP and outdoor temperature

T out	COP
40	8.673
50	6.502
60	5.104
70	4.12
80	3.383
90	2.801
100	2.32

According to the result of table 41, a cubic regression function fits quite well for COP and outdoor air temperature, which is shown as follows,

$$\boldsymbol{COP = a + bz + cz^2 + dz^3} \quad (129)$$

Where z is outdoor air temperature in °F, the coefficients of the model are further developed ---a=26.326238, b= -0.679772, c=0.0069813, d=-2.586e-5. Figure 233 shows the relationship between COP and outdoor air temperature and it indicates that the cubic regression curve fits quite well.

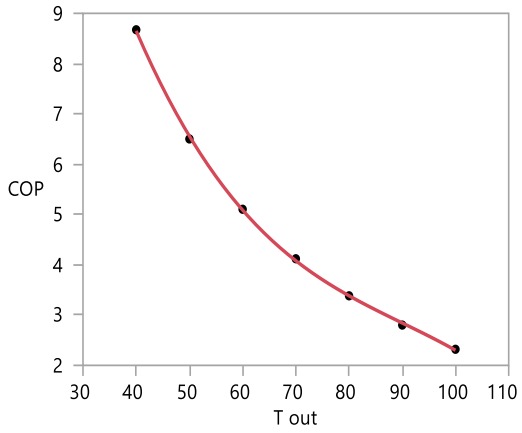

Figure 223 COP varied with outdoor air temperature

6.3.2.2 Weighted COP during Cooling Season

According to section 6.2, the weighting factor for each climate zone (totally 18) in the U.S. is a function of time of year. The correlation is directly used in this study. The weighted COP is defined as the summation of the product of monthly COP and weighting factor during the cooling season, which is shown as follows,

$$COP_{weighted} = \sum_{starting}^{ending} COP_{monthly} * \text{WF} \quad (130)$$

Where monthly COP is calculated by the simplified correlation derived in the previous section, and it is only related to the outdoor dry-bulb temperature. The outdoor dry-bulb temperature for each climate zone is from the correlated data in section 6.1 and the weighting factor is from the correlated data in section 6.2.

7. 100% OUTDOOR AIR FOR THE CONDENSER BUT 100% INDOOR AIR FOR THE EVAPORATOR

For all of the previous discussions, it is assumed that the outdoor air is both the heat source and heat sink, meaning that energy is removed in the vapor- compression system evaporator from the outdoor air as the air is dehumidified and cooled and then this energy plus compressor work is rejected from the condenser to the same outdoor air. This simplification is useful because since only one set of the conditions, namely the environment, is assumed for the theoretical analysis and system performance evaluation, rather than two sets, which would also include a return air condition entering the evaporator.

However in addition to the above, another simulation is used for the evaporative cooling case: namely use 100% outdoor air for the condenser, but also 100% indoor air for the evaporator. This case considers only external water, namely reconfigured system A1 since being that with the reason for this quite limited internal condensate results for this simulation, and for many cases no condensate occurs in the evaporator. Therefore, the author will not repeat these conditions for internal evaporative cooling, namely reconfigured system A2.

7.1 System Conditions and Assumptions

Unlike utilizing the outdoor air source for both the evaporator and condenser, outdoor air dry-bulb temperatures and relative humidities for this case study can both have a wider range (considering a Second Law limitation). For the case of a 100% indoor condition, indoor air conditions are set as: 23.9℃ (75℉), RH=50%, outdoor conditions are set as: 26.7, 32.2, 37.8, 43.3℃ (80, 90, 100, 110℉) with RH=40%, 50%, 60% 70%, 80%, 90%; Taeo=4.4, 10℃(40, 50℉); compressor efficiency: 80%. Three objectives are further studied, how outdoor air conditions

(namely the dry-bulb temperature and relative humidity) influence reference COP (dry condition), evaporative cooling COP and COP improvement with evaporative cooling.

The assumptions that follow are the same as those used for the study of outdoor air supply both the evaporator and condenser:

1. The isentropic efficiency of the compressor is 80%

2. Pressure drops in the condenser and evaporator are neglected.

3. The kinetic and potential energy changes in all cycle processes are neglected.

4. Both the evaporator and condenser are insulated from heat losses and gains to/from the surroundings.

5. The refrigerant condensing temperature is 30 °F higher than condenser inlet air temperature.

6. The evaporating temperature is 10 °F lower than the supply air temperature, which is the same as the evaporator outlet air temperature.

7.2 Results and Discussion

7.2.1 Baseline System (without evaporative cooling)

For the case without evaporative cooling along with the assumptions listed previsouly, the COP is just a function related to the outdoor dry-bulb temperature and the supply air temperature (Taeo) and remains the same with varied outdoor relative humidity. Figures 224 and 225 show how the baseline COP varies with different outdoor air conditions (dry-bulb temperature and relative humidity) and supply air temperatures. It can be observed that with increasing outdoor temperature, the COP is decreasing significantly in both figures. By comparing Figure 224 with Figure 225, increasing the supply air temperature (Taeo) from 4.44℃ to 10℃ results in the COP increasing as well, namely the COP range from 2---3.7 at the lower temperature and then increased

to 2.2—4.2 at the higher temperature. The trends of the baseline COP as it relates to the three aforementioned variables is summarized in Table 42.

Table 42 Baseline COP varied with Tout, RH and Taeo

case	T_{out}	RH	T_{aeo}	COP without EC
1	↑	→	→	↓
2	→	↑	→	→
3	→	→	↑	↑

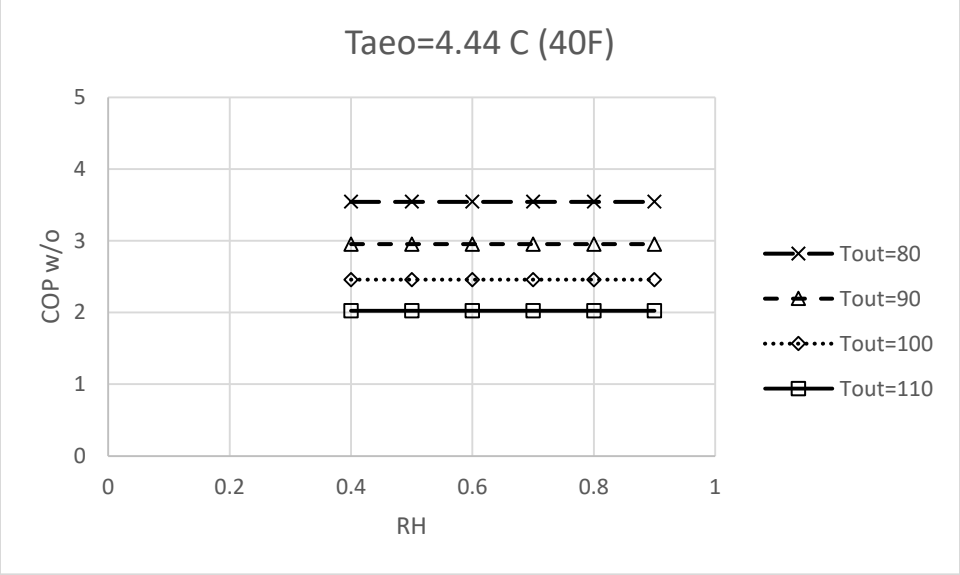

Figure 224 Baseline system varied with different outdoor air temperature and relative humidity when Taeo=4.4 ℃

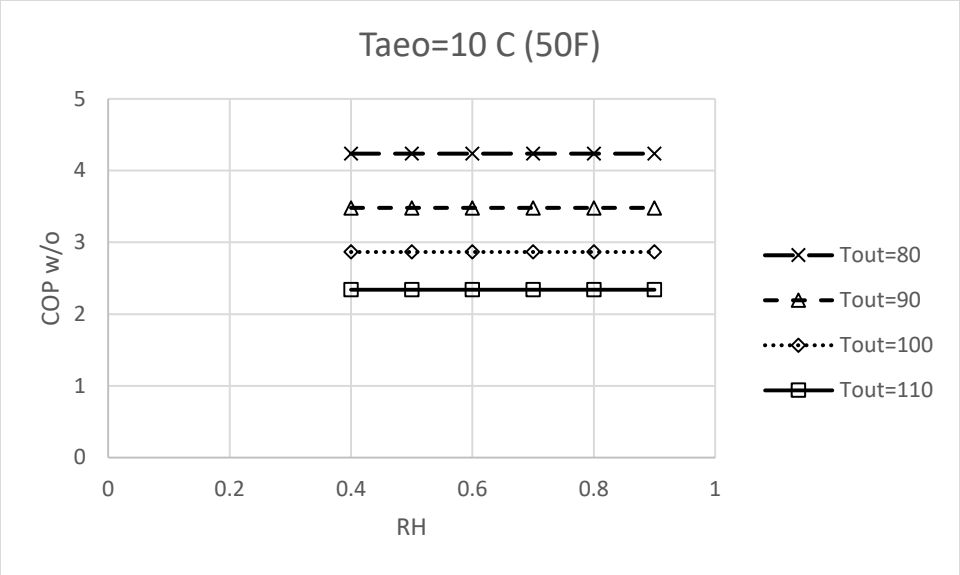

Figure 225 Baseline system varied with different outdoor air temperature and relative humidity when Taeo=10 ℃

7.2.2 Reconfigured System A1

The COP results for the external evaporative cooling at the condenser inlet, namely system A1, are shown in Figures 226 and 227. It can be observed that COP decreases with relative humidity, since with the boosting of relative humidity, the evaporative cooling effect is decreasing, which was discussed in the previous sections (5.1). These two figures also indicate that COP increases with the boosting of the evaporator air outlet temperature, Taeo and then decreases with increasing outdoor air temperatures. All of these trends are similar to those observed and discussed earlier in section 5.1 (the case used outdoor air for both the evaporator and condenser), as summarized in Table 43.

Table 43 COP with external evaporative cooling varied with Tout, RH and Taeo

case	T_{out}	RH	T_{aeo}	COP with EC
1	↑	→	→	↓
2	→	↑	→	↓
3	→	→	↑	↑

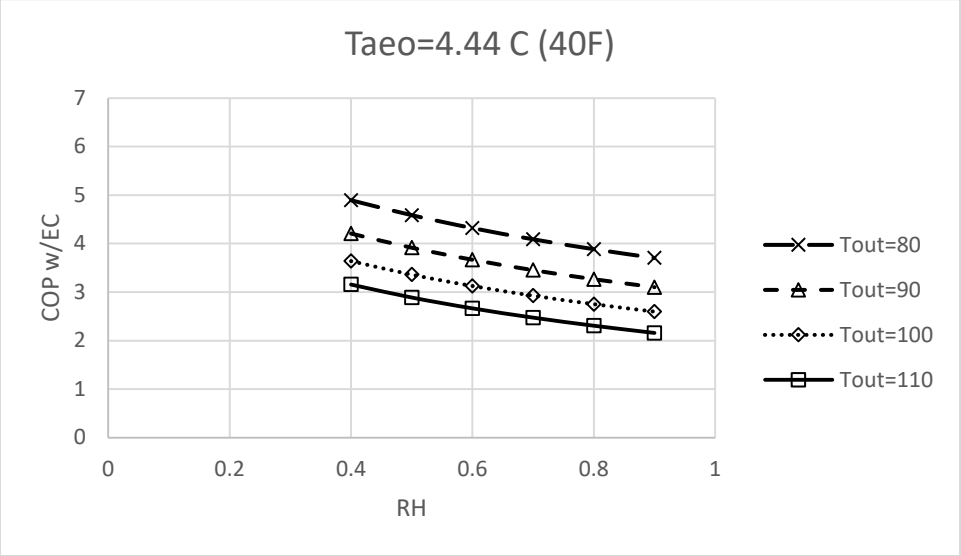

Figure 226 COP with external evaporative cooling varied with RH and Tout when Taeo=4.4℃

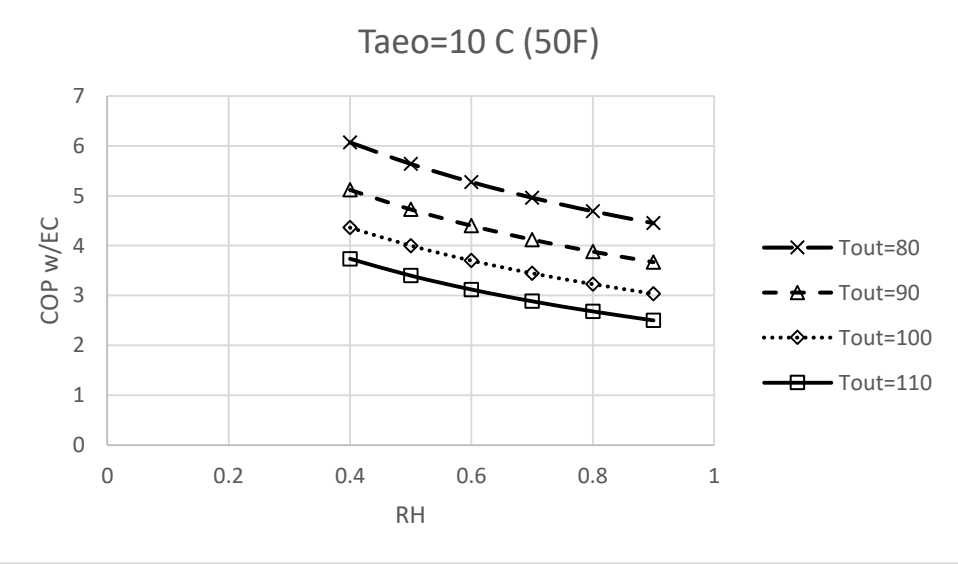

Figure 227 COP with external evaporative cooling varied with RH and Tout when Taeo=10℃

7.2.3 Comparison of Baseline System and Reconfigured System A1

According to Figures 228 and 229, the COP improvements decrease with increasing relative humidity. Also COP improvement increases with increasing outdoor air temperatures, however, at a high relative humidity (80%), COP improvements are quite similar for different outdoor air temperatures. By comparing Figures 228 and 229, it can be seen that the system performance increases with increasing Taeo--- from 4.44℃ to 10℃. The greatest improvement for a Taeo 4.4 to 10 ℃ can be up to almost 60% at the extreme condition of 110℉ outdoor air temperature and 40% relative humidity. The COP trends for the three variables, namely outdoor air conditions (dry-bulb temperatures and relative humidity), and supply air temperature (Taeo), are similar to the case of using outdoor air for both the evaporator and condenser, and they are summarized in Table 44. A final observation is that evaporative cooling using external water is better for the hot and dry regions with higher supply air temperatures (Taeo).

Table 44 COP improvement with external evaporative cooling varied with Tout, RH and Taeo

case	T_{out}	RH	T_{aeo}	% difference
1	↑	→	→	↑
2	→	↑	→	↓
3	→	→	↑	↑

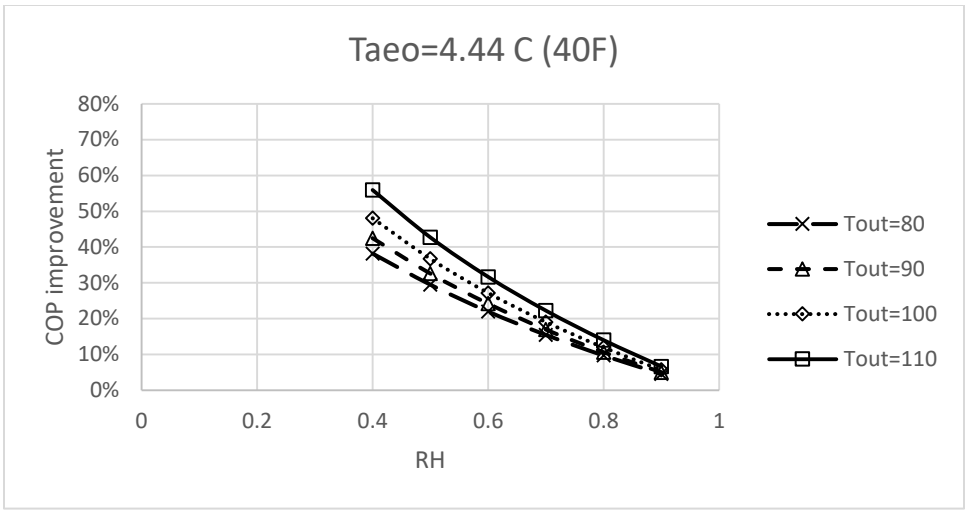

Figure 228 COP improvement under different outdoor air temperatures and relative humidity when Taeo=4.4 ℃

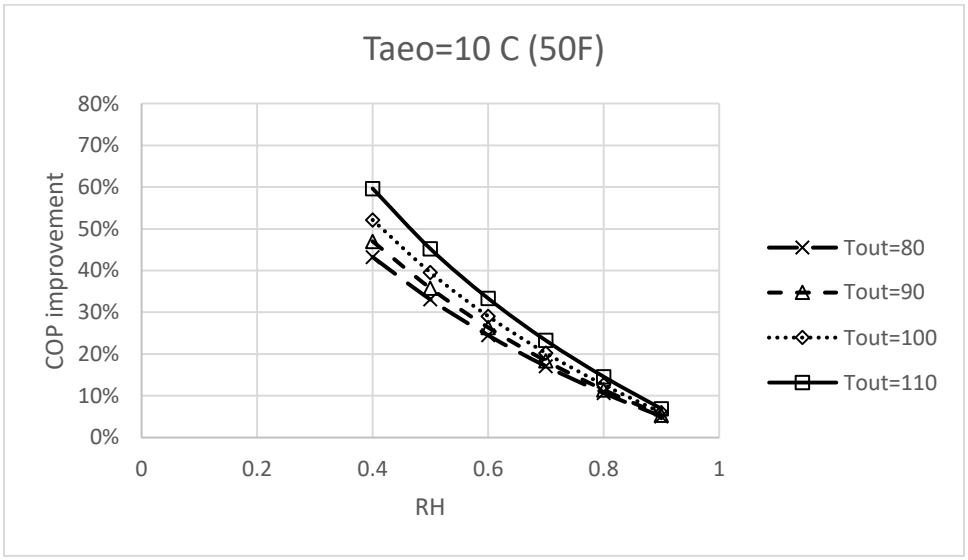

Figure 229 COP improvement under different outdoor air temperatures and relative humidity when Taeo=10 ℃

8. SYSTEM PERFORMANCE IMPROVEMENT COMPARISONS (RECONFIGURED SYSTEM A, B, C AND D)

8.1 Improvement Analysis among Four Reconfigured System Based on the Specified Conditions

Based on upper and lower limits of the cooling season weather report, the conditions below were obtained and used as imput simulation data. These input conditions are outdoor air temperatures of 26.7, 29.4, 32.2, 35 ℃ (80, 85, 90, 95℉) and relative humidities of 40%, 50%, 60%, 70%, 80% over a range of assumed evaporator exit air temperatures of 7.2, 10, 12.8℃ (45, 50, 55℉) with a typical compressor efficiency of 80%. The conditions above have a wider range compared to the real-world conditions in weather reports, meaning the simulation study will cover all geographical cooling seasons that would possibly be encountered. For reconfigured system B (HRV and ERV), the indoor air condition (exhaust air) is set the typical indoor conditions of 23.9℃ (75℉) and RH=50%, along with an HRV or ERV effectiveness of 60%. For reconfigured system C and D, the heat exchanger effectivenesses are set up as 0, 20%, 50%, 80%, and 100%.

Figure 230 presents an overview of COP improvements for Reconfigured systems A—D compared to the baseline system. The performance of reconfigured system B (ERV) is obviously the highest, followed by the reconfigured system A1 (internal evaporative cooling). Reconfigured system A2 (internal evaporative cooling) and B (HVR) performance improvement are similar to each other, but higher than reconfigured system D (internal heat exchanger). For reconfigured system C, improvements are limited, with the resulting COPs being close to the baseline system.

The baseline system COP performance under all conditions ranges from 2.8 to 4.8, and the COP of reconfigured system A1 is way higher than the baseline, ranging from 3.2 to 7, which can be observed in Figure 231. Under all conditions, the benefit from reconfigured system A1 (external

evaporative cooling) is always higher than that of reconfigured system A2 (internal evaporative cooling), which may or may not be the case if the cost of external water is factored in. Reconfigured system B2 (ERV) COPs under all conditions range from 4 to 8 and are higher than B1 (HRV) with the values ranging from 3 to 5.5, which is can be seen in Figure 232. Since energy recovery is the summation of heat recovery and moisture recovery, this difference in ERV and HRV performance further proves that latent heat recover can be a large portion of the total energy recovery. Figure 233 illustrates that reconfigured system C (utilizes condensate water to cool refrigerant exiting the condenser) has almost no improvements compared to the baseline system, being always less than 5%, which further shows that the evaporator condensate water is limited with regards to affecting heat transfer between the refrigerant and condensate water, meaning there is negligible subcooling effect on the condenser exit refrigerant. Reconfigured system D (internal heat exchanger) has obvious improvement, though not as high as Reconfigured system A1 (external evaporative cooling) and B2 (ERV). The improvement increases as the internal heat exchanger effectiveness increases. Figure 234 indicates that the highest COP (when the internal heat exchanger effectiveness is 100%) can reach 3.8 to 5.5, roughly as much as a 50% improvement, compared to the baseline system that ranges from 2.8 to 4.8.

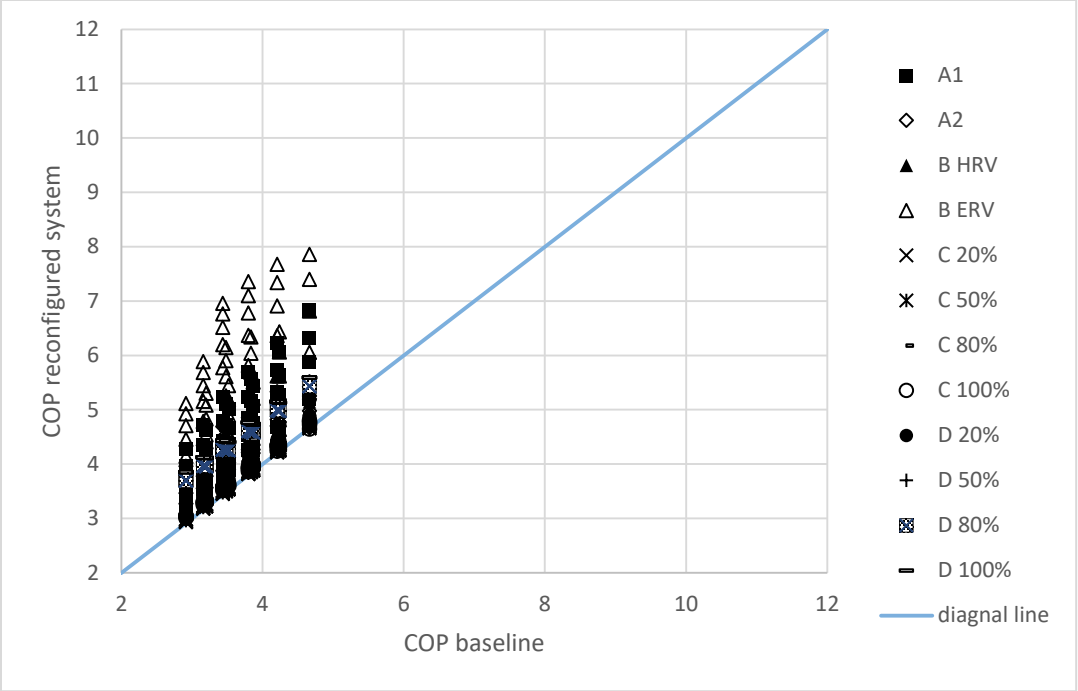

Figure 230 COP comparison between different reconfigured systems under typical conditions

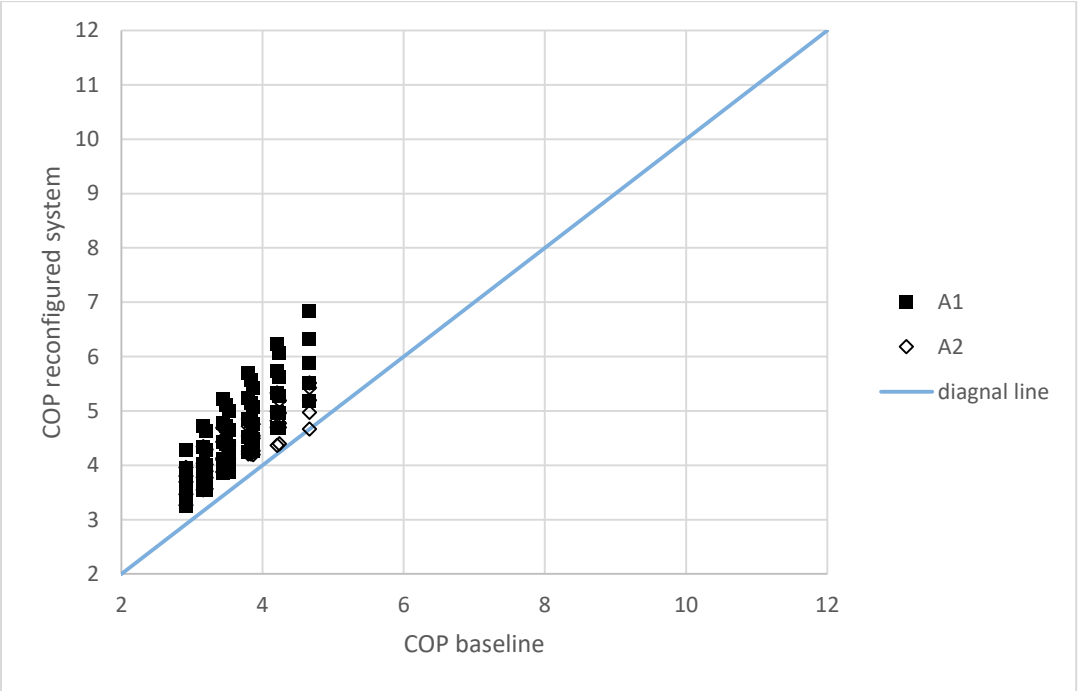

Figure 231 COP comparison between reconfigured system A and baseline system under typical conditions

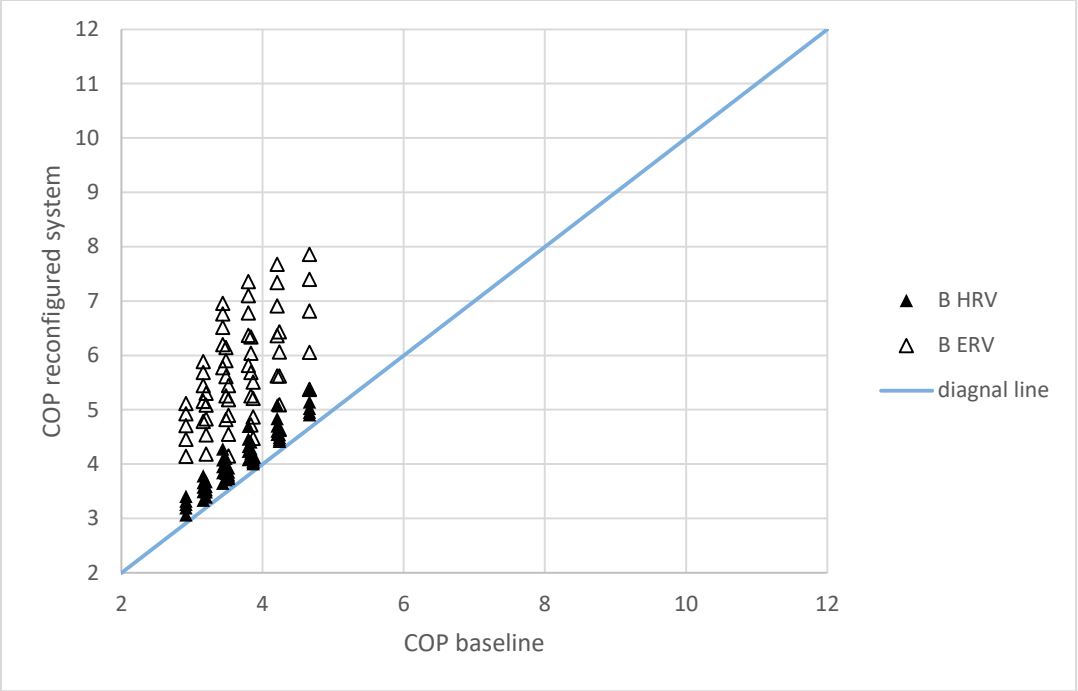

Figure 232 COP comparison between reconfigured system B and the baseline system under typical conditions

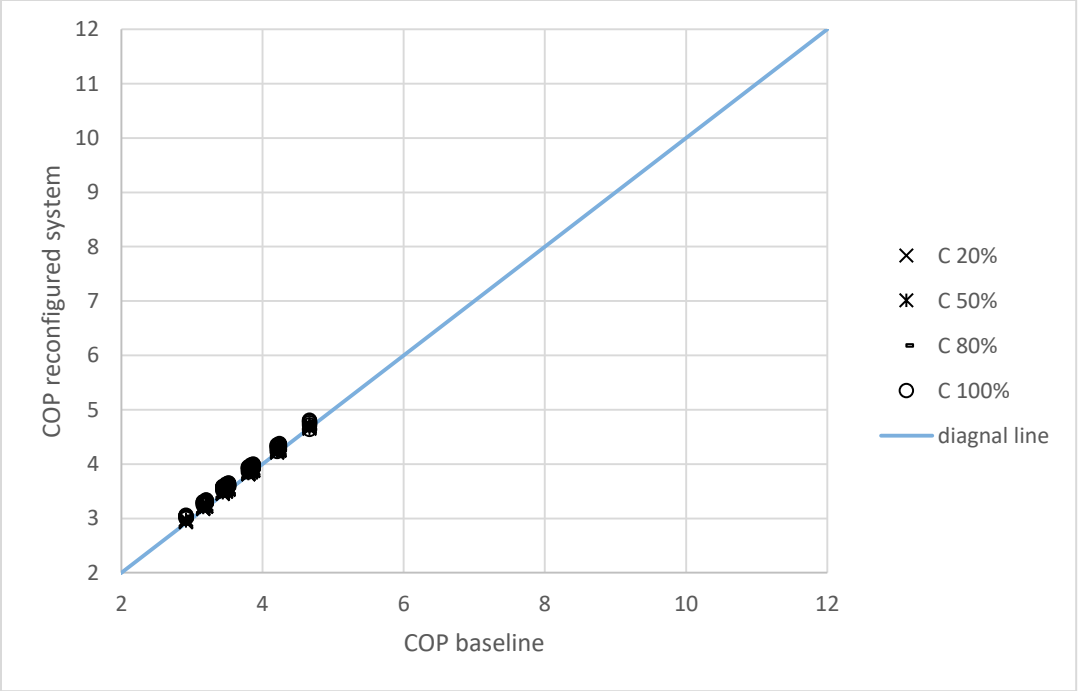

Figure 233 COP comparison between reconfigured system C and the baseline system under typical conditions

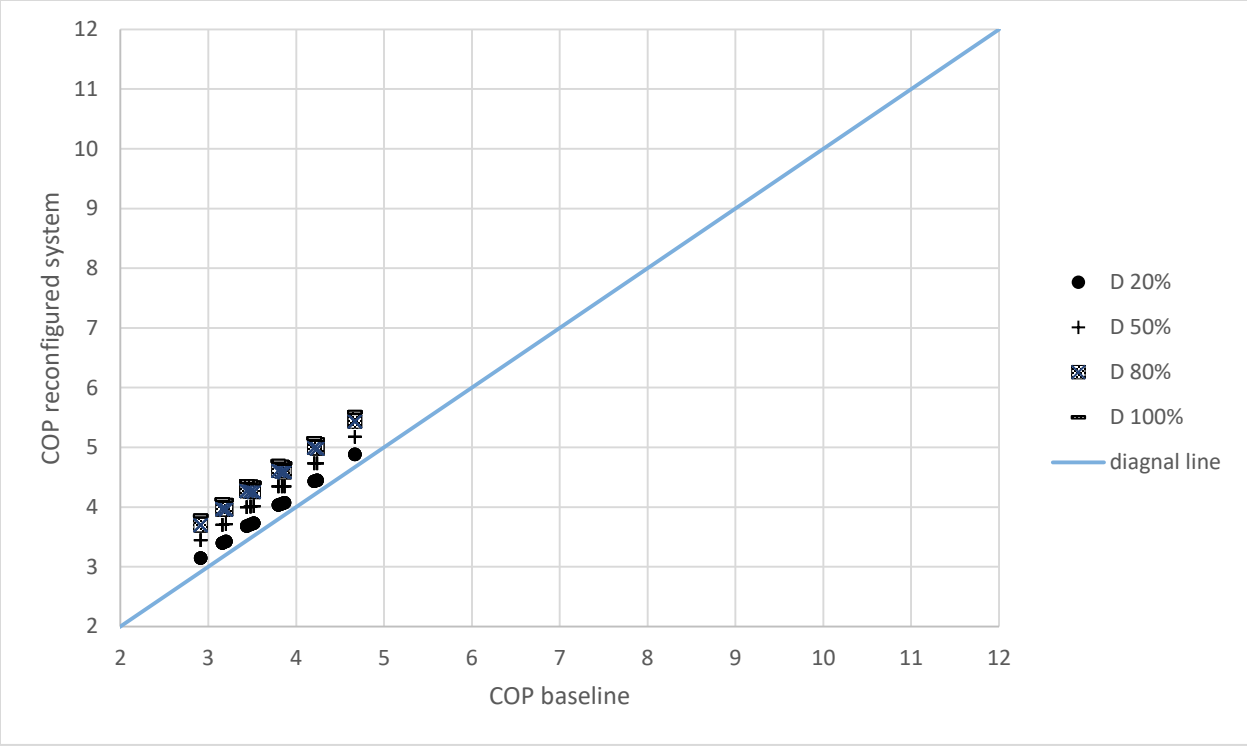

Figure 234 COP comparison between reconfigured system D and the baseline system under typical conditions

8.2 How Assumptions Influence COP Improvement

When apply the correlated equations derived on the four reconfigured system (section 5.1, 5.2, 5.3 and 5.4), it is necessary to check if the assumptions made in the model formulation have significant influence on the COP and COP ratio correlations. Thus, it is important to study the 6 (a---f) effects of on COP ratios for the four reconfigured system aforementioned.

a. compressor efficiency (80%, test 100%)

b. subcooling (0 F, test 10F)

c. superheated(0 F, test 10F)

d. Delta T aeo (10F, test 15F)

e. Delta T aci (30F, test 20F)

f. Change all assumptions (only change a,d,e since b and c are related to reconfigured system)

To further investigate how these 6 assumptions influence COP rations, three errors are defined and applied to the four reconfigured system aforementioned. Error 1 is a rating which is used to evaluate how different assumptions influence reconfigured system performance improvement, which is defined as follows,

$$E1=\frac{COPratio_{old\ assumption}-COPratio_{new\ assumption}}{COPratio_{old\ assumption}} \quad (131)$$

Error 2 is defined as the percentage difference between COP calculated---the product of baseline COP with new assumptions and COP ratio with old assumptions and the COP based on the new assumption---the product of baseline COP with new assumptions and COP ratio with new assumptions, and error 2 is expressed as follows

$$E2=\frac{COP_{cal}-COP_{new\ ass}}{COP_{new\ ass}} \quad (132)$$

where

$$COP_{baseline\ new\ assump} * funCOP_{ratio} = COP_{calculated} \quad (133)$$

Then combine Equation 132 and 133, E2 is further expressed as,

$$E2=\frac{COP_{baseline\ new\ ass}*fun\ COP_{ratio}-COP_{baseline\ new\ ass}*COP_{ratio\ new\ ass}}{COP_{baseline\ new\ ass}*COP_{ratio\ new\ ass}} \quad (134)$$

The term of $COP_{baseline\ new\ ass}$ is canceled on the numerator and denominator, and error 2 is simplified as

$$E2=\frac{funCOP_{ratio}-COP\ ratio\ _{new\ ass}}{COP_{ratio\ new\ ass}} \quad (135)$$

Thus, error 2 is a rating used to evaluate if COP correlation (Equation data) (under the original assumption) is applicable to the new assumptions.

Error 3 is expressed as follows,

$$E3=\frac{0.5*(improvement\ of\ original\ assumptions+improvement\ of\ new\ assumptions)}{Error\ 1} \quad (136)$$

Thus, error 3 is used for evaluating how error 1 influence the improvement, **the greater value, the better.**

The tables of three errors for the six effects are summarized in Appendix B. For compressor efficiency effect, error 1 is negligible; error 2 is negligible for most cases, but there is almost 5% error for internal evaporative cooling; error 3 are pretty large (larger than 10) except for reconfigured system C since its improvement is so little.

For subcooling effect, error 1 is negligible; error 2 is negligible for most cases, but there is as much as 5% for internal evaporative cooling; error 3 is large enough (larger than 10). For superheated effect, error 1 is negligible; error 2 is negligible for most cases, but there is as much as 5% for internal evaporative cooling; error 3 is large enough (larger than 10).

For Delta Taeo effect, error 1 is negligible; error 2 is negligible for most cases, but there is almost 4% error for internal evaporative cooling; error 3 is pretty large for all reconfigured system (larger than 10) except for reconfigured system C since its improvement is so little.

For Delta Taci effect, error 1 is negligible most cases but there is almost 5% error for external evaporative cooling/internal heat exchanger case. Error increases with the boosting heat exchanger effectiveness; Error 2 is negligible for most cases but there is almost 5% error for the external/internal evaporative cooling/internal heat exchanger case and this error increases with the boosting heat exchanger effectiveness; error 3 is small for most cases and only reconfigured B system has a great value.

When all the assumptions aforementioned change, error 1 is negligible for most cases but there is as much as 4% for internal heat exchanger (100%) case and error 1 increases with the boosting heat exchanger effectiveness. Error 2 is negligible for most cases but there is as much as 4% for internal heat exchanger (100%) case and error 2 increases with the boosting heat exchanger effectiveness. Also, there is as much as 5% error 2 for the internal evaporative cooling case. Error 3 for reconfigured system A1 and A2 and B (HRV and ERV) are OK (higher than 10). Other reconfigured system values are not high enough.

8.3 COP Improvement Comparison for Four Reconfigured Systems for the Real-world Weather Conditions

In section 8.1, the typical conditions (fixed conditions) are employed to simulate different reconfigured systems, and it is found that system B (ERV) and A1 (external evaporative cooling) are much higher than the other systems. On the other hand, it is meaningful to compare the four reconfigured system for real climate conditions during the cooling months across the U.S for the 18 climate zones using the correlated equations as well. The climate zone weather conditions and correlated equations are summarized in the previous sections (section 6.1). For simplification, only 50°F is considered for the supply air temperature (Taeo).

In figure 235, all monthly COPs for 18 climate zones in the cooling season are plotted and compared, and it showed that on the one hand reconfigured system A1 had the best improvement and for some cases, COP ratios are even less than 1. That is because, for reconfigured system A2 (internal condensate evaporative cooling) and reconfigured system C (internal condensate cool refrigerant exiting condenser) COP correlation development, all the equations derived previously are based on the existence of condensate water generated in the evaporator. However, in the real

weather data (18 climate zones), for lots of climate zones and some specific months, no condensate generated in the evaporator. Moreover, for reconfigured system B (HRV and ERV), the equations are based on no condensation occurred in the evaporator. However, considering the real condition, for lots of cases, condensation occurred in the evaporator. Basically that is the reason system B, C and A2 are not accurate. However, system A1 and system D (no pre-assumption) cases, the data is quite convincible.

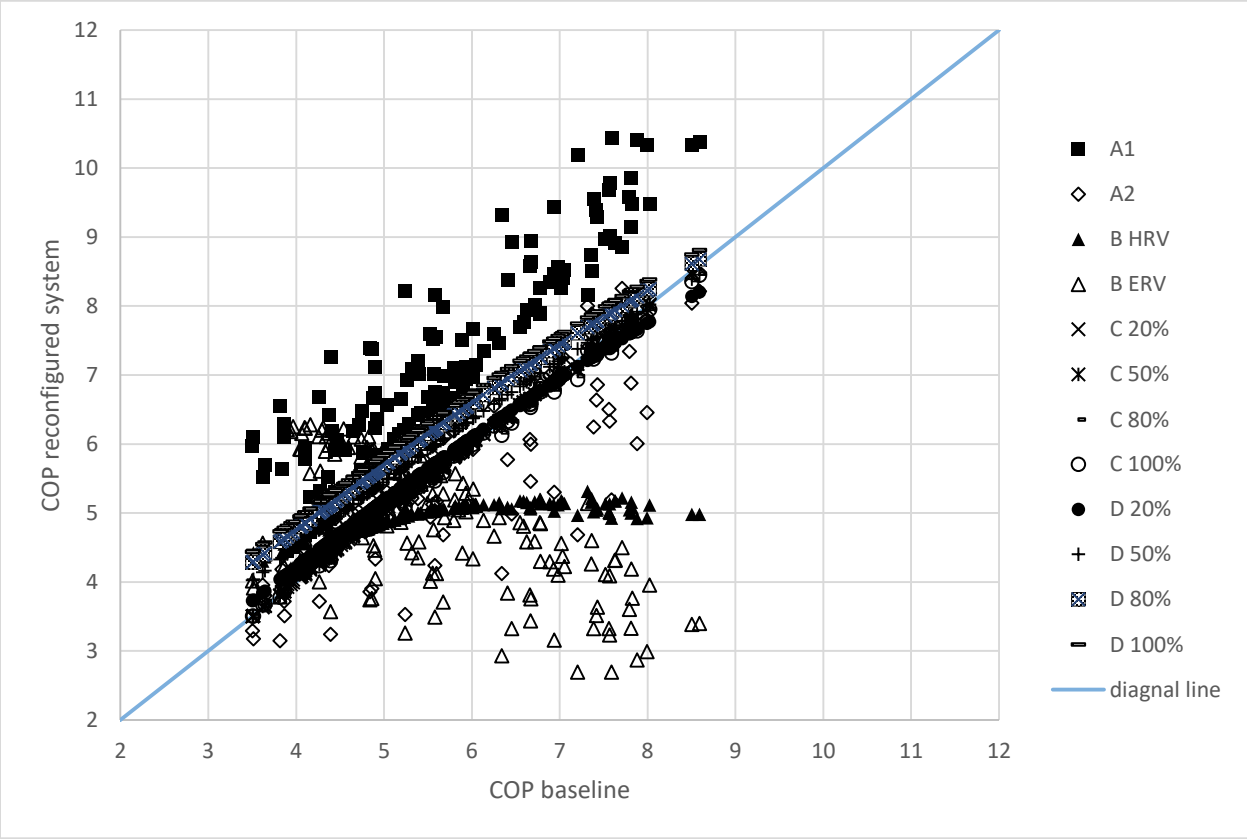

Figure 235 COP comparison between different reconfigured systems using real weather data and correlated equations

In Figure 236, the baseline system COPs under all weather conditions are ranging from 3.5 to 8.7 while the reconfigured COPs of A1 (external cooling) are increased from 4.5 to 10.5, which is an enormous amount of improvement. The reason that significant amount of spots of A2 (internal

evaporative cooling) are below the diagonal line is that, for lots of climate zones and specific months, there is no generated condensate in the evaporator at all. That further proved that internal evaporative cooling technology could be applied to very limited climate zones.

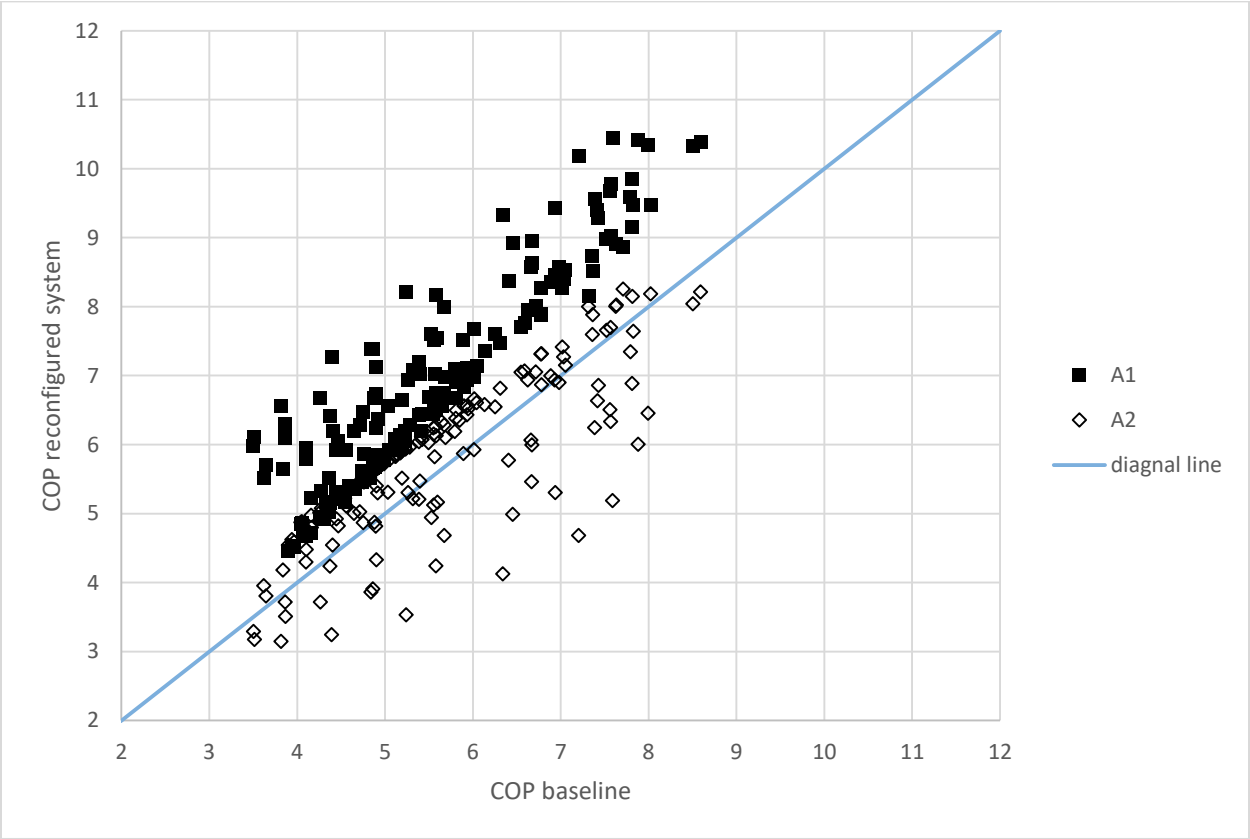

Figure 236 COP comparison between reconfigured system A and baseline system using real weather data and correlated equations

For lots of cases, the reason of reconfigured system B (HRV and ERV) system performance worse than baseline system is that for a large amount of climate zones at specific months (May, Sep. Oct…), outdoor air temperature is even lower than indoor air temperature (70---we used for our model). In that case, the outdoor air mixed with indoor exhaust air (higher temperature than

outdoor) would actually decrease COP during the cooling months and these scenarios are shown in Figure 237.

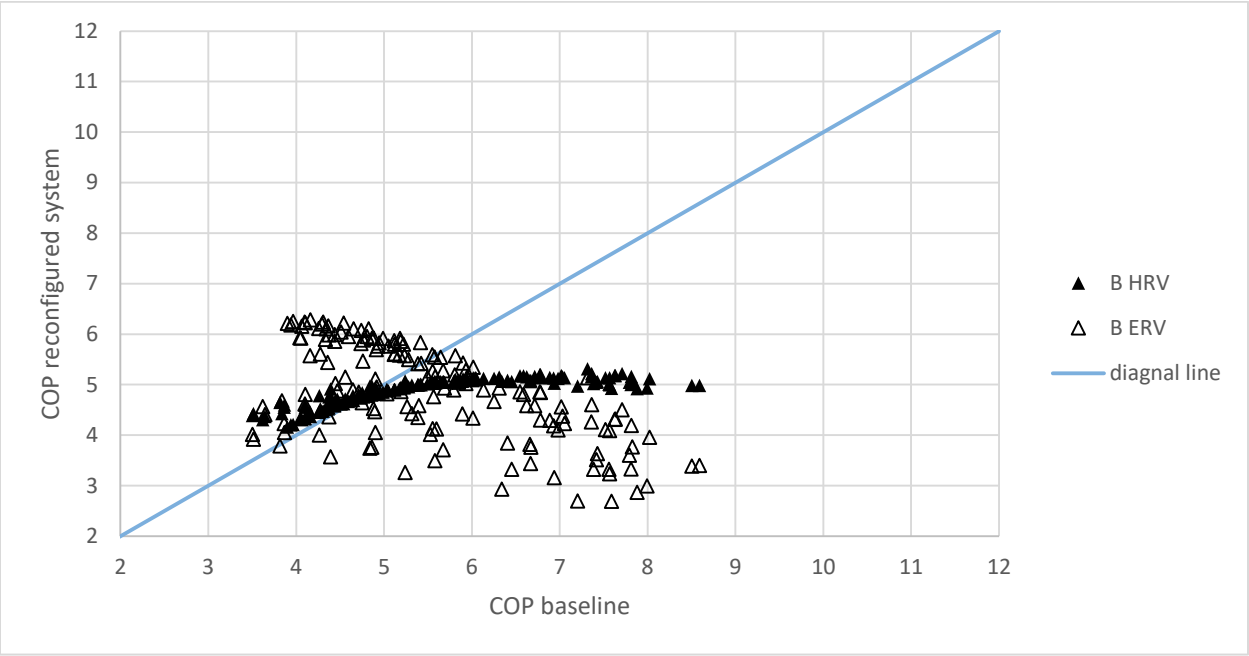

Figure 237 COP comparison between reconfigured system B and baseline system using real weather data and correlated equations

Since reconfigured system C performance improvement is very limited, condensate exists or not does not matter a lot, all the spots in Figure 238 are a little beyond the diagonal line.

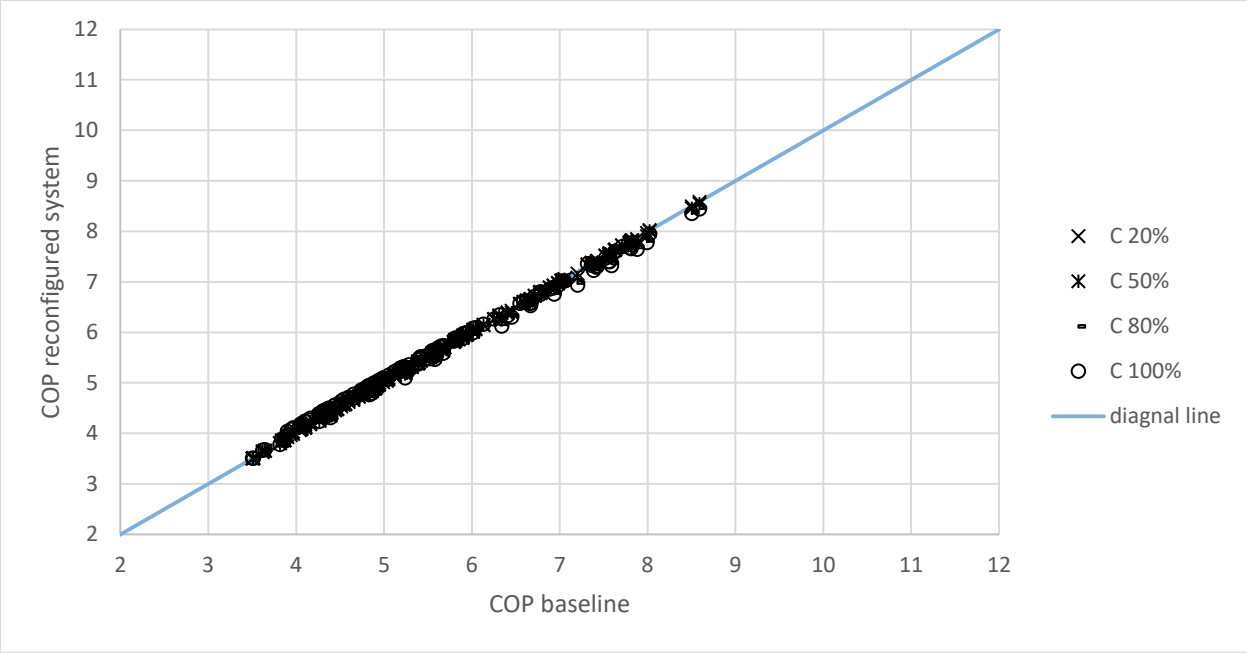

Figure 238 COP comparison between reconfigured system C and baseline system using real weather data and correlated equations

Reconfigured system D improvement is irrelevant to condensate; it is observed in Figure 239 that almost all spots of reconfigured system D are above the diagonal line, which means reconfigured system D always has a benefit over baseline system but the improvement is lower than system A1 (external evaporative cooling). When the heat exchanger effectiveness become 100%, COPs can reach from 4.7 to 8.9.

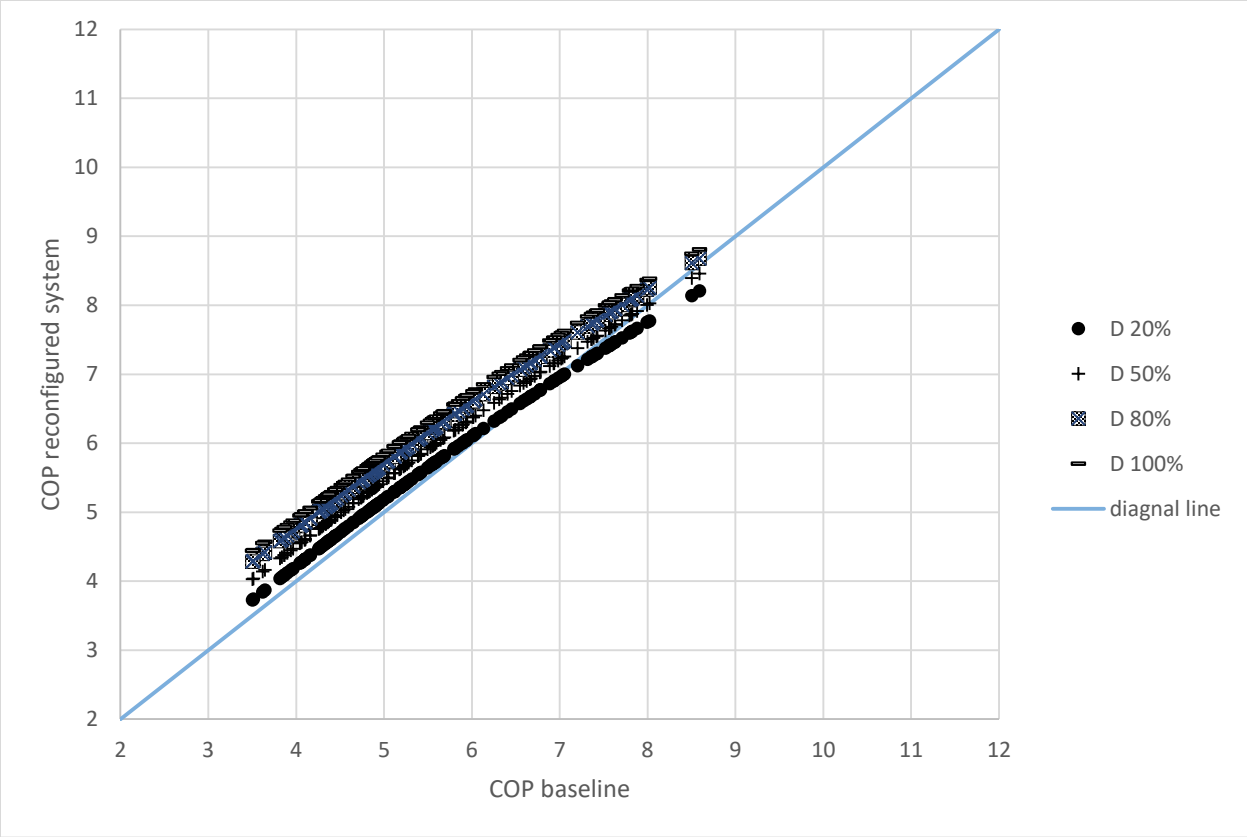

Figure 239 COP comparison between reconfigured system D and baseline system using real weather data and correlated equations

The weighting factors for each month of all the 18 climate zones are obtained from the section 6.2. Thus the weighted COP for each climate zone over the whole cooling season could be further calculated based on the known monthly COP and the weighting factor. Table 45 showed all the reconfigured systems' COP weighted improvement (ratio over the baseline system) over the whole cooling season for all the 18 climate zones. Table 46 summarized the ranking from the first to the third reconfigured method for improvement of all the 18 climate zones. In table 46, only for climate zone 1A, 2A, and 3Aw, reconfigured system B (ERV, effectiveness 60%) is the best since these three regions are hot and humid, which are the best conditions for heat/energy recovery. For all the other climate zones, reconfigured system A1 is the most efficient, followed by reconfigured system D (internal heat exchanger). Since the heat exchanger effectiveness of

reconfigured system B is 60%, it is necessary to use the same effectiveness for D, which is further shown in table 38, though the new data will not change the first 3 ranking order.

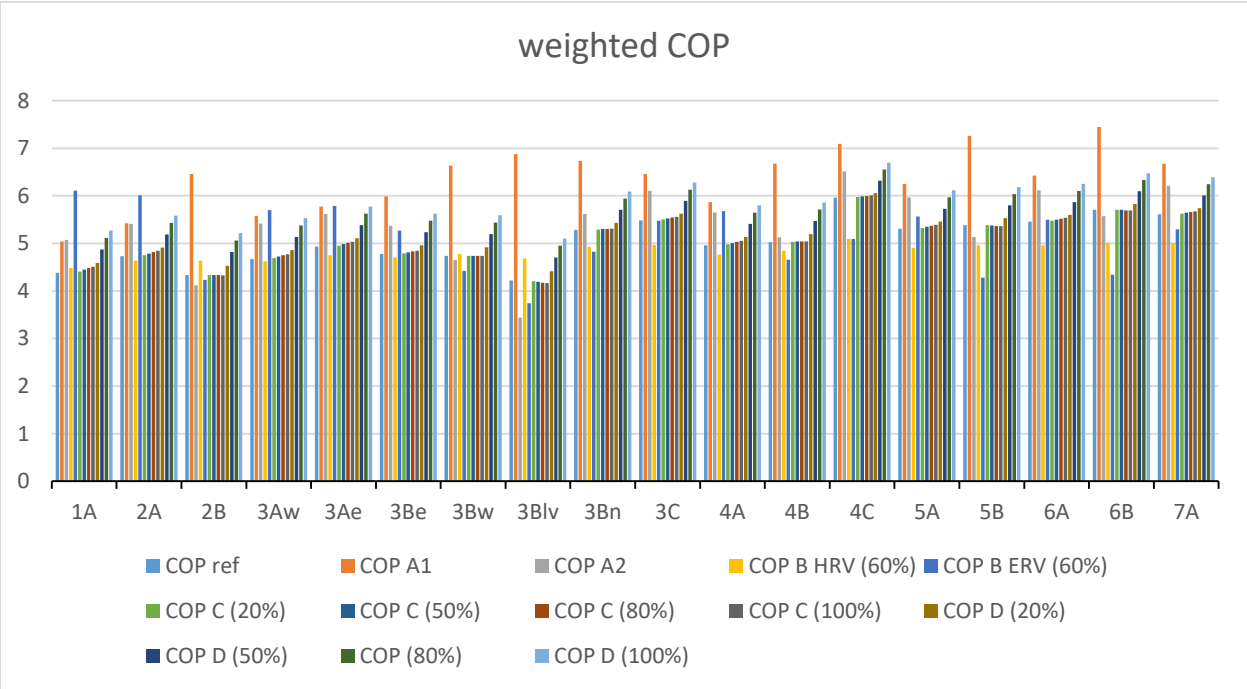

Figure 240 Weighted COP for all 18 climate zones over the whole cooling season

Table 45 All reconfigured systems (A to D) COP ratio for all 18 climate zones

	COP A1	COP A2	COP B HRV (60%)	COP B ERV (60%)	COP C (20%)	COP C (50%)	COP C (80%)	COP C (100%)	COP D (20%)	COP D (50%)	COP (80%)	COP D (100%)
1A	1.15	1.16	1.02	1.39	1.01	1.01	1.02	1.03	1.05	1.11	1.17	1.20
2A	1.15	1.14	0.98	1.27	1.01	1.01	1.02	1.02	1.04	1.10	1.15	1.18
2B	1.49	0.95	1.07	0.98	1.00	1.00	1.00	1.00	1.05	1.11	1.17	1.20
3Aw	1.19	1.16	0.99	1.22	1.00	1.01	1.02	1.02	1.04	1.10	1.15	1.18
3Ae	1.17	1.14	0.96	1.17	1.00	1.01	1.02	1.02	1.04	1.09	1.14	1.17
3Be	1.25	1.12	0.99	1.10	1.00	1.01	1.01	1.01	1.04	1.10	1.15	1.18

Table 45 continued

	COP A1	COP A2	COP B HRV (60%)	COP B ERV (60%)	COP C (20%)	COP C (50%)	COP C (80%)	COP C (100%)	COP D (20%)	COP D (50%)	COP (80%)	COP D (100%)
3Bw	1.40	0.98	1.01	0.93	1.00	1.00	1.00	1.00	1.04	1.10	1.15	1.18
3Blv	1.63	0.82	1.11	0.89	1.00	0.99	0.99	0.99	1.05	1.12	1.17	1.21
3Bn	1.28	1.06	0.93	0.91	1.00	1.00	1.00	1.01	1.03	1.08	1.13	1.15
3C	1.18	1.11	0.91	1.00	1.00	1.01	1.01	1.01	1.03	1.07	1.12	1.14
4A	1.18	1.14	0.96	1.14	1.00	1.01	1.01	1.02	1.03	1.09	1.14	1.17
4B	1.33	1.02	0.96	0.93	1.00	1.00	1.00	1.00	1.03	1.09	1.14	1.17
4C	1.19	1.09	0.85	0.86	1.00	1.00	1.01	1.01	1.02	1.06	1.10	1.12
5A	1.18	1.12	0.92	1.05	1.00	1.01	1.01	1.02	1.03	1.08	1.12	1.15
5B	1.35	0.95	0.92	0.79	1.00	1.00	1.00	1.00	1.03	1.08	1.12	1.15
6A	1.18	1.12	0.91	1.01	1.00	1.01	1.01	1.01	1.03	1.08	1.12	1.15
6B	1.30	0.98	0.88	0.76	1.00	1.00	1.00	1.00	1.02	1.07	1.11	1.13
7A	1.19	1.11	0.89	0.94	1.00	1.01	1.01	1.01	1.02	1.07	1.11	1.14

Table 46 First, second and third ranking modification method for each climate zone

	largest ratio	Largest	Second	Third
1A	1.39	ERV (60%)	D (100%)	D(80%)
2A	1.27	ERV (60%)	D (100%)	D(80%) or A1
2B	1.49	A1	D(100%)	D(80%)
3Aw	1.22	ERV (60%)	A1 or D (100%)	A1 or D (100%)
3Ae	1.17	A1 or D (100%)or ERV (60%)	--	--
3Be	1.25	A1	D(100%)	D(80%)
3Bw	1.40	A1	D(100%)	D(80%)
3Blv	1.63	A1	D(100%)	D(80%)
3Bn	1.28	A1	D(100%)	D(80%)
3C	1.18	A1	D(100%)	D(80%)
4A	1.18	A1 or D (100%)	A1 or D (100%)	D(80%) or A2 or ERV (60%)
4B	1.33	A1	D(100%)	D(80%)
4C	1.19	A1	D(100%)	D(80%)
5A	1.18	A1	D(100%)	D(80%) or A2
5B	1.35	A1	D(100%)	D(80%)

Table 46 continued

	largest ratio	Largest	Second	Third
6A	1.18	A1	D(100%)	D(80%) or A2
6B	1.30	A1	D(100%)	D(80%)
7A	1.19	A1	D(100%)	D(80%) or A2

Table 47 Reconfigured system D with the same heat exchanger effectiveness as B (60%)

	COP A1	COP A2	COP B HRV (60%)	COP B ERV (60%)	COP D(60%)
1A	1.15	1.16	1.02	1.39	1.13
2A	1.15	1.14	0.98	1.27	1.12
2B	1.49	0.95	1.07	0.98	1.13
3Aw	1.19	1.16	0.99	1.22	1.12
3Ae	1.17	1.14	0.96	1.17	1.11
3Be	1.25	1.12	0.99	1.10	1.11
3Bw	1.40	0.98	1.01	0.93	1.11
3Blv	1.63	0.82	1.11	0.89	1.14
3Bn	1.28	1.06	0.93	0.91	1.10
3C	1.18	1.11	0.91	1.00	1.09
4A	1.18	1.14	0.96	1.14	1.11
4B	1.33	1.02	0.96	0.93	1.10
4C	1.19	1.09	0.85	0.86	1.07
5A	1.18	1.12	0.92	1.05	1.09
5B	1.35	0.95	0.92	0.79	1.09
6A	1.18	1.12	0.91	1.01	1.09
6B	1.30	0.98	0.88	0.76	1.08
7A	1.19	1.11	0.89	0.94	1.08

8.4 Corrected COP Improvement Comparison for Four Reconfigured Systems for the Real-world Weather Conditions

Considering the extreme conditions occurred, namely no condensate occurred or outdoor air temperature lower than indoor air, some changes are made to the content in section 8.3 (but still using correlated equations for each reconfigured system). When the outdoor air condition is not suitable for reconfiguration, just use the baseline system (conventional vapor-compression

system) instead of always using reconfigured systems. Thus, the new plots actually illustrates the corrected COP improvement for all the reconfigured systems, and according to Figure 241, roughly all the test spots are above the diagonal line meaning system performance for the reconfigured systems are always better than the baseline system. Reconfigured system A1 (external evaporative cooling) and B (ERV) are still the best efficient retrofit methods compared to the baseline system.

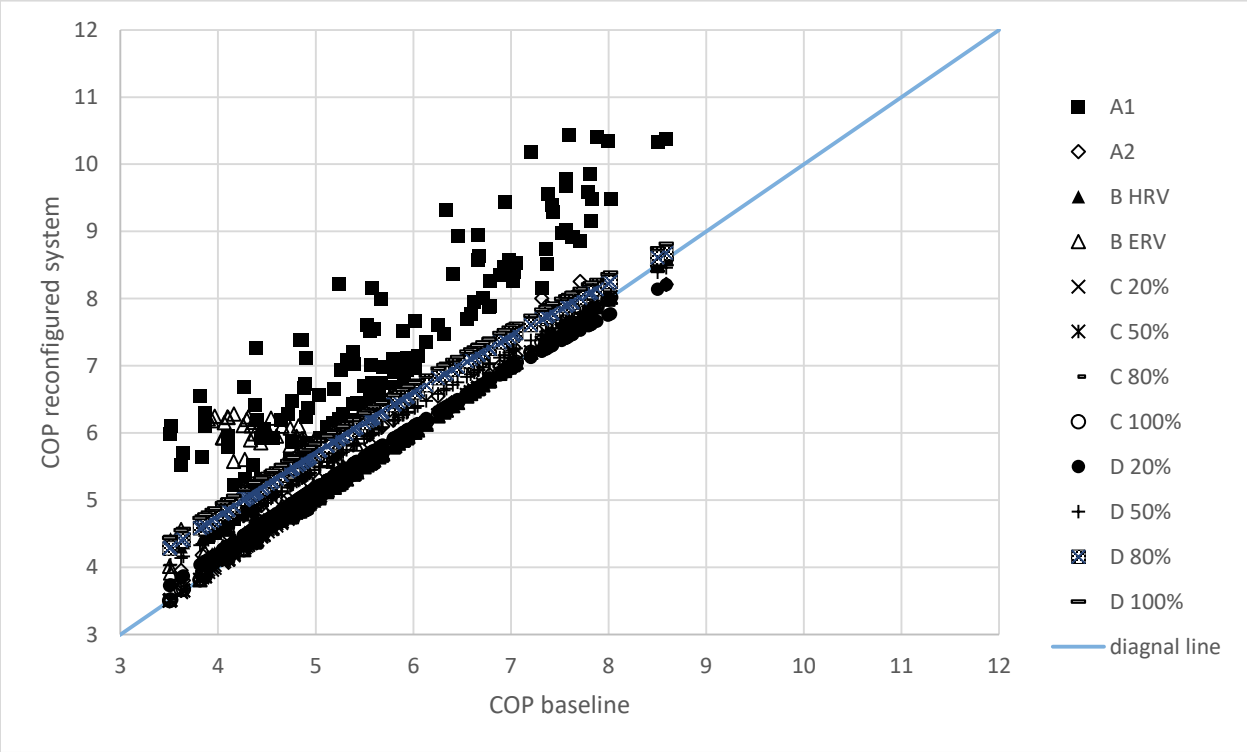

Figure 241 Corrected COP comparison between different reconfigured systems using real weather data and correlated equations

Unlike the plot in section 8.3, the corrected COPs for reconfigured system A2 (internal evaporative cooling) from Figured 242 are higher than that of the baseline system, though still not as significant as reconfigured system A1 (external evaporative cooling).

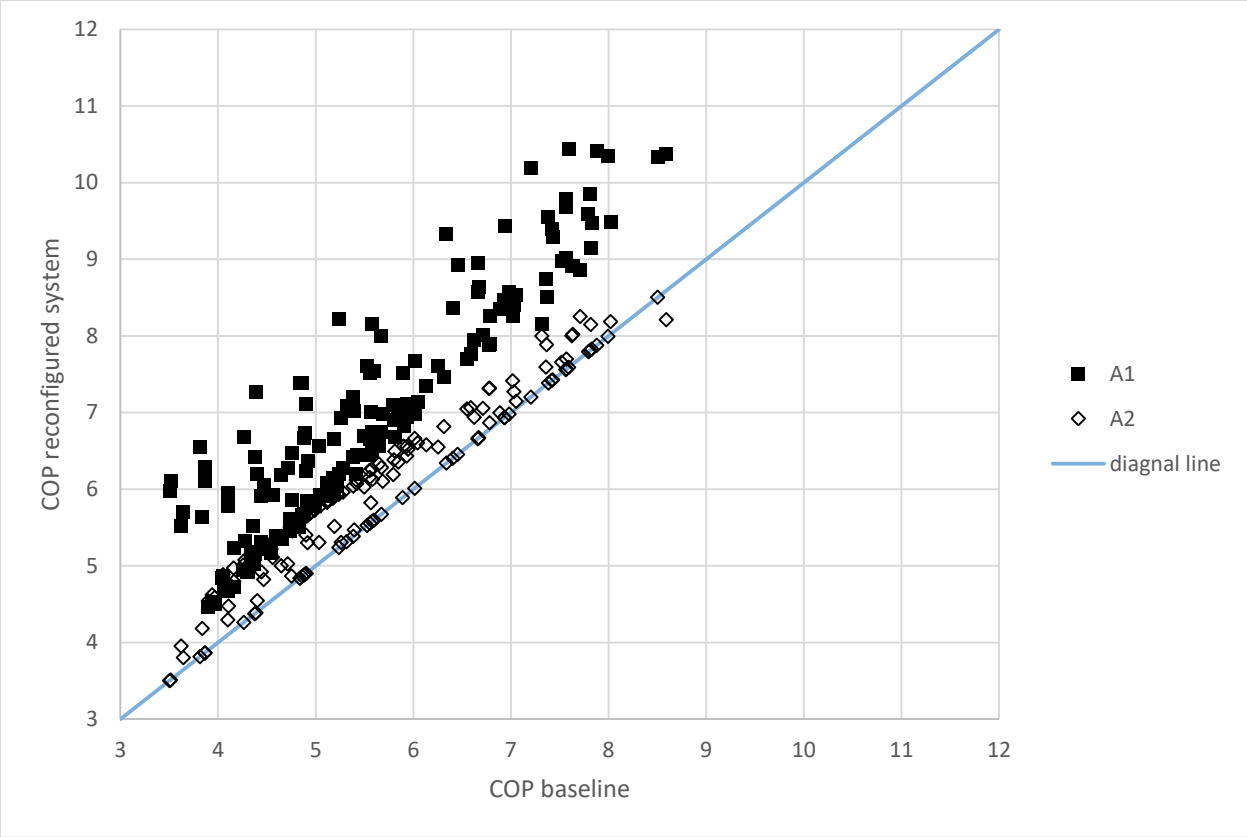

Figure 242 Corrected COP comparison between reconfigured system A and baseline system using real weather data and correlated equations

Figure 243 shows the comparison between HRV/ERV and the baseline system. Energy recovery is always more efficient than heat recovery, and the improvement of energy recovery over the conventional vapor compression cycle is significant almost all the climate zones (and months). Heat recovery method, much less efficient than energy recovery, just slightly improvement exist for most months since for most cooling months in different climate zones, the difference between the outdoor air temperature and indoor air temperature (70°F) is not significant. On the other hand, the big difference between energy recovery and heat recovery for most climate zones (most months) will also illustrate moisture recovery (latent load) takes a considerable portion in the total energy recovery. The results of system C and D are almost the same as mentioned in section 8.3.

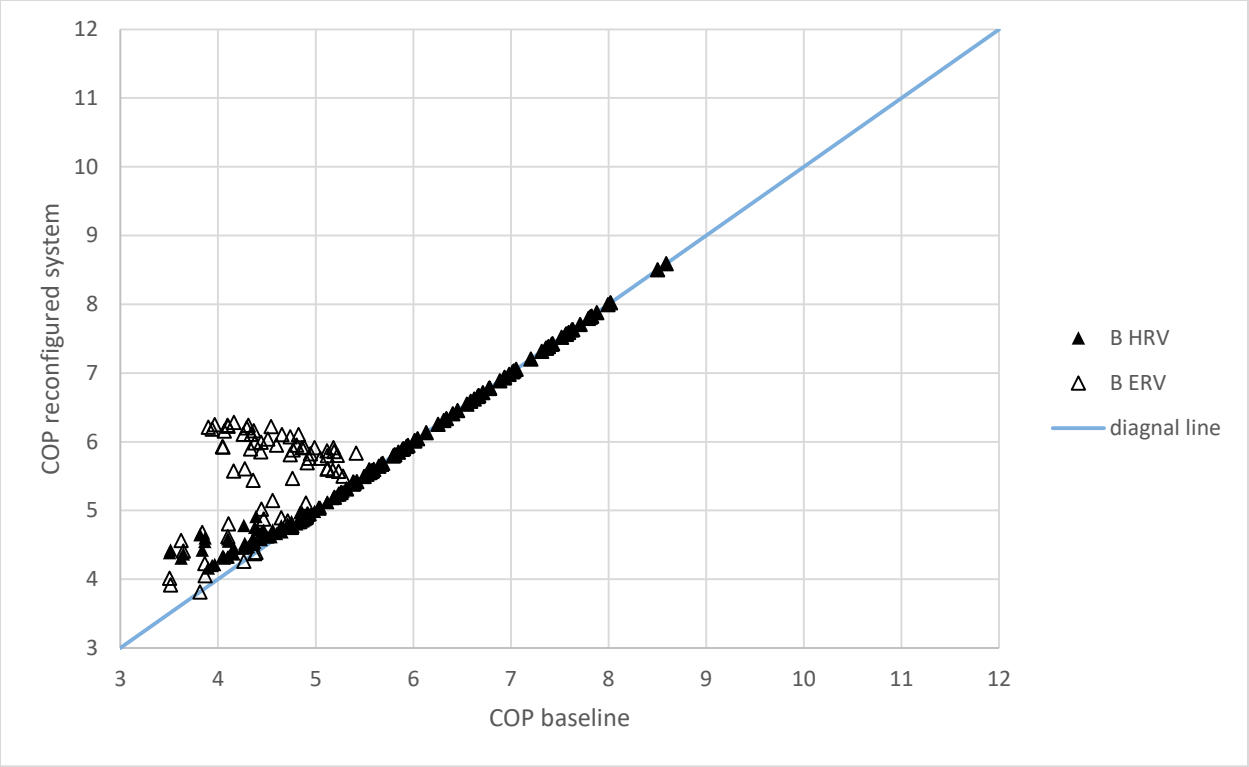

Figure 243 Corrected COP comparison between reconfigured system B and baseline system using real weather data and correlated equations

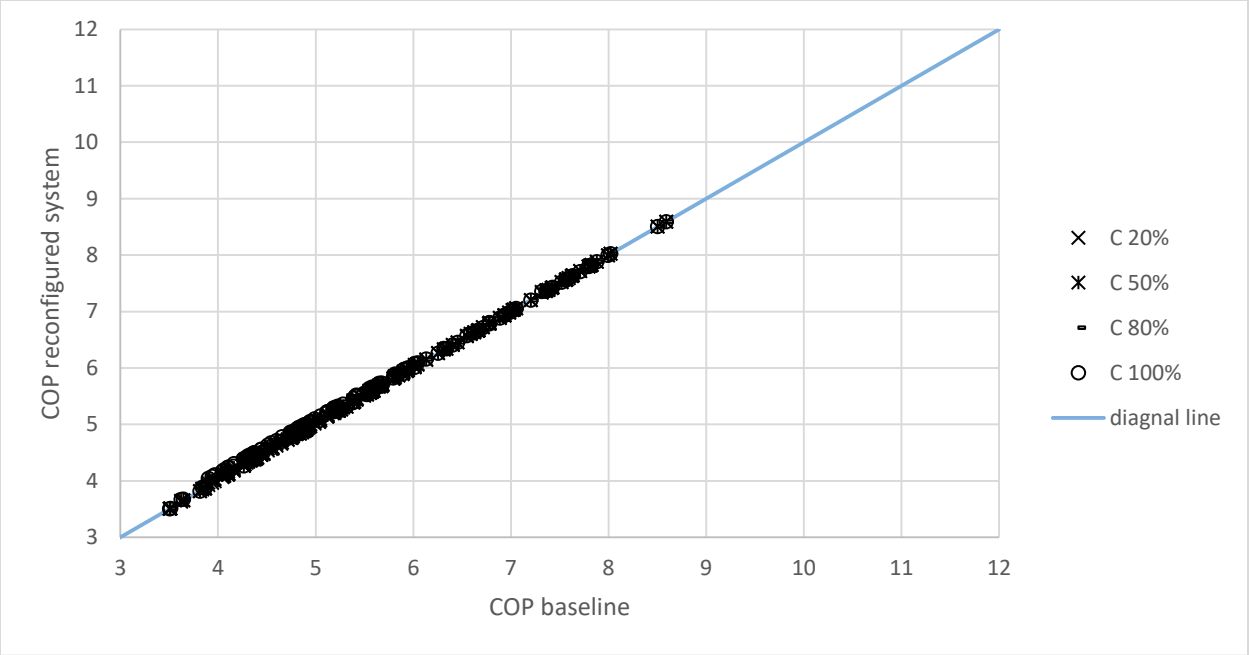

Figure 244 Corrected COP comparison between reconfigured system C and baseline system using real weather data and correlated equations

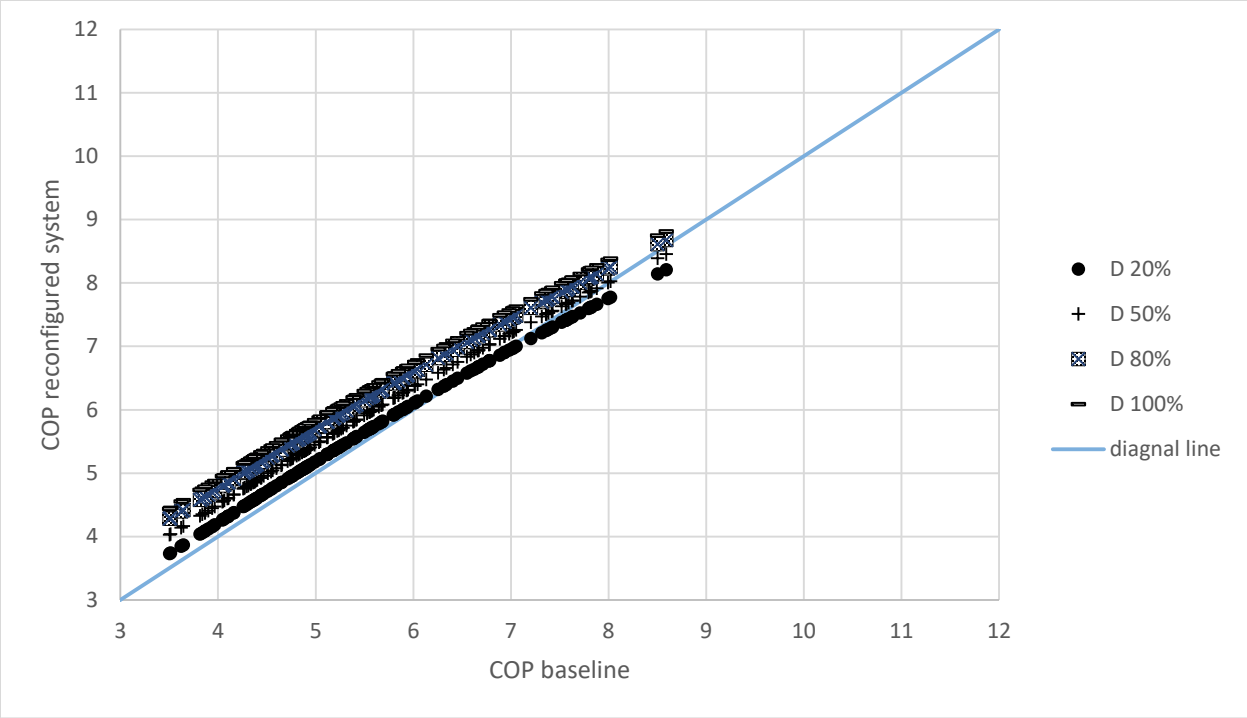

Figure 245 Corrected COP comparison between reconfigured system D and baseline system using real weather data and correlated equations

According to Table 48 and 49, for climate zone 3Ae and 4A, the most efficient reconfigured system become ERV (effectiveness 60%). All the other results remain the same with that of section 8.3. For most climate zones, the hot regions (small climate zone number) can always get more benefit from the reconfigured system than the cold regions. In climate zone 2B (hot and dry), the largest improvement can reach as much as 50%. Compared to the humid regions, dry regions (B) can always achiever larger improvement. In climate zone 3Blv---Las Vegas, the largest improvement can get almost 63% improvement. Since the heat exchanger effectiveness of reconfigured system B is 60%, it is necessary to use the same effectiveness for D, which is further shown in table 50, though the new data will not change the first 3 ranking order.

Table 48 All reconfigured systems (A to D) corrected COP ratio for all 18 climate zones

	COP A1	COP A2	COP B HRV (60%)	COP B ERV (60%)	COP C (20%)	COP C (50%)	COP C (80%)	COP C (100%)	COP D (20%)	COP D (50%)	COP (80%)	COP D (100%)
1A	1.15	1.16	1.04	1.39	1.01	1.01	1.02	1.03	1.05	1.11	1.17	1.20
2A	1.15	1.14	1.02	1.30	1.01	1.01	1.02	1.02	1.04	1.10	1.15	1.18
2B	1.49	1.03	1.11	1.10	1.00	1.00	1.00	1.00	1.05	1.11	1.17	1.20
3Aw	1.19	1.16	1.03	1.26	1.00	1.01	1.02	1.02	1.04	1.10	1.15	1.18
3Ae	1.17	1.14	1.01	1.22	1.00	1.01	1.02	1.02	1.04	1.09	1.14	1.17
3Be	1.25	1.13	1.03	1.17	1.00	1.01	1.01	1.02	1.04	1.10	1.15	1.18
3Bw	1.40	1.03	1.05	1.06	1.00	1.00	1.00	1.00	1.04	1.10	1.15	1.18
3Blv	1.63	1.00	1.14	1.04	1.00	1.00	1.00	1.00	1.05	1.12	1.17	1.21
3Bn	1.28	1.06	1.01	1.01	1.00	1.00	1.00	1.01	1.03	1.08	1.13	1.15
3C	1.18	1.11	1.00	1.08	1.00	1.01	1.01	1.01	1.03	1.07	1.12	1.14
4A	1.18	1.14	1.01	1.20	1.00	1.01	1.02	1.02	1.03	1.09	1.14	1.17
4B	1.33	1.06	1.02	1.05	1.00	1.00	1.01	1.01	1.03	1.09	1.14	1.17
4C	1.19	1.09	1.00	1.00	1.00	1.00	1.01	1.01	1.02	1.06	1.10	1.12
5A	1.18	1.13	1.00	1.11	1.00	1.01	1.01	1.02	1.03	1.08	1.12	1.15
5B	1.35	1.00	1.00	1.00	1.00	1.00	1.00	1.00	1.03	1.08	1.12	1.15
6A	1.18	1.12	1.00	1.07	1.00	1.01	1.01	1.01	1.03	1.08	1.12	1.15
6B	1.30	1.00	1.00	1.00	1.00	1.00	1.00	1.00	1.02	1.07	1.11	1.13
7A	1.19	1.11	1.00	1.04	1.00	1.01	1.01	1.01	1.02	1.07	1.11	1.14

Table 49 First to third ranking modification methods based on corrected model for each climate zone

	largest ratio	Largest	Second	Third
1A	1.394920307	ERV (60%)	D(100%)	D(80%)
2A	1.303636712	ERV (60%)	D(100%)	D(80%)orA1orA2
2B	1.490207937	A1	D(100%)	D(80%)

Table 49 continued

	largest ratio	Largest	Second	Third
3Aw	1.259734114	ERV 60%	A1	D(100%)
3Ae	1.220422052	ERV 60%	A1orD(100%)	A1orD(100%)
3Be	1.253975745	A1	D(100%)	ERV (60%)
3Bw	1.400056776	A1	D(100%)	D(80%)
3Blv	1.629992102	A1	D(100%)	D(80%)
3Bn	1.2757221	A1	D(100%)	D(80%)
3C	1.177235581	A1	D(100%)	D(80%) or A2
4A	1.198664952	ERV 60%	A1	D(100%)
4B	1.32792066	A1	D(100%)	D(80%)
4C	1.189293286	A1	D(100%)	D(80%)orA2
5A	1.178256392	A1	D(100%)	D(80%)orA2
5B	1.348311913	A1	D(100%)	D(80%)orA2
6A	1.177233907	A1	D(100%)	D(80%)orA2
6B	1.304606692	A1	D(100%)	D(80%)
7A	1.190073048	A1	D(100%)	D(80%)orA2

Table 50 Reconfigured system D has the same heat exchanger effectiveness as B of 60%--- based on the corrected model

	COP A1	COP A2	COP B HRV (60%)	COP B ERV (60%)	COP D (60%)
1A	1.15	1.16	1.04	1.39	1.13
2A	1.15	1.14	1.02	1.30	1.12
2B	1.49	1.03	1.11	1.10	1.13
3Aw	1.19	1.16	1.03	1.26	1.12
3Ae	1.17	1.14	1.01	1.22	1.11
3Be	1.25	1.13	1.03	1.17	1.11
3Bw	1.40	1.03	1.05	1.06	1.11
3Blv	1.63	1.00	1.14	1.04	1.14
3Bn	1.28	1.06	1.01	1.01	1.10
3C	1.18	1.11	1.00	1.08	1.09
4A	1.18	1.14	1.01	1.20	1.11
4B	1.33	1.06	1.02	1.05	1.10
4C	1.19	1.09	1.00	1.00	1.07
5A	1.18	1.13	1.00	1.11	1.09
5B	1.35	1.00	1.00	1.00	1.09

Table 50 continued

	COP A1	COP A2	COP B HRV (60%)	COP B ERV (60%)	COP D (60%)
6A	1.18	1.12	1.00	1.07	1.09
6B	1.30	1.00	1.00	1.00	1.08
7A	1.19	1.11	1.00	1.04	1.08

9. HOW REFRIGERANT TYPE INFLUENCE COP AND COP IMPROVEMENT

Today, many residential and light commercial AC systems in use still contain R22, which is being phased out globally and has been banned for use in new AC systems in the U.S since 2010. The vast majority of AC units sold today contain R-410A, which is an HFC mixture with a GWP (global warming potential)-a measure of its climate-warming compared to CO2—of 2,088. Therefore, R-410A is soon to follow the path of R-22 in that its phase-out has also been mandated. Thus, searching for a new replacement for R-410A considering Ozone Depleting Potential, GWP, flammability, toxicity, and safety issues are ongoing and paramount. An important consideration when phasing out R-410A is that any replacement refrigerants should not have a lower COP compared to R-410A because the net result should be all increase in global warming. Therefore, effects must be made to improve the energy efficiency of existing vapor- compression technology and components.

9.1 Potential Replacement of R410A --- Comparing System Performance (COP) of Conventional Vapor-Compression System (Ratio 1)

R134a, R32, R1234yf, R1234ze (z) and R1234ze (e) provide low global warming potential (GWP), zero depleting potential (ODP) and relative low flammability, which is shown in table 51. Previously performed tests with R32 were satisfactory and it seems possible that this substance could stay in the market. The HVAC industry in China is focusing on this refrigerant since R32's GWP level is moderate, but compared with R410A, R32 (GWP of 675) is only one-third of its GWP.

Table 51 ODP and GWP values of different refrigerant

Refrigerant	ODP (R11=1.0)	GWP IPCC AR4 (CO_2=1)
R22	0.055	1810
R410A	0	2088
R32	0	675
R1234yf	0	4
CO_2	0	1
R134a	0	1430

Even though R22 is totally phased out, a comparison of conventional vapor-compression system performance is made between R22, R410A, R32, R134a, R1234yf, R1234ze(e) and R1234ze(z) in Table 61 and Figure 238. The conditions are still the same as previous chapters, namely outdoor condition set as: 26.7, 32.2, 37.8, 43.3℃ (80, 90, 100, 110°F), RH=40%, 50%, 60% 70%, 80%, 90%; Taeo=4.4, 10℃(40, 50°F); compressor efficiency: 80%. Ratio 1 is defined as follows,

$$\text{R1}=\frac{COP_{baseline\ new\ ref}}{COP_{baseline\ R-410A}} \tag{137}$$

And it is the ratio of new refrigerant COP over R-410A COP for a conventional vapor-compression. If this ratio is less than 1, then the new refrigerant may have a lower GWP but increasing fuel to operate causes more GWP.

Figure 246 shows 6 refrigerants compared with R-410A for a conventional vapor compression system, and it indicates that all the ratios are greater than 1, which means all other refrigerants have larger COP than R410A at the same condition. The ranking of system performance for the 7 refrigerants are illustrated as follows, (R1234ze (z)> R22> R134a> R1234ze (e)> R32> R1234yf> R410A) and a comprehensive table of conventional vapor-compression

coefficient of system performance under typical conditions for the 7 refrigerants is listed in Appendix B.

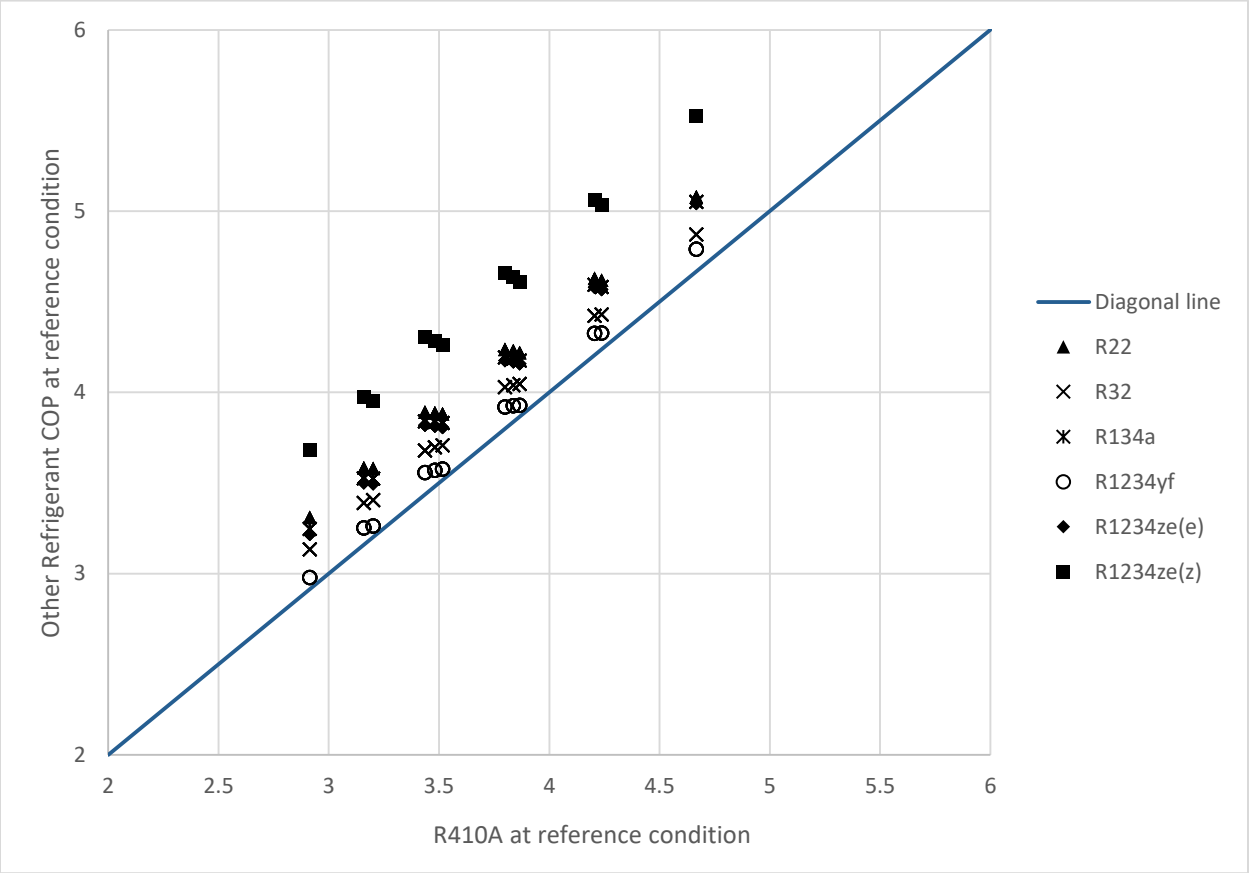

Figure 246 6 refrigerant compared with R-410A for a conventional vapor compression system

9.2 Reconfigured System Performance for the Other 6 Refrigerants (Ratio 2)

Ratio 2 is defined as

$$R2=\frac{COP_{recon\ new\ ref}}{COP_{baseline\ new\ ref}} \tag{138}$$

Ratio 2 is the ratio of system with modification over the baseline system using new refrigerant. If this ratio is greater than 1, then it is necessary to compare the new refrigerant modification improvement with R-410A modification improvement.

COP and COP ratios for six refrigerants under different conditions are shown in the Appendix C and Ratio 2 for any refrigerant under any modification is larger than 1.

9.3 Ratio 3 (a product of ratio 1 and ratio 2)

Now multiply the above two ratios together and get

$$R3=R1*R2=\frac{COP_{baseline\ new\ ref}}{COP_{baseline\ R-410A}} * \frac{COP_{recon\ new\ ref}}{COP_{baseline\ new\ ref}} \quad (139)$$

By simplification, R3 is defined as

$$R3=\frac{COP_{recon\ new\ ref}}{COP_{baseline\ R-410A}} \quad (140)$$

If this ratio is greater than 1, then we save the planet using a new refrigerant and reconfigured system--if less than 1 then GWP could increase because use more coal/natural gas, meaning we keep looking for a better refrigerant.

Based on the results of section 9.1 and 9.2, ratio 1 and ratio 2 are both larger than 1, meaning all ratio 3 is greater than 1, which further indicates we can save the planet using a new refrigerant and reconfigured systems.

9.4 COP Improvement Comparison between Different Refrigerant for the Reconfigured Systems

Since for all refrigerants, modified system performances are larger than the baseline system, it is necessary to compare COP ratio for all the reconfigured system---namely figure out which refrigerant is the best choice for each modification.

Figure 247 shows the performance of improvement with reconfigured system A1 (external evaporative cooling) over the baseline system. This figure indicates that the performance improvement is similar for the six refrigerant, but almost all the data is under the diagonal line, meaning R-410A has the highest benefit of this modification---R410A> R1234yf> R1234ze(e)> R32> R134a> R22> R1234ze(z). The details of COP and COP ratios under different conditions for all seven refrigerants are shown in Appendix C.

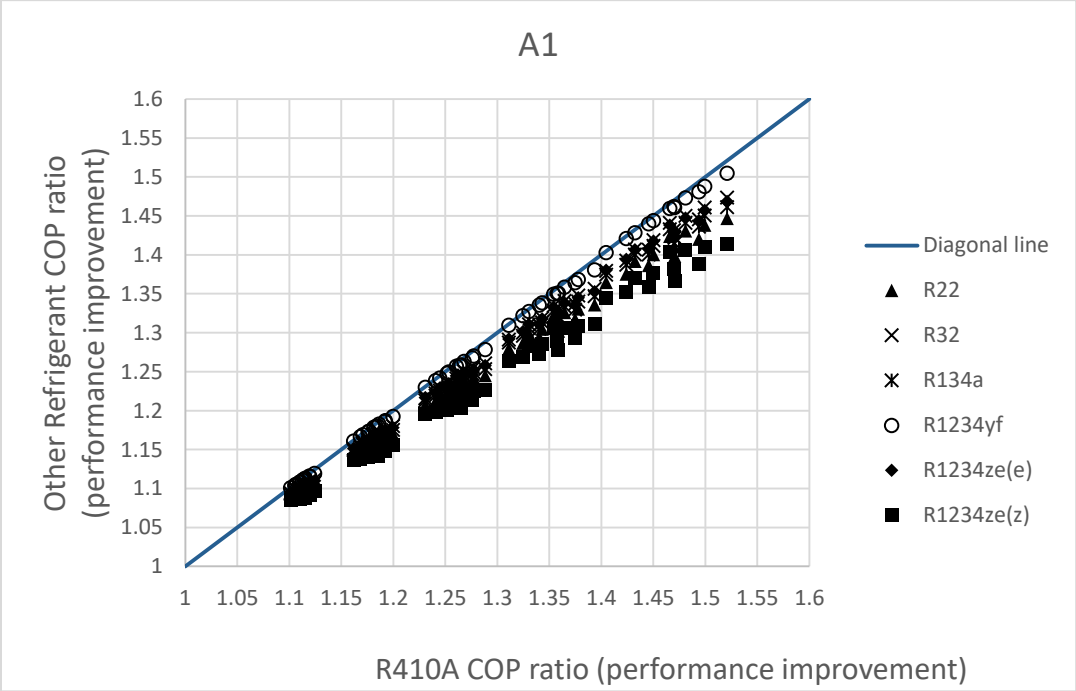

Figure 247 Reconfigured system A1 performance improvement comparison between different refrigerants

Figure 248 shows the performance of improvement with reconfigured system A2 (external evaporative cooling) over the baseline system. This figure indicates that the performance improvement is similar for the six refrigerant, but almost all the data is under the diagonal line, meaning R-410A still has the highest benefit of this modification and the ranking is the same as reconfigured system A1---R410A> R1234yf> R1234ze(e)> R32> R134a> R22> R1234ze(z). The

details of COP and COP ratios under different conditions for all seven refrigerants are shown in Appendix C.

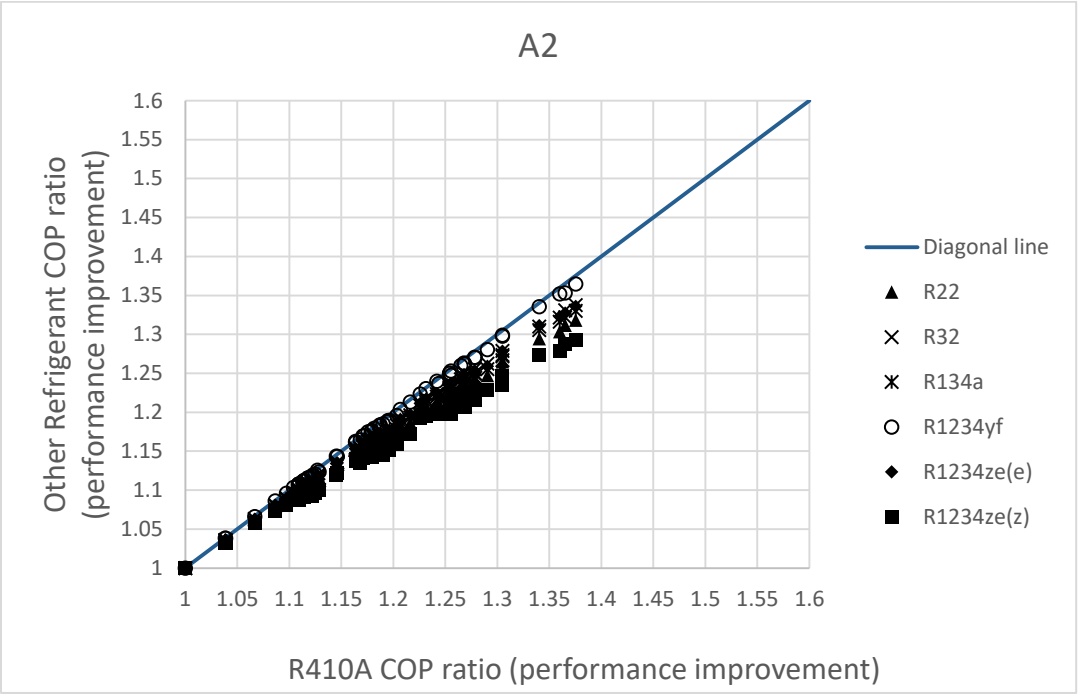

Figure 248 Reconfigured system A2 performance improvement comparison between different refrigerants

Figure 249 shows the performance of improvement with reconfigured system B1 (HRV) over the baseline system. This figure indicates that the performance improvement is quite similar for the six refrigerant, from 5% to 25% under the typical conditions. The details of COP and COP ratios under different conditions for all seven refrigerants are shown in Appendix C.

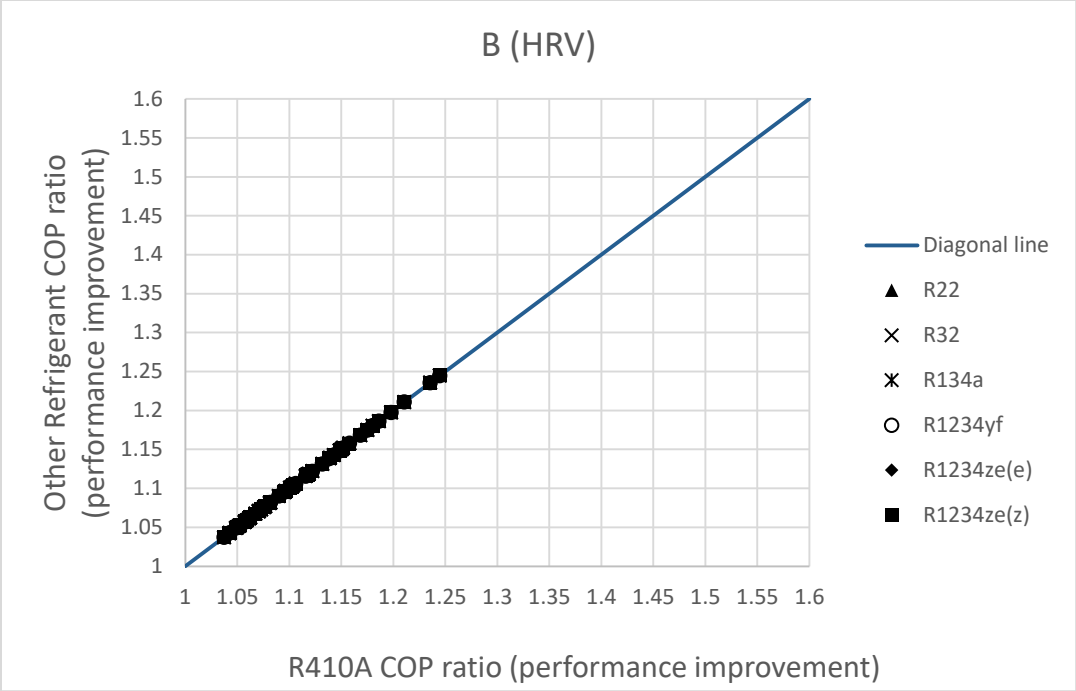

Figure 249 Reconfigured system B1 performance improvement comparison between different refrigerants

Figure 250 shows the performance of improvement with reconfigured system B2 (ERV) over the baseline system. This figure indicates that the performance improvement is quite similar for the six refrigerant, from 8% and reach up to 205% under the typical conditions. The details of COP and COP ratios under different conditions for all seven refrigerants are shown in Appendix C.

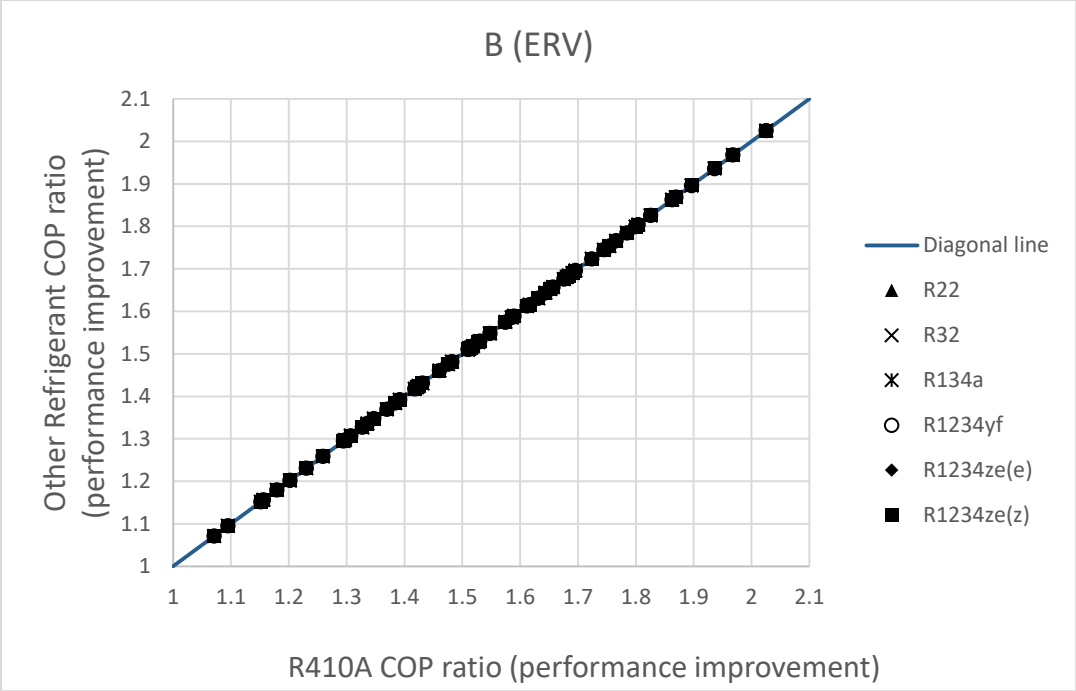

Figure 250 Reconfigured system B2 performance improvement comparison between different refrigerants

Figure 251, 252, 253 and 254 show the performance of improvement with reconfigured system C (condensing refrigerant subcooling) over the baseline system when heat exchanger effectiveness is 20%, 50%, 80% and 100%, respectively. These four figures indicate that the performance improvement is quite similar for the six refrigerant, and negligible. The highest improvement is only 1%, 2.5%, 4%, and 5% when heat exchanger effectiveness is 20%, 50%, 80% and 100%. The details of COP and COP ratios under different conditions for all seven refrigerants are shown in Appendix B.

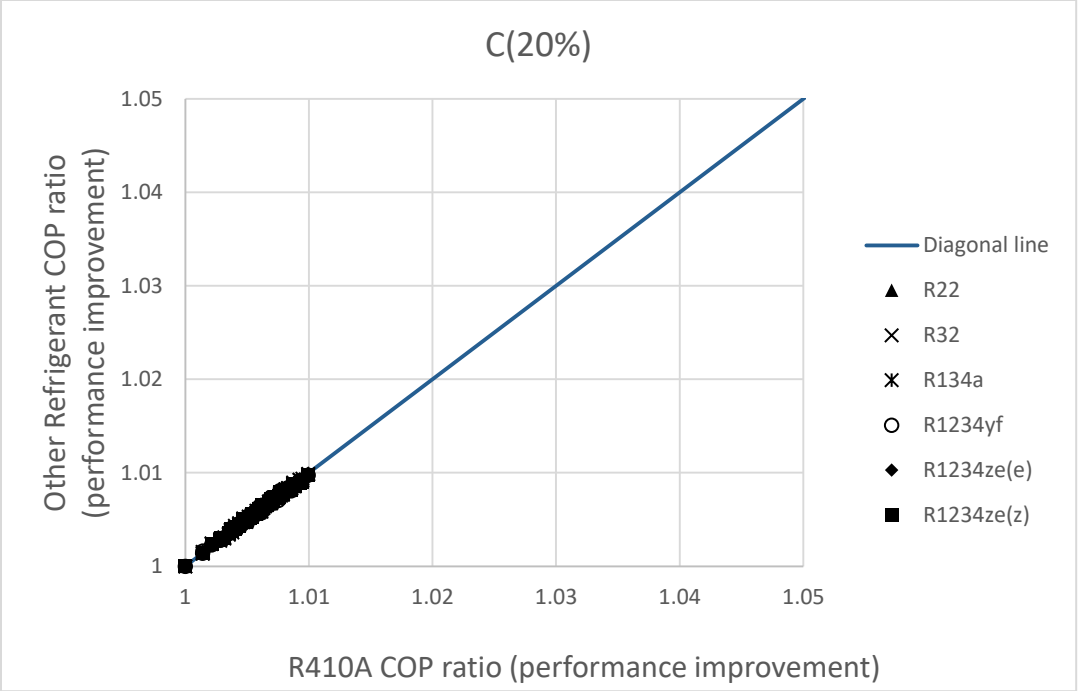

Figure 251 Reconfigured system C performance improvement comparison between different refrigerants when heat exchanger effectiveness is 20%

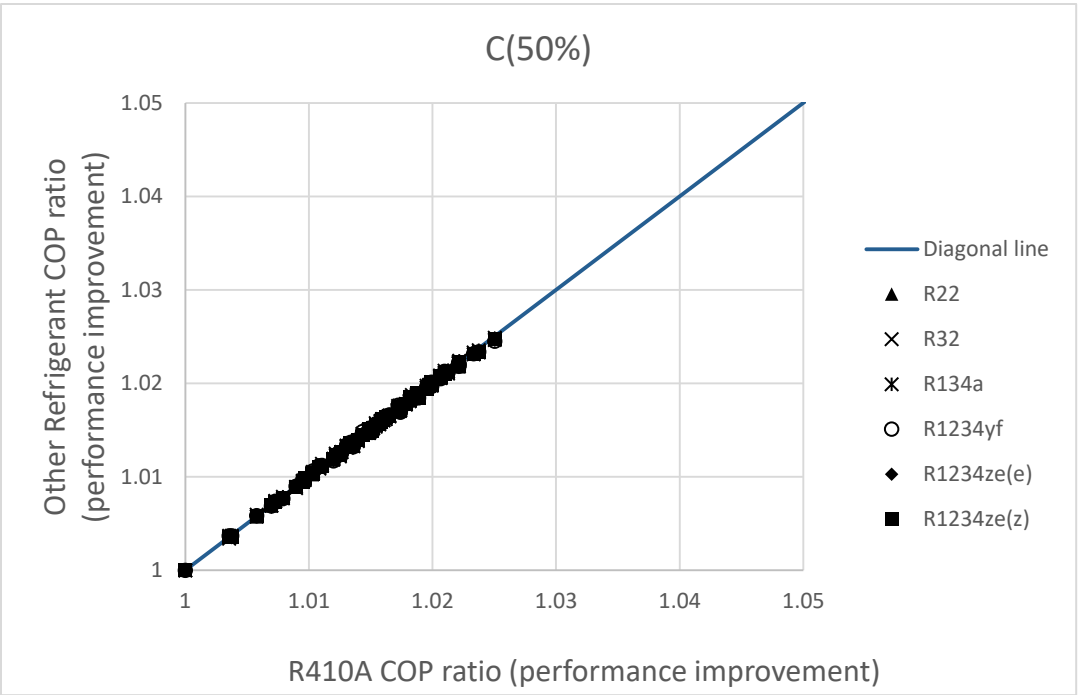

Figure 252 Reconfigured system C performance improvement comparison between different refrigerants when heat exchanger effectiveness is 50%

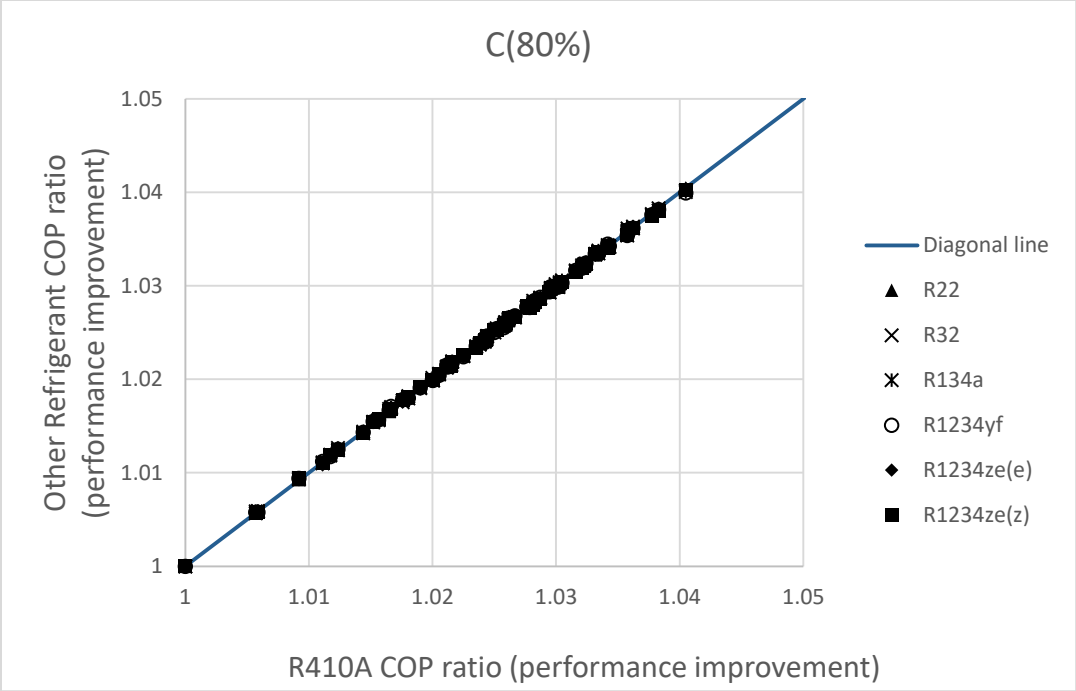

Figure 253 Reconfigured system C performance improvement comparison between different refrigerants when heat exchanger effectiveness is 80%

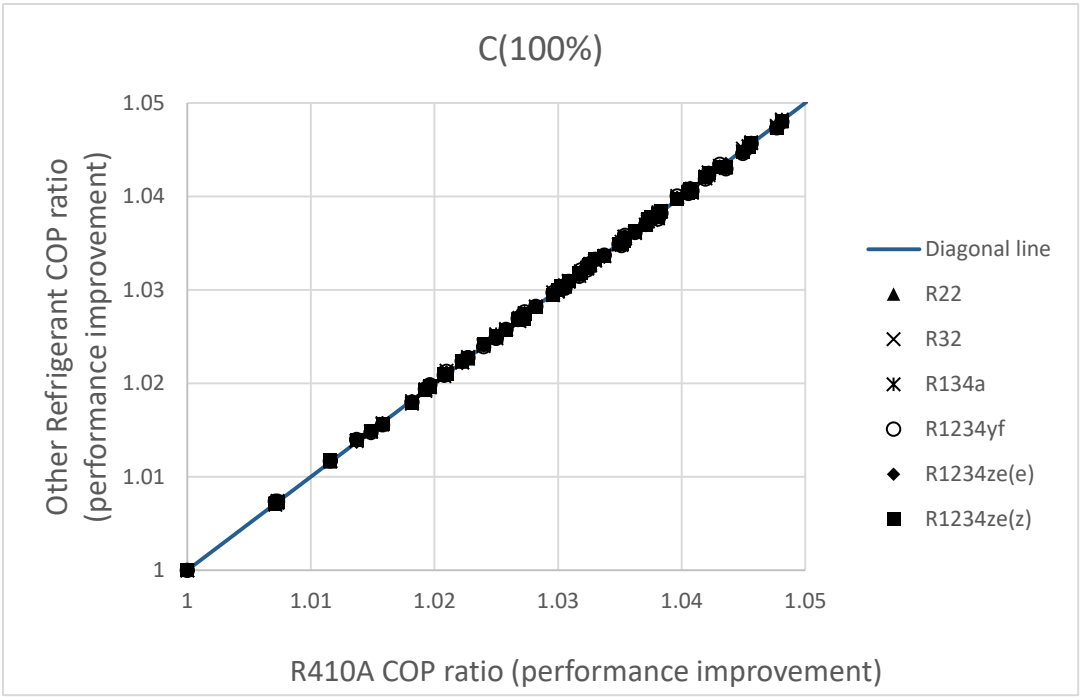

Figure 254 Reconfigured system C performance improvement comparison between different refrigerants when heat exchanger effectiveness is 100%

Figure 255, 256, 257 and 258 show the performance of improvement with reconfigured system D (internal heat exchanger) over the baseline system when internal heat exchanger effectiveness is 20%, 50%, 80% and 100%, respectively. These four figures indicate that several refrigerants have better improvement than R-410A while some others have worse improvement than R-410A, the ranking of performance improvement is shown as follows, R1234yf>R1234ze(e)> R134a>R410A>R22>R1234ze(z)>R32. The highest improvement is 14%, 34%, 46%, and 59% when heat exchanger effectiveness is 20%, 50%, 80% and 100%. The details of COP and COP ratios under different conditions for all seven refrigerants are shown in Appendix B.

Figure 255 Reconfigured system D performance improvement comparison between different refrigerants when heat exchanger effectiveness is 20%

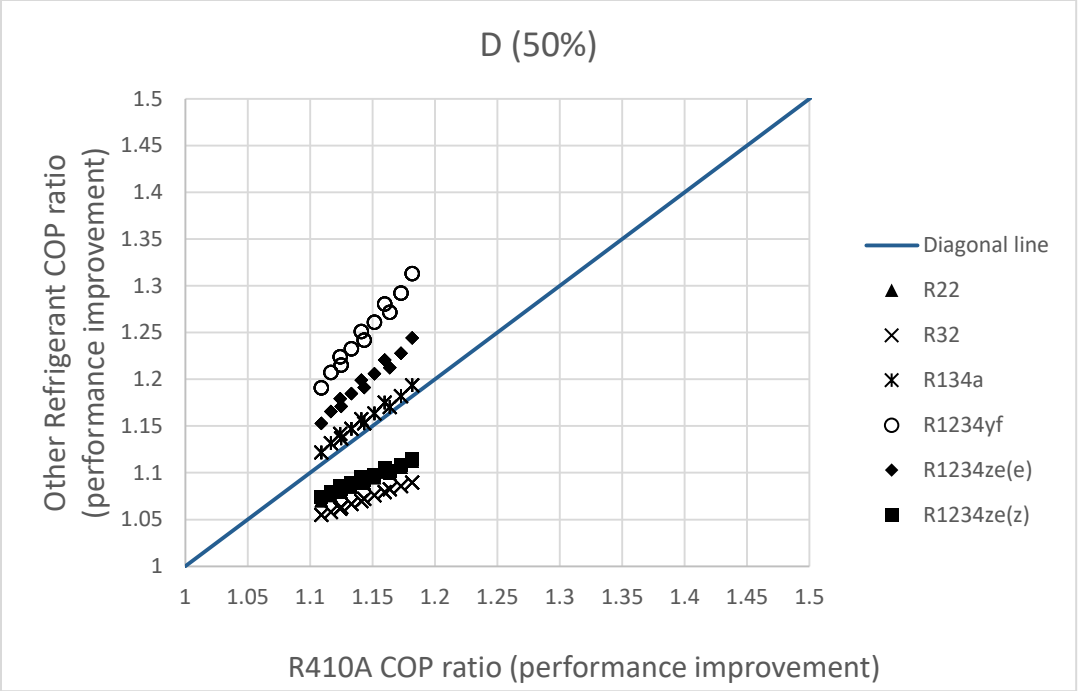

Figure 256 Reconfigured system D performance improvement comparison between different refrigerants when heat exchanger effectiveness is 50%

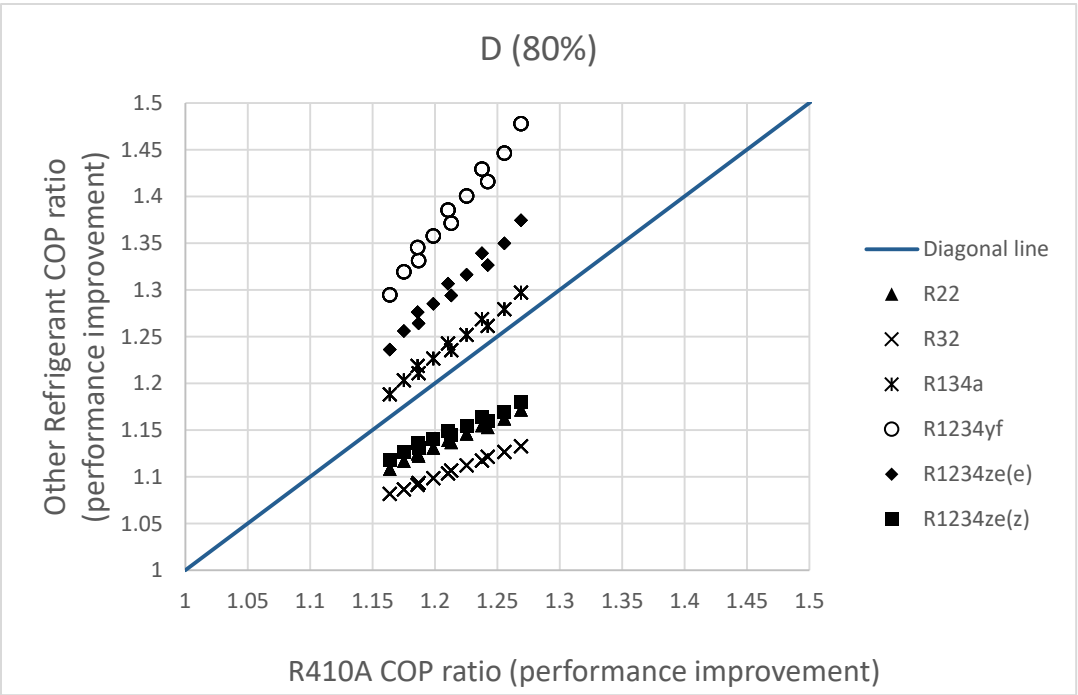

Figure 257 Reconfigured system D performance improvement comparison between different refrigerants when heat exchanger effectiveness is 80%

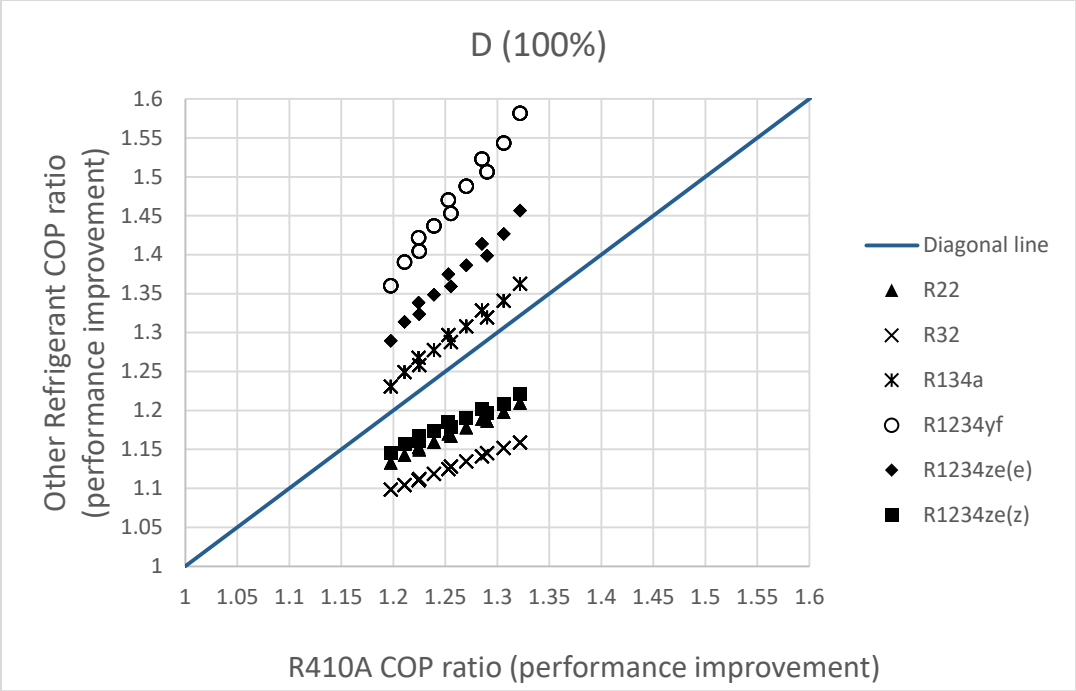

Figure 258 Reconfigured system D performance improvement comparison between different refrigerants when heat exchanger effectiveness is 100%

10. ECONOMIC ANALYSIS

Owning and operating cost information for the HVAC system are parts of the investment plan of a facility and this information can be used for preparing annual budgets, managing assets, and selecting options. A properly engineered system should be economical, however, it is difficult to assess because of the complexities surrounding effective money management and the inherent difficulty of predicting future operating along with maintenance expenses. Complex tax structures and the time value of money can affect the final engineering decision as well. In another word, it does not imply the use of either the cheapest or the most expensive system; instead, it demands intelligent analysis of financial objectives and the owner's requirements.

10.1 Engineering Economics

Codes and standards, equipment efficiencies, energy modeling, commissioning, energy-conservation incentive programs, and lifecycle cost analysis are the major components for determining the economics of HVAC systems. Thus, it is necessary for a mechanical engineer to consider when specifying HVAC systems into new or existing buildings, with a focus on the economic analysis provided to the client.

The economics of HVAC systems include capital costs and operating costs. The capital cost is related to the manufacture and the choice of the product/equipment. The operating cost comprises energy consumption, maintenance and repair, recommissioning, replacement, and asset preservation. Lifecycle analysis factors in escalation and time cost of money over the study's period.

Large amounts of articles and books have been written to guide engineers through the mathematical representation of HVAC economic analysis. Before we dig into the indirect cost

impacts, it is necessary to review some of the basic terminology of the economic engineering process.

$$\text{Lifecycle cost (LCC)} = \text{first cost} + \text{maintenance and repair} + \text{energy} + \text{water} + \text{replacement} - \text{salvage value} \quad (141)$$

Often, engineers are asked to determine the best option between one or more HVAC system options, which is also the focus of this study. There are several ways to represent the results when comparing the lifecycle costs of two or more options. Simple payback, net savings, the savings-to-investment ratio (SIR), the adjusted internal rate of return (IROR), and discounted payback are all methods to measure an HVAC option's economic performance over time. Simple payback and lifecycle payback are the two common methods used in HVAC analysis and they are defined as,

$$\text{Simple payback (years)} = (\text{first cost difference}) \div (\text{annual operating savings cost difference}) \quad (142)$$

$$\text{Lifecycle payback (years)} = (\text{first cost difference}) \div (\text{annual operating savings cost difference}) \quad (143)$$

Net savings, the savings-to-investment ratio and the adjusted internal rate of return are used often as well and they are defined as,

$$\text{Net savings (\$)} = \text{HVAC base option LCC} - \text{HVAC option 1 LCC} \quad (144)$$

$$\text{SIR} = (\text{option 1 net savings}) \div (\text{option 1 first cost increase}) \quad (145)$$

$$\text{Adjusted IROR} = (\text{average annual operating cost savings})^{**} \div (\text{initial investment}) \quad (146)$$

Of special note, * does not factor in the time cost of money or maintenance/repair, replacement, or salvage value while ** accounts for time cost of money and maintenance/repair, replacement, and salvage value

10.2 COP Analysis

10.2.1 Different City System Performance Comparison in the Same Climate Zone

Warm-season temperature and humidity conditions are based on annual percentiles of 0.4, 1.0 and 2.0. Cold-season conditions are based on annual percentiles of 99.6 and 99.0. The use of annual percentiles to define design conditions ensures that they represent the same probability of occurrence in any climate, regardless of the seasonal distribution of extreme temperature and humidity.

For example, 99.6% winter design dry-bulb temperature means that the outdoor temperature that your locations stay above the design temperature for 99.6% of the time. 0.4% summer design dry-bulb temperature and coincident dry-bulb temperature mean that the summer temperatures in a year for that location will exceed this design value about 0.4% of the time.

All the COP calculations are based on the section 6.3 model, a simplified vapor-compression refrigeration model, where COP is only related to outdoor air temperature. Since the three percentile design temperatures are collected from ASHRAE fundamental book, the design HVAC COPs (resiliency) are obtained. A comprehensive analysis of resiliency COPs under the aforementioned three percentile design temperatures for 53 cities are listed in Table 52. Furthermore, the different cities in the same climate zone are compared. Since the highest temperatures for the 53 cities are also collected in section 6.1, the highest-temperature-corresponding-COP for the 53 cities in 18 climate zones are shown in Table 53.

Table 52 Design HVAC COP (resiliency) under three different percentiles

		Design Temperature			Design HVAC COP (resiliency)			Zone Average resilient COP			City and average % diff		
		0.40%	1%	2%	0.40%	1%	2%	0.40%	1%	2%	0.40%	1%	2%
1A	Miami	91.9	90.8	89.8	2.713	2.77	2.822	2.713	2.77	2.822	0.00%	0.00%	0.00%
	Key west							2.713	2.77	2.822			
2A	Orlando	93.8	92.4	91.1	2.613	2.687	2.755	2.578	2.667	2.748	1.34%	0.74%	0.24%
	New Orleans	93.1	91.6	90.3	2.65	2.729	2.796	2.578	2.667	2.748	2.78%	2.31%	1.75%
	Mobile	94.1	92.2	90.5	2.597	2.697	2.786	2.578	2.667	2.748	0.73%	1.13%	1.37%
	Houston	96.8	94.9	93	2.45	2.554	2.655	2.578	2.667	2.748	-4.97%	-4.24%	-3.38%
2B	Phoenix	110.3	108.3	106.4	1.539	1.701	1.845	1.721	1.877	2.019	-10.54%	-9.37%	-8.65%
	Tucson	105.8	103.6	101.4	1.888	2.039	2.181	1.721	1.877	2.019	9.72%	8.64%	7.99%
3Aw	Dallas	101.4	99.1	96.9	2.181	2.319	2.445	2.23	2.38	2.516	-2.20%	-2.55%	-2.84%
	Little Rock	99.8	97	94.3	2.278	2.439	2.586	2.23	2.38	2.516	2.16%	2.49%	2.79%
	Oklahoma City							2.23	2.38	2.516			
3Ae	Charlotte	94.2	91.8	89.6	2.592	2.718	2.833	2.56	2.676	2.776	1.26%	1.57%	2.06%
	Atlanta	93.4	91.3	89.8	2.634	2.744	2.822	2.56	2.676	2.776	2.92%	2.54%	1.69%
	Montgomery	96.8	94.7	92.7	2.45	2.565	2.671	2.56	2.676	2.776	-4.27%	-4.16%	-3.77%
3Be	Lubbock	99.4	97.1	94.7	2.302	2.434	2.565	2.179	2.327	2.461	5.65%	4.58%	4.21%
	Wichita Falls	103.8	101.2	98.6	2.026	2.193	2.348	2.179	2.327	2.461	-7.00%	-5.75%	-4.59%
	Midland	101.1	98.6	96.5	2.199	2.348	2.467	2.179	2.327	2.461	0.95%	0.91%	0.22%
3Bw	Bakersfield							2.199	2.337	2.461			
	EL Paso	101.1	98.8	96.6	2.199	2.337	2.461	2.199	2.337	2.461	0.00%	0.00%	0.00%
3Blv	Las Vegas												
3Bn	Sacramento	100.5	97.6	94.6	2.236	2.405	2.57	2.248	2.397	2.565	-0.54%	0.35%	0.21%
	Stockton	100.1	97.9	94.8	2.26	2.388	2.56	2.248	2.397	2.565	0.53%	-0.36%	-0.21%
3C	Los Angeles	83.8	80.4	77.8	3.141	3.334	3.493	2.937	3.124	3.29	6.92%	6.72%	6.17%
	Long Beach	91.4	87.8	84.5	2.739	2.927	3.102	2.937	3.124	3.29	-6.74%	-6.32%	-5.71%
4A	Richmond	95.1	92.7	90.1	2.543	2.671	2.807	2.488	2.632	2.769	2.23%	1.48%	1.35%
	Nashville	94.6	92.3	90.2	2.57	2.692	2.802	2.488	2.632	2.769	3.32%	2.28%	1.16%
	Wichita	101.1	97.8	94.4	2.199	2.394	2.581	2.488	2.632	2.769	-11.60%	-9.04%	-6.80%
	St. Louis	96.2	93.5	91.1	2.483	2.629	2.755	2.488	2.632	2.769	-0.18%	-0.12%	-0.53%
	New York							2.488	2.632	2.769			
	Philadelphia	93.6	90.9	88.3	2.624	2.765	2.901	2.488	2.632	2.769	5.46%	5.06%	4.74%
	Washington DC							2.488	2.632	2.769			
4B	Albuquerque	95.5	93.3	91	2.522	2.64	2.76	2.842	3.045	3.243	-11.26%	-13.31%	-14.89%

Table 52 continued

		Design Temperature			Design HVAC COP (resiliency)			Zone Average resilient COP			City and average % diff		
		0.40%	1%	2%	0.40%	1%	2%	0.40%	1%	2%	0.40%	1%	2%
	Amarillo	98.6	95.8	93.2	2.348	2.505	2.645	2.842	3.045	3.243	-17.36%	-17.72%	-18.45%
4C	Portland	91.2	87.1	83.4	2.75	2.963	3.163	2.842	3.045	3.243	-3.23%	-2.67%	-2.48%
	Seattle	85.3	81.6	78.2	3.059	3.264	3.468	2.842	3.045	3.243	7.66%	7.20%	6.93%
	Eugene	91.8	88	84.3	2.718	2.916	3.113	2.842	3.045	3.243	-4.34%	-4.22%	-4.00%
5A	Omaha	94	90.9	88	2.602	2.765	2.916	2.724	2.872	3.018	-4.45%	-3.73%	-3.39%
	Chicago	91.9	89.4	86.6	2.713	2.843	2.99	2.724	2.872	3.018	-0.38%	-1.01%	-0.95%
	Pittsburgh	89.2	86.6	84.3	2.854	2.99	3.113	2.724	2.872	3.018	4.78%	4.09%	3.14%
	Des Moines	92.8	89.7	87.1	2.666	2.828	2.963	2.724	2.872	3.018	-2.12%	-1.56%	-1.82%
	Boston	90.6	87.6	84.3	2.781	2.937	3.113	2.724	2.872	3.018	2.10%	2.26%	3.14%
5B	Denver	94.8	92.2	89.5	2.56	2.697	2.838	2.461	2.608	2.75	3.99%	3.44%	3.22%
	Boise	98.6	95.7	92.8	2.348	2.511	2.666	2.461	2.608	2.75	-4.59%	-3.72%	-3.05%
	Reno	96.4	93.8	91.3	2.472	2.613	2.744	2.461	2.608	2.75	0.45%	0.20%	-0.19%
6A	Minneapolis	90.8	87.8	84.9	2.77	2.927	3.081	2.752	2.911	3.062	0.66%	0.54%	0.62%
	Milwaukee							2.752	2.911	3.062			
	Sioux Falls	91.5	88.4	85.6	2.734	2.895	3.043	2.752	2.911	3.062	-0.66%	-0.54%	-0.61%
6B	Helena							2.721	2.861	3.011			
	Cheyenne	89.5	86.9	84	2.838	2.974	3.13	2.721	2.861	3.011	4.31%	3.93%	3.94%
	Casper	94	91.2	88.4	2.602	2.75	2.895	2.721	2.861	3.011	-4.36%	-3.91%	-3.84%
7A	Fargo							2.747	2.924	3.089			
	Bismarck	93.1	89.4	86.1	2.65	2.843	3.016	2.747	2.924	3.089	-3.53%	-2.76%	-2.34%
	St. Cloud	89.4	86.3	83.4	2.843	3.006	3.163	2.747	2.924	3.089	3.50%	2.79%	2.39%

Table 53 Highest-temperature-corresponding-COP comparison

		Highest Temperature	City data	Average	% difference
1A	Miami	84	3.130	3.116	0.44%
	Key west	84.5	3.102	3.116	-0.44%
2A	Orlando	83	3.185	3.171	0.42%
	New Orleans	83	3.185	3.171	0.42%
	Mobile	82	3.241	3.171	2.20%
	Houston	85	3.075	3.171	-3.04%
2B	Phoenix	94.5	2.576	2.759	-6.65%
	Tucson	87.5	2.942	2.759	6.65%
3Aw	Dallas	86.5	2.995	3.122	-4.05%
	Little Rock	83	3.185	3.122	2.03%

Table 53 continued

		Highest Temperature	City data	Average	% difference
	Oklahoma City	83	3.185	3.122	2.03%
3Ae	Charlotte	78.5	3.449	3.349	2.98%
	Atlanta	80	3.358	3.349	0.25%
	Montgomery	82	3.241	3.349	-3.23%
3Be	Lubbock	80.5	3.328	3.214	3.54%
	Wichita Falls	84.5	3.102	3.214	-3.49%
	Midland	82.5	3.213	3.214	-0.05%
3Bw	Bakersfield	84	3.130	3.157	-0.88%
	EL Paso	83	3.185	3.157	0.88%
3Blv	Las Vegas	92.5	2.682	2.682	0.00%
3Bn	Sacramento	75	3.679	3.628	1.40%
	Stockton	76.5	3.577	3.628	-1.40%
3C	Los Angeles	74	3.749	3.732	0.48%
	Long Beach	74.5	3.714	3.732	-0.48%
4A	Richmond	79.5	3.388	3.411	-0.68%
	Nashville	79.5	3.388	3.411	-0.68%
	Wichita	81	3.299	3.411	-3.29%
	St. Louis	80	3.358	3.411	-1.56%
	New York	76.5	3.577	3.411	4.87%
	Philadelphia	78	3.480	3.411	2.03%
	Washington DC	79.5	3.388	3.411	-0.68%
4B	Albuquerque	78	3.480	3.480	0.00%
	Amarillo	78	3.480	3.480	0.00%
4C	Portland	69	4.143	4.277	-3.15%
	Seattle	66.5	4.368	4.277	2.13%
	Eugene	67	4.321	4.277	1.03%
5A	Omaha	76.5	3.577	3.682	-2.84%
	Chicago	76	3.611	3.682	-1.94%
	Pittsburgh	73	3.822	3.682	3.81%
	Des Moines	76.5	3.577	3.682	-2.84%
	Boston	73	3.822	3.682	3.81%
5B	Denver	73.5	3.786	3.703	2.23%
	Boise	75.5	3.644	3.703	-1.58%
	Reno	75	3.679	3.703	-0.65%
6A	Minneapolis	73.5	3.786	3.835	-1.30%
	Milwaukee	72	3.898	3.835	1.64%
	Sioux Falls	73	3.822	3.835	-0.34%
6B	Helena	70	4.058	4.058	-0.01%
	Cheyenne	69.5	4.100	4.058	1.03%

Table 53 continued

		Highest Temperature	City data	Average	% difference
	Casper	70.5	4.017	4.058	-1.02%
7A	Fargo	71.5	3.937	3.991	-1.34%
	Bismarck	71	3.977	3.991	-0.35%
	St. Cloud	70	4.058	3.991	1.69%

10.2.2 Three COPs Comparison

Three important COPs are introduced in this section,

Weighted COP during cooling season--- economic (sustainability)

Design temperature corresponding COP----HVAC design COP (resiliency)

Highest monthly temperature corresponding COP--- the value between the above two COPs

The three different COPs mentioned above are based on three different aspects. The first one is the weighted COP during the whole cooling season, and it is usually used for economic analysis and sustainability study. The weighted COP is calculated based on the monthly COP (derived from section 6.3) and weighting factors (derived from section 6.2) The monthly average temperature for each climate zone used for calculating COP is directly used in section 6.1. This COP is the highest value among these three COPs since the real outdoor temperature is below the highest temperature and design temperature. The second COP is the design HVAC COP (resiliency), which is the performance corresponding to three percentile design temperatures, and it is the lowest among the three types of COP. Of special importance, the highest temperature is higher than real outdoor temperature but lower than design temperature. Thus highest-temperature corresponding-COP is between sustainability COP and resiliency COP. A comparison between the three COP mentions above is made in Table 54 and Figure 259.

Table 54 Three COP comparison for 18 climate zones

CZ	Economic (sustainability)	Design HVAC COP (resiliency)			
CZ	COP weighted dry	0.40%	1%	2%	Highest temperature COP
1A	3.49	2.71	2.77	2.82	3.12
2A	3.76	2.58	2.67	2.75	3.17
2B	3.48	1.72	1.88	2.02	2.76
3Aw	3.72	2.23	2.38	2.52	3.12
3Ae	3.91	2.56	2.68	2.78	3.35
3Be	3.80	2.18	2.33	2.46	3.21
3Bw	3.77	2.20	2.34	2.46	3.16
3Blv	3.39				2.68
3Bn	4.16	2.25	2.40	2.56	3.63
3C	4.34	2.94	3.12	3.29	3.73
4A	3.93	2.49	2.63	2.77	3.41
4B	3.98	2.84	3.04	3.24	3.48
4C	4.73	2.84	3.04	3.24	4.28
5A	4.20	2.72	2.87	3.02	3.68
5B	4.26	2.46	2.61	2.75	3.70
6A	4.32	2.75	2.91	3.06	3.84
6B	4.52	2.72	2.86	3.01	4.06
7A	4.44	2.75	2.92	3.09	3.99

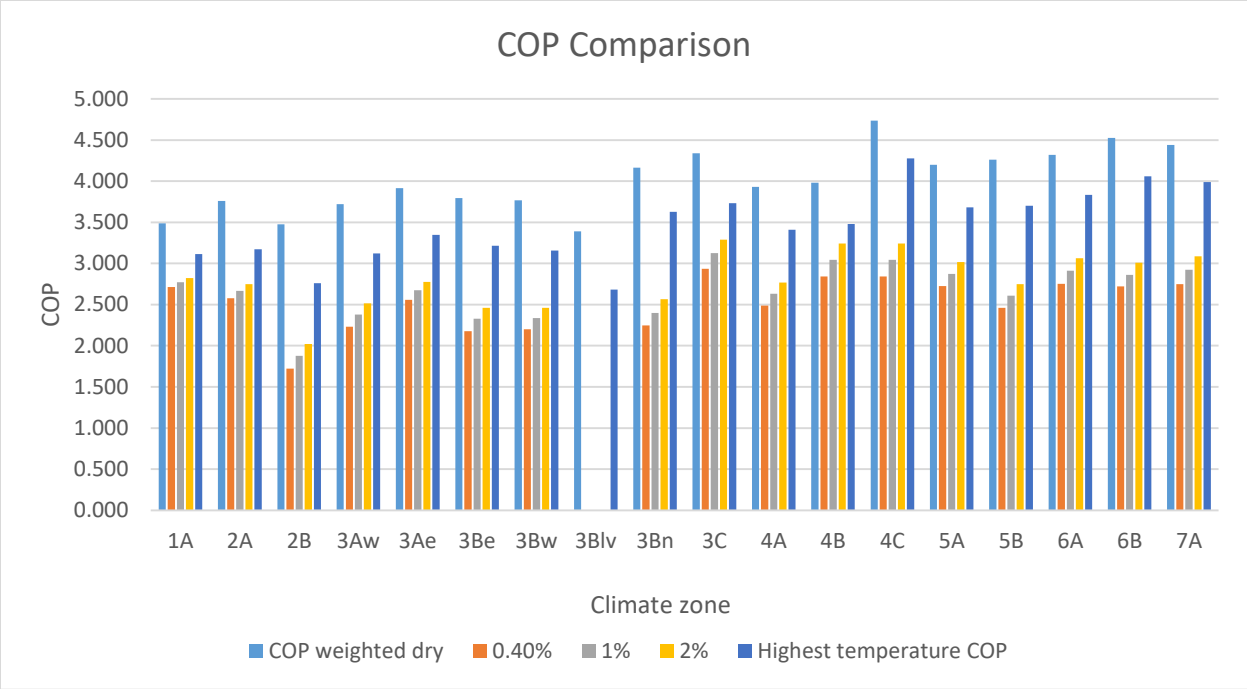

Figure 259 Three COP comparison for 18 climate zones

10.3 Economic Analysis for a Case Study

Energy cost for a whole cooling season is defined as,

$$\text{Energy}_{\text{kw hr/season}}=\frac{\frac{24\ hr}{day}*q_{design,cooling}*CDD}{\frac{1000W}{kW}*(T0-Ti)*SEER} \quad (147)$$

Where

$$q_{design,cooling}=A_w(T_o-T_i)/R_w+A_c(T_o-T_i)/R_c \quad (148)$$

R values of wall and ceiling are assumed as 11 and 25 hr ft^2°F/Btu, respectively. T_o is outside design term and T_i is inside temperature. Length, width, and height of this building is assumed to be 80ft, 40ft and 10 ft, respectively. SEER is COP/0.293, cooling degree-day values

are based on 50 °F and directly used from section 6.2. The electricity cost in this section is $0.2/kw hr.

Thus, a comprehensive analysis is listed in Table 55 and Figure 260 along with Figure 261. Climate zone 1A has the highest seasonal energy/operating cost, followed by 2B and 3Blv. Climate zones with higher temperatures and longer cooling season length/larger cooling degree days always have higher seasonal energy/operating costs.

Table 55 Seasonal operating cost for 18 climate zones

CZ	COP weighted dry	SEER	CDD (50)	Seasonal Kw hr	Operating cost ($)	Seasonal Kw hr/ft^2	Operating cost ($)/ft^2
1A	3.49	11.91	10027	6995.8	1399.2	2.19	0.44
2A	3.76	12.83	6973	4514.4	902.9	1.41	0.28
2B	3.48	11.86	8331	5834.7	1166.9	1.82	0.36
3Aw	3.72	12.69	5616	3675.6	735.1	1.15	0.23
3Ae	3.91	13.36	5042	3136.1	627.2	0.98	0.20
3Be	3.80	12.96	5145	3299.2	659.8	1.03	0.21
3Bw	3.77	12.86	5718	3693.0	738.6	1.15	0.23
3Blv	3.39	11.57	7219	5185.9	1037.2	1.62	0.32
3Bn	4.16	14.21	4478	2617.4	523.5	0.82	0.16
3C	4.34	14.81	5525	3099.7	619.9	0.97	0.19
4A	3.93	13.42	4023	2490.8	498.2	0.78	0.16
4B	3.98	13.59	3901	2384.2	476.8	0.75	0.15
4C	4.73	16.16	2176	1118.6	223.7	0.35	0.07
5A	4.20	14.33	3065	1776.8	355.4	0.56	0.11
5B	4.26	14.54	2851	1629.0	325.8	0.51	0.10
6A	4.32	14.74	2502	1410.7	282.1	0.44	0.09
6B	4.52	15.44	1853	996.9	199.4	0.31	0.06
7A	4.44	15.16	2113	1158.4	231.7	0.36	0.07

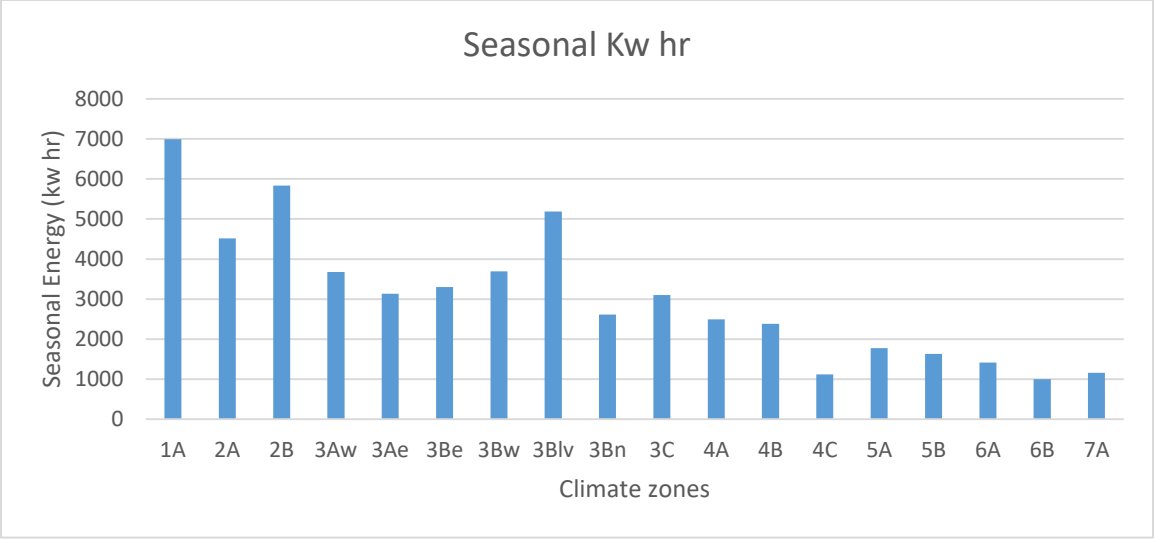

Figure 260 Season energy (kW ·hr) for 18 climate zones

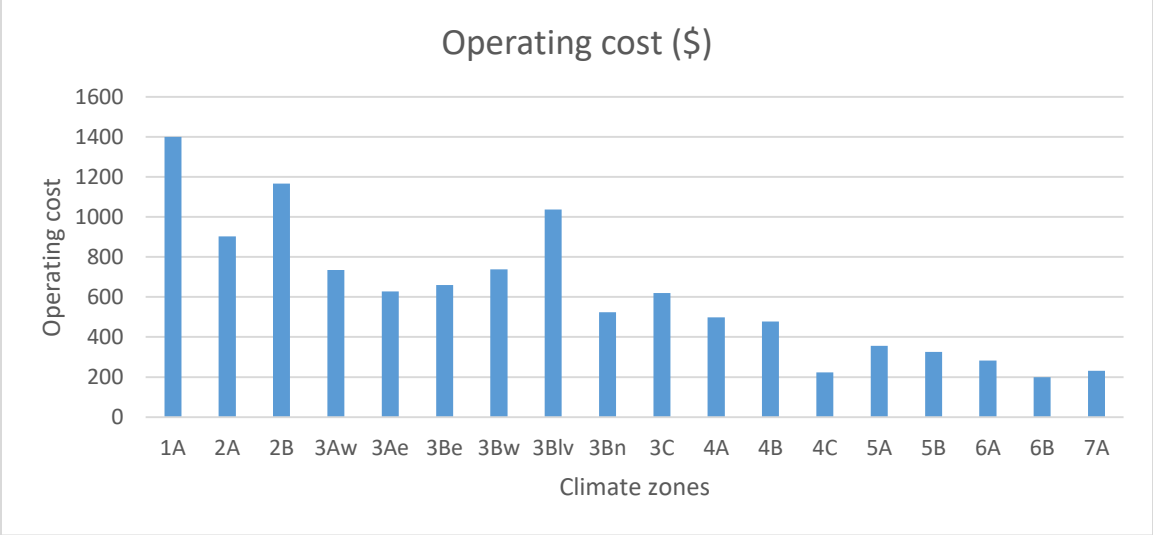

Figure 261 Seasonal operating cost for 18 climate zones

11. CONCLUSION

Searching for replacements for R-410A is ongoing and paramount, primarily based on Ozone Depleting Potential (ODP), GWP, flammability, toxicity, and safety issues. The study reported herein focuses on this by search by performing two important tasks that are necessary for identifying possible replacement refrigerants. The first task performed is to investigate more efficient modified cycles by determining performance improvements (COP ratios) for these cycles, which is important because most replacement refrigerants compared to R-410A produce reduced cycle performances. The second task is to develop a comprehensive climate zone model so that one can evaluate and compare modified cycle performances for the full range of a cooling-season weather conditions found throughout the U.S, which is a necessary step because cycle performances are dependent on outdoor temperatures and humidities.

The modified cycles evaluated in this study were all created by reconfiguring a conventional vapor-compression cycle with additional components that increase cycle energy performances. The first set of modifications investigated are based on installing evaporative cooling at the condenser air inlet with the supply water source being either external or internal, which in the latter case is supplied by the evaporator condensate. The second set of modifications investigated are based on installing HRV or ERV units at the evaporator inlet, which is a variation of DOAS (dedicated outdoor air system) technology. The final two modifications both cool the refrigerant exiting the condenser and entering the evaporator by either using evaporator condensate water or by transferring energy to the refrigerant exiting the evaporator and entering the compressor with the aid of an internal heat exchanger, which is commonly called a liquid-line and suction-line heat exchanger.

The energy performances of the six aforementioned refrigeration systems, based on modifications to the conventional vapor-compression cycle, which was also used herein as the baseline case, were investigated and compared by simulating each system with five potential replacement refrigerants, namely R-134a, R-32, R-1234yf, R-1234ze (z) and R-1234ze (e), along with the conventional and baseline refrigerant R-410A.

To fully evaluate cycle modifications and replacement refrigerants in support of the R-410A phase-out, the investigation must be performed for not only typical outdoor temperature/ humidity conditions but also for variable real-world weather conditions that occur over large U.S. geographical regions, which can be divided into representative climate zones. Therefore, an important and necessary task reported herein was to develop climate zone models that correlated dry-bulb temperatures, relative humidities, and wet-bulb temperatures to geography and time of year. Once developed, these models were used to determine cooling degree-days and cycle performance weighting factors, based on climate data for the time of year (month/day) for 53 major cities, representing all climate zones all across the U.S., which maximizes the usefulness of the study results. The final step to determine the reconfiguration effectiveness for any modified cycle with any phase-out replacement refrigerant at any location is to merge the two sets of models, namely the climate zone models and the refrigeration cycle models, and then to use them to perform a comprehensive analysis over the cooling seasons, where lengths in days vary with each climate zone.

Prior to evaluating the modified cycles at real-world, climate-zone conditions for the full cooling season, they were evaluated and compared at specific outdoor temperatures and relative humidities for the aforementioned reference refrigerant R-410A and the replacement. This modeling step is important because it provides insight into the behavior characteristics of the

modified cycles, while forming the basis for the cycle models by correlating performance with outdoor conditions and other parameters. These evaluations and comparisons were performed for outdoor air temperatures ranging from 26.7 to 35 ℃ (80 to 95℉) and relative humidities ranging from 40% to 80% for assumed evaporator exit air temperatures of 7.2, 10, 12.8℃ (45, 50, 55℉) with a typical compressor efficiency of 80%. The modified cycle that had the highest COP percentage increase of 60% with R-410A was the case of evaporative cooling condenser air with not only external water but also 38% of the water supplied by internal evaporator condensate, which improves sustainability. It was also found that in most humid climate areas (especially when RH is higher than 70%), evaporator condensate water alone is sufficient to precool air to the wet-bulb temperature, which is the lowest condenser inlet air temperature achievable with evaporative cooling. In contrast, dry/moderate humidity regions require some external water to supplement the internal condensate water in order to achieve the 100% evaporative cooling effect. Obviously, any effort to reduce external water is desirable because it reduces operating cost and promotes sustainability.

Modifying the system by using an HRV to precool evaporator air, increase the R-410A COP by as much as 25% for a modest and achievable heat exchanger effectiveness of 60%, depending on the specific outdoor conditions. Furthermore, precooling and pre-dehumidifying the incoming outdoor air entering the evaporator by using an ERV can increase the R-410A COP by as much as 100%. Of special note, modifying the conventional system with an ERV always results in better improvements to COP compared to the use of the HRV; however, the degree of improvement is dependent on outdoor conditions.

The least effective cycle modification is the use of evaporator condensate water to cool the refrigerant exiting the condenser and entering the evaporator with COP percentage increases of

less than 5%, even for high heat exchanger effectivenesses of 80% and 100%. Even though this COP improvement was formed to be small, quantifying this result was worthwhile because HVAC engineers often raise the possibility of using low temperature evaporator condensate to improve COP by cooling the refrigerant entering the evaporator. In contrast, achieve the same effect by using an internal heat exchanger can increase the COP over the baseline system by 32% for an internal heat exchanger effectiveness of 100% with this decreasing to 27% and 18% when the heat exchanger effectiveness drops to 80% and 50%, respectively. As a side note, COP improvements from an internal heat exchanger modification increases with increasing outdoor air temperature and decreases with increasing evaporator outlet air temperature. Thus, an HVAC system reconfigured with an internal heat exchanger is more suitable for hot temperature regions and for those situations that require lower room-supply air temperatures.

The most promising modified cycles were further compared over varying cooling seasons that occur over a large range of geographical locations represented by climate zones models and real-world weather conditions. The two best performing reconfigured systems, namely the external evaporative cooling of condenser inlet air and the ERV unit installation at the evaporator air inlet were shown to improve the system COP performance over a cooling season as much as 63% and 39%, respectively for R-410A. Compared to the conventional cycle, depending on the climate zone, the hot regions that are represented by small climate zone numbers show benefits from the reconfigured systems that are larger than those achievable in the cold regions that are represented by large climate zone numbers. For example, in climate zone 2B (hot and dry), the largest improvements were as much as 50%, again for R-410A.

In addition to using the R-410 as the baseline refrigerant, which in fact was able to quantify cycle modification developments over cooling seasons, the modified systems were also compared

and evaluated for replacement refrigerants. The order of COPs for the seven refrigerants based on the baseline system was R1234ze (z) > R22 > R134a > R1234ze (e) > R32 > R1234yf > R410A, thus R-410 always had the lowest system performance. Similarly, the orders of COPs for the seven refrigerants based on each of the four modifided systems remained constant (the same order as the baseline system) and R-410A still had the lowest system performance for any modified cycle. The COP increases or performance improvements for the different modified cycles vary and are quite different. With the external evaporative cooling modification, with R410A always benefitting the most, followed by the other replacements in this order, namely R410A > R1234yf > R1234ze(e) > R32 > R134a > R22 > R1234ze(z). For the internal evaporative cooling modification, the R410A improvement was still the highest (same as the external case), followed by R1234yf with R1234ze(z) achieving the lowest benefit, which is similar to the otehrs, namely for external water. For the HRV/ERV modifications and the case of using condensate to cool the condenser exiting refrigerant, all of the refrigerants had similar COP increases. For the internal heat exchanger modification case, R1234yf benefits the most from the modification, follows by R1234yf> R1234ze(e)> R134a> R410A> R22> R1234ze(z)> R32.

The above results prove that replacement refrigerants can be used in the phaseout of R-410A without increasing energy consumption, with otherwise could have increased the release of CO2, providing cycle modification are implemented as identified and quantified in this study. Of special importance, the effect using cycle modification to aid the phaseout of R-410A has been investigated and quantified for all climate zones in the U.S. for the full range of possible cooling season that vary with geographical locations.

The major tasks that have been fully or partially completed to date. In addition, significant efforts have gone into developing a methodology for utilizing the model outputs to determine

meaningful comparisons between R-410A and replacement refrigerants. Other efforts have gone into developing a property comparison methodology for identifying promising replacements and then verifying this approved with R-134a and well-known replacements. Major tasks to complete the research effort that are either finished or ongoing are listed below:

- Developed models and simulations for the reconfigured vapor compression cycles.
- Modeled and correlated the climate zone over the cooling seasons.
- Developing a property comparison methodology for identifying promising replacements and then verifying this approved with R-134a and well-known replacements
- For each reconfigured system, investigate how different assumptions influence COP ratios (compressor efficiency, subcooling effect, superheated effect, etc)
- Use 100% outdoor air for the condenser but 100% indoor air for the evaporator
- Use cycle models to evaluate several replacement refrigerants as substitute for R-410A (for different configurations and climate zones)
- Summarize which reconfigured system has the largest COP improvement
- For the cases utilizing external water, evaluate net cost and cost ratio, where net$=$electricity bill (pay)-$water bill (sell) and cost ratio is defined as $\frac{\$ total\ water}{\$\ total\ electricity}$
- Economic analysis for a case study of 18 climate zones in the U.S.

From the result of Dr. Domanski Nature Communication paper, a dilemma of R410A was found as followed. The viable candidates for single component low-GWP alternatives for small AC systems are very limited, especially for refrigerants with volumetric capacities similar to R410A. Fluids with good COP and low toxicity are available, but all are at least slightly flammable. Nonflammable candidates exist among the fluid with low volumetric capacity, but the use of such fluids in small AC systems would require extensive redesign and may result in lower COP. Blends

offer possibilities, and refrigeration industry is actively reducing or eliminating flammability with the trade-off of increased GWP. The thesis will attempt to solve this major problem (Dr. Domanski /NIST R-410A dilemma) of finding nonflammable replacement refrigerants (for R-410A) that can reduce global warming effects. Then quantify the solution efficiency of replacement refrigerants and reconfigured cycle compared to existing R-410A system.

Another motive for this paper is to combine two separate ideas (climate zone models and refrigeration cycle models), one can determine and evaluate reconfiguration effectiveness for any refrigerant and any location at any time, including over a complete cooling season.

REFERENCE

1. Gagge, A.P., A. Fobelets, and L. Berglund, *A standard predictive index of human response to the thermal environment.* ASHRAE Trans.;(United States), 1986. **92**(CONF-8606125-).

2. Domanski, P. A., J. S. Brown, J. Heo, J. Wojtusiak and M. O. McLinden, *A thermodynamic analysis of refrigerants: Performance limits of the vapor compression cycle.* International Journal of Refrigeration, 2014. **38**: p. 71-79.

3. Mclinden, M. O., A. F. Kazakov, J. S. Brown and P. A. Domanski, *A thermodynamic analysis of refrigerants: Possibilities and tradeoffs for Low-GWP refrigerants.* International Journal of Refrigeration, 2014. **38**: p. 80-92.

4. McLinden, M. O., J. S. Brown, R. Brignoli, A. F. Kazakov and P. A. Domanski, *Limited options for low-global-warming-potential refrigerants.* Nature Communications, 2017. **8**: p. 14476.

5. Casvendi, B., U. Calli, and A. Hebpasli. *Improving the Energy Performance of Air-Cooled Chillers with Water-Spray Mist Pre-Cooling: An Application*. in *International Conference "Clima*. 2010.

6. Hajidavalloo, E., *Application of evaporative cooling on the condenser of window-air-conditioner.* Applied Thermal Engineering, 2007. **27**: p. 1937-1943.

7. Faramarzi, R., J. Lutton, and S. Gouw, *Performance comparison of evaporatively-cooled condenser versus air-cooled condenser air conditioners.* ACEEE Summer Study Proceedings, Irvine, CA Southern California Edison, 2010.

8. Goswami, D.Y., G.D. Mathur, and S.M. Kulkarni, *Experimental investigation of performance of a residential air conditioning system with an evaporatively cooled condenser.* Journal of Solar Energy Engineering, 1993(4): p. 206.

9. Wang, T., C. Sheng, and A.A. Nnanna, *Experimental investigation of air conditioning system using evaporative cooling condenser.* Energy and Buildings, 2014. **81**: p. 435-443.

10. Yang, J., K. Chan, X. Wu, X. Yang and H. Zhang, *Performance enhancement of air-cooled chillers with water mist: Experimental and analytical investigation.* Applied Thermal Engineering, 2012. **40**: p. 114-120.

11. Dixit, A.M., A. Desai, and A. Vyas, *IMPROVING EFFICIENCY OF AIR CONDITIONER BY CELLULOSE PAD.*

12. Hajidavalloo, E. and H. Eghtedari, *Performance improvement of air-cooled refrigeration system by using evaporatively cooled air condenser.* international journal of refrigeration, 2010. **33**(5): p. 982-988.

13. Chaktranond, C. and P. Doungsong, *Energy Saving in a Domestic Split-Type Air Conditioner with Evaporative Cooling Systems.* Department of Mechanical Engineering, Faculty of Engineering, Thammasat University, Thailand, 2009.

14. Yu, F.W. and K.T. Chan, *Application of direct evaporative coolers for improving the energy efficiency of air-cooled chillers.* JOURNAL OF SOLAR ENERGY ENGINEERING-TRANSACTIONS OF THE ASME, 2005. **127**(3): p. 430-433.

15. Yu, F. and K. Chan, *Improved condenser design and condenser-fan operation for air-cooled chillers.* Applied Energy, 2006. **83**(6): p. 628-648.

16. Shen, B., M. R. Ally, C. K. Rice and W. G. Craddick, *Direct Evaporative Precooling Model and Analysis*. 2011.

17. Hao, X., C. Zhu, Y. Lin, H. Wang, G. Zhang and Y. Chen, *Optimizing the pad thickness of evaporative air-cooled chiller for maximum energy saving.* Energy and Buildings, 2013. **61**: p. 146-152.

18. Youbi-Idrissi, M., H. Macchi-Tejeda, L. Fournaison and J. Guilpart, *Numerical model of sprayed air cooled condenser coupled to refrigerating system.* Energy conversion and management, 2007. **48**(7): p. 1943-1951.

19. Huan, Z., Y. Shijun, Y. Hongxing and N. Jianlei, *Enhanced performance of air-cooled chillers using evaporative cooling.* Building Services Engineering Research and Technology, 2000. **21**(4): p. 213-217.

20. Yang, J., K. Chan, X. Wu, F. Yu and X. Yang, *An analysis on the energy efficiency of air-cooled chillers with water mist system.* Energy and Buildings, 2012. **55**: p. 273-284.

21. Sarntichartsak, P. and S. Thepa, *Modeling and experimental study on the performance of an inverter air conditioner using R-410A with evaporatively cooled condenser.* Applied Thermal Engineering, 2013. **51**(1): p. 597-610.

22. Li, P., J. Chen, and C. Wang, *Recycling and utilizing the condensed water with decentralized air-conditioning.*

23. Licina, D. and C. Sekhar, *Energy and water conservation from air handling unit condensate in hot and humid climates.* Energy and Buildings, 2012. **45**: p. 257-263.

24. Sawan, R., K. Ghali, and M. Al-Hindi, *Use of condensate drain to pre-cool the inlet air to the condensers: A technique to improve the performance of split air-conditioning units.* HVAC&R Research, 2012. **18**(3): p. 417-431.

25. Besant, R.W. and C.J. Simonson, *Air-to-air energy recovery.* ASHRAE journal, 2000. **42**(5): p. 31.

26. Lazzarin, R.M. and A. Gasparella, *Technical and economical analysis of heat recovery in building ventilation systems.* Applied Thermal Engineering, 1998. **18**(1-2): p. 47-67.

27. Fehrm, M., W. Reiners, and M. Ungemach, *Exhaust air heat recovery in buildings.* International Journal of Refrigeration, 2002. **25**(4): p. 439-449.

28. Zhong, K. and Y. Kang, *Applicability of air-to-air heat recovery ventilators in China.* Applied Thermal Engineering, 2009. **29**(5-6): p. 830-840.

29. Niu, J., L. Zhang, and H. Zuo, *Energy savings potential of chilled-ceiling combined with desiccant cooling in hot and humid climates.* Energy and Buildings, 2002. **34**(5): p. 487-495.

30. Simonson, C.J., D.L. Ciepliski, and R.W. Besant, *Determining the performance of energy wheels: Part II--experimental data and numerical validation.* ASHRAE Transactions, 1999. **105**: p. 188.

31. Asiedu, Y., R.W. Besant, and C.J. Simonson, *Cost-Effective Design of Dual Heat and Energy Recovery Exchangers for 100% Ventilation Air in HVAC Cabinet Units.* ASHRAE Transactions, 2005. **111**(1).

32. Dodoo, A., L. Gustavsson, and R. Sathre, *Primary energy implications of ventilation heat recovery in residential buildings.* Energy and Buildings, 2011. **43**(7): p. 1566-1572.

33. El Fouih, Y., P. Stabat, P. Rivière, P. Hoang and V. Archambault, *Adequacy of air-to-air heat recovery ventilation system applied in low energy buildings.* Energy and Buildings, 2012. **54**: p. 29-39.

34. Laverge, J. and A. Janssens, *Heat recovery ventilation operation traded off against natural and simple exhaust ventilation in Europe by primary energy factor, carbon dioxide emission, household consumer price and exergy*. Energy and Buildings, 2012. **50**: p. 315-323.

35. Roulet, C.-A., F. Heidt, F. Foradini and M.-C. Pibiri, *Real heat recovery with air handling units.* Energy and Buildings, 2001. **33**(5): p. 495-502.

36. Yaïci, W., M. Ghorab, and E. Entchev, *Numerical analysis of heat and energy recovery ventilators performance based on CFD for detailed design.* Applied Thermal Engineering, 2013. **51**(1-2): p. 770-780.

37. Nasif, M., R. Al-Waked, G. Morrison and M. Behnia, *Membrane heat exchanger in HVAC energy recovery systems, systems energy analysis.* Energy and Buildings, 2010. **42**(10): p. 1833-1840.

38. Rasouli, M., C.J. Simonson, and R.W. Besant, *Applicability and optimum control strategy of energy recovery ventilators in different climatic conditions.* Energy and Buildings, 2010. **42**(9): p. 1376-1385.

39. Mahmud, K., G. I. Mahmood, C. J. Simonson and R. W. Besant, *Performance testing of a counter-cross-flow run-around membrane energy exchanger (RAMEE) system for HVAC applications.* Energy and Buildings, 2010. **42**(7): p. 1139-1147.

40. O'Connor, D., J.K.S. Calautit, and B.R. Hughes, *A review of heat recovery technology for passive ventilation applications.* Renewable and Sustainable Energy Reviews, 2016. **54**: p. 1481-1493.

41. Linton, J., W. Snelson, and P. Hearty. *Effect of condenser liquid subcooling on system performance for refrigerants CFC-12, HFC-134 a, and HFC-152 a*. in *ASHRAE Winter Meeting, Anaheim, CA, USA, 01/25-29/92*. 1992.

42. Yumrutaş, R., M. Kunduz, and M. Kanoğlu, *Exergy analysis of vapor compression refrigeration systems.* Exergy, an International Journal, 2002. **2**(4): p. 266-272.

43. Dalkilic, A. and S. Wongwises, *A performance comparison of vapour-compression refrigeration system using various alternative refrigerants.* International Communications in Heat and Mass Transfer, 2010. **37**(9): p. 1340-1349.

44. Jensen, J.B. and S. Skogestad, *Optimal operation of simple refrigeration cycles: Part I: Degrees of freedom and optimality of sub-cooling.* Computers & chemical engineering, 2007. **31**(5-6): p. 712-721.

45. Pottker, G. and P.S. Hrnjak, *Effect of condenser subcooling of the performance of vapor compression systems: experimental and numerical investigation.* 2012.

46. Zhang, J., W. Hu, and M.S. Hashmi, *Super-subcooling with R12 and R22 refrigeration plants using reciprocating compressors.* Applied energy, 1993. **45**(2): p. 157-166.

47. Thornton, J., S. Klein, and J. Mitchell, *Dedicated mechanical subcooling design strategies for supermarket applications.* International Journal of Refrigeration, 1994. **17**(8): p. 508-515.

48. Khan, J.-u.-R. and S. Zubair, *Design and rating of dedicated mechanical-subcooling vapour compression refrigeration systems.* Proceedings of the Institution of Mechanical Engineers, Part A: Journal of Power and Energy, 2000. **214**(5): p. 455-471.

49. Qureshi, B.A. and S.M. Zubair, *The effect of refrigerant combinations on performance of a vapor compression refrigeration system with dedicated mechanical sub-cooling.* International Journal of Refrigeration, 2012. **35**(1): p. 47-57.

50. Qureshi, B. A., M. Inam, M. A. Antar and S. M. Zubair, *Experimental energetic analysis of a vapor compression refrigeration system with dedicated mechanical sub-cooling.* Applied energy, 2013. **102**: p. 1035-1041.

51. Zubair, S.M., *Thermodynamics of a vapor-compression refrigeration cycle with mechanical subcooling.* Energy, 1994. **19**(6): p. 707-715.

52. Zubair, S.M., *Improvement of refrigeration/air-conditioning performance with mechanical sub-cooling.* Energy, 1990. **15**(5): p. 427-433.

53. Yang, L. and C.-L. Zhang, *On subcooler design for integrated two-temperature supermarket refrigeration system.* Energy and Buildings, 2011. **43**(1): p. 224-231.

54. Yu, J., Y. Ren, H. Chen and Y. Li, *Applying mechanical subcooling to ejector refrigeration cycle for improving the coefficient of performance.* Energy Conversion and Management, 2007. **48**(4): p. 1193-1199.

55. Xing, M., G. Yan, and J. Yu, *Performance evaluation of an ejector subcooled vapor-compression refrigeration cycle.* Energy Conversion and Management, 2015. **92**: p. 431-436.

56. Boewe, D. E., C. W. Bullard, J. M. Yin and P. S. Hrnjak, *Contribution of internal heat exchanger to transcritical R-744 cycle performance.* HVAC&R RESEARCH, 2001. **7**(2): p. 155-168.

57. Cho, H., C. Ryu, and Y. Kim, *Cooling performance of a variable speed CO 2 cycle with an electronic expansion valve and internal heat exchanger.* International Journal of Refrigeration, 2007. **30**(4): p. 664-671.

58. Aprea, C. and A. Maiorino, *An experimental evaluation of the transcritical CO 2 refrigerator performances using an internal heat exchanger.* International journal of refrigeration, 2008. **31**(6): p. 1006-1011.

59. Sarkar, J., S. Bhattacharyya, and M.R. Gopal, *Optimization of a transcritical CO 2 heat pump cycle for simultaneous cooling and heating applications.* International Journal of Refrigeration, 2004. **27**(8): p. 830-838.

60. Torrella, E., D. Sánchez, R. Llopis and R. Cabello, *Energetic evaluation of an internal heat exchanger in a CO2 transcritical refrigeration plant using experimental data.* International Journal of refrigeration, 2011. **34**(1): p. 40-49.

61. Mathur, G.D., *Enhancing AC system performance with a suction line heat exchanger with refrigerant HFO-1234yf.* 2011, SAE Technical Paper.

62. Preissner, M., B. Cutler, R. Radermacher and C. Zhang, *Suction line heat exchanger for R134a automotive air-conditioning system.* 2000.

63. Zhang, C.A., B.L. Graham, and T.R. Dickson, *How to improve vehicle R134a A/C system performance with a liquid line suction line heat exchanger (IHX).* 2002, SAE Technical Paper.

64. Selbaş, R., Ö. Kızılkan, and A. Şencan, *Thermoeconomic optimization of subcooled and superheated vapor compression refrigeration cycle.* Energy, 2006. **31**(12): p. 2108-2128.

65. Jarall, S., *Study of refrigeration system with HFO-1234yf as a working fluid.* International journal of refrigeration, 2012. **35**(6): p. 1668-1677.

66. Şencan, A., R. Selbaş, Ö. Kızılkan and S. A. Kalogirou, *Thermodynamic analysis of subcooling and superheating effects of alternative refrigerants for vapour compression refrigeration cycles.* International journal of energy research, 2006. **30**(5): p. 323-347.

67. Hermes, C.J., *Alternative evaluation of liquid-to-suction heat exchange in the refrigeration cycle.* International Journal of Refrigeration, 2013. **36**(8): p. 2119-2127.

68. Klein, S., D. Reindl, and K. Brownell, *Refrigeration system performance using liquid-suction heat exchangers.* International Journal of Refrigeration, 2000. **23**(8): p. 588-596.

69. Navarro-Esbri, J., R. Cabello, and E. Torrella, *Experimental evaluation of the internal heat exchanger influence on a vapour compression plant energy efficiency working with R22, R134a and R407C.* Energy, 2005. **30**(5): p. 621-636.

70. Navarro-Esbrí, J., F. Moles, and Á. Barragán-Cervera, *Experimental analysis of the internal heat exchanger influence on a vapour compression system performance working with R1234yf as a drop-in replacement for R134a.* Applied Thermal Engineering, 2013. **59**(1-2): p. 153-161.

71. Vijayan, R. and P. Srinivasan, *Influence of internal heat exchanger on performance of window AC retrofitted with R407C.* 2009.

72. Pottker, G. and P. Hrnjak, *Experimental investigation of the effect of condenser subcooling in R134a and R1234yf air-conditioning systems with and without internal heat exchanger.* International Journal of Refrigeration, 2015. **50**: p. 104-113.

73. Domanski, P.A., D.A. Didion, and J. Doyle, *Evaluation of suction-line/liquid-line heat exchange in the refrigeration cycle.* International Journal of Refrigeration, 1994. **17**(7): p. 487-493.

74. Domanski, P.A. and P.A. Domanski, *Theoretical evaluation of the vapor compression cycle with a liquid-line/suction-line heat exchanger, economizer, and ejector*. 1995: National Institute of Standards and Technology Gaithersburg, USA.

75. Mastrullo, R., A. Mauro, S. Tino and G. Vanoli, *A chart for predicting the possible advantage of adopting a suction/liquid heat exchanger in refrigerating system.* Applied Thermal Engineering, 2007. **27**(14-15): p. 2443-2448.

76. ASHRAE Technical Committees, T.G., and Technical Resource Groups, *2018 ASHRAE HANDBOOK REFRIGERATION*. 2018.

77. Akasaka, R., K. Tanaka, and Y. Higashi, *Thermodynamic property modeling for 2, 3, 3, 3-tetrafluoropropene (HFO-1234yf).* International Journal of Refrigeration, 2010. **33**(1): p. 52-60.

78. Akasaka, R., K. Tanaka, and Y. Higashi, *Measurements of saturated densities and critical parameters for the binary mixture of 2, 3, 3, 3-tetrafluoropropene (R-1234yf)+ difluoromethane (R-32).* International Journal of Refrigeration, 2013. **36**(4): p. 1341-1346.

79. Mota-Babiloni, A., J. Navarro-Esbrí, F. Molés, Á. B. Cervera, B. Peris and G. Verdú, *A review of refrigerant R1234ze (E) recent investigations.* Applied Thermal Engineering, 2016. **95**: p. 211-222.

80. Agrawal, N., S. Patil, and P. Nanda, *Experimental Studies of a Domestic Refrigerator Using R290/R600a Zeotropic Blends.* Energy Procedia, 2017. **109**: p. 425-430.

81. Fatouh, M. and M. El Kafafy, *Assessment of propane/commercial butane mixtures as possible alternatives to R134a in domestic refrigerators.* Energy Conversion and Management, 2006. **47**(15): p. 2644-2658.

82. Katare, P.K. and V.M. Kriplani, *Comparative assessment for drop in replacement of R134a in domestic refrigerator.*

83. Sah, R.P., R.K. Das, and V. Tiwari, *Analysis of Vapour Compression Refrigeration System with Refrigerants R134a, R143a, R152a, R290 and R32.* International Journal of Innovative Research and Development, 2014.

84. Kneifel, J. and E. O'Rear, *An Assessment of Typical Weather Year Data Impacts vs. Multi-year Weather Data on Net-Zero Energy Building Simulations*. 2014, Technical report, National Institute of Standards and Technology.

85. Huang, Y.J. and D. Crawley, *Does it matter which weather data you use in energy simulations?* 1996, Lawrence Berkeley National Lab., CA (United States).

86. Crawley, D.B., *Which weather data should you use for energy simulations of commercial buildings?/Discussion.* Ashrae Transactions, 1998. **104**: p. 498.

87. Hong, T., W.-K. Chang, and H.-W. Lin, *A fresh look at weather impact on peak electricity demand and energy use of buildings using 30-year actual weather data.* Applied Energy, 2013. **111**: p. 333-350.

88. Wang, L., P. Mathew, and X. Pang, *Uncertainties in energy consumption introduced by building operations and weather for a medium-size office building.* Energy and Buildings, 2012. **53**: p. 152-158.

89. Braun, M., H. Altan, and S. Beck, *Using regression analysis to predict the future energy consumption of a supermarket in the UK.* Applied Energy, 2014. **130**: p. 305-313.

90. Powell, K. M., A. Sriprasad, W. J. Cole and T. F. Edgar, *Heating, cooling, and electrical load forecasting for a large-scale district energy system.* Energy, 2014. **74**: p. 877-885.

91. Bhandari, M., S. Shrestha, and J. New, *Evaluation of weather datasets for building energy simulation.* Energy and Buildings, 2012. **49**: p. 109-118.

92. Lei, F. and P. Hu. *A baseline model for office building energy consumption in hot summer and cold winter region*. in *Management and Service Science, 2009. MASS'09. International Conference on*. 2009. IEEE.

93. Pang, X., P. Bhattacharya, Z. O'Neill, P. Haves, M. Wetter and T. Bailey. *Real-time building energy simulation using EnergyPlus and the Building Controls Virtual Test Bed*. in *Proceeding of the 12th IBPSA Conference*. 2011. Citeseer.

94. CIBSE, T., *Degree-days: theory and application.* London, UK: Chartered Institution of Building Services Engineers, 2006.

95. Lee, K., H.-J. Baek, and C. Cho, *The estimation of base temperature for heating and cooling degree-days for South Korea.* Journal of Applied Meteorology and Climatology, 2014. **53**(2): p. 300-309.

96. Mourshed, M., *The impact of the projected changes in temperature on heating and cooling requirements in buildings in Dhaka, Bangladesh.* Applied Energy, 2011. **88**(11): p. 3737-3746.

97. Mourshed, M., *Relationship between annual mean temperature and degree-days.* Energy and buildings, 2012. **54**: p. 418-425.

98. Oktay, Z., C. Coskun, and I. Dincer, *A new approach for predicting cooling degree-hours and energy requirements in buildings.* Energy, 2011. **36**(8): p. 4855-4863.

99. Petri, Y. and K. Caldeira, *Impacts of global warming on residential heating and cooling degree-days in the United States.* Scientific reports, 2015. **5**.

100. Krese, G., M. Prek, and V. Butala, *Analysis of building electric energy consumption data using an improved cooling degree day method.* Strojniški vestnik-Journal of Mechanical Engineering, 2012. **58**(2): p. 107-114.

101. Shin, M. and S.L. Do, *Prediction of cooling energy use in buildings using an enthalpy-based cooling degree days method in a hot and humid climate.* Energy and Buildings, 2016. **110**: p. 57-70.

102. Papakostas, K., T. Mavromatis, and N. Kyriakis, *Impact of the ambient temperature rise on the energy consumption for heating and cooling in residential buildings of Greece.* Renewable Energy, 2010. **35**(7): p. 1376-1379.

103. Al-Hadhrami, L., *Comprehensive review of cooling and heating degree days characteristics over Kingdom of Saudi Arabia.* Renewable and sustainable energy reviews, 2013. **27**: p. 305-314.

104. Csáky, I. and T. Kalmár, *Analysis of degree day and cooling energy demand in educational buildings.* Environmental Engineering and Management Journal, 2014. **13**(11): p. 2765-2770.

105. Cheng-wen, Y. and Y. Jian. *Application of ANN for the prediction of building energy consumption at different climate zones with HDD and CDD*. in *Future Computer and Communication (ICFCC), 2010 2nd International Conference on*. 2010. IEEE.

106. De Rosa, M., V. Bianco, F. Scarpa and L. A. Tagliafico, *Heating and cooling building energy demand evaluation; a simplified model and a modified degree days approach.* Applied energy, 2014. **128**: p. 217-229.

107. Xu, P., Y. J. Huang, N. Miller, N. Schlegel and P. Shen, *Impacts of climate change on building heating and cooling energy patterns in California.* Energy, 2012. **44**(1): p. 792-804.

APPENDIX A TABLES

Table 56 Thermodynamic and Transport Properties Comparisons between R-134a, R-1234yf and R-1234ze

			Thermodynamic Properties						Transport Properties		
			Saturation pressure (kPa)	Density (kg/m3)	Specific volume (m3/kg)	Specific heat Cp (kJ/kg K)	Enthalpy (kJ/kg)	Enthalpy Vaporization (kJ/kg)	Viscosities (mPa s)	Thermal Cond. (W/m K)	Pr
Liquid phase	TL= -20 °C	R-290	244.52	554.45	0.0018036	2.3608	151.36	400.77	0.15473	0.11662	3.1322
		R-600a	72.477	602.88	0.0016587	2.1824	155.3	372.31	0.2519	0.10665	5.1548
		R134a	132.73	1358.3	0.0007362	1.293	173.64	212.92	0.34758	0.10107	4.4469
		% difference 290,134a	84.22%	-59.18 %	144.98%	82.58 %	-12.83%	88.23%	-55.48%	15.39%	-29.56 %
		% difference600a,134a	-45.40%	-55.62 %	125.30%	68.79 %	-10.56%	74.86%	-27.53%	5.52%	15.92 %
		% difference290, 600a	237.38%	-8.03%	8.74%	8.17%	-2.54%	7.64%	-38.57%	9.35%	-39.24 %
	TH = 30 °C	R-290	1079	484.39	0.0020644	2.7767	278.83	326.7	0.092188	0.091409	2.8004
		R-600a	404.72	544.31	0.0018372	2.4633	271.24	323.33	0.14343	0.087489	4.0385
		R134a	770.2	1187.5	0.0008421	1.4465	241.72	173.1	0.18313	0.078992	3.3533
		% difference290,134a	40.09%	-59.21 %	145.14%	91.96 %	15.35%	88.73%	-49.66%	15.72%	-16.49 %
		% difference600a,134a	-47.45%	-54.16 %	118.16%	70.29 %	12.21%	86.79%	-21.68%	10.76%	20.43 %
		% difference290,600a	166.60%	-11.01 %	12.37%	12.72 %	2.80%	1.04%	-35.73%	4.48%	-30.66 %
Vapor phase	TL= -20 °C	R-290	244.52	5.5046	0.18167	1.5803	552.13	400.77	0.006887	0.013631	0.79842
		R-600a	72.477	2.0687	0.48339	1.4989	527.61	372.31	0.00638	0.012454	0.76789

Table 56 continued

			Thermodynamic Properties						Transport Properties		
			Saturation pressure (kPa)	Density (kg/m3)	Specific volume (m3/kg)	Specific heat Cp (kJ/kg K)	Enthalpy (kJ/kg)	Enthalpy Vaporization (kJ/kg)	Viscosities (mPa s)	Thermal Cond. (W/m K)	Pr
		R134a	132.73	6.7845	0.14739	0.8158	386.55	212.92	0.01	0.0098164	0.83101
		% differenceyf,134a	84.22%	-18.87%	23.26%	93.71%	42.84%	88.23%	-31.13%	38.86%	-3.92%
		% differenceze,134a	-45.40%	-69.51%	227.97%	83.73%	36.49%	74.86%	-36.19%	26.87%	-7.60%
		% difference yf,ze	237.38%	166.09%	-62.42%	5.43%	4.65%	7.64%	7.94%	9.45%	3.98%
	TH= 30 °C	R-290	1079	23.451	0.042643	2.0877	605.54	326.7	0.008463	0.019724	0.89573
		R-600a	404.72	10.48	0.095422	1.8353	594.57	323.33	0.007631	0.017371	0.80624
		R134a	770.2	37.535	0.026642	1.0655	414.82	173.1	0.011907	0.014336	0.88493
		% differenceyf,134a	40.09%	-37.52%	60.06%	95.94%	45.98%	88.73%	-28.93%	37.58%	1.22%
		% differenceze,134a	-47.45%	-72.08%	258.16%	72.25%	43.33%	86.79%	-35.91%	21.17%	-8.89%
		% difference yf,ze	166.60%	123.77%	-55.31%	13.75%	1.85%	1.04%	10.90%	13.55%	11.10%

Table 57 Condenser-to-evaporator cfm ratio for different manufactures—part 1

Configuration	Nominal Tons	Net Cooling Capacities (KBtu/h)	Evaporator		Condenser		EER (Btu/h-W)	Condenser-to-Evaporator Air Ratio	Manufacturer and model
			Airflow (Standard ft^3/min)	Face Area (ft^2)	Airflow (Standard ft^3/min)	Face Area (ft^2)			
Rooftop, electric cooling and gas heating	2	23	800	3.7	2800	10.2	11	3.50	Carrier 48ES-A
	2 1/2	28.4	1000	3.7	3000	11.9	11.2	3.00	
	3	34.4	1200	3.7	3200	15.4	11	2.67	
	3 1/2	40.5	1400	4.7	3600	13.6	11.2	2.57	
	4	46.5	1600	4.7	4000	15.5	11.2	2.50	
	5	57	1750	5.7	3200	15.5	11	1.83	

Table 57 continued

Configuration	Nominal Tons	Net Cooling Capacities (KBtu/h)	Evaporator		Condenser		EER (Btu/h-W)	Condenser-to-Evaporator Air Ratio	Manufacturer and model
			Airflow (Standard ft^3/min)	Face Area (ft^2)	Airflow (Standard ft^3/min)	Face Area (ft^2)			
Rooftop, electric cooling and gas heating	2	23.6	800	5.54	2500	10.56	11.1	3.13	Rheem RRNL-B
	2.5	28.6	1000	5.54	2500	10.56	11.1	2.5	
	3	35.6	1200	5.54	2700	14.8	11.3	2.25	
	3.5	42	1400	7.39	3500	16.65	11.2	2.5	
	4	48	1600	7.39	3300	16.23	11.2	2.06	
	5	57.5	1850	7.39	3300	16.23	10.5	1.78	
Rooftop, heat pump	2	24	800	3.7	2700	11.9	missing	3.38	Carrier 50SZ
	2.5	30	1000	3.7	2700	13.6		2.7	
	3	36	1200	4.7	2800	15.5		2.33	
	3.5	41.5	1400	4.7	2800	19.4		2	
	4	47	1600	5.6	3300	19.4		2.06	
	5	57	1750	5.6	3300	19.4		1.89	
	2	23.8	800	3.7	2700	11.9	11.5	3.38	Carrier 50EZ-A
	2.5	29	1000	3.7	2700	11.9	11.5	2.7	
	3	35	1200	3.7	2700	11.9	11.5	2.25	
	3.5	40	1400	4.7	3100	13.6	11.5	2.21	
	4	47	1600	4.7	3100	13.6	11.5	1.94	
	5	57	1850	5.7	3100	17.5	11.5	1.68	

Table 58 Condenser-to-evaporator cfm ratio for different manufactures—part 2

Configuration	Nominal Tons	Evaporator		Condenser		Condenser-to-Evaporator Air Ratio	Manufacturer and model
		Airflow (Standard ft^3/min)	Face Area (ft^2)	Airflow (Standard ft^3/min)	Face Area (ft^2)		
Split system cooling units	7.5	3000	8.1	5670	19.25	1.89	Trane
	10	4000	11.2	8120	24	2.03	
	15	6000	16.3	10900	33.3	1.82	
	20	8000	21.6	16120	50.2	2.02	
DCC Commercial packaged air conditioner	6	2350	8.9	4200	19	1.79	Daikin
	7.5	3000	8.9	7200	28.8	2.40	
	8.5	3200	10.2	8200	28.8	2.56	
	10	3500	10.2	8200	35.2	2.34	
	12.5	3900	14.7	8400	39	2.15	

Table 58 continued

Configuration	Nominal Tons	Evaporator		Condenser		Condenser-to-Evaporator Air Ratio	Manufacturer and model
		Airflow (Standard ft^3/min)	Face Area (ft^2)	Airflow (Standard ft^3/min)	Face Area (ft^2)		
DTC Commercial packaged air conditioner	3---5	1200	7.8	3800	13	3.17	Daikin
	3---5	1600	7.8	3800	13	2.38	
	3---5	2000	8.9	4200	19	2.1	
DSC Commercial packaged air conditioner	3---5	1250	7	3800	17.1	3.04	
	3----5	1200	7	3800	17.1	3.17	
	3---5	1600	7.8	3800	12.5	2.38	
	3---5	1800	7.8	3800	13	2.11	
DCH Commercial packaged heat pump	6	2350	8.9	4300	18.7	1.83	
	6	2400	8.9	4300	18.7	1.79	
	7 1/2	3000	10.2	7600	32.4	2.53	
	8 1/2	3400	10.2	7600	32.4	2.24	
	10	3500	10.2	8200	32.4	2.34	
	12 1/2	4000	14.7	8200	35.3	2.05	
DTH Commercial packaged heat pump	3----5	1200	7.8	3800	17	3.17	
	3----5	1600	7.8	3800	17	2.38	
	3----5	2000	8.9	4200	19	2.1	
DSH Commercial packaged heat pump	3----5	1250	7	3800	17	3.04	
	3----5	1200	7	3800	17	3.17	
	3----5	1650	7.8	3800	17	2.3	
	3----5	1600	7.8	3800	17	2.38	
	3----5	2000	8.9	4200	18.7	2.1	
	3----5	1800	8.9	4200	18.7	2.33	
DCG Commercial packaged gas/electric units	6	2350	8.9	4200	19	1.79	
	7 1/2	3000	8.9	7200	28.8	2.4	
	8 1/2	3200	10.2	8200	28.8	2.56	
	10	3500	10.2	8200	35.2	2.34	
	12 1/2	3900	14.7	8400	39	2.15	
	15	5600	20	9000	53.3	1.61	
	20	7000	20	9000	53.3	1.29	
	25	8200	17.2	15000	53.3	1.83	
DTG Commercial packaged gas/electric units	3---5	1200	7.8	3800	13	3.17	
	3---5	1600	7.8	3800	13	2.38	
	3---5	2000	8.9	4200	19	2.1	
DTG Commercial packaged gas/electric units	3--5	1250	7	3800	17.1	3.04	
	3---5	1200	7	3800	17.1	3.17	

Table 58 continued

Configuration	Nominal Tons	Evaporator		Condenser		Condenser-to-Evaporator Air Ratio	Manufacturer and model
		Airflow (Standard ft^3/min)	Face Area (ft^2)	Airflow (Standard ft^3/min)	Face Area (ft^2)		
residential packaged gas/electric units GPG 16M	2---5	800	4.3	2200	12.3	2.75	Goodman
	2---5	950	4.3	2200	8.7	2.32	
	2---5	1200	5.7	2600	14.9	2.17	
	2---5	1250	5.7	3200	14.9	2.56	
	2---5	1300	5.7	3100	14.4	2.38	
	2---5	2000	8.9	3800	19	1.9	
residential packaged gas/electric units GPG 14M	2---5	800	4.3	2150	12.3	2.69	
	2---5	1000	4.3	3050	12.3	3.05	
	2---5	1200	4.3	2250	8.8	1.88	
	2---5	1300	4.3	2850	11.1	2.19	
	2---5	1525	5.7	3300	15.4	2.16	

Table 59 Baseline and external evaporative cooling system performance and percentage difference

Tout	RH	Taeo	COP ref	COP ex	%difference
80	0.4	45	3.866	5.431	40.5%
80	0.5	45	3.866	5.069	31.1%
80	0.6	45	3.866	4.759	23.1%
80	0.7	45	3.866	4.492	16.2%
80	0.8	45	3.866	4.258	10.1%
80	0.4	50	4.237	6.069	43.2%
80	0.5	50	4.237	5.638	33.1%
80	0.6	50	4.237	5.274	24.5%
80	0.7	50	4.237	4.961	17.1%
80	0.8	50	4.237	4.689	10.7%
80	0.4	55	4.667	6.841	46.6%
80	0.5	55	4.667	6.32	35.4%
80	0.6	55	4.667	5.884	26.1%
80	0.7	55	4.667	5.513	18.1%
80	0.8	55	4.667	5.193	11.3%
85	0.4	45	3.516	5.007	42.4%
85	0.5	45	3.516	4.658	32.5%
85	0.6	45	3.516	4.362	24.1%

Table 59 continued

Tout	RH	Taeo	COP ref	COP ex	%difference
85	0.7	45	3.516	4.108	16.8%
85	0.8	45	3.516	3.886	10.5%
85	0.4	50	3.837	5.564	45.0%
85	0.5	50	3.837	5.154	34.3%
85	0.6	50	3.837	4.809	25.3%
85	0.7	50	3.837	4.515	17.7%
85	0.8	50	3.837	4.26	11.0%
85	0.4	55	4.206	6.229	48.1%
85	0.5	55	4.206	5.74	36.5%
85	0.6	55	4.206	5.334	26.8%
85	0.7	55	4.206	4.989	18.6%
85	0.8	55	4.206	4.692	11.6%
90	0.4	45	3.201	4.627	44.5%
90	0.5	45	3.201	4.291	34.1%
90	0.6	45	3.201	4.007	25.2%
90	0.7	45	3.201	3.764	17.6%
90	0.8	45	3.201	3.553	11.0%
90	0.4	50	3.481	5.117	47.0%
90	0.5	50	3.481	4.726	35.8%
90	0.6	50	3.481	4.399	26.4%
90	0.7	50	3.481	4.12	18.4%
90	0.8	50	3.481	3.879	11.4%
90	0.4	55	3.799	5.696	49.9%
90	0.5	55	3.799	5.235	37.8%
90	0.6	55	3.799	4.853	27.7%
90	0.7	55	3.799	4.53	19.2%
90	0.8	55	3.799	4.253	12.0%
95	0.4	45	2.914	4.285	47.0%
95	0.5	45	2.914	3.96	35.9%
95	0.6	45	2.914	3.687	26.5%
95	0.7	45	2.914	3.454	18.5%
95	0.8	45	2.914	3.251	11.6%
95	0.4	50	3.159	4.719	49.4%
95	0.5	50	3.159	4.343	37.5%
95	0.6	50	3.159	4.031	27.6%
95	0.7	50	3.159	3.766	19.2%
95	0.8	50	3.159	3.537	12.0%
95	0.4	55	3.436	5.226	52.1%
95	0.5	55	3.436	4.788	39.3%

Table 59 continued

Tout	RH	Taeo	COP ref	COP ex	%difference
95	0.6	55	3.436	4.427	28.8%
95	0.7	55	3.436	4.123	20.0%
95	0.8	55	3.436	3.863	12.4%

Table 60 Quadratic and exponential functions for baseline system

Tout	RH	Taeo	qua predicted	ex predicted	model	qua rs	ex rs	% qua	% ex
80	0.4	45	3.867542	3.866415	3.866	-0.00154	-0.00042	-0.04%	-0.01%
80	0.5	45	3.867542	3.866415	3.866	-0.00154	-0.00042	-0.04%	-0.01%
80	0.6	45	3.867542	3.866415	3.866	-0.00154	-0.00042	-0.04%	-0.01%
80	0.7	45	3.867542	3.866415	3.866	-0.00154	-0.00042	-0.04%	-0.01%
80	0.8	45	3.867542	3.866415	3.866	-0.00154	-0.00042	-0.04%	-0.01%
80	0.4	50	4.241467	4.238074	4.237	-0.00447	-0.00107	-0.11%	-0.03%
80	0.5	50	4.241467	4.238074	4.237	-0.00447	-0.00107	-0.11%	-0.03%
80	0.6	50	4.241467	4.238074	4.237	-0.00447	-0.00107	-0.11%	-0.03%
80	0.7	50	4.241467	4.238074	4.237	-0.00447	-0.00107	-0.11%	-0.03%
80	0.8	50	4.241467	4.238074	4.237	-0.00447	-0.00107	-0.11%	-0.03%
80	0.4	55	4.659642	4.664504	4.667	0.007358	0.002496	0.16%	0.05%
80	0.5	55	4.659642	4.664504	4.667	0.007358	0.002496	0.16%	0.05%
80	0.6	55	4.659642	4.664504	4.667	0.007358	0.002496	0.16%	0.05%
80	0.7	55	4.659642	4.664504	4.667	0.007358	0.002496	0.16%	0.05%
80	0.8	55	4.659642	4.664504	4.667	0.007358	0.002496	0.16%	0.05%
85	0.4	45	3.512125	3.51531	3.516	0.003875	0.00069	0.11%	0.02%
85	0.5	45	3.512125	3.51531	3.516	0.003875	0.00069	0.11%	0.02%
85	0.6	45	3.512125	3.51531	3.516	0.003875	0.00069	0.11%	0.02%
85	0.7	45	3.512125	3.51531	3.516	0.003875	0.00069	0.11%	0.02%
85	0.8	45	3.512125	3.51531	3.516	0.003875	0.00069	0.11%	0.02%
85	0.4	50	3.8396	3.838133	3.837	-0.0026	-0.00113	-0.07%	-0.03%
85	0.5	50	3.8396	3.838133	3.837	-0.0026	-0.00113	-0.07%	-0.03%
85	0.6	50	3.8396	3.838133	3.837	-0.0026	-0.00113	-0.07%	-0.03%
85	0.7	50	3.8396	3.838133	3.837	-0.0026	-0.00113	-0.07%	-0.03%
85	0.8	50	3.8396	3.838133	3.837	-0.0026	-0.00113	-0.07%	-0.03%
85	0.4	55	4.211325	4.207782	4.206	-0.00533	-0.00178	-0.13%	-0.04%
85	0.5	55	4.211325	4.207782	4.206	-0.00533	-0.00178	-0.13%	-0.04%
85	0.6	55	4.211325	4.207782	4.206	-0.00533	-0.00178	-0.13%	-0.04%
85	0.7	55	4.211325	4.207782	4.206	-0.00533	-0.00178	-0.13%	-0.04%
85	0.8	55	4.211325	4.207782	4.206	-0.00533	-0.00178	-0.13%	-0.04%

Table 60 continued

Tout	RH	Taeo	qua predicted	ex predicted	model	qua rs	ex rs	% qua	% ex
90	0.4	45	3.196542	3.199625	3.201	0.004458	0.001375	0.14%	0.04%
90	0.5	45	3.196542	3.199625	3.201	0.004458	0.001375	0.14%	0.04%
90	0.6	45	3.196542	3.199625	3.201	0.004458	0.001375	0.14%	0.04%
90	0.7	45	3.196542	3.199625	3.201	0.004458	0.001375	0.14%	0.04%
90	0.8	45	3.196542	3.199625	3.201	0.004458	0.001375	0.14%	0.04%
90	0.4	50	3.477567	3.479779	3.481	0.003433	0.001221	0.10%	0.04%
90	0.5	50	3.477567	3.479779	3.481	0.003433	0.001221	0.10%	0.04%
90	0.6	50	3.477567	3.479779	3.481	0.003433	0.001221	0.10%	0.04%
90	0.7	50	3.477567	3.479779	3.481	0.003433	0.001221	0.10%	0.04%
90	0.8	50	3.477567	3.479779	3.481	0.003433	0.001221	0.10%	0.04%
90	0.4	55	3.802842	3.79998	3.799	-0.00384	-0.00098	-0.10%	-0.03%
90	0.5	55	3.802842	3.79998	3.799	-0.00384	-0.00098	-0.10%	-0.03%
90	0.6	55	3.802842	3.79998	3.799	-0.00384	-0.00098	-0.10%	-0.03%
90	0.7	55	3.802842	3.79998	3.799	-0.00384	-0.00098	-0.10%	-0.03%
90	0.8	55	3.802842	3.79998	3.799	-0.00384	-0.00098	-0.10%	-0.03%
95	0.4	45	2.920792	2.915511	2.914	-0.00679	-0.00151	-0.23%	-0.05%
95	0.5	45	2.920792	2.915511	2.914	-0.00679	-0.00151	-0.23%	-0.05%
95	0.6	45	2.920792	2.915511	2.914	-0.00679	-0.00151	-0.23%	-0.05%
95	0.7	45	2.920792	2.915511	2.914	-0.00679	-0.00151	-0.23%	-0.05%
95	0.8	45	2.920792	2.915511	2.914	-0.00679	-0.00151	-0.23%	-0.05%
95	0.4	50	3.155367	3.158375	3.159	0.003633	0.000625	0.12%	0.02%
95	0.5	50	3.155367	3.158375	3.159	0.003633	0.000625	0.12%	0.02%
95	0.6	50	3.155367	3.158375	3.159	0.003633	0.000625	0.12%	0.02%
95	0.7	50	3.155367	3.158375	3.159	0.003633	0.000625	0.12%	0.02%
95	0.8	50	3.155367	3.158375	3.159	0.003633	0.000625	0.12%	0.02%
95	0.4	55	3.434192	3.435497	3.436	0.001808	0.000503	0.05%	0.01%
95	0.5	55	3.434192	3.435497	3.436	0.001808	0.000503	0.05%	0.01%
95	0.6	55	3.434192	3.435497	3.436	0.001808	0.000503	0.05%	0.01%
95	0.7	55	3.434192	3.435497	3.436	0.001808	0.000503	0.05%	0.01%
95	0.8	55	3.434192	3.435497	3.436	0.001808	0.000503	0.05%	0.01%

Table 61 Quadratic and exponential functions for system with external evaporative cooling

Tout	RH	Taeo	qua predicted	ex predicted	model	qua rs	ex rs	% qua	% ex
80	0.4	45	5.451355	5.43818	5.431	-0.02036	-0.00718	-0.37%	-0.13%
80	0.5	45	5.075719	5.068855	5.069	-0.00672	0.000145	-0.13%	0.00%
80	0.6	45	4.751761	4.75442	4.759	0.007239	0.00458	0.15%	0.10%

Table 61 continued

Tout	RH	Taeo	qua predicted	ex predicted	model	qua rs	ex rs	% qua	% ex
80	0.7	45	4.479482	4.487627	4.492	0.012518	0.004373	0.28%	0.10%
80	0.8	45	4.258882	4.26253	4.258	-0.00088	-0.00453	-0.02%	-0.11%
80	0.4	50	6.080465	6.074925	6.069	-0.01147	-0.00593	-0.19%	-0.10%
80	0.5	50	5.655504	5.641917	5.638	-0.0175	-0.00392	-0.31%	-0.07%
80	0.6	50	5.282221	5.272832	5.274	-0.00822	0.001168	-0.16%	0.02%
80	0.7	50	4.960617	4.958983	4.961	0.000383	0.002017	0.01%	0.04%
80	0.8	50	4.690692	4.69324	4.689	-0.00169	-0.00424	-0.04%	-0.09%
80	0.4	55	6.784475	6.825092	6.841	0.056525	0.015908	0.83%	0.23%
80	0.5	55	6.310189	6.315733	6.32	0.009811	0.004267	0.16%	0.07%
80	0.6	55	5.887581	5.881261	5.884	-0.00358	0.002739	-0.06%	0.05%
80	0.7	55	5.516652	5.511231	5.513	-0.00365	0.001769	-0.07%	0.03%
80	0.8	55	5.197402	5.197067	5.193	-0.0044	-0.00407	-0.08%	-0.08%
85	0.4	45	5.011582	5.009191	5.007	-0.00458	-0.00219	-0.09%	-0.04%
85	0.5	45	4.653236	4.657463	4.658	0.004764	0.000537	0.10%	0.01%
85	0.6	45	4.346568	4.357753	4.362	0.015432	0.004247	0.35%	0.10%
85	0.7	45	4.091579	4.103055	4.108	0.016421	0.004945	0.40%	0.12%
85	0.8	45	3.888269	3.887617	3.886	-0.00227	-0.00162	-0.06%	-0.04%
85	0.4	50	5.575752	5.568572	5.564	-0.01175	-0.00457	-0.21%	-0.08%
85	0.5	50	5.168081	5.158877	5.154	-0.01408	-0.00488	-0.27%	-0.09%
85	0.6	50	4.812088	4.809477	4.809	-0.00309	-0.00048	-0.06%	-0.01%
85	0.7	50	4.507774	4.512031	4.515	0.007226	0.002969	0.16%	0.07%
85	0.8	50	4.255139	4.259687	4.26	0.004861	0.000313	0.11%	0.01%
85	0.4	55	6.214822	6.225875	6.229	0.014178	0.003125	0.23%	0.05%
85	0.5	55	5.757826	5.746999	5.74	-0.01783	-0.007	-0.31%	-0.12%
85	0.6	55	5.352508	5.338427	5.334	-0.01851	-0.00443	-0.35%	-0.08%
85	0.7	55	4.998869	4.990189	4.989	-0.00987	-0.00119	-0.20%	-0.02%
85	0.8	55	4.696909	4.694098	4.692	-0.00491	-0.0021	-0.10%	-0.04%
90	0.4	45	4.621609	4.625536	4.627	0.005391	0.001464	0.12%	0.03%
90	0.5	45	4.280552	4.290119	4.291	0.010448	0.000881	0.24%	0.02%
90	0.6	45	3.991175	4.004129	4.007	0.015825	0.002871	0.39%	0.07%
90	0.7	45	3.753476	3.760783	3.764	0.010524	0.003217	0.28%	0.09%
90	0.8	45	3.567455	3.554512	3.553	-0.01446	-0.00151	-0.41%	-0.04%
90	0.4	50	5.120839	5.117139	5.117	-0.00384	-0.00014	-0.08%	0.00%
90	0.5	50	4.730457	4.728942	4.726	-0.00446	-0.00294	-0.09%	-0.06%
90	0.6	50	4.391755	4.397767	4.399	0.007245	0.001233	0.16%	0.03%
90	0.7	50	4.104731	4.115588	4.12	0.015269	0.004412	0.37%	0.11%
90	0.8	50	3.869385	3.875815	3.879	0.009615	0.003185	0.25%	0.08%
90	0.4	55	5.694969	5.693412	5.696	0.001031	0.002588	0.02%	0.05%
90	0.5	55	5.255262	5.242505	5.235	-0.02026	-0.0075	-0.39%	-0.14%
90	0.6	55	4.867235	4.857766	4.853	-0.01423	-0.00477	-0.29%	-0.10%

Table 61 continued

Tout	RH	Taeo	qua predicted	ex predicted	model	qua rs	ex rs	% qua	% ex
90	0.7	55	4.530886	4.529662	4.53	-0.00089	0.000338	-0.02%	0.01%
90	0.8	55	4.246215	4.250367	4.253	0.006785	0.002633	0.16%	0.06%
95	0.4	45	4.281435	4.281903	4.285	0.003565	0.003097	0.08%	0.07%
95	0.5	45	3.957669	3.961591	3.96	0.002331	-0.00159	0.06%	-0.04%
95	0.6	45	3.685581	3.688365	3.687	0.001419	-0.00136	0.04%	-0.04%
95	0.7	45	3.465172	3.455649	3.454	-0.01117	-0.00165	-0.32%	-0.05%
95	0.8	45	3.296442	3.258043	3.251	-0.04544	-0.00704	-1.40%	-0.22%
95	0.4	50	4.715725	4.714014	4.719	0.003275	0.004986	0.07%	0.11%
95	0.5	50	4.342634	4.345634	4.343	0.000366	-0.00263	0.01%	-0.06%
95	0.6	50	4.021221	4.031316	4.031	0.009779	-0.00032	0.24%	-0.01%
95	0.7	50	3.751487	3.763328	3.766	0.014513	0.002672	0.39%	0.07%
95	0.8	50	3.533432	3.53532	3.537	0.003568	0.00168	0.10%	0.05%
95	0.4	55	5.224915	5.219455	5.226	0.001085	0.006545	0.02%	0.13%
95	0.5	55	4.802499	4.794209	4.788	-0.0145	-0.00621	-0.30%	-0.13%
95	0.6	55	4.431761	4.431392	4.427	-0.00476	-0.00439	-0.11%	-0.10%
95	0.7	55	4.112702	4.121875	4.123	0.010298	0.001125	0.25%	0.03%
95	0.8	55	3.845322	3.858167	3.863	0.017678	0.004833	0.46%	0.13%

Table 62 Quadratic and exponential functions for COP ratio of external evaporative cooling over baseline

Tout	RH	Taeo	qua predicted	ex predicted	model	qua rs	ex rs	% qua	% ex
80	0.4	45	1.407342	1.406517	1.404811	-0.00253	-0.00171	-0.18%	-0.12%
80	0.5	45	1.310669	1.310996	1.311174	0.000506	0.000178	0.04%	0.01%
80	0.6	45	1.228012	1.229671	1.230988	0.002976	0.001317	0.24%	0.11%
80	0.7	45	1.159373	1.160669	1.161924	0.002552	0.001256	0.22%	0.11%
80	0.8	45	1.104751	1.10245	1.101397	-0.00335	-0.00105	-0.30%	-0.10%
80	0.4	50	1.43386	1.433417	1.432381	-0.00148	-0.00104	-0.10%	-0.07%
80	0.5	50	1.331541	1.331246	1.330658	-0.00088	-0.00059	-0.07%	-0.04%
80	0.6	50	1.24324	1.244158	1.244749	0.001508	0.000591	0.12%	0.05%
80	0.7	50	1.168957	1.170103	1.170876	0.001919	0.000773	0.16%	0.07%
80	0.8	50	1.10869	1.107399	1.106679	-0.00201	-0.00072	-0.18%	-0.07%
80	0.4	55	1.462752	1.463198	1.465824	0.003072	0.002626	0.21%	0.18%
80	0.5	55	1.354789	1.353999	1.354189	-0.0006	0.00019	-0.04%	0.01%
80	0.6	55	1.260843	1.260855	1.260767	-7.6E-05	-8.8E-05	-0.01%	-0.01%
80	0.7	55	1.180915	1.181526	1.181273	0.000358	-0.00025	0.03%	-0.02%
80	0.8	55	1.115004	1.114173	1.112706	-0.0023	-0.00147	-0.21%	-0.13%
85	0.4	45	1.42567	1.424964	1.424061	-0.00161	-0.0009	-0.11%	-0.06%
85	0.5	45	1.325059	1.324908	1.324801	-0.00026	-0.00011	-0.02%	-0.01%

Table 62 continued

Tout	RH	Taeo	qua predicted	ex predicted	model	qua rs	ex rs	% qua	% ex
85	0.6	45	1.238466	1.23965	1.240614	0.002148	0.000965	0.17%	0.08%
85	0.7	45	1.16589	1.167196	1.168373	0.002483	0.001177	0.21%	0.10%
85	0.8	45	1.107332	1.10591	1.105233	-0.0021	-0.00068	-0.19%	-0.06%
85	0.4	50	1.4511	1.450855	1.450091	-0.00101	-0.00076	-0.07%	-0.05%
85	0.5	50	1.344846	1.344111	1.343237	-0.00161	-0.00087	-0.12%	-0.07%
85	0.6	50	1.252608	1.253077	1.253323	0.000715	0.000246	0.06%	0.02%
85	0.7	50	1.174388	1.17558	1.176701	0.002313	0.001121	0.20%	0.10%
85	0.8	50	1.110184	1.109833	1.110242	5.79E-05	0.000409	0.01%	0.04%
85	0.4	55	1.478906	1.47961	1.48098	0.002074	0.00137	0.14%	0.09%
85	0.5	55	1.367006	1.365802	1.364717	-0.00229	-0.00109	-0.17%	-0.08%
85	0.6	55	1.269124	1.268703	1.268188	-0.00094	-0.00052	-0.07%	-0.04%
85	0.7	55	1.185259	1.185943	1.186163	0.000903	0.00022	0.08%	0.02%
85	0.8	55	1.115412	1.115575	1.115549	0.000137	-2.6E-05	0.01%	0.00%
90	0.4	45	1.445922	1.445649	1.445486	-0.00044	-0.00016	-0.03%	-0.01%
90	0.5	45	1.341375	1.340819	1.340519	-0.00086	-0.0003	-0.06%	-0.02%
90	0.6	45	1.250845	1.251437	1.251796	0.000951	0.000359	0.08%	0.03%
90	0.7	45	1.174333	1.175382	1.175883	0.00155	0.0005	0.13%	0.04%
90	0.8	45	1.111837	1.110915	1.109966	-0.00187	-0.00095	-0.17%	-0.09%
90	0.4	50	1.470265	1.470535	1.46998	-0.00029	-0.00056	-0.02%	-0.04%
90	0.5	50	1.360074	1.358977	1.357656	-0.00242	-0.00132	-0.18%	-0.10%
90	0.6	50	1.2639	1.263806	1.263717	-0.00018	-8.9E-05	-0.01%	-0.01%
90	0.7	50	1.181743	1.182715	1.183568	0.001825	0.000853	0.15%	0.07%
90	0.8	50	1.113603	1.113811	1.114335	0.000732	0.000524	0.07%	0.05%
90	0.4	55	1.496984	1.498274	1.499342	0.002358	0.001068	0.16%	0.07%
90	0.5	55	1.381148	1.379614	1.377994	-0.00315	-0.00162	-0.23%	-0.12%
90	0.6	55	1.279329	1.278366	1.277441	-0.00189	-0.00092	-0.15%	-0.07%
90	0.7	55	1.191528	1.192023	1.192419	0.000891	0.000396	0.07%	0.03%
90	0.8	55	1.117744	1.118524	1.119505	0.001761	0.000982	0.16%	0.09%
95	0.4	45	1.468098	1.468663	1.470487	0.002389	0.001825	0.16%	0.12%
95	0.5	45	1.359614	1.358798	1.358957	-0.00066	0.000159	-0.05%	0.01%
95	0.6	45	1.265148	1.265083	1.265271	0.000123	0.000188	0.01%	0.01%
95	0.7	45	1.184699	1.185263	1.185312	0.000613	4.9E-05	0.05%	0.00%
95	0.8	45	1.118268	1.117486	1.115649	-0.00262	-0.00184	-0.23%	-0.16%
95	0.4	50	1.491355	1.492544	1.493827	0.002472	0.001283	0.17%	0.09%
95	0.5	50	1.377227	1.375908	1.374802	-0.00242	-0.00111	-0.18%	-0.08%
95	0.6	50	1.277116	1.276389	1.276037	-0.00108	-0.00035	-0.08%	-0.03%
95	0.7	50	1.191023	1.191539	1.192149	0.001127	0.00061	0.09%	0.05%
95	0.8	50	1.118947	1.119348	1.119658	0.000712	0.00031	0.06%	0.03%
95	0.4	55	1.516986	1.519272	1.520955	0.003968	0.001682	0.26%	0.11%
95	0.5	55	1.397214	1.395492	1.393481	-0.00373	-0.00201	-0.27%	-0.14%

Table 62 continued

Tout	RH	Taeo	qua predicted	ex predicted	model	qua rs	ex rs	% qua	% ex
95	0.6	55	1.291459	1.289884	1.288417	-0.00304	-0.00147	-0.24%	-0.11%
95	0.7	55	1.199721	1.19979	1.199942	0.000221	0.000152	0.02%	0.01%
95	0.8	55	1.122	1.12303	1.124272	0.002272	0.001242	0.20%	0.11%

Table 63 Wet-bulb temperatures of outdoor air, incoming air temperatures for the condenser and different humidity ratios under different conditions

Tout	T supply air	RH	Tsat	Taci	△w internal	△w total	△w internal/△w total/2.5
80	45	0.4	63.36	75.71	0.00232	0.003703	0.25
		0.5	66.5	71.74	0.00449	0.002977	0.60
		0.6	69.46	69.46	0.006674	0.002289	1.17
		0.7	72.26	72.26	0.008874	0.001636	2.17
		0.8	74.9	74.9	0.01109	0.001012	4.38
	50	0.4	63.38	78.12	0.001024	0.003715	0.11
		0.5	66.53	74.15	0.003193	0.002993	0.43
		0.6	69.5	70.19	0.005378	0.002308	0.93
		0.7	72.3	72.3	0.007577	0.001658	1.83
		0.8	74.94	74.94	0.009792	0.001038	3.77
	55	0.4	63.41	80.94	0	0.003726	0.00
		0.5	66.56	76.97	0.00166	0.003006	0.22
		0.6	69.53	73.01	0.003845	0.002325	0.66
		0.7	72.33	72.33	0.006044	0.001678	1.44
		0.8	74.98	74.98	0.008259	0.001062	3.11
85	45	0.4	67.16	77.89	0.003836	0.00395	0.39
		0.5	70.56	73.21	0.006398	0.003157	0.81
		0.6	73.75	73.75	0.008982	0.00241	1.49
		0.7	76.74	76.74	0.01159	0.001702	2.72
		0.8	79.56	79.56	0.01421	0.001028	5.53
	50	0.4	67.19	80.31	0.002539	0.003966	0.26
		0.5	70.6	75.63	0.005102	0.003178	0.64
		0.6	73.79	73.79	0.007685	0.002434	1.26

Table 63 continued

Tout	T supply air	RH	Tsat	Taci	△w internal	△w total	△w internal/△w total/2.5
		0.7	76.78	76.78	0.01029	0.00173	2.38
		0.8	79.6	79.6	0.01292	0.001061	4.87
		0.4	67.22	83.15	0.001007	0.003981	0.10
		0.5	70.63	78.47	0.003569	0.003196	0.45
	55	0.6	73.83	73.83	0.006153	0.002457	1.00
		0.7	76.82	76.82	0.008757	0.001757	1.99
		0.8	79.64	79.64	0.01138	0.001092	4.17
		0.4	70.96	79.62	0.005586	0.004189	0.53
		0.5	74.63	74.63	0.008605	0.003327	1.03
	45	0.6	78.04	78.04	0.01165	0.002517	1.85
		0.7	81.23	81.23	0.01473	0.001752	3.36
		0.8	84.21	84.21	0.01784	0.001026	6.96
		0.4	71	82.06	0.00429	0.00421	0.41
		0.5	74.67	76.57	0.007309	0.003352	0.87
90	50	0.6	78.09	78.09	0.01036	0.002547	1.63
		0.7	81.27	81.27	0.01344	0.001787	3.01
		0.8	84.26	84.26	0.01654	0.001067	6.20
		0.4	71.03	84.91	0.002757	0.00423	0.26
		0.5	74.71	79.42	0.005776	0.003377	0.68
	55	0.6	78.13	78.13	0.008825	0.002576	1.37
		0.7	81.32	81.32	0.0119	0.001821	2.61
		0.8	84.31	84.31	0.01501	0.001106	5.43
		0.4	74.77	80.85	0.007602	0.004418	0.69
		0.5	78.71	78.71	0.01115	0.003483	1.28
	45	0.6	82.34	82.34	0.01474	0.002607	2.26
		0.7	85.72	85.72	0.01837	0.001782	4.12
		0.8	88.87	88.87	0.02204	0.001001	8.81
95		0.4	74.81	83.31	0.006306	0.004444	0.57
		0.5	78.75	78.75	0.009856	0.003515	1.12
	50	0.6	82.39	82.39	0.01345	0.002645	2.03
		0.7	85.77	85.77	0.01708	0.001826	3.74
		0.8	88.93	88.93	0.02075	0.001051	7.90

Table 63 continued

Tout	T supply air	RH	Tsat	Taci	△w internal	△w total	△w internal/△w total/2.5
	55	0.4	74.85	86.18	0.004773	0.004469	0.43
		0.5	78.8	79.75	0.008323	0.003545	0.94
		0.6	82.44	82.44	0.01191	0.002681	1.78
		0.7	85.82	85.82	0.01554	0.001868	3.33
		0.8	88.98	88.98	0.01921	0.001099	6.99

Table 64 Baseline and external evaporative cooling system performance and percentage difference

Tout	RH	Taeo	COP ref	COP in	COP % diff
80	0.4	45	3.866	4.201	8.67%
80	0.5	45	3.866	4.546	17.59%
80	0.6	45	3.866	4.761	23.15%
80	0.7	45	3.866	4.499	16.37%
80	0.8	45	3.866	4.269	10.42%
80	0.4	50	4.237	4.401	3.87%
80	0.5	50	4.237	4.776	12.72%
80	0.6	50	4.237	5.194	22.59%
80	0.7	50	4.237	4.966	17.21%
80	0.8	50	4.237	4.698	10.88%
80	0.4	55	4.667	4.667	0.00%
80	0.5	55	4.667	4.979	6.69%
80	0.6	55	4.667	5.431	16.37%
80	0.7	55	4.667	5.515	18.17%
80	0.8	55	4.667	5.2	11.42%
85	0.4	45	3.516	4.027	14.53%
85	0.5	45	3.516	4.414	25.54%
85	0.6	45	3.516	4.367	24.20%
85	0.7	45	3.516	4.117	17.09%
85	0.8	45	3.516	3.899	10.89%
85	0.4	50	3.837	4.211	9.75%
85	0.5	50	3.837	4.631	20.69%
85	0.6	50	3.837	4.812	25.41%

Table 64 continued

85	0.7	50	3.837	4.523	17.88%
85	0.8	50	3.837	4.271	11.31%
85	0.4	55	4.206	4.369	3.88%
85	0.5	55	4.206	4.821	14.62%
85	0.6	55	4.206	5.334	26.82%
85	0.7	55	4.206	4.995	18.76%
85	0.8	55	4.206	4.702	11.79%
90	0.4	45	3.201	3.894	21.65%
90	0.5	45	3.201	4.291	34.05%
90	0.6	45	3.201	4.015	25.43%
90	0.7	45	3.201	3.776	17.96%
90	0.8	45	3.201	3.568	11.47%
90	0.4	50	3.481	4.067	16.83%
90	0.5	50	3.481	4.543	30.51%
90	0.6	50	3.481	4.404	26.52%
90	0.7	50	3.481	4.13	18.64%
90	0.8	50	3.481	3.893	11.84%
90	0.4	55	3.799	4.213	10.90%
90	0.5	55	3.799	4.725	24.37%
90	0.6	55	3.799	4.856	27.82%
90	0.7	55	3.799	4.539	19.48%
90	0.8	55	3.799	4.266	12.29%
95	0.4	45	2.914	3.803	30.51%
95	0.5	45	2.914	3.963	36.00%
95	0.6	45	2.914	3.697	26.87%
95	0.7	45	2.914	3.468	19.01%
95	0.8	45	2.914	3.269	12.18%
95	0.4	50	3.159	3.967	25.58%
95	0.5	50	3.159	4.345	37.54%
95	0.6	50	3.159	4.04	27.89%
95	0.7	50	3.159	3.779	19.63%
95	0.8	50	3.159	3.554	12.50%
95	0.4	55	3.436	4.105	19.47%
95	0.5	55	3.436	4.691	36.53%
95	0.6	55	3.436	4.434	29.05%
95	0.7	55	3.436	4.135	20.34%
95	0.8	55	3.436	3.878	12.86%

Table 65 Quadratic and exponential functions for system with internal evaporative cooling

Tout	RH	Taeo	qua predicted	ex predicted	model	qua rs	ex rs	% qua	% ex
80	0.4	45	4.181	4.194	4.201	0.020	0.007	0.47%	0.18%
80	0.5	45	4.546	4.550	4.546	0.000	-0.004	-0.01%	-0.10%
80	0.6	45	4.685	4.689	4.761	0.076	0.072	1.61%	1.51%
80	0.7	45	4.596	4.588	4.499	-0.097	-0.089	-2.15%	-1.98%
80	0.8	45	4.280	4.263	4.269	-0.011	0.006	-0.25%	0.13%
80	0.4	50	4.412	4.394	4.401	-0.011	0.007	-0.25%	0.17%
80	0.5	50	4.834	4.833	4.776	-0.058	-0.057	-1.21%	-1.20%
80	0.6	50	5.029	5.049	5.194	0.165	0.145	3.18%	2.79%
80	0.7	50	4.997	5.009	4.966	-0.031	-0.043	-0.62%	-0.87%
80	0.8	50	4.738	4.719	4.698	-0.040	-0.021	-0.85%	-0.44%
80	0.4	55	4.657	4.592	4.667	0.010	0.075	0.21%	1.60%
80	0.5	55	5.136	5.122	4.979	-0.157	-0.143	-3.15%	-2.86%
80	0.6	55	5.388	5.424	5.431	0.043	0.007	0.79%	0.12%
80	0.7	55	5.413	5.455	5.515	0.102	0.060	1.86%	1.08%
80	0.8	55	5.210	5.210	5.2	-0.010	-0.010	-0.20%	-0.19%
85	0.4	45	4.036	4.059	4.027	-0.009	-0.032	-0.22%	-0.80%
85	0.5	45	4.329	4.329	4.414	0.085	0.085	1.92%	1.92%
85	0.6	45	4.395	4.385	4.367	-0.028	-0.018	-0.65%	-0.40%
85	0.7	45	4.234	4.217	4.117	-0.117	-0.100	-2.85%	-2.42%
85	0.8	45	3.846	3.851	3.899	0.053	0.048	1.35%	1.23%
85	0.4	50	4.249	4.258	4.211	-0.038	-0.047	-0.91%	-1.11%
85	0.5	50	4.599	4.604	4.631	0.032	0.027	0.69%	0.59%
85	0.6	50	4.722	4.727	4.812	0.090	0.085	1.87%	1.77%
85	0.7	50	4.618	4.609	4.523	-0.095	-0.086	-2.10%	-1.90%
85	0.8	50	4.287	4.267	4.271	-0.016	0.004	-0.37%	0.09%
85	0.4	55	4.477	4.455	4.369	-0.108	-0.086	-2.47%	-1.97%
85	0.5	55	4.884	4.884	4.821	-0.063	-0.063	-1.30%	-1.30%
85	0.6	55	5.063	5.084	5.334	0.271	0.250	5.07%	4.70%
85	0.7	55	5.016	5.025	4.995	-0.021	-0.030	-0.42%	-0.60%
85	0.8	55	4.742	4.717	4.702	-0.040	-0.015	-0.85%	-0.31%
90	0.4	45	3.910	3.928	3.894	-0.016	-0.034	-0.40%	-0.87%
90	0.5	45	4.131	4.117	4.291	0.160	0.174	3.74%	4.05%
90	0.6	45	4.125	4.098	4.015	-0.110	-0.083	-2.73%	-2.07%
90	0.7	45	3.892	3.874	3.776	-0.116	-0.098	-3.06%	-2.59%
90	0.8	45	3.431	3.477	3.568	0.137	0.091	3.83%	2.55%
90	0.4	50	4.105	4.125	4.067	-0.038	-0.058	-0.94%	-1.41%
90	0.5	50	4.383	4.383	4.543	0.160	0.160	3.52%	3.52%
90	0.6	50	4.434	4.423	4.404	-0.030	-0.019	-0.68%	-0.43%
90	0.7	50	4.258	4.239	4.13	-0.128	-0.109	-3.09%	-2.63%

Table 65 continued

Tout	RH	Taeo	qua predicted	ex predicted	model	qua rs	ex rs	% qua	% ex
90	0.8	50	3.854	3.857	3.893	0.039	0.036	0.99%	0.92%
90	0.4	55	4.315	4.321	4.213	-0.102	-0.108	-2.43%	-2.55%
90	0.5	55	4.650	4.655	4.725	0.075	0.070	1.59%	1.49%
90	0.6	55	4.758	4.762	4.856	0.098	0.094	2.03%	1.93%
90	0.7	55	4.638	4.627	4.539	-0.099	-0.088	-2.18%	-1.93%
90	0.8	55	4.292	4.268	4.266	-0.026	-0.002	-0.60%	-0.05%
95	0.4	45	3.802	3.799	3.803	0.001	0.004	0.03%	0.11%
95	0.5	45	3.951	3.914	3.963	0.012	0.049	0.31%	1.24%
95	0.6	45	3.873	3.829	3.697	-0.176	-0.132	-4.75%	-3.57%
95	0.7	45	3.567	3.557	3.468	-0.099	-0.089	-2.87%	-2.57%
95	0.8	45	3.035	3.138	3.269	0.234	0.131	7.15%	4.00%
95	0.4	50	3.980	3.994	3.967	-0.013	-0.027	-0.32%	-0.67%
95	0.5	50	4.185	4.171	4.345	0.160	0.174	3.67%	4.00%
95	0.6	50	4.164	4.137	4.04	-0.124	-0.097	-3.07%	-2.40%
95	0.7	50	3.916	3.897	3.779	-0.137	-0.118	-3.62%	-3.11%
95	0.8	50	3.441	3.485	3.554	0.113	0.069	3.19%	1.94%
95	0.4	55	4.172	4.188	4.105	-0.067	-0.083	-1.64%	-2.02%
95	0.5	55	4.435	4.435	4.691	0.256	0.256	5.46%	5.46%
95	0.6	55	4.470	4.459	4.434	-0.036	-0.025	-0.82%	-0.57%
95	0.7	55	4.279	4.258	4.135	-0.144	-0.123	-3.48%	-2.97%
95	0.8	55	3.860	3.861	3.878	0.018	0.017	0.46%	0.44%

Table 66 Quadratic and exponential functions for COP ratio of internal evaporative cooling over baseline

Tout	RH	Taeo	qua pre	ex pre	model	qua re	ex re	% qua	% ex
80	0.4	45	1.084	1.085	1.087	0.003	0.002	0.26%	0.19%
80	0.5	45	1.179	1.177	1.176	-0.003	-0.001	-0.28%	-0.09%
80	0.6	45	1.214	1.213	1.232	0.018	0.019	1.45%	1.52%
80	0.7	45	1.187	1.187	1.164	-0.024	-0.023	-2.04%	-1.97%
80	0.8	45	1.100	1.103	1.104	0.004	0.002	0.35%	0.15%
80	0.4	50	1.032	1.037	1.039	0.006	0.002	0.60%	0.19%
80	0.5	50	1.144	1.140	1.127	-0.016	-0.013	-1.45%	-1.18%
80	0.6	50	1.194	1.191	1.226	0.032	0.034	2.61%	2.81%
80	0.7	50	1.183	1.182	1.172	-0.011	-0.010	-0.97%	-0.84%
80	0.8	50	1.112	1.113	1.109	-0.003	-0.005	-0.31%	-0.41%
80	0.4	55	0.974	0.984	1.000	0.026	0.016	2.60%	1.55%
80	0.5	55	1.101	1.098	1.067	-0.034	-0.031	-3.19%	-2.92%
80	0.6	55	1.167	1.163	1.164	-0.003	0.001	-0.28%	0.07%

Table 66 continued

Tout	RH	Taeo	qua pre	ex pre	model	qua re	ex re	% qua	% ex
80	0.7	55	1.172	1.170	1.182	0.009	0.012	0.79%	1.03%
80	0.8	55	1.117	1.117	1.114	-0.003	-0.003	-0.24%	-0.24%
85	0.4	45	1.157	1.155	1.145	-0.012	-0.009	-1.05%	-0.82%
85	0.5	45	1.232	1.232	1.255	0.023	0.024	1.84%	1.90%
85	0.6	45	1.246	1.247	1.242	-0.004	-0.005	-0.36%	-0.42%
85	0.7	45	1.200	1.200	1.171	-0.029	-0.029	-2.47%	-2.44%
85	0.8	45	1.092	1.095	1.109	0.017	0.013	1.49%	1.21%
85	0.4	50	1.111	1.109	1.097	-0.014	-0.012	-1.26%	-1.08%
85	0.5	50	1.202	1.199	1.207	0.005	0.007	0.41%	0.62%
85	0.6	50	1.232	1.232	1.254	0.022	0.023	1.77%	1.80%
85	0.7	50	1.201	1.201	1.179	-0.022	-0.022	-1.89%	-1.87%
85	0.8	50	1.109	1.112	1.113	0.004	0.001	0.33%	0.12%
85	0.4	55	1.058	1.059	1.039	-0.019	-0.020	-1.85%	-1.93%
85	0.5	55	1.165	1.161	1.146	-0.018	-0.014	-1.60%	-1.26%
85	0.6	55	1.210	1.208	1.268	0.058	0.060	4.57%	4.74%
85	0.7	55	1.195	1.194	1.188	-0.008	-0.007	-0.64%	-0.56%
85	0.8	55	1.119	1.121	1.118	-0.001	-0.003	-0.13%	-0.27%
90	0.4	45	1.231	1.228	1.216	-0.014	-0.011	-1.17%	-0.91%
90	0.5	45	1.285	1.287	1.341	0.055	0.054	4.12%	4.01%
90	0.6	45	1.279	1.281	1.254	-0.025	-0.027	-1.97%	-2.12%
90	0.7	45	1.212	1.211	1.180	-0.032	-0.031	-2.74%	-2.63%
90	0.8	45	1.084	1.087	1.115	0.031	0.028	2.74%	2.51%
90	0.4	50	1.190	1.185	1.168	-0.021	-0.017	-1.84%	-1.45%
90	0.5	50	1.260	1.260	1.305	0.045	0.045	3.44%	3.49%
90	0.6	50	1.270	1.271	1.265	-0.005	-0.006	-0.36%	-0.47%
90	0.7	50	1.218	1.218	1.186	-0.032	-0.032	-2.70%	-2.67%
90	0.8	50	1.106	1.108	1.118	0.012	0.010	1.07%	0.89%
90	0.4	55	1.142	1.137	1.109	-0.033	-0.028	-2.96%	-2.53%
90	0.5	55	1.228	1.225	1.244	0.016	0.019	1.27%	1.51%
90	0.6	55	1.253	1.253	1.278	0.025	0.025	1.96%	1.96%
90	0.7	55	1.218	1.218	1.195	-0.023	-0.023	-1.92%	-1.90%
90	0.8	55	1.122	1.123	1.123	0.001	0.000	0.12%	-0.03%
95	0.4	45	1.304	1.303	1.305	0.001	0.002	0.11%	0.16%
95	0.5	45	1.338	1.342	1.360	0.022	0.018	1.63%	1.29%
95	0.6	45	1.311	1.313	1.269	-0.042	-0.045	-3.35%	-3.51%
95	0.7	45	1.224	1.220	1.190	-0.034	-0.030	-2.83%	-2.52%
95	0.8	45	1.076	1.076	1.122	0.046	0.045	4.12%	4.05%
95	0.4	50	1.268	1.264	1.256	-0.012	-0.009	-0.98%	-0.69%
95	0.5	50	1.318	1.321	1.375	0.057	0.055	4.18%	3.98%
95	0.6	50	1.307	1.310	1.279	-0.028	-0.031	-2.21%	-2.42%

Table 66 continued

Tout	RH	Taeo	qua pre	ex pre	model	qua re	ex re	% qua	% ex
95	0.7	50	1.236	1.234	1.196	-0.039	-0.037	-3.28%	-3.13%
95	0.8	50	1.103	1.103	1.125	0.022	0.022	1.95%	1.92%
95	0.4	55	1.225	1.219	1.195	-0.031	-0.024	-2.56%	-2.04%
95	0.5	55	1.291	1.291	1.365	0.074	0.074	5.44%	5.45%
95	0.6	55	1.296	1.298	1.290	-0.005	-0.008	-0.42%	-0.58%
95	0.7	55	1.240	1.239	1.203	-0.037	-0.036	-3.05%	-2.99%
95	0.8	55	1.123	1.124	1.129	0.005	0.005	0.46%	0.43%

Table 67 Baseline and system with HRV COP and COP percentage difference

Tout	RH	Taeo	COP ref	COP HRV	% difference
80	0.4	45	3.866	4.14	7.09%
80	0.5	45	3.866	4.09	5.79%
80	0.6	45	3.866	4.055	4.89%
80	0.7	45	3.866	4.03	4.24%
80	0.8	45	3.866	4.01	3.72%
80	0.4	50	4.237	4.64	9.51%
80	0.5	50	4.237	4.546	7.29%
80	0.6	50	4.237	4.488	5.92%
80	0.7	50	4.237	4.448	4.98%
80	0.8	50	4.237	4.419	4.30%
80	0.4	55	4.667	5.376	15.19%
80	0.5	55	4.667	5.144	10.22%
80	0.6	55	4.667	5.026	7.69%
80	0.7	55	4.667	4.955	6.17%
80	0.8	55	4.667	4.908	5.16%
85	0.4	45	3.516	3.93	11.77%
85	0.5	45	3.516	3.855	9.64%
85	0.6	45	3.516	3.804	8.19%
85	0.7	45	3.516	3.765	7.08%
85	0.8	45	3.516	3.736	6.26%
85	0.4	50	3.837	4.409	14.91%
85	0.5	50	3.837	4.284	11.65%
85	0.6	50	3.837	4.204	9.56%
85	0.7	50	3.837	4.149	8.13%
85	0.8	50	3.837	4.108	7.06%
85	0.4	55	4.206	5.092	21.07%
85	0.5	55	4.206	4.84	15.07%

Table 67 continued

Tout	RH	Taeo	COP ref	COP HRV	% difference
85	0.6	55	4.206	4.7	11.75%
85	0.7	55	4.206	4.611	9.63%
85	0.8	55	4.206	4.549	8.16%
90	0.4	45	3.201	3.676	14.84%
90	0.5	45	3.201	3.592	12.21%
90	0.6	45	3.201	3.533	10.37%
90	0.7	45	3.201	3.489	9.00%
90	0.8	45	3.201	3.397	6.12%
90	0.4	50	3.481	4.108	18.01%
90	0.5	50	3.481	3.978	14.28%
90	0.6	50	3.481	3.892	11.81%
90	0.7	50	3.481	3.832	10.08%
90	0.8	50	3.481	3.716	6.75%
90	0.4	55	3.799	4.694	23.56%
90	0.5	55	3.799	4.464	17.50%
90	0.6	55	3.799	4.328	13.92%
90	0.7	55	3.799	4.239	11.58%
90	0.8	55	3.799	4.087	7.58%
95	0.4	45	2.914	3.405	16.85%
95	0.5	45	2.914	3.318	13.86%
95	0.6	45	2.914	3.258	11.81%
95	0.7	45	2.914	3.196	9.68%
95	0.8	45	2.914	3.067	5.25%
95	0.4	50	3.159	3.784	19.78%
95	0.5	50	3.159	3.658	15.80%
95	0.6	50	3.159	3.575	13.17%
95	0.7	50	3.159	3.495	10.64%
95	0.8	50	3.159	3.339	5.70%
95	0.4	55	3.436	4.277	24.48%
95	0.5	55	3.436	4.076	18.63%
95	0.6	55	3.436	3.953	15.05%
95	0.7	55	3.436	3.844	11.87%
95	0.8	55	3.436	3.65	6.23%

Table 68 Predicted and actual data of COP and COP ratio for reconfigured system with HRV

Tout	RH	Taeo	COP HRV	COP HRV predicted	COP % error	COP ratio	COP ratio predicted	COP ratio % error
80	0.4	45	4.140	4.127	0.31%	1.07	1.07	0.32%
80	0.5	45	4.090	4.080	0.24%	1.06	1.06	0.25%
80	0.6	45	4.055	4.046	0.21%	1.05	1.05	0.22%
80	0.7	45	4.030	4.025	0.11%	1.04	1.04	0.12%
80	0.8	45	4.010	4.017	-0.18%	1.04	1.04	-0.17%
80	0.4	50	4.640	4.655	-0.32%	1.10	1.10	-0.29%
80	0.5	50	4.546	4.569	-0.52%	1.07	1.08	-0.49%
80	0.6	50	4.488	4.500	-0.27%	1.06	1.06	-0.24%
80	0.7	50	4.448	4.445	0.06%	1.05	1.05	0.08%
80	0.8	50	4.419	4.405	0.31%	1.04	1.04	0.33%
80	0.4	55	5.376	5.317	1.10%	1.15	1.14	1.04%
80	0.5	55	5.144	5.183	-0.76%	1.10	1.11	-0.81%
80	0.6	55	5.026	5.068	-0.85%	1.08	1.09	-0.90%
80	0.7	55	4.955	4.972	-0.35%	1.06	1.07	-0.40%
80	0.8	55	4.908	4.893	0.31%	1.05	1.05	0.25%
85	0.4	45	3.930	3.926	0.11%	1.12	1.12	0.09%
85	0.5	45	3.855	3.859	-0.11%	1.10	1.10	-0.13%
85	0.6	45	3.804	3.806	-0.04%	1.08	1.08	-0.06%
85	0.7	45	3.765	3.765	0.00%	1.07	1.07	-0.02%
85	0.8	45	3.736	3.736	-0.01%	1.06	1.06	-0.03%
85	0.4	50	4.409	4.408	0.02%	1.15	1.15	0.05%
85	0.5	50	4.284	4.303	-0.44%	1.12	1.12	-0.41%
85	0.6	50	4.204	4.214	-0.23%	1.10	1.10	-0.20%
85	0.7	50	4.149	4.139	0.23%	1.08	1.08	0.26%
85	0.8	50	4.108	4.079	0.70%	1.07	1.06	0.73%
85	0.4	55	5.092	5.013	1.55%	1.21	1.19	1.59%
85	0.5	55	4.840	4.859	-0.40%	1.15	1.15	-0.36%
85	0.6	55	4.700	4.725	-0.54%	1.12	1.12	-0.50%
85	0.7	55	4.611	4.610	0.03%	1.10	1.10	0.07%
85	0.8	55	4.549	4.511	0.84%	1.08	1.07	0.88%
90	0.4	45	3.676	3.684	-0.23%	1.15	1.15	-0.27%
90	0.5	45	3.592	3.602	-0.27%	1.12	1.13	-0.31%
90	0.6	45	3.533	3.532	0.03%	1.10	1.10	-0.01%
90	0.7	45	3.489	3.474	0.42%	1.09	1.09	0.37%
90	0.8	45	3.397	3.429	-0.94%	1.06	1.07	-0.98%
90	0.4	50	4.108	4.119	-0.27%	1.18	1.18	-0.30%
90	0.5	50	3.978	3.998	-0.51%	1.14	1.15	-0.55%
90	0.6	50	3.892	3.894	-0.04%	1.12	1.12	-0.07%
90	0.7	50	3.832	3.803	0.74%	1.10	1.09	0.71%

Table 68 continued

Tout	RH	Taeo	COP HRV	COP HRV predicted	COP % error	COP ratio	COP ratio predicted	COP ratio % error
90	0.8	50	3.716	3.727	-0.30%	1.07	1.07	-0.34%
90	0.4	55	4.694	4.664	0.64%	1.24	1.23	0.67%
90	0.5	55	4.464	4.496	-0.71%	1.18	1.18	-0.68%
90	0.6	55	4.328	4.347	-0.45%	1.14	1.14	-0.42%
90	0.7	55	4.239	4.217	0.52%	1.12	1.11	0.54%
90	0.8	55	4.087	4.104	-0.41%	1.08	1.08	-0.38%
95	0.4	45	3.405	3.412	-0.21%	1.17	1.17	-0.16%
95	0.5	45	3.318	3.317	0.04%	1.14	1.14	0.09%
95	0.6	45	3.258	3.234	0.72%	1.12	1.11	0.78%
95	0.7	45	3.196	3.164	1.00%	1.10	1.09	1.05%
95	0.8	45	3.067	3.105	-1.24%	1.05	1.06	-1.18%
95	0.4	50	3.784	3.798	-0.37%	1.20	1.20	-0.39%
95	0.5	50	3.658	3.666	-0.22%	1.16	1.16	-0.24%
95	0.6	50	3.575	3.550	0.70%	1.13	1.12	0.68%
95	0.7	50	3.495	3.448	1.33%	1.11	1.09	1.31%
95	0.8	50	3.339	3.360	-0.64%	1.06	1.06	-0.66%
95	0.4	55	4.277	4.282	-0.11%	1.24	1.25	-0.12%
95	0.5	55	4.076	4.104	-0.69%	1.19	1.19	-0.70%
95	0.6	55	3.953	3.946	0.17%	1.15	1.15	0.15%
95	0.7	55	3.844	3.807	0.97%	1.12	1.11	0.95%
95	0.8	55	3.650	3.684	-0.92%	1.06	1.07	-0.94%

Table 69 Baseline and system with HRV COP and COP percentage difference

Tout	RH	Taeo	COP ref	COP ERV	% difference
80	0.4	45	3.866	4.140	7.09%
80	0.5	45	3.866	4.471	15.65%
80	0.6	45	3.866	4.867	25.89%
80	0.7	45	3.866	5.209	34.74%
80	0.8	45	3.866	5.508	42.47%
80	0.4	50	4.237	4.640	9.51%
80	0.5	50	4.237	5.093	20.20%
80	0.6	50	4.237	5.623	32.71%
80	0.7	50	4.237	6.063	43.10%
80	0.8	50	4.237	6.434	51.85%
80	0.4	55	4.667	5.376	15.19%
80	0.5	55	4.667	6.054	29.72%

Table 69 continued

Tout	RH	Taeo	COP ref	COP ERV	% difference
80	0.6	55	4.667	6.815	46.03%
80	0.7	55	4.667	7.399	58.54%
80	0.8	55	4.667	7.860	68.42%
85	0.4	45	3.516	4.147	17.95%
85	0.5	45	3.516	4.552	29.47%
85	0.6	45	3.516	4.894	39.19%
85	0.7	45	3.516	5.188	47.55%
85	0.8	45	3.516	5.443	54.81%
85	0.4	50	3.837	4.722	23.06%
85	0.5	50	3.837	5.255	36.96%
85	0.6	50	3.837	5.686	48.19%
85	0.7	50	3.837	6.042	57.47%
85	0.8	50	3.837	6.341	65.26%
85	0.4	55	4.206	5.619	33.59%
85	0.5	55	4.206	6.361	51.24%
85	0.6	55	4.206	6.913	64.36%
85	0.7	55	4.206	7.339	74.49%
85	0.8	55	4.206	7.678	82.55%
90	0.4	45	3.201	4.184	30.71%
90	0.5	45	3.201	4.538	41.77%
90	0.6	45	3.201	4.834	51.02%
90	0.7	45	3.201	5.087	58.92%
90	0.8	45	3.201	5.304	65.70%
90	0.4	50	3.481	4.818	38.41%
90	0.5	50	3.481	5.258	51.05%
90	0.6	50	3.481	5.612	61.22%
90	0.7	50	3.481	5.903	69.58%
90	0.8	50	3.481	6.147	76.59%
90	0.4	55	3.799	5.813	53.01%
90	0.5	55	3.799	6.367	67.60%
90	0.6	55	3.799	6.780	78.47%
90	0.7	55	3.799	7.101	86.92%
90	0.8	55	3.799	7.357	93.66%
95	0.4	45	2.914	4.143	42.18%
95	0.5	45	2.914	4.453	52.81%
95	0.6	45	2.914	4.710	61.63%
95	0.7	45	2.914	4.927	69.08%
95	0.8	45	2.914	5.112	75.43%
95	0.4	50	3.159	4.786	51.50%

Table 69 continued

Tout	RH	Taeo	COP ref	COP ERV	% difference
95	0.5	50	3.159	5.153	63.12%
95	0.6	50	3.159	5.446	72.40%
95	0.7	50	3.159	5.686	79.99%
95	0.8	50	3.159	5.885	86.29%
95	0.4	55	3.436	5.775	68.07%
95	0.5	55	3.436	6.198	80.38%
95	0.6	55	3.436	6.516	89.64%
95	0.7	55	3.436	6.762	96.80%
95	0.8	55	3.436	6.959	102.53%

Table 70 Predicted and actual data of COP and COP ratio for reconfigured system with ERV

Tout	RH	Taeo	COP ERV	COP ERV predicted	COP % error	COP ratio	COP ratio predicted	COP ratio % error
80	0.4	45	4.140	4.021	2.87%	1.07	1.04	2.88%
80	0.5	45	4.471	4.461	0.22%	1.16	1.15	0.23%
80	0.6	45	4.867	4.872	-0.11%	1.26	1.26	-0.10%
80	0.7	45	5.209	5.238	-0.56%	1.35	1.35	-0.55%
80	0.8	45	5.508	5.544	-0.65%	1.42	1.43	-0.64%
80	0.4	50	4.640	4.613	0.58%	1.10	1.09	0.61%
80	0.5	50	5.093	5.134	-0.81%	1.20	1.21	-0.79%
80	0.6	50	5.623	5.626	-0.05%	1.33	1.33	-0.02%
80	0.7	50	6.063	6.068	-0.08%	1.43	1.43	-0.06%
80	0.8	50	6.434	6.443	-0.13%	1.52	1.52	-0.11%
80	0.4	55	5.376	5.509	-2.48%	1.15	1.18	-2.54%
80	0.5	55	6.054	6.152	-1.62%	1.30	1.32	-1.68%
80	0.6	55	6.815	6.763	0.77%	1.46	1.45	0.71%
80	0.7	55	7.399	7.318	1.10%	1.59	1.57	1.04%
80	0.8	55	7.860	7.795	0.83%	1.68	1.67	0.77%
85	0.4	45	4.147	4.149	-0.06%	1.18	1.18	-0.08%
85	0.5	45	4.552	4.551	0.03%	1.29	1.29	0.01%
85	0.6	45	4.894	4.913	-0.39%	1.39	1.40	-0.41%
85	0.7	45	5.188	5.222	-0.65%	1.48	1.49	-0.67%
85	0.8	45	5.443	5.463	-0.36%	1.55	1.55	-0.38%
85	0.4	50	4.722	4.760	-0.81%	1.23	1.24	-0.78%
85	0.5	50	5.255	5.238	0.33%	1.37	1.36	0.35%
85	0.6	50	5.686	5.673	0.22%	1.48	1.48	0.25%

Table 70 continued

Tout	RH	Taeo	COP ERV	COP ERV predicted	COP % error	COP ratio	COP ratio predicted	COP ratio % error
85	0.7	50	6.042	6.049	-0.12%	1.57	1.58	-0.09%
85	0.8	50	6.341	6.349	-0.13%	1.65	1.65	-0.10%
85	0.4	55	5.619	5.686	-1.19%	1.34	1.35	-1.15%
85	0.5	55	6.361	6.276	1.33%	1.51	1.49	1.37%
85	0.6	55	6.913	6.820	1.34%	1.64	1.62	1.38%
85	0.7	55	7.339	7.296	0.59%	1.74	1.73	0.63%
85	0.8	55	7.678	7.682	-0.06%	1.83	1.83	-0.02%
90	0.4	45	4.184	4.202	-0.42%	1.31	1.31	-0.46%
90	0.5	45	4.538	4.555	-0.38%	1.42	1.42	-0.42%
90	0.6	45	4.834	4.862	-0.57%	1.51	1.52	-0.62%
90	0.7	45	5.087	5.108	-0.41%	1.59	1.60	-0.45%
90	0.8	45	5.304	5.282	0.41%	1.66	1.65	0.36%
90	0.4	50	4.818	4.821	-0.05%	1.38	1.39	-0.09%
90	0.5	50	5.258	5.243	0.28%	1.51	1.51	0.24%
90	0.6	50	5.612	5.614	-0.04%	1.61	1.61	-0.08%
90	0.7	50	5.903	5.918	-0.25%	1.70	1.70	-0.28%
90	0.8	50	6.147	6.140	0.12%	1.77	1.76	0.08%
90	0.4	55	5.813	5.758	0.94%	1.53	1.52	0.97%
90	0.5	55	6.367	6.283	1.31%	1.68	1.65	1.34%
90	0.6	55	6.780	6.750	0.45%	1.78	1.78	0.47%
90	0.7	55	7.101	7.138	-0.51%	1.87	1.88	-0.49%
90	0.8	55	7.357	7.430	-0.99%	1.94	1.96	-0.96%
95	0.4	45	4.143	4.175	-0.77%	1.42	1.43	-0.72%
95	0.5	45	4.453	4.474	-0.48%	1.53	1.53	-0.43%
95	0.6	45	4.710	4.721	-0.23%	1.62	1.62	-0.18%
95	0.7	45	4.927	4.903	0.49%	1.69	1.68	0.54%
95	0.8	45	5.112	5.012	1.95%	1.75	1.72	2.00%
95	0.4	50	4.786	4.790	-0.09%	1.52	1.52	-0.11%
95	0.5	50	5.153	5.151	0.05%	1.63	1.63	0.03%
95	0.6	50	5.446	5.452	-0.11%	1.72	1.73	-0.13%
95	0.7	50	5.686	5.681	0.10%	1.80	1.80	0.08%
95	0.8	50	5.885	5.826	0.99%	1.86	1.84	0.98%
95	0.4	55	5.775	5.722	0.92%	1.68	1.67	0.90%
95	0.5	55	6.198	6.173	0.41%	1.80	1.80	0.39%
95	0.6	55	6.516	6.555	-0.60%	1.90	1.91	-0.61%
95	0.7	55	6.762	6.852	-1.33%	1.97	1.99	-1.35%
95	0.8	55	6.959	7.051	-1.32%	2.03	2.05	-1.34%

Table 71 Baseline and system with condensing refrigerant subcooloing COP and COP percentage difference

			HX 20%		HX 50%		HX 80%		HX 100%	
Tout	RH	Taeo	COP ref	% difference	COP subcooling	% difference	COP subcooling	% difference	COP subcooling	% difference
80	0.4	45	3.866	0.28%	3.893	0.70%	3.909	1.11%	3.919	1.37%
80	0.5	45	3.866	0.44%	3.908	1.09%	3.934	1.76%	3.952	2.22%
80	0.6	45	3.866	0.54%	3.92	1.40%	3.953	2.25%	3.975	2.82%
80	0.7	45	3.866	0.65%	3.928	1.60%	3.966	2.59%	3.992	3.26%
80	0.8	45	3.866	0.70%	3.935	1.78%	3.977	2.87%	4.006	3.62%
80	0.4	50	4.237	0.14%	4.253	0.38%	4.262	0.59%	4.268	0.73%
80	0.5	50	4.237	0.35%	4.275	0.90%	4.298	1.44%	4.314	1.82%
80	0.6	50	4.237	0.50%	4.29	1.25%	4.322	2.01%	4.343	2.50%
80	0.7	50	4.237	0.59%	4.3	1.49%	4.338	2.38%	4.364	3.00%
80	0.8	50	4.237	0.66%	4.307	1.65%	4.35	2.67%	4.38	3.38%
80	0.4	55	4.667	-0.11%	4.655	-0.26%	4.648	-0.41%	4.643	-0.51%
80	0.5	55	4.667	0.21%	4.694	0.58%	4.71	0.92%	4.721	1.16%
80	0.6	55	4.667	0.41%	4.715	1.03%	4.744	1.65%	4.764	2.08%
80	0.7	55	4.667	0.51%	4.728	1.31%	4.766	2.12%	4.792	2.68%
80	0.8	55	4.667	0.60%	4.738	1.52%	4.781	2.44%	4.811	3.09%
85	0.4	45	3.516	0.37%	3.55	0.97%	3.571	1.56%	3.585	1.96%
85	0.5	45	3.516	0.54%	3.563	1.34%	3.592	2.16%	3.612	2.73%
85	0.6	45	3.516	0.63%	3.573	1.62%	3.608	2.62%	3.632	3.30%
85	0.7	45	3.516	0.71%	3.58	1.82%	3.62	2.96%	3.647	3.73%
85	0.8	45	3.516	0.77%	3.586	1.99%	3.63	3.24%	3.659	4.07%
85	0.4	50	3.837	0.29%	3.865	0.73%	3.882	1.17%	3.894	1.49%
85	0.5	50	3.837	0.47%	3.883	1.20%	3.91	1.90%	3.929	2.40%
85	0.6	50	3.837	0.60%	3.894	1.49%	3.93	2.42%	3.953	3.02%
85	0.7	50	3.837	0.68%	3.903	1.72%	3.943	2.76%	3.971	3.49%
85	0.8	50	3.837	0.76%	3.909	1.88%	3.954	3.05%	3.984	3.83%
85	0.4	55	4.206	0.14%	4.221	0.36%	4.23	0.57%	4.236	0.71%
85	0.5	55	4.206	0.38%	4.246	0.95%	4.27	1.52%	4.287	1.93%
85	0.6	55	4.206	0.52%	4.261	1.31%	4.295	2.12%	4.319	2.69%
85	0.7	55	4.206	0.62%	4.272	1.57%	4.312	2.52%	4.34	3.19%

Table 71 continued

Tout	RH	Taeo	COP ref	% difference	COP subcooling	% difference	COP subcooling	% difference	COP subcooling	% difference
85	0.8	55	4.206	0.69%	4.279	1.74%	4.325	2.83%	4.355	3.54%
90	0.4	45	3.201	0.47%	3.24	1.22%	3.265	2.00%	3.281	2.50%
90	0.5	45	3.201	0.62%	3.252	1.59%	3.284	2.59%	3.305	3.25%
90	0.6	45	3.201	0.72%	3.261	1.87%	3.298	3.03%	3.323	3.81%
90	0.7	45	3.201	0.81%	3.267	2.06%	3.308	3.34%	3.336	4.22%
90	0.8	45	3.201	0.87%	3.272	2.22%	3.317	3.62%	3.347	4.56%
90	0.4	50	3.481	0.40%	3.517	1.03%	3.539	1.67%	3.554	2.10%
90	0.5	50	3.481	0.57%	3.531	1.44%	3.563	2.36%	3.584	2.96%
90	0.6	50	3.481	0.69%	3.541	1.72%	3.579	2.82%	3.604	3.53%
90	0.7	50	3.481	0.78%	3.549	1.95%	3.591	3.16%	3.619	3.96%
90	0.8	50	3.481	0.83%	3.554	2.10%	3.6	3.42%	3.631	4.31%
90	0.4	55	3.799	0.32%	3.829	0.79%	3.846	1.24%	3.859	1.58%
90	0.5	55	3.799	0.50%	3.847	1.26%	3.877	2.05%	3.897	2.58%
90	0.6	55	3.799	0.63%	3.859	1.58%	3.897	2.58%	3.922	3.24%
90	0.7	55	3.799	0.71%	3.868	1.82%	3.911	2.95%	3.94	3.71%
90	0.8	55	3.799	0.79%	3.874	1.97%	3.921	3.21%	3.953	4.05%
95	0.4	45	2.914	0.62%	2.958	1.51%	2.985	2.44%	3.003	3.05%
95	0.5	45	2.914	0.75%	2.969	1.89%	3.002	3.02%	3.025	3.81%
95	0.6	45	2.914	0.86%	2.976	2.13%	3.014	3.43%	3.041	4.36%
95	0.7	45	2.914	0.93%	2.982	2.33%	3.024	3.77%	3.053	4.77%
95	0.8	45	2.914	1.00%	2.987	2.51%	3.032	4.05%	3.062	5.08%
95	0.4	50	3.159	0.54%	3.202	1.36%	3.227	2.15%	3.245	2.72%
95	0.5	50	3.159	0.70%	3.214	1.74%	3.247	2.79%	3.27	3.51%
95	0.6	50	3.159	0.79%	3.222	1.99%	3.261	3.23%	3.288	4.08%
95	0.7	50	3.159	0.89%	3.229	2.22%	3.272	3.58%	3.301	4.50%
95	0.8	50	3.159	0.95%	3.234	2.37%	3.28	3.83%	3.311	4.81%
95	0.4	55	3.436	0.44%	3.474	1.11%	3.498	1.80%	3.514	2.27%
95	0.5	55	3.436	0.61%	3.489	1.54%	3.522	2.50%	3.545	3.17%
95	0.6	55	3.436	0.73%	3.499	1.83%	3.539	3.00%	3.565	3.75%
95	0.7	55	3.436	0.81%	3.507	2.07%	3.55	3.32%	3.58	4.19%
95	0.8	55	3.436	0.87%	3.512	2.21%	3.559	3.58%	3.592	4.54%

Table 72 log $COP_{subcooling}$ Model Coefficients when HX effectiveness is 50%

a0+a1*RH^2+a2*RH+a3*Taeo^2+a4*Taeo+a5*Tout^2+a6*Tout+a7*RH*Taeo+a8*Taeo*Tout+a9*RH*Tout									
a0	a1	a2	a3	a4	a5	a6	a7	a8	a9
1.78	-0.489	0.0946	6.89e-5	0.0226	2.14e-5	-0.152	0.000801	-0.000146	-0.000544

Table 73 log $COP_{subcooling}$ Model Coefficients when HX effectiveness is 80%

a0+a1*RH^2+a2*RH+a3*Taeo^2+a4*Taeo+a5*Tout^2+a6*Tout+a7*RH*Taeo+a8*Taeo*Tout+a9*RH*Tout									
a0	a1	a2	a3	a4	a5	a6	a7	a8	a9
1.74	-0.0788	0.152	6.36e-5	0.0220	1.80e-5	-0.0144	0.000129	-0.000139	-0.000871

Table 74 log $COP_{subcooling}$ Model Coefficients when HX effectiveness is 100%

a0+a1*RH^2+a2*RH+a3*Taeo^2+a4*Taeo+a5*Tout^2+a6*Tout+a7*RH*Taeo+a8*Taeo*Tout+a9*RH*Tout									
a0	a1	a2	a3	a4	a5	a6	a7	a8	a9
1.72	-0.0997	0.195	6.03e-5	0.0216	1.75e-5	-0.0142	0.00162	-0.000134	-0.00113

Table 75 log COP ratio (condensing refrigerant subcooling over baseline system) Model Coefficients for HX effectiveness=50%

a0+a1*RH^2+a2*RH+a3*Taeo^2+a4*Taeo+a5*Tout^2+a6*Tout+a7*RH*Taeo+a8*Taeo*Tout+a9*RH*Tout									
a0	a1	a2	a3	a4	a5	a6	a7	a8	a9
-0.0430	-0.0489	0.0946	-1.29e-5	-0.000488	-6.94e-7	0.000455	0.000801	1.07e-5	-0.000544

Table 76 log COP ratio (condensing refrigerant subcooling over baseline system) Model Coefficients for HX effectiveness=80%

a0+a1*RH^2+a2*RH+a3*Taeo^2+a4*Taeo+a5*Tout^2+a6*Tout+a7*RH*Taeo+a8*Taeo*Tout+a9*RH*Tout									
a0	a1	a2	a3	a4	a5	a6	a7	a8	a9
-0.0819	-0.0788	0.152	-1.83e-5	-0.00111	-4.12e-6	0.000121	0.000129	1.81e-5	-0.000871

Table 77 log COP ratio (condensing refrigerant subcooling over baseline system) Model Coefficients for HX effectiveness=100%

a0+a1*RH^2+a2*RH+a3*Taeo^2+a4*Taeo+a5*Tout^2+a6*Tout+a7*RH*Taeo+a8*Taeo*Tout+a9*RH*Tout									
a0	a1	a2	a3	a4	a5	a6	a7	a8	a9
-0.0981	-0.0997	0.195	-2.16e-5	-0.00152	-4.65e-6	0.00145	0.00162	2.27e-5	-0.00113

Table 78 Baseline and system with internal heat exchanger COP and COP percentage difference

				HX 20%		HX 50%		HX 80%		HX 100%	
Tout	RH	Taeo	COP ref	COP	% diff	COP	% diff	COP	% diff	COP	% diff
80	0.4	45	3.866	4.072	5.33%	4.346	12.42%	4.586	18.62%	4.733	22.43%
80	0.5	45	3.866	4.072	5.33%	4.346	12.42%	4.586	18.62%	4.733	22.43%
80	0.6	45	3.866	4.072	5.33%	4.346	12.42%	4.586	18.62%	4.733	22.43%
80	0.7	45	3.866	4.072	5.33%	4.346	12.42%	4.586	18.62%	4.733	22.43%
80	0.8	45	3.866	4.072	5.33%	4.346	12.42%	4.586	18.62%	4.733	22.43%
80	0.4	50	4.237	4.448	4.98%	4.732	11.68%	4.979	17.51%	5.131	21.10%
80	0.5	50	4.237	4.448	4.98%	4.732	11.68%	4.979	17.51%	5.131	21.10%
80	0.6	50	4.237	4.448	4.98%	4.732	11.68%	4.979	17.51%	5.131	21.10%
80	0.7	50	4.237	4.448	4.98%	4.732	11.68%	4.979	17.51%	5.131	21.10%
80	0.8	50	4.237	4.448	4.98%	4.732	11.68%	4.979	17.51%	5.131	21.10%
80	0.4	55	4.667	4.883	4.63%	5.176	10.91%	5.432	16.39%	5.589	19.76%
80	0.5	55	4.667	4.883	4.63%	5.176	10.91%	5.432	16.39%	5.589	19.76%
80	0.6	55	4.667	4.883	4.63%	5.176	10.91%	5.432	16.39%	5.589	19.76%
80	0.7	55	4.667	4.883	4.63%	5.176	10.91%	5.432	16.39%	5.589	19.76%
80	0.8	55	4.667	4.883	4.63%	5.176	10.91%	5.432	16.39%	5.589	19.76%
85	0.4	45	3.516	3.731	6.11%	4.012	14.11%	4.256	21.05%	4.406	25.31%
85	0.5	45	3.516	3.731	6.11%	4.012	14.11%	4.256	21.05%	4.406	25.31%
85	0.6	45	3.516	3.731	6.11%	4.012	14.11%	4.256	21.05%	4.406	25.31%
85	0.7	45	3.516	3.731	6.11%	4.012	14.11%	4.256	21.05%	4.406	25.31%
85	0.8	45	3.516	3.731	6.11%	4.012	14.11%	4.256	21.05%	4.406	25.31%

Table 78 continued

Tout	RH	Taeo	COP ref	COP	% diff	COP	% diff	COP	% diff	COP	% diff
85	0.4	50	3.837	4.058	5.76%	4.348	13.32%	4.6	19.89%	4.755	23.92%
85	0.5	50	3.837	4.058	5.76%	4.348	13.32%	4.6	19.89%	4.755	23.92%
85	0.6	50	3.837	4.058	5.76%	4.348	13.32%	4.6	19.89%	4.755	23.92%
85	0.7	50	3.837	4.058	5.76%	4.348	13.32%	4.6	19.89%	4.755	23.92%
85	0.8	50	3.837	4.058	5.76%	4.348	13.32%	4.6	19.89%	4.755	23.92%
85	0.4	55	4.206	4.432	5.37%	4.732	12.51%	4.993	18.71%	5.152	22.49%
85	0.5	55	4.206	4.432	5.37%	4.732	12.51%	4.993	18.71%	5.152	22.49%
85	0.6	55	4.206	4.432	5.37%	4.732	12.51%	4.993	18.71%	5.152	22.49%
85	0.7	55	4.206	4.432	5.37%	4.732	12.51%	4.993	18.71%	5.152	22.49%
85	0.8	55	4.206	4.432	5.37%	4.732	12.51%	4.993	18.71%	5.152	22.49%
90	0.4	45	3.201	3.425	7.00%	3.713	16.00%	3.962	23.77%	4.114	28.52%
90	0.5	45	3.201	3.425	7.00%	3.713	16.00%	3.962	23.77%	4.114	28.52%
90	0.6	45	3.201	3.425	7.00%	3.713	16.00%	3.962	23.77%	4.114	28.52%
90	0.7	45	3.201	3.425	7.00%	3.713	16.00%	3.962	23.77%	4.114	28.52%
90	0.8	45	3.201	3.425	7.00%	3.713	16.00%	3.962	23.77%	4.114	28.52%
90	0.4	50	3.481	3.711	6.61%	4.009	15.17%	4.266	22.55%	4.422	27.03%
90	0.5	50	3.481	3.711	6.61%	4.009	15.17%	4.266	22.55%	4.422	27.03%
90	0.6	50	3.481	3.711	6.61%	4.009	15.17%	4.266	22.55%	4.422	27.03%
90	0.7	50	3.481	3.711	6.61%	4.009	15.17%	4.266	22.55%	4.422	27.03%
90	0.8	50	3.481	3.711	6.61%	4.009	15.17%	4.266	22.55%	4.422	27.03%
90	0.4	55	3.799	4.036	6.24%	4.344	14.35%	4.609	21.32%	4.77	25.56%
90	0.5	55	3.799	4.036	6.24%	4.344	14.35%	4.609	21.32%	4.77	25.56%
90	0.6	55	3.799	4.036	6.24%	4.344	14.35%	4.609	21.32%	4.77	25.56%
90	0.7	55	3.799	4.036	6.24%	4.344	14.35%	4.609	21.32%	4.77	25.56%
90	0.8	55	3.799	4.036	6.24%	4.344	14.35%	4.609	21.32%	4.77	25.56%
95	0.4	45	2.914	3.148	8.03%	3.444	18.19%	3.698	26.90%	3.852	32.19%
95	0.5	45	2.914	3.148	8.03%	3.444	18.19%	3.698	26.90%	3.852	32.19%
95	0.6	45	2.914	3.148	8.03%	3.444	18.19%	3.698	26.90%	3.852	32.19%
95	0.7	45	2.914	3.148	8.03%	3.444	18.19%	3.698	26.90%	3.852	32.19%
95	0.8	45	2.914	3.148	8.03%	3.444	18.19%	3.698	26.90%	3.852	32.19%
95	0.4	50	3.159	3.4	7.63%	3.705	17.28%	3.967	25.58%	4.126	30.61%
95	0.5	50	3.159	3.4	7.63%	3.705	17.28%	3.967	25.58%	4.126	30.61%
95	0.6	50	3.159	3.4	7.63%	3.705	17.28%	3.967	25.58%	4.126	30.61%
95	0.7	50	3.159	3.4	7.63%	3.705	17.28%	3.967	25.58%	4.126	30.61%
95	0.8	50	3.159	3.4	7.63%	3.705	17.28%	3.967	25.58%	4.126	30.61%
95	0.4	55	3.436	3.683	7.19%	3.999	16.39%	4.269	24.24%	4.433	29.02%
95	0.5	55	3.436	3.683	7.19%	3.999	16.39%	4.269	24.24%	4.433	29.02%
95	0.6	55	3.436	3.683	7.19%	3.999	16.39%	4.269	24.24%	4.433	29.02%
95	0.7	55	3.436	3.683	7.19%	3.999	16.39%	4.269	24.24%	4.433	29.02%
95	0.8	55	3.436	3.683	7.19%	3.999	16.39%	4.269	24.24%	4.433	29.02%

Table 79 COP_{IHX} Model Coefficients when HX effectiveness is 50%

a0+a1*Taeo^2+a2*Taeo+a3*Tout^2+a4*Tout+a5*Taeo*Tout					
a0	a1	a2	a3	a4	a5
7.242	0.00089	0.139	0.000813	-0.120	-0.00183

Table 80 COP_{IHX} Model Coefficients when HX effectiveness is 80%

a0+a1*Taeo^2+a2*Taeo+a3*Tout^2+a4*Tout+a5*Taeo*Tout					
a0	a1	a2	a3	a4	a5
7.386	0.000905	0.140	0.000817	-0.119	-0.00183

Table 81 COP_{IHX} Model Coefficients when HX effectiveness is 100%

a0+a1*Taeo^2+a2*Taeo+a3*Tout^2+a4*Tout+a5*Taeo*Tout					
a0	a1	a2	a3	a4	a5
7.454	0.000905	0.141	0.000817	-0.119	-0.00183

Table 82 COP_{IHX} ratio Model Coefficients when HX effectiveness is 50%

a0+a1*Taeo^2+a2*Taeo+a3*Tout^2+a4*Tout+a5*Taeo*Tout					
a0	a1	a2	a3	a4	a5
1.172	-2.78e-5	0.000260	4.74e-5	-0.000363	-1.86e-5

Table 83 COP_{IHX} ratio Model Coefficients when HX effectiveness is 80%

a0+a1*Taeo^2+a2*Taeo+a3*Tout^2+a4*Tout+a5*Taeo*Tout					
a0	a1	a2	a3	a4	a5
1.236	-1.81e-6	0.000218	6.55e-5	-0.00468	-2.809e-5

Table 84 COP_{IHX} ratio Model Coefficients when HX effectiveness is 100%

a0+a1*Taeo^2+a2*Taeo+a3*Tout^2+a4*Tout+a5*Taeo*Tout					
a0	a1	a2	a3	a4	a5
1.27	-3.12e-6	0.000292	7.52e-4	-0.00517	-3.33e-5

Table 85 Weather report of 53 cities

			Daily Highest(°F)	Daily lowest(°F)	Daily Temp (°F)	Daily Highest RH	Daily Lowest RH	Daily Average RH	wet bulb Temp (°F)
1A	Miami	Jan	76	60	68	0.84	0.59	0.72	62.01
		Feb	78	62	70	0.83	0.57	0.70	63.36
		March	80	65	72.5	0.82	0.56	0.69	65.37
		April	83	68	75.5	0.80	0.53	0.67	67.55
		May	87	73	80	0.83	0.59	0.71	72.67
		June	90	76	83	0.86	0.65	0.76	76.8
		July	91	77	84	0.86	0.63	0.74	77.17
		August	91	77	84	0.86	0.65	0.75	77.45
		Sep	89	77	83	0.88	0.66	0.77	77.08
		Oct	86	74	80	0.86	0.62	0.74	73.49
		Nov	82	68	75	0.85	0.61	0.73	68.64
		Dec	78	63	70.5	0.83	0.59	0.71	64.05
	Key west	Jan	74	64	69	0.81	0.69	0.75	63.61
		Feb	76	66	71	0.80	0.67	0.73	64.98
		March	78	68	73	0.79	0.66	0.72	66.56
		April	81	72	76.5	0.77	0.63	0.70	69.23
		May	85	76	80.5	0.77	0.65	0.71	73.13
		June	88	79	83.5	0.79	0.68	0.74	76.71
		July	89	80	84.5	0.78	0.66	0.72	77.06
		August	89	80	84.5	0.79	0.68	0.73	77.34
		Sep	88	79	83.5	0.81	0.69	0.75	76.99
		Oct	85	76	80.5	0.81	0.68	0.75	74.21
		Nov	80	72	76	0.82	0.69	0.76	70.31
		Dec	76	67	71.5	0.82	0.69	0.75	65.91
2A	Orlando	Jan	71	49	60	0.87	0.53	0.70	54.34
		Feb	74	52	63	0.87	0.50	0.68	56.63
		March	78	56	67	0.88	0.48	0.68	60.2
		April	83	60	71.5	0.87	0.45	0.66	63.74
		May	88	66	77	0.90	0.49	0.70	69.69
		June	91	72	81.5	0.92	0.57	0.74	74.87
		July	92	74	83	0.92	0.59	0.75	76.53

Table 85 continued

			Daily Highest(°F)	Daily lowest(°F)	Daily Temp (°F)	Daily Highest RH	Daily Lowest RH	Daily Average RH	wet bulb Temp (°F)
		August	92	74	83	0.93	0.60	0.76	76.8
		Sep	90	73	81.5	0.92	0.61	0.76	75.41
		Oct	85	66	75.5	0.88	0.55	0.72	68.84
		Nov	78	59	68.5	0.89	0.55	0.72	62.47
		Dec	73	52	62.5	0.87	0.55	0.71	56.81
	New Orleans	Jan	62	45	53.5	0.84	0.63	0.73	49
		Feb	65	48	56.5	0.83	0.58	0.71	51.37
		March	72	54	63	0.85	0.58	0.71	57.26
		April	78	60	69	0.88	0.57	0.72	62.92
		May	85	68	76.5	0.89	0.58	0.74	70.27
		June	90	74	82	0.90	0.62	0.76	75.87
		July	91	75	83	0.92	0.66	0.79	77.62
		August	91	75	83	0.92	0.66	0.79	77.62
		Sep	88	72	80	0.89	0.63	0.76	74.02
		Oct	80	63	71.5	0.88	0.56	0.72	65.2
		Nov	72	54	63	0.87	0.61	0.74	57.88
		Dec	64	47	55.5	0.86	0.62	0.74	51.01
	Mobile	Jan	61	40	50.5	0.81	0.57	0.69	45.61
		Feb	64	43	53.5	0.82	0.53	0.68	48.13
		March	71	49	60	0.84	0.52	0.68	53.95
		April	78	55	66.5	0.87	0.50	0.69	59.98
		May	85	64	74.5	0.87	0.53	0.70	67.43
		June	89	70	79.5	0.88	0.55	0.72	72.49
		July	91	73	82	0.89	0.60	0.75	75.6
		August	91	73	82	0.91	0.61	0.76	75.87
		Sep	87	68	77.5	0.89	0.59	0.74	71.19
		Oct	79	58	68.5	0.85	0.50	0.68	61.55
		Nov	71	49	60	0.85	0.54	0.70	54.34
		Dec	63	42	52.5	0.83	0.58	0.71	47.75
	Houston	Jan	63	43	53	0.85	0.58	0.72	48.37
		Feb	66	47	56.5	0.86	0.55	0.71	51.37
		March	73	53	63	0.87	0.54	0.71	57.26
		April	80	59	69.5	0.89	0.54	0.71	63.15
		May	86	68	77	0.91	0.57	0.74	70.73
		June	91	73	82	0.92	0.56	0.74	75.33
		July	94	75	84.5	0.93	0.55	0.74	77.63
		August	95	75	85	0.93	0.55	0.74	78.09
		Sep	90	70	80	0.93	0.57	0.75	73.75
		Oct	82	61	71.5	0.91	0.53	0.72	65.2

Table 85 continued

			Daily Highest(°F)	Daily lowest(°F)	Daily Temp (°F)	Daily Highest RH	Daily Lowest RH	Daily Average RH	wet bulb Temp (°F)
		Nov	73	52	62.5	0.89	0.55	0.72	57.01
		Dec	64	45	54.5	0.87	0.57	0.72	49.74
2B	Phoenix	Jan	69	46	57.5	0.67	0.32	0.49	47.96
		Feb	72	49	60.5	0.60	0.27	0.43	49.1
		March	78	54	66	0.56	0.24	0.40	52.67
		April	86	60	73	0.43	0.16	0.29	54.76
		May	95	69	82	0.35	0.13	0.24	59.19
		June	104	77	90.5	0.31	0.11	0.21	63.45
		July	106	83	94.5	0.45	0.20	0.33	71.57
		August	104	82	93	0.51	0.23	0.37	72.16
		Sep	100	75	87.5	0.50	0.23	0.37	68.03
		Oct	89	64	76.5	0.51	0.23	0.37	59.78
		Nov	76	52	64	0.58	0.27	0.43	51.85
		Dec	67	45	56	0.67	0.33	0.50	46.93
	Tucson	Jan	65	42	53.5	0.62	0.30	0.46	44.13
		Feb	68	44	56	0.58	0.26	0.42	45.34
		March	74	48	61	0.53	0.22	0.38	48.36
		April	82	55	68.5	0.41	0.16	0.29	51.59
		May	91	64	77.5	0.35	0.13	0.24	56.2
		June	99	72	85.5	0.33	0.13	0.23	61.09
		July	99	76	87.5	0.58	0.26	0.42	69.89
		August	97	75	86	0.64	0.29	0.47	70.48
		Sep	94	71	82.5	0.57	0.27	0.42	66
		Oct	84	59	71.5	0.53	0.24	0.38	56.32
		Nov	73	48	60.5	0.56	0.26	0.41	48.65
		Dec	64	41	52.5	0.63	0.32	0.47	43.5
3Aw	Dallas	Feb	61	41	51	0.80	0.51	0.65	45.39
		March	69	49	59	0.79	0.49	0.64	52.26
		April	77	56	66.5	0.82	0.50	0.66	59.3
		May	84	65	74.5	0.87	0.53	0.70	67.43
		June	92	73	82.5	0.85	0.48	0.67	73.81
		July	96	77	86.5	0.81	0.42	0.61	75.53
		August	96	77	86.5	0.80	0.41	0.61	75.53
		Sep	89	69	79	0.85	0.48	0.66	70.4
		Oct	79	58	68.5	0.82	0.47	0.65	60.84
		Nov	67	48	57.5	0.81	0.50	0.66	51.33
	Little Rock	Feb	55	35	45	0.80	0.53	0.67	40.36
		March	64	43	53.5	0.79	0.51	0.65	47.6
		April	73	51	62	0.82	0.51	0.67	55.53

Table 85 continued

			Daily Highest(°F)	Daily lowest(°F)	Daily Temp (°F)	Daily Highest RH	Daily Lowest RH	Daily Average RH	wet bulb Temp (°F)
		May	81	61	71	0.87	0.54	0.70	64.27
		June	89	69	79	0.86	0.52	0.69	71.22
		July	93	73	83	0.88	0.54	0.71	75.4
		August	93	72	82.5	0.88	0.53	0.70	74.67
		Sep	86	65	75.5	0.89	0.54	0.71	68.59
		Oct	75	53	64	0.86	0.48	0.67	57.31
		Nov	63	42	52.5	0.83	0.53	0.68	47.23
	Oklahoma City	Feb	55	33	44	0.77	0.51	0.64	39.03
		March	63	41	52	0.75	0.46	0.61	45.58
		April	72	50	61	0.77	0.45	0.61	53.39
		May	80	60	70	0.83	0.51	0.67	62.65
		June	88	68	78	0.84	0.51	0.67	69.78
		July	94	72	83	0.80	0.44	0.62	72.78
		August	93	71	82	0.80	0.43	0.62	71.9
		Sep	85	63	74	0.83	0.49	0.66	65.96
		Oct	73	52	62.5	0.79	0.46	0.62	54.91
		Nov	62	40	51	0.79	0.50	0.64	45.22
3Ae	Charlotte	Feb	55	33	44	0.76	0.48	0.62	38.75
		March	63	39	51	0.79	0.46	0.62	44.88
		April	72	47	59.5	0.78	0.43	0.60	51.89
		May	79	56	67.5	0.83	0.50	0.66	60.19
		June	86	65	75.5	0.85	0.53	0.69	68.07
		July	89	68	78.5	0.87	0.55	0.71	71.31
		August	88	67	77.5	0.89	0.55	0.72	70.66
		Sep	81	60	70.5	0.89	0.55	0.72	64.29
		Oct	72	49	60.5	0.87	0.50	0.68	54.39
		Nov	62	39	50.5	0.83	0.50	0.67	45.28
	Atlanta	Feb	57	38	47.5	0.76	0.49	0.62	41.82
		March	65	44	54.5	0.78	0.47	0.62	47.94
		April	73	52	62.5	0.78	0.44	0.61	54.69
		May	80	60	70	0.83	0.50	0.67	62.65
		June	86	68	77	0.85	0.53	0.69	69.42
		July	89	71	80	0.89	0.58	0.73	73.22
		August	88	71	79.5	0.90	0.57	0.73	72.76
		Sep	82	65	73.5	0.88	0.57	0.73	67.27
		Oct	73	54	63.5	0.84	0.50	0.67	56.86
		Nov	64	45	54.5	0.81	0.52	0.66	48.67
	Montgomery	Feb	62	39	50.5	0.80	0.49	0.65	44.95
		March	70	45	57.5	0.83	0.48	0.65	51.13

Table 85 continued

			Daily Highest(°F)	Daily lowest(°F)	Daily Temp (°F)	Daily Highest RH	Daily Lowest RH	Daily Average RH	wet bulb Temp (°F)
		April	77	52	64.5	0.86	0.47	0.66	57.53
		May	84	61	72.5	0.88	0.51	0.69	65.37
		June	90	68	79	0.89	0.52	0.70	71.5
		July	92	72	82	0.90	0.58	0.74	75.33
		August	92	71	81.5	0.91	0.57	0.74	74.87
		Sep	87	65	76	0.89	0.53	0.71	69.04
		Oct	78	54	66	0.89	0.47	0.68	59.31
		Nov	69	44	56.5	0.87	0.50	0.68	50.82
3Be	Lubbock	March	67	37	52	0.68	0.32	0.50	43.64
		April	75	46	60.5	0.67	0.30	0.48	50.2
		May	84	56	70	0.75	0.33	0.54	59.43
		June	91	64	77.5	0.78	0.36	0.57	66.57
		July	93	68	80.5	0.73	0.38	0.56	68.83
		August	91	67	79	0.78	0.42	0.60	68.71
		Sep	85	59	72	0.82	0.46	0.64	63.68
		Oct	75	48	61.5	0.78	0.39	0.58	53.19
		Nov	64	36	50	0.74	0.38	0.56	43
	Wichita Falls	March	67	37	52	0.79	0.43	0.61	45.58
		April	75	46	60.5	0.80	0.43	0.61	52.96
		May	84	60	72	0.86	0.46	0.66	64.18
		June	91	68	79.5	0.85	0.44	0.64	70.29
		July	97	72	84.5	0.78	0.36	0.57	72.54
		August	97	71	84	0.80	0.38	0.59	72.73
		Sep	88	63	75.5	0.86	0.46	0.66	67.29
		Oct	75	48	61.5	0.84	0.44	0.64	54.46
		Nov	65	40	52.5	0.83	0.46	0.65	46.72
	Midland	March	70	41	55.5	0.66	0.27	0.46	45.74
		April	79	49	64	0.66	0.26	0.46	52.56
		May	88	60	74	0.75	0.29	0.52	62.23
		June	93	67	80	0.77	0.32	0.55	68.1
		July	95	70	82.5	0.73	0.33	0.53	69.59
		August	94	69	81.5	0.75	0.35	0.55	69.37
		Sep	87	52	69.5	0.81	0.42	0.61	60.76
		Oct	78	52	65	0.79	0.38	0.59	56.4
		Nov	67	39	53	0.76	0.37	0.56	45.56
3Bw	Bakersfield	Feb	63	42	52.5	0.82	0.51	0.66	46.89
		March	69	47	58	0.75	0.42	0.59	50.4
		April	75	50	62.5	0.67	0.33	0.50	52.27
		May	84	58	71	0.57	0.26	0.42	57.06

Table 85 continued

			Daily Highest(°F)	Daily lowest(°F)	Daily Temp (°F)	Daily Highest RH	Daily Lowest RH	Daily Average RH	wet bulb Temp (°F)
		June	91	64	77.5	0.51	0.23	0.37	60.53
		July	97	71	84	0.48	0.21	0.35	64.68
		August	96	69	82.5	0.54	0.24	0.39	64.97
		Sep	90	64	77	0.58	0.29	0.43	62.03
		Oct	79	55	67	0.64	0.34	0.49	55.7
		Nov	66	45	55.5	0.78	0.50	0.64	49.18
	EL Paso	Feb	63	37	50	0.56	0.27	0.41	40.42
		March	70	43	56.5	0.46	0.20	0.33	43.87
		April	79	51	65	0.40	0.17	0.28	48.85
		May	88	60	74	0.41	0.16	0.29	55.46
		June	96	68	82	0.46	0.18	0.32	62.14
		July	95	71	83	0.63	0.29	0.46	67.73
		August	92	70	81	0.67	0.32	0.50	67.4
		Sep	88	63	75.5	0.69	0.34	0.52	63.47
		Oct	78	52	65	0.65	0.30	0.48	53.84
		Nov	66	40	53	0.61	0.30	0.46	43.72
3Blv	Las Vegas	Feb	63	43	53	0.52	0.26	0.39	42.41
		March	70	49	59.5	0.44	0.21	0.33	46.09
		April	78	56	67	0.35	0.16	0.25	49.43
		May	89	66	77.5	0.31	0.13	0.22	55.5
		June	99	75	87	0.24	0.11	0.17	59.48
		July	104	81	92.5	0.29	0.15	0.22	65.2
		August	102	79	90.5	0.35	0.17	0.26	65.69
		Sep	94	71	82.5	0.34	0.17	0.25	59.9
		Oct	81	59	70	0.38	0.19	0.29	52.65
		Nov	66	47	56.5	0.47	0.26	0.37	44.71
3Bn	Sacramento	Feb	60	41	50.5	0.88	0.59	0.74	46.42
		March	65	44	54.5	0.85	0.53	0.69	49.2
		April	71	46	58.5	0.82	0.43	0.62	51.42
		May	80	51	65.5	0.81	0.35	0.58	56.6
		June	87	56	71.5	0.78	0.31	0.54	60.69
		July	92	58	75	0.76	0.28	0.52	63.06
		August	91	58	74.5	0.78	0.29	0.53	62.92
		Sep	87	56	71.5	0.77	0.31	0.54	60.69
		Oct	78	50	64	0.82	0.38	0.60	55.77
		Nov	64	43	53.5	0.88	0.58	0.73	49
	Stockton	Feb	63	41	52	0.89	0.60	0.75	47.97
		March	68	45	56.5	0.85	0.51	0.68	50.82
		April	74	47	60.5	0.78	0.41	0.60	52.75

Table 85 continued

			Daily Highest(°F)	Daily lowest(°F)	Daily Temp (°F)	Daily Highest RH	Daily Lowest RH	Daily Average RH	wet bulb Temp (°F)
		May	82	53	67.5	0.73	0.32	0.52	56.85
		June	89	57	73	0.68	0.28	0.48	60.3
		July	94	59	76.5	0.66	0.26	0.46	62.54
		August	93	58	75.5	0.67	0.28	0.47	62.03
		Sep	90	56	73	0.70	0.30	0.50	60.86
		Oct	80	50	65	0.78	0.37	0.58	56.18
		Nov	66	42	54	0.87	0.60	0.73	49.46
3C	Los Angeles	Jan	68	48	58	0.70	0.51	0.60	50.59
		Feb	69	49	59	0.75	0.57	0.66	52.66
		March	70	51	60.5	0.78	0.60	0.69	54.59
		April	73	54	63.5	0.80	0.60	0.70	57.5
		May	75	57	66	0.83	0.63	0.73	60.41
		June	78	60	69	0.85	0.64	0.75	63.61
		July	83	64	73.5	0.86	0.65	0.75	67.76
		August	84	64	74	0.85	0.64	0.75	68.22
		Sep	83	63	73	0.83	0.62	0.72	66.56
		Oct	79	59	69	0.78	0.58	0.68	61.99
		Nov	73	52	62.5	0.72	0.52	0.62	54.91
		Dec	68	48	58	0.69	0.49	0.59	50.4
	Long Beach	Jan	67	46	56.5	0.75	0.47	0.61	49.49
		Feb	67	48	57.5	0.77	0.52	0.64	50.94
		March	69	51	60	0.78	0.53	0.66	53.54
		April	72	53	62.5	0.79	0.50	0.65	55.55
		May	74	58	66	0.80	0.54	0.67	59.09
		June	77	61	69	0.82	0.55	0.68	61.99
		July	82	65	73.5	0.82	0.52	0.67	65.77
		August	84	65	74.5	0.81	0.52	0.67	66.66
		Sep	82	63	72.5	0.82	0.52	0.67	64.88
		Oct	77	58	67.5	0.81	0.49	0.65	59.96
		Nov	72	51	61.5	0.78	0.48	0.63	54.25
		Dec	67	46	56.5	0.77	0.46	0.61	49.49
4A	Richmond	April	70	46	58	0.78	0.42	0.60	50.59
		May	78	55	66.5	0.86	0.51	0.69	59.98
		June	86	65	75.5	0.86	0.51	0.69	68.07
		July	90	69	79.5	0.90	0.54	0.72	72.49
		August	88	67	77.5	0.91	0.57	0.74	71.19
		Sep	81	60	70.5	0.91	0.57	0.74	64.76
		Oct	71	48	59.5	0.89	0.52	0.70	53.89
	Nashville	April	71	48	59.5	0.80	0.47	0.64	52.7

Table 85 continued

			Daily Highest(°F)	Daily lowest(°F)	Daily Temp (°F)	Daily Highest RH	Daily Lowest RH	Daily Average RH	wet bulb Temp (°F)
		May	78	57	67.5	0.86	0.52	0.69	60.88
		June	86	65	75.5	0.87	0.52	0.70	68.33
		July	89	70	79.5	0.89	0.55	0.72	72.49
		August	89	68	78.5	0.90	0.54	0.72	71.58
		Sep	82	61	71.5	0.90	0.54	0.72	65.2
		Oct	72	49	60.5	0.86	0.48	0.67	54.19
	Wichita	April	68	45	56.5	0.78	0.47	0.62	49.68
		May	77	55	66	0.83	0.51	0.67	59.09
		June	87	65	76	0.82	0.47	0.64	67.2
		July	92	70	81	0.78	0.42	0.60	70.44
		August	91	69	80	0.79	0.44	0.62	70.16
		Sep	83	60	71.5	0.83	0.49	0.66	63.74
		Oct	70	47	58.5	0.80	0.47	0.63	51.62
	St. Louis	April	67	47	57	0.78	0.49	0.64	50.5
		May	76	57	66.5	0.82	0.51	0.67	59.53
		June	85	67	76	0.83	0.52	0.67	68
		July	89	71	80	0.85	0.52	0.68	71.85
		August	88	69	78.5	0.88	0.52	0.70	71.04
		Sep	80	61	70.5	0.89	0.53	0.71	64.05
		Oct	69	49	59	0.84	0.51	0.68	53.05
	New York	April	61	45	53	0.64	0.45	0.55	45.38
		May	71	54	62.5	0.73	0.52	0.63	55.12
		June	79	64	71.5	0.76	0.55	0.65	63.49
		July	84	69	76.5	0.75	0.53	0.64	67.64
		August	83	68	75.5	0.77	0.54	0.65	67.03
		Sep	75	61	68	0.78	0.56	0.67	60.87
		Oct	64	50	57	0.75	0.54	0.65	50.69
	Philadelphia	April	64	44	54	0.73	0.48	0.60	47.14
		May	74	54	64	0.79	0.52	0.65	56.87
		June	83	64	73.5	0.85	0.54	0.69	66.27
		July	87	69	78	0.84	0.55	0.70	70.59
		August	85	68	76.5	0.84	0.55	0.70	69.23
		Sep	78	60	69	0.85	0.55	0.70	62.46
		Oct	67	48	57.5	0.83	0.54	0.69	51.9
	Washington DC	April	67	47	57			0.58	49.34
		May	75	57	66			0.65	58.64
		June	84	66	75			0.66	66.85
		July	88	71	79.5			0.67	71.12
		August	87	70	78.5			0.69	70.77

Table 85 continued

			Daily Highest(°F)	Daily lowest(°F)	Daily Temp (°F)	Daily Highest RH	Daily Lowest RH	Daily Average RH	wet bulb Temp (°F)
		Sep	82	60	71			0.70	64.27
		Oct	68	51	59.5			0.67	53.3
4B	Albuquerque	April	69	43	56	0.49	0.19	0.34	43.71
		May	79	53	66	0.48	0.18	0.33	50.87
		June	88	62	75	0.46	0.17	0.32	57.11
		July	90	66	78	0.60	0.25	0.42	62.5
		August	87	65	76	0.66	0.29	0.48	62.73
		Sep	81	58	69.5	0.66	0.30	0.48	57.48
		Oct	69	46	57.5	0.62	0.29	0.46	47.35
	Amarillo	April	71	42	56.5	0.68	0.30	0.49	47.15
		May	80	52	66	0.74	0.35	0.55	56.33
		June	88	61	74.5	0.77	0.38	0.57	64.02
		July	91	65	78	0.74	0.36	0.55	66.42
		August	89	64	76.5	0.78	0.40	0.59	66.28
		Sep	83	56	69.5	0.80	0.42	0.61	60.76
		Oct	72	45	58.5	0.73	0.36	0.54	49.81
4C	Portland	April	62	43	52.5	0.85	0.55	0.70	47.58
		May	69	48	58.5	0.84	0.52	0.68	52.6
		June	73	52	62.5	0.82	0.49	0.65	55.55
		July	81	56	68.5	0.80	0.44	0.62	60.13
		August	81	57	69	0.82	0.44	0.63	60.81
		Sep	75	52	63.5	0.86	0.48	0.67	56.86
		Oct	62	47	54.5	0.90	0.60	0.75	50.27
	Seattle	April	60	43	51.5	0.83	0.57	0.70	46.68
		May	66	49	57.5	0.82	0.54	0.68	51.71
		June	71	53	62	0.81	0.53	0.67	55.53
		July	76	57	66.5	0.81	0.49	0.65	59.08
		August	76	57	66.5	0.83	0.50	0.67	59.53
		Sep	71	53	62	0.86	0.57	0.71	56.35
		Oct	61	47	54	0.87	0.67	0.77	50.16
	Eugene	April	61	40	50.5	0.90	0.58	0.74	46.42
		May	67	44	55.5	0.90	0.54	0.72	50.65
		June	73	48	60.5	0.89	0.49	0.69	54.59
		July	82	51	66.5	0.87	0.39	0.63	58.62
		August	83	51	67	0.87	0.40	0.64	59.29
		Sep	77	47	62	0.89	0.45	0.67	55.53
		Oct	64	41	52.5	0.94	0.61	0.77	48.76
5A	Omaha	April	64	40	52	0.76	0.45	0.61	45.58
		May	74	51	62.5	0.79	0.49	0.64	55.33

Table 85 continued

			Daily Highest(°F)	Daily lowest(°F)	Daily Temp (°F)	Daily Highest RH	Daily Lowest RH	Daily Average RH	wet bulb Temp (°F)
		June	83	61	72	0.82	0.49	0.66	64.18
		July	87	66	76.5	0.84	0.52	0.68	68.71
		August	85	64	74.5	0.87	0.54	0.70	67.43
		Sep	78	54	66	0.87	0.53	0.70	59.75
		Oct	65	42	53.5	0.82	0.48	0.65	47.6
	Chicago	April	59	42	50.5	0.77	0.53	0.65	44.95
		May	70	52	61	0.77	0.51	0.64	54.02
		June	80	62	71	0.79	0.52	0.66	63.29
		July	84	68	76	0.82	0.54	0.68	68.26
		August	82	66	74	0.85	0.55	0.70	66.97
		Sep	75	58	66.5	0.85	0.55	0.70	60.2
		Oct	63	46	54.5	0.81	0.53	0.67	48.85
	Pittsburgh	April	62	40	51	0.73	0.48	0.60	44.54
		May	71	49	60	0.77	0.50	0.63	52.94
		June	79	58	68.5	0.82	0.51	0.66	61.08
		July	83	63	73	0.84	0.57	0.71	66.32
		August	81	62	71.5	0.86	0.54	0.70	64.72
		Sep	74	54	64	0.86	0.55	0.70	57.95
		Oct	63	43	53	0.81	0.53	0.67	47.51
	Des Moines	April	62	41	51.5	0.77	0.50	0.64	45.66
		May	72	52	62	0.77	0.50	0.63	54.68
		June	82	62	72	0.79	0.51	0.65	63.93
		July	86	67	76.5	0.82	0.53	0.67	68.44
		August	84	65	74.5	0.85	0.54	0.69	67.17
		Sep	76	55	65.5	0.85	0.54	0.70	59.3
		Oct	63	43	53	0.79	0.51	0.65	47.16
	Boston	April	56	41	48.5	0.71	0.55	0.63	42.85
		May	66	50	58	0.77	0.58	0.68	52.16
		June	76	60	68	0.80	0.58	0.69	61.33
		July	81	65	73	0.80	0.57	0.69	65.82
		August	80	65	72.5	0.82	0.59	0.70	65.62
		Sep	72	57	64.5	0.82	0.59	0.71	58.62
		Oct	61	47	54	0.78	0.57	0.67	48.4
5B	Denver	April	61	34	47.5	0.67	0.33	0.50	39.91
		May	71	44	57.5	0.70	0.35	0.53	48.77
		June	81	53	67	0.70	0.35	0.52	56.44
		July	88	59	73.5	0.69	0.32	0.50	61.27
		August	86	57	71.5	0.68	0.28	0.48	59.09
		Sep	77	48	62.5	0.69	0.31	0.50	52.27

Table 85 continued

			Daily Highest(°F)	Daily lowest(°F)	Daily Temp (°F)	Daily Highest RH	Daily Lowest RH	Daily Average RH	wet bulb Temp (°F)
		Oct	65	36	50.5	0.65	0.30	0.47	41.88
	Boise	April	62	39	50.5	0.68	0.35	0.52	42.74
		May	72	47	59.5	0.67	0.31	0.49	49.6
		June	81	54	67.5	0.65	0.28	0.46	55.36
		July	91	60	75.5	0.54	0.21	0.38	59.34
		August	90	60	75	0.53	0.23	0.38	58.97
		Sep	79	52	65.5	0.60	0.29	0.44	53.27
		Oct	65	41	53	0.66	0.37	0.51	44.65
	Reno	April	64	38	51	0.67	0.28	0.47	42.28
		May	74	46	60	0.67	0.26	0.47	49.57
		June	83	52	67.5	0.66	0.22	0.44	54.85
		July	92	58	75	0.64	0.18	0.41	59.87
		August	91	56	73.5	0.67	0.20	0.43	59.29
		Sep	82	49	65.5	0.69	0.22	0.45	53.52
		Oct	69	39	54	0.73	0.27	0.50	45.29
6A	Minneapolis	May	69	49	59	0.76	0.47	0.61	51.66
		June	79	59	69	0.78	0.50	0.64	61.05
		July	83	64	73.5	0.80	0.50	0.65	65.26
		August	81	62	71.5	0.83	0.52	0.68	64.23
		Sep	72	52	62	0.85	0.54	0.70	56.15
		Oct	58	40	49	0.81	0.53	0.67	43.94
	Milwaukee	May	65	47	56	0.79	0.58	0.68	50.37
		June	75	57	66	0.81	0.59	0.70	59.75
		July	80	64	72	0.83	0.60	0.71	65.41
		August	79	63	71	0.87	0.62	0.74	65.22
		Sep	71	55	63	0.87	0.63	0.75	58.09
		Oct	59	43	51	0.82	0.61	0.72	46.55
	Sioux Falls	May	70	46	58	0.80	0.48	0.64	51.38
		June	79	56	67.5	0.82	0.49	0.65	59.96
		July	84	62	73	0.83	0.48	0.65	64.82
		August	82	60	71	0.85	0.49	0.67	63.54
		Sep	73	49	61	0.86	0.51	0.68	54.84
		Oct	60	36	48	0.81	0.48	0.65	42.73
6B	Helena	May	67	41	54	0.72	0.38	0.55	46.22
		June	76	49	62.5	0.71	0.36	0.54	53.16
		July	86	54	70	0.66	0.29	0.47	57.62
		August	85	52	68.5	0.67	0.30	0.48	56.67
		Sep	73	43	58	0.73	0.36	0.54	49.39
	Cheyenne	May	65	40	52.5	0.71	0.41	0.56	45.13

Table 85 continued

			Daily Highest(°F)	Daily lowest(°F)	Daily Temp (°F)	Daily Highest RH	Daily Lowest RH	Daily Average RH	wet bulb Temp (°F)
		June	75	49	62	0.71	0.38	0.54	52.74
		July	83	56	69.5	0.70	0.33	0.52	58.51
		August	81	54	67.5	0.69	0.33	0.51	56.61
		Sep	72	45	58.5	0.67	0.34	0.50	48.99
	Casper	May	67	37	52	0.77	0.37	0.57	44.88
		June	79	46	62.5	0.75	0.30	0.52	52.72
		July	88	53	70.5	0.69	0.24	0.46	57.75
		August	86	52	69	0.66	0.23	0.44	56.03
		Sep	74	41	57.5	0.68	0.29	0.48	47.76
7A	Fargo	May	69	45	57	0.77	0.46	0.61	49.92
		June	77	55	66	0.82	0.50	0.66	58.86
		July	83	60	71.5	0.85	0.49	0.67	63.98
		August	81	57	69	0.86	0.47	0.67	61.76
		Sep	71	47	59	0.85	0.51	0.68	53.05
	Bismarck	May	68	43	55.5	0.78	0.43	0.61	48.62
		June	77	52	64.5	0.84	0.46	0.65	57.31
		July	85	57	71	0.84	0.41	0.62	62.31
		August	84	56	70	0.84	0.39	0.61	61.19
		Sep	72	45	58.5	0.83	0.43	0.63	51.62
	St. Cloud	May	69	44	56.5	0.82	0.46	0.64	50.06
		June	78	54	66	0.85	0.50	0.68	59.31
		July	82	58	70	0.88	0.50	0.69	63.13
		August	80	56	68	0.91	0.53	0.72	62.01
		Sep	70	47	58.5	0.91	0.55	0.73	53.57

Table 86 Coefficient of a, b, c and d for monthly/daily models

	Dry-bulb Temperature								RH								Wet-bulb							
	Month data				Daily data				Month data				Daily data				Month data				Daily data			
	a	b	c	d	a	b	c	d	a	b	c	d	a	b	c	d	a	b	c	d	a	b	c	d
1A	65.65	1.82	0.43	-0.05	65.51	0.18	0.00	-1.6E-06	0.77	-0.04	0.01	-4.3E-04	0.75	-1.2E-03	8.6E-06	-1.5E-08	61.11	0.15	0.62	-0.05	61.39	0.04	5.5E-04	-1.9E-06
2A	43.97	5.96	0.43	-0.07	46.68	0.22	0.00	-2.5E-06	0.70	0.00	0.00	-2.1E-04	0.70	-4.6E-05	2.7E-06	-7.3E-09	40.07	0.15	0.49	-0.07	42.42	0.19	3.4E-04	-2.5E-06

Table 86 continued

	a	b	c	d	a	b	c	d	a	b	c	d	a	b	c	d	a	b	c	d	a	b	c	d
2B	47.779	4.32	0.955	-0.111	49.777	0.118	0.000	-3.7E-06	0.64	-0.16	0.002	-8.4E-04	0.57	-4.7E-03	2.3E-05	-3.1E-08	45.72	-1.74	1.445	-0.111	45.04	-0.001	1.3E-03	-3.9E-06
3Aw	29.688	6.333	1.116	-0.114	32.699	0.226	0.000	-4.8E-06	0.600	0.003	0.000	1.3E-04	0.61	7.8E-04	-3.5E-06	4.8E-09	25.028	6.489	0.889	-0.112	28.077	0.25	6.8E-04	-4.1E-06
3Ae	29.955	7.12	0.776	-0.111	33.229	0.227	0.000	-3.8E-06	0.69	0.006	0.002	-9.4E-04	0.66	-1.4E-03	1.5E-05	-3.3E-08	28.10	4.70	1.08	-0.112	30.311	0.220	8.8E-04	-4.2E-06
3Be	1.18	20.007	-0.933	-0.004	11.881	0.622	0.000	-1.6E-06	0.51	0.001	0.001	-3.4E-04	0.51	-1.3E-04	5.0E-06	-1.2E-08	2.25	15.889	-0.52	-0.005	10.071	0.550	6.6E-04	-1.8E-06
3Bw	39.667	2.96	1.488	-0.155	41.088	0.166	0.000	-5.1E-06	0.90	-0.24	0.003	-1.2E-03	0.79	-6.9E-03	3.3E-05	-4.5E-08	44.20	-3.85	2.03	-0.155	42.455	-0.005	1.9E-03	-5.3E-06
3Blv	41.24	1.788	2.111	-0.209	42.094	0.144	0.000	-6.8E-06	0.66	-0.16	0.002	-4.1E-04	0.58	-4.8E-03	1.8E-05	-1.5E-08	41.61	-2.93	1.887	-0.144	40.303	-0.003	1.7E-03	-5.0E-06
3Bn	48.799	-2.089	1.888	-0.155	47.866	0.000	0.000	-5.2E-06	0.84	-0.03	0.001	1.1E-03	0.83	-1.5E-03	-9.0E-06	4.0E-08	46.455	-1.87	1.288	-0.100	45.611	-0.001	1.2E-03	-3.5E-06
3C	57.552	-1.506	1.006	-0.008	56.933	-0.001	0.000	-2.8E-06	0.57	0.004	0.000	-6.5E-05	0.59	1.2E-03	-2.8E-06	-2.0E-09	49.61	-0.556	0.911	-0.007	49.444	0.001	8.4E-04	-2.5E-06
4A	2.76	12.355	0.855	-0.155	9.588	0.433	0.000	-5.3E-06	0.29	0.012	-0.001	2.8E-04	0.35	3.5E-03	-1.1E-05	9.7E-09	-3.811	12.944	0.600	-0.013	3.277	0.444	3.9E-04	-4.6E-06
4B	-12.30	20.144	-0.411	-0.009	-1.552	0.644	0.000	-3.1E-06	1.06	-0.035	0.006	-3.0E-03	0.88	-9.3E-03	5.8E-05	-1.0E-07	14.711	3.550	1.774	-0.018	16.966	0.017	1.5E-03	-6.1E-06
4C	57.266	-12.006	3.644	-0.255	51.507	-0.027	0.000	-8.6E-06	0.35	0.058	-0.010	5.6E-03	0.06	1.6E-02	-1.0E-04	1.9E-07	47.577	-7.552	2.555	-0.018	44.036	-0.016	2.4E-03	-6.2E-06
5A	-14.199	17.002	0.030	-0.013	-4.998	0.057	0.000	-4.6E-06	0.84	-0.014	0.003	-1.5E-03	0.77	-3.5E-03	2.6E-05	-5.3E-08	-5.550	10.81	1.005	-0.016	0.503	0.039	8.2E-04	-5.6E-06
5B	14.999	2.186	2.556	-0.024	16.665	0.166	0.000	-8.4E-06	0.17	0.020	-0.004	2.1E-03	0.27	5.1E-03	-3.6E-05	7.2E-08	4.04	7.411	1.044	-0.014	8.233	0.028	8.5E-04	-4.8E-06
6A	-96.40	48.355	-3.665	0.003	-70.33	1.444	0.000	8.77E-07	1.555	-0.42	0.006	-3.0E-03	1.34	-1.2E-02	6.2E-05	-1.0E-07	-73.64	36.85	-2.27	-0.002	-53.64	1.12	-2.4E-03	-8.9E-07

Table 86 continued

	a	b	c	d	a	b	c	d	a	b	c	d	a	b	c	d	a	b	c	d	a	b	c	d
6B	67.18	-30.73	8.40	-0.57	51.25	-0.70	0.01	-2E-05	-0.70	0.66	-0.11	5.8E-03	-0.35	1.8E-02	-1.1E-04	2.0E-07	19.08	-6.17	3.83	-0.31	15.99	-0.06	3.5E-03	-1.1E-05
7A	25.85	-8.12	4.76	-0.38	22.10	-0.09	0.00	-1.3E-05	-1.16	0.77	-0.11	5.0E-03	-0.76	2.1E-02	-1.1E-04	1.7E-07	-5.50	4.67	2.60	-0.27	-2.68	0.25	2.3E-03	-9.2E-06

Table 87 Monthly/total cooling degree-days and weighting factor under different base temperatures

		50		55		60		65	
CZ	Month	CDD	WF	CDD	WF	CDD	WF	CDD	WF
	1	554.0	0.0552	399.0	0.0486	244.0	0.0383	89.0	0.0195
	2	578.7	0.0577	438.7	0.0535	298.7	0.0468	158.7	0.0349
	3	735.3	0.0733	580.3	0.0707	425.3	0.0667	270.3	0.0594
	4	806.1	0.0804	656.1	0.0800	506.1	0.0794	356.1	0.0782
	5	922.4	0.0920	767.4	0.0936	612.4	0.0960	457.4	0.1005
	6	963.4	0.0961	813.4	0.0992	663.4	0.1040	513.4	0.1128
	7	1043.6	0.1041	888.6	0.1083	733.6	0.1150	578.6	0.1271
	8	1058.7	0.1056	903.7	0.1102	748.7	0.1174	593.7	0.1304
	9	998.5	0.0996	848.5	0.1034	698.5	0.1095	548.5	0.1205
	10	954.7	0.0952	799.7	0.0975	644.7	0.1011	489.7	0.1076
	11	793.4	0.0791	643.4	0.0784	493.4	0.0774	343.4	0.0754
	12	618.1	0.0616	463.1	0.0565	308.1	0.0483	153.1	0.0336
	total	10026.9	1.0000	8201.9	1.0000	6376.9	1.0000	4551.9	1.0000
2A	1	31.5	0.0045						
	2	196.0	0.0281	59.1	0.0110	0.1	0.0000		
	3	422.1	0.0605	267.1	0.0498	112.1	0.0286	9.0	0.0034
	4	598.1	0.0858	448.1	0.0836	298.1	0.0761	148.1	0.0560
	5	784.8	0.1125	629.8	0.1174	474.8	0.1212	319.8	0.1209
	6	880.2	0.1262	730.2	0.1361	580.2	0.1481	430.2	0.1627
	7	978.8	0.1404	823.8	0.1536	668.8	0.1707	513.8	0.1944
	8	979.7	0.1405	824.7	0.1538	669.7	0.1710	514.7	0.1947
	9	870.0	0.1248	720.0	0.1342	570.0	0.1455	420.0	0.1588
	10	723.6	0.1038	568.6	0.1060	413.6	0.1056	258.6	0.0978
	11	427.4	0.0613	277.4	0.0517	129.9	0.0332	29.6	0.0112
	12	80.8	0.0116	14.4	0.0027				
	total	6972.9	1.0000	5363.1	1.0000	3917.2	1.0000	2643.8	1.0000
2B	1	91.3	0.0110	3.3	0.0005				

Table 87 continued

CZ	Month	CDD	WF	CDD	WF	CDD	WF	CDD	WF
	2	263.5	0.0316	123.5	0.0185	15.1	0.0029		
	3	506.8	0.0608	351.8	0.0527	196.8	0.0381	53.2	0.0139
	4	702.0	0.0843	552.0	0.0827	402.0	0.0777	252.0	0.0659
	5	920.8	0.1105	765.8	0.1148	610.8	0.1181	455.8	0.1192
	6	1039.2	0.1247	889.2	0.1333	739.2	0.1430	589.2	0.1541
	7	1164.4	0.1398	1009.4	0.1513	854.4	0.1652	699.4	0.1829
	8	1172.7	0.1408	1017.7	0.1525	862.7	0.1669	707.7	0.1850
	9	1044.1	0.1253	894.1	0.1340	744.1	0.1439	594.1	0.1553
	10	863.3	0.1036	708.3	0.1062	553.3	0.1070	398.3	0.1041
	11	491.3	0.0590	341.3	0.0512	192.0	0.0371	74.8	0.0196
	12	72.0	0.0086	15.0	0.0022				
	total	8331.5	1.0000	6671.5	1.0000	5170.6	1.0000	3824.6	1.0000
3Aw	1								
	2	0.1	0.0000						
	3	160.4	0.0286	40.5	0.0093				
	4	433.8	0.0772	283.8	0.0651	133.8	0.0416	25.0	0.0113
	5	700.9	0.1248	545.9	0.1253	390.9	0.1214	235.9	0.1067
	6	864.7	0.1540	714.7	0.1640	564.7	0.1754	414.7	0.1876
	7	999.8	0.1780	844.8	0.1939	689.8	0.2143	534.8	0.2420
	8	993.8	2.0580	838.8	0.1925	683.8	0.2124	528.8	0.2393
	9	822.7	0.1465	672.7	0.1544	522.7	0.1624	372.7	0.1686
	10	542.9	0.0967	387.9	0.0890	232.9	0.0723	98.1	0.0444
	11	97.1	0.0173	27.5	0.0063	0.2	0.0001		
	12								
	total	5616.1	1.0000	4356.5	1.0000	3218.6	1.0000	2209.9	1.0000
3Ae	1								
	2	0.4	0.0001						
	3	155.2	0.0308	34.7	0.0092				
	4	401.6	0.0797	251.6	0.0666	102.3	0.0385	9.7	0.0058
	5	637.3	0.1264	482.3	0.1276	327.3	0.1233	172.3	0.1028
	6	776.5	0.1540	626.5	0.1658	476.5	0.1796	326.5	0.1948
	7	889.8	0.1765	734.8	0.1944	579.8	0.2185	424.8	0.2534
	8	878.9	0.1743	723.9	0.1915	568.9	0.2144	413.9	0.2469
	9	725.9	0.1440	575.9	0.1524	425.9	0.1605	275.9	0.1646
	10	482.9	0.0958	327.9	0.0868	173.1	0.0652	53.2	0.0318
	11	93.3	0.0185	21.9	0.0058				
	12								
	total	5041.8	1.0000	3779.5	1.0000	2653.8	1.0000	1676.3	1.0000
3Be	1								
	2								

Table 87 continued

CZ	Month	CDD	WF	CDD	WF	CDD	WF	CDD	WF
	3	83.0	0.0161	13.3	0.0034				
	4	409.5	0.0796	259.5	0.0657	113.4	0.0396	20.7	0.0109
	5	701.7	0.1364	546.7	0.1384	391.7	0.1367	236.7	0.1242
	6	853.6	0.1659	703.6	0.1781	553.6	0.1932	403.6	0.2118
	7	955.1	0.1856	800.1	0.2026	645.1	0.2251	490.1	0.2572
	8	911.6	0.1772	756.6	0.1915	601.6	0.2099	446.6	0.2344
	9	720.7	0.1401	570.7	0.1445	420.7	0.1468	270.7	0.1421
	10	445.4	0.0866	290.4	0.0735	139.9	0.0488	37.1	0.0195
	11	64.0	0.0124	9.2	0.0023				
	12								
	total	5144.6	1.0000	3950.1	1.0000	2866.0	1.0000	1905.5	1.0000
3Bw	1								
	2	28.6	0.0050						
	3	240.1	0.0420	88.1	0.0201	6.0	0.0019		
	4	467.1	0.0817	317.1	0.0722	167.1	0.0521	37.5	0.0173
	5	704.3	0.1232	549.3	0.1251	394.3	0.1231	239.3	0.1106
	6	850.2	0.1487	700.2	0.1595	550.2	0.1717	400.2	0.1850
	7	977.5	0.1710	822.5	0.1874	667.5	0.2083	512.5	0.2369
	8	973.9	0.1703	818.9	0.1865	663.9	0.2072	508.9	0.2353
	9	813.5	0.1423	663.5	0.1512	513.5	0.1603	363.5	0.1680
	10	550.3	0.0962	395.3	0.0900	240.3	0.0750	101.4	0.0469
	11	111.9	0.0196	34.9	0.0327	1.1	0.0003		
	12								
	total	5717.5	1.0000	4389.8	1.0000	3203.9	1.0000	2163.3	1.0000
3Blv	1								
	2	55.6	0.0077	0.5	0.0001				
	3	315.6	0.0437	160.6	0.0274	39.1	0.0085		
	4	584.2	0.0809	434.2	0.0742	284.2	0.0617	134.2	0.0385
	5	874.2	0.1211	719.2	0.1229	564.2	0.1224	409.2	0.1174
	6	1056.7	0.1464	906.7	0.1549	756.7	0.1642	606.7	0.1741
	7	1220.2	0.1690	1065.2	0.1820	910.2	0.1975	755.2	0.2167
	8	1222.8	0.1694	1067.8	0.1824	912.8	0.1980	757.8	0.2175
	9	1029.4	0.1426	879.4	0.1502	729.4	0.1583	579.4	0.1663
	10	706.8	0.0979	551.8	0.0943	396.8	0.0861	242.0	0.0694
	11	153.8	0.0213	68.0	0.0116	15.8	0.0034		
	12								
	total	7219.2	1.0000	5853.4	1.0000	4609.2	1.0000	3484.5	1.0000
3Bn	1								
	2	30.0	0.0067						
	3	167.3	0.0374	26.8	0.0085				

Table 87 continued

CZ	Month	CDD	WF	CDD	WF	CDD	WF	CDD	WF
	4	327.1	0.0730	177.1	0.0561	36.8	0.0180		
	5	512.5	0.1144	357.5	0.1132	202.5	0.0992	51.8	0.0461
	6	642.0	0.1434	492.0	0.1558	342.0	0.1675	192.0	0.1708
	7	762.7	0.1703	607.7	0.1925	452.7	0.2217	297.7	0.2648
	8	782.7	0.1748	627.7	0.1988	472.7	0.2315	317.7	0.2827
	9	672.8	0.1502	522.8	0.1656	372.8	0.1826	222.8	0.1982
	10	472.5	0.1055	317.5	0.1006	162.5	0.0796	42.0	0.0373
	11	108.6	0.0243	27.9	0.0088				
	12								
	total	4478.0	1.0000	3156.9	1.0000	2041.9	1.0000	1123.9	1.0000
3C	1	218.3	0.0395	63.3	0.0170				
	2	229.8	0.0416	89.8	0.0240				
	3	324.2	0.0587	169.2	0.0453	18.9	0.0087		
	4	403.5	0.0730	253.5	0.0679	103.5	0.0479		
	5	516.4	0.0935	361.4	0.0968	206.4	0.0955	51.4	0.0508
	6	588.5	0.1065	438.5	0.1174	288.5	0.1334	138.5	0.1368
	7	677.2	0.1226	522.2	0.1399	367.2	0.1698	212.2	0.2097
	8	709.4	0.1284	554.4	0.1485	399.4	0.1847	244.4	0.2415
	9	666.8	0.1207	516.8	0.1384	366.8	0.1696	216.8	0.2142
	10	601.7	0.1089	446.7	0.1196	291.7	0.1349	136.7	0.1351
	11	419.8	0.0760	269.8	0.0723	119.8	0.0554	12.0	0.0119
	12	169.5	0.0307	48.0	0.0129	0.2	0.0001		
	total	5525.1	1.0000	3733.6	1.0000	2162.4	1.0000	1012.0	1.0000
4A	1								
	2								
	3								
	4	176.7	0.0439	58.0	0.0193	3.2	0.0015		
	5	511.9	0.1272	356.9	0.1185	201.9	0.0958	64.6	0.0489
	6	728.1	0.1810	578.1	0.1919	428.1	0.2032	278.1	0.2108
	7	874.8	0.2174	719.8	0.2390	564.8	0.2681	409.8	0.3106
	8	850.5	0.2114	695.5	0.2309	540.5	0.2566	385.5	0.2921
	9	630.8	0.1568	480.8	0.1596	330.8	0.1570	180.8	0.1370
	10	250.6	0.0623	122.6	0.0407	37.3	0.0177	0.8	0.0006
	11								
	12								
	total	4023.4	1.0000	3011.7	1.0000	2106.7	1.0000	1319.5	1.0000
4B	1								
	2								
	3								
	4	174.7	0.0448	59.3	0.0205	4.0	0.0020		

Table 87 continued

CZ	Month	CDD	WF	CDD	WF	CDD	WF	CDD	WF
	5	518.1	0.1328	363.1	0.1255	208.1	0.1044	68.5	0.0565
	6	723.4	0.1855	573.4	0.1982	423.4	0.2125	273.4	0.2254
	7	850.6	0.2181	695.6	0.2404	540.6	0.2713	385.6	0.3179
	8	809.8	0.2076	654.8	0.2264	499.8	0.2509	344.8	0.2844
	9	590.3	0.1513	440.3	0.1522	290.3	0.1457	140.4	0.1158
	10	233.8	0.0599	106.5	0.0368	26.3	0.0132		
	11								
	12								
	total	3900.6	1.0000	2892.9	1.0000	1992.4	1.0000	1212.7	1.0000
4C	1								
	2								
	3								
	4	47.8	0.0220						
	5	218.7	0.1005	65.7	0.0514				
	6	374.1	0.1719	224.1	0.1754	74.1	0.1285		
	7	504.2	0.2317	349.2	0.2733	194.2	0.3368	39.5	0.3835
	8	525.8	0.2417	370.8	0.2902	215.8	0.3742	60.8	0.5903
	9	391.8	0.1801	241.8	0.1892	92.6	0.1605	2.7	0.0262
	10	113.3	0.0521	26.2	0.0205				
	11								
	12								
	total	2175.6	1.0000	1277.7	1.0000	576.6	1.0000	102.9	1.0000
5A	1								
	2								
	3								
	4	49.8	0.0162	2.2	0.0010				
	5	362.5	0.1182	207.5	0.0956	70.8	0.0511	4.0	0.0055
	6	597.2	0.1948	447.2	0.2061	297.2	0.2144	147.2	0.2014
	7	741.7	0.2419	586.7	0.2704	431.7	0.3114	276.7	0.3786
	8	710.9	0.2319	555.9	0.2562	400.9	0.2892	245.9	0.3364
	9	484.9	0.1582	334.9	0.1543	184.9	0.1334	57.1	0.0781
	10	118.5	0.0387	35.7	0.0164	0.6	0.0005		
	11								
	12								
	total	3065.5	1.0000	2170.0	1.0000	1386.2	1.0000	730.9	1.0000
5B	1								
	2								
	3								
	4	29.5	0.0104						
	5	298.9	0.1048	144.2	0.0726	32.6	0.0264		

Table 87 continued

CZ	Month	CDD	WF	CDD	WF	CDD	WF	CDD	WF
	6	539.8	0.1893	389.8	0.1963	239.8	0.1939	90.5	0.1457
	7	706.5	0.2478	551.5	0.2777	396.5	0.3205	241.5	0.3887
	8	700.0	0.2455	545.0	0.2745	390.0	0.3153	235.0	0.3782
	9	478.0	0.1676	328.0	0.1652	178.0	0.1439	54.3	0.0874
	10	98.6	0.0346	27.1	0.0137				
	11								
	12								
	total	2851.3	1.0000	1985.5	1.0000	1236.9	1.0000	621.2	1.0000
6A	1								
	2								
	3								
	4								
	5	223.5	0.0893	95.3	0.0554	18.4	0.0176		
	6	536.0	0.2142	386.0	0.2245	236.0	0.2266	88.6	0.1815
	7	688.5	0.2752	533.5	0.3102	378.5	0.3633	223.5	0.4579
	8	631.0	0.2522	476.0	0.2768	321.0	0.3082	166.0	0.3402
	9	375.5	0.1501	225.5	0.1311	87.8	0.0843	10.0	0.0205
	10	47.6	0.0190	3.3	0.0019				
	11								
	12								
	total	2502.2	1.0000	1719.7	1.0000	1041.7	1.0000	488.1	1.0000
6B	1								
	2								
	3								
	4								
	5	93.7	0.0506	13.7	0.0115				
	6	379.1	0.2046	229.1	0.1917	84.8	0.1306	5.8	0.0248
	7	588.6	0.3177	433.6	0.3628	278.6	0.4291	123.6	0.5312
	8	568.2	0.3067	413.2	0.3457	258.2	0.3977	103.3	0.4439
	9	223.2	0.1205	105.6	0.0883	27.6	0.0426		
	10								
	11								
	12								
	total	1852.9	1.0000	1195.2	1.0000	649.3	1.0000	232.7	1.0000
7A	1								
	2								
	3								
	4								
	5	191.9	0.0908	62.7	0.0449	3.1	0.0040		
	6	462.8	0.2190	312.8	0.2241	162.8	0.2059	34.8	0.1100

Table 87 continued

CZ	Month	CDD	WF	CDD	WF	CDD	WF	CDD	WF
	7	631.6	0.2989	476.6	0.3414	321.6	0.4068	166.6	0.5262
	8	580.2	0.2745	425.2	0.3046	270.2	0.3418	115.2	0.3638
	9	246.9	0.1168	118.6	0.0850	32.8	0.0415		
	10								
	11								
	12								
	total	2113.4	1.0000	1395.9	1.0000	790.5	1.0000	316.6	1.0000

Table 88 Error 1 for compressor efficiency effect

	COP A1	COP A2	COP B HRV (60%)	COP B ERV (60%)	COP C (20%)	COP C (50%)	COP C (80%)	COP C (100%)	COP D (20%)	COP D (50%)	COP (80%)	COP D (100%)
max	0.03%	0.02%	0.03%	0.03%	0.03%	0.03%	0.03%	0.03%	0.01%	0.02%	0.02%	0.02%
min	-0.02%	-0.02%	-0.02%	-0.02%	-0.03%	-0.03%	-0.02%	-0.52%	-0.01%	-0.02%	-0.02%	-0.02%

Table 89 Error 2 for compressor efficiency effect

	COP A1	COP A2	COP B HRV (60%)	COP B ERV (60%)	COP C (20%)	COP C (50%)	COP C (80%)	COP C (100%)	COP D (20%)	COP D (50%)	COP (80%)	COP D (100%)
max	0.17%	3.53%	1.19%	2.52%	0.03%	0.05%	0.08%	0.10%	0.01%	0.02%	0.02%	0.01%
min	-0.19%	-5.45%	-1.60%	-2.87%	-0.05%	-0.10%	-0.20%	-0.24%	-0.01%	-0.01%	-0.02%	-0.02%

Table 90 Error 3 for compressor effect

	COP A1	COP A2	COP B HRV (60%)	COP B ERV (60%)	COP C (20%)	COP C (50%)	COP C (80%)	COP C (100%)	COP D (20%)	COP D (50%)	COP (80%)	COP D (100%)
min	513	211	209	685	9	36	42	75	515	605	976	1786

Table 91 Error 1 for subcooling effect

	COP A1	COP A2	COP B HRV (60%)	COP B ERV (60%)
max	2.25%	1.94%	0.03%	0.04%
min	0.42%	0.00%	-0.03%	-0.03%

Table 92 Error 2 for subcooling effect

	COP A1	COP A2	COP B HRV (60%)	COP B ERV (60%)
max	2.18%	5.20%	1.21%	2.54%
min	0.49%	-3.79%	-1.61%	-2.89%

Table 93 Error 3 for subcooling effect

	COP A1	COP A2	COP B HRV (60%)	COP B ERV (60%)
min	13	13	181	717

Table 94 Error 1 for superheated effect

	COP A1	COP A2	COP B HRV (60%)	COP B ERV (60%)
max	0.20%	0.13%	-0.25%	-0.27%
min	-0.29%	-0.35%	-0.40%	-0.40%

Table 95 Error 2 for superheated effect

	COP A1	COP A2	COP B HRV (60%)	COP B ERV (60%)
max	0.22%	3.58%	0.87%	2.14%
min	-0.33%	-5.40%	-1.96%	-3.22%

Table 96 Error 3 for superheated effect

	COP A1	COP A2	COP B HRV (60%)	COP B ERV (60%)
min	38.87084	11.62517318	11.83121328	20.95012886

Table 97 Error 1 for Delta Taeo effect

	COP A1	COP A2	COP B HRV (60%)	COP B ERV (60%)	COP C (20%)	COP C (50%)	COP C (80%)	COP C (100%)	COP D (20%)	COP D (50%)	COP (80%)	COP D (100%)
max	2.33 %	1.25 %	0.02%	0.03%	0.03%	0.03%	0.04%	0.03%	-0.33%	-0.66%	-0.94%	-1.10%
min	0.33 %	0.00 %	-0.03%	-0.03%	-0.03%	-0.04%	-0.04%	-0.52%	-0.41%	-0.77%	-1.07%	-1.24%

Table 98 Error 2 for Delta Taeo effect

	COP A1	COP A2	COP B HRV (60%)	COP B ERV (60%)	COP C (20%)	COP C (50%)	COP C (80%)	COP C (100%)	COP D (20%)	COP D (50%)	COP (80%)	COP D (100%)
max	2.20 %	4.35 %	1.20%	2.53%	0.04%	0.06%	0.08%	0.10%	-0.33%	-0.66%	-0.93%	-1.08%
min	0.30 %	-4.25 %	-1.61%	-2.91%	-0.05%	-0.12%	-0.17%	-0.25%	-0.40%	-0.76%	-1.05%	-1.22%

Table 99 Error 3 for Delta Taeo effect

	COP A1	COP A2	COP B HRV (60%)	COP B ERV (60%)	COP C (20%)	COP C (50%)	COP C (80%)	COP C (100%)	COP D (20%)	COP D (50%)	COP (80%)	COP D (100%)
min	19	19	236	280	10	24	41	44	14	16	18	18

Table 100 Error 1 for Delta Taci effect

	COP A1	COP A2	COP B HRV (60%)	COP B ERV (60%)	COP C (20%)	COP C (50%)	COP C (80%)	COP C (100%)	COP D (20%)	COP D (50%)	COP (80%)	COP D (100%)
max	-0.16 %	0.00 %	0.03%	0.04%	0.15%	0.34%	0.53%	0.66%	1.77%	3.45%	4.62%	5.20%
min	-5.56 %	-2.36 %	-0.03%	-0.02%	0.00%	0.00%	0.00%	-0.52%	1.25%	2.50%	3.43%	3.95%

Table 101 Error 2 for Delta Taci effect

	COP A1	COP A2	COP B HRV (60%)	COP B ERV (60%)	COP C (20%)	COP C (50%)	COP C (80%)	COP C (100%)	COP D (20%)	COP D (50%)	COP (80%)	COP D (100%)
max	0.00%	2.82%	1.20%	2.53%	0.15%	0.36%	0.57%	0.70%	1.80%	3.56%	4.82%	5.48%
min	-5.44%	-7.21%	-1.61%	-2.89%	0.01%	0.03%	0.03%	0.04%	1.27%	2.58%	3.57%	4.12%

Table 102 Error 3 for Delta Taci effect

	COP A1	COP A2	COP B HRV (60%)	COP B ERV (60%)	COP C (20%)	COP C (50%)	COP C (80%)	COP C (100%)	COP D (20%)	COP D (50%)	COP (80%)	COP D (100%)
min	9	10	196	1413	5	5	5	5	3	4	4	4

Table 103 Error 1 for all assumptions changing

	COP A1	COP A2	COP B HRV (60%)	COP B ERV (60%)	COP C (20%)	COP C (50%)	COP C (80%)	COP C (100%)	COP D (20%)	COP D (50%)	COP (80%)	COP D (100%)
max	0.35%	0.35%	0.04%	0.02%	0.00%	0.34%	0.53%	0.64%	1.43%	2.76%	3.67%	4.13%
min	-1.92%	-0.63%	-0.03%	-0.06%	-0.14%	0.00%	0.00%	-0.52%	0.92%	1.87%	2.55%	2.92%

Table 104 Error 2 for all assumptions changing

	COP A1	COP A2	COP B HRV (60%)	COP B ERV (60%)	COP C (20%)	COP C (50%)	COP C (80%)	COP C (100%)	COP D (20%)	COP D (50%)	COP (80%)	COP D (100%)
max	0.44%	3.88%	1.19%	2.53%	0.15%	0.34%	0.55%	1.47%	1.45%	2.83%	3.79%	4.30%
min	-2.06%	-5.55%	-1.60%	-2.88%	0.01%	0.03%	0.03%	0.04%	0.93%	1.91%	2.63%	3.02%

Table 105 Error 3 for all assumptions changing

	COP A1	COP A2	COP B HRV (60%)	COP B ERV (60%)	COP C (20%)	COP C (50%)	COP C (80%)	COP C (100%)	COP D (20%)	COP D (50%)	COP (80%)	COP D (100%)
min	25	30	185	1224	4	5	5	5	5	5	6	6

Table 106 Conventional vapor-compression system performance under different conditions for 7 refrigerants

R410A	R22	R32	R134a	R1234yf	R1234ze(e)	R1234ze(z)
3.866	4.22	4.046	4.176	3.929	4.157	4.608
3.866	4.22	4.046	4.176	3.929	4.157	4.608
3.866	4.22	4.046	4.176	3.929	4.157	4.608
3.866	4.22	4.046	4.176	3.929	4.157	4.608
3.866	4.22	4.046	4.176	3.929	4.157	4.608
4.237	4.618	4.429	4.582	4.328	4.568	5.033
4.237	4.618	4.429	4.582	4.328	4.568	5.033
4.237	4.618	4.429	4.582	4.328	4.568	5.033
4.237	4.618	4.429	4.582	4.328	4.568	5.033
4.237	4.618	4.429	4.582	4.328	4.568	5.033
4.667	5.079	4.871	5.051	4.789	5.043	5.523
4.667	5.079	4.871	5.051	4.789	5.043	5.523
4.667	5.079	4.871	5.051	4.789	5.043	5.523
4.667	5.079	4.871	5.051	4.789	5.043	5.523
4.667	5.079	4.871	5.051	4.789	5.043	5.523
3.516	3.882	3.707	3.831	3.577	3.807	4.261
3.516	3.882	3.707	3.831	3.577	3.807	4.261
3.516	3.882	3.707	3.831	3.577	3.807	4.261
3.516	3.882	3.707	3.831	3.577	3.807	4.261
3.516	3.882	3.707	3.831	3.577	3.807	4.261
3.837	4.23	4.04	4.186	3.926	4.168	4.634
3.837	4.23	4.04	4.186	3.926	4.168	4.634
3.837	4.23	4.04	4.186	3.926	4.168	4.634
3.837	4.23	4.04	4.186	3.926	4.168	4.634
3.837	4.23	4.04	4.186	3.926	4.168	4.634
4.206	4.629	4.422	4.593	4.325	4.58	5.062
4.206	4.629	4.422	4.593	4.325	4.58	5.062
4.206	4.629	4.422	4.593	4.325	4.58	5.062
4.206	4.629	4.422	4.593	4.325	4.58	5.062
4.206	4.629	4.422	4.593	4.325	4.58	5.062

Table 107 continued

R410A	R22	R32	R134a	R1234yf	R1234ze(e)	R1234ze(z)
3.201	3.581	3.405	3.523	3.263	3.496	3.954
3.201	3.581	3.405	3.523	3.263	3.496	3.954
3.201	3.581	3.405	3.523	3.263	3.496	3.954
3.201	3.581	3.405	3.523	3.263	3.496	3.954
3.201	3.581	3.405	3.523	3.263	3.496	3.954
3.481	3.888	3.696	3.837	3.569	3.814	4.285
3.481	3.888	3.696	3.837	3.569	3.814	4.285
3.481	3.888	3.696	3.837	3.569	3.814	4.285
3.481	3.888	3.696	3.837	3.569	3.814	4.285
3.481	3.888	3.696	3.837	3.569	3.814	4.285
3.799	4.237	4.028	4.193	3.919	4.176	4.66
3.799	4.237	4.028	4.193	3.919	4.176	4.66
3.799	4.237	4.028	4.193	3.919	4.176	4.66
3.799	4.237	4.028	4.193	3.919	4.176	4.66
3.799	4.237	4.028	4.193	3.919	4.176	4.66
2.914	3.311	3.133	3.247	2.979	3.216	3.68
2.914	3.311	3.133	3.247	2.979	3.216	3.68
2.914	3.311	3.133	3.247	2.979	3.216	3.68
2.914	3.311	3.133	3.247	2.979	3.216	3.68
2.914	3.311	3.133	3.247	2.979	3.216	3.68
3.159	3.584	3.39	3.525	3.251	3.5	3.975
3.159	3.584	3.39	3.525	3.251	3.5	3.975
3.159	3.584	3.39	3.525	3.251	3.5	3.975
3.159	3.584	3.39	3.525	3.251	3.5	3.975
3.159	3.584	3.39	3.525	3.251	3.5	3.975
3.436	3.891	3.679	3.84	3.558	3.819	4.307
3.436	3.891	3.679	3.84	3.558	3.819	4.307
3.436	3.891	3.679	3.84	3.558	3.819	4.307
3.436	3.891	3.679	3.84	3.558	3.819	4.307
3.436	3.891	3.679	3.84	3.558	3.819	4.307

APPENDIX B FIGURES

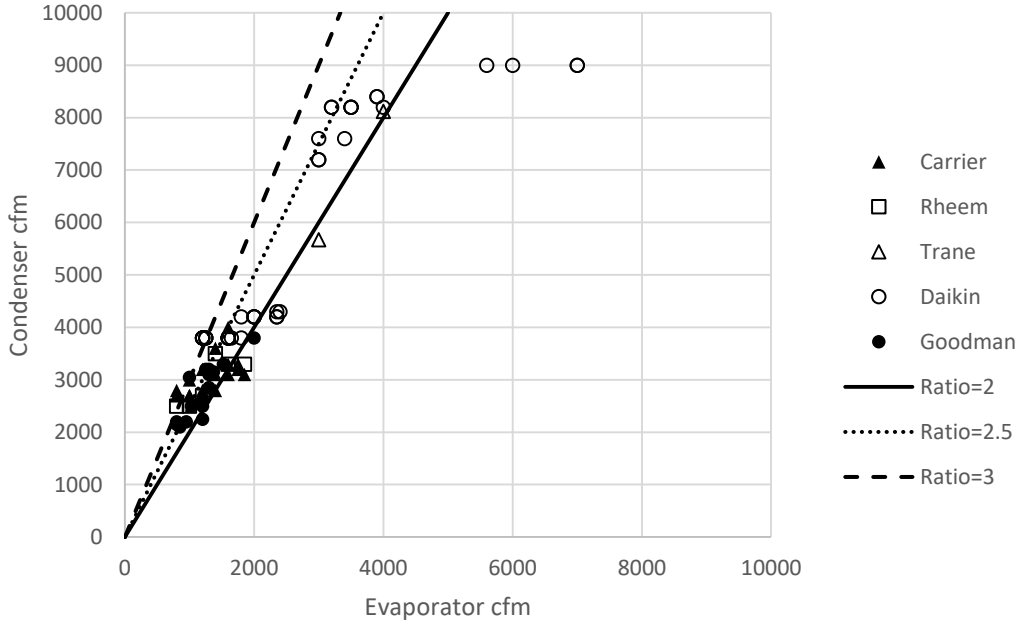

Figure 262 Condenser-to-evaporator cfm ratio less than 10000 cfm

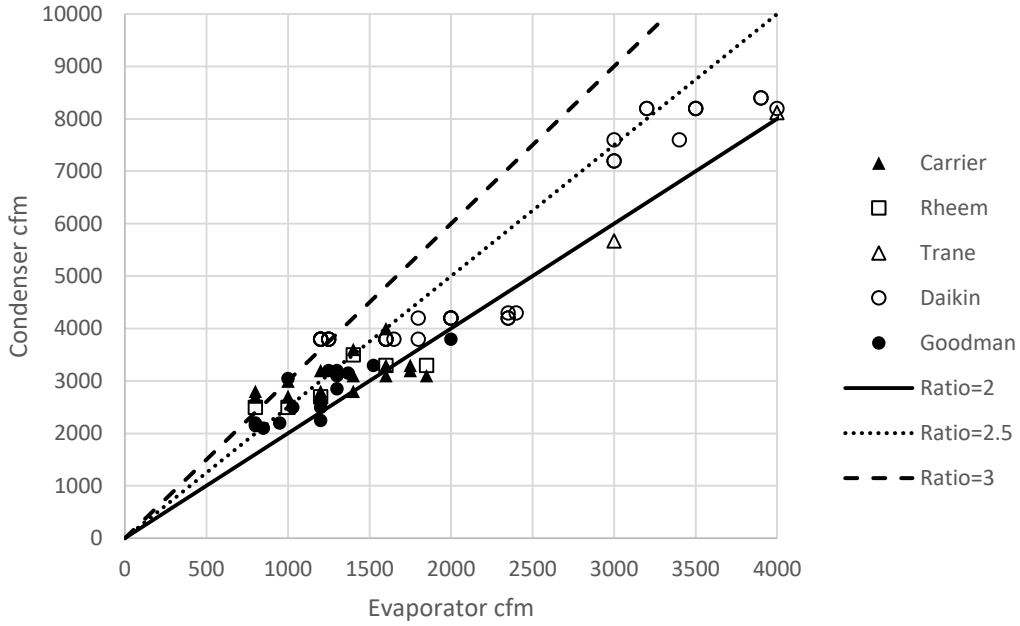

Figure 263 Condenser-to-evaporator cfm ratio less than 4000 cfm

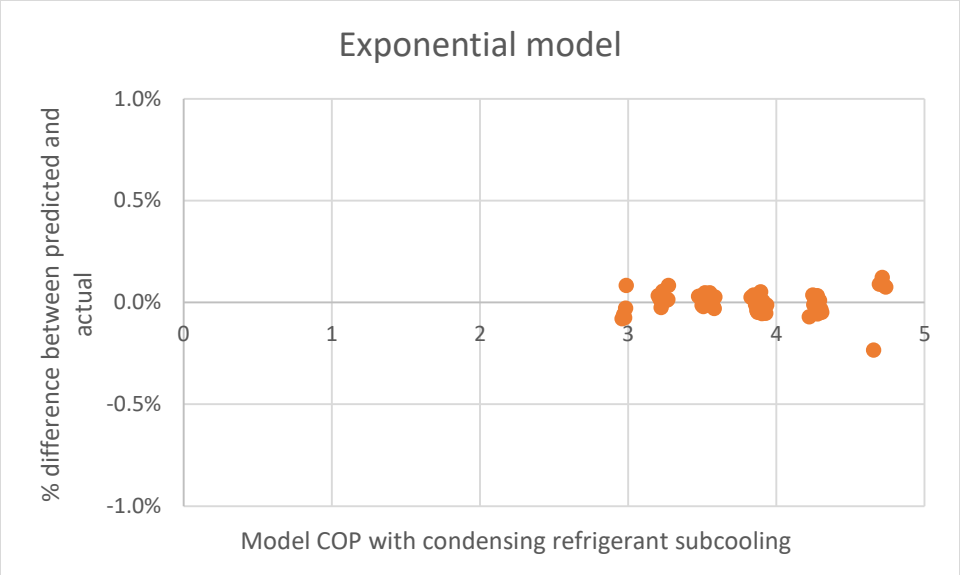

Figure 264 Percentage difference comparison of predicted and actual data of exponential method for COP with condensing refrigerant subcooling when HX effectiveness is 50%

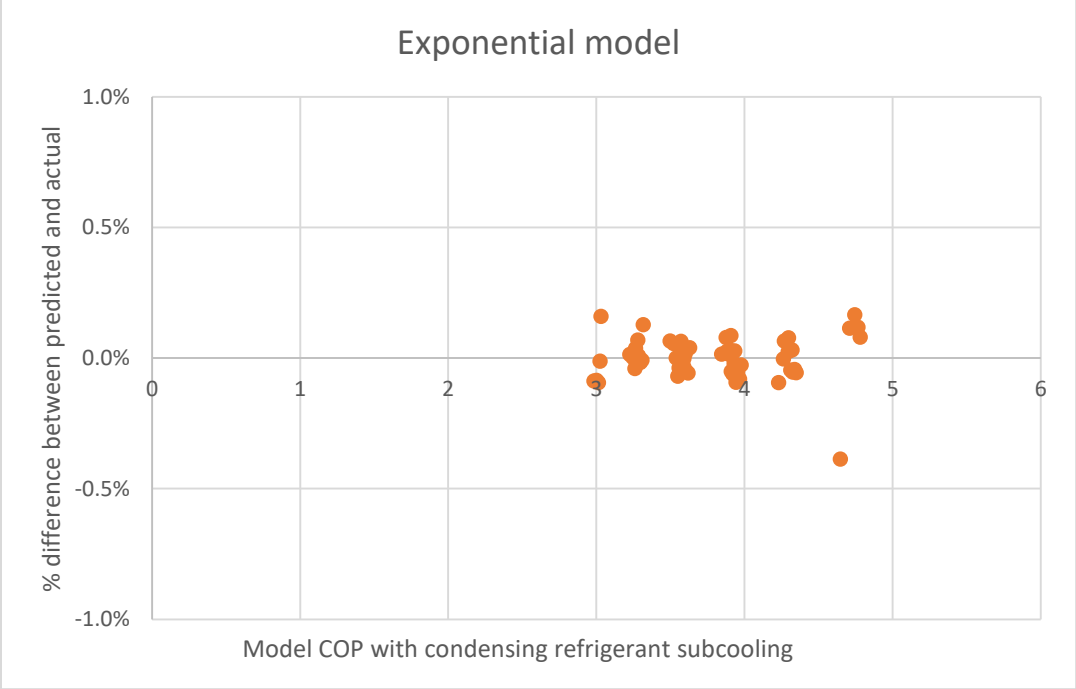

Figure 265 Percentage difference comparison of predicted and actual data of exponential method for COP with condensing refrigerant subcooling when HX effectiveness is 80%

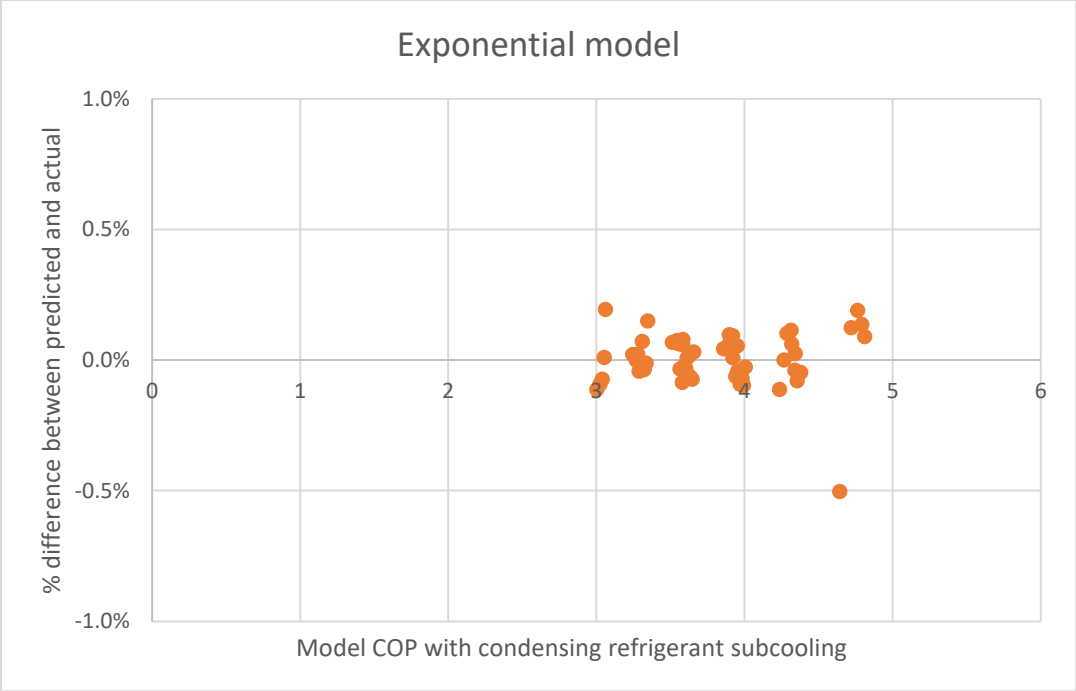

Figure 266 Percentage difference comparison of predicted and actual data of exponential method for COP with condensing refrigerant subcooling when HX effectiveness is 100%

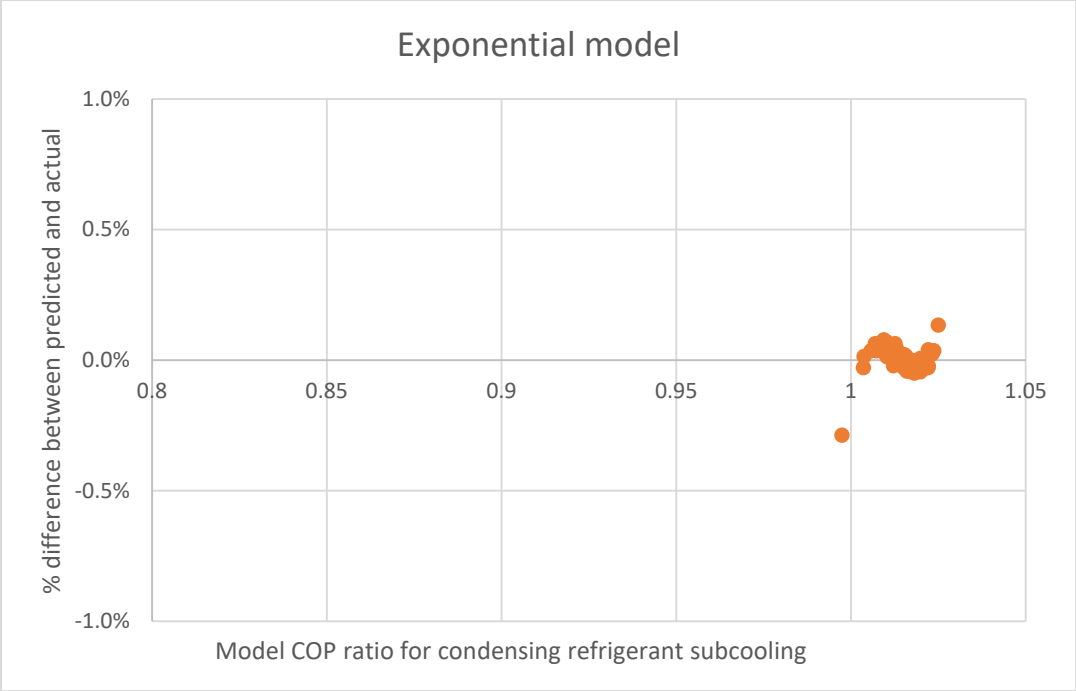

Figure 267 Percentage difference comparison of predicted and actual data of exponential method for COP ratio of condensing refrigerant subcooling over baseline when HX effectiveness is 50%

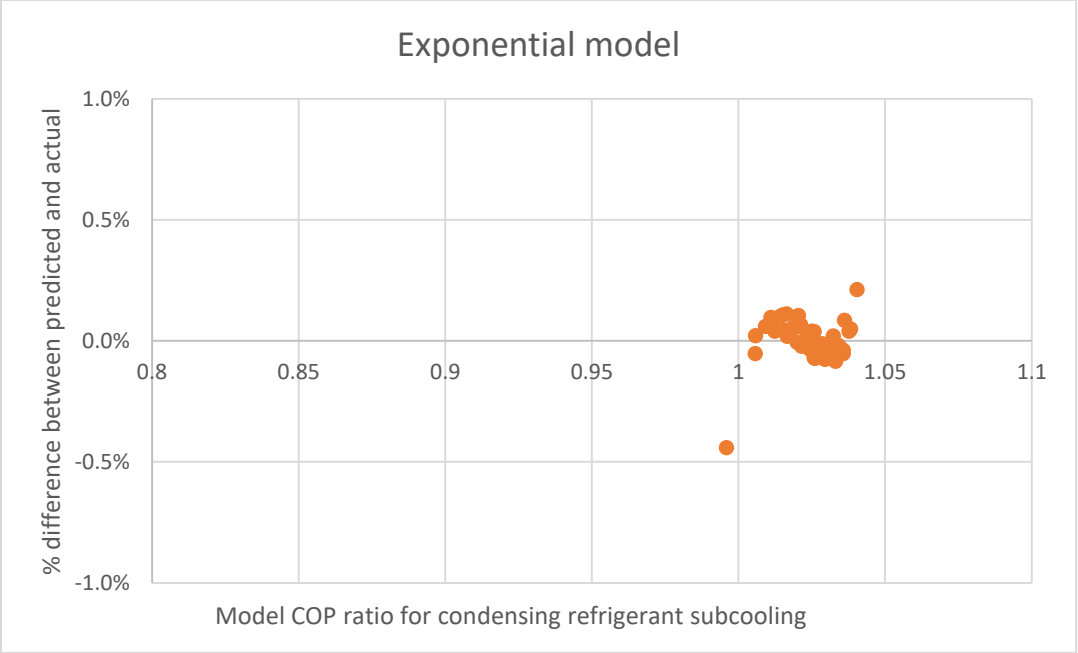

Figure 268 Percentage difference comparison of predicted and actual data of exponential method for COP ratio of condensing refrigerant subcooling over baseline when HX effectiveness is 80%

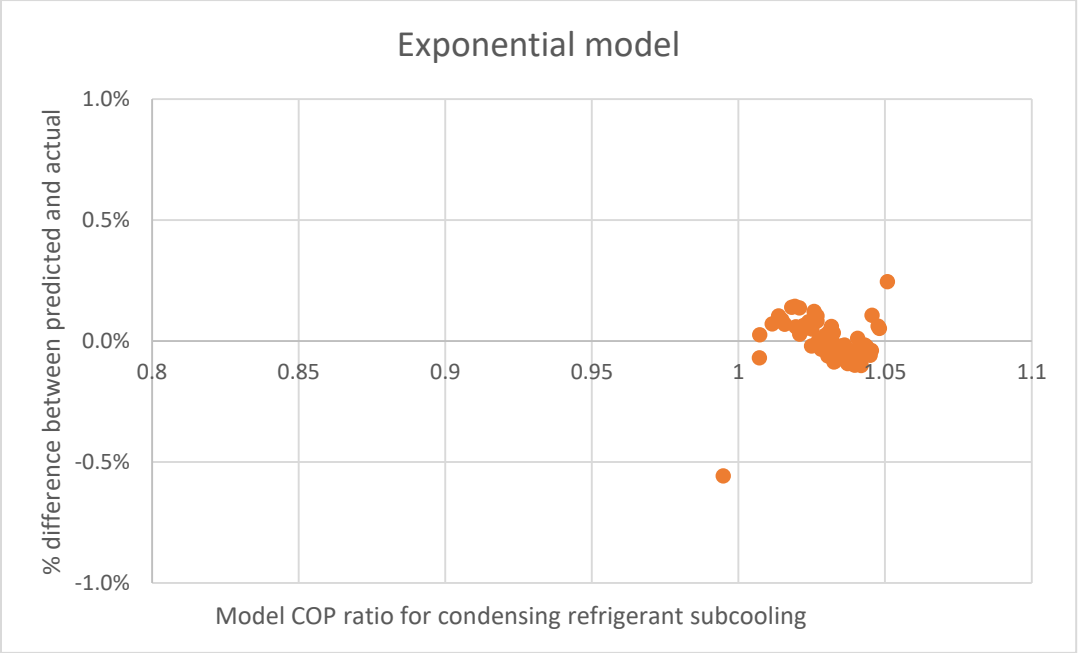

Figure 269 Percentage difference comparison of predicted and actual data of exponential method for COP ratio of condensing refrigerant subcooling over baseline when HX effectiveness is 100%

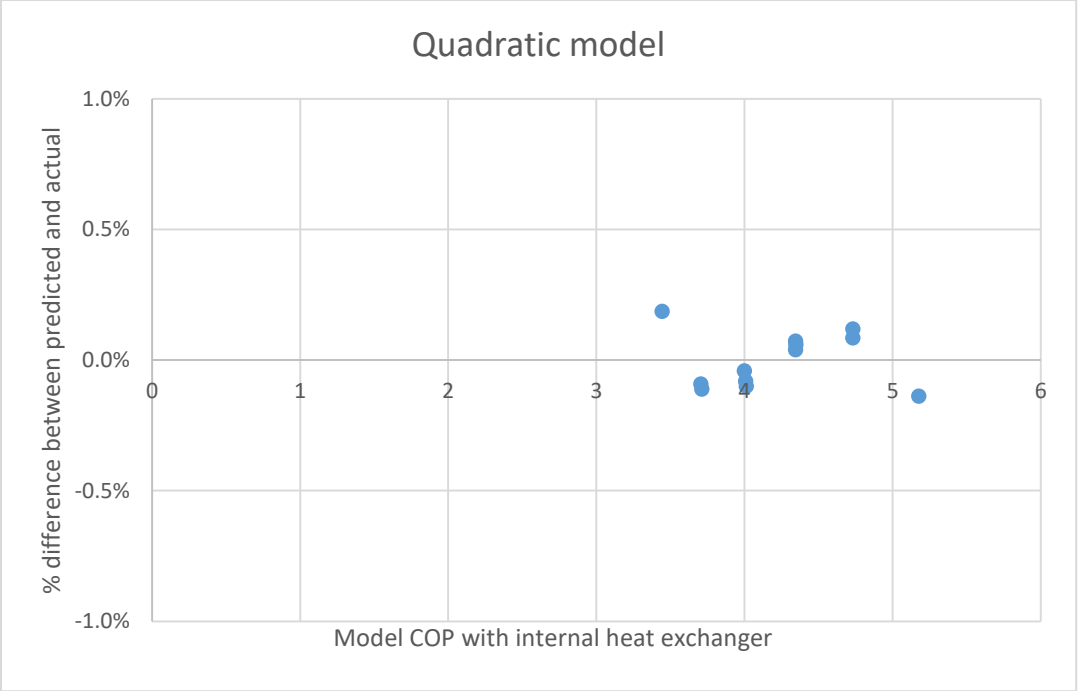

Figure 270 Percentage difference comparison of predicted and actual data of exponential method for COP with internal heat exchanger when HX effectiveness is 50%

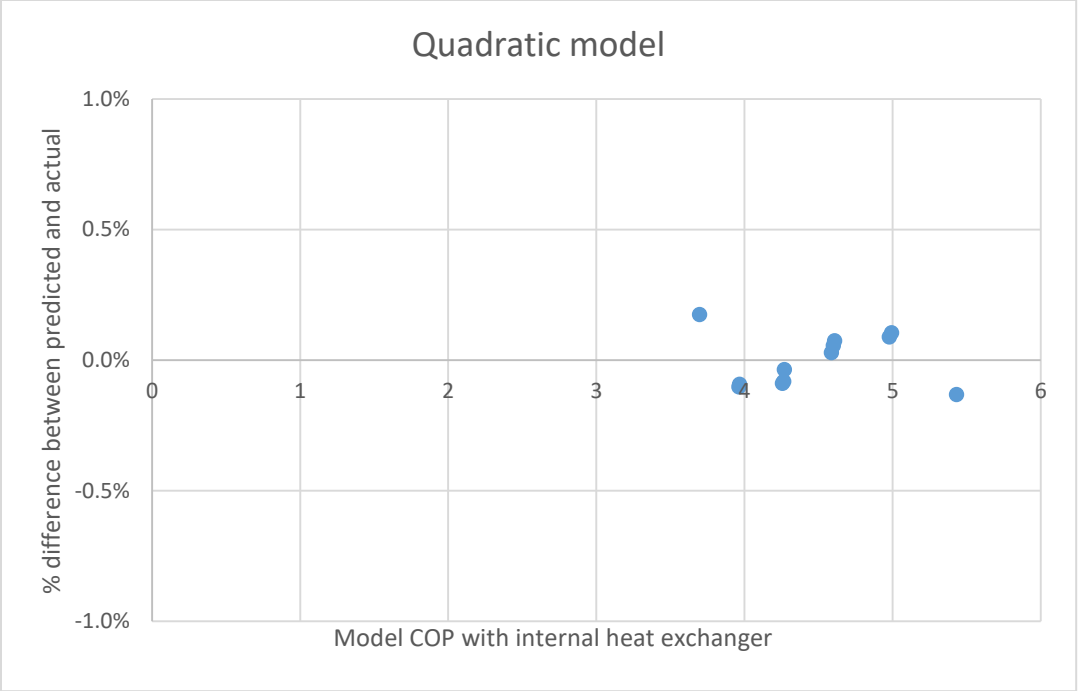

Figure 271 Percentage difference comparison of predicted and actual data of exponential method for COP with internal heat exchanger when HX effectiveness is 80%

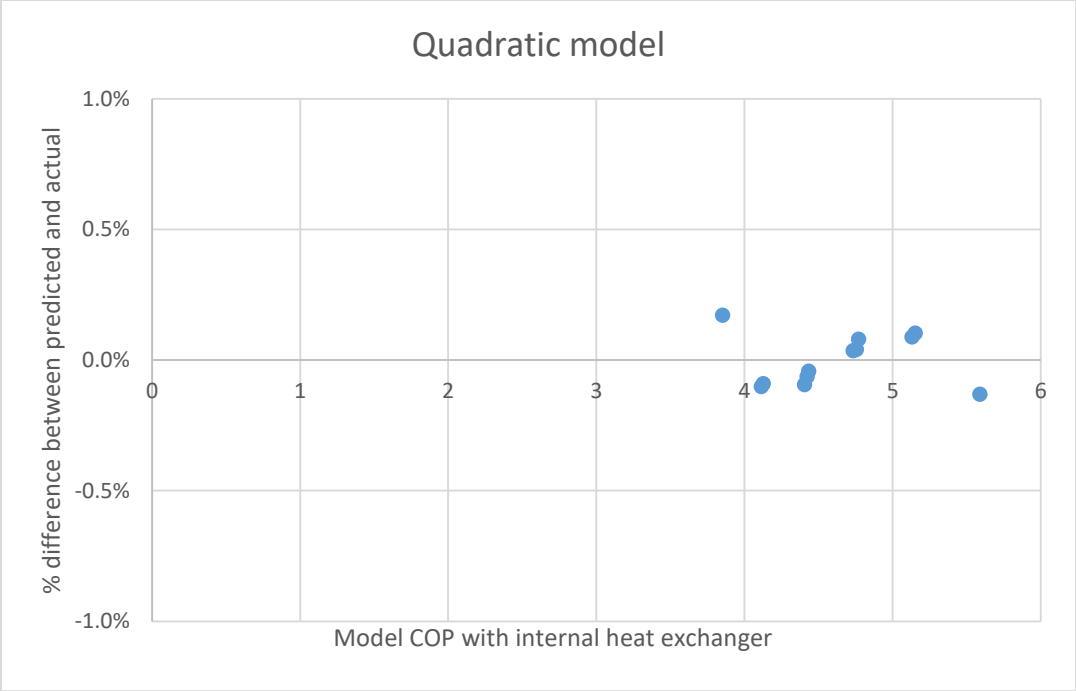

Figure 272 Percentage difference comparison of predicted and actual data of exponential method for COP with internal heat exchanger when HX effectiveness is 100%

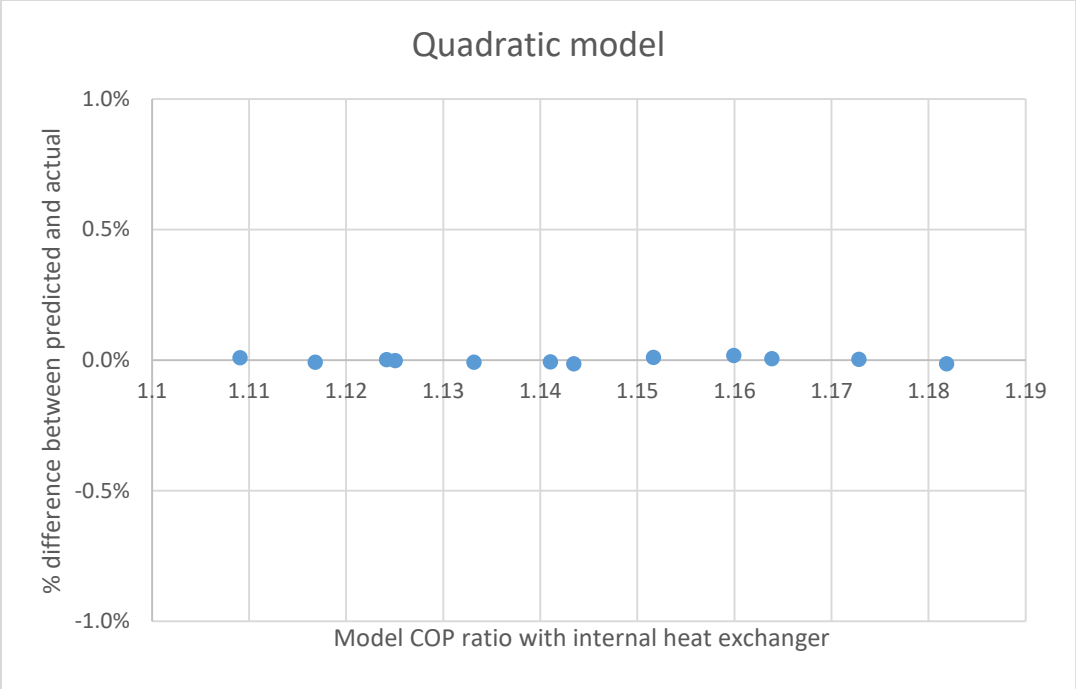

Figure 273 Percentage difference comparison of predicted and actual data of exponential method for COP ratio of internal heat exchanger over baseline when HX effectiveness is 50%

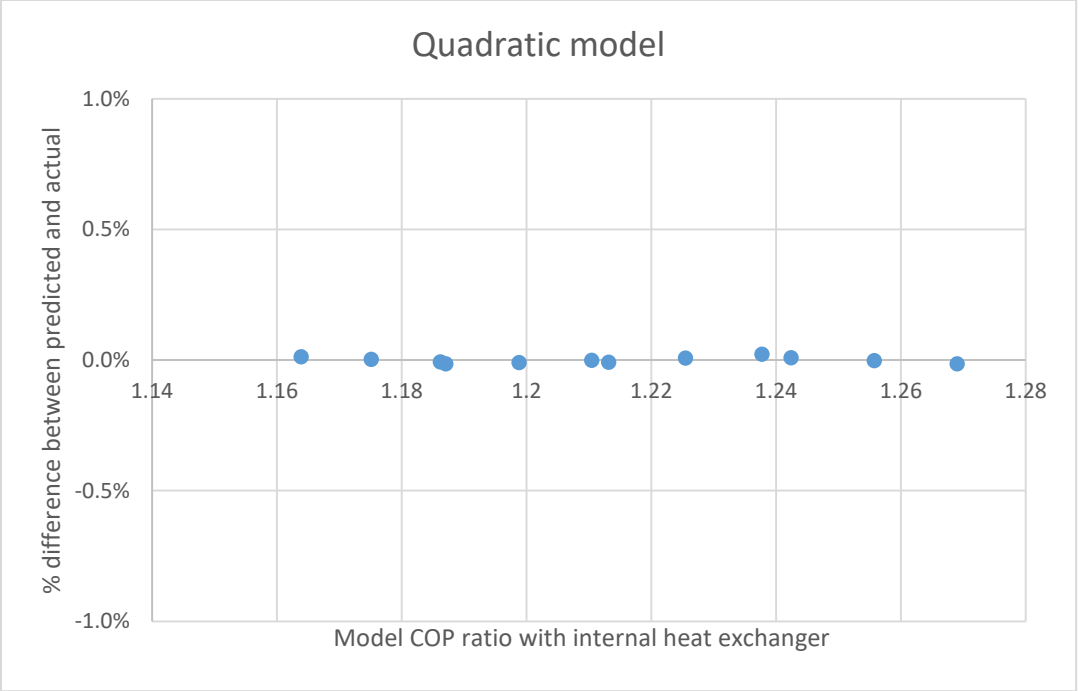

Figure 274 Percentage difference comparison of predicted and actual data of exponential method for COP ratio of internal heat exchanger over baseline when HX effectiveness is 80%

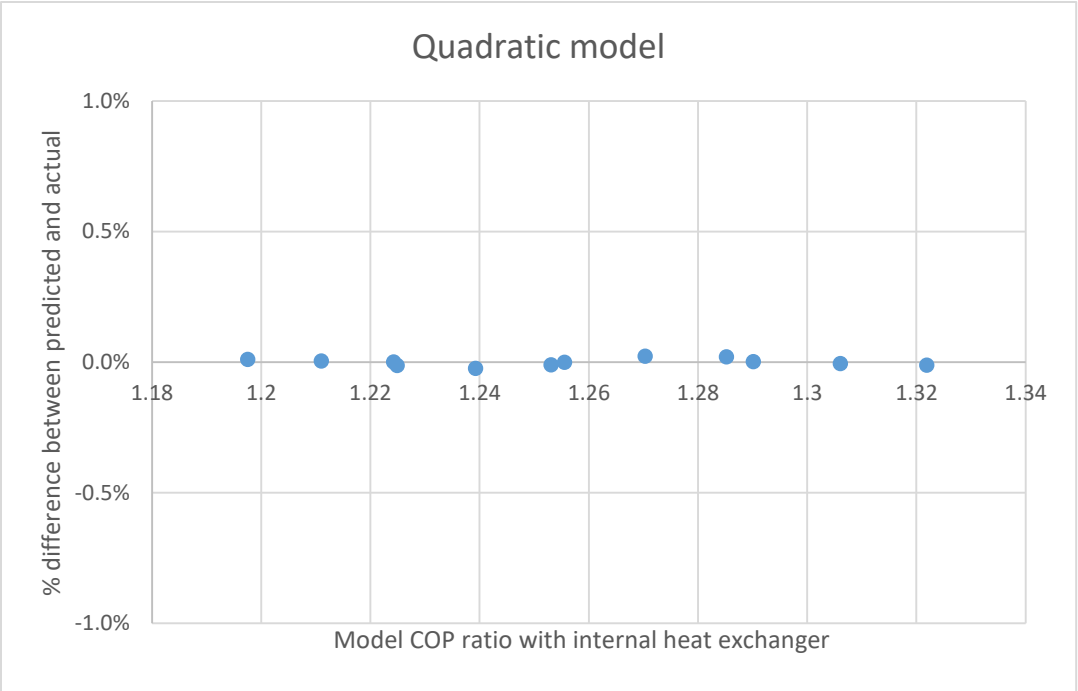

Figure 275 Percentage difference comparison of predicted and actual data of exponential method for COP ratio of internal heat exchanger over baseline when HX effectiveness is 100%

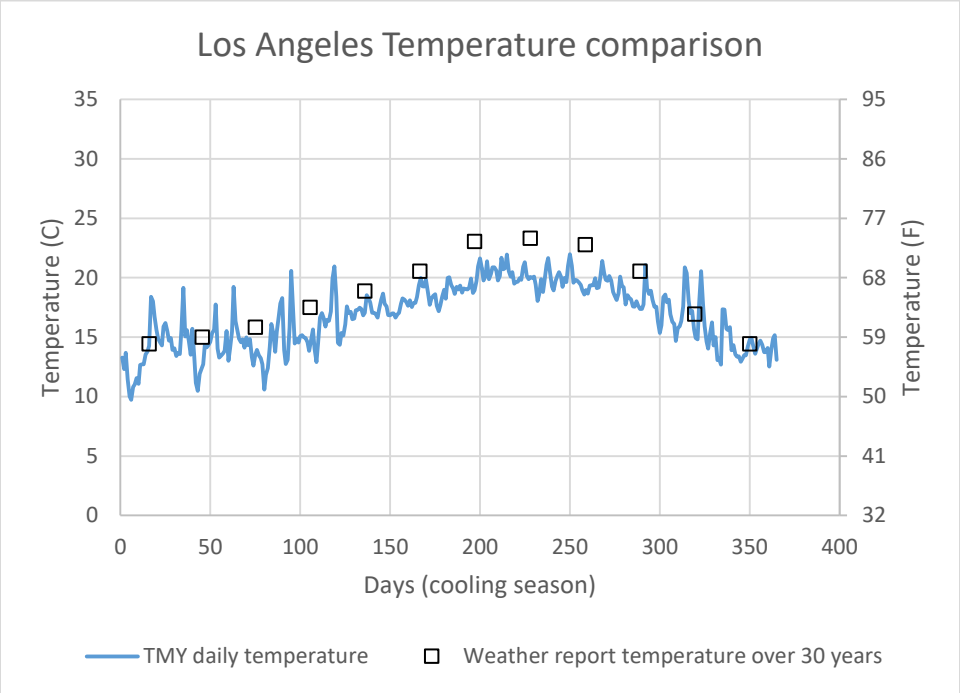

Figure 276 Temperature for Los Angeles comparison between TMY data and NOAA

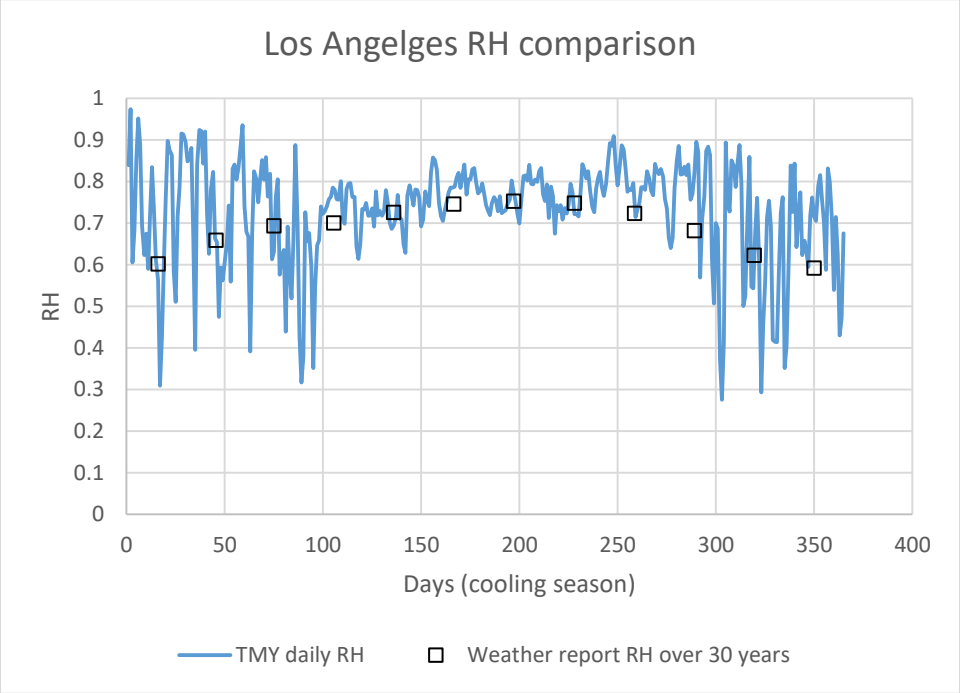

Figure 277 Relative humidity for Los Angeles comparison between TMY data and NOAA

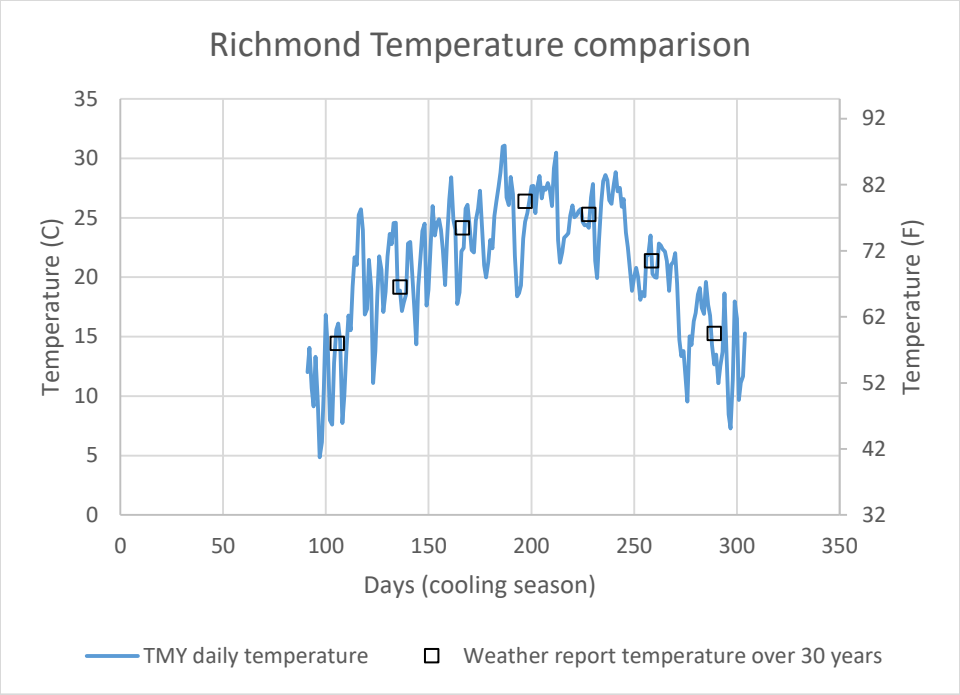

Figure 278 Temperature for Richmond comparison between TMY data and NOAA

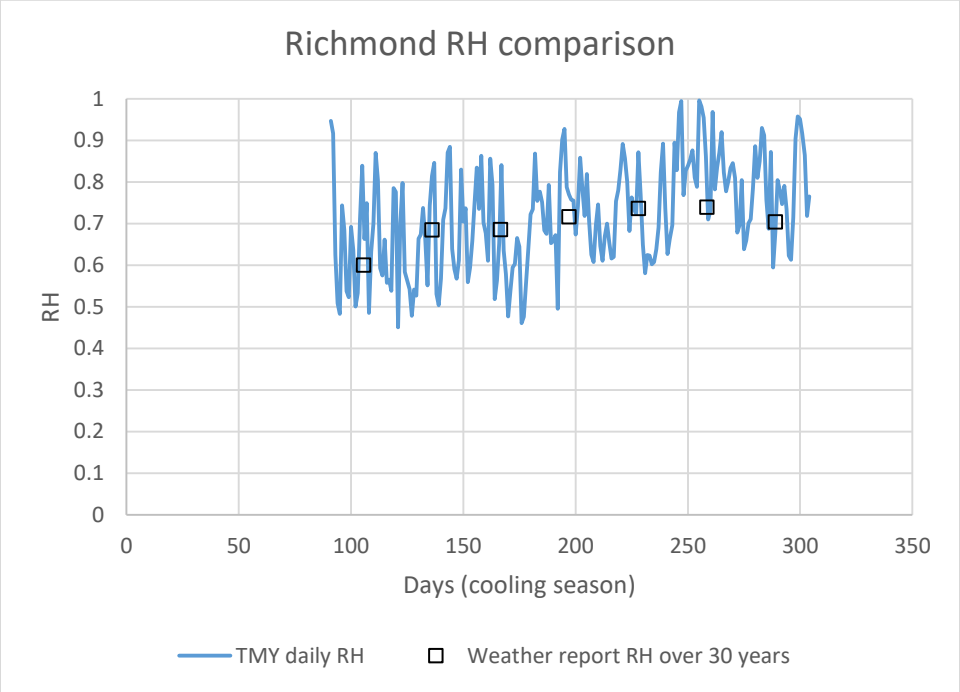

Figure 279 Relative humidity for Richmond comparison between TMY data and NOAA

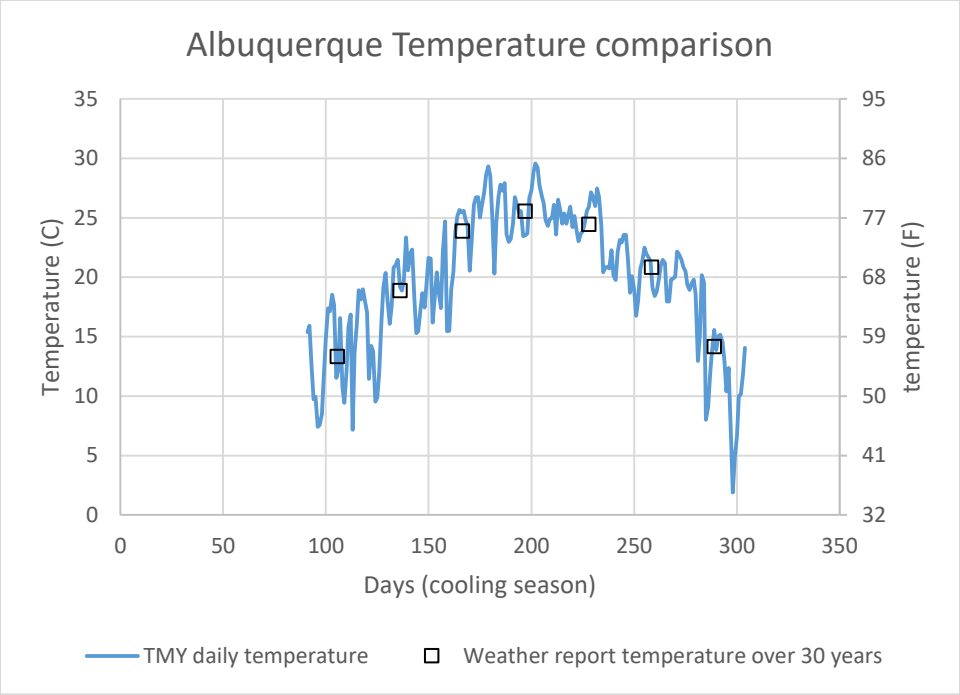

Figure 280 Temperature for Albuquerque comparison between TMY data and NOAA

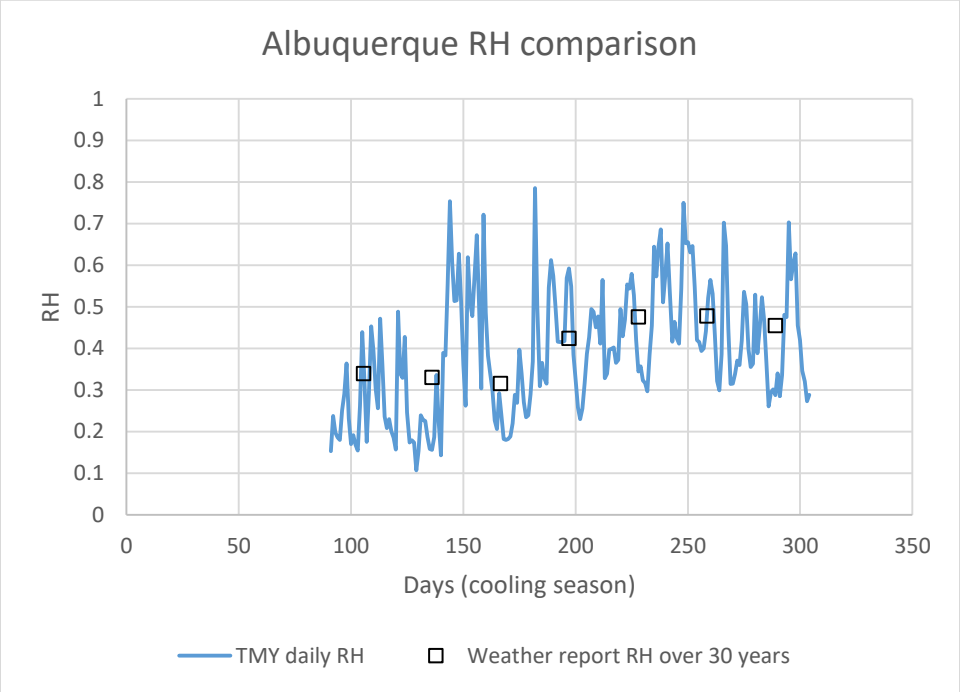

Figure 281 Relative humidity for Albuquerque comparison between TMY data and NOAA

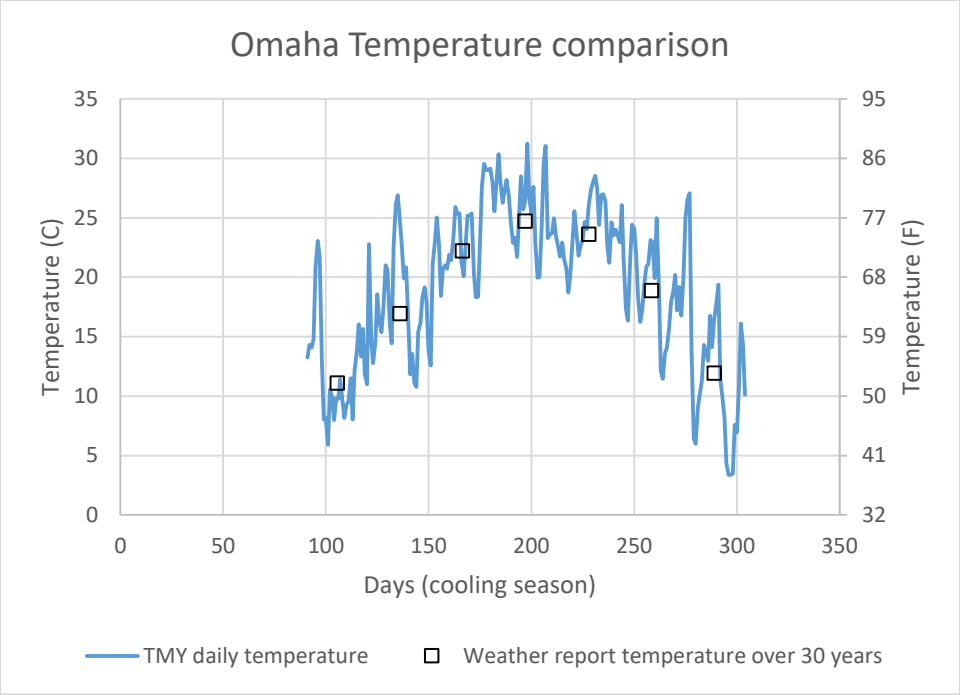

Figure 282 Temperature for Omaha comparison between TMY data and NOAA

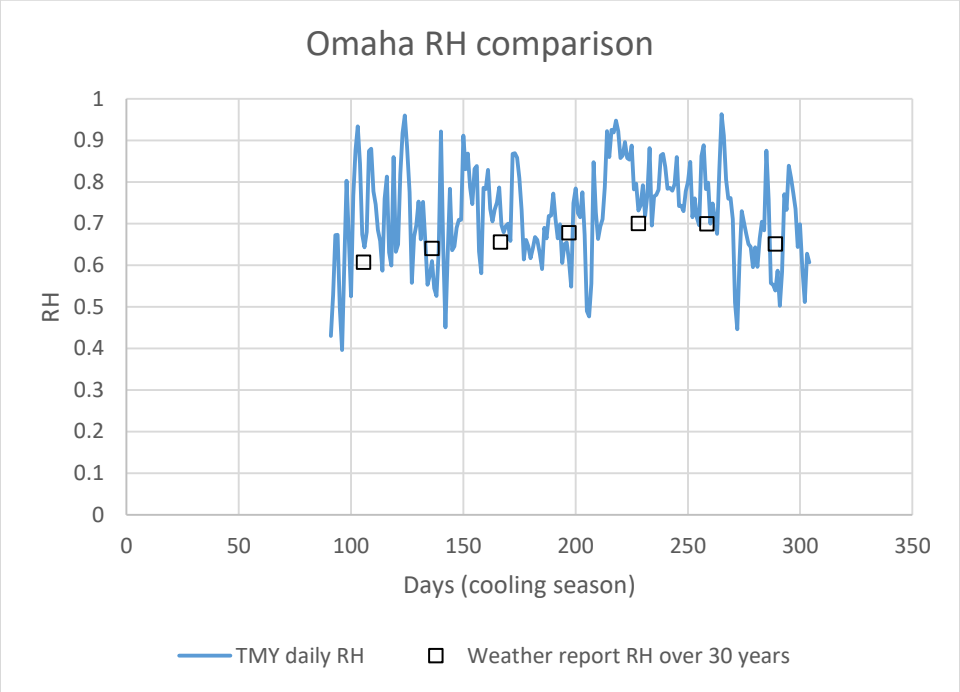

Figure 283 Temperature for Omaha comparison between TMY data and NOAA

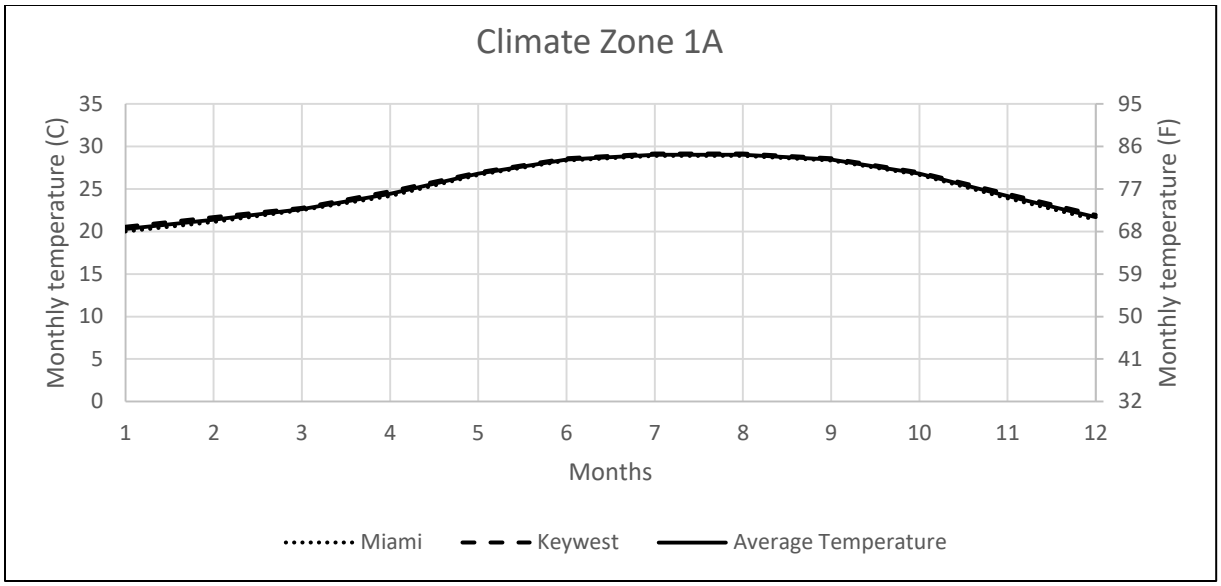

Figure 284 Monthly temperature comparison for climate zone 1A

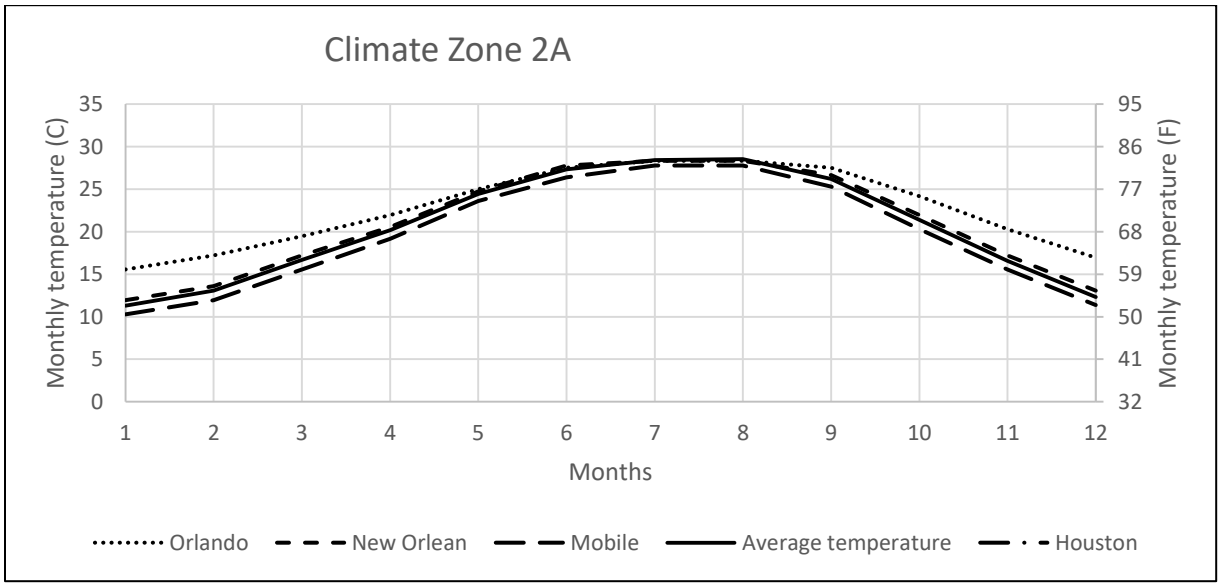

Figure 285 Monthly temperature comparison for climate zone 2A

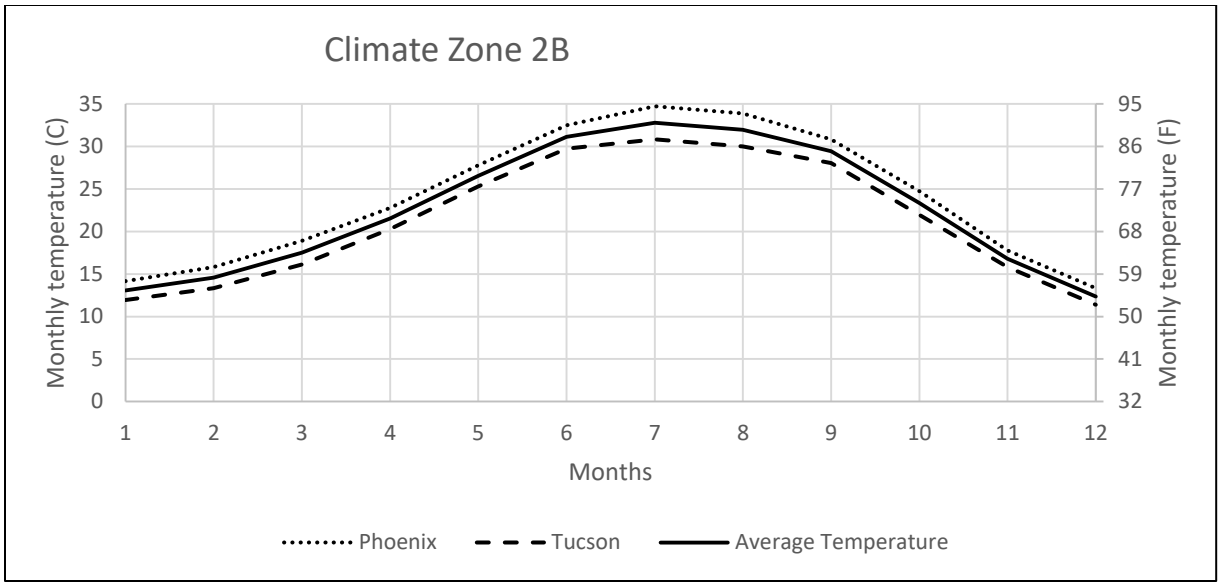

Figure 286 Monthly temperature comparison for climate zone 2B

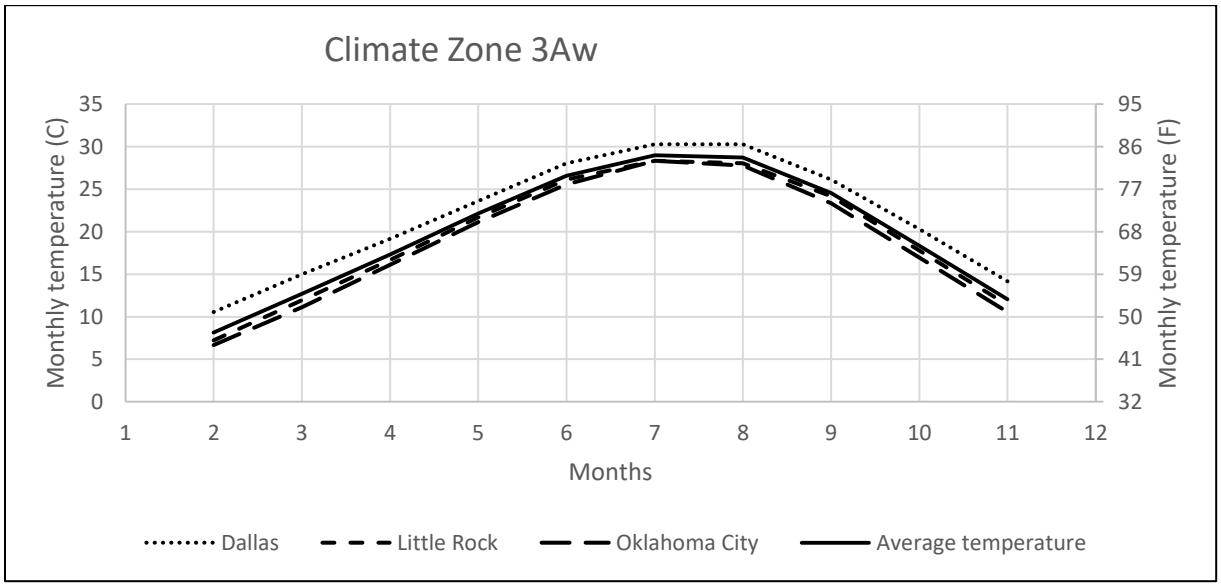

Figure 287 Monthly temperature comparison for climate zone 3Aw

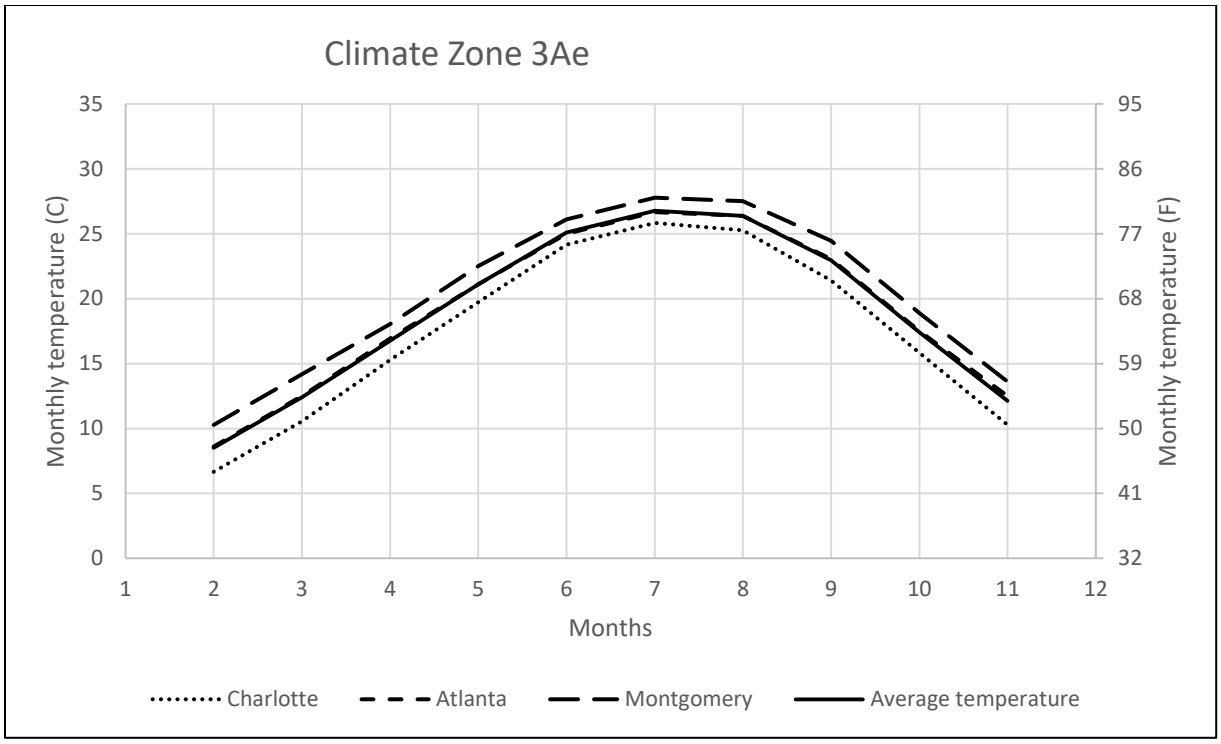

Figure 288 Monthly temperature comparison for climate zone 3Ae

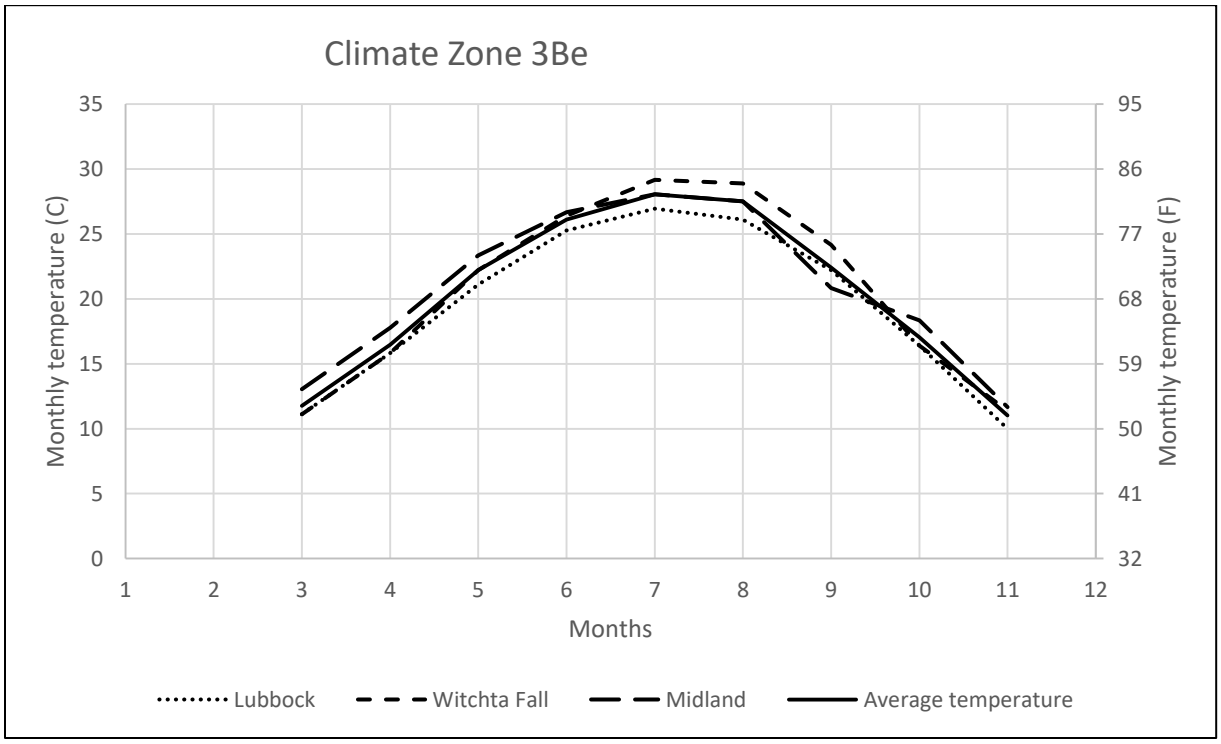

Figure 289 Monthly temperature comparison for climate zone 3Be

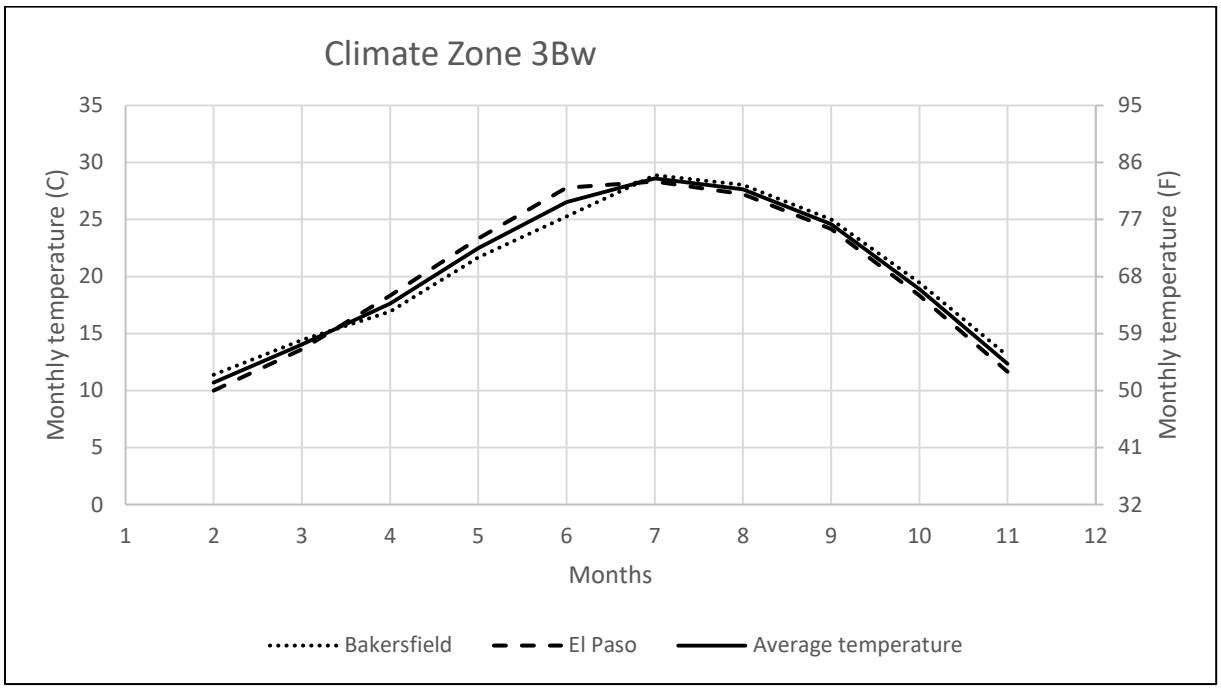

Figure 290 Monthly temperature comparison for climate zone 3Bw

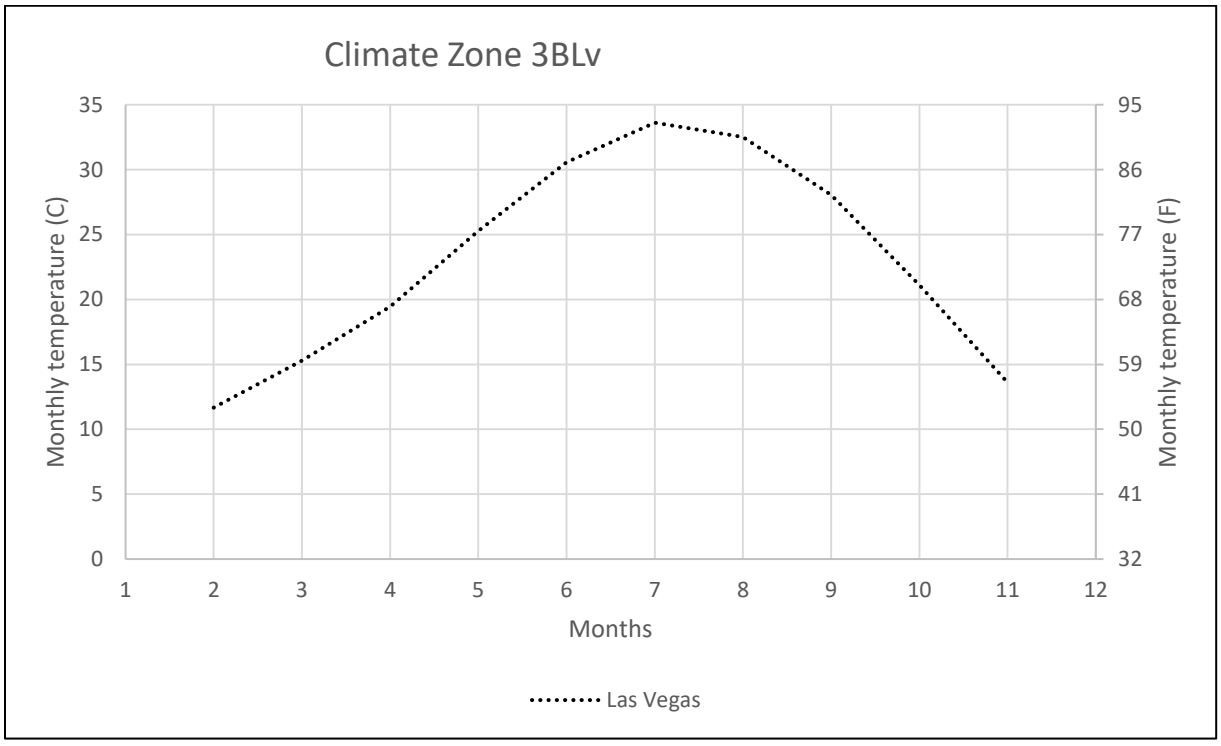

Figure 291 Monthly temperature comparison for climate zone 3Blv

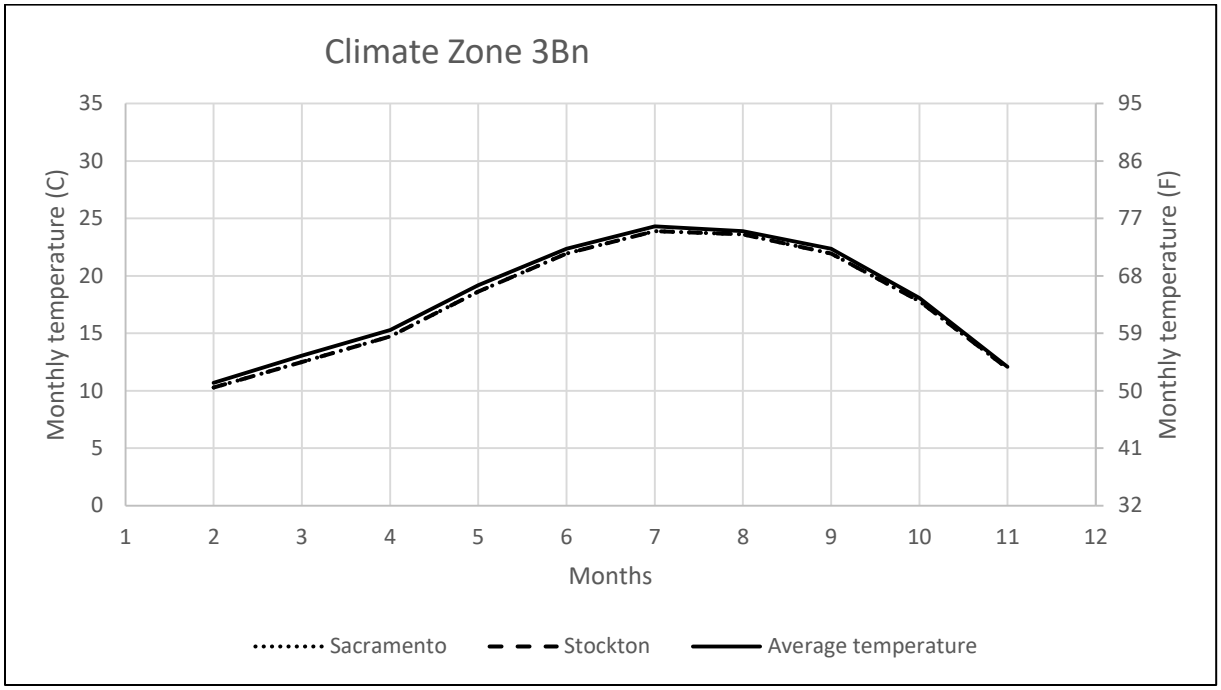

Figure 292 Monthly temperature comparison for climate zone 3Bn

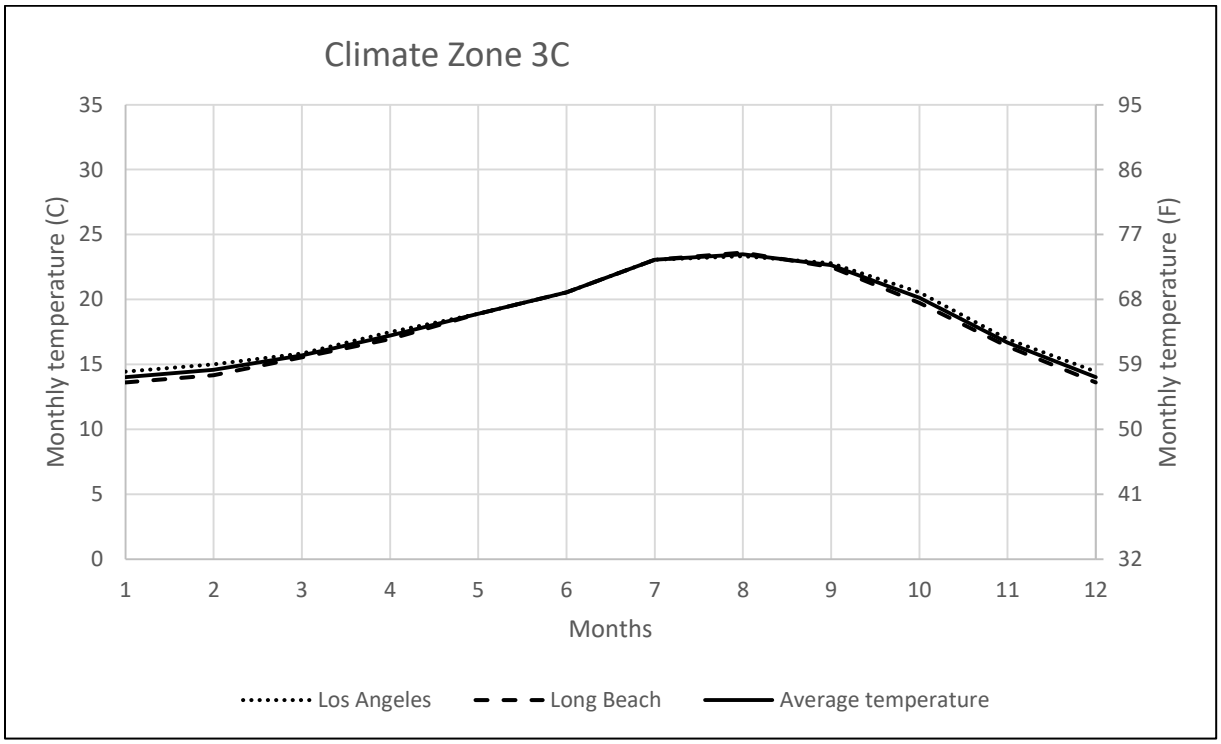

Figure 293 Monthly temperature comparison for climate zone 3C

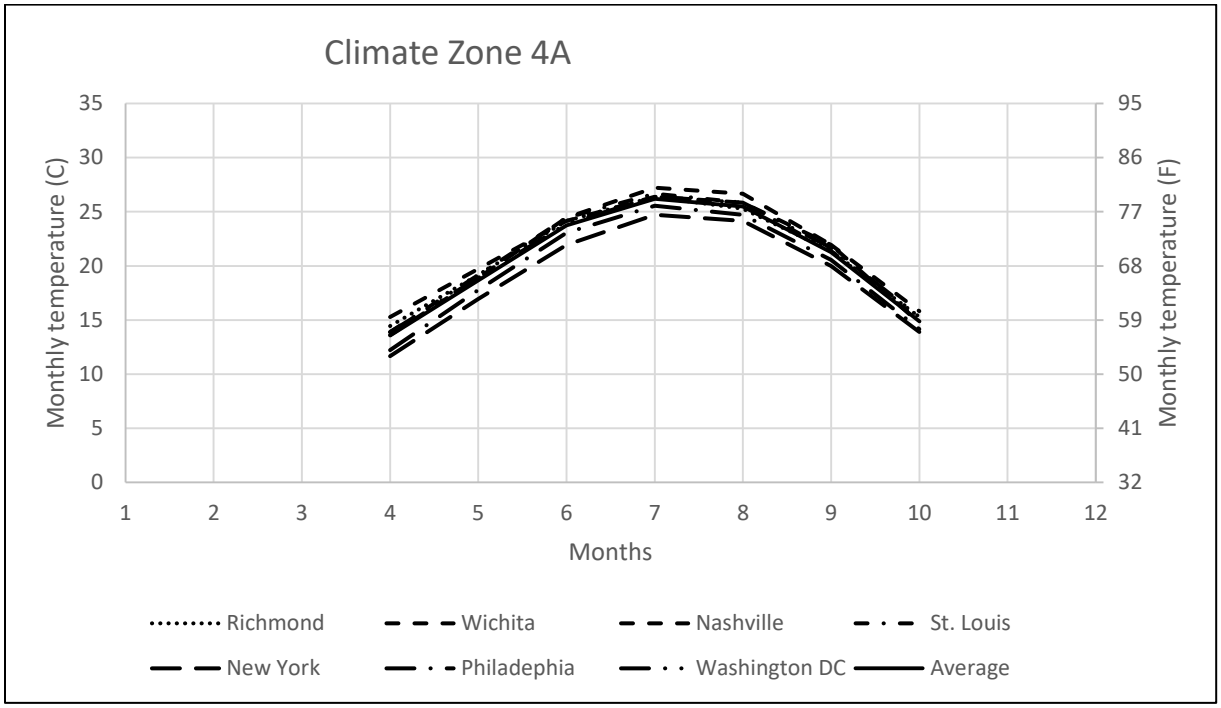

Figure 294 Monthly temperature comparison for climate zone 4A

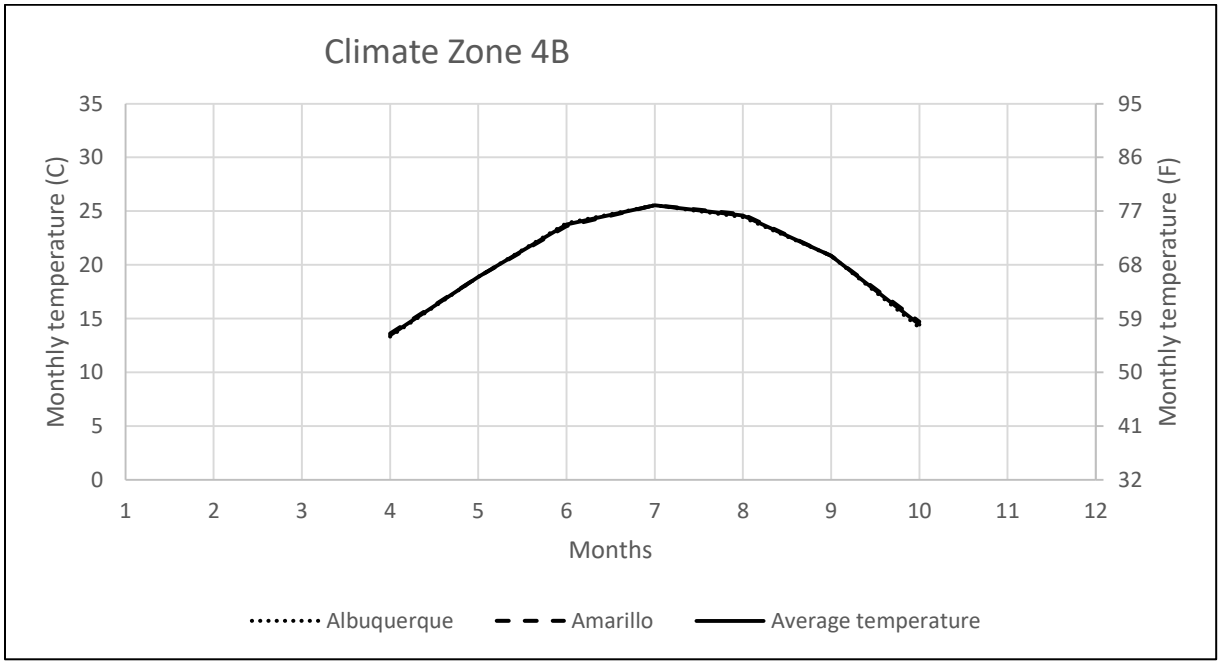

Figure 295 Monthly temperature comparison for climate zone 4B

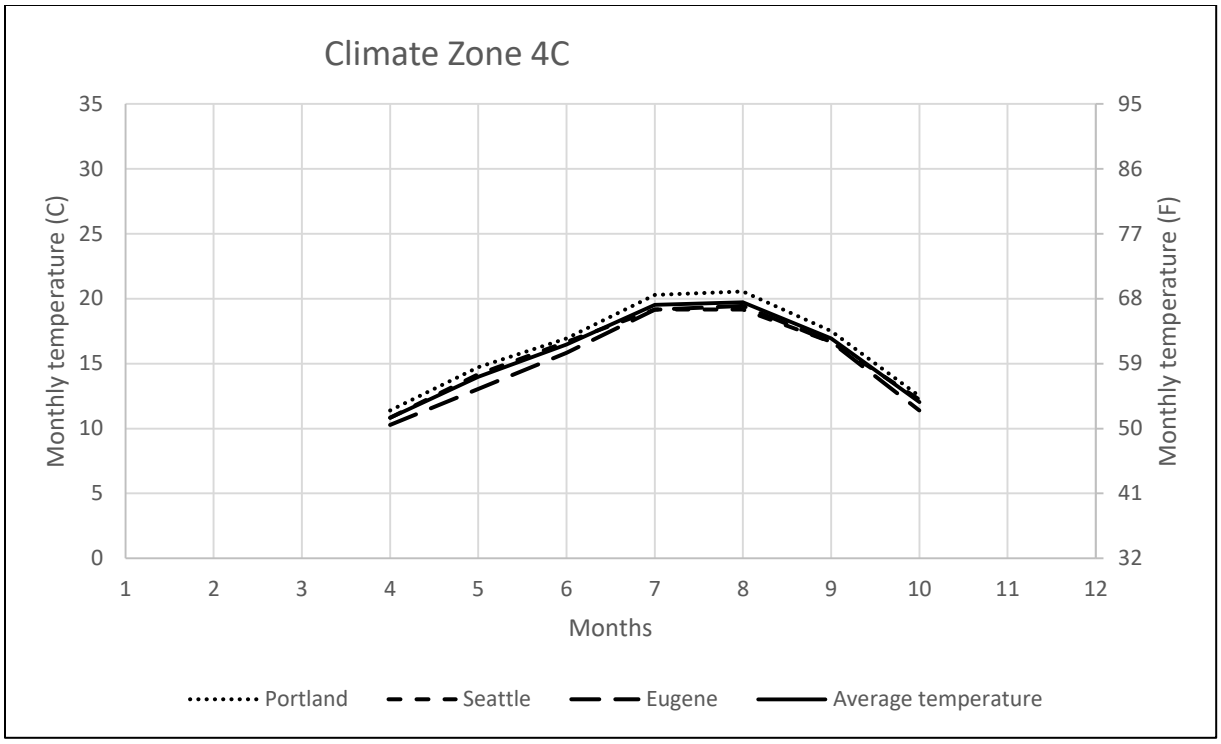

Figure 296 Monthly temperature comparison for climate zone 4C

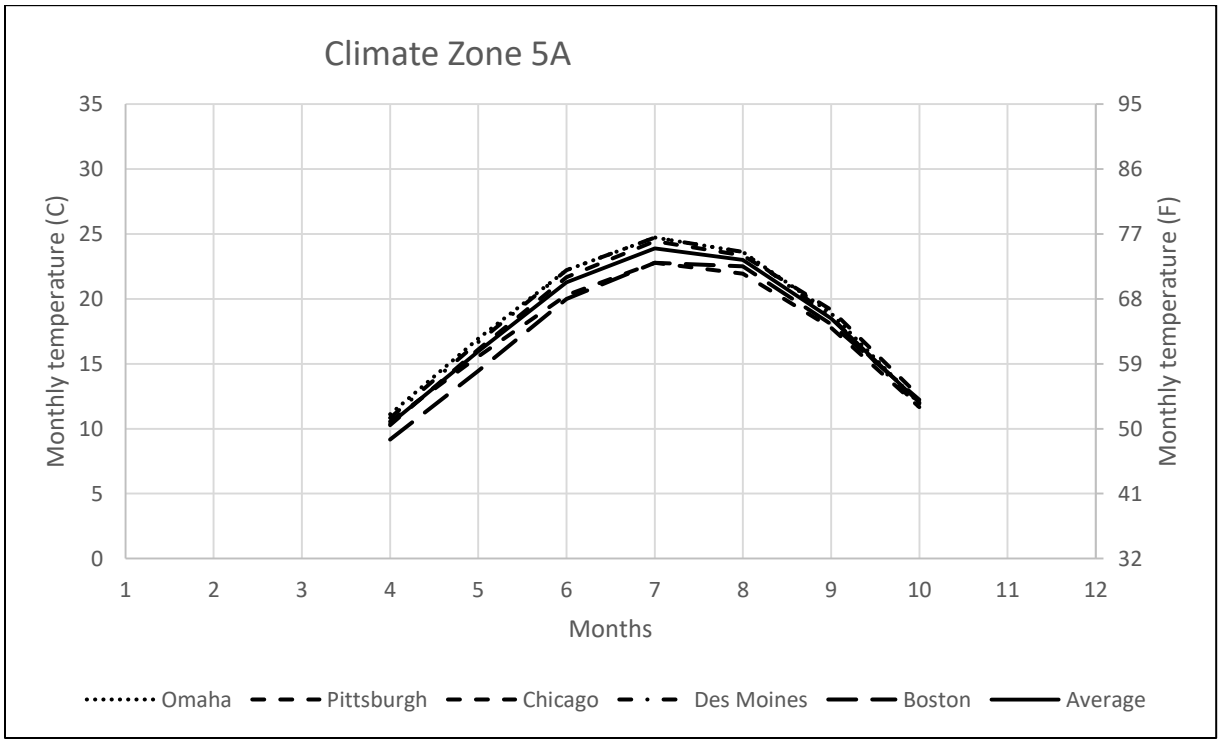

Figure 297 Monthly temperature comparison for climate zone 5A

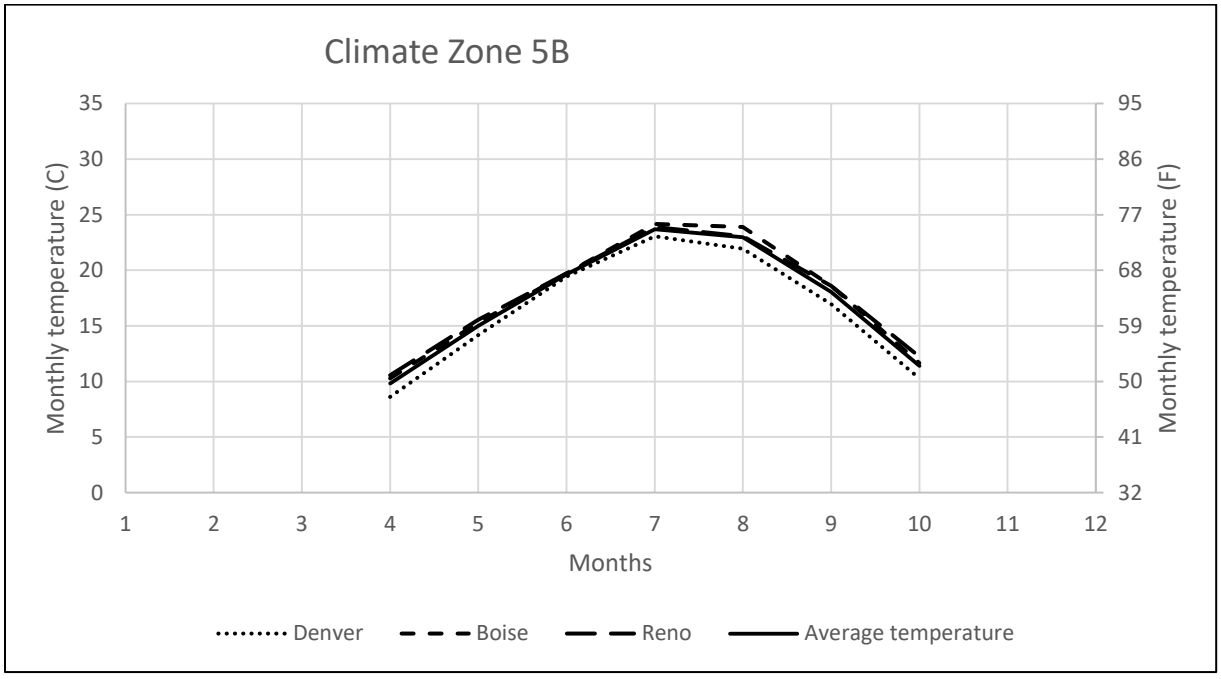

Figure 298 Monthly temperature comparison for climate zone 5B

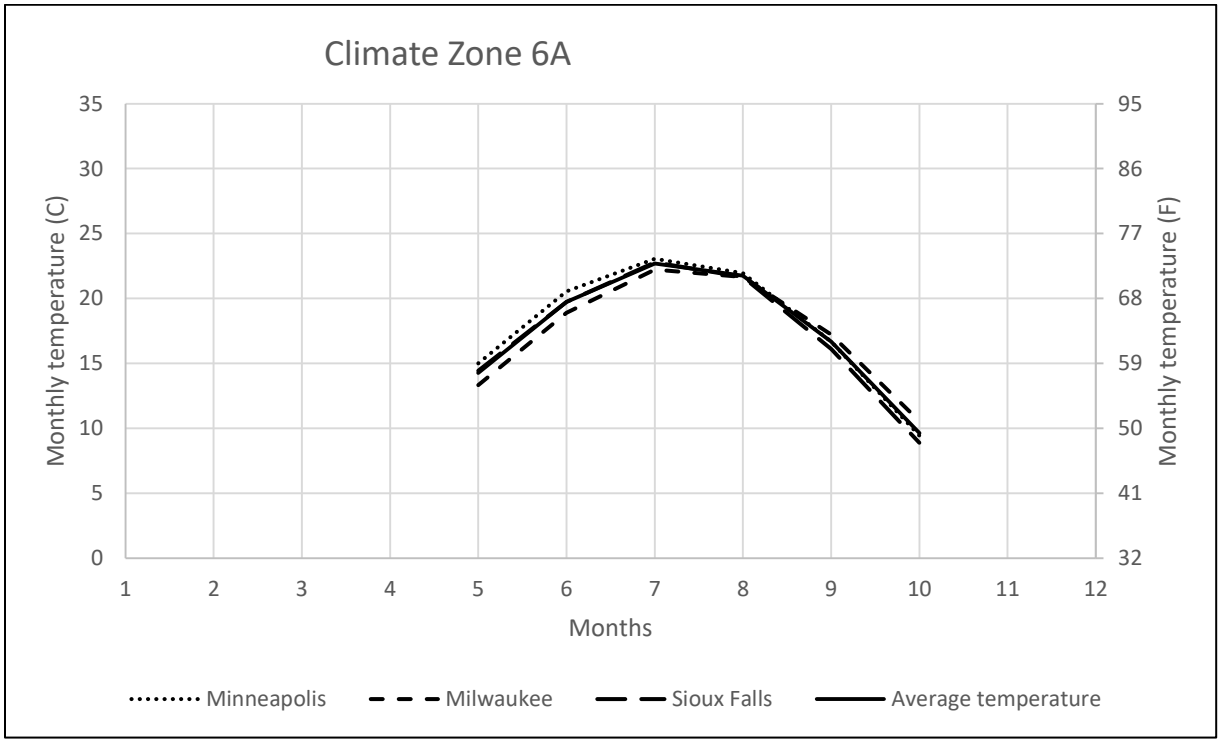

Figure 299 Monthly temperature comparison for climate zone 6A

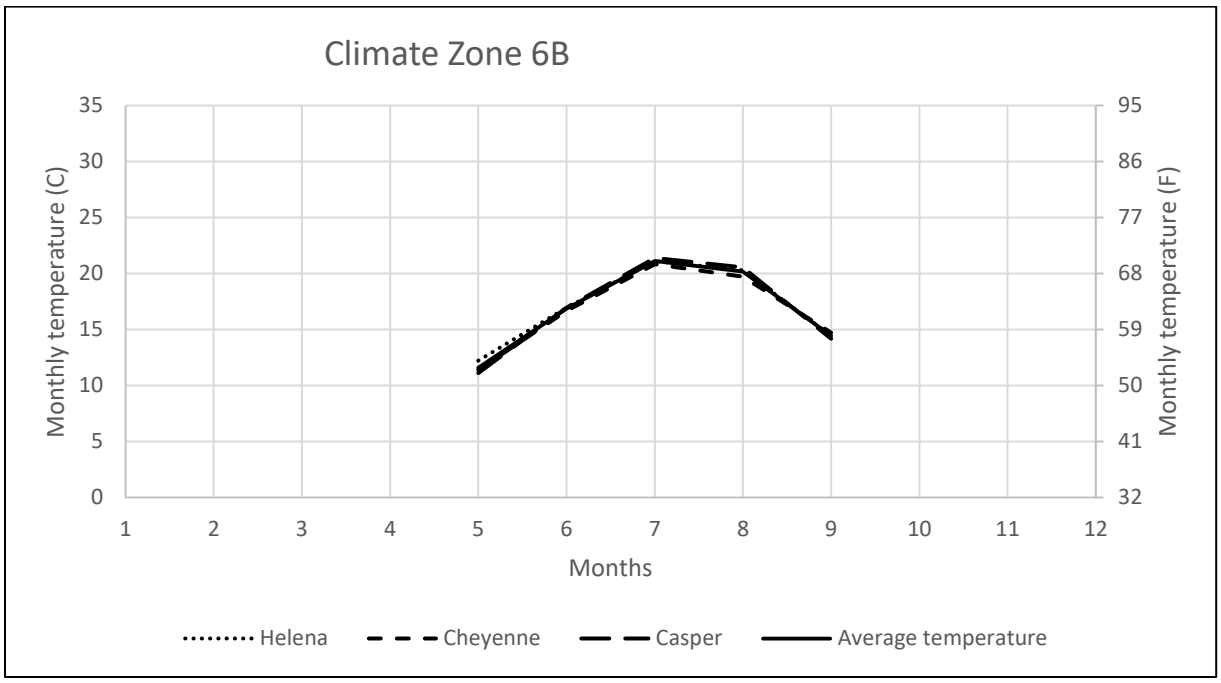

Figure 300 Monthly temperature comparison for climate zone 6B

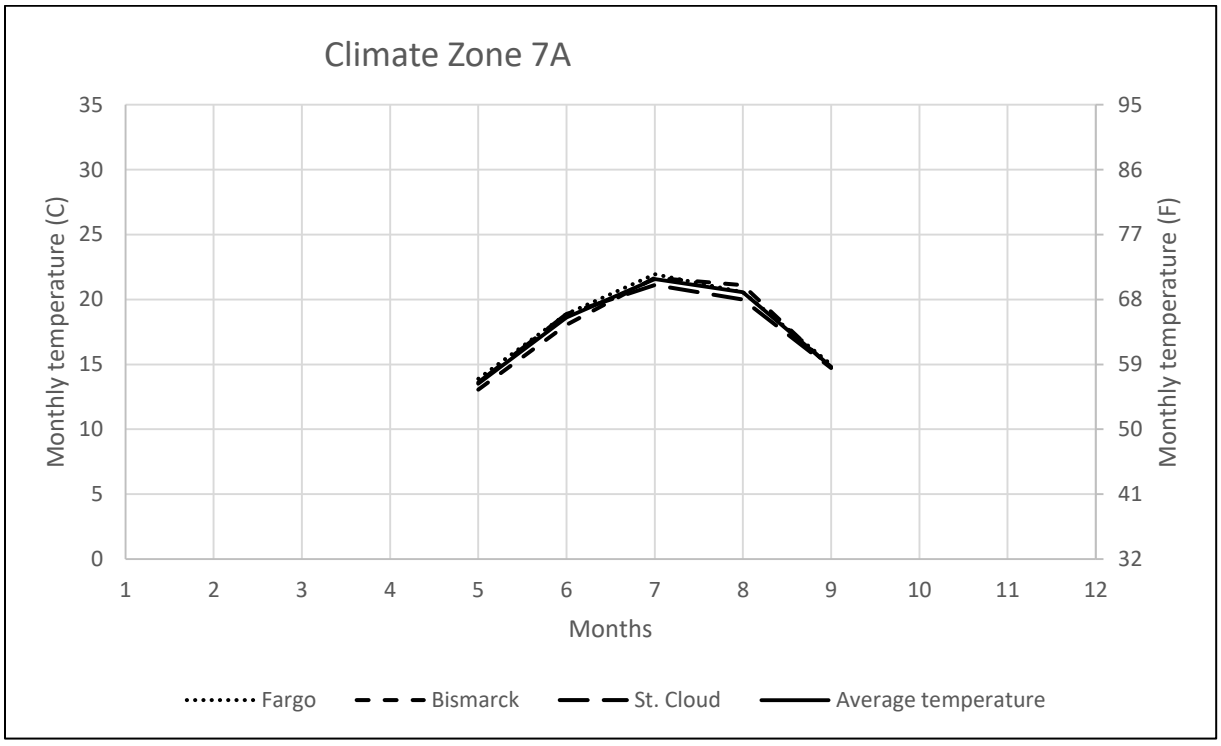

Figure 301 Monthly temperature comparison for climate zone 7A

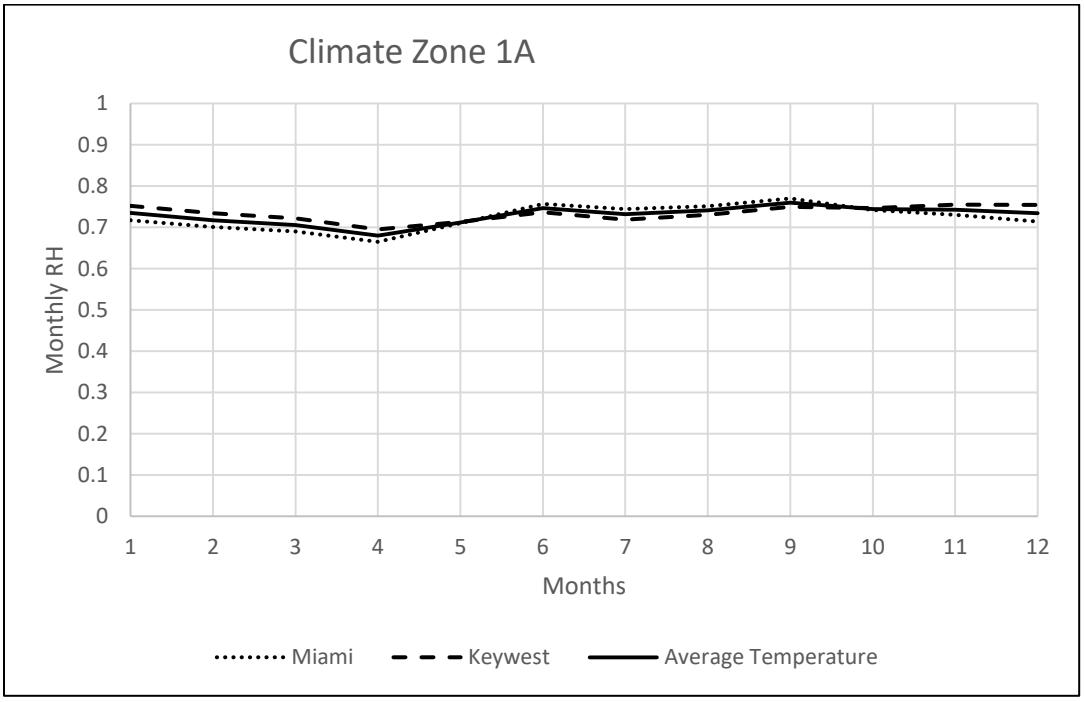

Figure 302 Relative humidity comparison for climate zone 1A

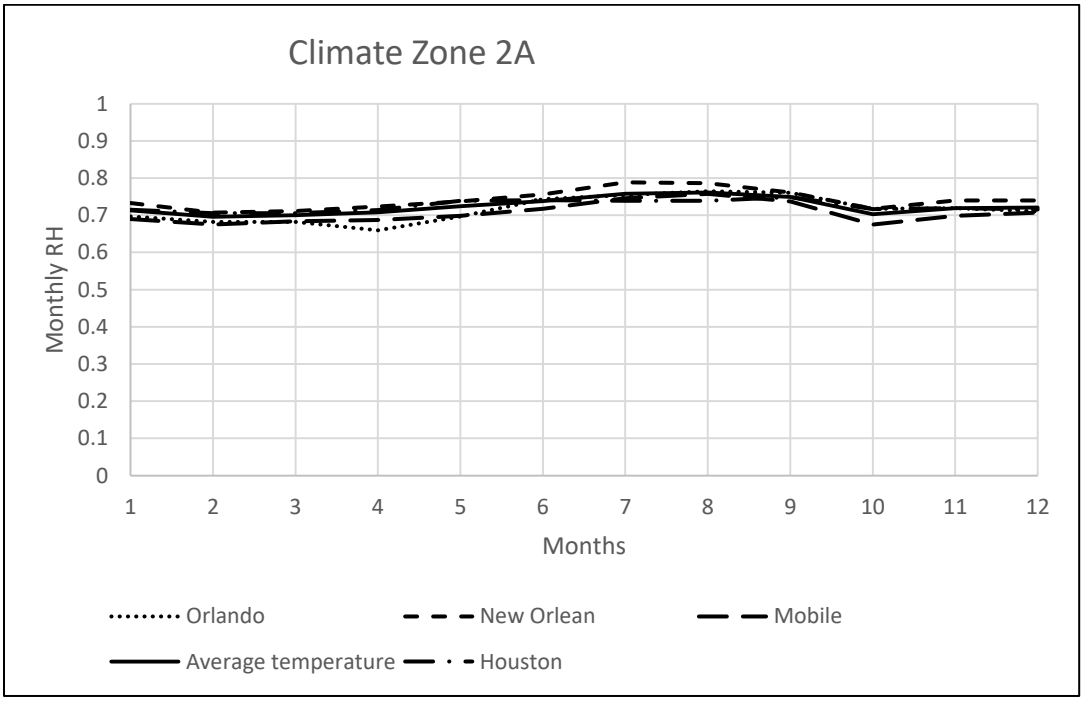

Figure 303 Relative humidity comparison for climate zone 2A

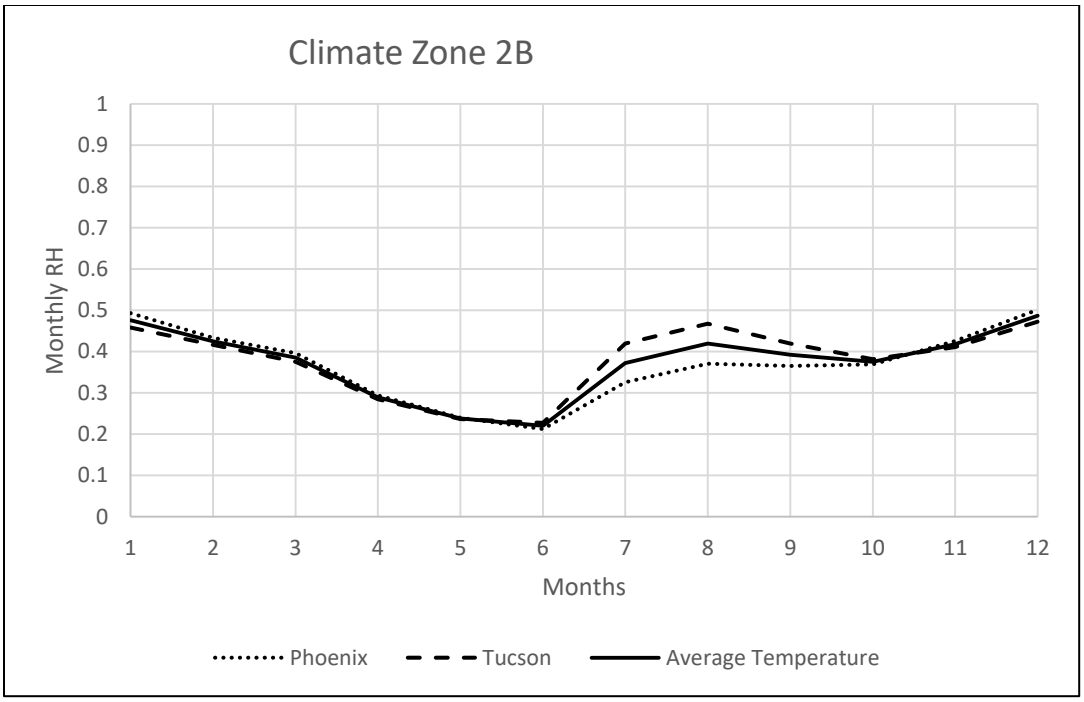

Figure 304 Relative humidity comparison for climate zone 2B

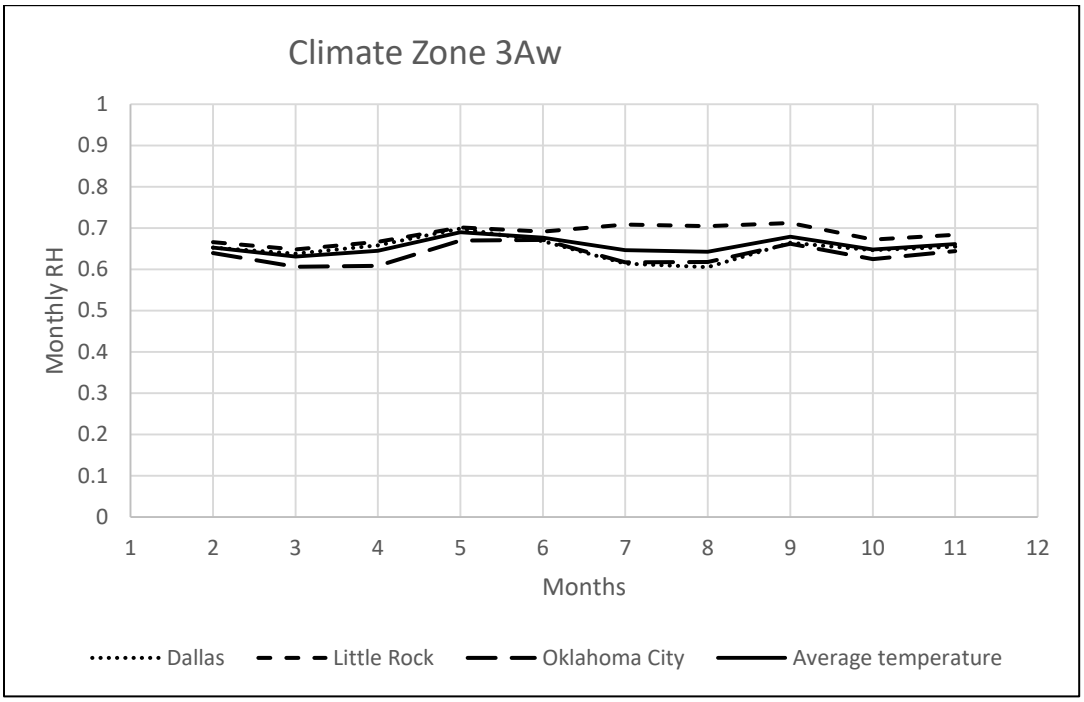

Figure 305 Relative humidity comparison for climate zone 3Aw

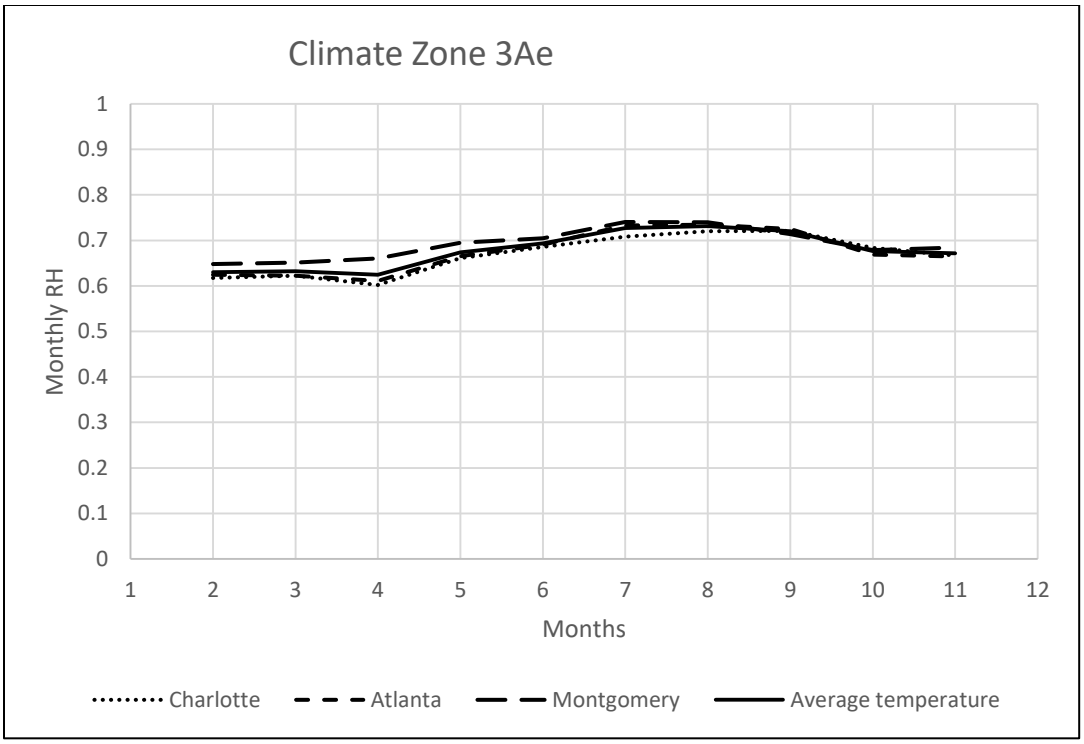

Figure 306 Relative humidity comparison for climate zone 3Ae

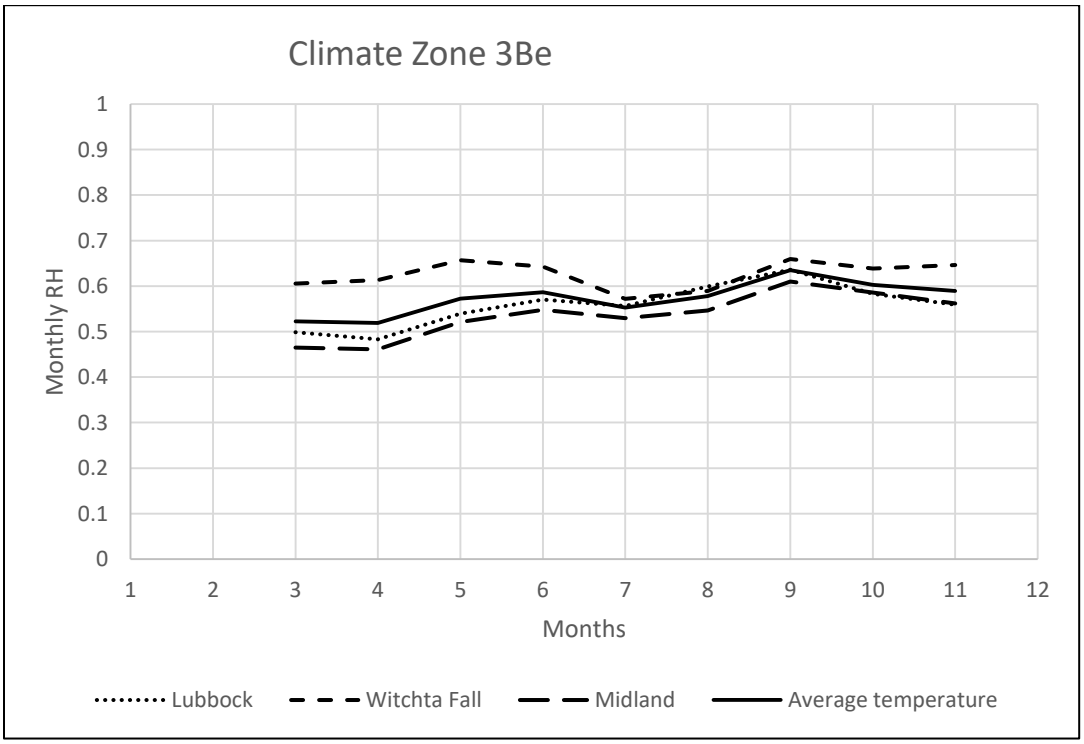

Figure 307 Relative humidity comparison for climate zone 3Be

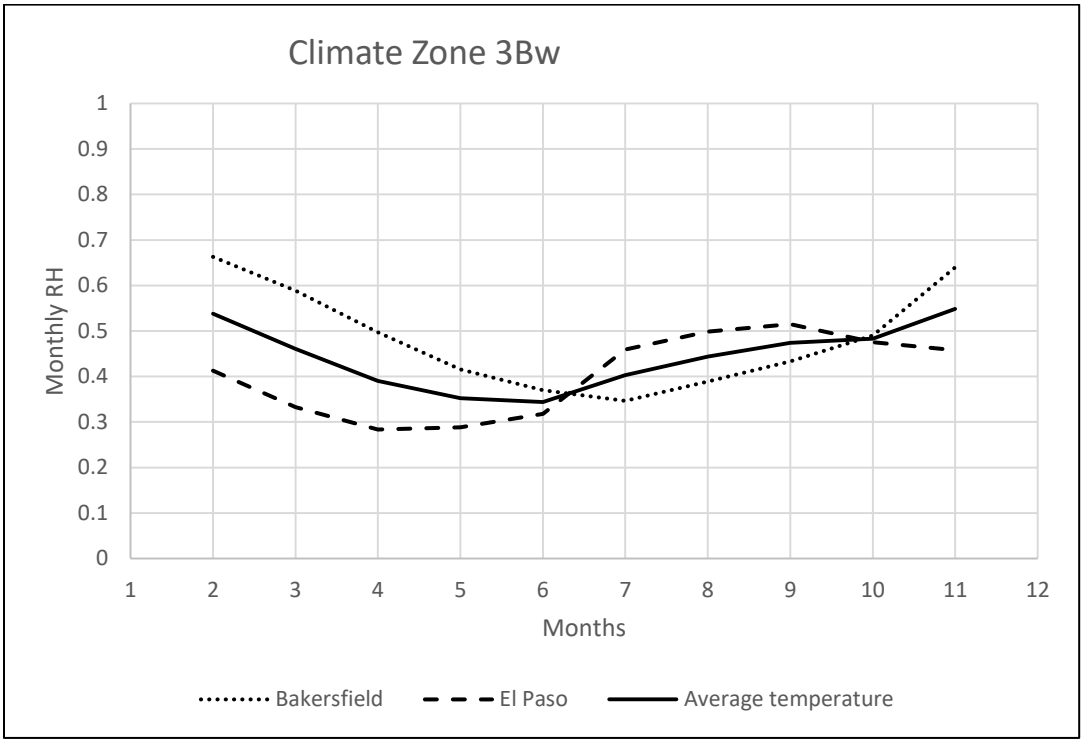

Figure 308 Relative humidity comparison for climate zone 3Bw

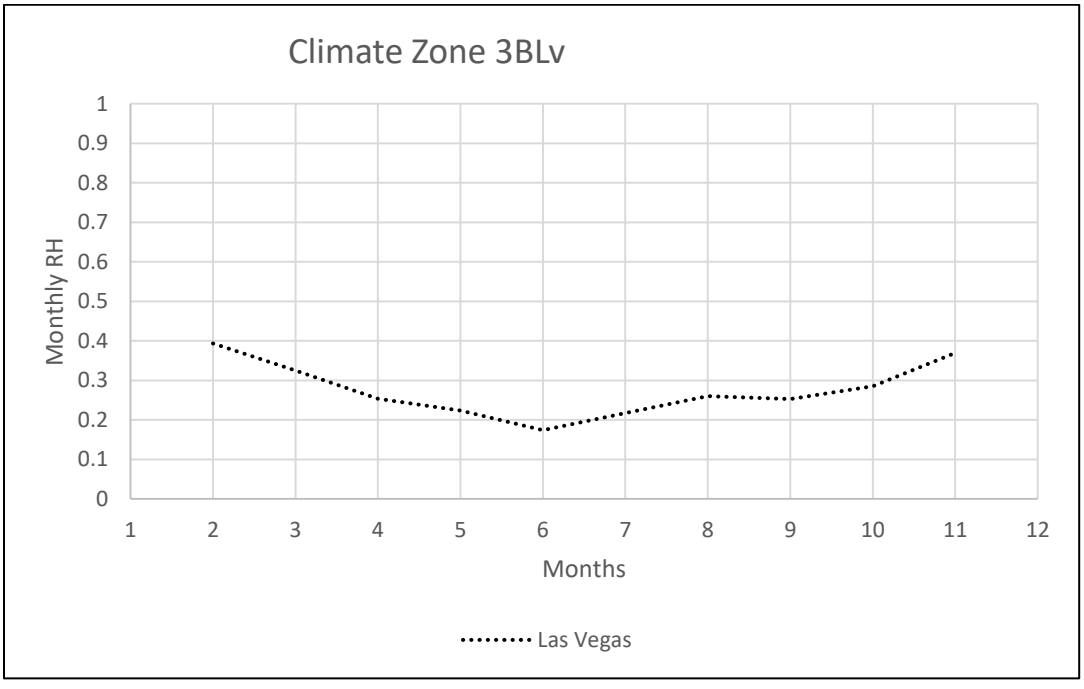

Figure 309 Relative humidity comparison for climate zone 3Blv

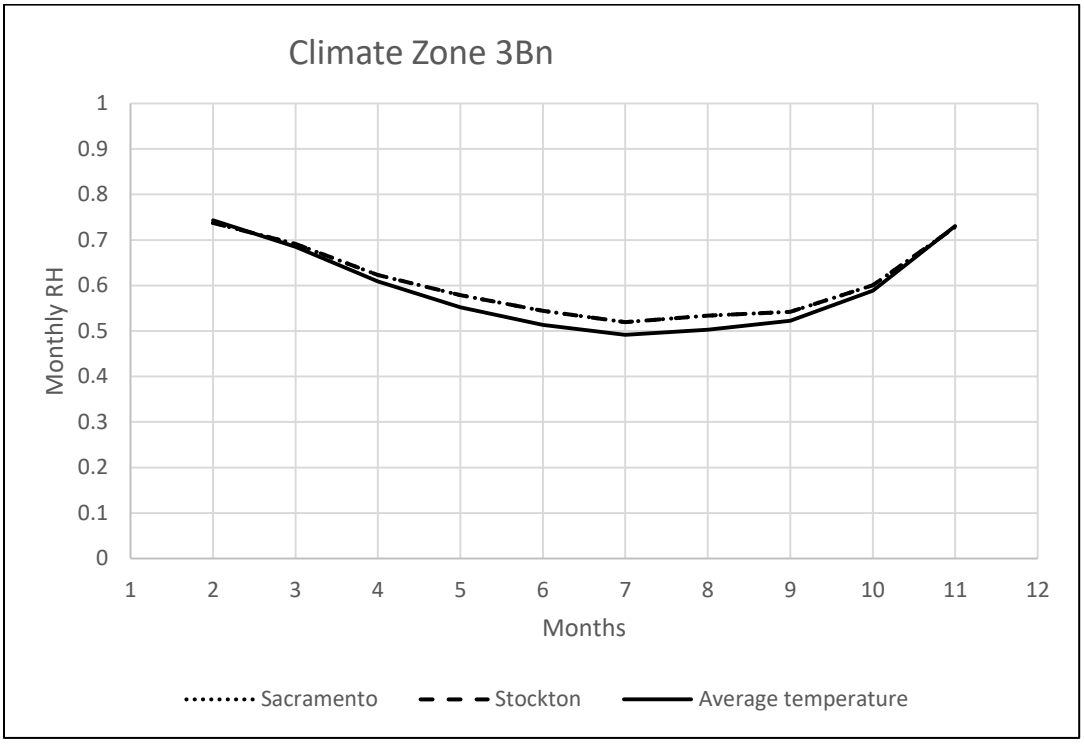

Figure 310 Relative humidity comparison for climate zone 3Bn

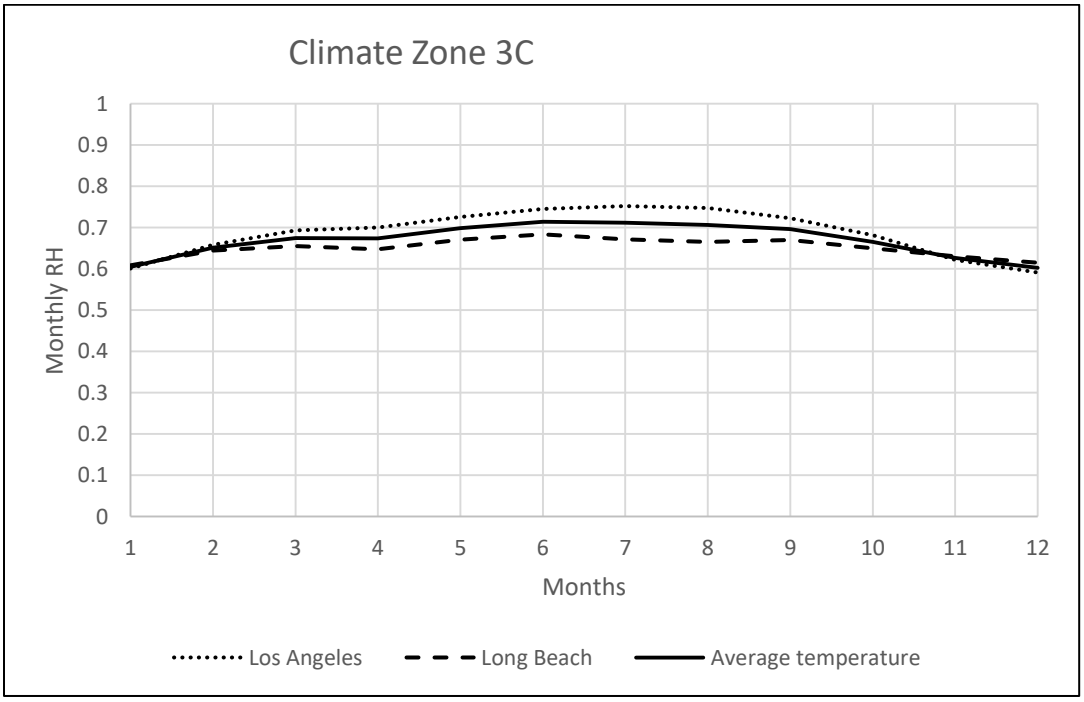

Figure 311 Relative humidity comparison for climate zone 3C

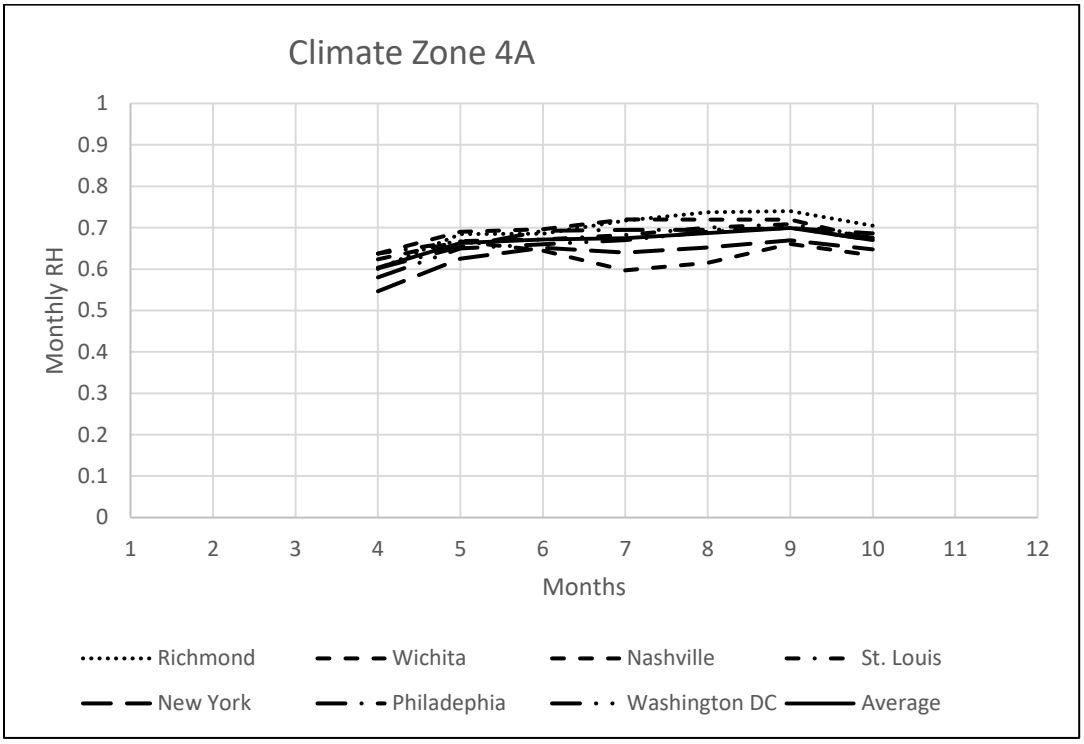

Figure 312 Relative humidity comparison for climate zone 4A

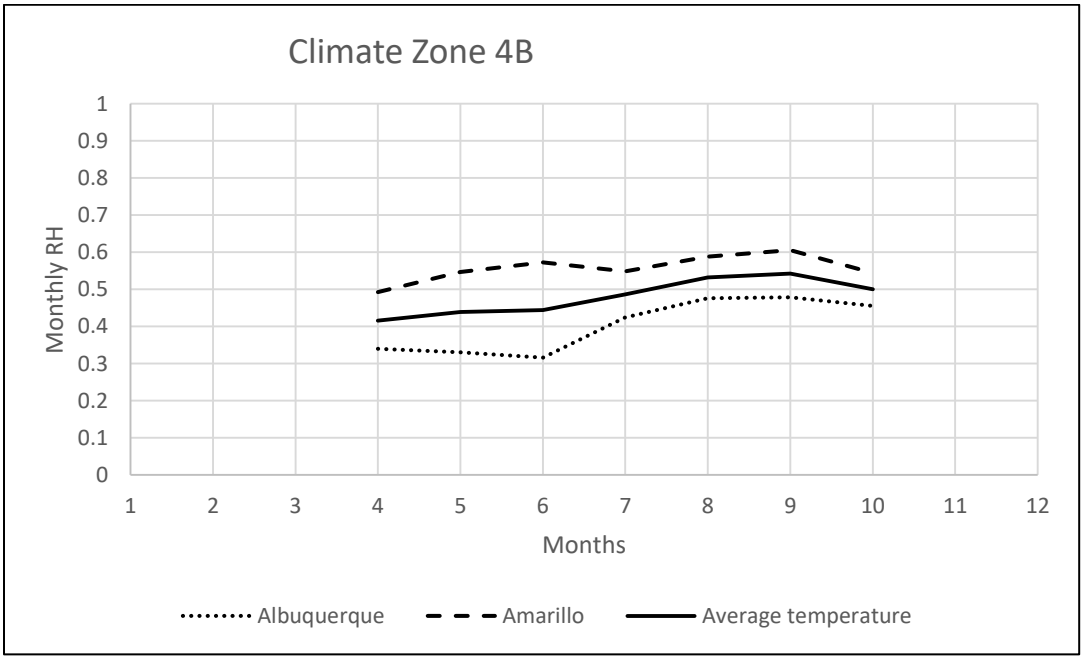

Figure 313 Relative humidity comparison for climate zone 4B

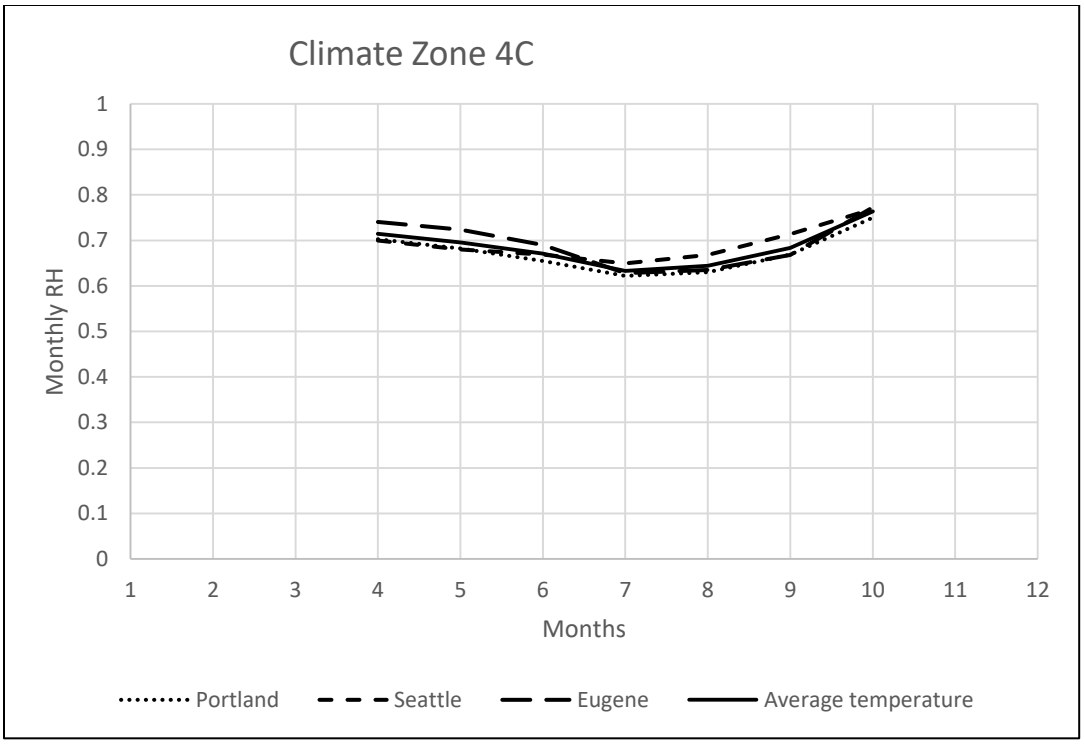

Figure 314 Relative humidity comparison for climate zone 4C

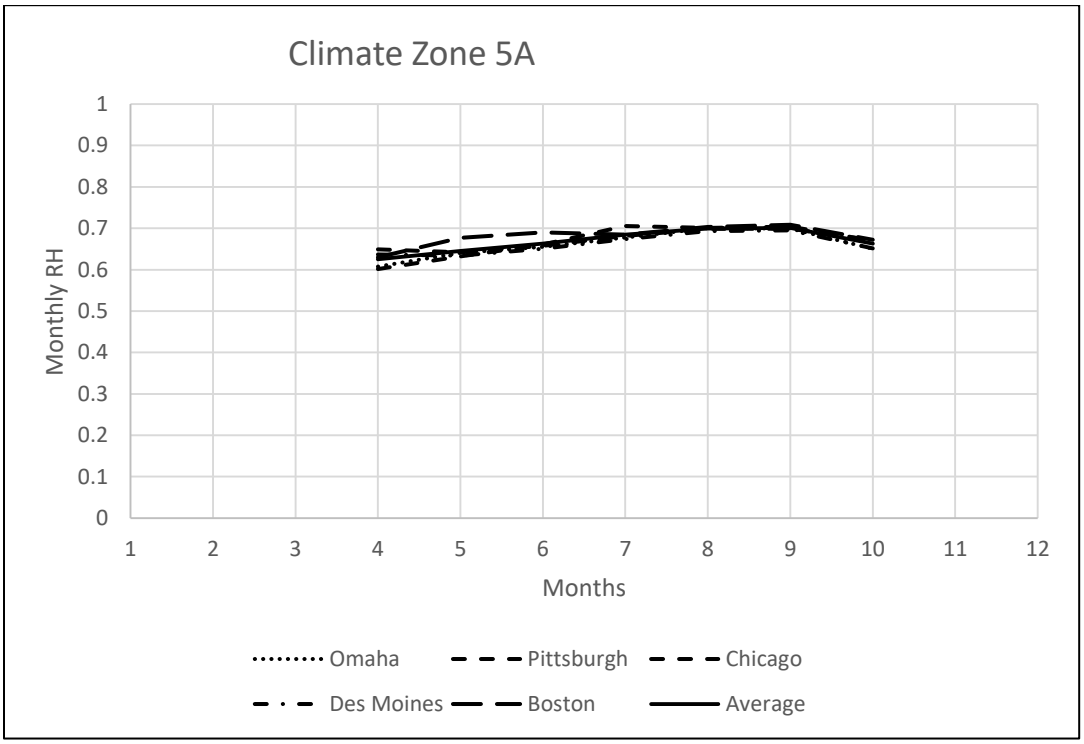

Figure 315 Relative humidity comparison for climate zone 5A

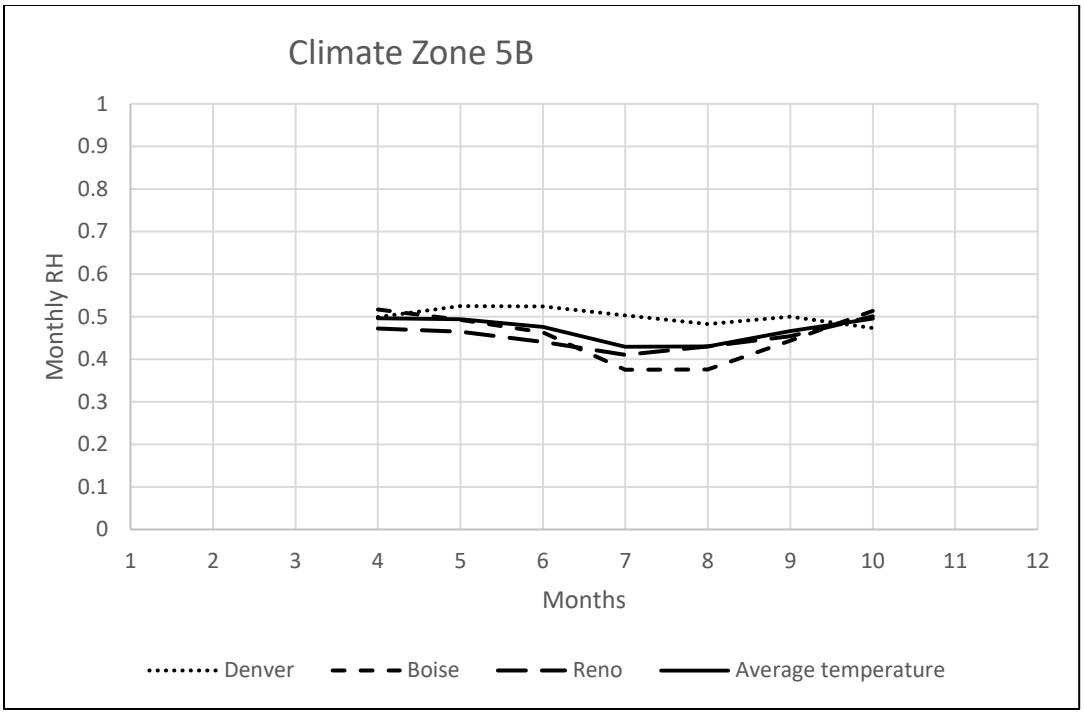

Figure 316 Relative humidity comparison for climate zone 5B

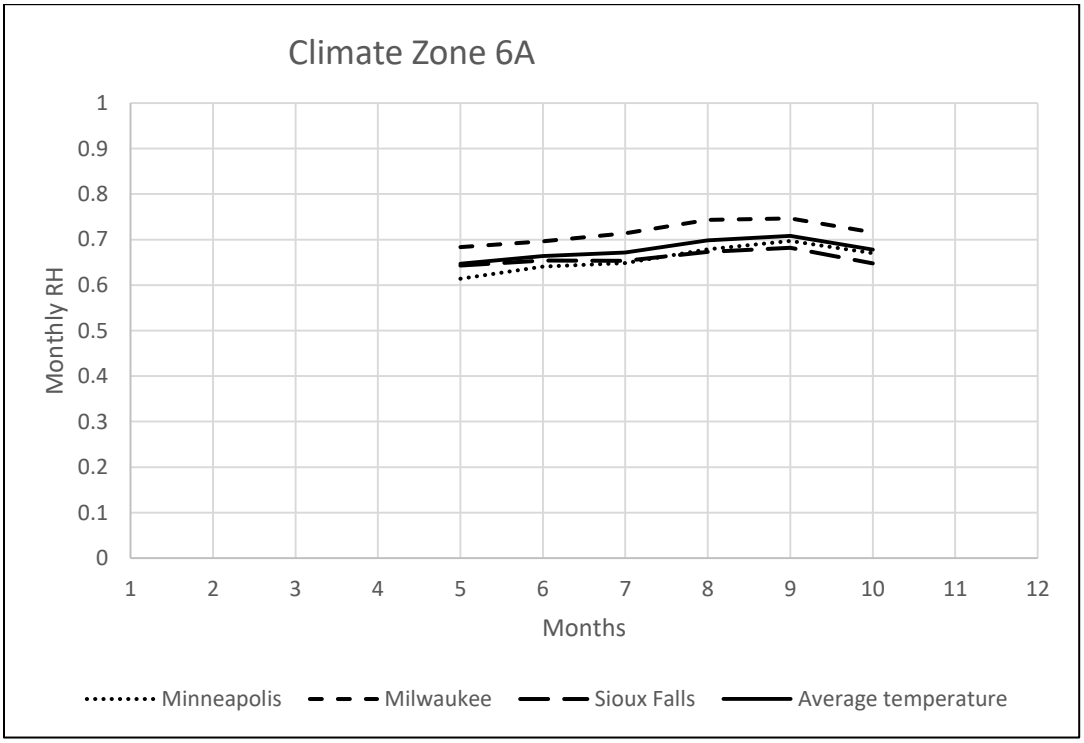

Figure 317 Relative humidity comparison for climate zone 6A

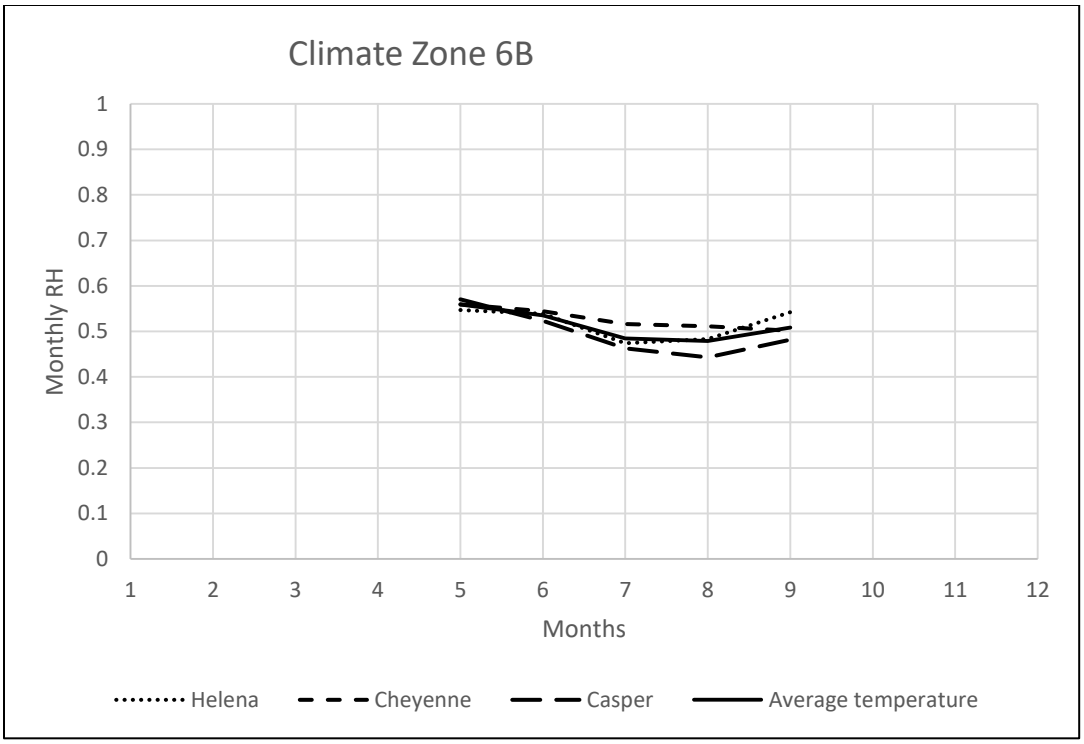

Figure 318 Relative humidity comparison for climate zone 6B

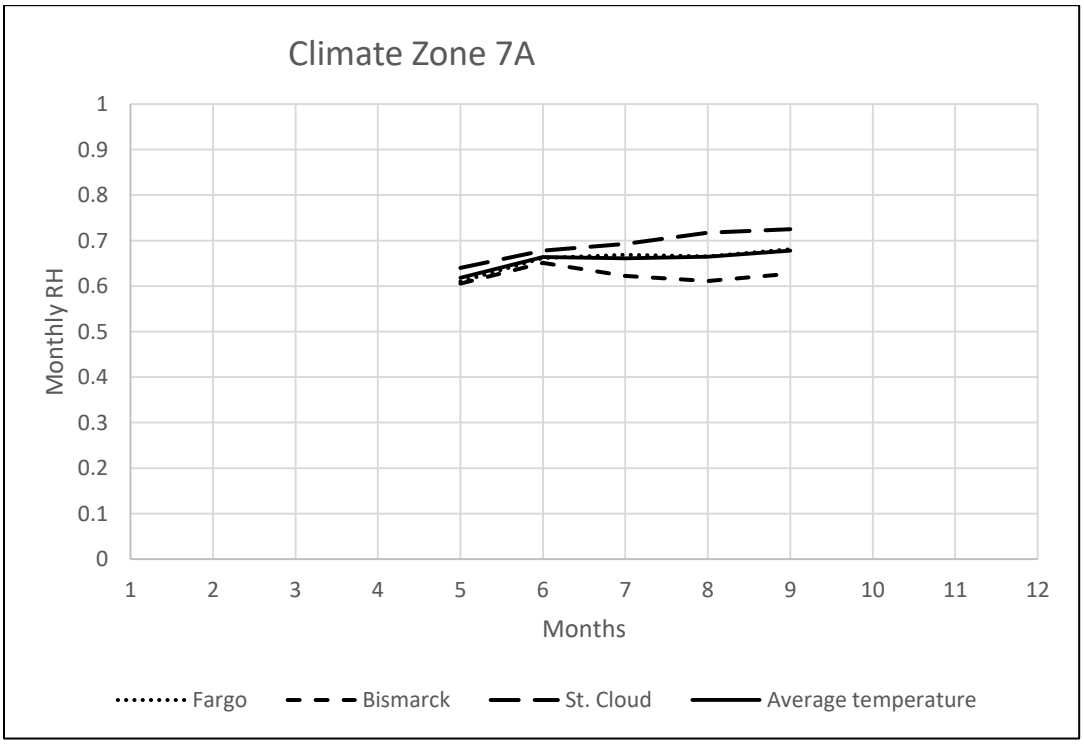

Figure 319 Relative humidity comparison for climate zone 7A

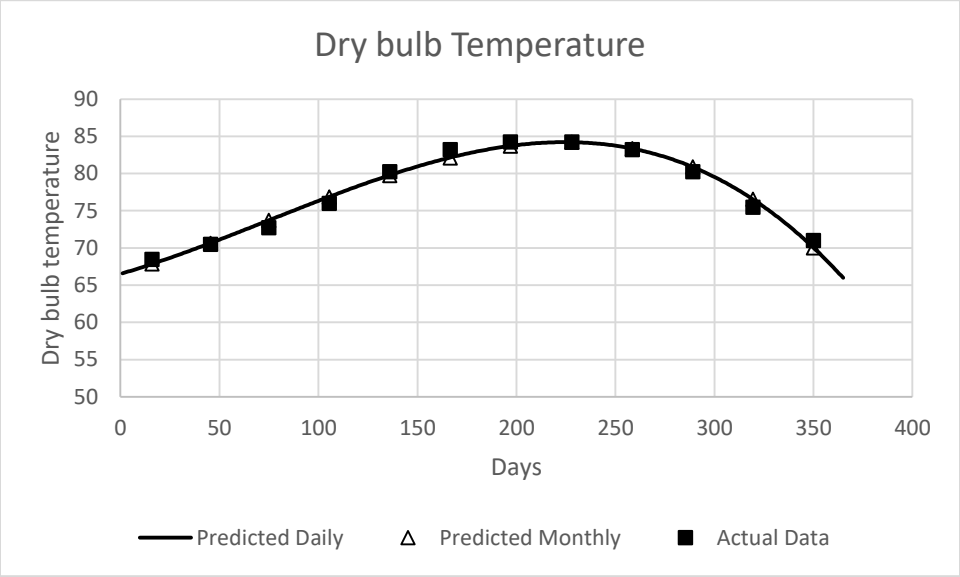

Figure 320 Monthly and daily predicted data versus actual data of dry-bulb temperature for climate zone 1A

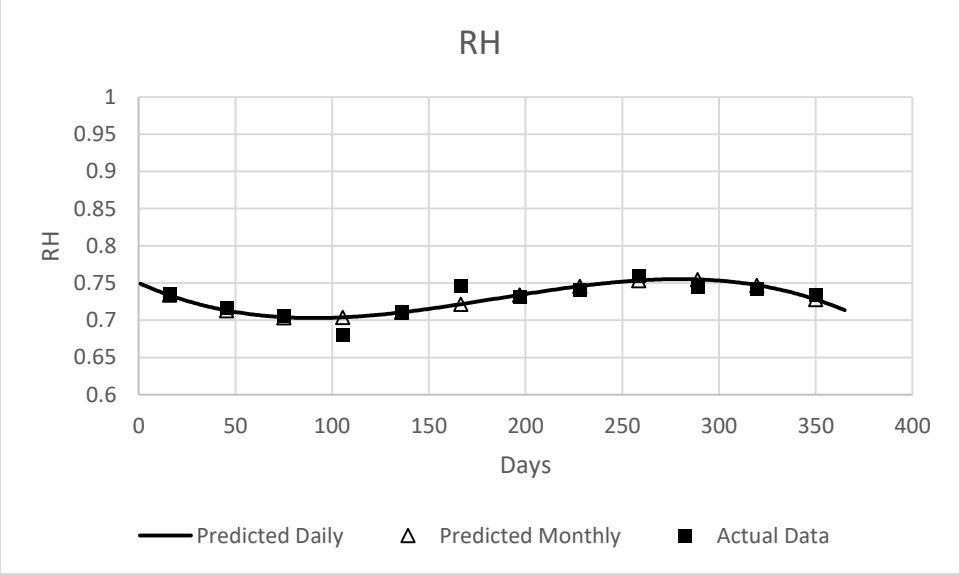

Figure 321 Monthly and daily predicted data versus actual data of relative humidity for climate zone 1A

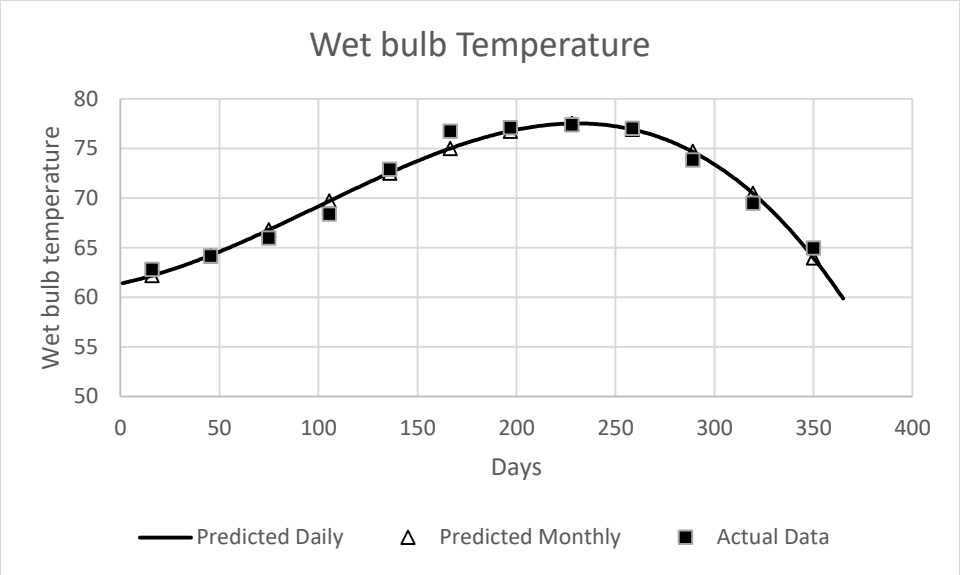

Figure 322 Monthly and daily predicted data versus actual data of wet-bulb temperature for climate zone 1A

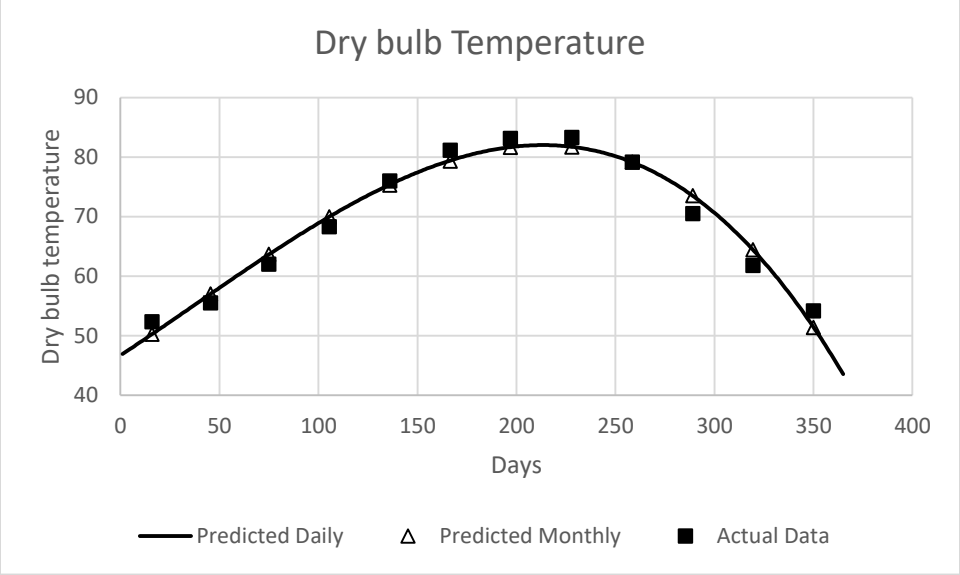

Figure 323 Monthly and daily predicted data versus actual data of dry-bulb temperature for climate zone 2A

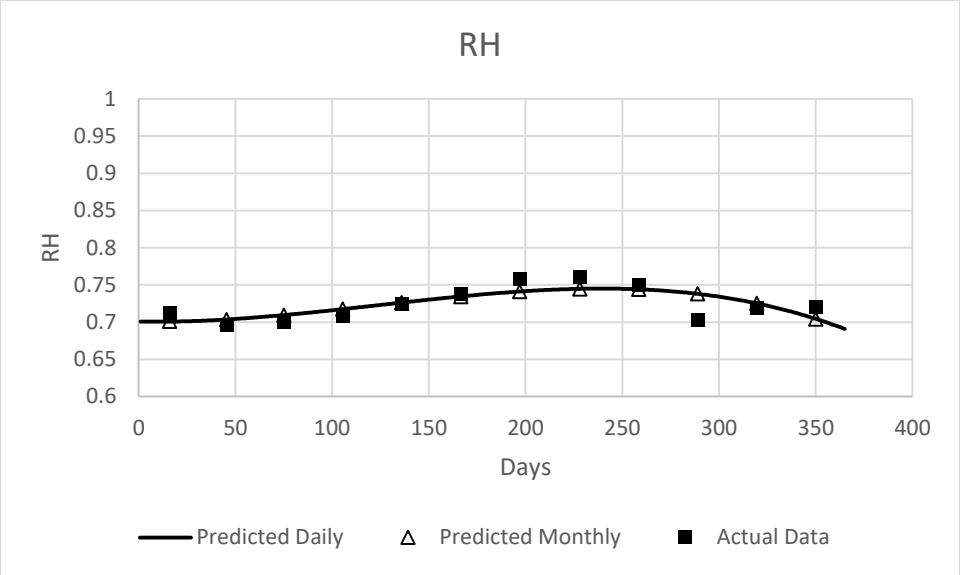

Figure 324 Monthly and daily predicted data versus actual data of relative humidity for climate zone 2A

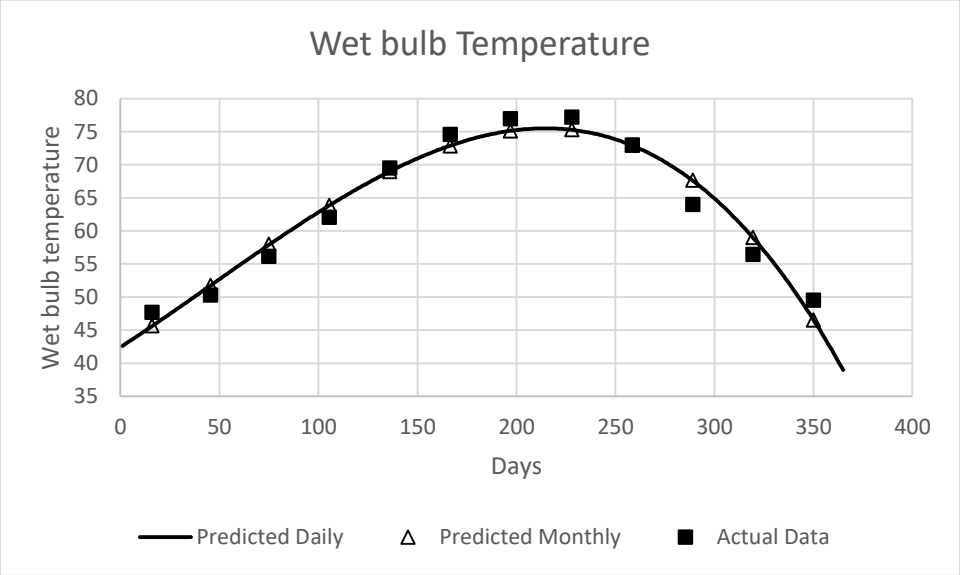

Figure 325 Monthly and daily predicted data versus actual data of wet-bulb temperature for climate zone 2A

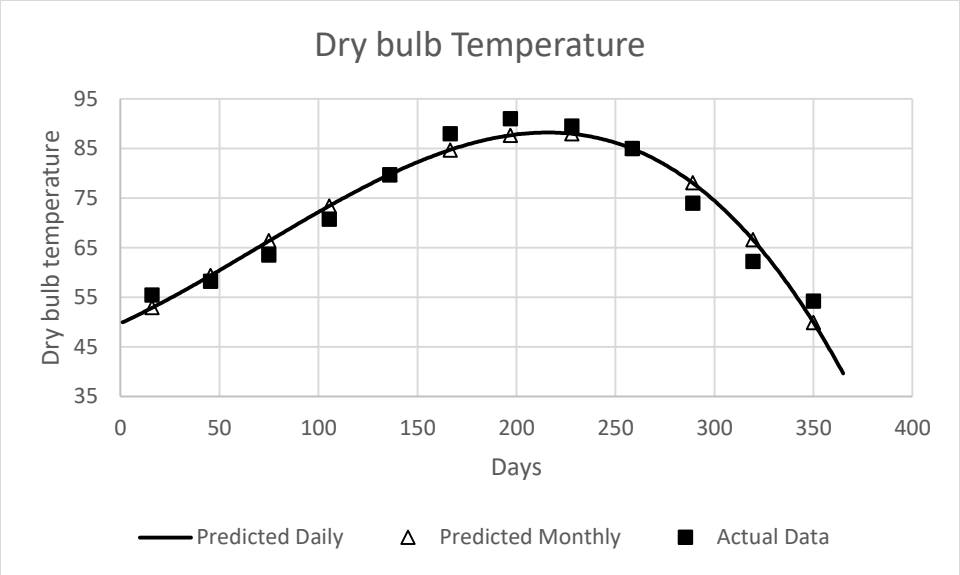

Figure 326 Monthly and daily predicted data versus actual data of dry-bulb temperature for climate zone 2B

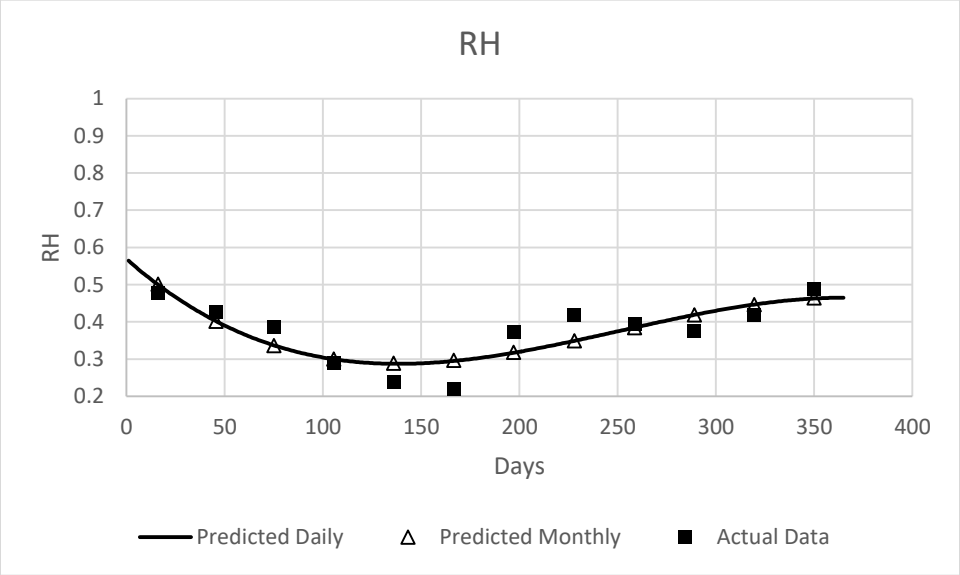

Figure 327 Monthly and daily predicted data versus actual data of relative humidity for climate zone 2B

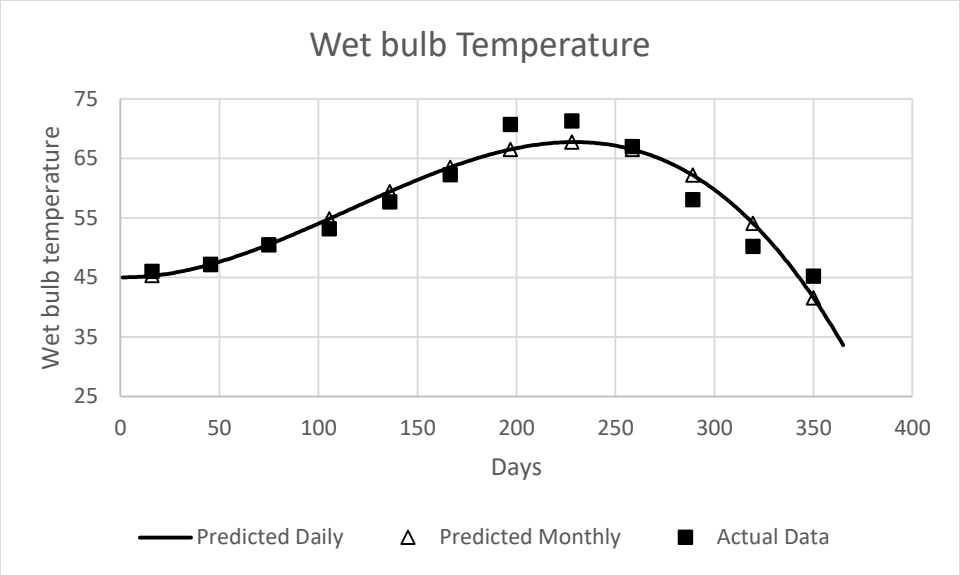

Figure 328 Monthly and daily predicted data versus actual data of wet-bulb temperature for climate zone 2B

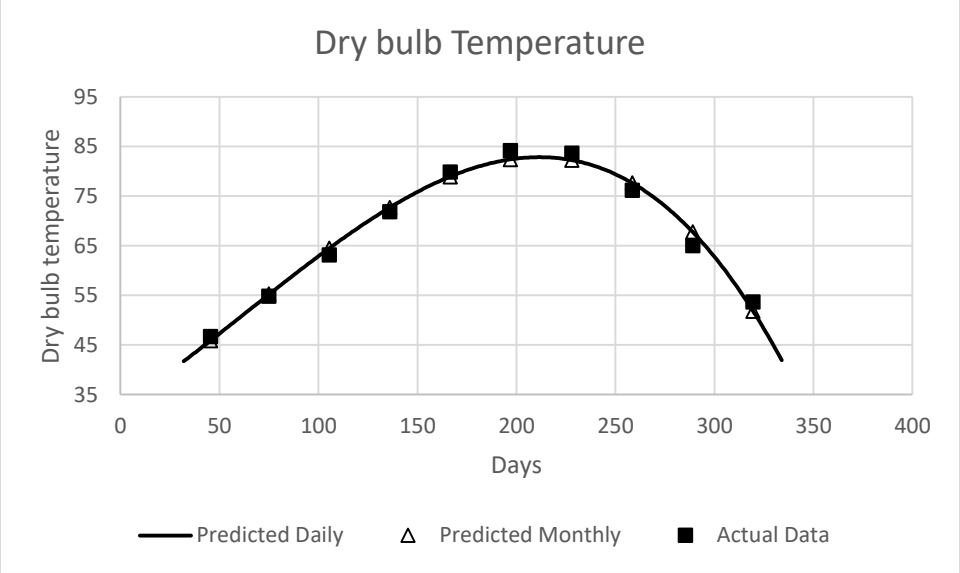

Figure 329 Monthly and daily predicted data versus actual data of dry-bulb temperature for climate zone 3Aw

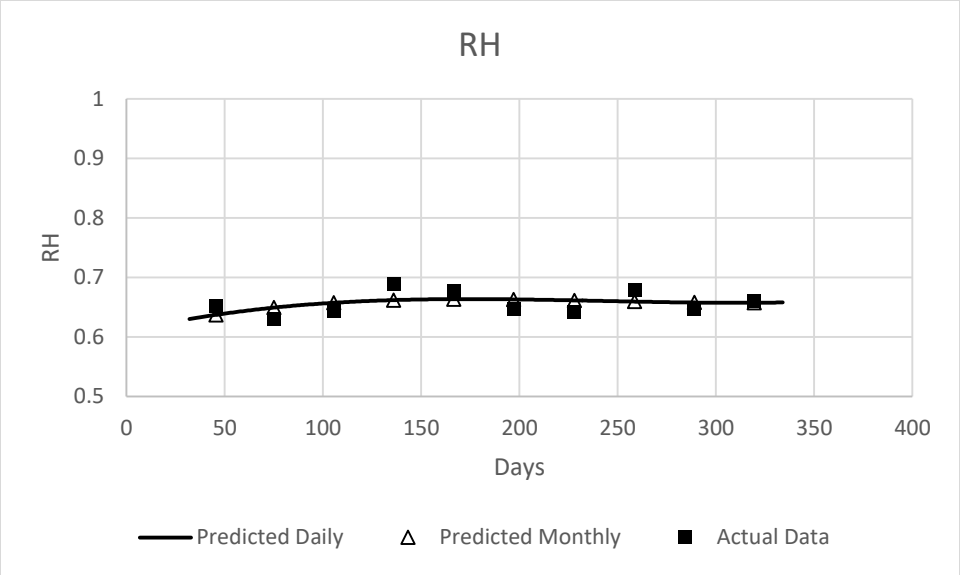

Figure 330 Monthly and daily predicted data versus actual data of relative humidity for climate zone 3Aw

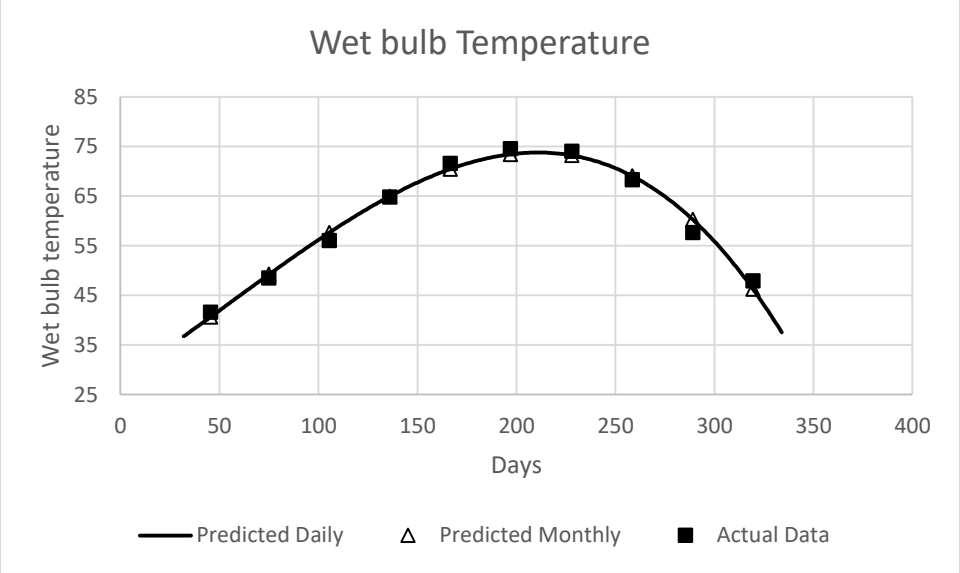

Figure 331 Monthly and daily predicted data versus actual data of wet-bulb temperature for climate zone 3Aw

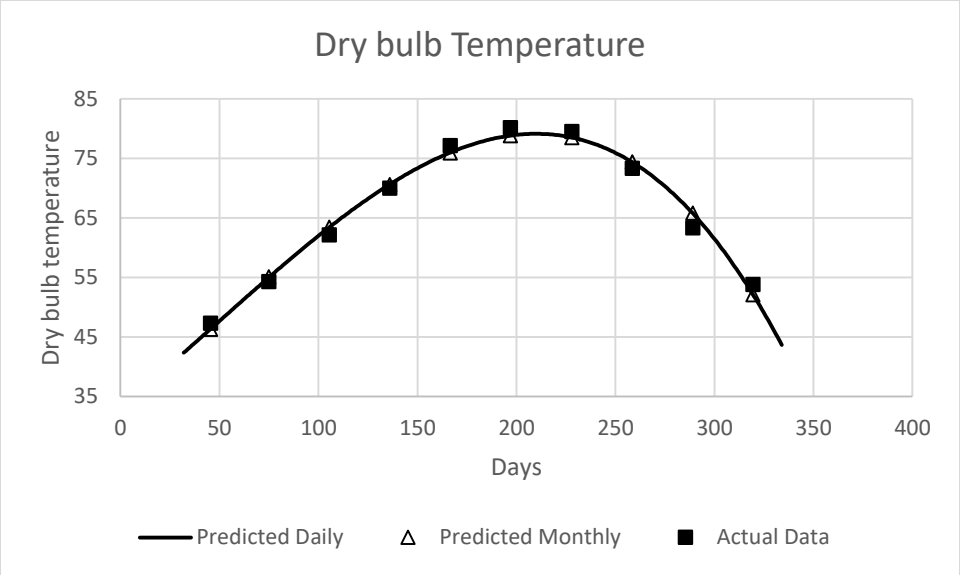

Figure 332 Monthly and daily predicted data versus actual data of dry-bulb temperature for climate zone 3Ae

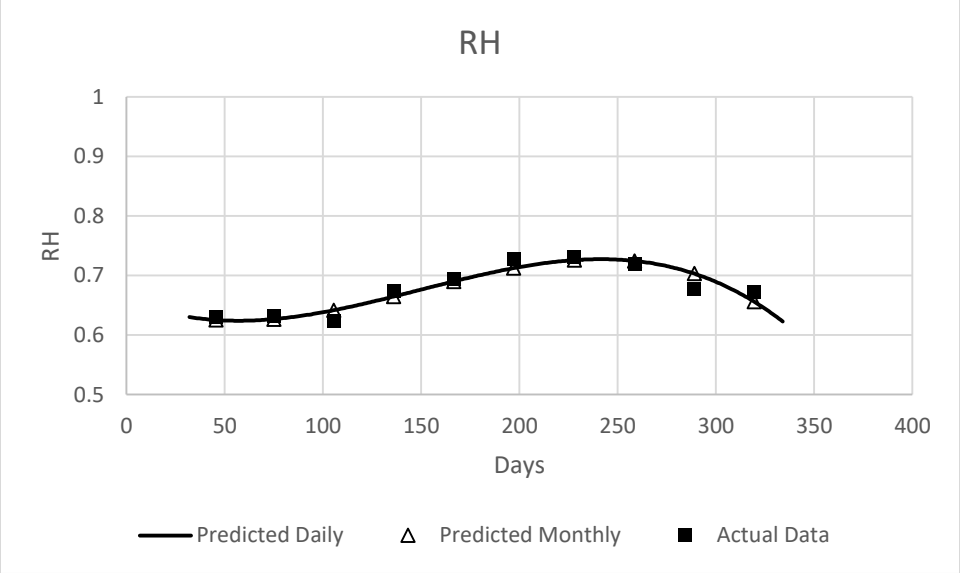

Figure 333 Monthly and daily predicted data versus actual data of relative humidity for climate zone 3Ae

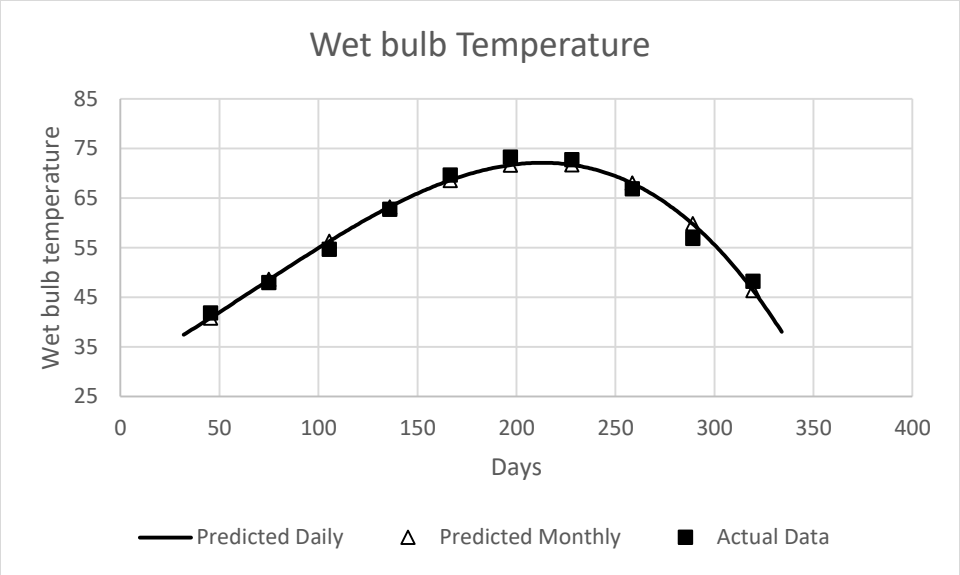

Figure 334 Monthly and daily predicted data versus actual data of wet-bulb temperature for climate zone 3Ae

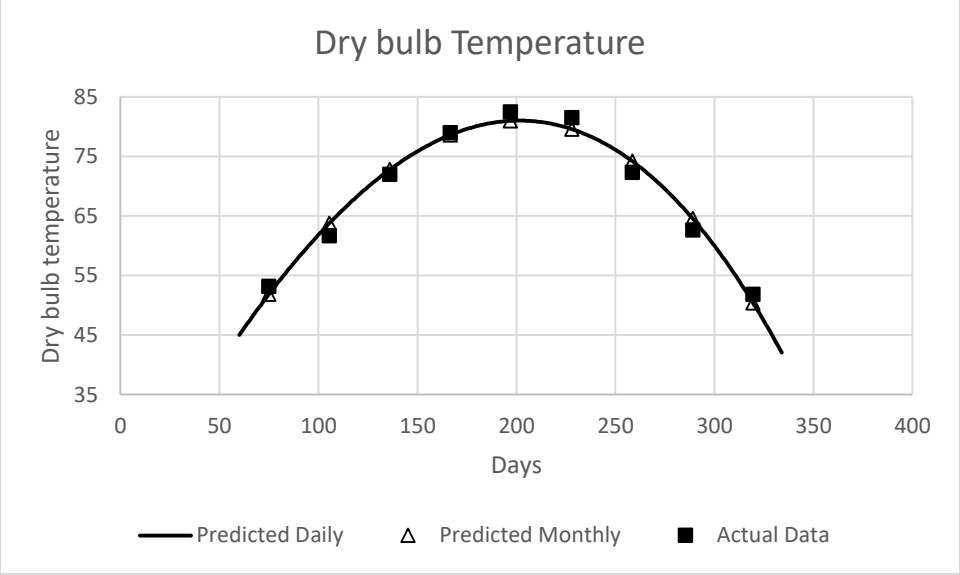

Figure 335 Monthly and daily predicted data versus actual data of dry-bulb temperature for climate zone 3Be

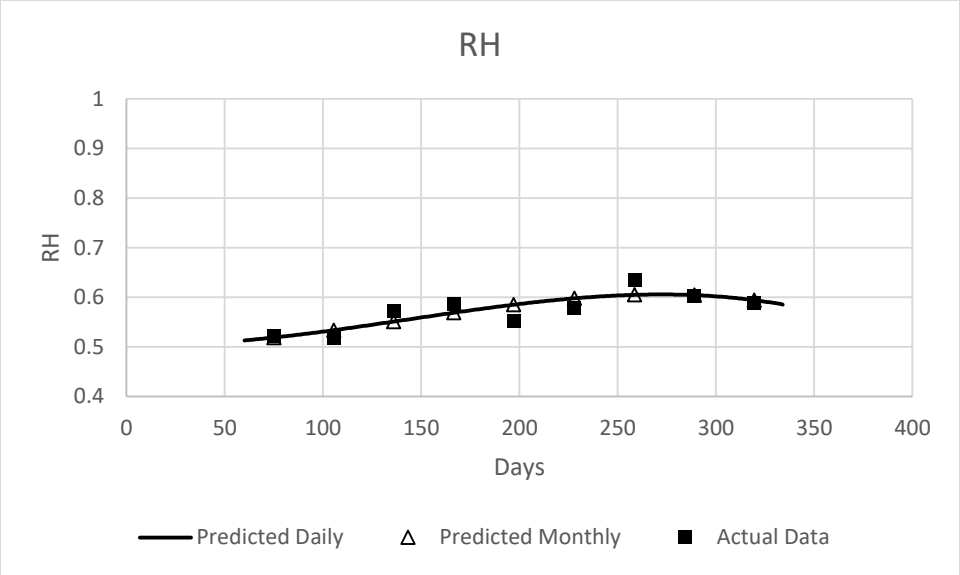

Figure 336 Monthly and daily predicted data versus actual data of relative humidity for climate zone 3Be

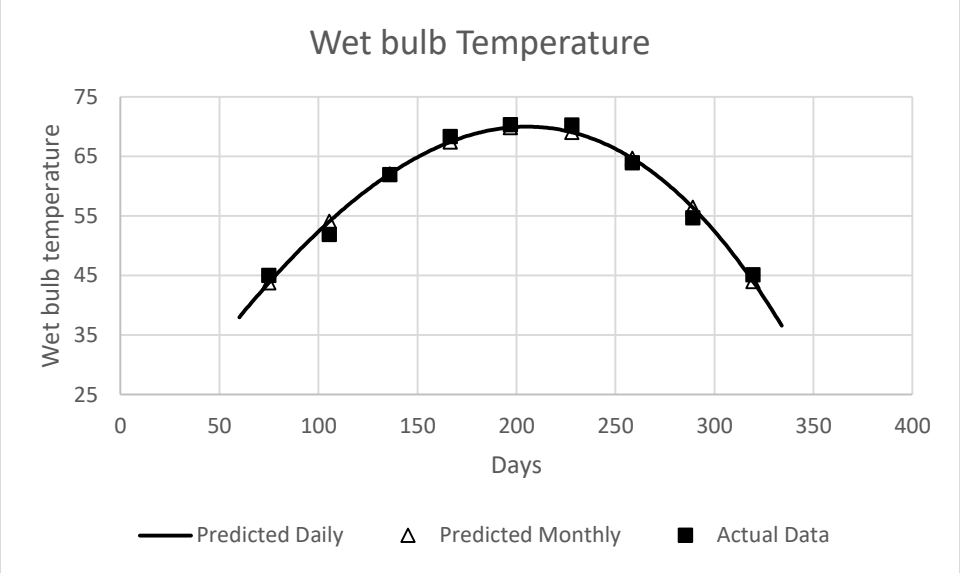

Figure 337 Monthly and daily predicted data versus actual data of wet-bulb temperature for climate zone 3Be

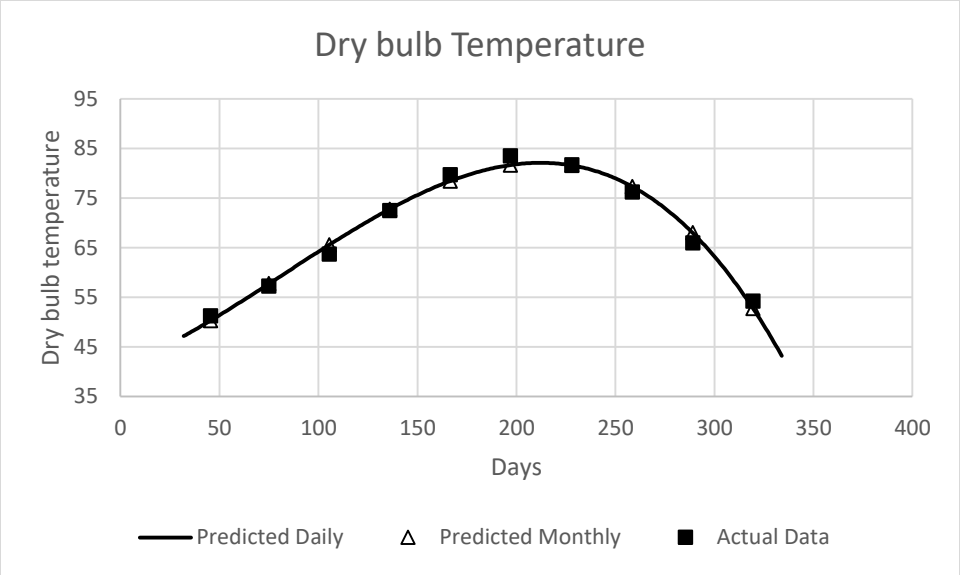

Figure 338 Monthly and daily predicted data versus actual data of dry-bulb temperature for climate zone 3Bw

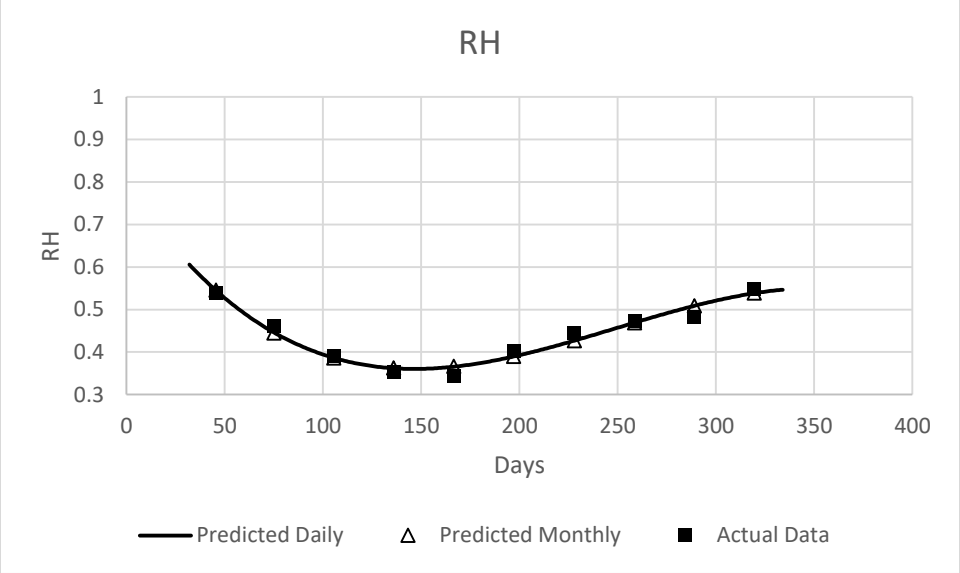

Figure 339 Monthly and daily predicted data versus actual data of relative humidity for climate zone 3Bw

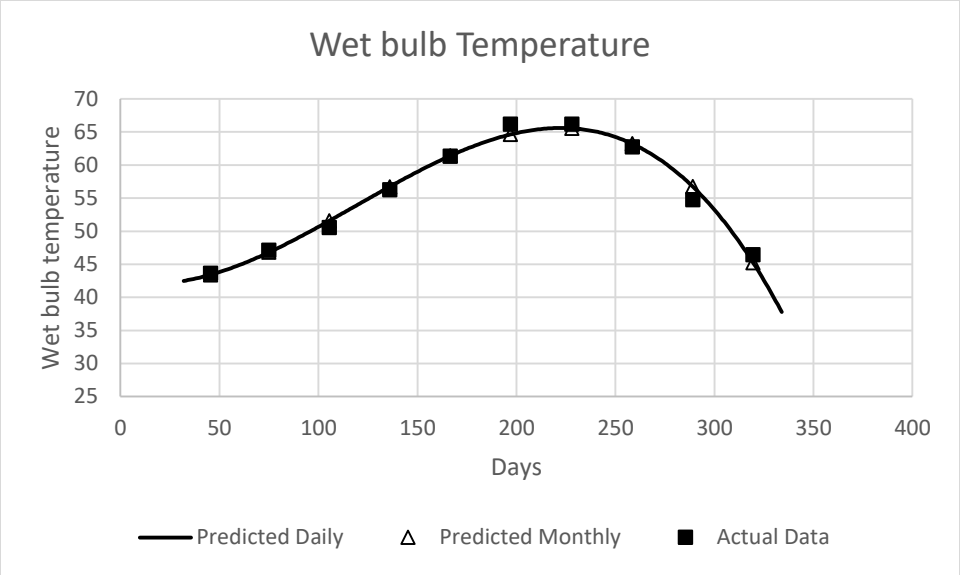

Figure 340 Monthly and daily predicted data versus actual data of wet-bulb temperature for climate zone 3Bw

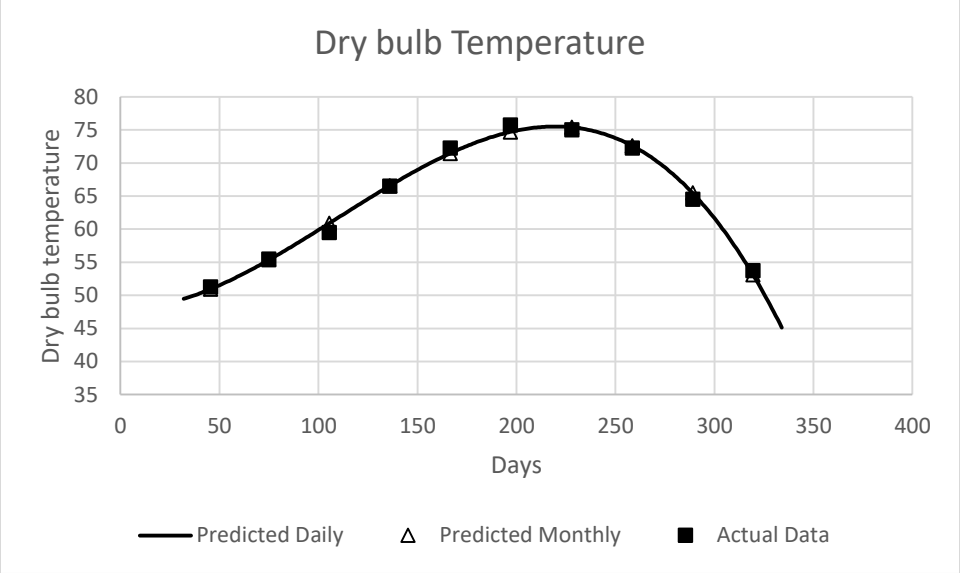

Figure 341 Monthly and daily predicted data versus actual data of dry-bulb temperature for climate zone 3Bn

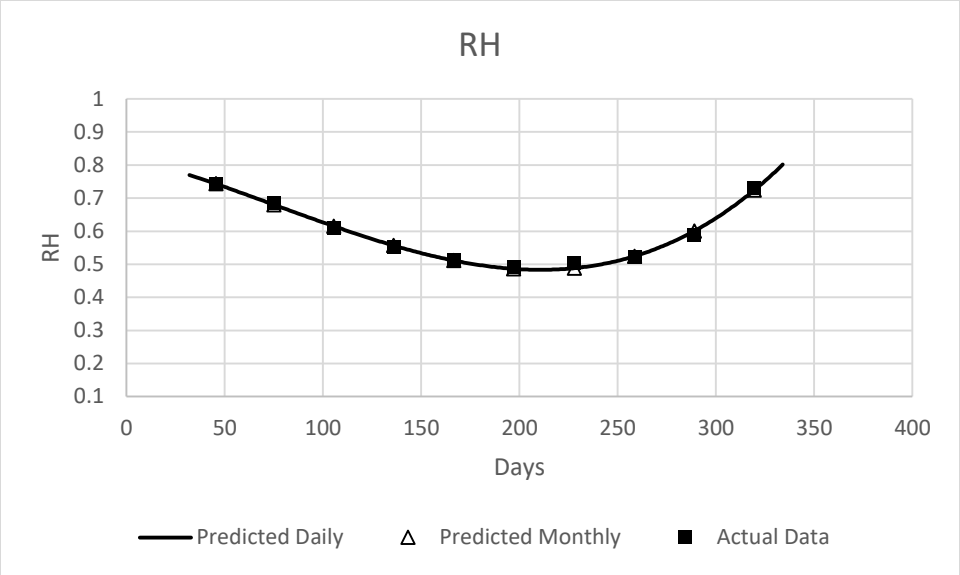

Figure 342 Monthly and daily predicted data versus actual data of relative humidity for climate zone 3Bn

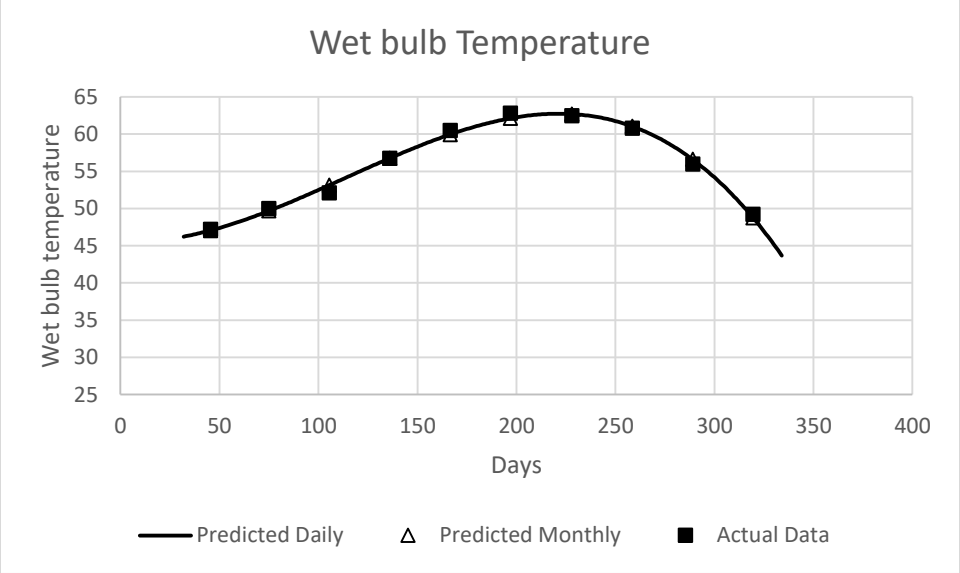

Figure 343 Monthly and daily predicted data versus actual data of wet-bulb temperature for climate zone 3Bn

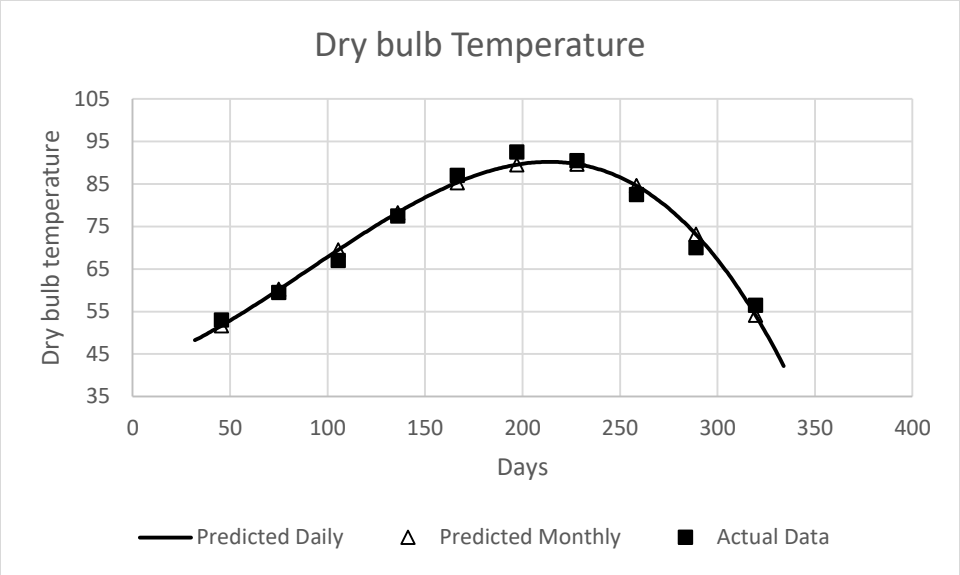

Figure 344 Monthly and daily predicted data versus actual data of dry-bulb temperature for climate zone 3Blv

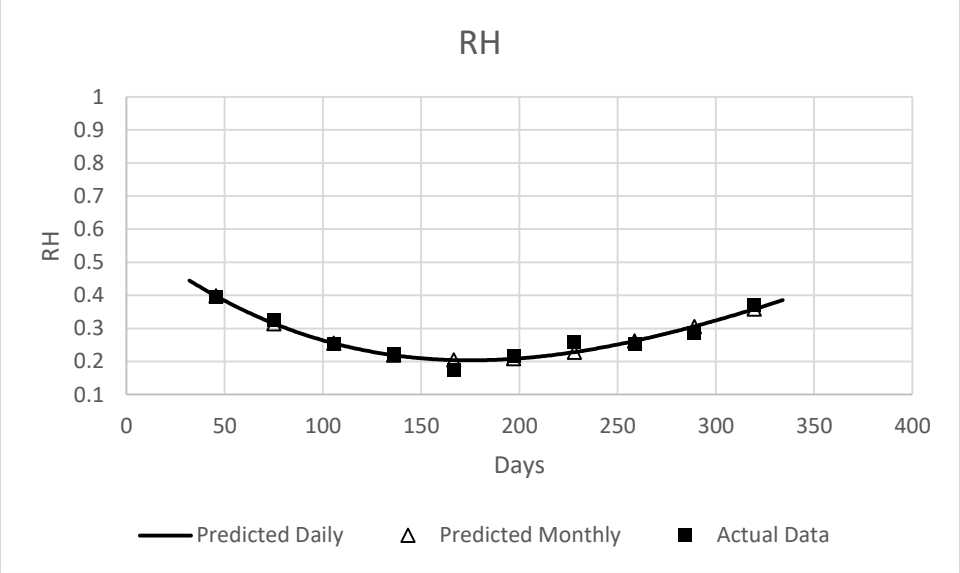

Figure 345 Monthly and daily predicted data versus actual data of relative humidity for climate zone 3Blv

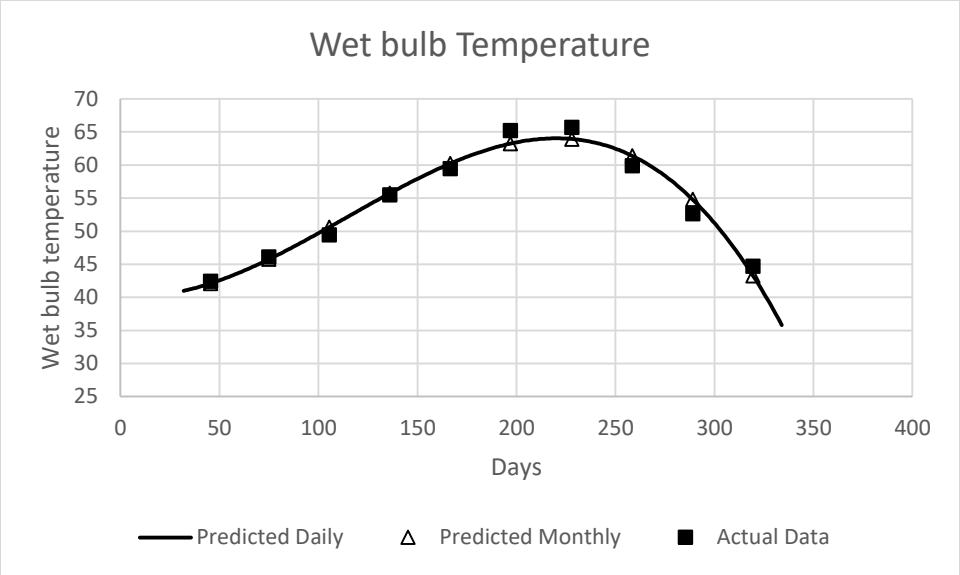

Figure 346 Monthly and daily predicted data versus actual data of wet-bulb temperature for climate zone 3Blv

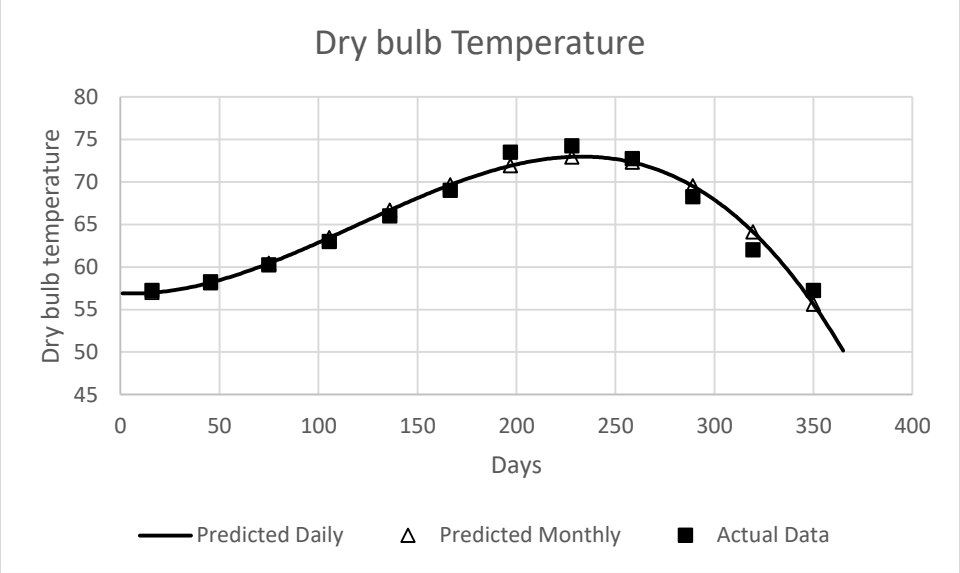

Figure 347 Monthly and daily predicted data versus actual data of dry-bulb temperature for climate zone 3C

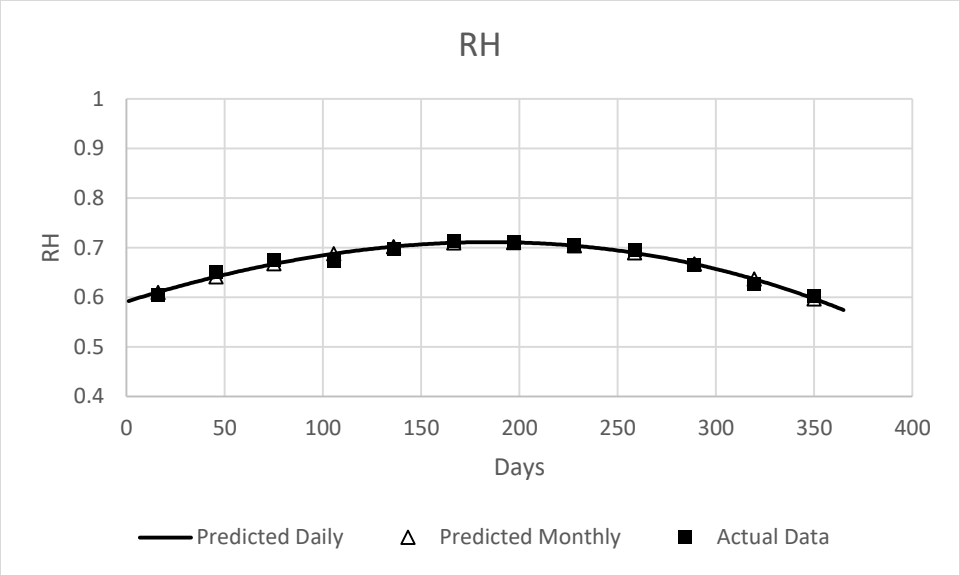

Figure 348 Monthly and daily predicted data versus actual data of relative humidity for climate zone 3C

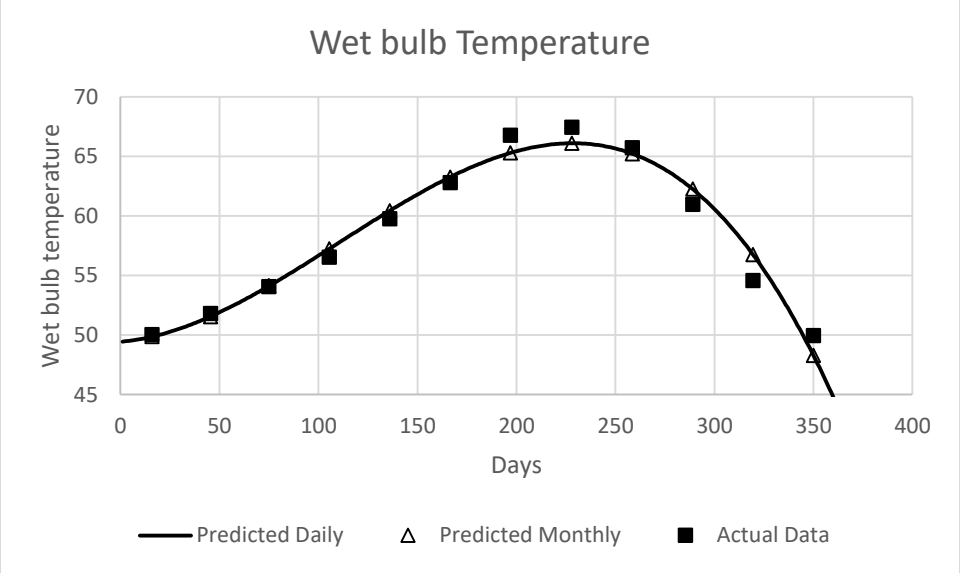

Figure 349 Monthly and daily predicted data versus actual data of wet-bulb temperature for climate zone 3C

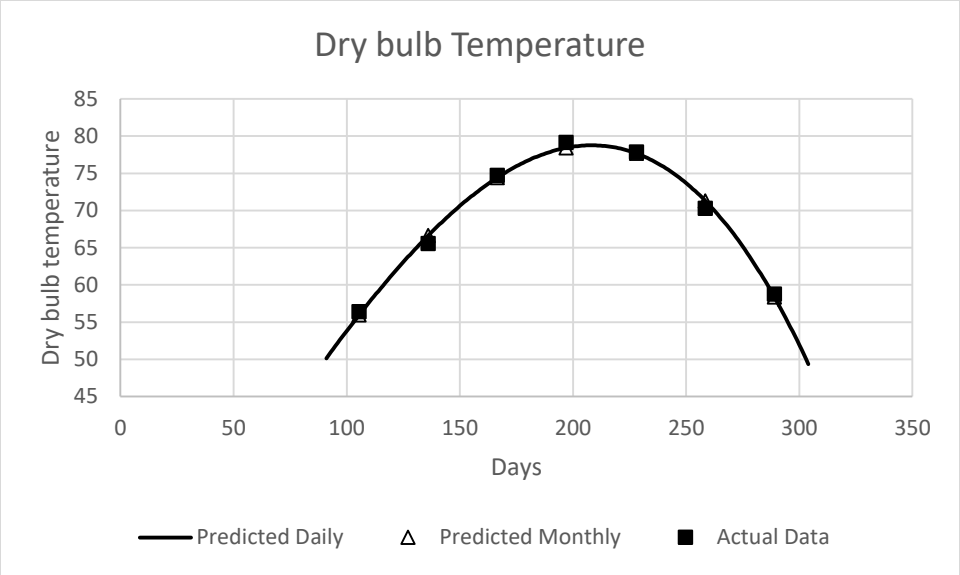

Figure 350 Monthly and daily predicted data versus actual data of dry-bulb temperature for climate zone 4A

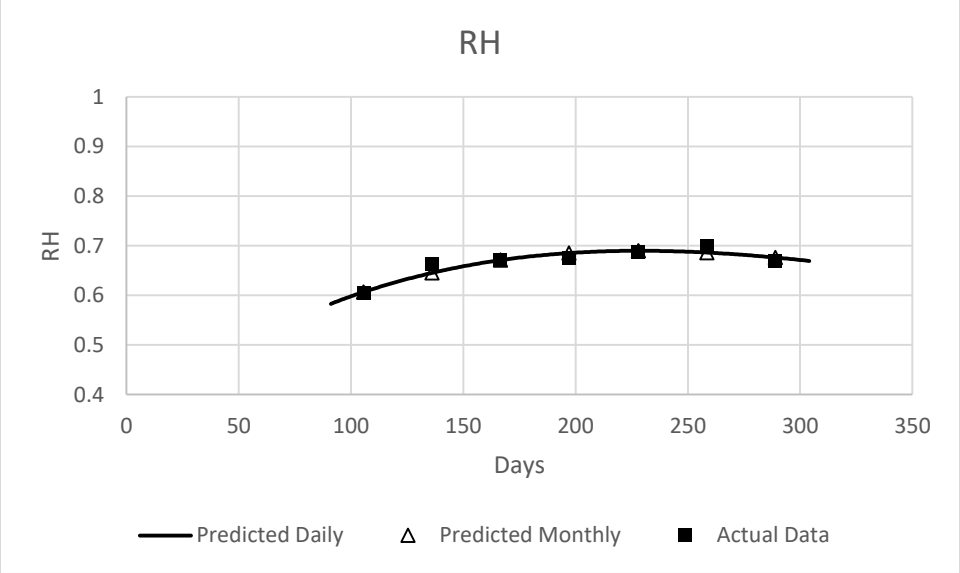

Figure 351 Monthly and daily predicted data versus actual data of relative humidity for climate zone 4A

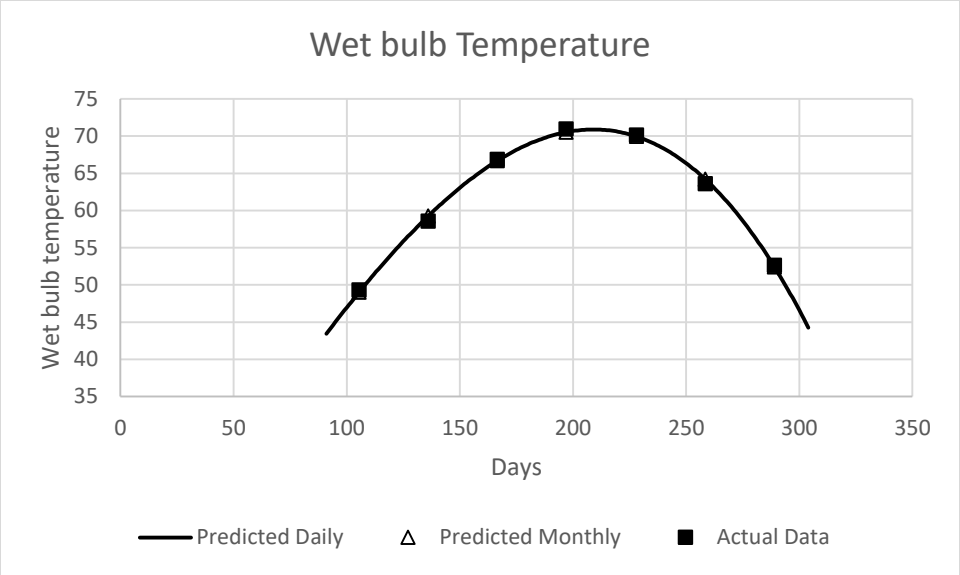

Figure 352 Monthly and daily predicted data versus actual data of wet-bulb temperature for climate zone 4A

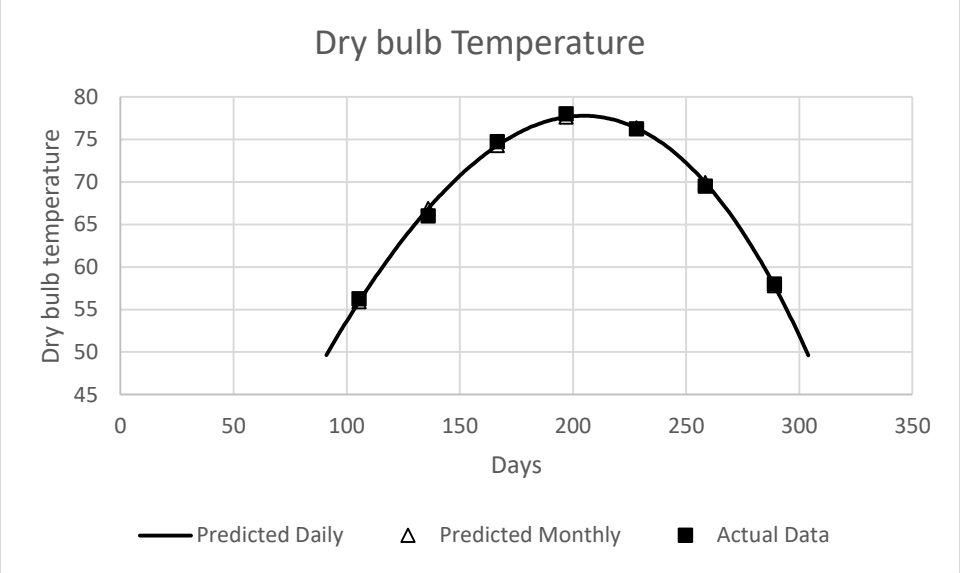

Figure 353 Monthly and daily predicted data versus actual data of dry-bulb temperature for climate zone 4B

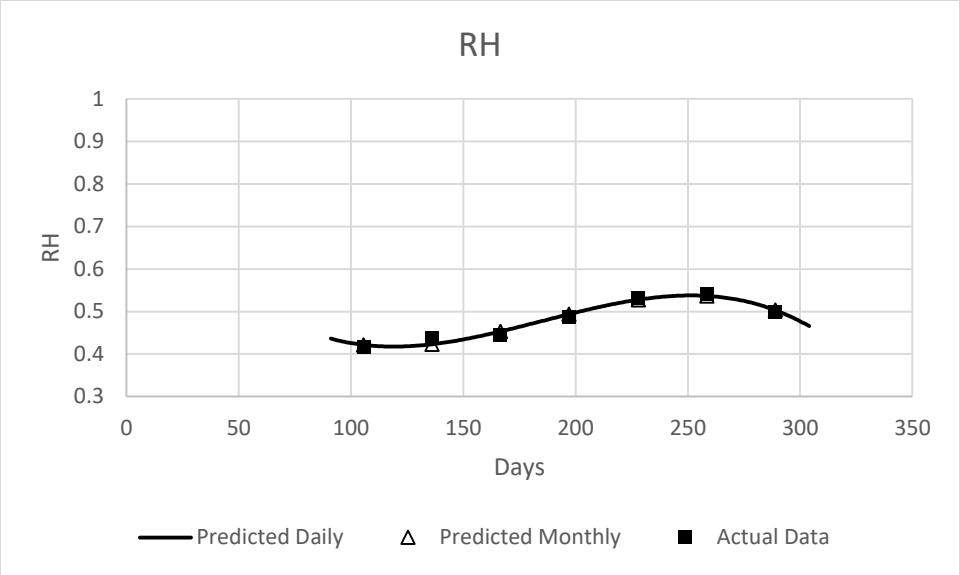

Figure 354 Monthly and daily predicted data versus actual data of relative humidity for climate zone 4B

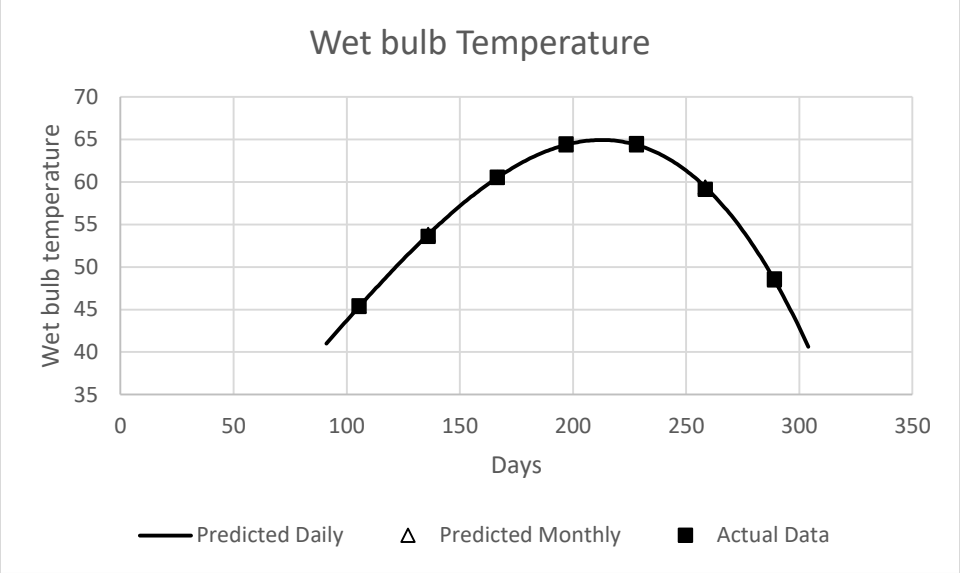

Figure 355 Monthly and daily predicted data versus actual data of wet-bulb temperature for climate zone 4B

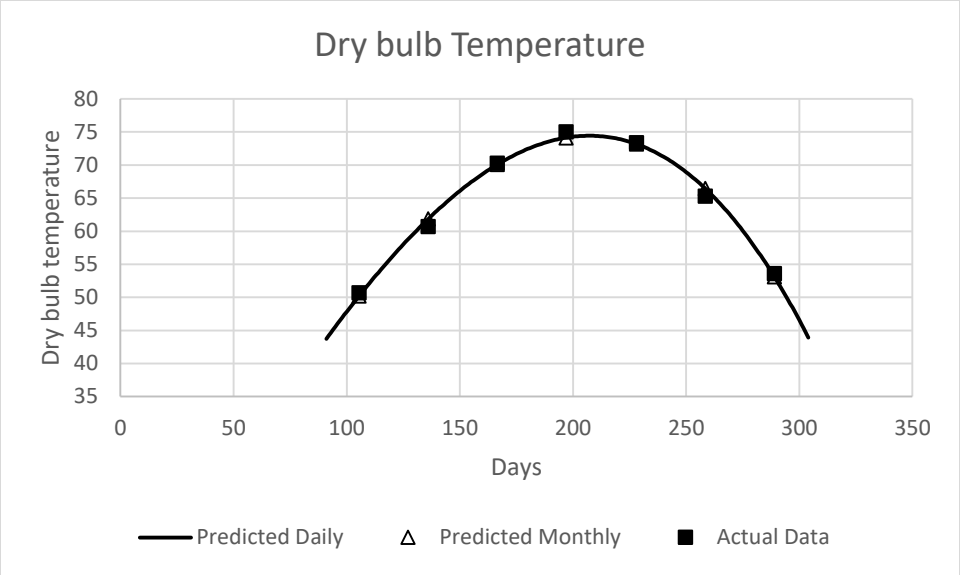

Figure 356 Monthly and daily predicted data versus actual data of dry-bulb temperature for climate zone 5A

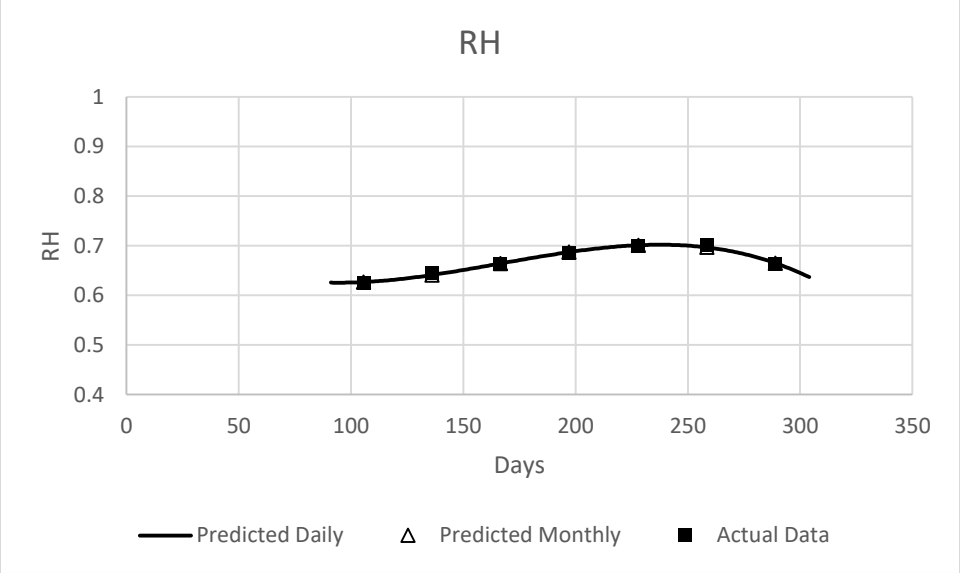

Figure 357 Monthly and daily predicted data versus actual data of relative humidity for climate zone 5A

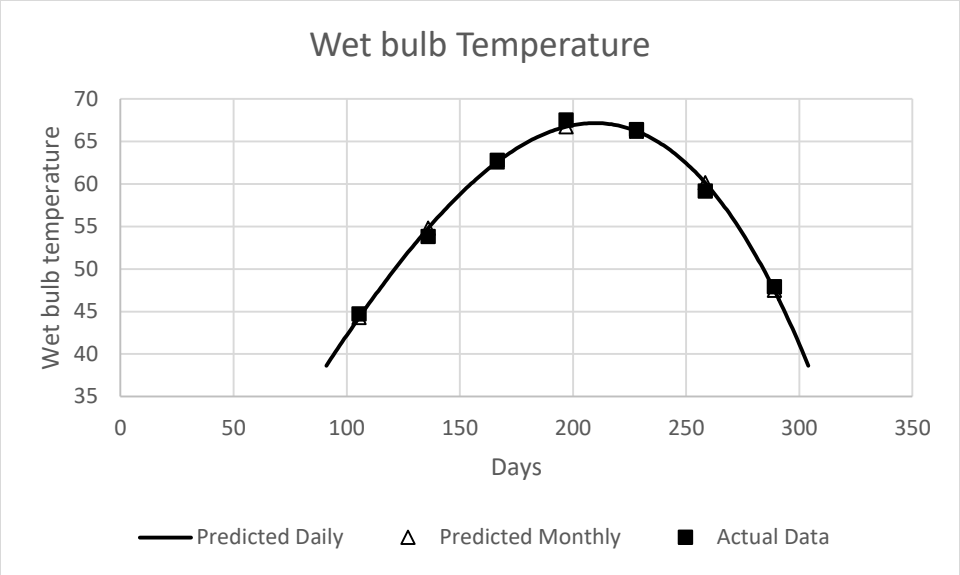

Figure 358 Monthly and daily predicted data versus actual data of wet-bulb temperature for climate zone 5A

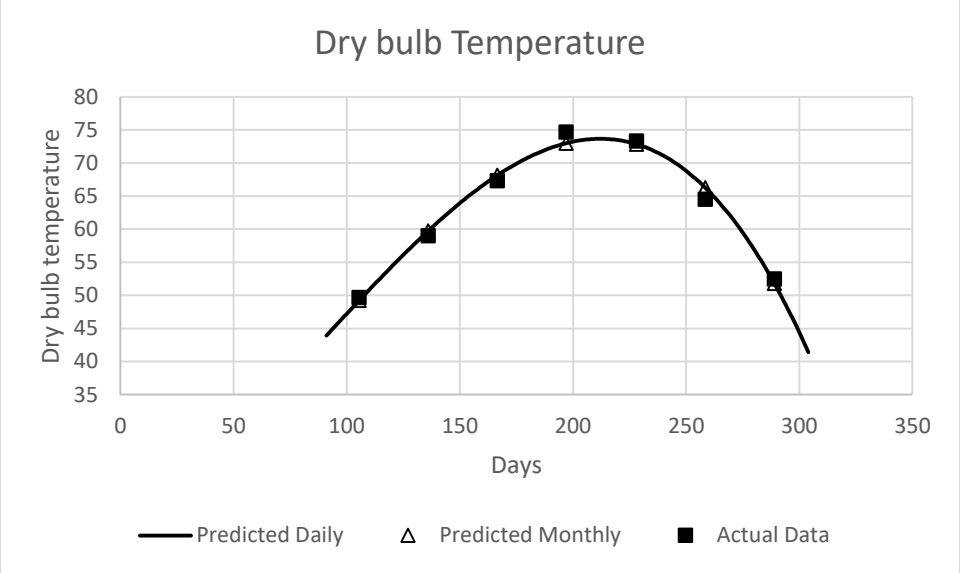

Figure 359 Monthly and daily predicted data versus actual data of dry-bulb temperature for climate zone 5B

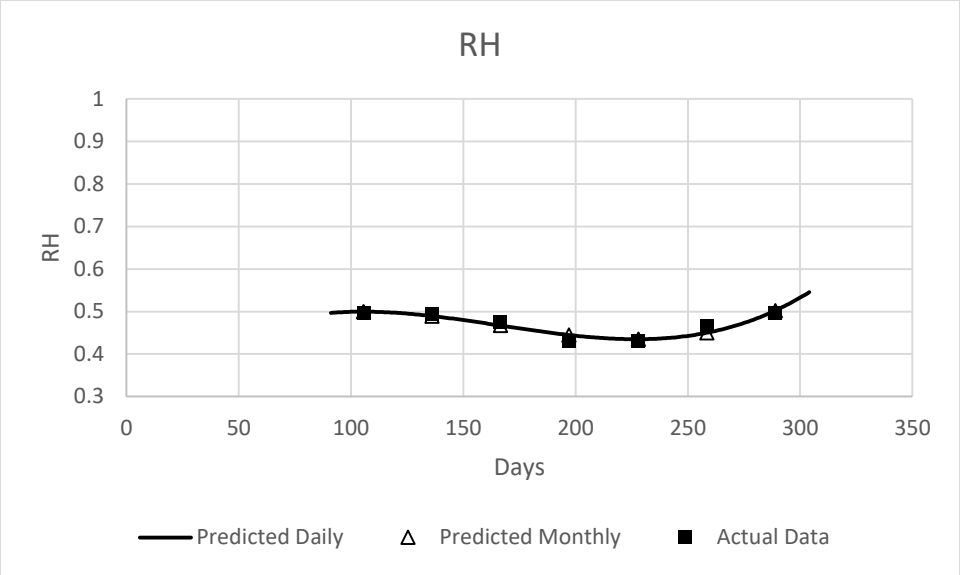

Figure 360 Monthly and daily predicted data versus actual data of relative humidity for climate zone 5B

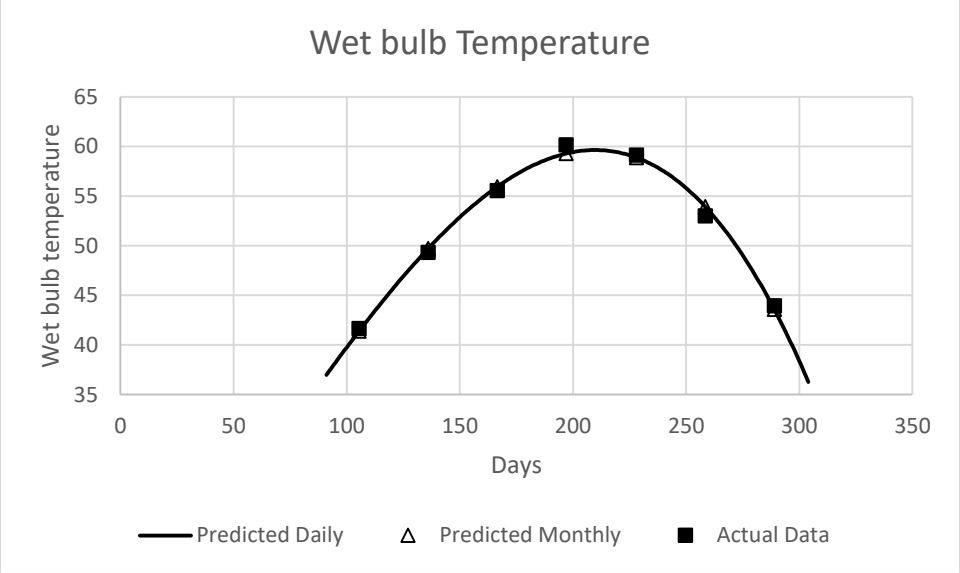

Figure 361 Monthly and daily predicted data versus actual data of wet-bulb temperature for climate zone 5B

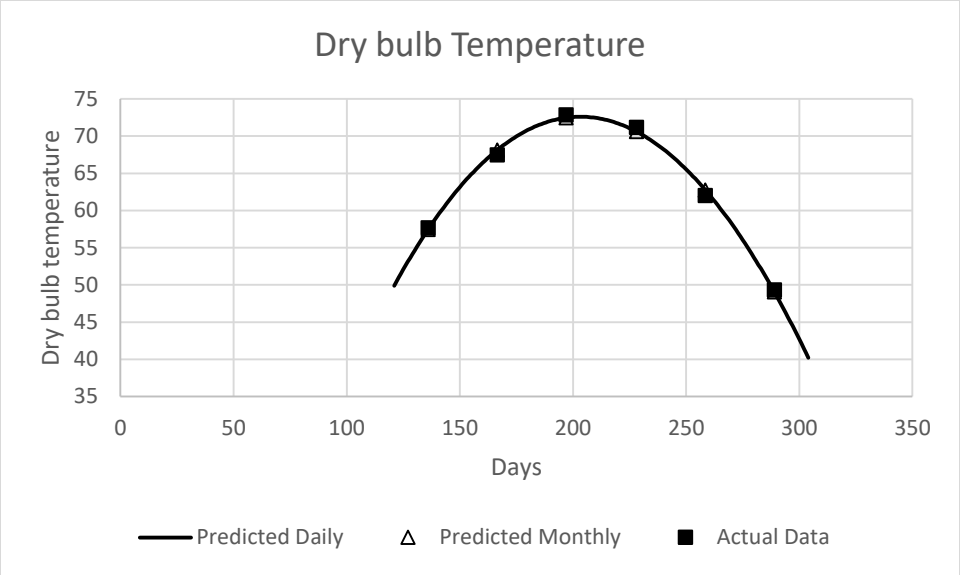

Figure 362 Monthly and daily predicted data versus actual data of dry-bulb temperature for climate zone 6A

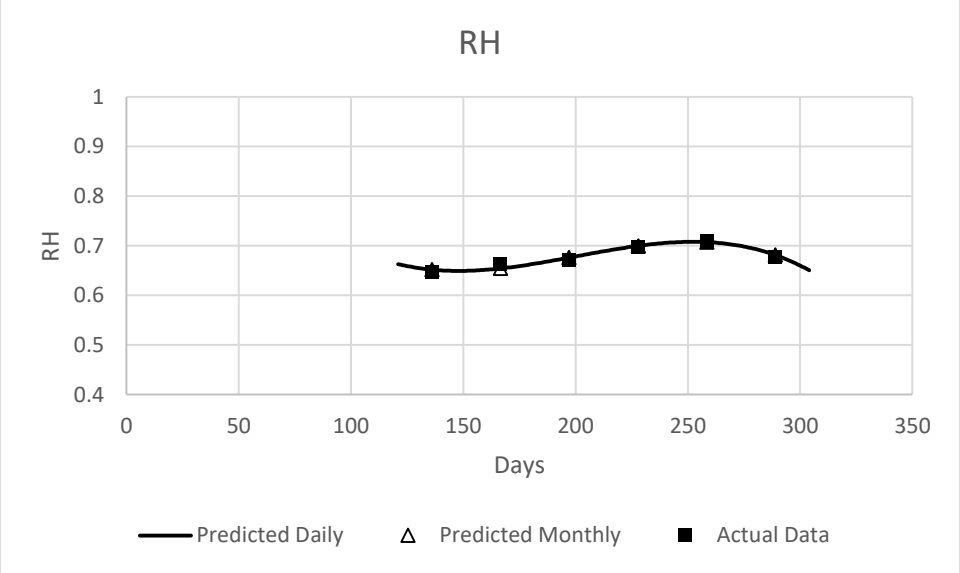

Figure 363 Monthly and daily predicted data versus actual data of relative humidity for climate zone 6A

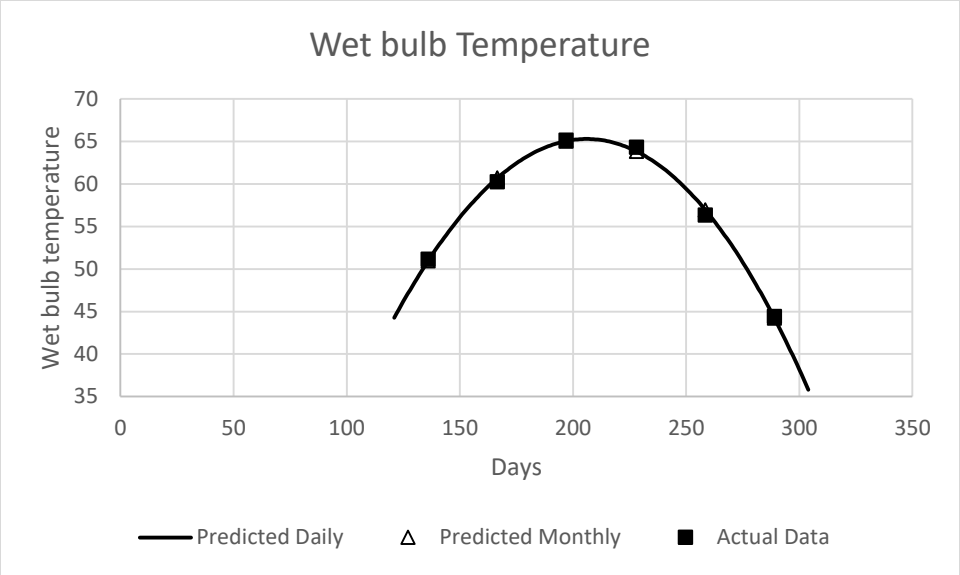

Figure 364 Monthly and daily predicted data versus actual data of wet-bulb temperature for climate zone 6A

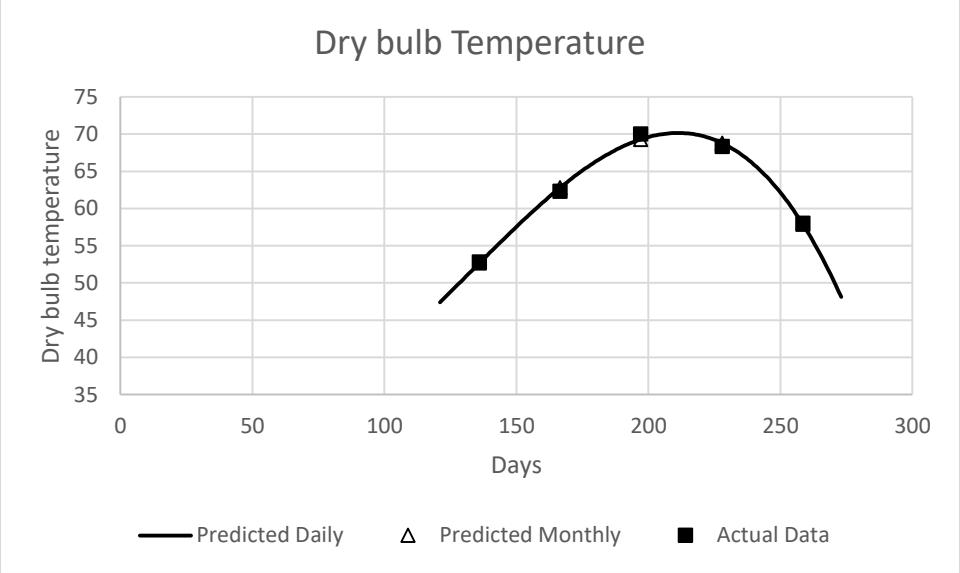

Figure 365 Monthly and daily predicted data versus actual data of dry-bulb temperature for climate zone 6B

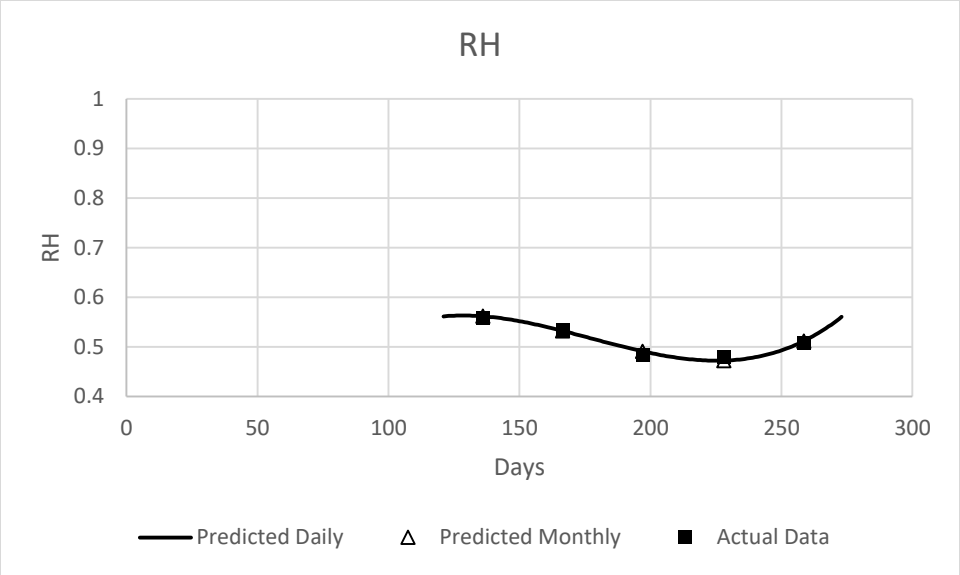

Figure 366 Monthly and daily predicted data versus actual data of relative humidity for climate zone 6B

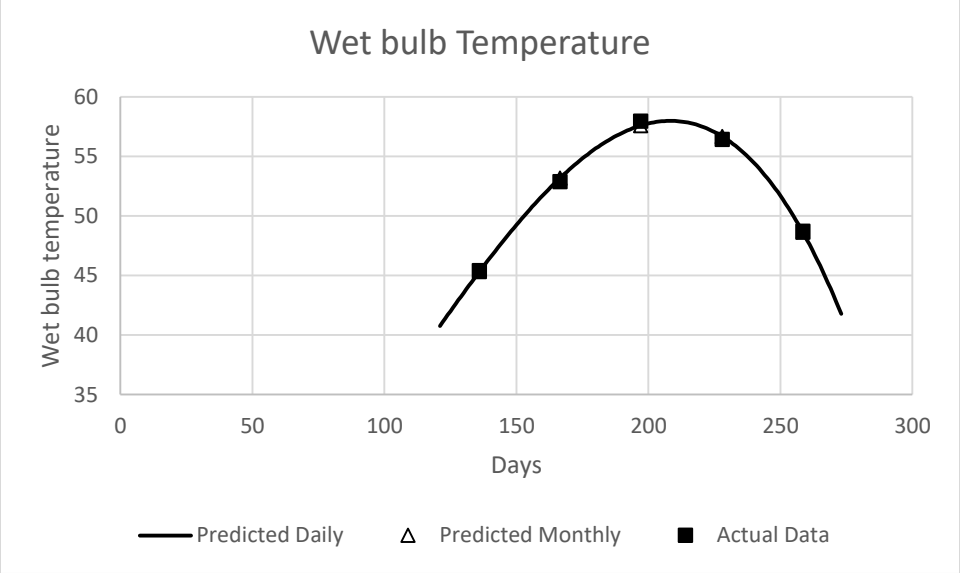

Figure 367 Monthly and daily predicted data versus actual data of wet-bulb temperature for climate zone 6B

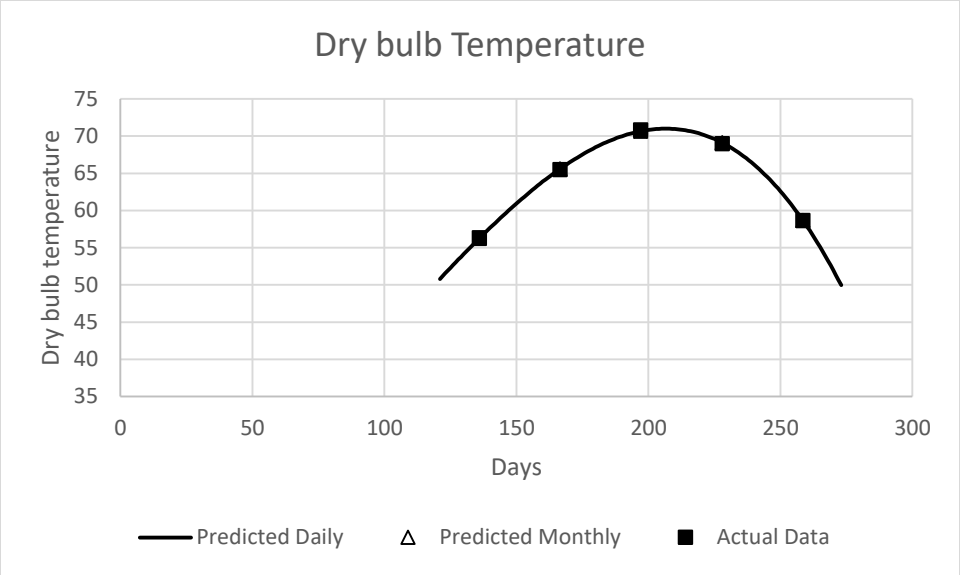

Figure 368 Monthly and daily predicted data versus actual data of dry-bulb temperature for climate zone 7A

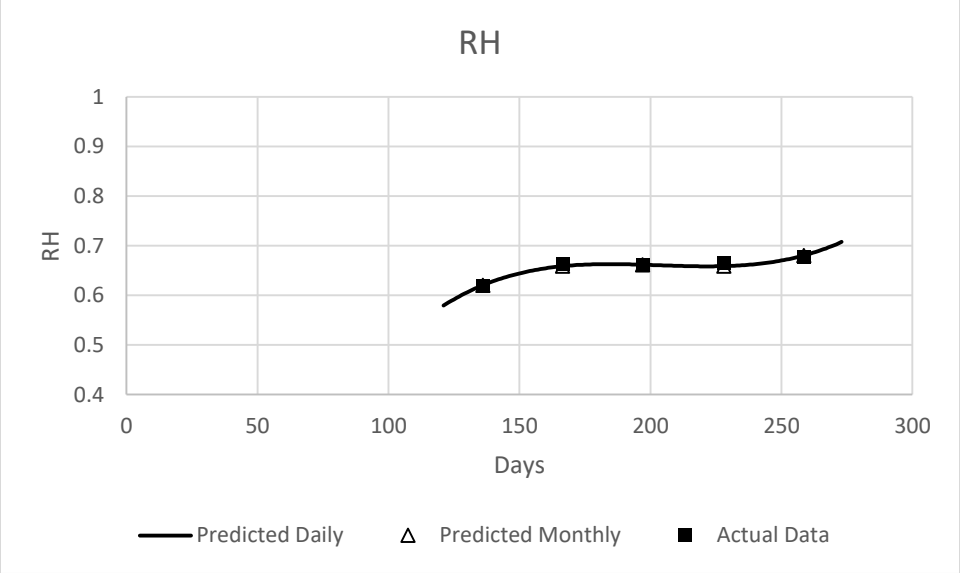

Figure 369 Monthly and daily predicted data versus actual data of relative humidity for climate zone 7A

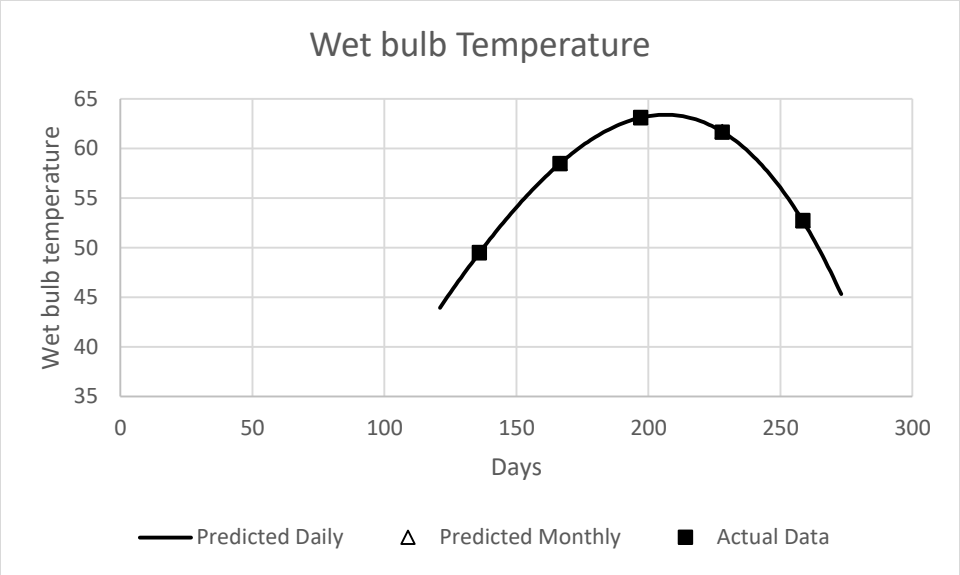

Figure 370 Monthly and daily predicted data versus actual data of wet-bulb temperature for climate zone 7A

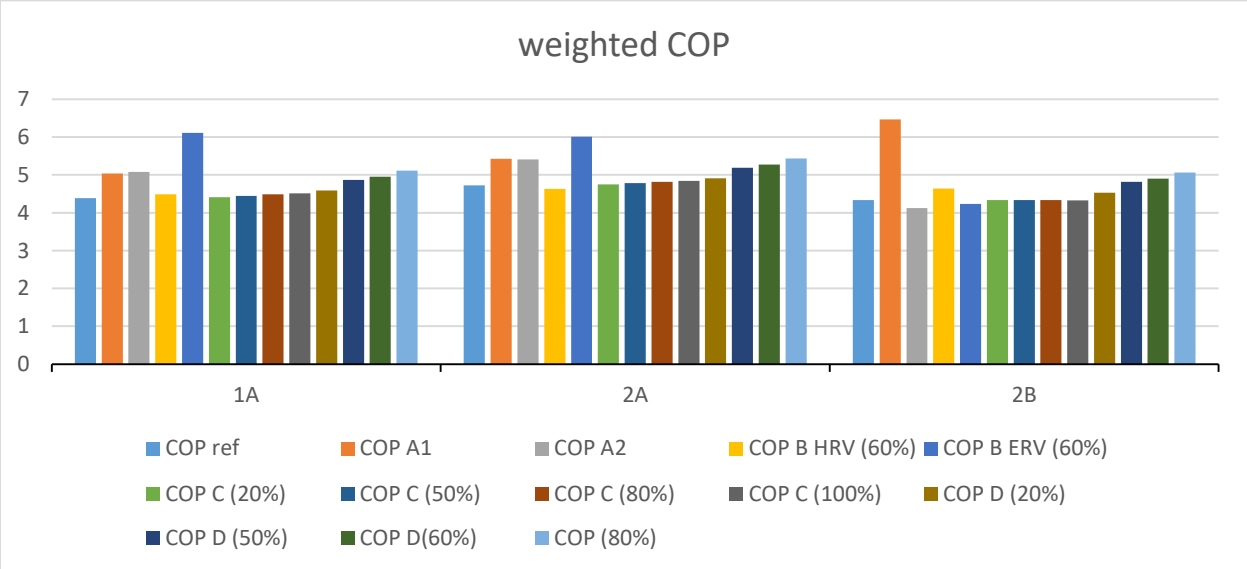

Figure 371 Weighted COP comparison between different reconfigured systems based on the old model for climate zone 1A, 2A and 2B during the whole cooling season

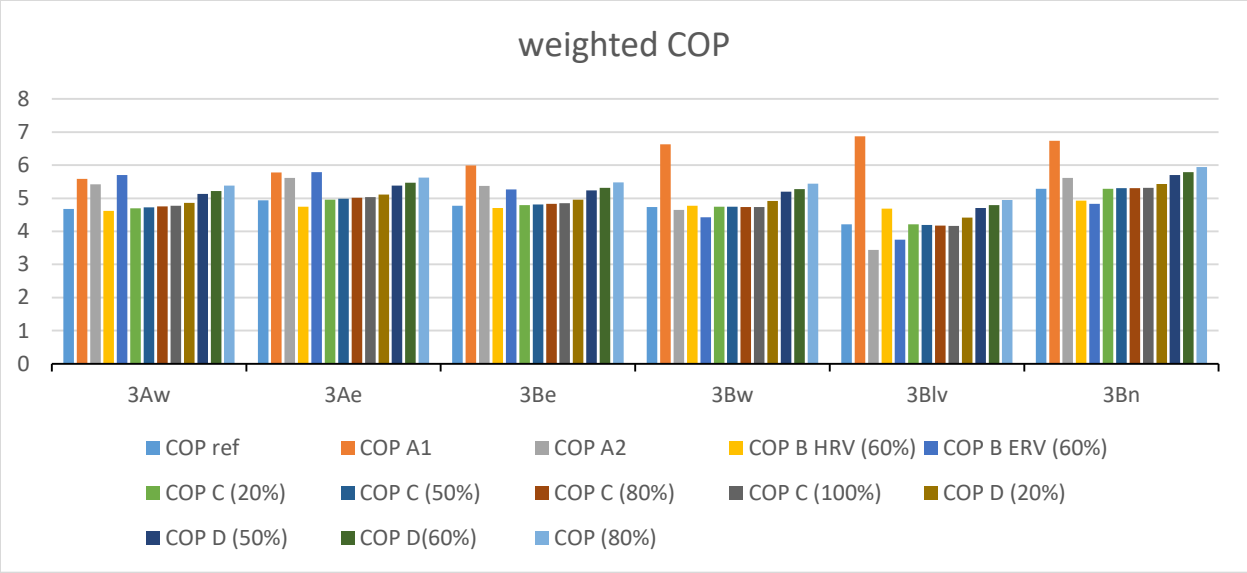

Figure 372 Weighted COP comparison between different reconfigured systems based on the old model for climate zone 3Aw, 3Ae, 3Be, 3Bw, 3Blv, and 3Bn during the whole cooling season

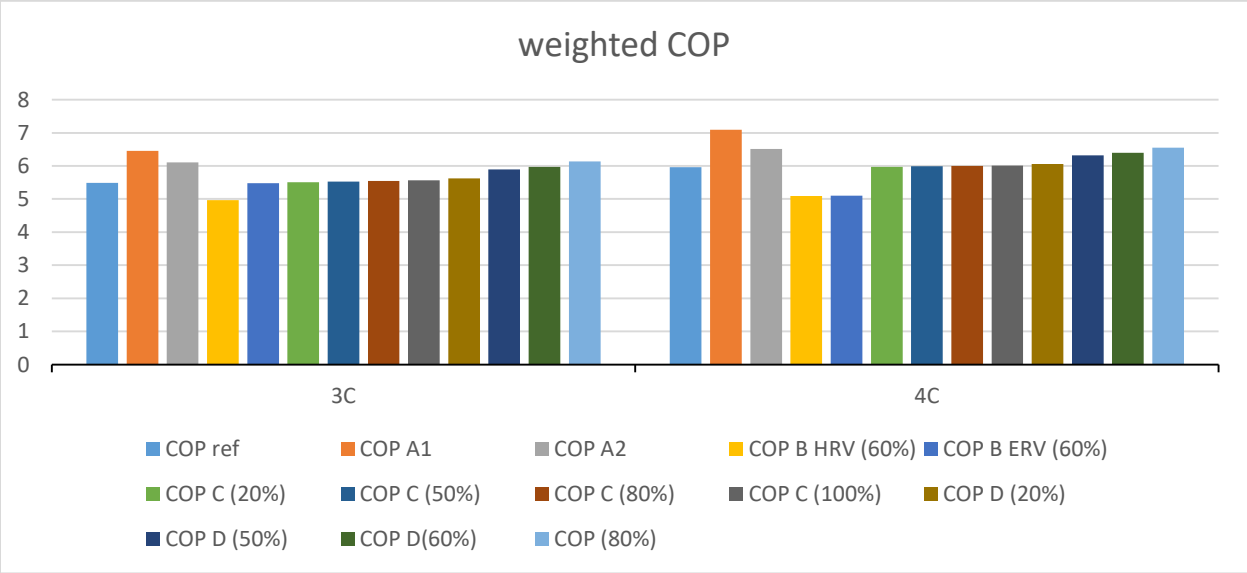

Figure 373 Weighted COP comparison between different reconfigured systems based on the old model for climate zone 3C and 4C during the whole cooling season

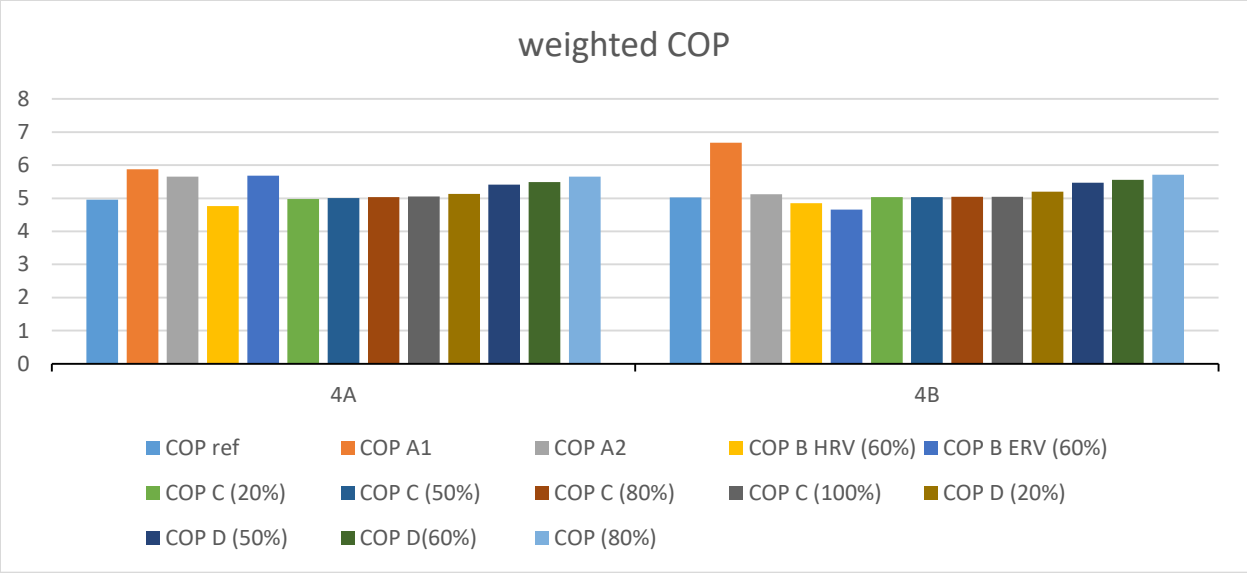

Figure 374 Weighted COP comparison between different reconfigured systems based on the old model for climate zone 4A and 4B during the whole cooling season

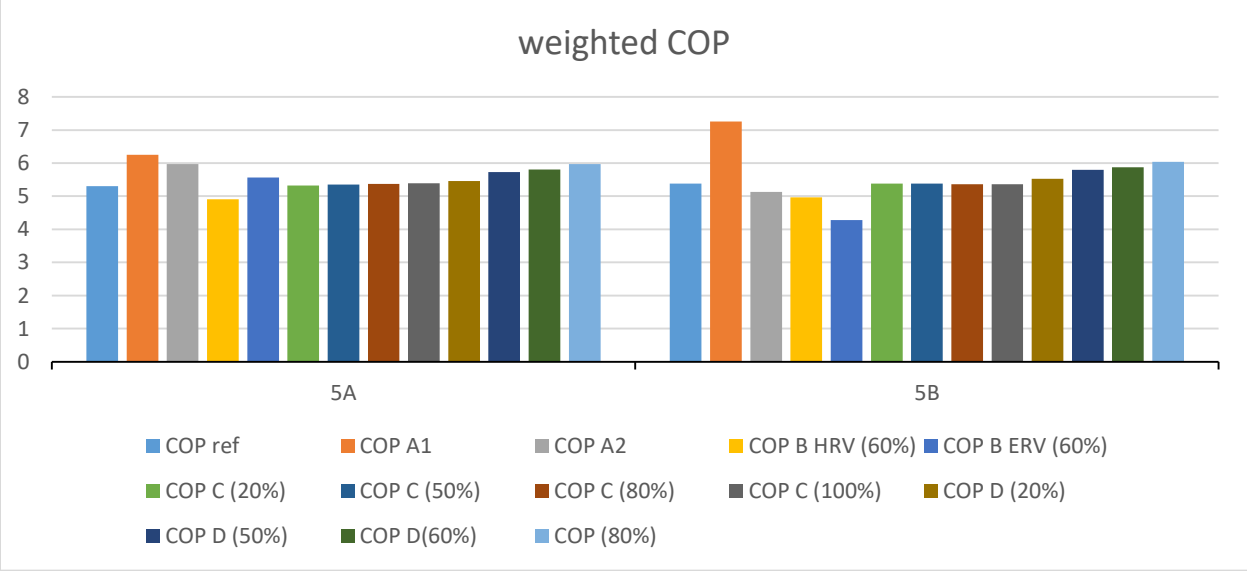

Figure 375 Weighted COP comparison between different reconfigured systems based on the old model for climate zone 5A and 5B during the whole cooling season

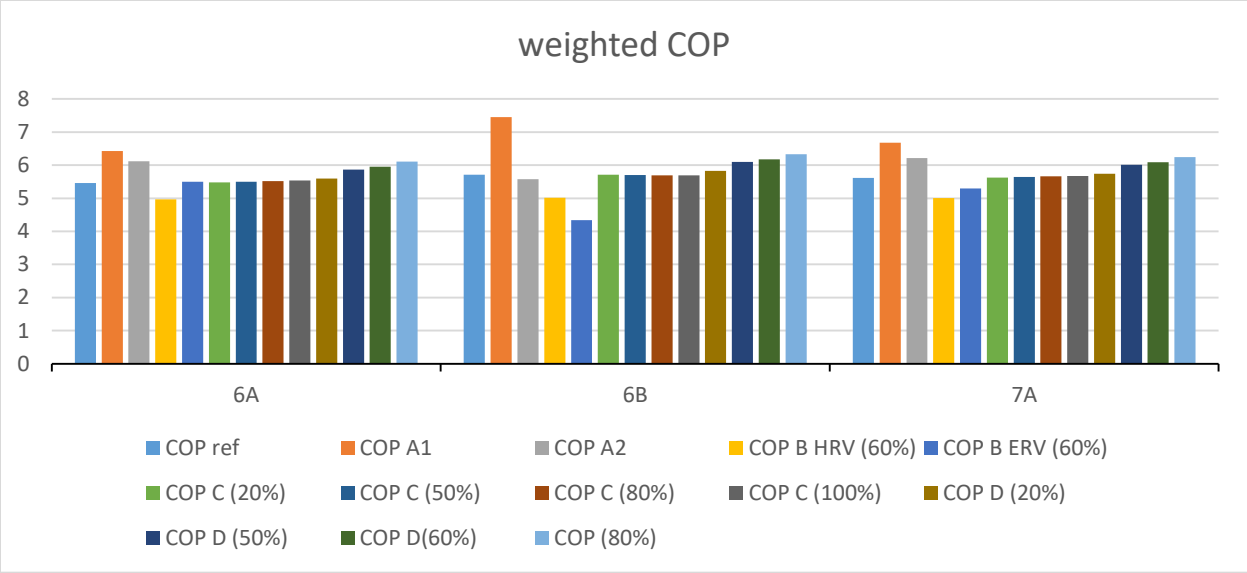

Figure 376 Weighted COP comparison between different reconfigured systems based on the old model for climate zone 6A, 6B and 7A during the whole cooling season

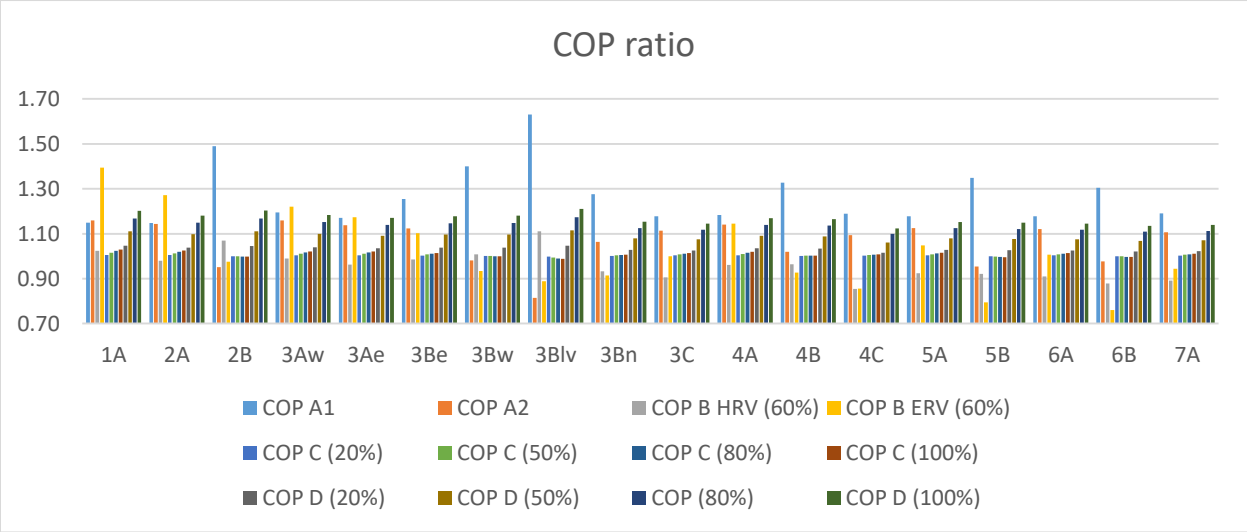

Figure 377 Weighted COP ratio comparison between different reconfigured systems based on the old model for all climate zones during the whole cooling season

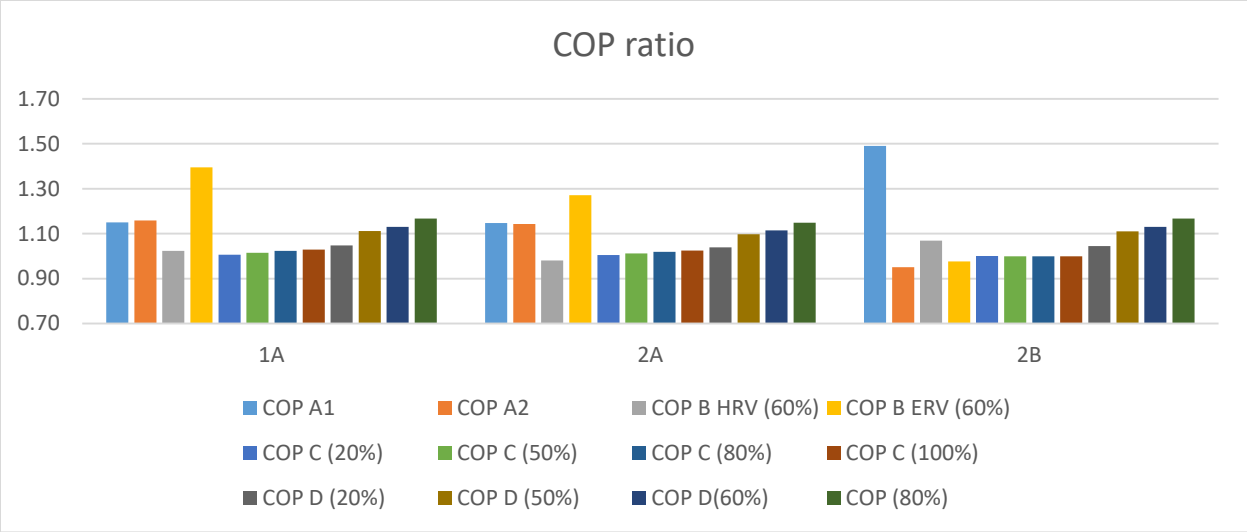

Figure 378 Weighted COP ratio comparison between different reconfigured systems based on the old model for climate zone 1A, 2A and 2B during the whole cooling season

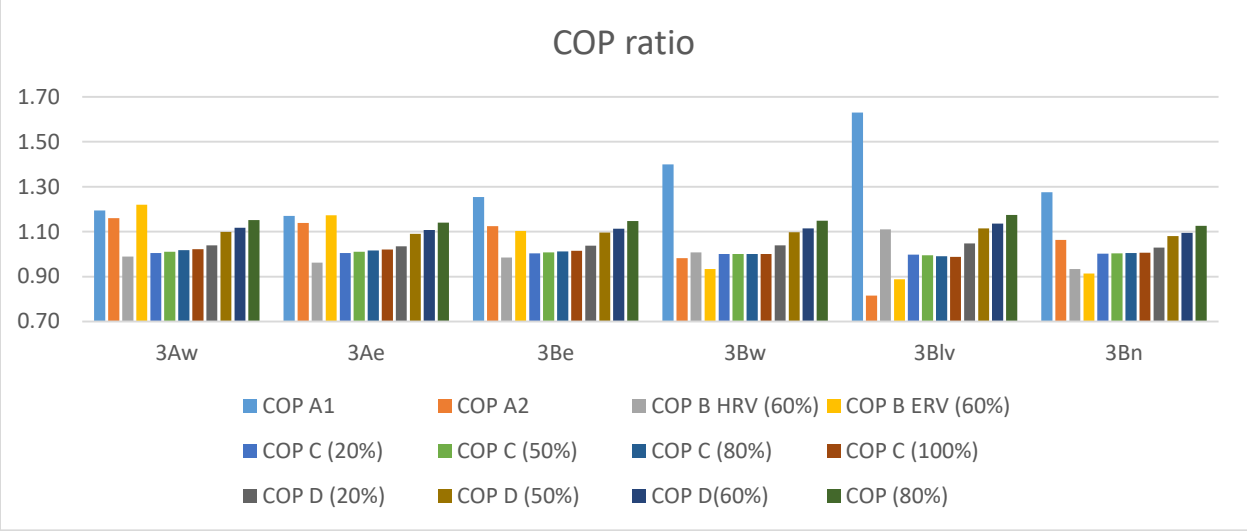

Figure 379 Weighted COP ratio comparison between different reconfigured systems based on the old model for climate zone 3Aw, 3Ae, 3Be, 3Bw, 3Blv, and 3Bn during the whole cooling season

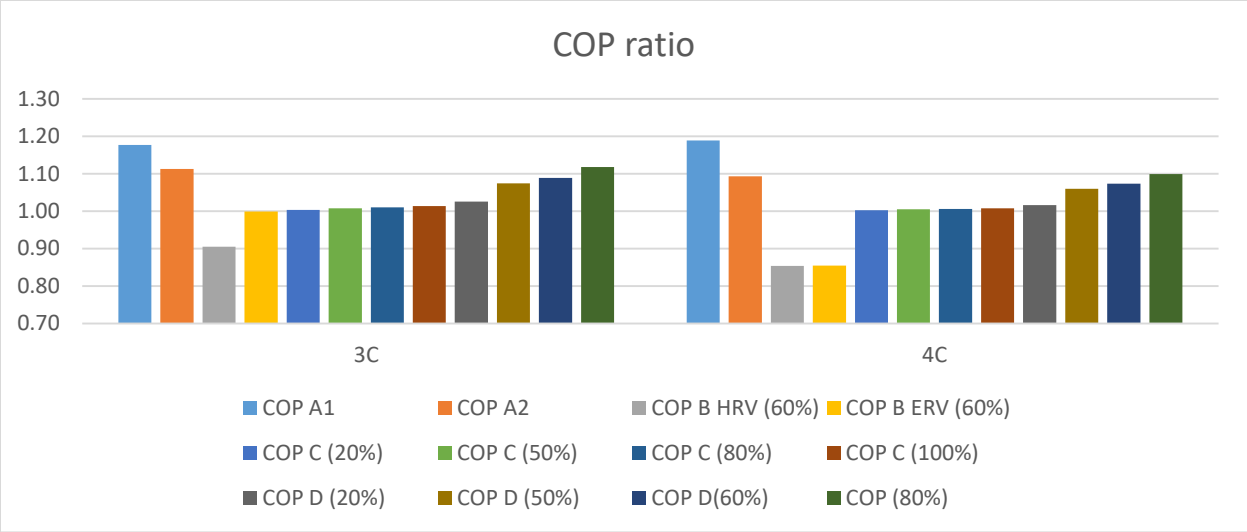

Figure 380 Weighted COP ratio comparison between different reconfigured systems based on the old model for climate zone 3C and 4C during the whole cooling season

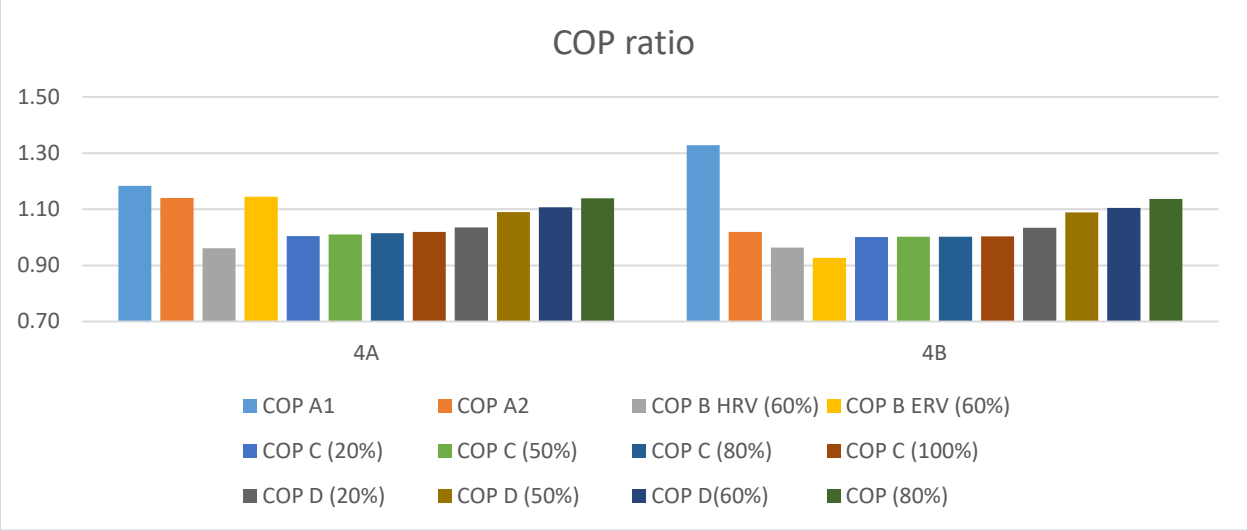

Figure 381 Weighted COP ratio comparison between different reconfigured systems based on the old model for climate zone 4A and 4B during the whole cooling season

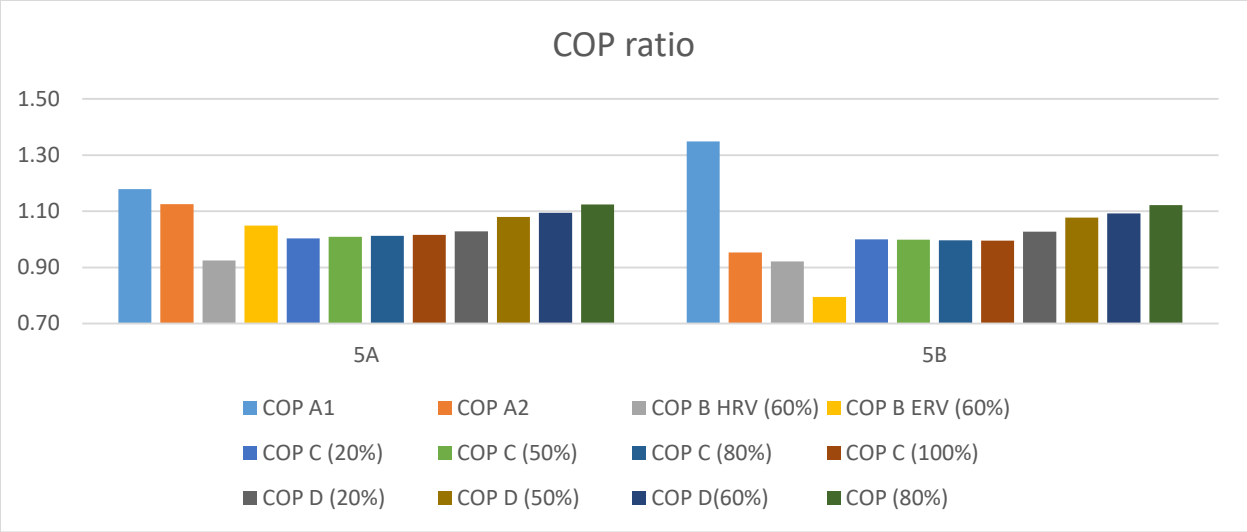

Figure 382 Weighted COP ratio comparison between different reconfigured systems based on the old model for climate zone 5A and 5B during the whole cooling season

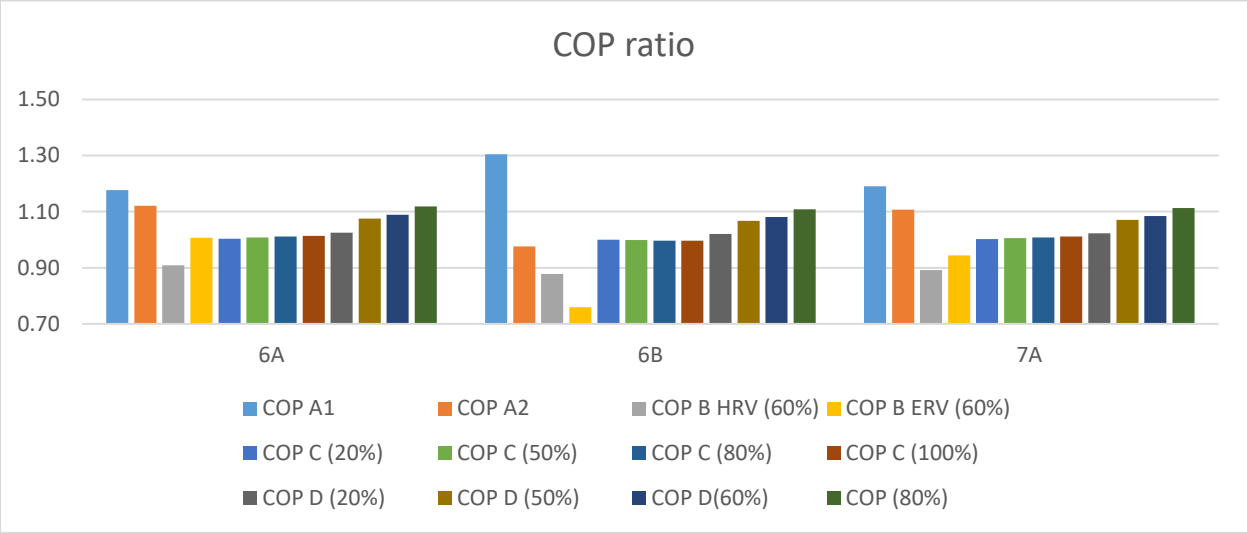

Figure 383 Weighted COP ratio comparison between different reconfigured systems based on the old model for climate zone 6A, 6B and 7A during the whole cooling season

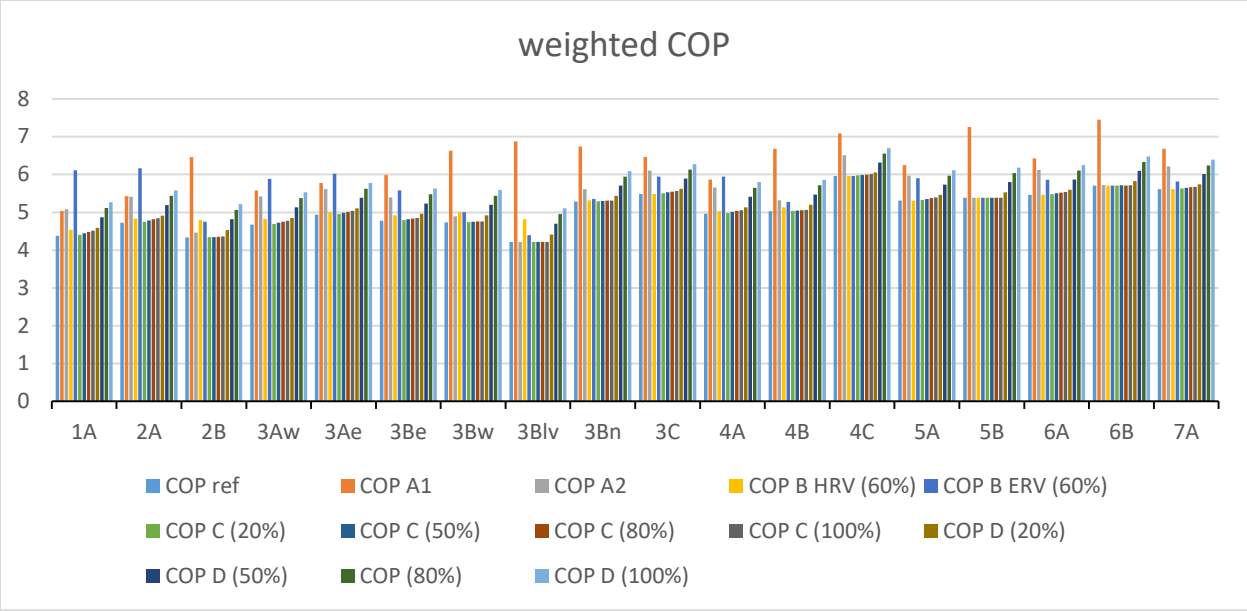

Figure 384 Weighted COP comparison between different reconfigured systems based on the corrected model for all climate zones during the whole cooling season

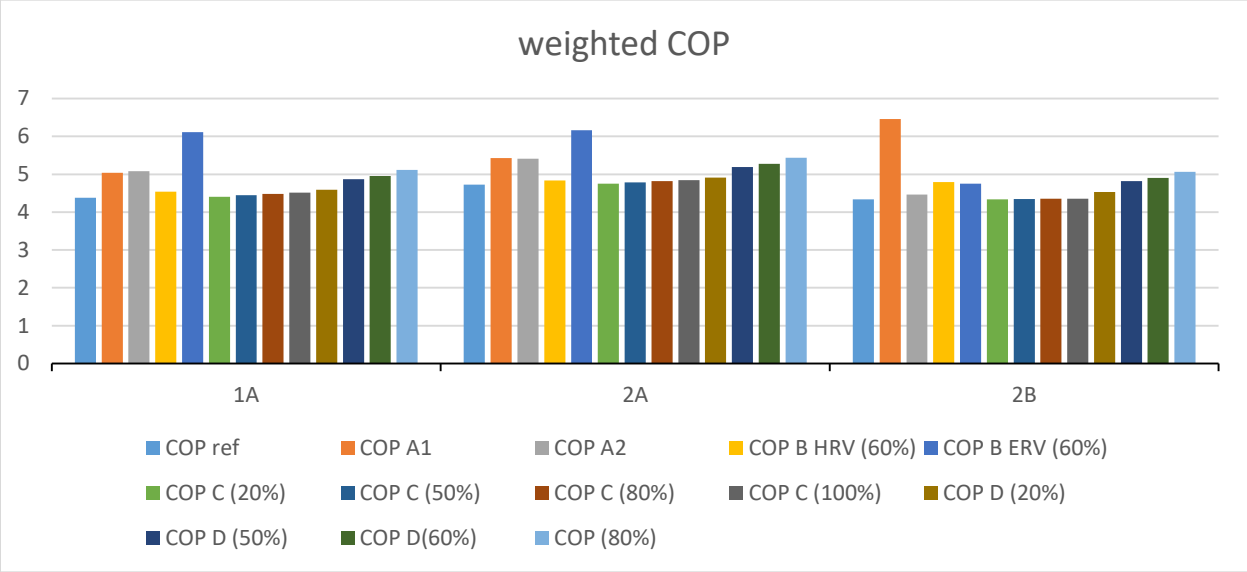

Figure 385 Weighted COP comparison between different reconfigured systems based on the corrected model for climate zone 1A, 2A and 2B during the whole cooling season

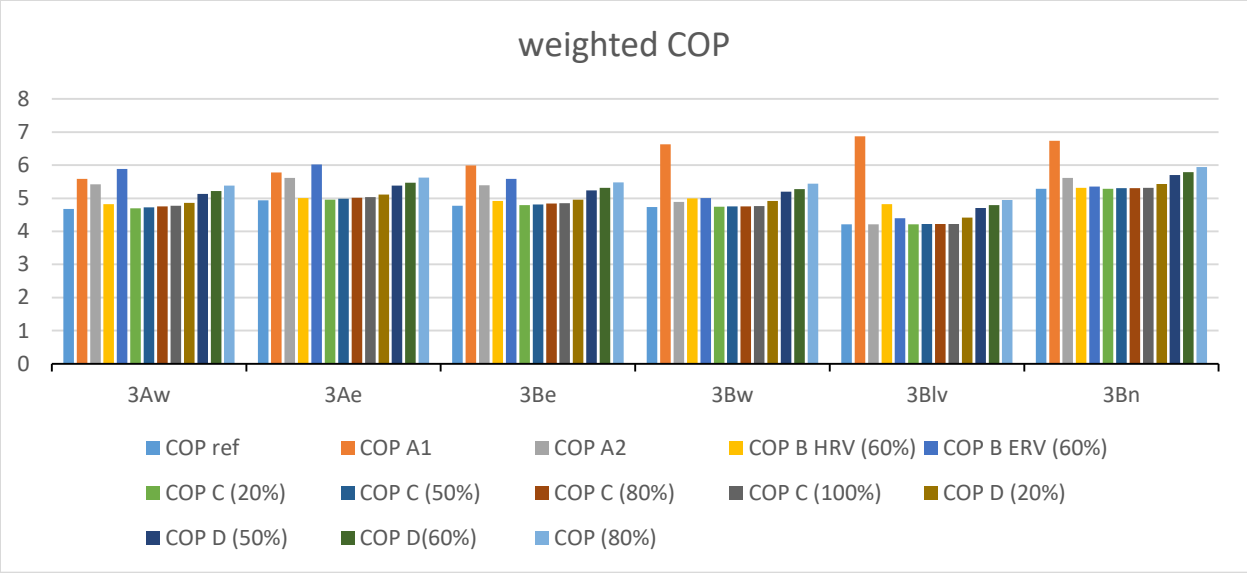

Figure 386 Weighted COP comparison between different reconfigured systems based on the corrected model for climate zone 3Aw, 3Ae, 3Be, 3Bw, 3Blv and 3Bn during the whole cooling season

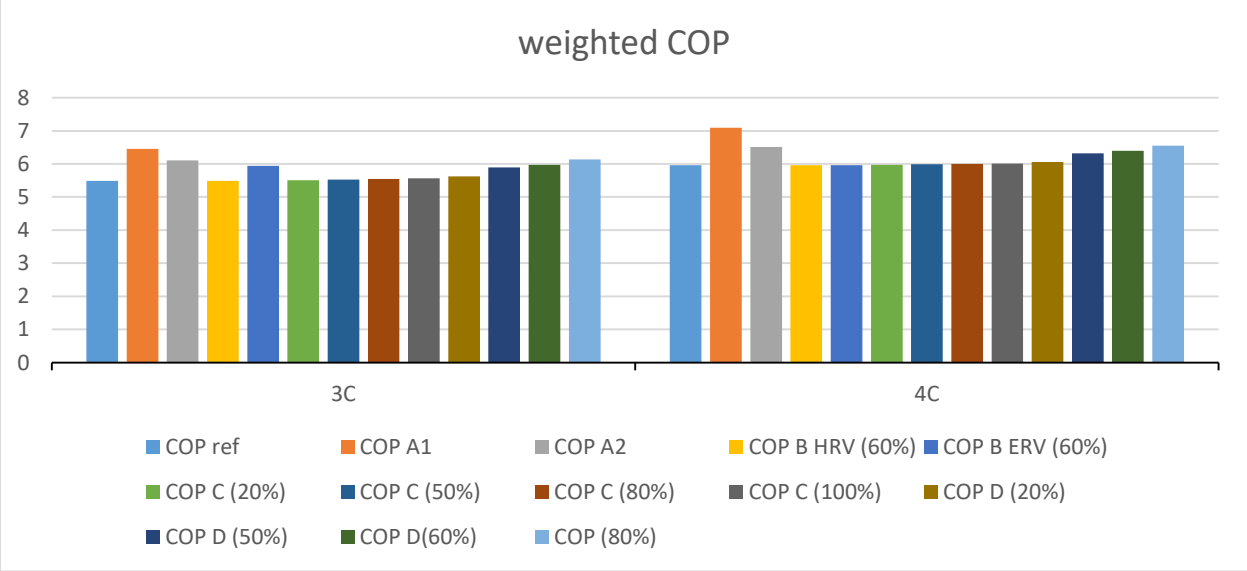

Figure 387 Weighted COP comparison between different reconfigured systems based on the corrected model for climate zone 3C and 4Cduring the whole cooling season

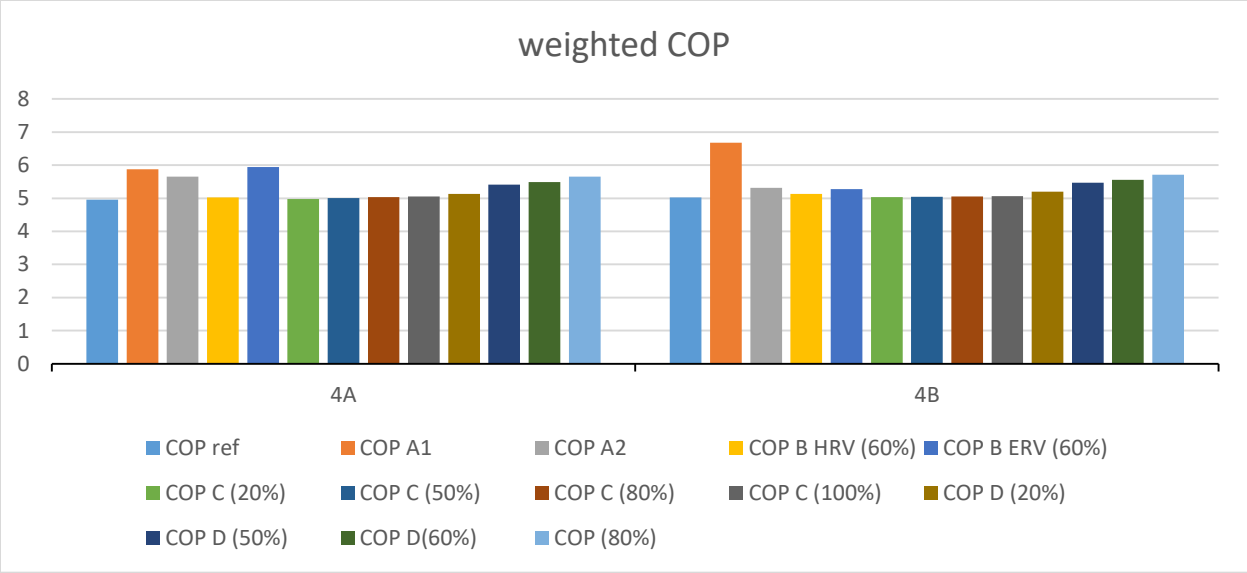

Figure 388 Weighted COP comparison between different reconfigured systems based on the corrected model for climate zone 4A and 4B during the whole cooling season

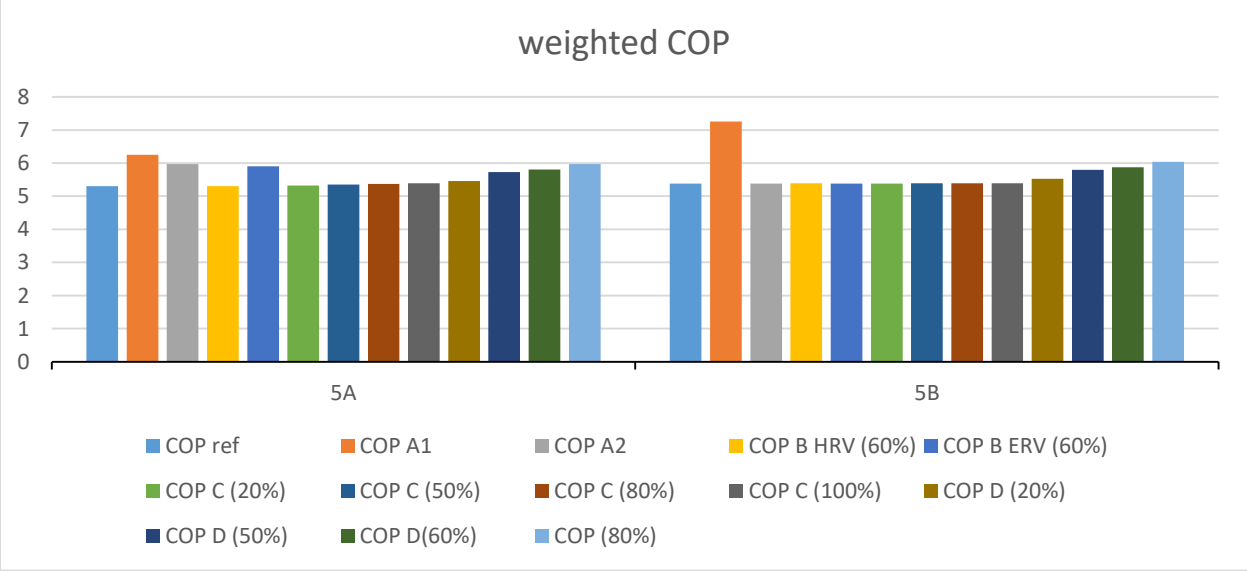

Figure 389 Weighted COP comparison between different reconfigured systems based on the corrected model for climate zone 5A and 5B during the whole cooling season

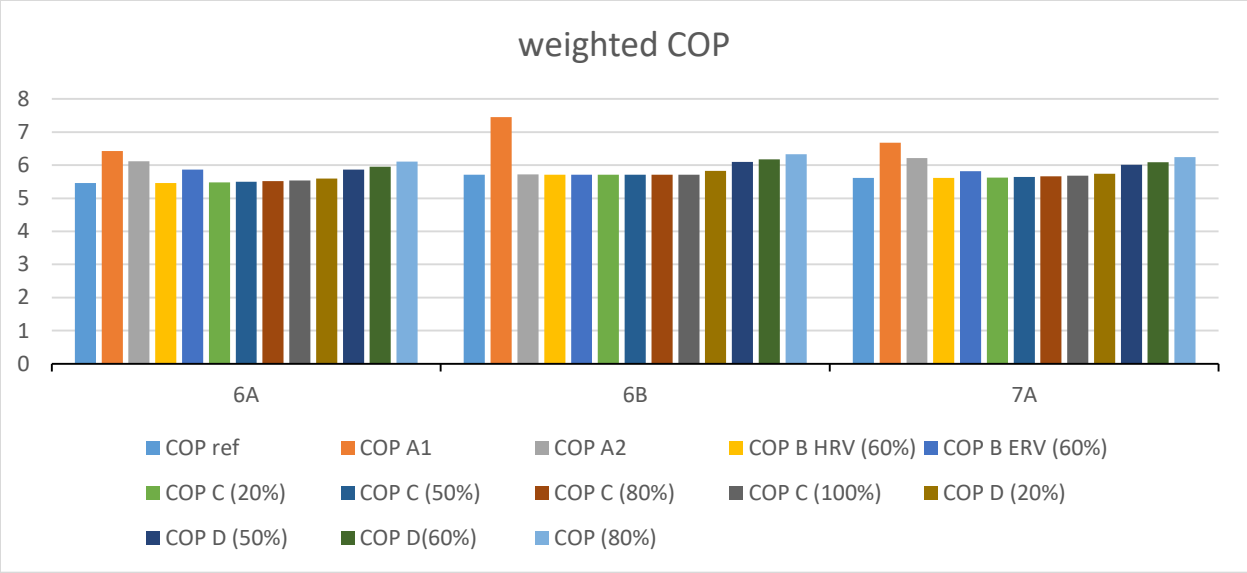

Figure 390 Weighted COP comparison between different reconfigured systems based on the corrected model for climate zone 6A, 6B and 7A during the whole cooling season

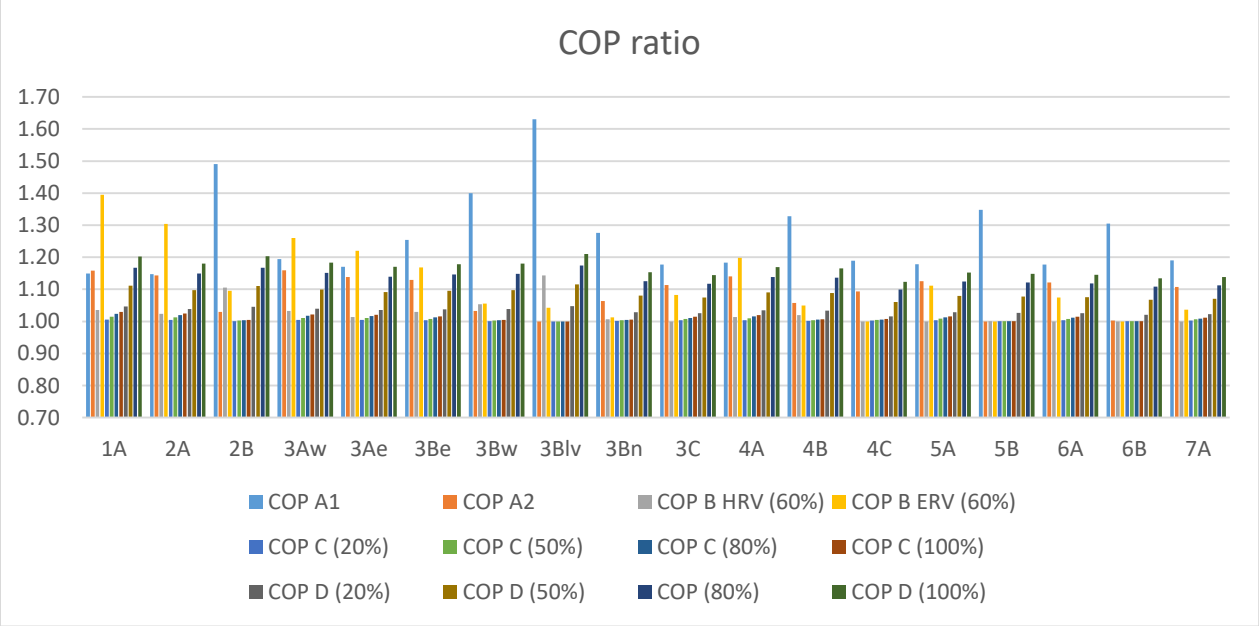

Figure 391 Weighted COP ratio comparison between different reconfigured systems based on the corrected model for all climate zones during the whole cooling season

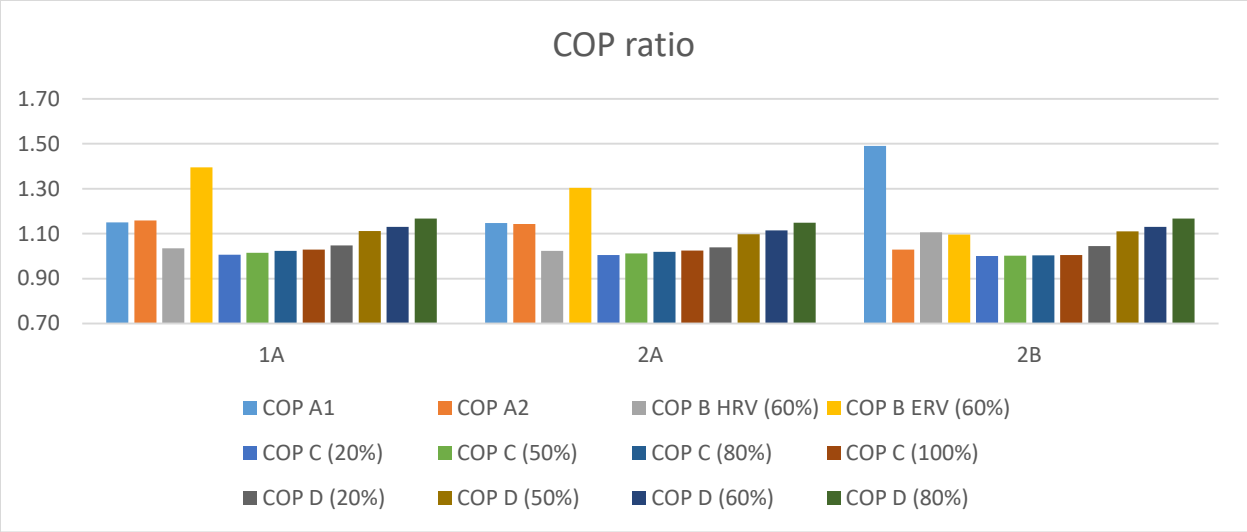

Figure 392 Weighted COP ratio comparison between different reconfigured systems based on the corrected model for climate zone 1A, 2A and 2B during the whole cooling season

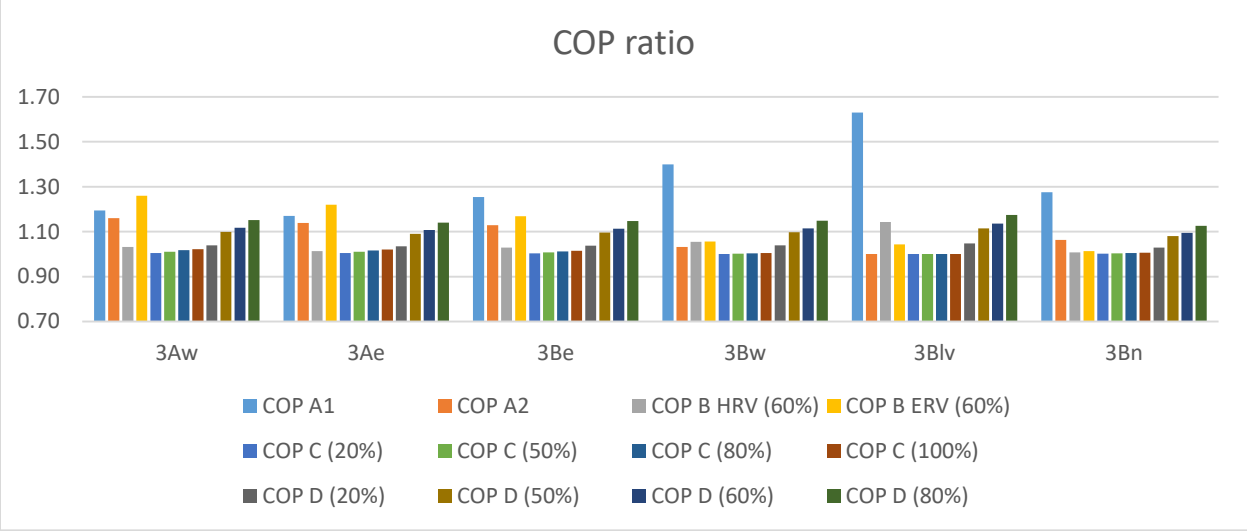

Figure 393 Weighted COP ratio comparison between different reconfigured systems based on the corrected model for climate zone 3Aw, 3Ae, 3Be, 3Bw, 3Blv and 3Bn during the whole cooling season

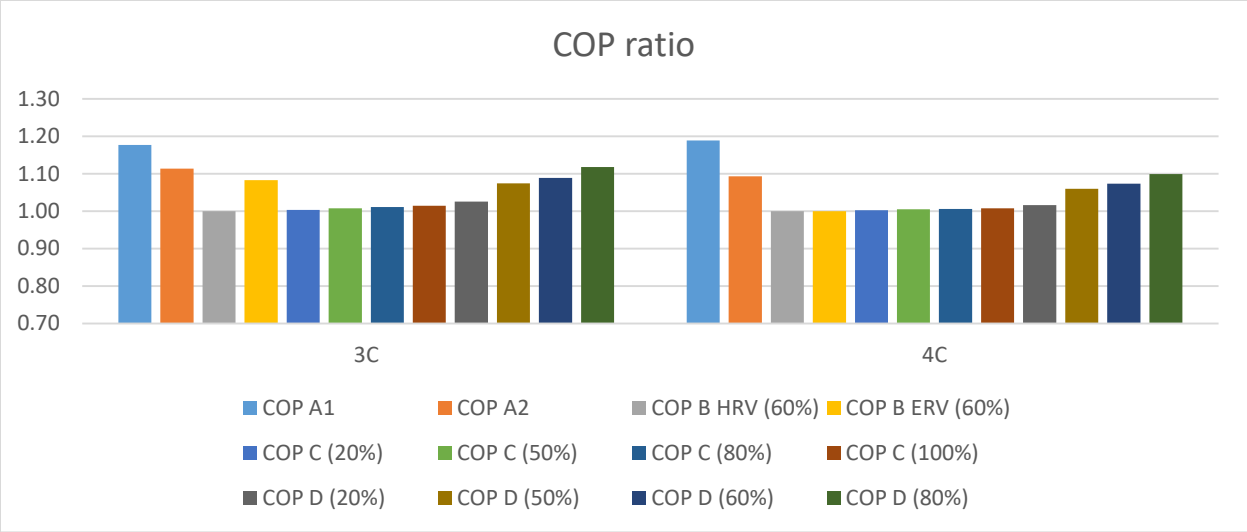

Figure 394 Weighted COP ratio comparison between different reconfigured systems based on the corrected model for climate zone 3C and 4C during the whole cooling season

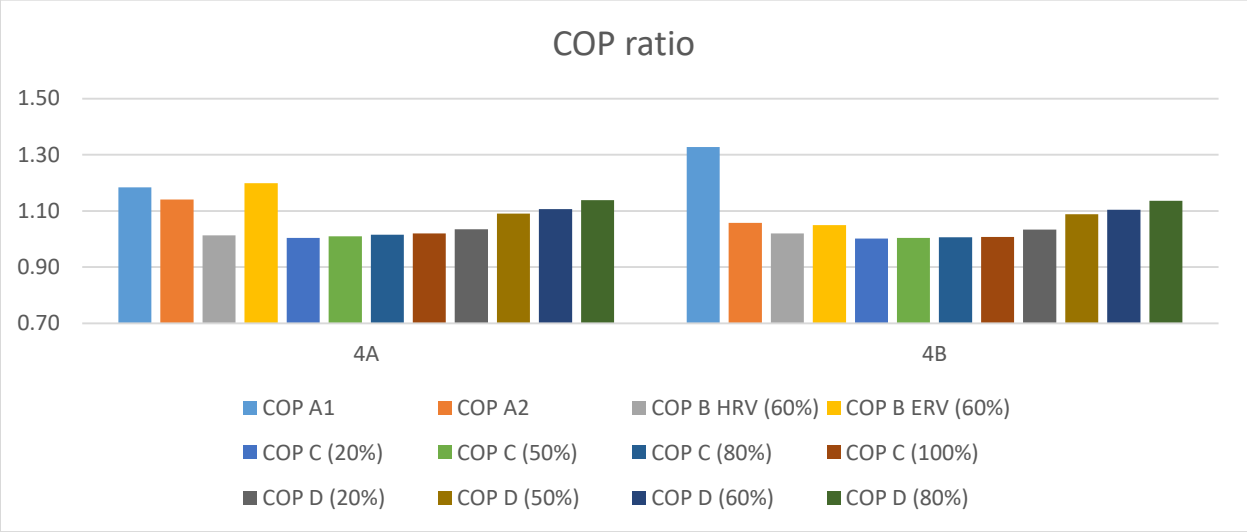

Figure 395 Weighted COP ratio comparison between different reconfigured systems based on the corrected model for climate zone 4A and 4B during the whole cooling season

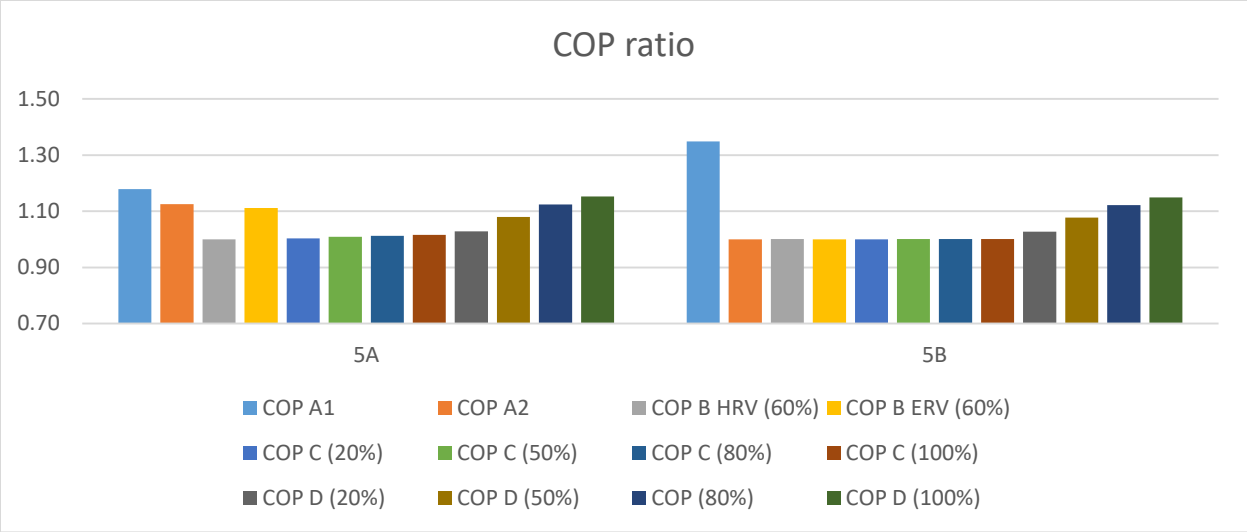

Figure 396 Weighted COP ratio comparison between different reconfigured systems based on the corrected model for climate zone 5A and 5B during the whole cooling season

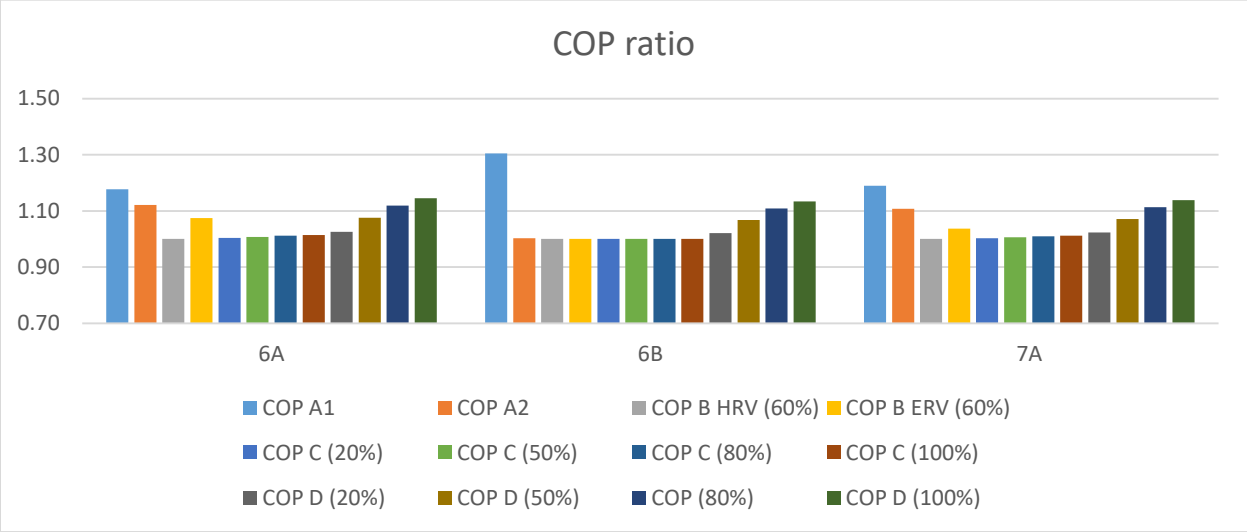

Figure 397 Weighted COP ratio comparison between different reconfigured systems based on the corrected model for climate zone 6A, 6B and 7A during the whole cooling season

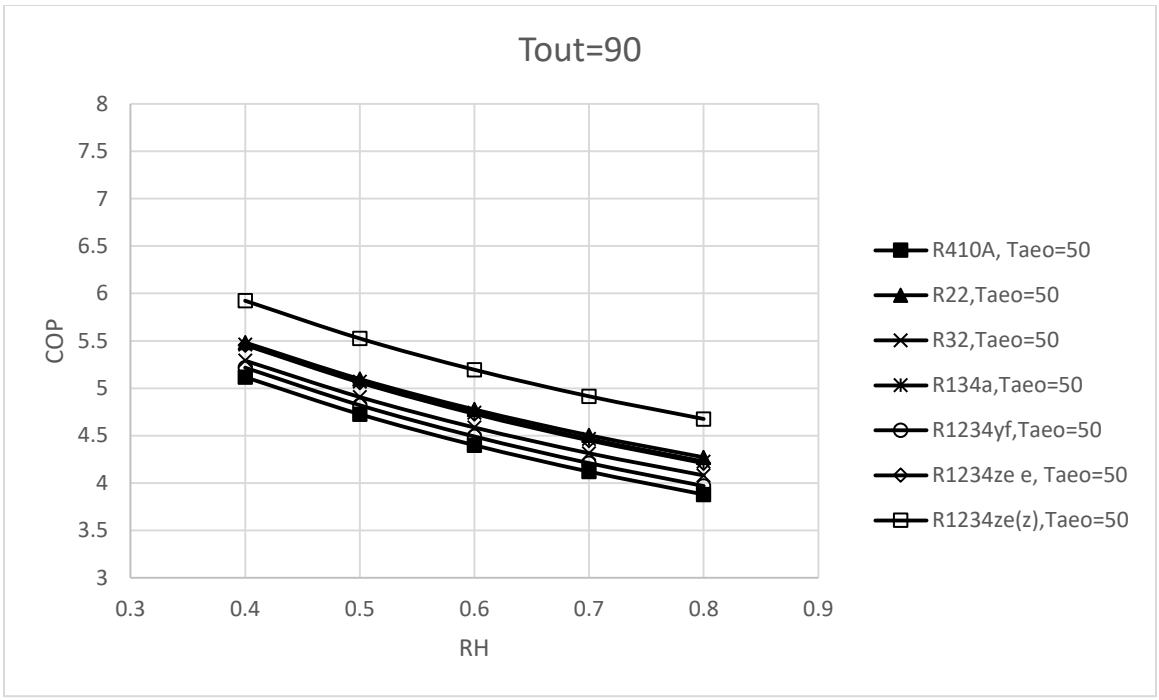

Figure 398 7 refrigerants COP comparison based on reconfigured system A1 when Tout=90°F *and Taeo=50*°F

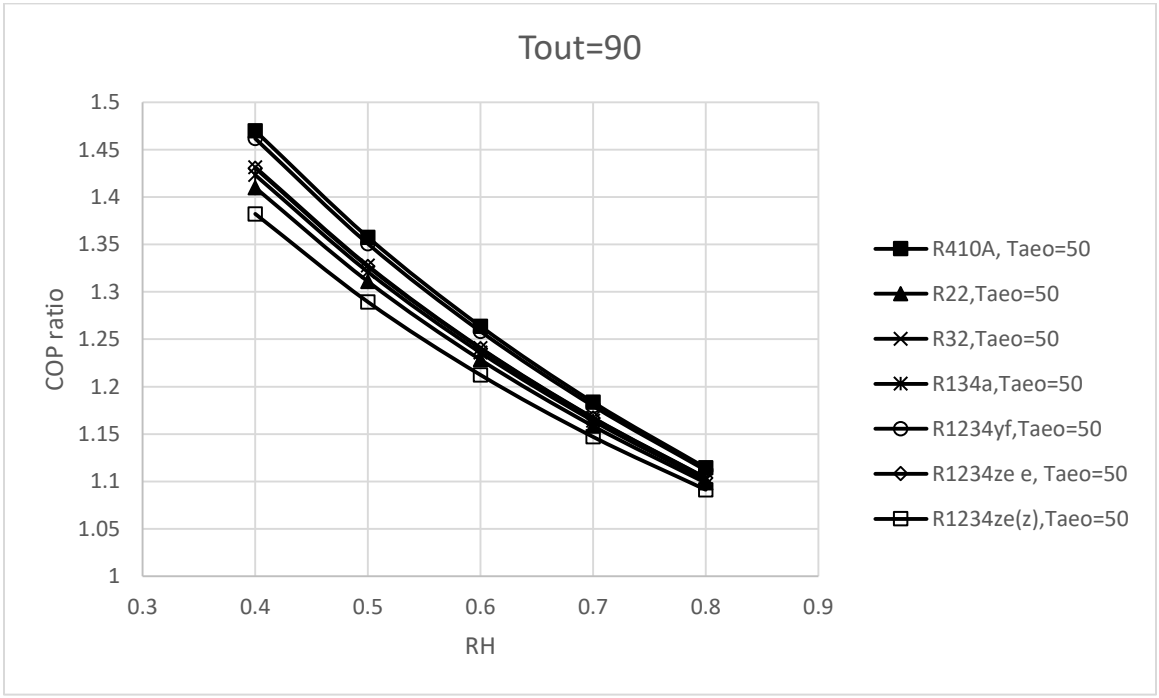

Figure 399 7 refrigerants COP ratio comparison based on reconfigured system A1 when Tout=90°F *and Taeo=50*°F

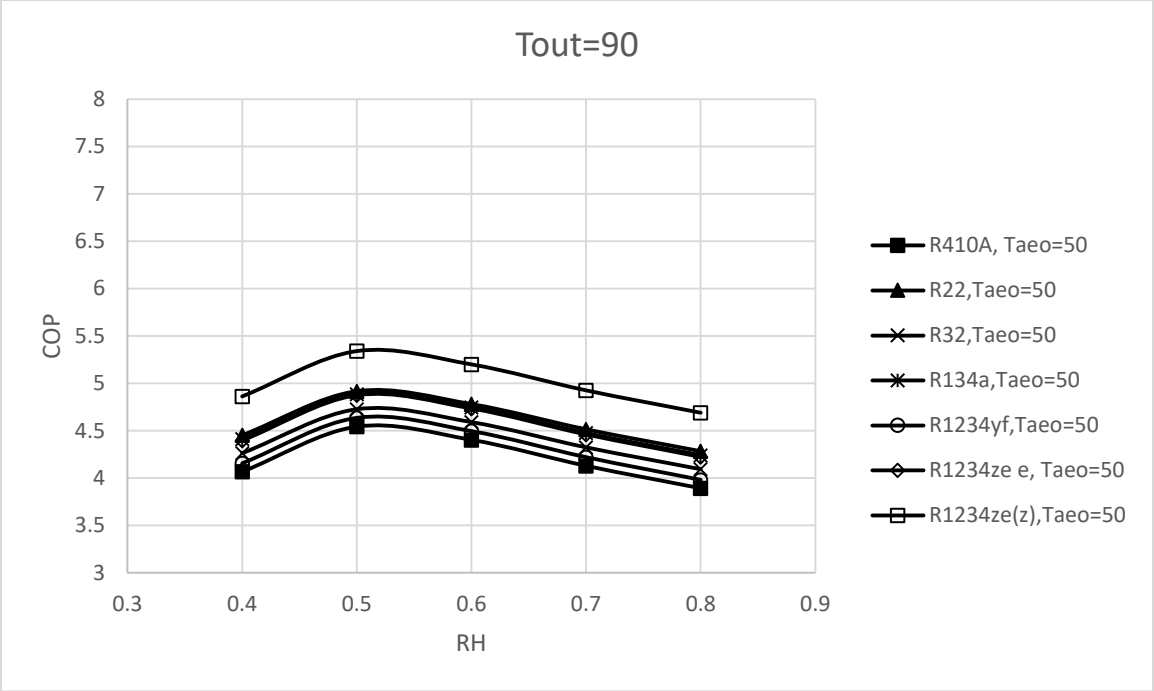

Figure 400 7 refrigerants COP comparison based on reconfigured system A2 when Tout=90℉ and Taeo=50℉

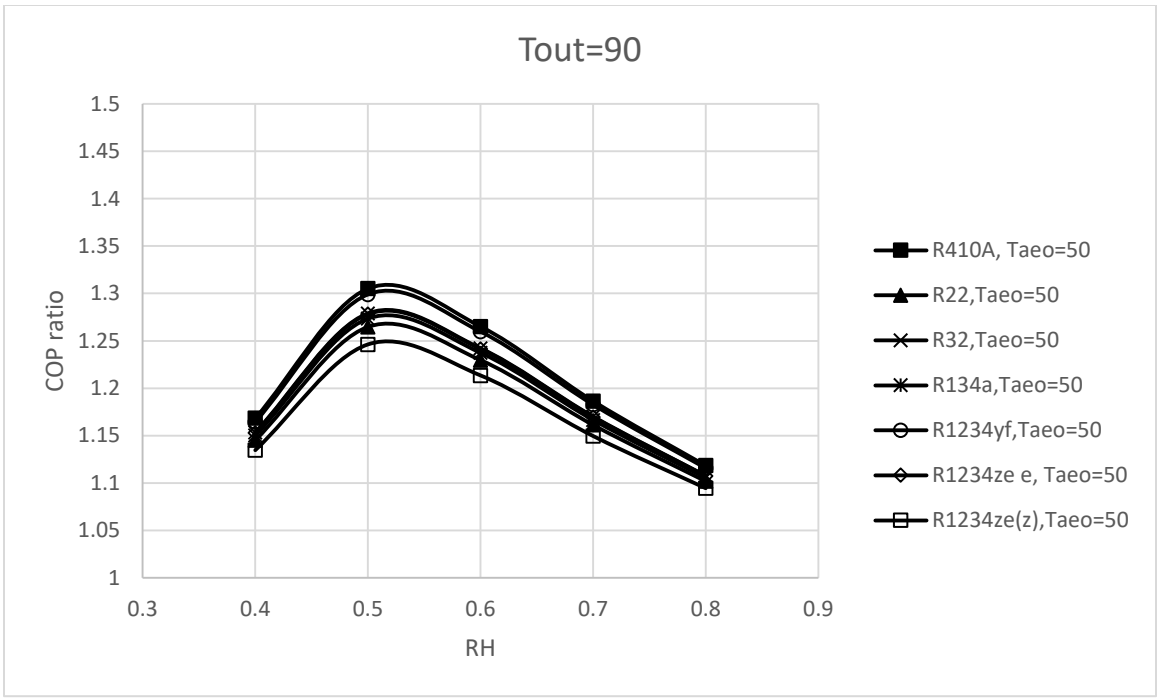

Figure 401 7 refrigerants COP ratio comparison based on reconfigured system A2 when Tout=90°F and Taeo=50°F

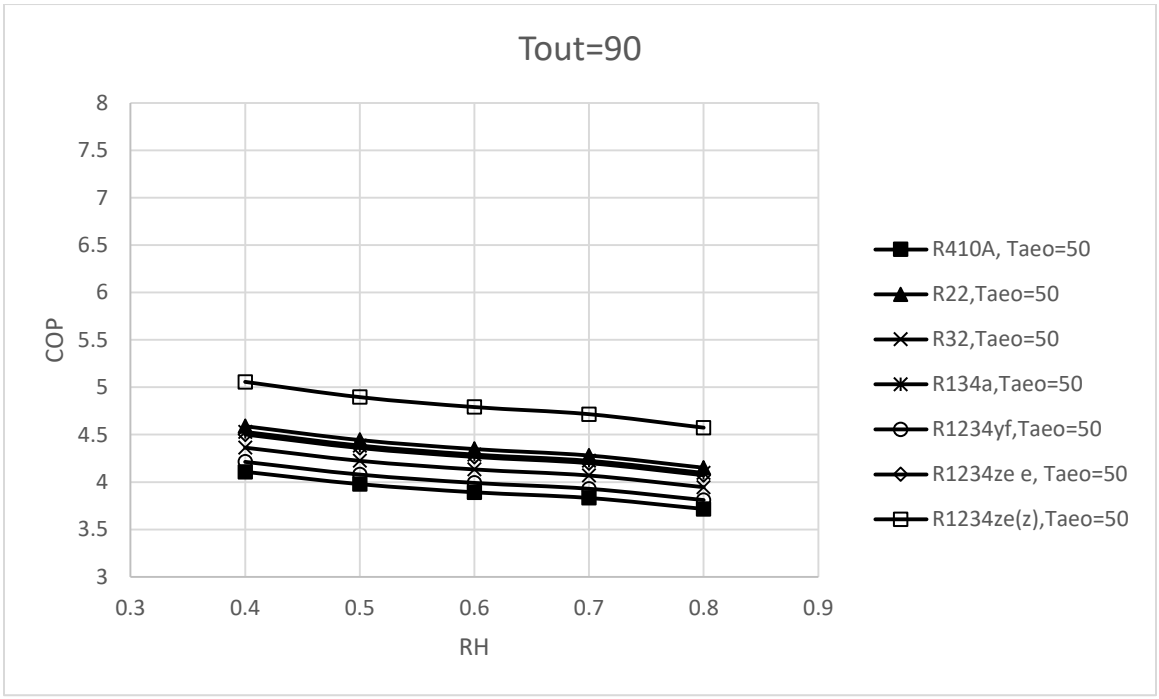

Figure 402 7 refrigerants COP comparison based on reconfigured system B1 when Tout=90°F and Taeo=50°F

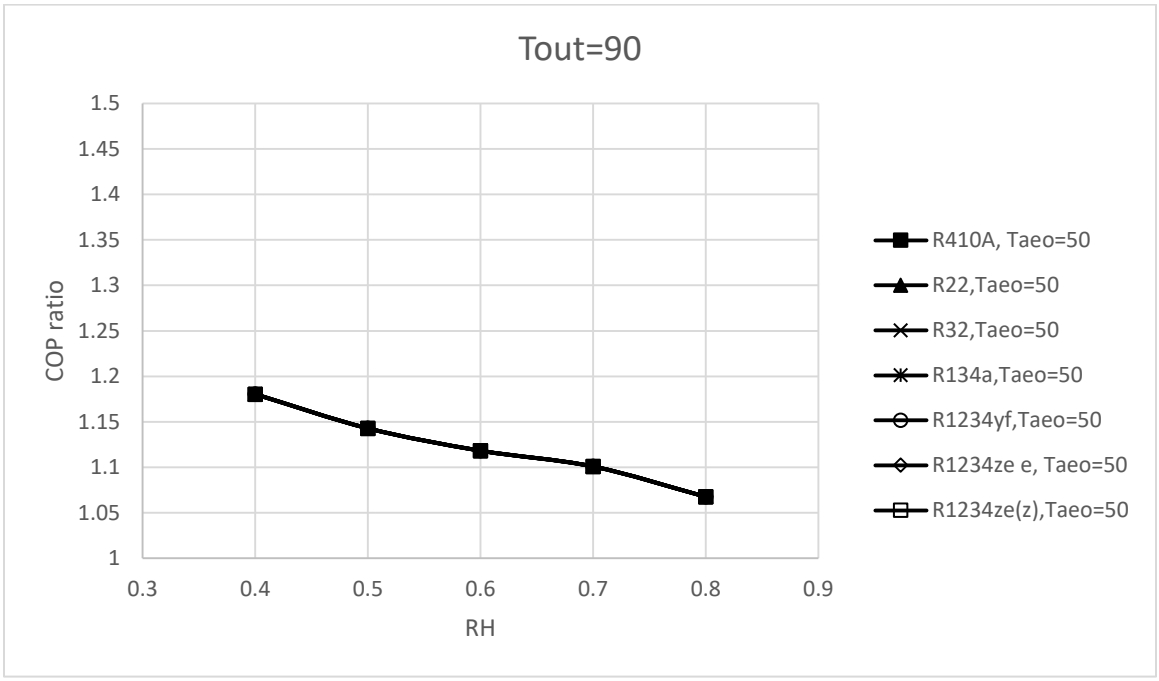

Figure 403 7 refrigerants COP ratio comparison based on reconfigured system B1 when Tout=90°F and Taeo=50°F

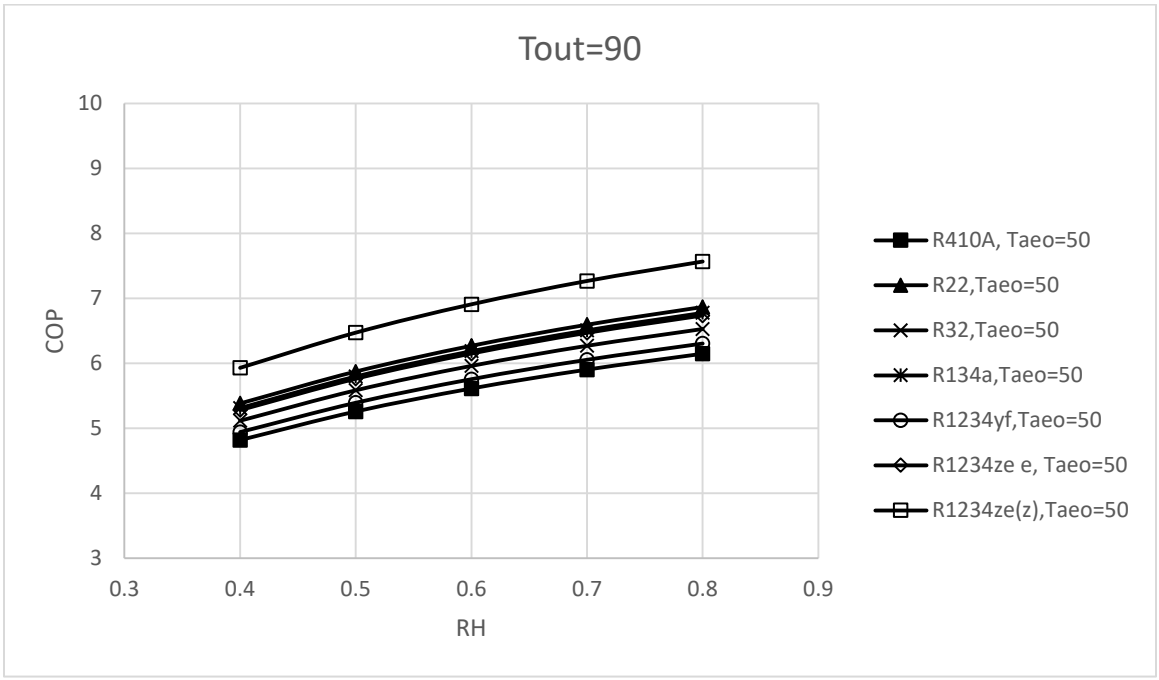

Figure 404 7 refrigerants COP comparison based on reconfigured system B2 when Tout=90°F and Taeo=50°F

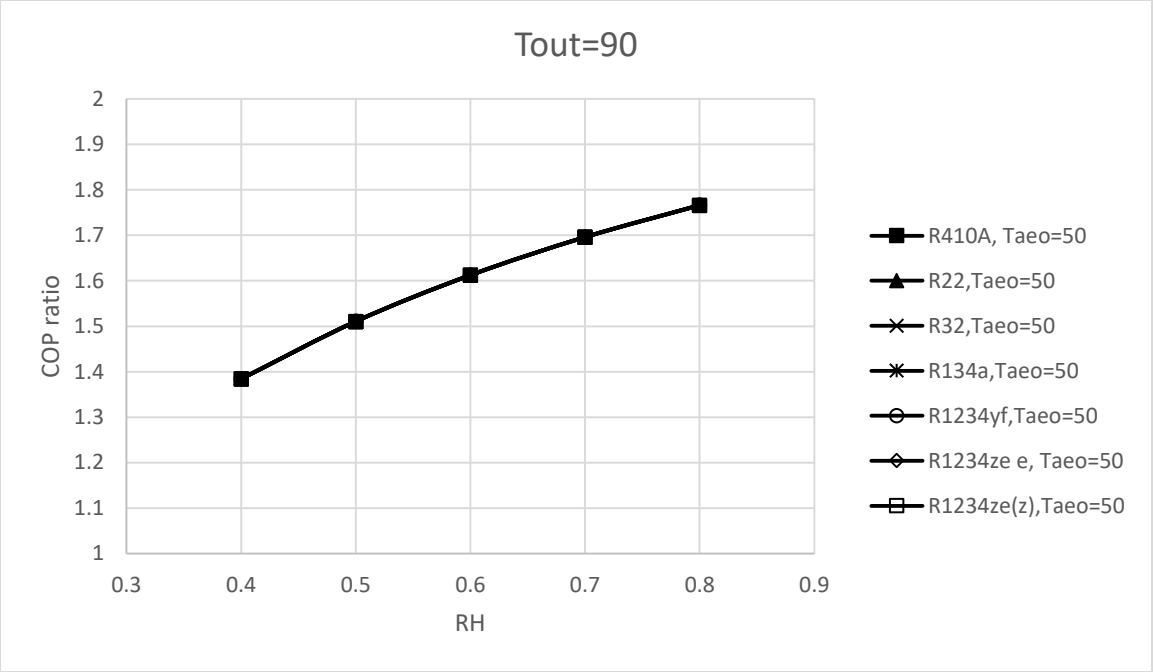

Figure 405 7 refrigerants COP ratio comparison based on reconfigured system B2 when Tout=90°F and Taeo=50°F

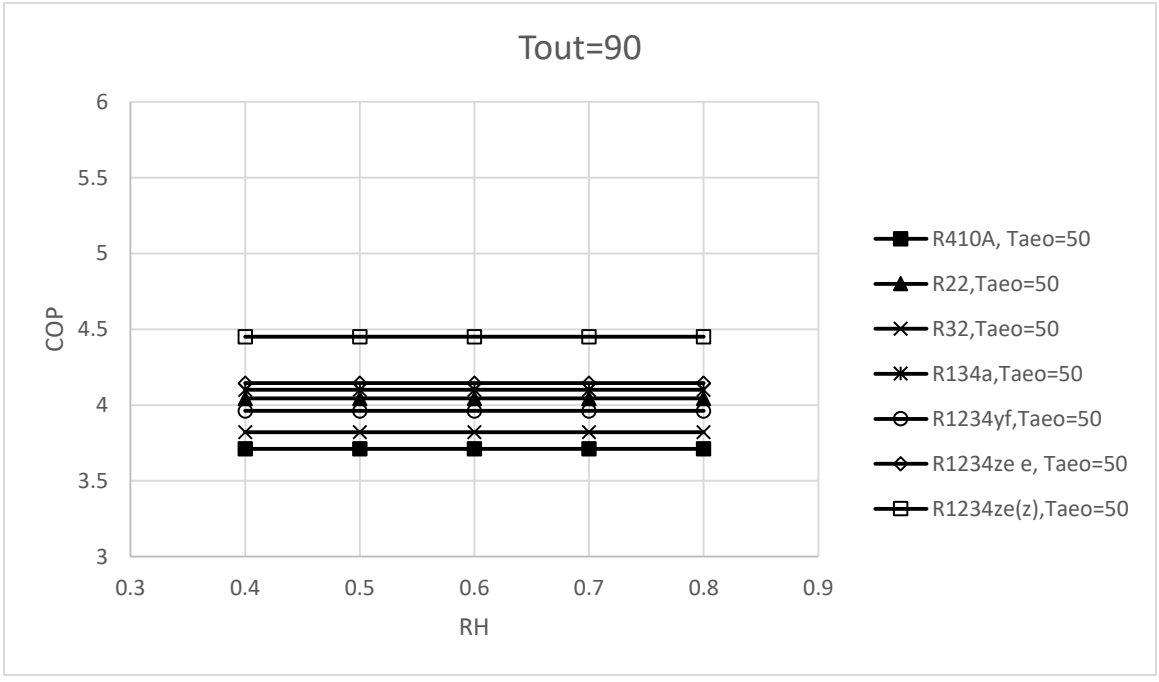

Figure 406 7 refrigerants COP comparison based on reconfigured system D with 20% internal heat exchanger effectiveness when Tout=90°F and Taeo=50°F

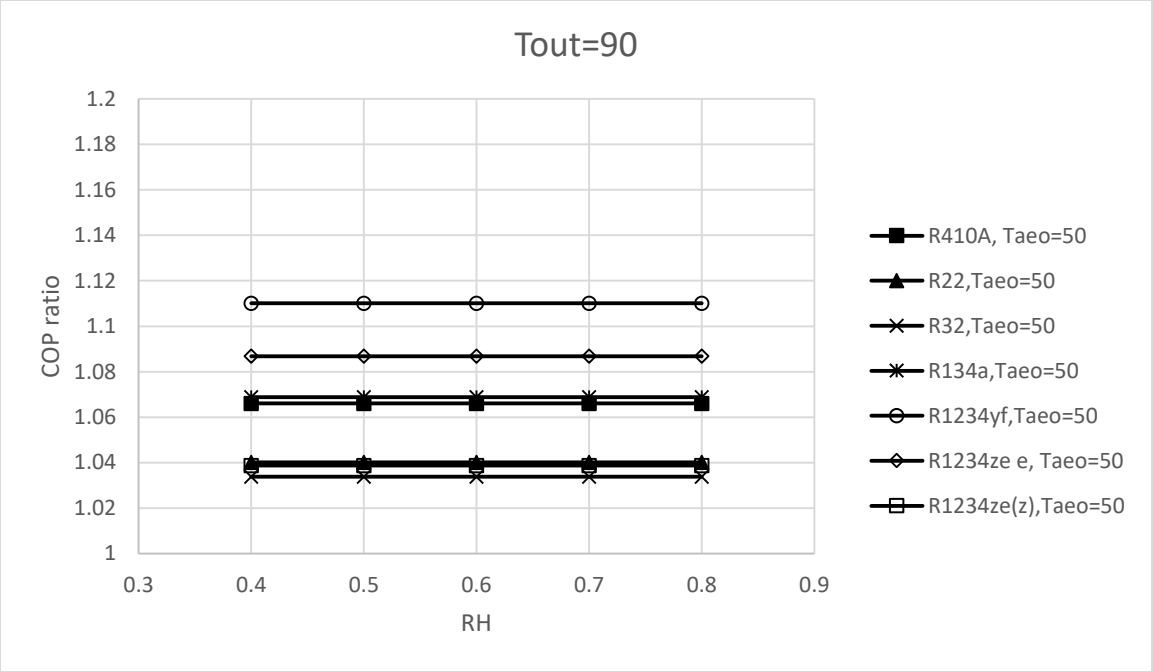

Figure 407 7 refrigerants COP ratio comparison based on reconfigured system D with 20% internal heat exchanger effectiveness when Tout=90℉ and Taeo=50℉

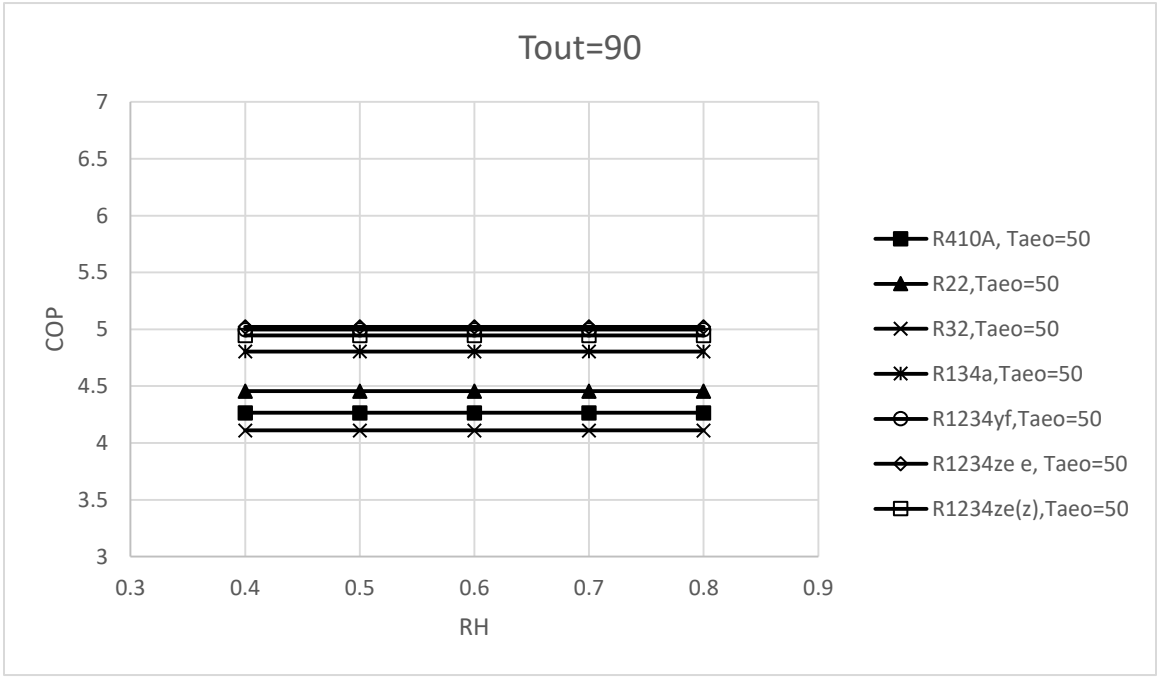

Figure 408 7 refrigerants COP comparison based on reconfigured system D with 80% internal heat exchanger effectiveness when Tout=90℉ and Taeo=50℉

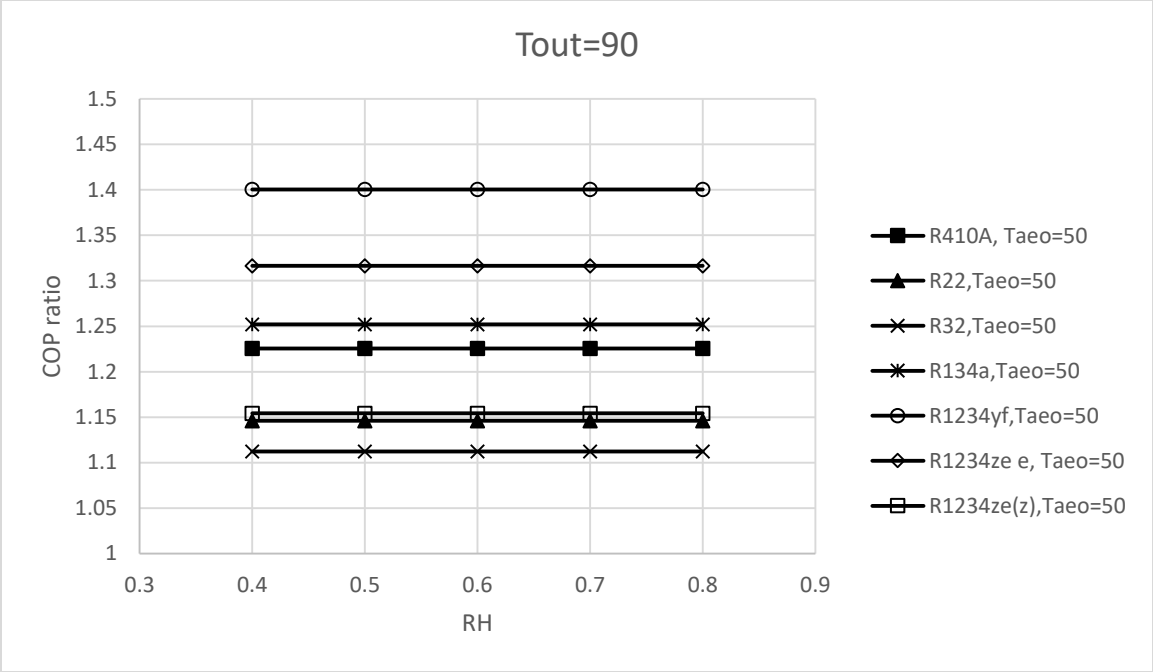

Figure 409 7 refrigerants COP ratio comparison based on reconfigured system D with 80% internal heat exchanger effectiveness when Tout=90°F and Taeo=50°F

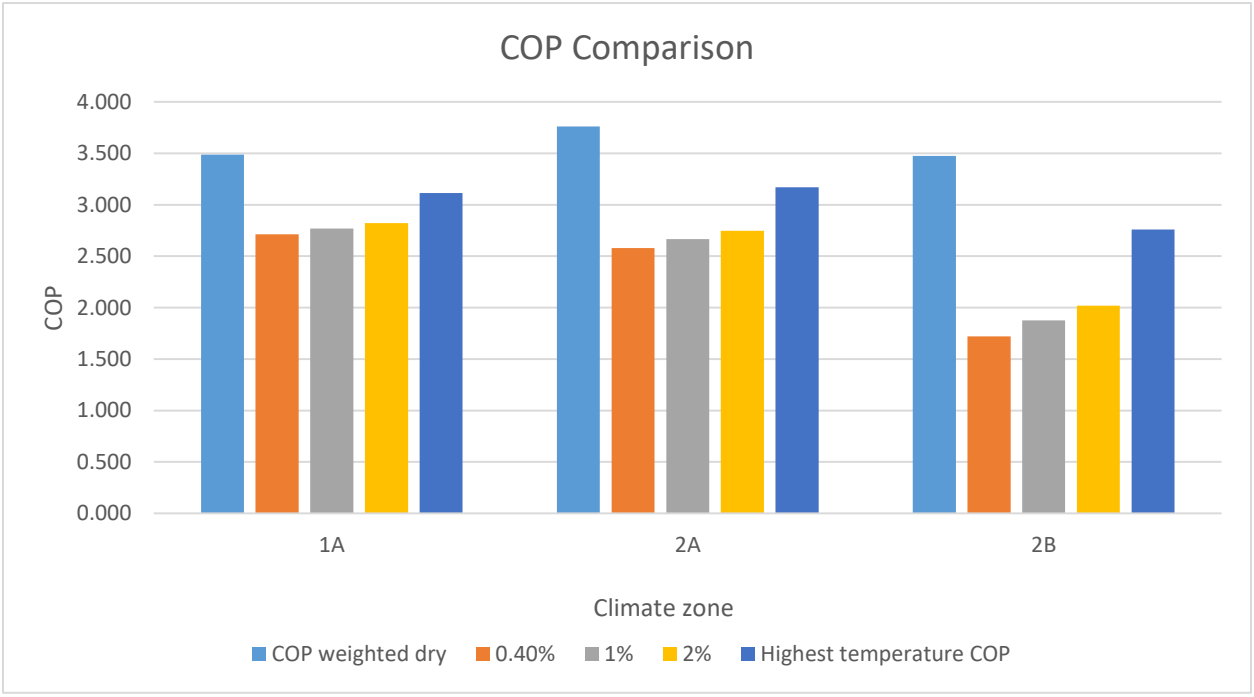

Figure 410 Three COP comparison for climate zone 1A, 2A and 2B

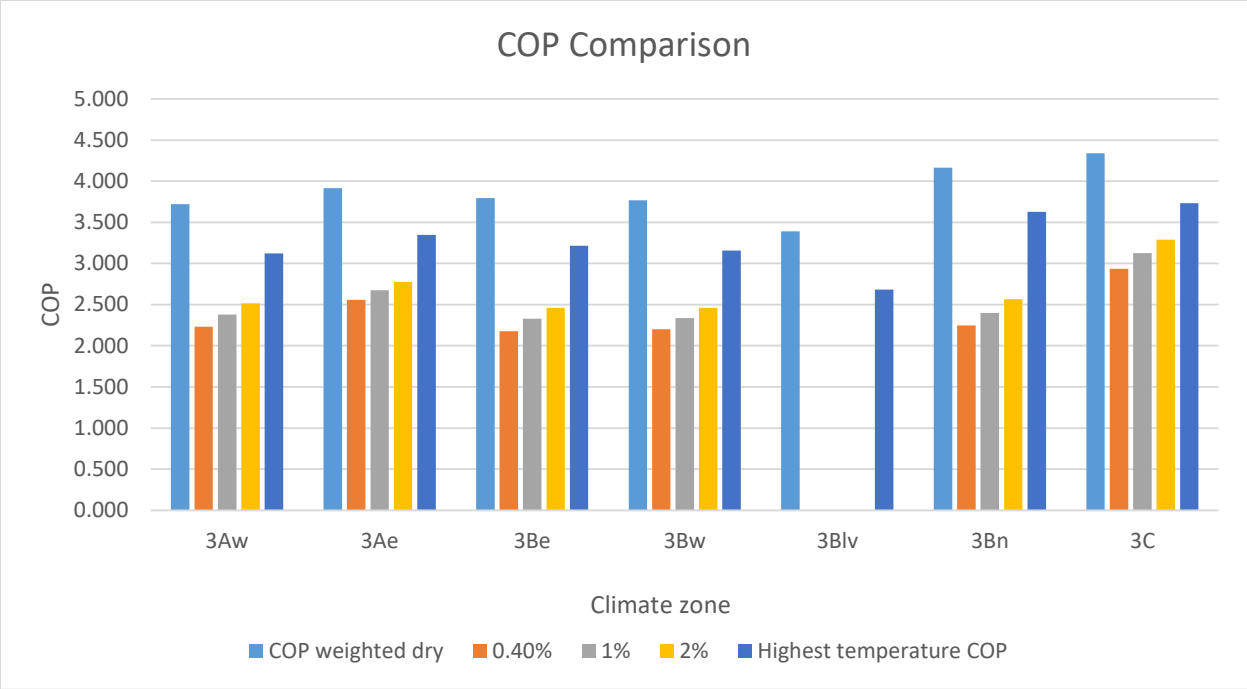

Figure 411 Three COP comparison for climate zone 3Aw, 3Ae, 3Be, 3Bw, 3Blv, 3Bn and 3C

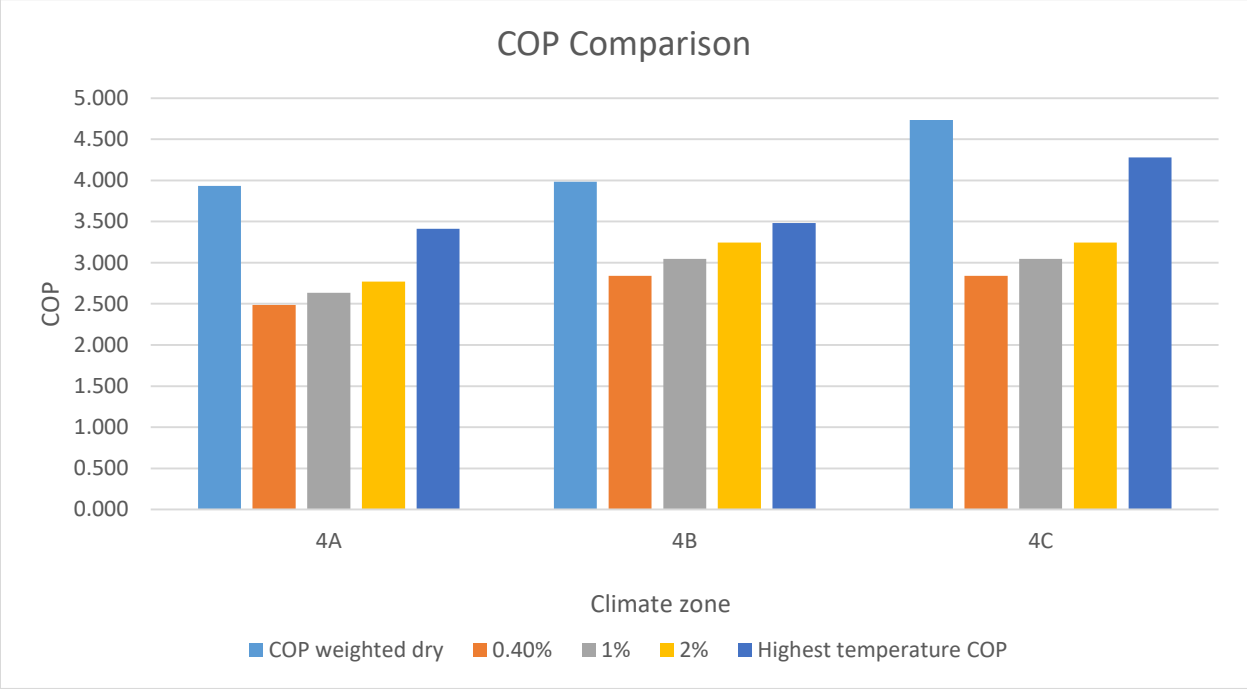

Figure 412 Three COP comparison for climate zone 4A, 4B and 4C

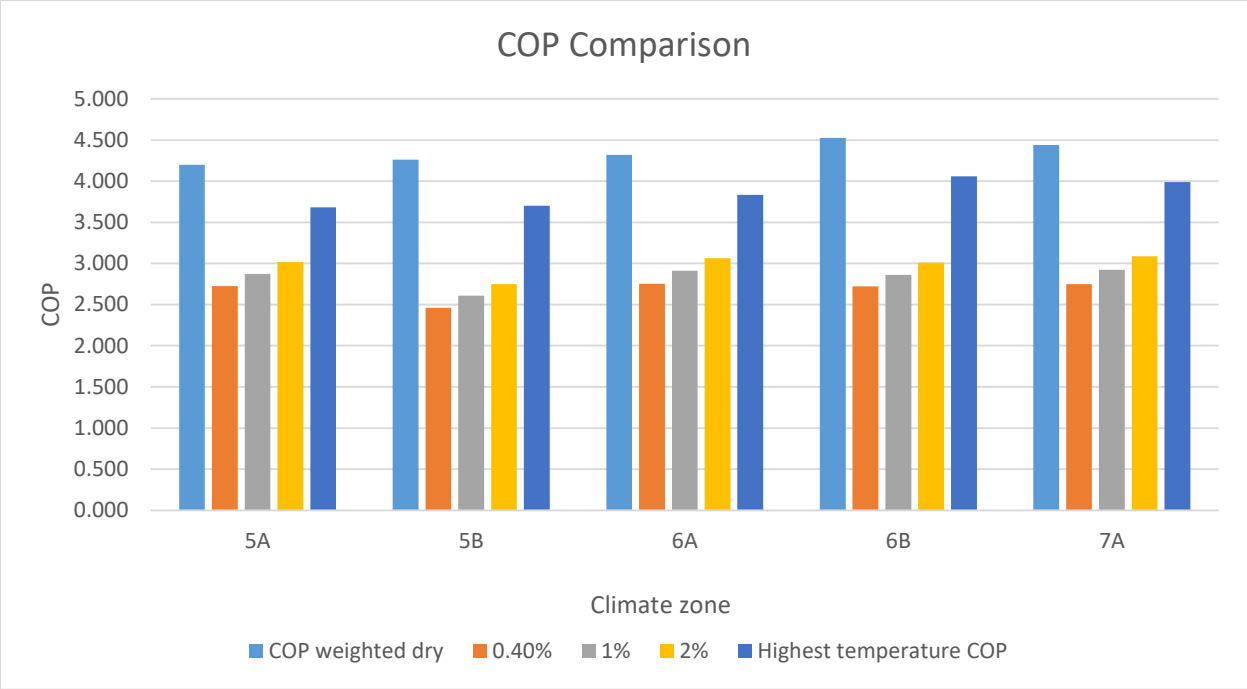

Figure 413 Three COP comparison for climate zone 5A, 5B, 6A, 6B and 7A

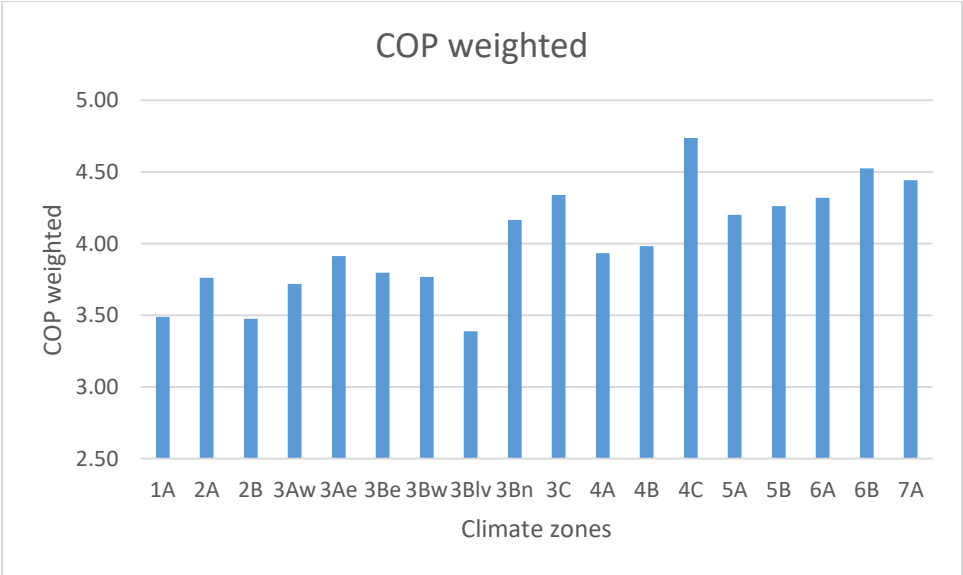

Figure 414 Weighted COP for 18 climate zones

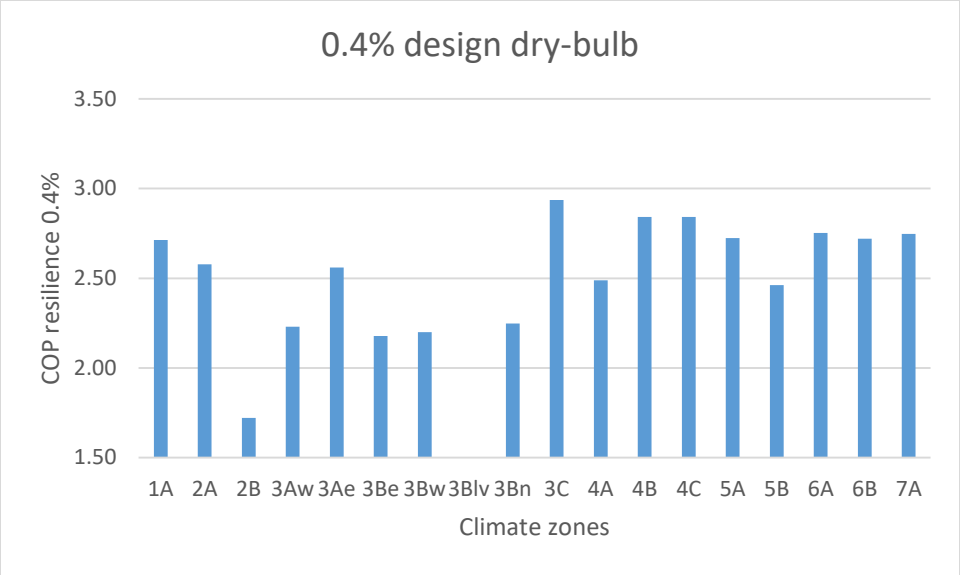

Figure 415 Design COP under 0.4% design dry-bulb temperature for 18 climate zones

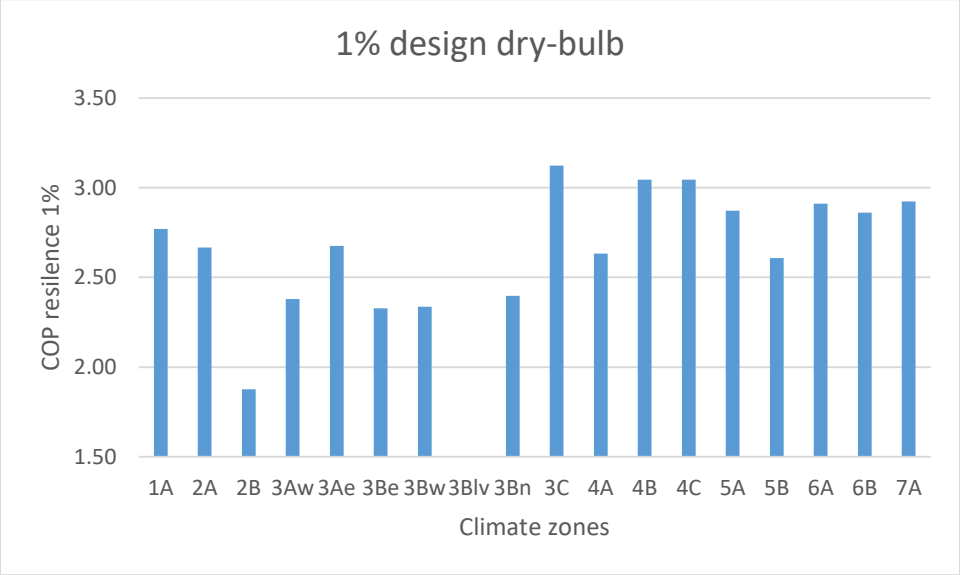

Figure 416 Design COP under 1% design dry-bulb temperature for 18 climate zones

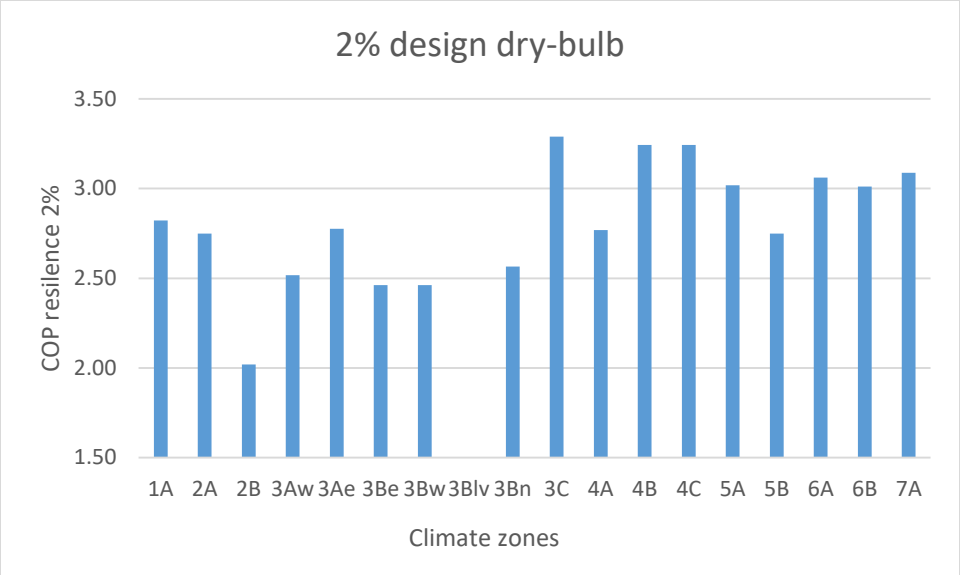

Figure 417 Design COP under 2% design dry-bulb temperature for 18 climate zones

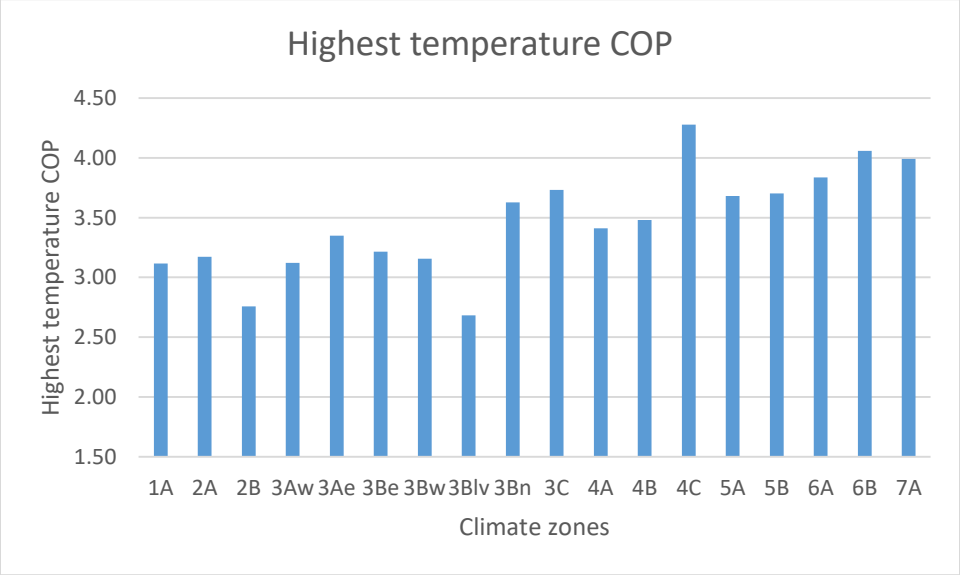

Figure 418 Highest-temperature-corresponding-COP for 18 climate zones